Determination of Synchronous-Machine-Stability Study Constants
Volume 2

EL-1424, Volume 2
Research Project 997-2

Final Report, December 1980
Work Completed, July 1980

Prepared by

ONTARIO HYDRO
700 University Avenue
Toronto, Ontario, Canada
M5G 1X6

Principal Investigators
M. E. Coultes
P. L. Dandeno
P. Kundur
A. T. Poray
W. Watson
H. M. Zein El-Din

Prepared for

Electric Power Research Institute
3412 Hillview Avenue
Palo Alto, California 94304

EPRI Project Managers
P. M. Anderson
D. T. Bewley
J. C. White

Rotating Electrical Machinery Program
Electrical Systems Division

ORDERING INFORMATION

Requests for copies of this report should be directed to Research Reports Center (RRC), Box 50490, Palo Alto, CA 94303, (415) 965-4081. There is no charge for reports requested by EPRI member utilities and affiliates, contributing nonmembers, U.S. utility associations, U.S. government agencies (federal, state, and local), media, and foreign organizations with which EPRI has an information exchange agreement. On request, RRC will send a catalog of EPRI reports.

NOTICE

This report was prepared by the organization(s) named below as an account of work sponsored by the Electric Power Research Institute, Inc. (EPRI). Neither EPRI, members of EPRI, the organization(s) named below, nor any person acting on their behalf: (a) makes any warranty or representation, express or implied, with respect to the accuracy, completeness, or usefulness of the information contained in this report, or that the use of any information, apparatus, method, or process disclosed in this report may not infringe privately owned rights; or (b) assumes any liabilities with respect to the use of, or for damages resulting from the use of, any information, apparatus, method, or process disclosed in this report.

Prepared by
Ontario Hydro
Toronto, Ontario, Canada

ABSTRACT

Data for two different 500 MW turbogenerators was gathered from standstill, on-line, and rated-speed open-circuit frequency response, dc inductance, 60 Hz field impedance, and line switching tests. The relative merits of generator models computed from standstill and on-line frequency response tests, stator decrement tests and sudden short circuit tests were judged by their ability to reproduce the measured line switching transients. From the results, an equivalent circuit model with three rotor windings in each axis and d-axis rotor circuit mutual leakage elements is recommended, with the parameters of the model being obtained from standstill, and in some cases also on-line frequency response measurements. Magnetic non-linearity of the iron was significant in all parts of the work. Q-axis saturation could not be estimated adequately from d-axis characteristics. Steady state measurements, on load, were used to compute the q-axis saturation curve.

EPRI PERSPECTIVE

PROJECT DESCRIPTION

Synchronous machines may be represented by passive electrical models for use in computer simulation studies involving network behavior under the influence of switching phenomena. For years the parameters of the model have been determined by calculation methods performed by the machine manufacturer. Computer results, involving switching disturbances introduced into the modeled network system, do not always compare well with switching tests performed on the actual system. In an effort to evaluate the validity of the calculated parameters utilized in the machine model, this project was designed to determine the generator model parameters through test methods.

Four contractors were asked to develop generator model parameters utilizing test methods. This Volume 2 report under RP997-2 details the conclusions reached by Ontario Hydro using frequency response techniques. Volumes 1 and 4 detail the conclusions reached by Westinghouse Electric Corporation and NEI Parsons, Ltd., respectively, also using frequency response techniques. Volume 3 details the conclusions reached by Power Technologies, Inc., using load-rejection techniques.

PROJECT OBJECTIVES

This was a 40-month project begun April 1, 1977. The goals of the project were:

1. To obtain a comprehensive set of test data on two machines known to be of distinctly different designs
2. To evaluate the performance of various equivalent circuit structures and recommend one that will adequately model most existing synchronous generators
3. To experiment with and evaluate different tests for obtaining parameters for this model and recommend a test procedure
4. To implement the suggested generator model in the EPRI and Ontario Hydro transient stability programs and determine the effect on program execution time
5. To recommend an improved way of handling iron saturation in transient stability programs

PROJECT RESULTS

It was concluded that a model incorporating three rotor windings in each of the direct- and quadrature-axis equivalent circuits, with parameters derived from a combination of standstill and on-line frequency response tests, best reproduced the measured line switching transients on the two different machines tested. For many machines, the standstill frequency response test would be sufficient for establishing the circuit parameters; for machines with complex, low-resistance damper structures, the on-line test was found to be necessary to adequately establish the parameters. Implementation of the suggested models in transient stability computer programs resulted in no significant increase in program execution time. Some recommendations for improved handling of iron saturation are made.

In companion projects (RP997-4 with Westinghouse Electric Corporation and RP997-1 with NEI Parsons, Ltd.) other machines were tested, other calculations were made, and the conclusions reached differed from those of Ontario Hydro. Therefore, no definite conclusions accepting or denying the frequency response test approach for obtaining model parameters can be stated.

Power Technologies, Inc., utilized a testing approach other than the standstill frequency response method; consequently, no comparison of their results with those of the other three contractors is made here.

D. T. Bewley, Project Manager
Electrical Systems Division

CONTENTS

Part 1: PRINCIPAL RESULTS
AND RECOMMENDATIONS

CONTENTS (Cont'd)

Part 2: SECONDARY MODELS
AND ANCILLARY TESTS

Part 3: IMPLEMENTATION OF RECOMMENDED MODELS
IN THE EPRI TRANSIENT AND MIDTERM
STABILITY PROGRAM

CONTENTS (Cont'd)

Part 4: LAMBTON TEST DATA

CONTENTS (Cont'd)

Part 5: NANTICOKE TEST DATA

ILLUSTRATIONS

Part 1: PRINCIPAL RESULTS
AND RECOMMENDATIONS

ILLUSTRATIONS (Cont'd)

ILLUSTRATIONS (Cont'd)

Part 2: SECONDARY MODELS
AND ANCILLARY TESTS

Part 3: IMPLEMENTATION OF RECOMMENDED MODELS IN THE EPRI TRANSIENT AND MIDTERM STABILITY PROGRAM

Part 4: LAMBTON TEST DATA

ILLUSTRATIONS (Cont'd)

Part 5: NANTICOKE TEST DATA

TABLES

Part 1: PRINCIPAL RESULTS
AND RECOMMENDATIONS

Part 2: SECONDARY MODELS
AND ANCILLARY TESTS

Part 3: IMPLEMENTATION OF RECOMMENDED MODELS
IN THE EPRI TRANSIENT AND MIDTERM
STABILITY PROGRAM

TABLES (Cont'd)

Part 4: LAMBTON TEST DATA

Part 5: NANTICOKE TEST DATA

TABLES (Cont'd)

SUMMARY

INTRODUCTION

The electric utility industry needs accurate models for its major generators to be able to predict the performance of the power system in the event of a disturbance. These models, usually in the form of direct and quadrature axis equivalent circuits, are used in transient stability programs which are run on digital computers. Using these programs, power system analysts can study the effect of a given disturbance on different system configurations to see which of them are likely to maintain stable operation following the event, and which are likely to break up with accompanying power interruptions to customers. These studies are the basis for decisions on what configurations (transmission capacity, reserve generation, etc) are tolerable with regard to the required system security. As such, they have a direct bearing on such things as timing of planned maintenance outages, and economic generation scheduling.

The ability of a power system to survive a major distrubance depends largely on whether or not the large generators can maintain synchronous operation during and following the transient. For this reason, models that will reliably predict the behaviour of large generators are crucial to the accuracy of transient stability studies.

The industry's standard test procedure for the performance of synchronous generators (IEEE No 115) is based on the three phase sudden short circuit test. For hydraulic machines, it is satisfactory, for large turbogenerators which now make up the bulk of North American generation, it is not. It provides no quadrature axis data, which is important for these machines; neither does it contain enough information to obtain a satisfactory direct axis model. Even if these fundamental deficiencies in the test procedure are ignored, the risks and practical difficulties associated with sudden short circuit tests on large turbine generators are such that they are never done after the machine is delivered, and only rarely in the factory.

This leaves the industry in the unenviable position of having a standard test which is practically never used, or alternatively, having, at the present time, no accepted standard for measuring the performance of large turbine generators. The project described herein addressed this problem and had as its objectives:

- Define d- and q-axis equivalent circuit structures with sufficient detail to model solid iron rotor turbogenerators.
- Develop a test procedure from which the elements for these equivalent circuits can be computed.
- Implement and test the performance of the new equivalent circuit structures in existing transient stability programs.
- Investigate saturation and other magnetic non-linearities as well as methods of accounting for them in transient stability programs.

RESULTS

A model including three rotor windings in each of the direct and quadrature axis equivalent circuits with parameters derived from a combination of standstill and on-line frequency response tests is recommended. Figures S-1 and S-2 demonstrate the ability of such a model to reproduce measured line switching transients on two different 500 MW turbogenerators on the Ontario Hydro system.

Note that both the power and the field current transients were reproduced with precision. This shows that the field winding has been properly separated from the multitude of other rotor circuits formed by the solid iron rotor forging, slot wedges, and damper windings. This is an important point where auxiliary controls such as power system stabilizers are used. These devices act to damp out oscillations by modulating the field current, so a proper representation of the field winding is essential if their effect is to be simulated correctly in a transient stability program.

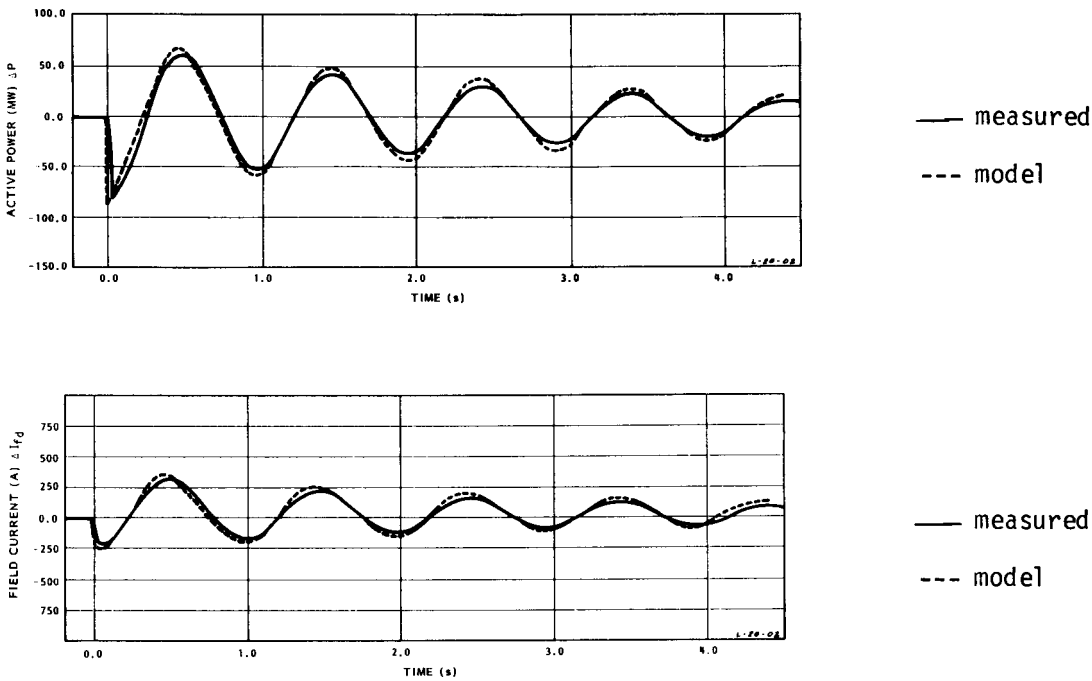

Figure S-1. Simulation of Lambton Generator Power and Field Current During a Transient Caused By Line Switching.

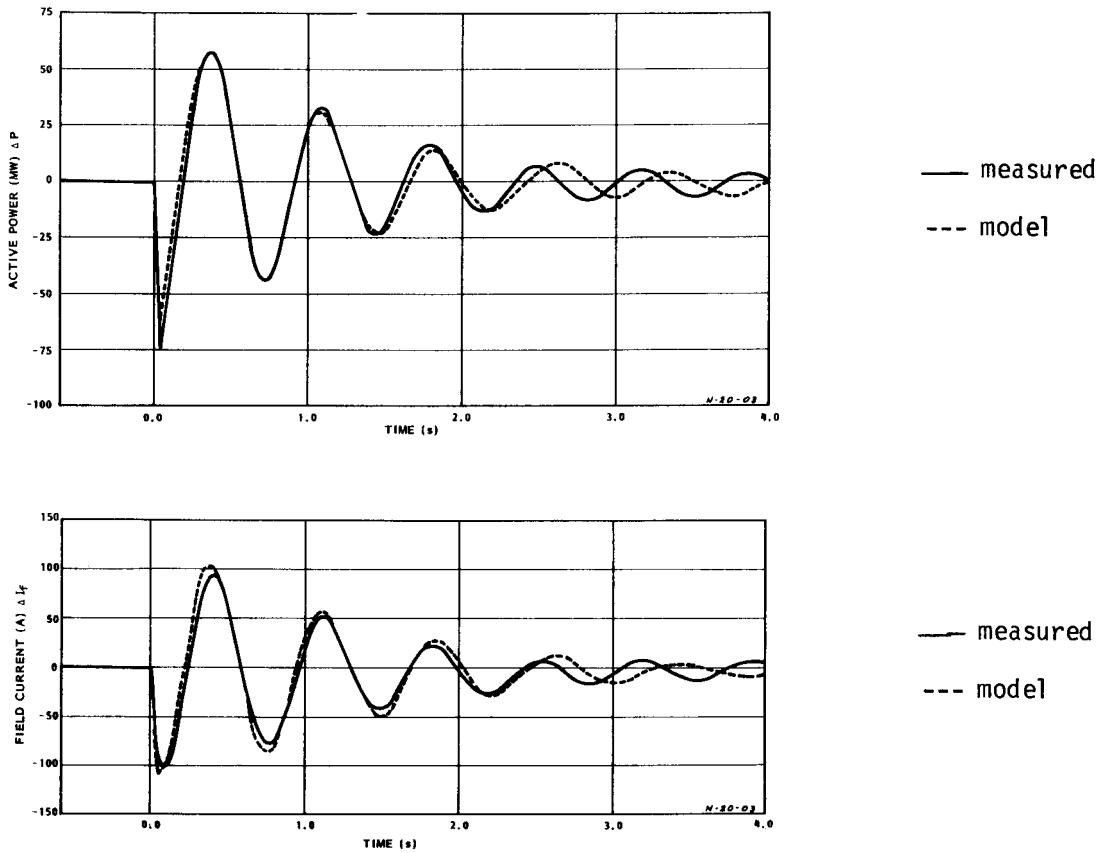

Figure S-2. Simulation of Nanticoke Generator Power and Field Current During a Transient Caused By Line Switching.

MODEL STRUCTURE

The proposed d- and q-axis equivalent circuits are shown in Figure S-3. They are estimated to contain sufficient detail to model all machines. In addition to three rotor circuits in each axis, there are rotor circuit mutual leakage elements, L_{fkd1} and L_{fkd2} in the direct axis equivalent circuit. These latter elements are necessary to model the field winding correctly.

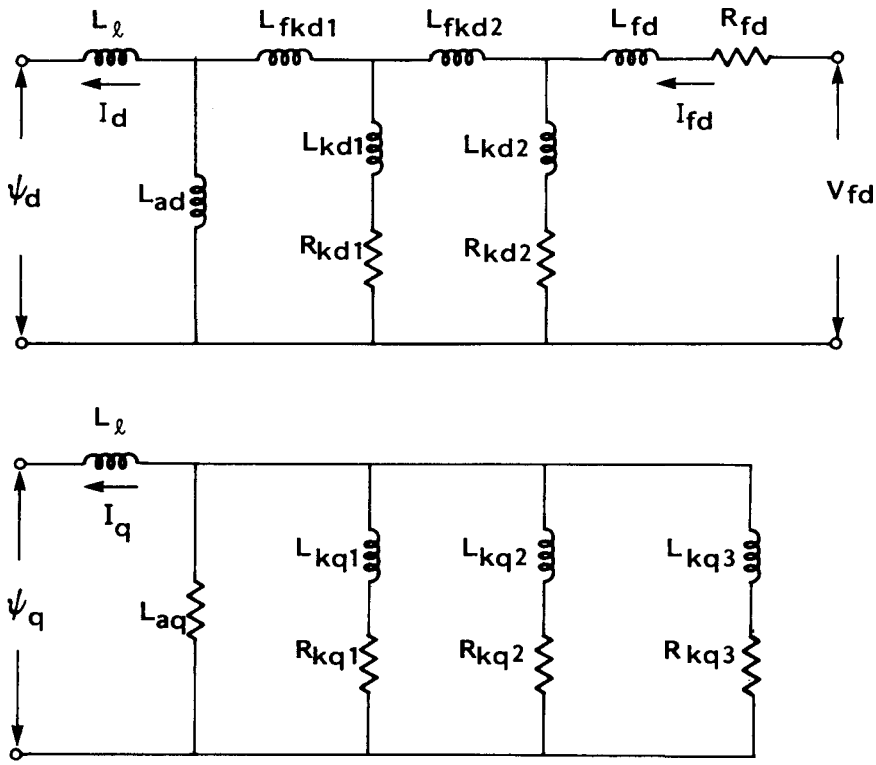

Figure S-3. Recommended Model Structure.

TEST METHOD

The foundation of the recommended procedure is the standstill frequency response test. This is done with the generator assembled, stationary, and disconnected from everything else. As such, it can be done either in the factory or on site. Stator winding impedance and stator to field transfer functions are measured with a low voltage (less than 50 V), low current (less than 100 A), variable frequency power supply connected to two terminals of the stator winding. From these measurements, d- and q-axis equivalent circuits of the form shown in Figure S-3 can be derived.

This equivalent circuit model is valid for the conditions existing during the standstill frequency response tests. However, for small signal conditions such as these, the permeability of iron is lower than it is for larger flux changes. This means that the iron-dependent inductances in the model derived from standstill frequency response tests are lower than they would be in an "unsaturated" model.

To get an unsaturated model, L_{ad} and L_{aq} in Figure S-3 must be adjusted upward to their unsaturated values. In the case of L_{ad}, this is the value corresponding to the air-gap line of the open-circuit saturation curve. To obtain the unsaturated value of L_{ad}, the mutual inductance between the field and stator windings is measured over a range of flux densities from zero to about half of the normal operating value. The amount by which it changes between flux densities corresponding to standstill frequency response tests and the maximum value is the factor by which L_{ad} and L_{aq} are multiplied to convert them to unsaturated values. With this done, the equivalent circuits are now ready for use in transient stability programs, and for many machines; eg, Lambton, no further tests are necessary.

However, if the generator rotor has a low resistance damper structure, such as full length slot wedges, the influence of this damper is likely to be significant at the frequency at which the generator oscillates against the rest of the system (typically 1 to 2 Hz). The electrical connections in the damper are by contact only; therefore, their resistance is sensitive to central forces produced by the rotor's turning. For such machines, a limited set of on-line frequency response tests may be necessary to represent the damper correctly at rated speed.

This was the case for one of the two generators tested in this project (Nanticoke). An algorithm was devised which began with the model derived from stationary tests, and adjusted the rotor circuit parameters in an iterative manner until the resulting model matched the measured performance from the on-line frequency response test. This resulted in a good model for the Nanticoke generator as was demonstrated in Figure S-2. This aproach also produced a good model for the Lambton machine, even though just the stationary tests would have been sufficient for it.

Consequently, a general procedure which includes standstill frequency response tests, direct current inductance measurements for adjusting L_{ad} and L_{aq} to unsaturated values, and on-line frequency response tests is recommended.

However, on-line tests will not be necessary for all machines. The rate at which the direct axis operational inductance changes through the frequency range around 1 to 2 Hz is the critical factor and the standstill test provides this information. Therefore, the stationary test results can be used to decide whether or not on-line frequency response measurements will be necessary for a particular machine.

APPLICATION OF THE RESULTS

The recommended models have been implemented in both the Ontario Hydro and EPRI transient stability programs with no significant increase in program execution time. Test cases run with both programs produced consistent results.

D- and q-axis equivalent circuits for the Nanticoke generator, derived by the recommended test procedure have successfully simulated both line switching transients and small signal step responses used to study power system stabilizer actions. It was the only model capable of doing this, and thus proved itself superior to all others tried which included those from standard data, sudden short circuit tests, and stator decrement tests.

MAGNETIC NON-LINEARITIES

Saturation

Q-axis saturation was found to be quite different from that on the direct axis. Therefore, estimation of q-axis saturation on the basis of d-axis test date; ie, the open-circuit saturation curve, is not valid. A set of steady state measurements of: terminal voltage, active power, reactive power, and internal angle over a wide range of generator loads was used to measure the q-axis saturation curve.

Small Signal Effects

Inductances measured with small flux changes around a zero flux density operating point during the standstill frequency response tests were lower than for larger flux changes. This same phenomenon was observed at normal operating flux density. The magnitude of the open-circuit transfer function between field voltage and terminal voltage was measured with varying sizes of perturbation and found to be lower at lower signal levels.

There was also evidence that the rotor leakage inductances are affected by magnetic non-linearities just as much as L_{ad}. This is at odds with the frequently employed assumption that they behave as linear, air-core devices.

Part 1

PRINCIPAL RESULTS AND RECOMMENDATIONS

Part 1

CONTENTS

CONTENTS (Cont'd)

CONTENTS (Cont'd)

ILLUSTRATIONS

ILLUSTRATIONS (Cont't)

ILLUSTRATIONS (Cont'd)

TABLES

Section 1

INTRODUCTION

HISTORICAL BACKGROUND

In the past, equivalent circuit models for synchronous generators were supplied on the basis of design calculations and, in some instances, sudden short circuit tests. Often, this is still the practice, and, in fact, the sudden short circuit test is a cornerstone of the current standard (1). As well, however, the manufacturers have continued to refine their design calculations, and this has resulted in substantial advances in both the detail and accuracy of the resulting models for round rotor machines (2,3,4). Nevertheless, some problems have become apparent during the past ten or fifteen years.

The first is that standard test procedures (1) have not kept pace with the advances in turbogenerator models. For example, the sudden short circuit test cannot even cope with the detail of generator equivalent circuits published thirty-five years ago (5), much less with that of the more recent ones (2). Consequently, there has not been a recognized standard method for verifying the accuracy of the more advanced and detailed turbogenerator models; this fact has delayed their acceptance by the industry.

A second difficulty arose with the advent of high initial response exciters and high gain automatic voltage regulators. These fast acting excitation systems raised steady state stability limits, making it possible to deliver more power from a generator over a given transmission system (6). However, auxiliary control loops such as power system stabilizers are essential for the normal, stable operation of most of these excitation systems. The gain and phase margins of these control loops are functions of the generator parameters; consequently, if they are to be properly designed, the response of the generator, in the frequency domain, must be accurately known over their active bandwidth. This requirement overtaxed the capabilities of most of the existing models which were accurate, typically, at only three widely separated points in the frequency domain.

Ontario Hydro began to investigate test methods for obtaining synchronous machine parameters because of precisely this problem (7), and conducted early experiments with both stationary (8) and running (9) tests.

About the same time, the industry was also becoming concerned about the performance of existing synchronous machine models in transient stability programs (10). The IEEE (Institute of Electrical and Electronics Engineers) formed a working group on "Determination of Synchronous Machine Stability Study Constants" to study the problem. This group, consisting of utility, manufacturing, and university members has been quite active, laying the groundwork for revised standards (11), and providing moral support for research into improved generator models.

EPRI responded to the need by establishing a research project, RP 997, on "Determination of Synchronous Machine Stability Study Models", and providing funds for research on the subject. This report is an account of Ontario Hydro's role in this effort.

OBJECTIVES

Ontario Hydro's part in the project had the following aims:

1. To provide a comprehensive set of test data for two machines, Lambton and Nanticoke which were known to be of distinctly different designs.

2. To evaluate the performance of various equivalent circuit structures and recommend one that will adequately model most existing synchronous generators.

3. To experiment with, and evaluate different tests for obtaining parameters for this model, and recommend a test procedure.

4. To implement the suggested generator model in the EPRI and Ontario Hydro transient stability programs, and determine the effect on the program execution time.

5. To recommend an improved way of handling iron saturation in transient stability programs.

FORMAT

Descriptions of the most successful and significant work, the conclusions drawn from all the work, and the recommendations have been assembled in Part 1. Part 2

is an account of results which are significant in their own right, but are not fundamental to the principal conclusions and recommendations. Part 3 discusses implementation of the recommended models in the EPRI transient stability program and Parts 4 and 5 document the considerable volume of test data that was accumulated for the Lambton and Nanticoke generators. Because the tests described in Parts 4 and 5 are the foundation for most of this report, it is suggested that the reader peruse either or both of these parts before continuing.

REFERENCES

1. Test Procedures for Synchronous Machines. IEEE No 115, March 1965.

2. W.B. Jackson and R.L. Winchester. Direct and Quadrature - Axis Equivalent Circuits for Solid-Rotor Turbine Generators. IEEE Trans PAS-88, July 1969, p 1121.

3. P.L. Dandeno, P. Kundur, R.P. Shulz. Recent Trends and Progress in Synchronous Machine Modelling in the Electric Utility Industry. Proc IEEE, vol 62, no 7, July 1974.

4. R.P. Shulz, W.D. Jones, and D.N. Ewart. Dynamic Models of Turbine Generators Derived From Solid Rotor Equivalent Circuits. IEEE Trans PAS-92, May/June 1973, p 926.

5. A.W. Rankin. The Direct and Quadrature Axis Equivalent Circuits of the Synchronous Machine. AIEE Trans, vol 64, Dec 1945, p 861.

6. P.L. Dandeno, A. Karas, K.R. McClymont, and W. Watson. Effect of High Speed Rectifier Excitation Systems on Generator Stability Limits. IEEE Trans PAS-87, Jan 1968, p 190.

7. W. Watson and M.E. Coultes. Static Exciter Stabilizing Signals On Large Generators - Mechanical Problems. IEEE Trans PAS-92, Jan/Feb 1973, p 204.

8. W. Watson and G. Manchur. Synchronous Machine Operational Impedances from Low Voltage Measurements at the Stator Terminals. IEEE Trans PAS-93, May/June 1974, p 777.

9. G. Manchur, et al. Generator Models Established by Frequency Response Tests On A 555 MVA Machine. IEEE Trans PAS-91, Sept/Oct 1972, p 2077.

10. P.L. Dandeno and P. Kundur. Stability Performance of 555 MVA Turboalternators - Digital Comparisons With System Operating Tests. IEEE Trans PAS-93, May/June 1974, p 767.

11. Supplementary Definitions and Associated Test Methods for Obtaining Parameters for Synchronous Machine Stability Study Constants. Working Group paper presented at the IEEE Summer Power Meeting, 1979, Vancouver, BC.

Section 2

STATIONARY TESTS

STANDSTILL FREQUENCY RESPONSE

The standstill frequency response test is a method of measuring synchronous machine parameters in transfer function form with the machine stationary. From these transfer functions, direct and quadrature axis equivalent circuits can be computed if required; most existing transient stability programs need the data in this form.

The principal advantages of the method are:

- It yields information in as much, or as little detail as required by the end use.
- Both direct and quadrature axis parameters are obtained with comparable accuracy and detail.
- There is no risk of damage to the machine because of the low power levels used.
- The tests can be done in the factory, or during a scheduled maintenance outage thus eliminating any replacement power costs.

In spite of its many virtues, the method is not perfect. The very low flux densities used result in test values for the iron-dependent inductances which are lower than unsaturated values. However, compensation for this effect is easily achieved using the results of a set of simple inductance measurements which will be discussed later in this section.

Theoretical Basis

The d-q-o components of the stator voltage of a synchronous machine are (1):

$$\left.\begin{aligned} V_d &= s\psi_d - \omega\psi_q - R_a I_d \\ V_q &= s\psi_q - \omega\psi_d - R_a I_q \\ V_o &= s\psi_o - R I_o \end{aligned}\right\} \qquad (2\text{-}1)$$

With the rotor stationary, $\omega=0$, and these equations reduce to:

$$\left.\begin{aligned} V_d &= s\psi_d - R_a I_d \\ V_q &= s\psi_q - R_a I_q \\ V_o &= s\psi_o - R_a I_o \end{aligned}\right\} \qquad (2\text{-}2)$$

Direct and quadrature axis operational inductances are defined (2) as:

$$\left.\begin{aligned} L_d(s) &= \frac{-\psi_d}{I_d} \\ L_q(s) &= \frac{-\psi_q}{I_q} \end{aligned}\right\} \qquad (2\text{-}3)$$

Substituting (2-2) in (2-3),

$$L_d(s) = -\frac{1}{s}\left[\frac{V_d}{I_d} + R_a\right] \qquad (2\text{-}4)$$

$$L_q(s) = -\frac{1}{s}\left[\frac{V_q}{I_q} + R_a\right] \qquad (2\text{-}5)$$

The standstill frequency response tests were done by positioning the rotor at the appropriate place, and supplying a sinusoidal test voltage to two of the stator terminals; the third terminal was left open.

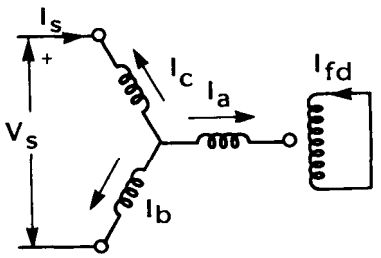

Figure 2-1. Schematic Of Connections For Standstill Frequency Response Tests.

For the direct axis measurements, the magnetic axis of the field winding was aligned with that of the series combination of phases b and c of the stator winding (Figure 2-1). In this position, θ, the angle between phase a and the field, is 90°. Also,

$$I_s = I_b = -I_c \tag{2-6}$$

$$I_a = 0 \tag{2-7}$$

$$V_s = V_c - V_b \tag{2-8}$$

Because of symmetry, $V_b = -V_c$

Furthermore, $V_a = 0$ since $I_a = 0$ and there is no flux linking phase a as a result of I_b, I_c, or I_{fd}. Then, applying the d-q-o transformation (1), the direct axis component of the stator current is

$$I_d = \frac{2}{3} \left[I_a \cos \theta + I_b \cos (\theta - 120) + I_c \cos (\theta + 120) \right] \qquad (2\text{-}9)$$

$$= \frac{2}{3} \left[I_a \cos (90) + I_b \cos (-30) + I_c \cos (210) \right]$$

$$= \frac{2}{3} \left[I_a (0) + I_b \left(\frac{\sqrt{3}}{2} \right) + I_c \left(\frac{\sqrt{3}}{2} \right) \right]$$

$$= \frac{2}{\sqrt{3}} I_s$$

The quadrature axis component of stator current is

$$I_q = -\frac{2}{3} \left[I_a \sin \theta + I_b \sin (\theta - 120) + I_c \sin (\theta + 120) \right] \qquad (2\text{-}10)$$

$$= \frac{2}{3} \left[0 + I_s \sin (-30) - I_s \sin (210) \right]$$

$$= 0$$

The zero sequence component is

$$I_o = \frac{1}{3} (I_a + I_b + I_c) \qquad (2\text{-}11)$$

$$= \frac{1}{3} (0 + I_s - I_s)$$

$$= 0$$

Similarly, the d-q-o components of the stator voltage are:

$$V_d = \frac{2}{3}\left[V_a \cos\theta + V_b \cos(\theta-120) + V_c \cos(\theta+120)\right] \qquad (2\text{-}12)$$

$$= \frac{2}{3}\left[V_a \cos(90) + V_b \cos(-30) + V_c \cos(210)\right]$$

$$= \frac{2}{3}\left[0 + \frac{\sqrt{3}}{2}(V_b - V_c)\right]$$

$$= -\frac{1}{\sqrt{3}} V_s$$

$$V_q = -\frac{2}{3}\left[V_a \sin\theta + V_b \sin(\theta-120) + V_c \sin(\theta+120)\right] \qquad (2\text{-}13)$$

$$= -\frac{2}{3}\left[0 + V_b \sin(-30) + V_c \sin(210)\right]$$

$$= -\frac{2}{3}\left[V_b\left(-\frac{1}{2}\right) - V_b\left(-\frac{1}{2}\right)\right]$$

$$= 0$$

$$V_o = \frac{1}{3}(V_a + V_b + V_c) \qquad (2\text{-}14)$$

$$= \frac{1}{3}(0 + V_b - V_b)$$

$$= 0$$

which establishes that only direct axis components are present in the stator voltages and currents for this connection, with $\theta = 90°$.

To measure the quadrature axis impedance, the rotor was turned 90° so that the magnetic axes of the field and phase a were aligned (θ=0). In this case,

$$I_d = \frac{2}{3} \left[I_a \cos(0) + I_b \cos(-120) + I_c \cos(120)\right] \quad (2\text{-}15)$$

$$= \frac{2}{3} \left[0 + I_s \left(-\frac{1}{2}\right) - I_s \left(-\frac{1}{2}\right)\right]$$

$$= 0$$

$$I_q = -\frac{2}{3} \left[I_a \sin(0) + I_b \sin(-120) + I_c \sin(120)\right] \quad (2\text{-}16)$$

$$= -\frac{2}{3} \left[0 + I_s \sin(-120) - I_s \sin(120)\right]$$

$$= \frac{2}{\sqrt{3}} I_s$$

$$I_o = \frac{1}{3} (0 + I_s - I_s) \quad (2\text{-}17)$$

$$= 0$$

$$V_d = \frac{2}{3} \left[V_a \cos(0) + V_b \cos(-120) + V_o \cos(120)\right] \quad (2\text{-}18)$$

$$= \frac{2}{3} \left[0 + V_b \cos(-120) - V_b \cos(120)\right]$$

$$= 0$$

$$V_q = -\frac{2}{3} \left[V_a \sin 0 + V_b \sin(-120) + V_c \sin(120)\right] \quad (2\text{-}19)$$

$$= -\frac{2}{3} \left[0 + V_b \left(-\frac{\sqrt{3}}{2}\right) + V_c \left(\frac{\sqrt{3}}{2}\right)\right]$$

$$= -\frac{1}{\sqrt{3}} \quad V_s$$

$$V_o = \frac{1}{3} \quad (0 + V_b - V_b)$$

$$= 0$$

Thus, it is evident that only q-axis components are present in the stator voltages and currents in this case.

Test Procedure

Standstill frequency response measurements were made over the range 0.001 Hz to 1 kHz. Test frequencies were selected to produce a logarithmic spacing and a density of at least 10 points per decade of frequency. For reasons which will be discussed later, 40 points were measured in the lowest decade, from 0.001 Hz to 0.01 Hz.

The following functions were measured:

$\frac{\Delta V_d}{I_d}$, $\frac{\Delta I_{fd}}{\Delta I_d}$ — rotor in d-axis position, field shorted

$\frac{\Delta V_d}{\Delta I_d}$, $\frac{\Delta V_{fd}}{\Delta I_d}$ — rotor in d-axis position, field open

$\frac{\Delta V_q}{\Delta I_q}$ — rotor in q-axis position

$\left.\frac{V_{fd}}{I_{fd}}\right\}$ stator winding open

Three power amplifiers, operated in parallel, with a combined capability of 15V, 60A peak supplied the test current in the set-up shown in Figure 2-2.

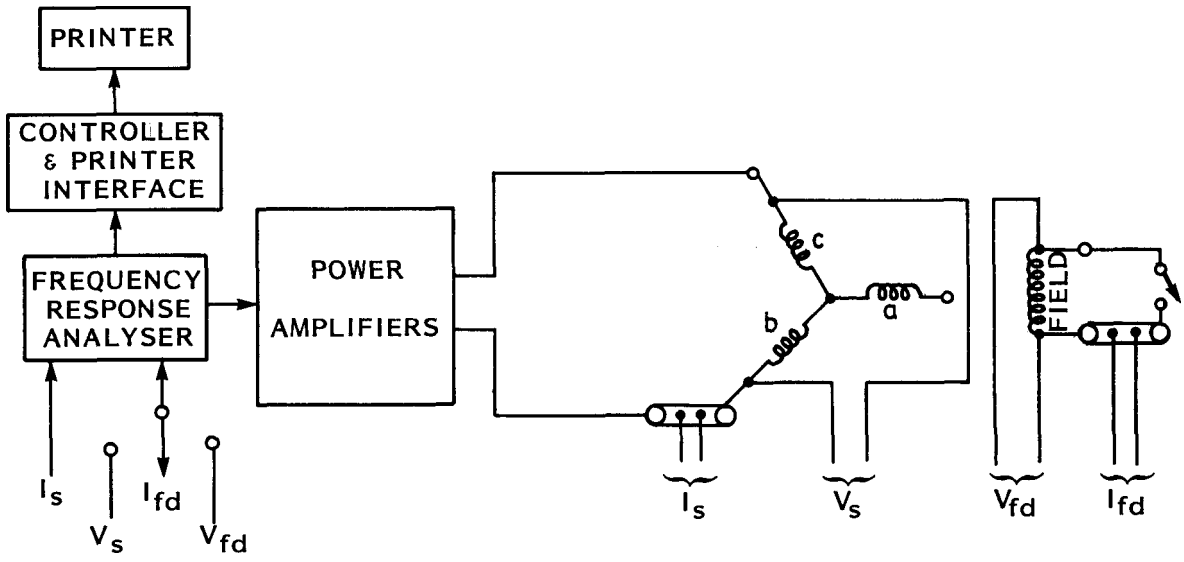

Figure 2-2. Test Set-Up For Standstill Frequency Response Measurements.

The frequency response analyzer generates a sinusoidal reference which drives the power amplifiers at the test frequency. It also measures the two variables of interest, cross-correlates them with the reference waveform, and computes the transfer function between the two variables as the ratio of the results of the two cross-correlations. An important feature of this method is that the phase angle between the two measured variables is computed from the complete cycle of the waveform. In contrast, a phase angle measurement based on detection of zero crossings depends only on a small portion of the waveform near the zero crossing; consequently, it is inordinately sensitive to imperfections such as crossover distortion in the power amplifiers. This is most important in the impedance measurements where angles less than one degree must be measured as accurately as possible.

Practical Considerations During the Tests

The operational inductance was calculated from the reactive component of the stator winding impedance. At very low frequencies, this impedance is almost totally resistive. Therefore, it was important to hold the stator resistance as constant as possible during the tests. To this end, the generator was allowed to reach ambient temperature before the tests began, and the stator cooling water was shut off during the tests.

Differential input amplifiers were used to measure stator voltage and current (from the metering shunt), thus avoiding inclusion of the contact resistance between the shunt and the stator terminal in the measured impedance.

It is important that the low frequency limit of the operational inductance be determined with precision. However, the resolution of instruments that are currently on the market is not sufficient to avoid some scatter in the test points at the lowest frequencies. To get around this problem, 40 points, rather than the usual 10, were measured in the lowest frequency decade (0.001 Hz to 0.01 Hz). Then, the imaginary part (inductive component) of the stator impedance was plotted against frequency on a linear scale, Figure 2-3.

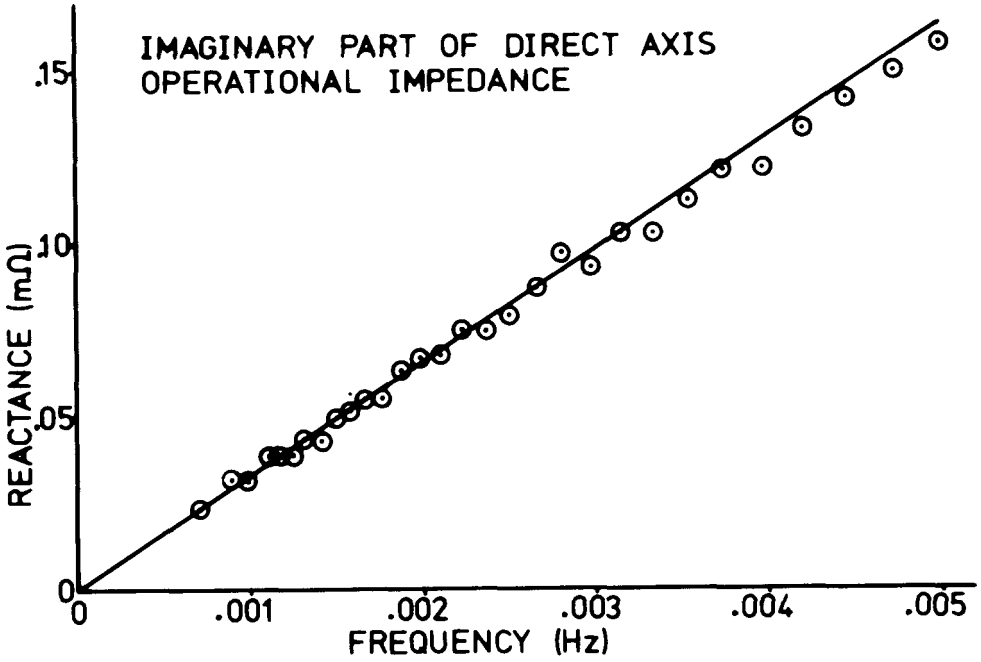

Figure 2-3. Reactive Component of Direct Axis Operational Impedance.

Since an inductive reactance must be zero when the frequency in zero, these points must pass through the origin. The slope of the best straight line through the origin and the low frequency test points is the low frequency limit of the operational inductance.

The dc resistance of the stator winding which is to be subtracted from the stator impedance can be obtained in a similar manner by taking the best line through the real part of the stator impedance at the lowest frequencies.

INDUCTANCE MEASUREMENTS

The magnetic characteristics of iron include both saturation and hysteresis. This makes any iron-core inductor a highly non-linear device whose parameters must be determined carefully and circumstantially if its performance is to be predicted accurately. Synchronous machinery, used for power generation, is a sub-group of this class of devices. Accordingly, the properties of its magnetic iron deserve considerable attention.

The self and mutual inductances of the accessible windings on the Lambton and Nanticoke generators were measured with the generator rotors in different position and over as wide a range of flux densities as was practical.

An electronic version of the classic ballistic galvanameter (3) was used to measure mutual inductance. With the arrangement in Figure 2-4, it can be shown that when switch S is closed, the mutual inductance between coil 1 and coil 2 is

$$L_{12} = \frac{\int_0^\infty V_2 dt}{i_1} \qquad (2\text{-}20)$$

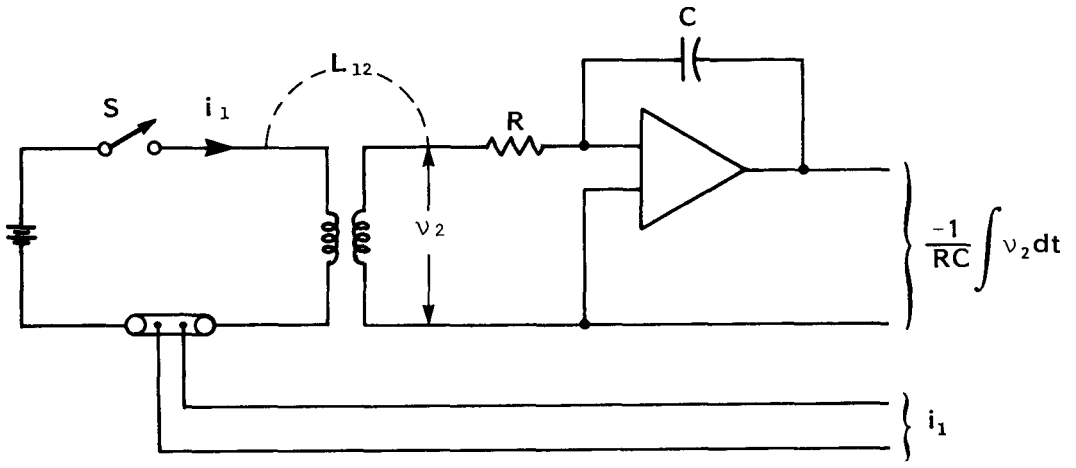

Figure 2-4. An Electronic Integrator Used To Measure Mutual Inductance.

Furthermore, it can also be proven that this result is not influenced by any induced currents, such as i_3, in other coupled windings. An extension of this method which cancels the effect of the IR drop in the inductance being measured (3) was used to obtain the self inductances of the generator windings.

REFERENCES

1. C. Concordia. Synchronous Machines Theory and Performance. New York: Wiley, 1951, pp 14-17.

2. IEEE Working Group. Supplementary Definitions and Associated Test Methods For Obtaining Parameters For Synchronous Machine Stability Study Simulations. F79 647-9.

3. E.P. Dick and W. Watson. Transformer Models For Transient Studies Based On Field Measurements. IEEE Paper No F80 244-4. Presented at the Power Engineering Society Winter Meeting, New York, February 1980.

Section 3

DERIVATION OF MODELS FROM STATIONARY TESTS

INTRODUCTION

In this section, techniques are developed for obtaining d- and q-axis equivalent circuit models from standstill frequency response measurements. These techniques are then applied to the test data from Lambton and Nanticoke as well as the Monticello measurements done by Westinghouse.

The equivalent circuit models for solid iron rotor turbogenerators are based on the widely used structure in which the rotor is represented by parallel branches of passive resistance and inductance elements. The mutual effects between the stator and rotor are known to be affected by iron non-linearities, so these parameters are allowed to vary depending on the operating conditions.

In the standstill frequency response tests performed by Watson and Manchur(1), only measurements at the stator terminals were used and there was some doubt regarding the field winding representation in the derived models. Umans et al(2) extended the technique to use the measurements of both stator and field quantities. However, the particular method of analysis did not appear to account fully for amortisseur and rotor body effects. This was evident when the models were used to simulate "field open" responses, and produced results which were markedly different from standstill frequency response measurements with the field open. The present work aims to overcome these discrepancies and other shortcomings of the foregoing methods by developing procedures of similar complexity while using a modified data reduction and model derivation process.

DERIVATION OF EQUIVALENT CIRCUITS

Direct Axis

The standstill frequency response tests in the d-axis yield, among other responses, two functions $Z_d(s)$ and $sG(s)$ which represent the operational impedance and stator to field transfer function with the field winding closed. The operational inductance $L_d(s)$ can be readily obtained from the operational impedance since, under standstill conditions, the following relationship holds:

$$Z_d(s) = R_a + sL_d(s) \tag{3-1}$$

Typical plots of these functions, $L_d(s)$ and $sG(s)$, over a range of frequencies from 0.001 to 100 Hz are shown in Figures 3-1 and 3-2, in which the circles represent the magnitude of the function and the squares its corresponding phase angle. It has been the practice to utilize such plots by fitting transfer function to the data. For a machine model with two damper windings plus the field on the direct axis, the $L_d(s)$ and $sG(s)$ functions are:

$$L_d(s) = L_d(o)\ \frac{(1+sT_1)(1+sT_2)(1+sT_3)}{(1+sT_4)(1+sT_5)(1+sT_6)} \tag{3-2}$$

$$sG(s) = sG_o\ \frac{(1+sT_7)(1+sT_8)}{(1+sT_4)(1+sT_5)(1+sT_6)} \tag{3-3}$$

$L_d(o)$ and G_o are the very low frequency asymptotes to the $L_d(s)$ and $sG(s)$ functions respectively, and the poles and zeroes result from a curve fitting procedure carried out to obtain a fit of both functions. It should be noted that $L_d(s)$ and $sG(s)$ have the same poles, with the number of poles corresponding to the number of rotor circuits (including the field).

If a two-rotor-circuit model were required, the above equations would be simplified by omitting T_3, T_6 and T_8 and adjusting the remaining time constants to obtain the best fit to the measured data. In general, the greater the number of modelled rotor windings, the better will be the fit since, in theory, the solid iron rotor body consists of an infinite number of circuits. The general approach to deriving the equivalent circuit models from the time constants (poles and zeros) of the above equations is outlined in the block diagram of Figure 3-3.

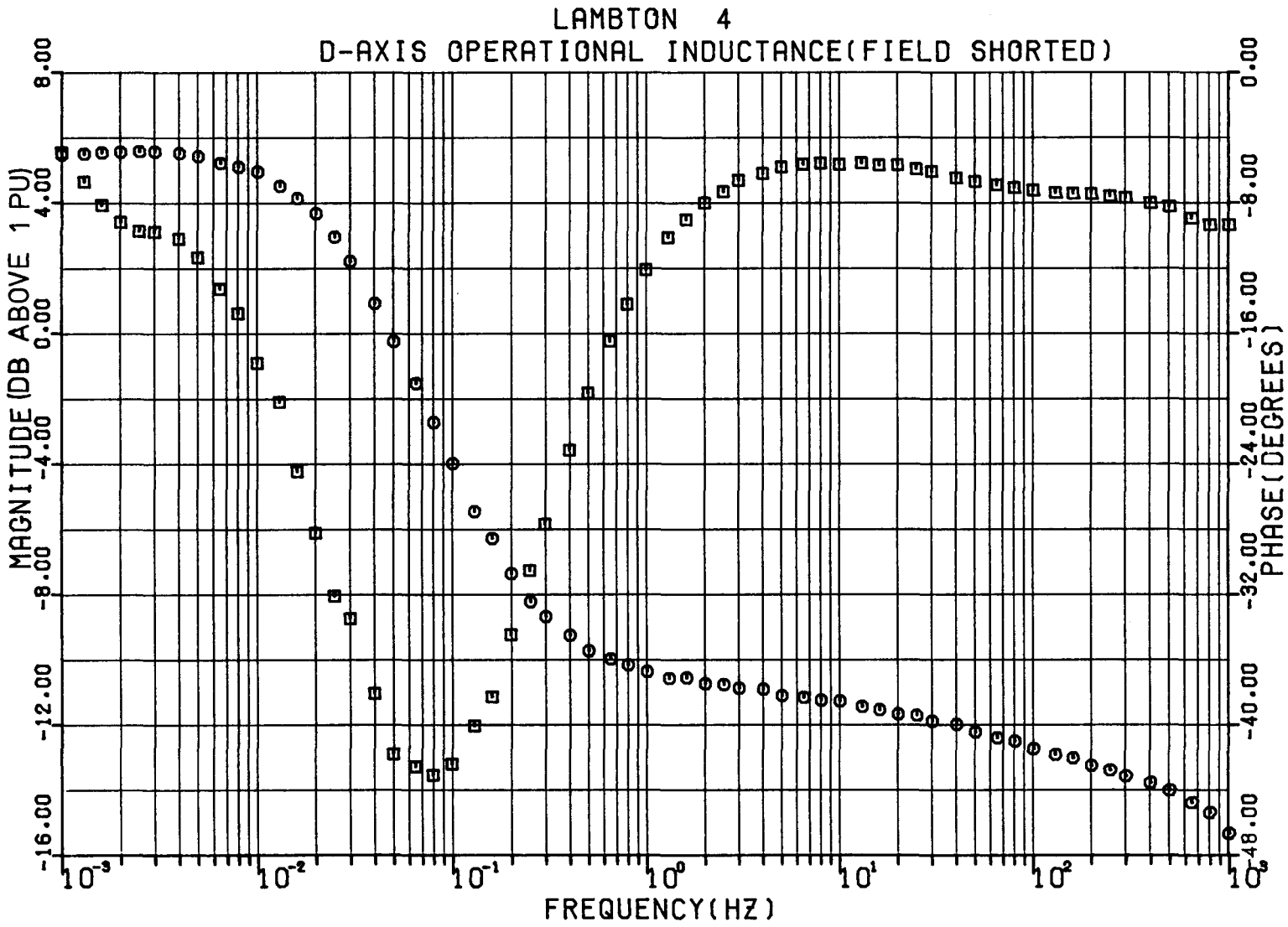

Figure 3-1. Lambton Direct-Axis Operational Inductance.

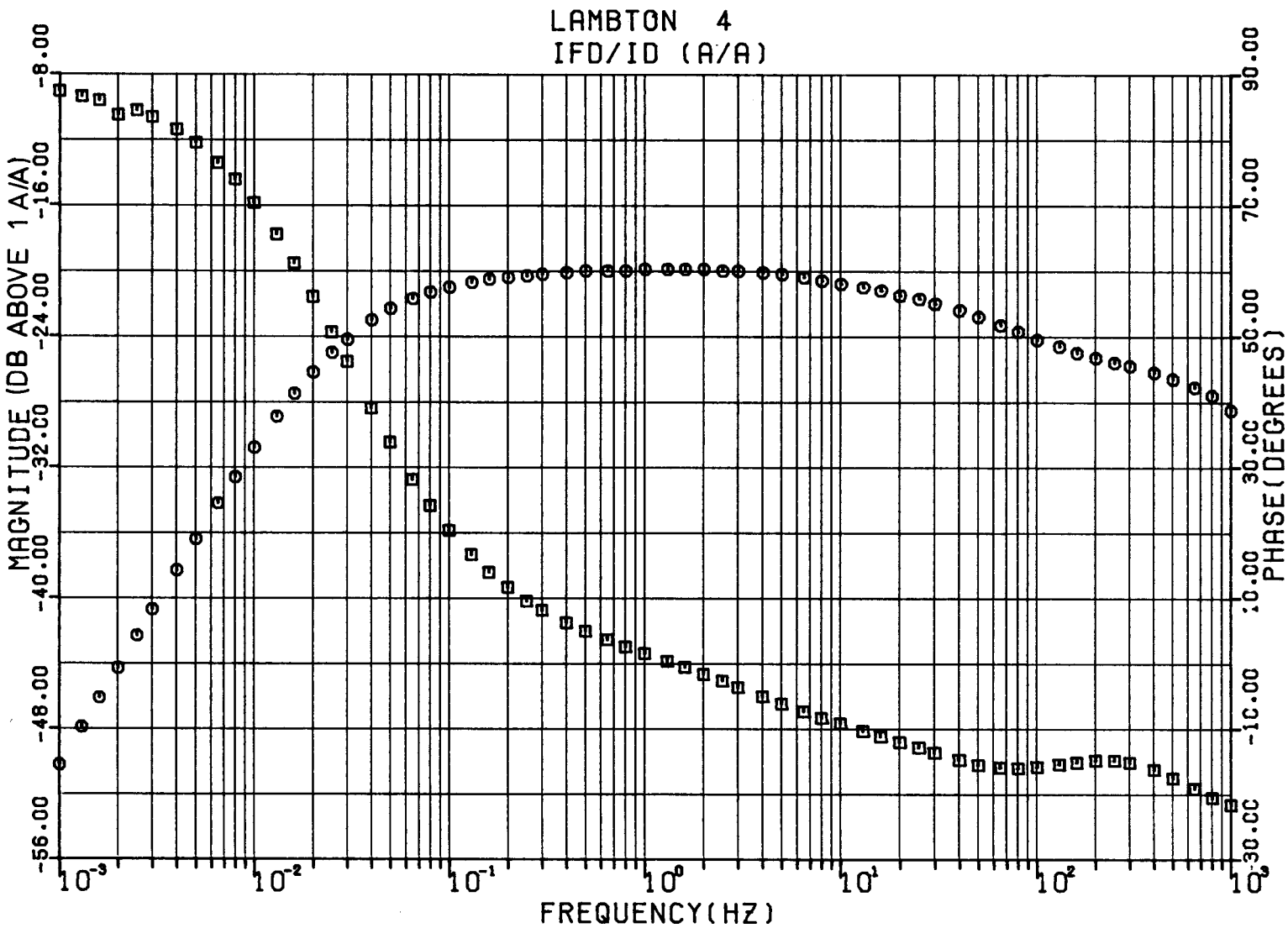

Figure 3-2. Lambton Stationary Stator-To-Field Transfer Function.

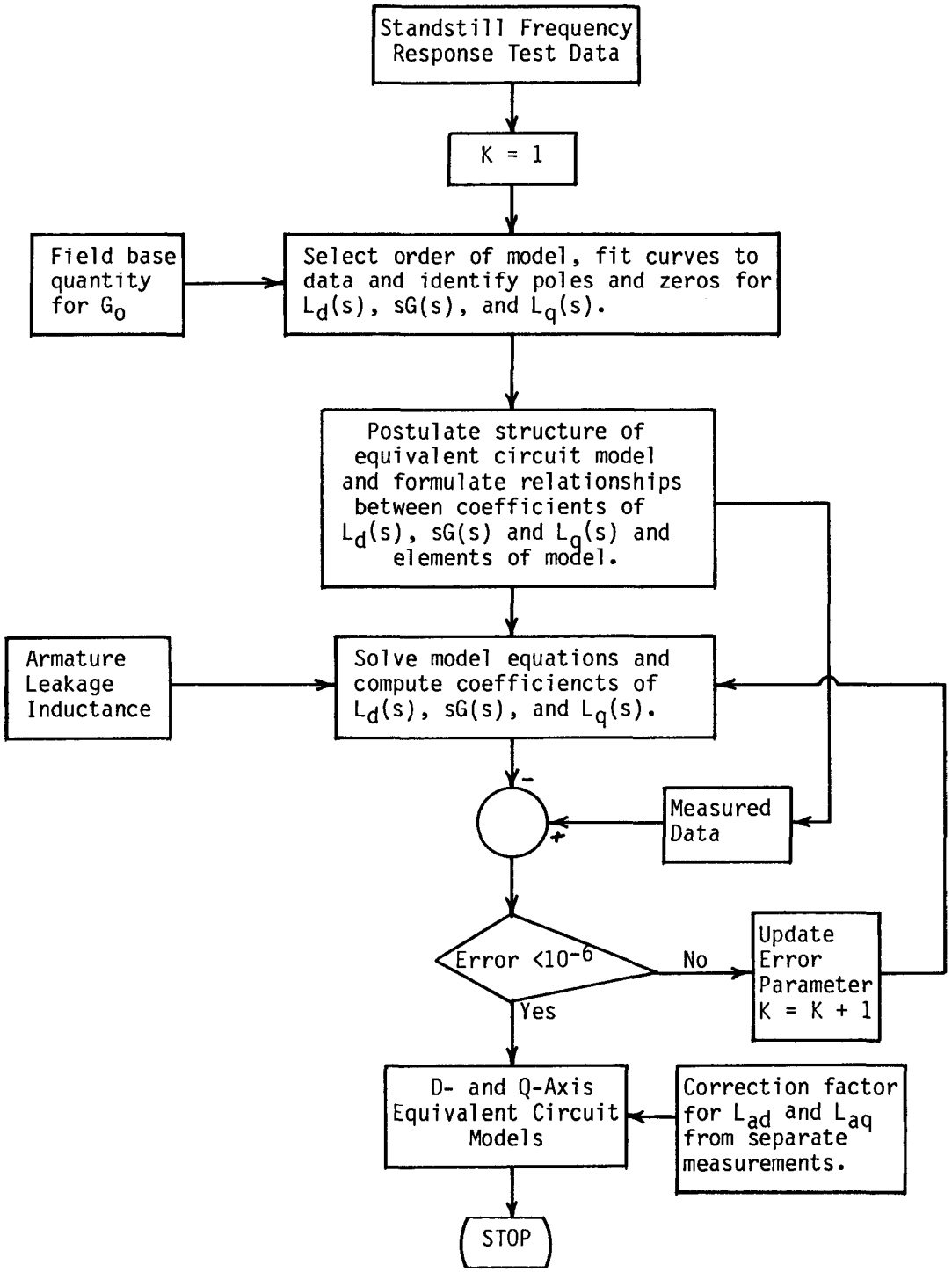

Figure 3-3. Flow Chart for Computing Direct and Quadrature Axis Models From Standstill Frequency Response Test Data.

The models developed herein are based on the well known method of representing the stator and rotor of the machine by equivalent windings, which consist of inductance and resistance elements. Usually, the rotor is represented in the direct axis by a field winding plus one or two amortisseur or damper windings. The distinction between the rotor body circuits and the rotor field circuit is obtained by using the transfer function sG(s). This also highlights the difference in coupling between rotor field and rotor body circuits relative to the stator circuits, an important factor when considering the simulation of rotor field quantities. Figure 3-4 shows the structure of the d-axis equivalent circuit. The curve-fitting procedure is the same as that used by Umans (2). However, it has been extended to use both magnitude and phase data, instead of magnitude only.

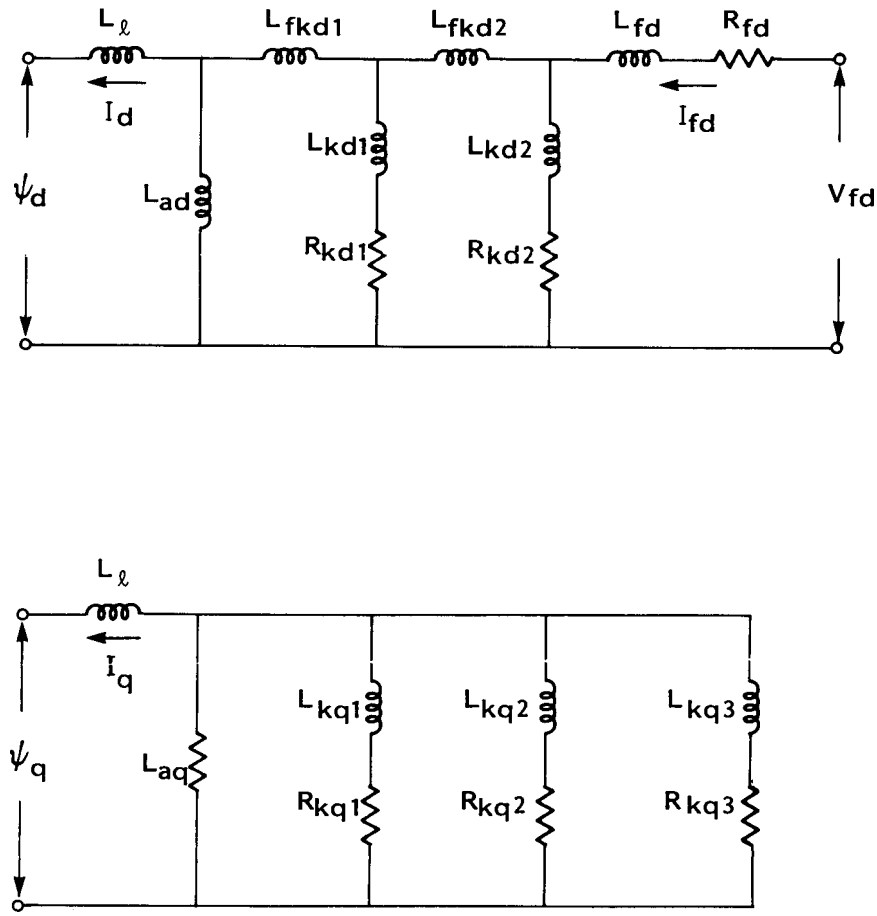

Figure 3-4. Third Order Equivalent Circuits For Turbogenerators

Appendix A describes the relationship between the poles and zeros of the above operational functions and the equivalent circuit elements in Figure 3-2. Both two and three rotor winding representations are considered and equations are developed to solve for the circuit elements. However, the relevant equations, nine in the case of the three rotor winding model and six in the case of the two rotor winding model, contain one less unknown than the number of test data parameters. In general, this means that these equations cannot be solved exactly unless they form a consistent set with the input data. Thus, the equations cannot be solved exactly unless the mathematical model is an exact representation of the generator and there are no errors in the test data. Obviously, neither of these conditions can be met. Two or three, or even thirty circuits will never be an exact model of the continuum of the rotor body, and there will always be some errors in the test data. Thus, some inaccuracy must be accepted in one or more of the input parameters.

An important part of the present method is to use the derived model to recalculate the input data from which the model is derived. From this, information is available about the locations of the inaccuracies mentioned above. The solution of the model equations considered in Appendix A gives rise to errors in the numerator coefficients of $L_d(s)$. These coefficients are obtained by expanding the numerator of $L_d(s)$ in Equation 3-2 to form a polynomial in "s". It was found that the largest error occurs in the coefficient representing the product of the numerator time constants. An iterative solution was adopted as shown in Figure 3-3, which minimizes this error by allowing the smallest time constant in the numerator of $L_d(s)$ to vary from its initial value. In other words, a three-rotor-winding model will reproduce exactly five out of the six time constants in equation 3-2, with the sixth time constant taking up the error. Experience has shown that this error always causes an increase in the value of the smallest numerator time constant. In practical terms this means that the existing model cannot represent accurately rotor body effects at frequencies near 60 Hz. This means that the subtransient inductance presented by the model will be higher than the actual value. For the present purpose, this is not a disadvantage, since the models are to be used for the study of system dynamics in which subtransient effects are not important.

In developing the above models, it has been assumed, at the outset, that there exists a prior knowledge of the value of armature leakage inductance L_l, so one is able to fix the rotor base quantities using the "L_{ad}" method. It would, of course, be equally valid to derive models in which no such assumption is made, but in which the rotor base quantities were chosen to make the mutual effects between the different rotor circuits and the stator circuits all equal. In Figure 3-4 we define L_{fkd1} to reflect the leakage flux which links all the rotor circuits, but not the stator circuits. Similarly, L_{fkd2} reflects the leakage flux which links only winding kd2 and the field winding, but not winding kd1 and the stator.

It is possible, of course, to omit the L_{fkd} elements in the equivalent circuit of Figure 3-4, since many computer stability programs are structured in such a way that the consideration of this series branch is awkward. Canay, among others shows how a direct concordance between the "conventional" d-axis circuit and the advanced circuit of Figure 3-4 may be obtained. This concordance is only valid for one operating point, since the requirement for adjusting L_{ad} for saturation would result in changing all the elements in Canay's simplified circuit. In addition, the rotor base quantities would also change with the change in L_{ad}.

We suggest that the addition of the L_{fkd1} branch (and even the L_{fkd2} branch) can be readily accounted for in any advanced stability program by structuring the generator equations in terms of flux linkages, resistances and reactances. Thus the advantage of retaining the L_{ad} base for rotor quantities is evident, as well as the capability of adjusting L_{ad} (or L_{aq}) as a function of total air gap flux, particularly in these advanced models.

The equivalent circuit derivation process considered here requires that a value for L_d, the synchronous inductance, be known. This value is obtained from the standstill tests as $L_d(o)$, the asymptote to the low frequency points of $L_d(s)$.

Quadrature Axis

$Z_q(s)$ is the input function which is obtained from the standstill frequency response test in the q-axis (3). It is the only function available since there is no field winding on the q-axis. The operational inductance $L_q(s)$ can be obtained in a similar manner to $L_d(s)$ and a typical plot of $L_q(s)$ is shown in Figure 3-5. As for the d-axis, $L_q(s)$ can be utilized by fitting second or third order rational polynomial expressions to the data. For example, $L_q(s)$ may be approximated by an equation similar to 3-2. The poles and zeros can then be used to obtain the equivalent circuit parameters. The process involved is fairly straightforward since in this case there is no field winding. The equations governing the q-axis models are identical to those developed by Umans et al (2) and are therefore not reproduced here. The equivalent circuit structure is identical to the d-axis model except that the mutual effects between the different rotor windings are the same as those between the stator and rotor windings; ie, L_{aq} is the common element. It is not possible to identify unequal mutual effects in the q-axis because there is no information available about the rotor currents in this axis. That is not to say that these effects do not exist, but rather that their representation is not necessary since, in general, one is not interested in the q-axis rotor currents to the same extent as the d-axis field current. It is important that accurate representation of the overall effects of the rotor in this axis be achieved, but the relative values of the different branches are not important in stability analysis.

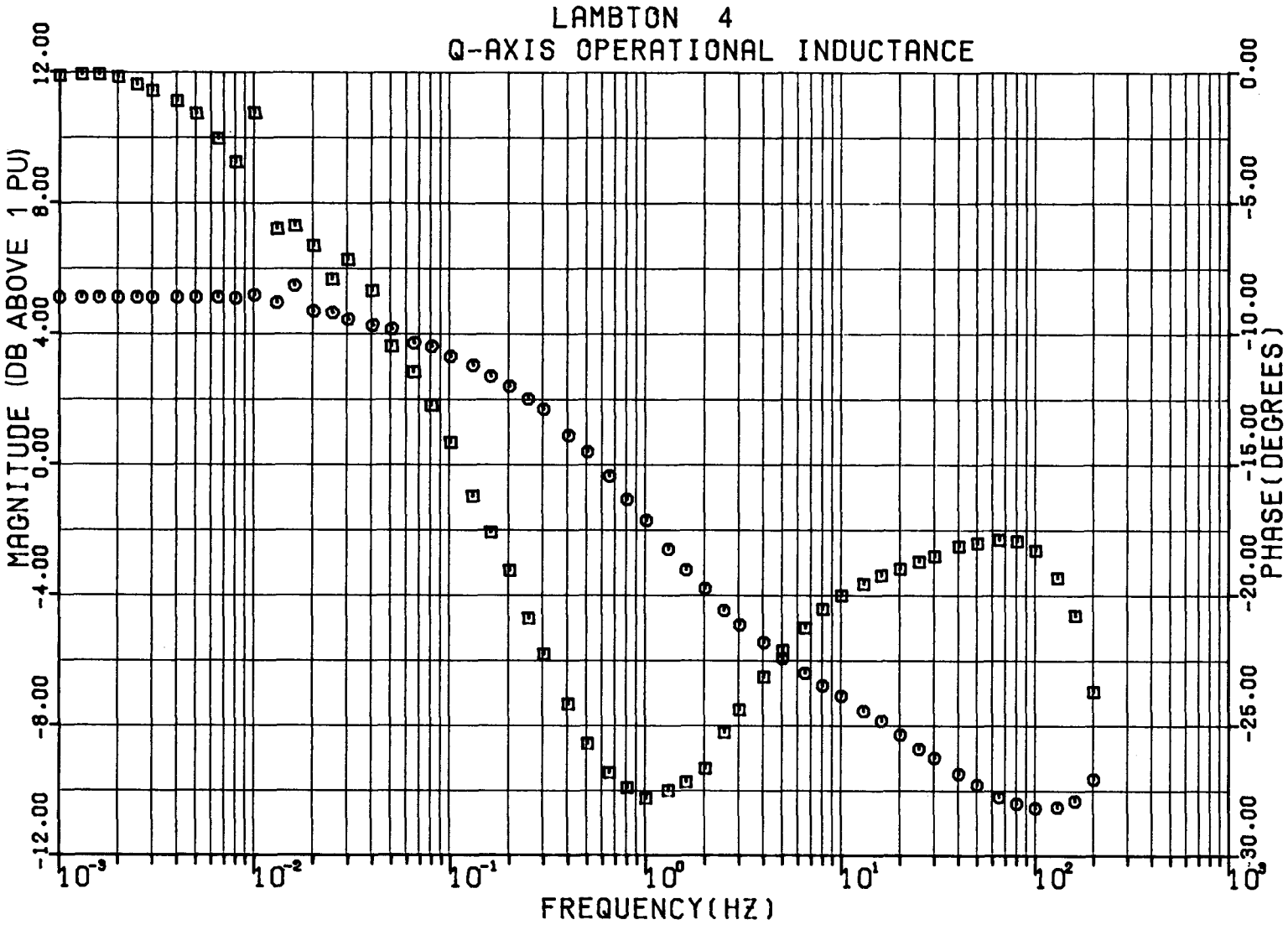

Figure 3-5. Lambton Quadrature-Axis Operational Inductance.

IRON NON-LINEARITY

At this point, we have d and q-axis equivalent circuits which are valid for the conditions for which they were derived, specifically, very low flux densities when compared to typical operating levels. As will be evident from the test data in Parts 3 and 4, the iron-dependent inductances in these circuits are substantially lower than what are usually called "unsaturated values". On the assumption that L_{ad} and L_{aq} are the only elements affected by iron non-linearity, the equivalent circuits derived from standstill frequency response tests will be converted to unsaturated models by multiplying L_{ad} and L_{aq} by (L_{afdu}/L_{afdss}) where L_{afdu} is the unsaturated value of L_{afd} measured at approximately half of typical operating flux density, and L_{afdss} is the low level value of L_{afd} measured at the level of air gap flux density produced by the standstill frequency response test current. These values will be obtained from the inductance measurements described in Section 2 and reported in Parts 4 and 5.

LAMB TON

Figures 3-6, 3-7 and 3-8 show the results of fitting the d and q-axis standstill frequency response data with second and third order rational polynomials or transfer functions. The order of the polynomial corresponds to the number of rotor circuits modelled. It is quite clear that the d-axis data, $L_d(s)$ and $sG(s)$, is well approximated by second order expressions whilst the q-axis data, $L_q(s)$, is best approximated by a third order model.

Using the time constants in the fitted expressions for $L_d(s)$, $sG(s)$, and $L_q(s)$, together with the unsaturated values of $L_d(o)$, $L_q(o)$, and the armature leakage inductance L_l from Table 3-1, two and three-rotor-winding equivalent circuits were obtained by the method described in Appendix A. L_{ad} and L_{aq} were then converted to unsaturated values, based on the inductance measurements in Part 4. The parameters for these equivalent circuits are listed in Table 3-2. This table also contains the corresponding parameters for the STANDARD model which were calculated from the inductances and time constants in Table 3-1.

Table 3-1

MANUFACTURER'S DATA FOR LAMBTON

MVA	555.5
kV	24.0
L_{du}	1.970 pu
L_{qu}	1.867 pu
L'_d	0.270 pu
L''_d	0.215 pu
L'_q	0.473 pu
L''_q	0.213 pu
T'_{do}	4.30 s
T''_{do}	0.031 s
T'_{qo}	0.560 s
T''_{qo}	0.061 s
L_l	0.16 pu

Table 3-2

LAMBTON GENERATOR PARAMETERS

Parameter	SSFR3 Model	SSFR2 Model	STANDARD Model
L_{ad}	1.858	1.858	1.810
L_{aq}	1.762	1.762	1.707
L_{l}	0.155	0.155	0.160
L_{fd}	0.00991	0.01051	0.1171
R_{fd}	0.001084	0.001084	0.001189
L_{kd1}	20.450	0.01136	0.01737
R_{kd1}	0.1216	0.01065	0.0109
L_{fkd1}	1.0470	0.1328	0
L_{kq1}	2.1010	0.5677	0.0638
R_{kq1}	0.01060	0.0147	0.0164
L_{kq2}	0.4504	0.1717	0.3833
R_{kq2}	0.03010	0.1765	0.0099
L_{fkd2}	-0.8786	-	-
L_{kd2}	0.00989	-	-
R_{kd2}	0.00879	-	-
L_{kq3}	0.11310	-	-
R_{kq3}	0.2610	-	-

The large and almost mutually offsetting values of "mutual leakage" inductances observed in model SSFR3 are more a result of the peculiar solution of the model equations than a measure of the unequal coupling between the rotor circuits. The same reasoning applies to the large value of leakage inductance in the damper winding, L_{kd1}. What these results demonstrate is that a three winding model is really unnecessary for this machine as the third winding assumes rather absurd values. It should be noted that the net effect of the mutual leakage inductances in model SSFR3 (0.1684) is very similar to that in model SSFR2 (0.1328).

The differences between the STANDARD and standstill model SSFR2 manifest themselves as a lower field time constant and a higher q-axis amortisseur time constant (T_{kq2}) in the former. It remains to be seen how these differences affect the relative performance of the model in the validation tests which consist of simulating measured line switching transients.

Verification of Equivalent Circuits

As a check on their accuracy, the equivalent circuits obtained from the standstill frequency response tests were used to reproduce that same test data. At first glance, this might seem a trivial step; however, for two reasons, it is not. First, a two or three discrete winding model cannot perfectly represent the infinity of circuits on a solid iron rotor, so the errors resulting from this simplification should be evaluated. Second, the model derivation method does not use all of the available data; for example, direct axis measurements with the field open are not included. Consequently, it is important to check that the derived models are not inconsistent with this extra data.

Figures 3-6 to 3-10 demonstrate the ability of the second and third order models to duplicate the standstill frequency response of the generator. In general, the largest errors are at the highest frequencies. This is because the curve fitting was biased toward frequencies below 10 Hz which was the most important range for this study. If turbine generator shaft dynamics were a concern, more weight would be given to the subtransient region.

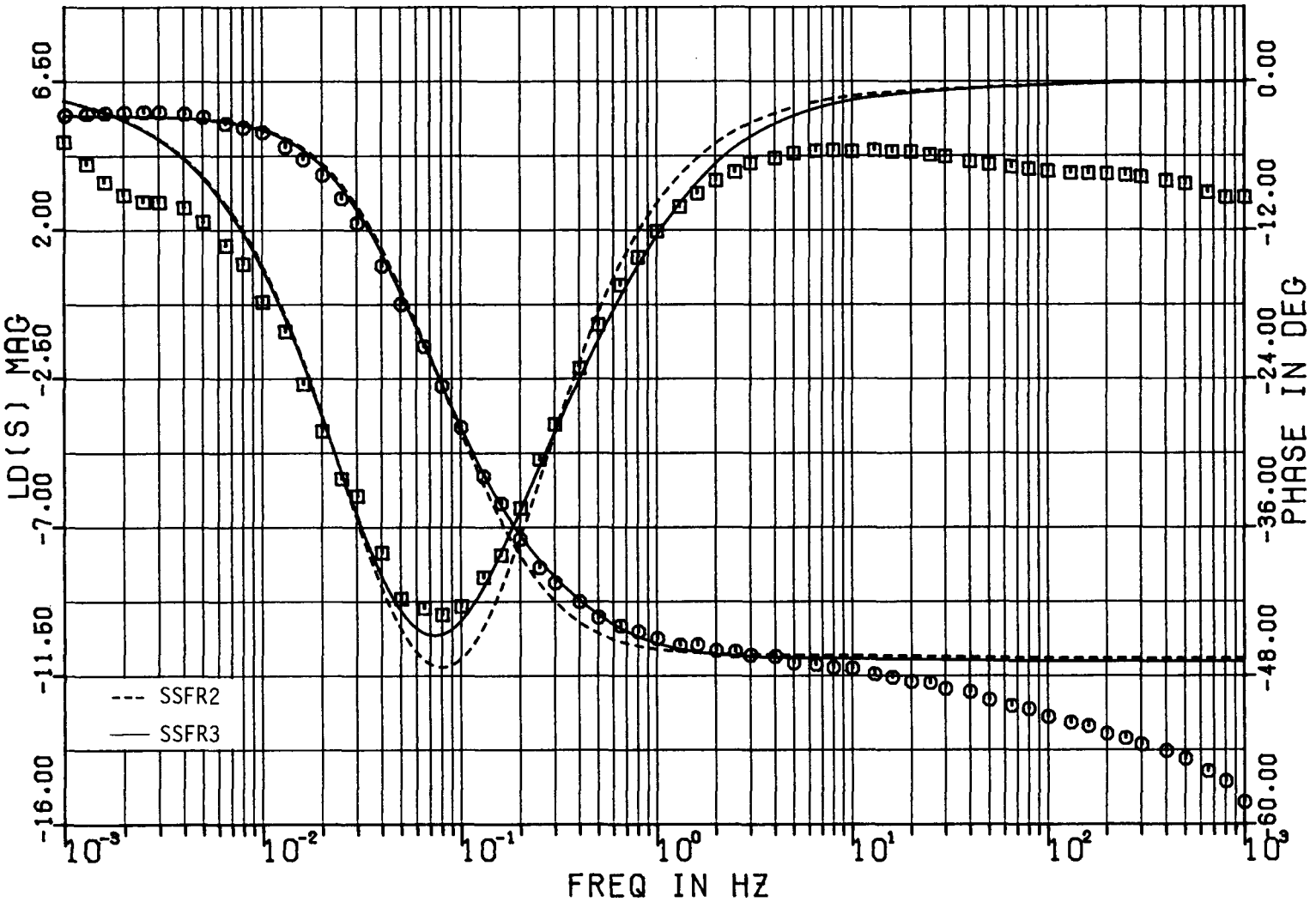

Figure 3-6. Two- and Three-Rotor-Winding Fits of Lambton $L_d(s)$.

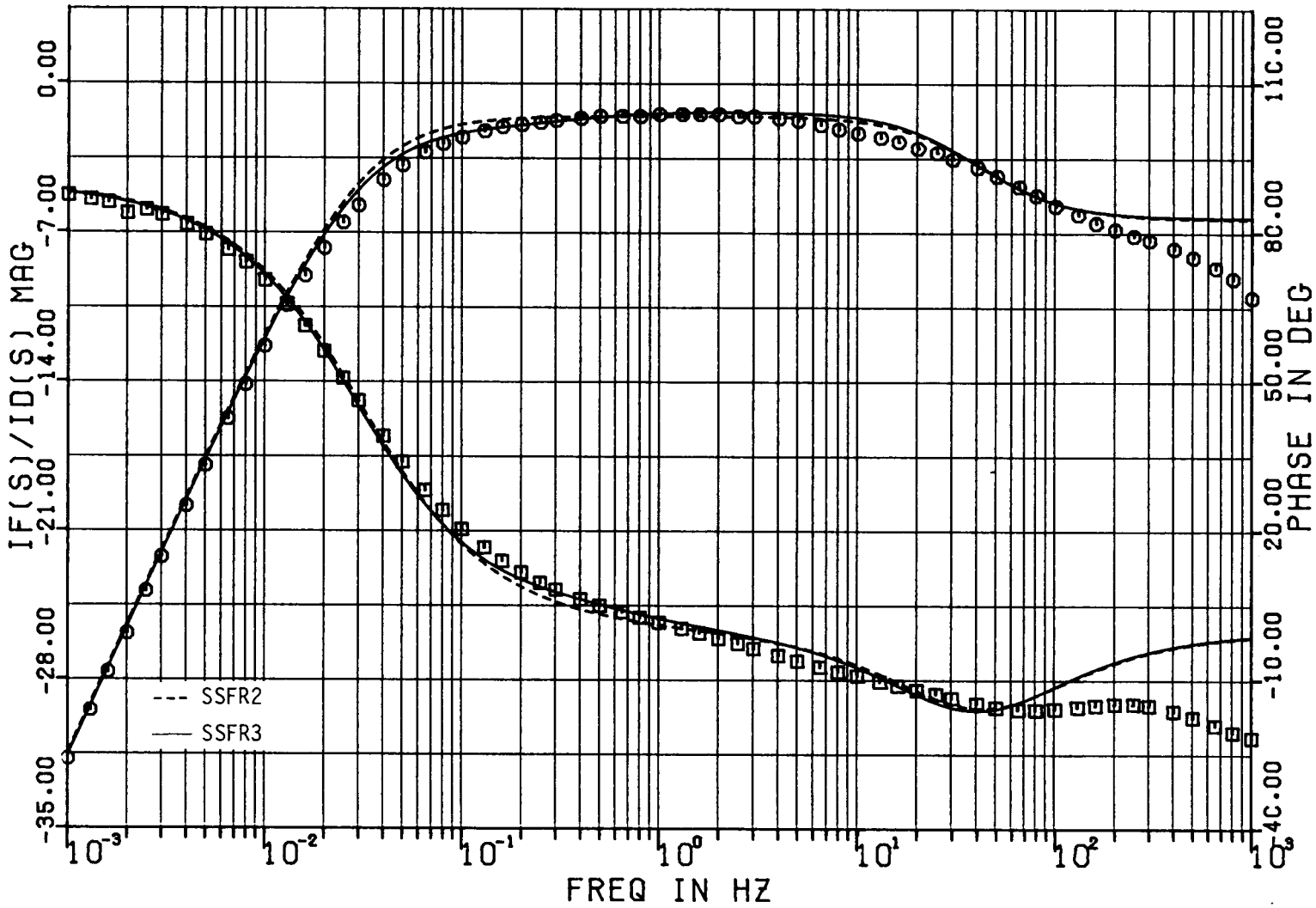

Figure 3-7. Two- and Three-Rotor-Winding Fits of Lambton sG(s).

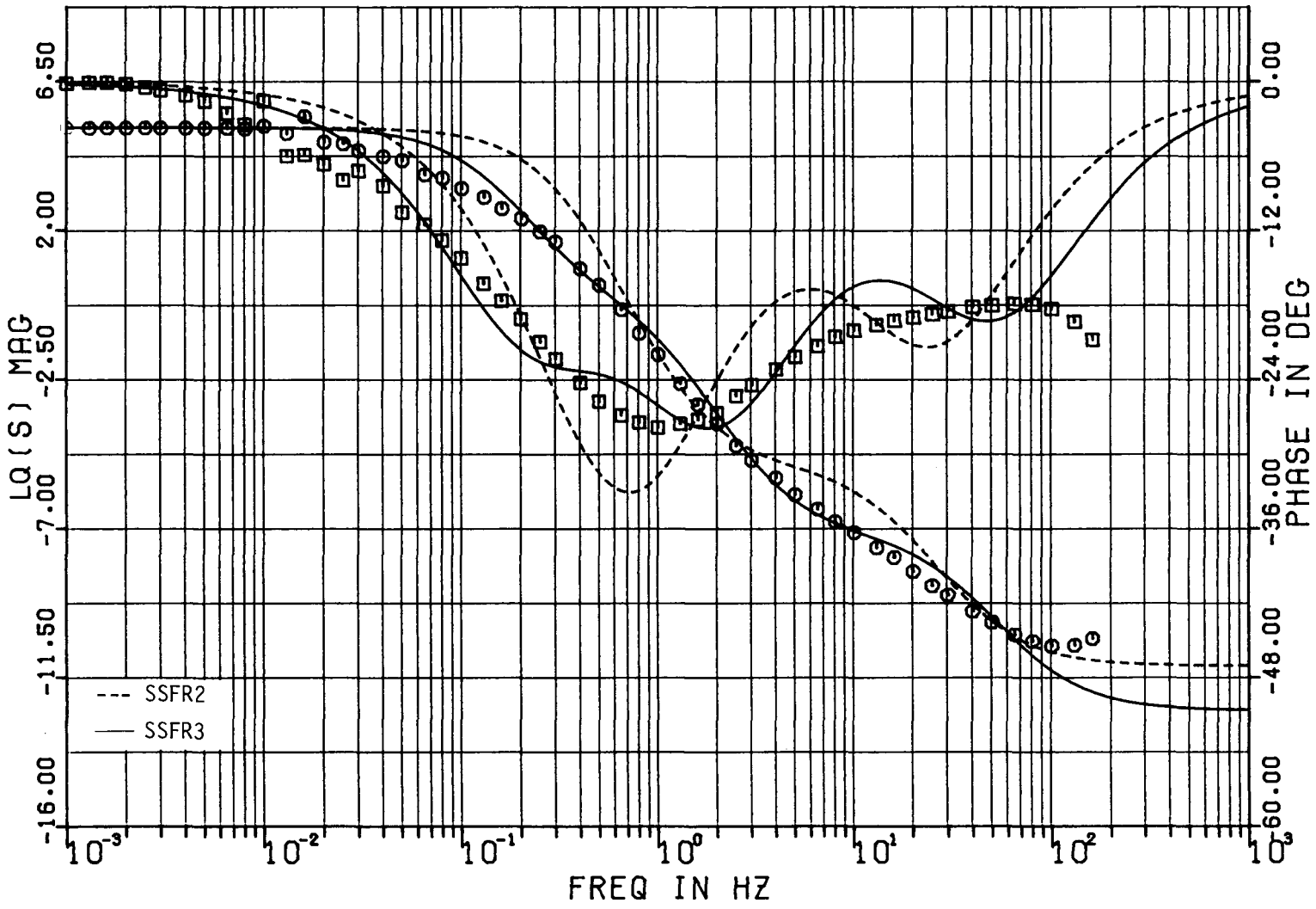

Figure 3-8. Two- and Three-Rotor-Winding Fits of Lambton $L_q(s)$.

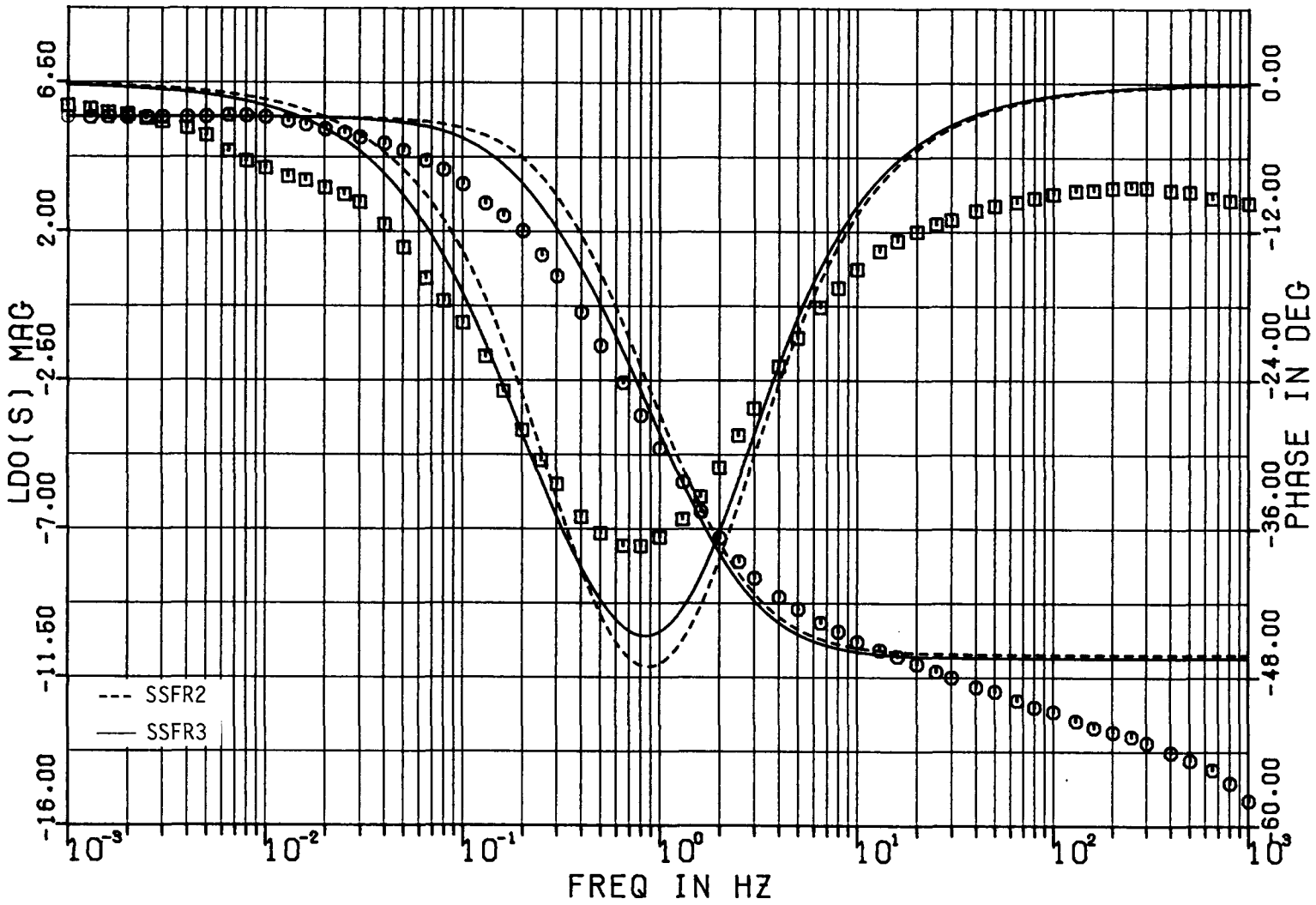

Figure 3-9. Two- and Three-Rotor-Winding Fits of Lambton $L_{do}(s)$.

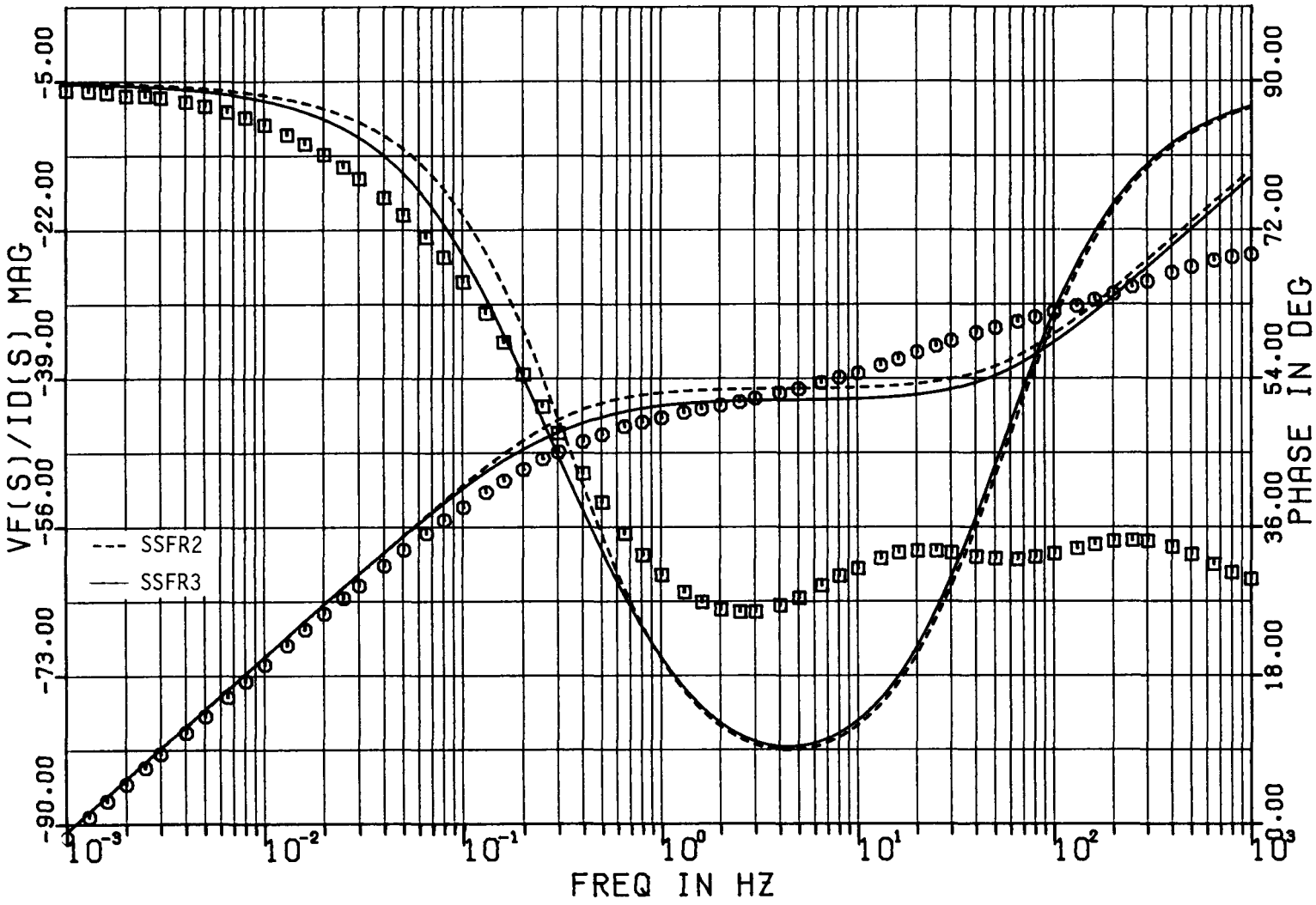

Figure 3-10. Two- and Three-Rotor Winding Fits of Lambton Stator-To-Field Transfer Impedance.

NANTICOKE

Standstill frequency response test data was fitted with second and third order rational polynomials. Using the time constants so obtained together with the unsaturated synchronous inductance and the armature leakage inductance L_1, the d- and q-axis equivalent circuits for models SSFR2 and SSFR3 were obtained. It is evident from Figures 3-11, 3-12 and 3-13 that both d- and q-axis test data for this machine is best approximated by third order polynomials, which implies a three rotor winding representation in both the d- and q-axis equivalent circuit models. Second order polynomials do not give such a good approximation. This is particularly noticeable in the phase angle of $L_d(s)$ and $L_q(s)$.

The standstill model was derived on the basis of equations used by Umans et al (2) in which the second "mutual leakage" inductance was neglected and an iterative solution was adopted for the remaining parameters. The corresponding parameters are shown in Table 3-4 as are those pertaining to the STANDARD d- and q-axis models which were computed from the data in Table 3-3. The model parameters in Table 3-4 are in pu on the generator base.

Figures 3-14 and 3-15 demonstrate the ability of the SSFR2 and SSFR3 models to reproduce the standstill measurements made on the direct axis with the field open. Here, it is evident that the rotor would have to be represented in much more detail than even the three circuit model provides, if operation of the generator with the field open were important.

Table 3-3

MANUFACTURER'S DATA FOR NANTICOKE

MVA	588
kV	22.0
L_{du}	2.360 pu
L'_d	0.286 pu
L''_d	0.211 pu
T'_{do}	7.606 s
T''_{do}	0.052 s
L_{qu}	2.242 pu
L'_q	0.340 pu
L''_q	0.225 pu
T'_{qo}	1.50 s
T''_{qo}	0.350 s
L_l	0.195 pu

Table 3-4

NANTICOKE STANDARD AND SSFR MODEL PARAMETERS

Parameter	SSFR3 Model	SSFR2 Model	STANDARD Model
L_{ad}	2.152	2.152	2.165
L_{aq}	2.057	2.057	2.047
L_{l}	0.172	0.172	0.195
L_{fd}	0.0155	0.0231	0.0908
R_{fd}	0.00094	0.00094	0.00076
L_{kd1}	2.732	0.0101	0.0457
R_{kd1}	0.1142	0.00416	0.00703
L_{fkd1}	-0.5215	0.2728	-
L_{kq1}	1.657	0.8006	0.1560
R_{kq1}	0.00538	0.00842	0.00390
L_{kq2}	0.1193	0.1243	0.0378
R_{kq2}	0.1081	0.04893	0.00139
L_{fkd2}	0.8975	-	-
L_{kd2}	0.00753	-	-
R_{kd2}	0.00592	-	-
L_{kq3}	0.4513	-	-
R_{kq3}	0.0188	-	-

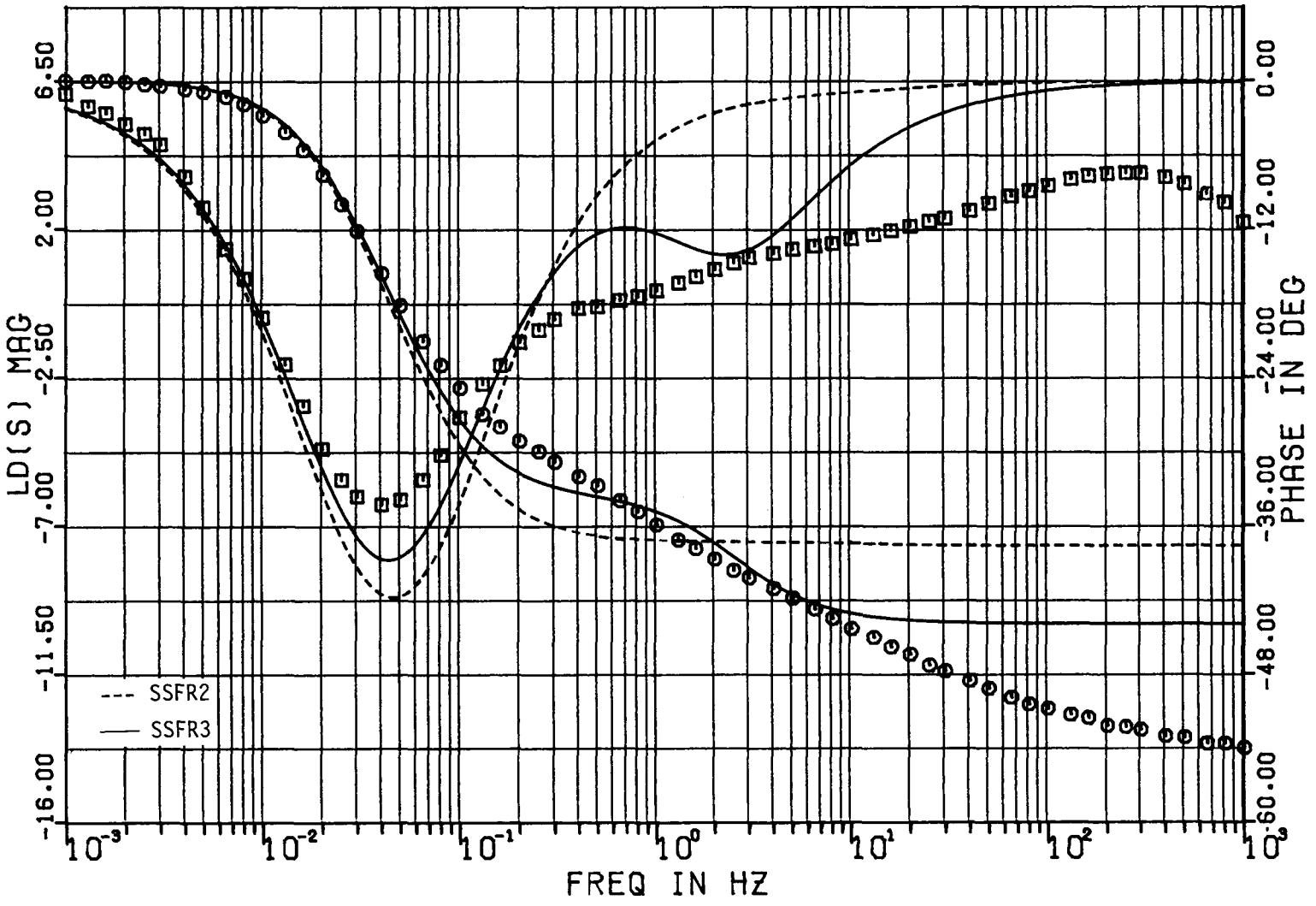

Figure 3-11. Two- and Three-Rotor Winding Fits of Nanticoke $L_d(s)$.

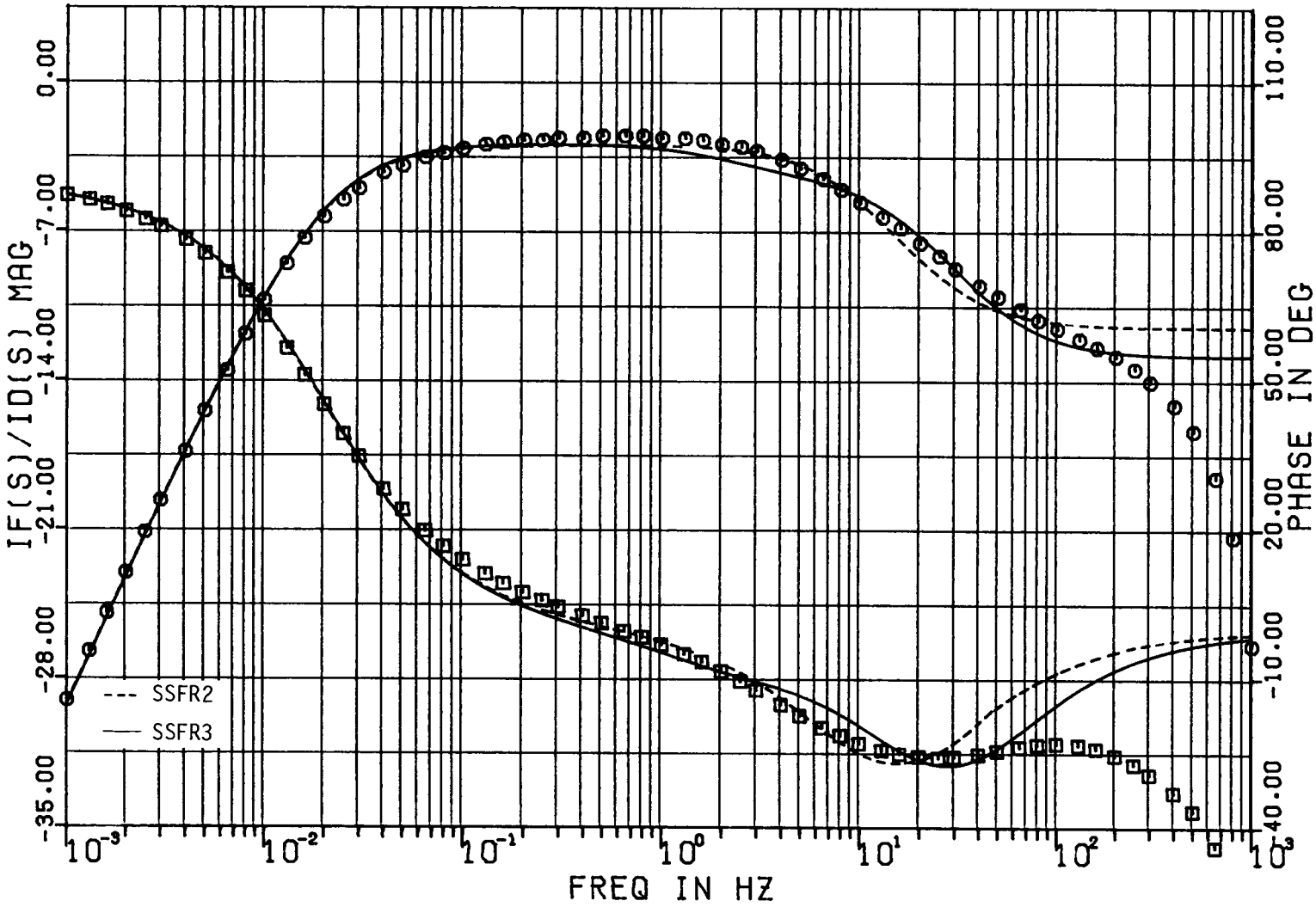

Figure 3-12. Two- and Three-Rotor Winding Fits of Nanticoke sG(s).

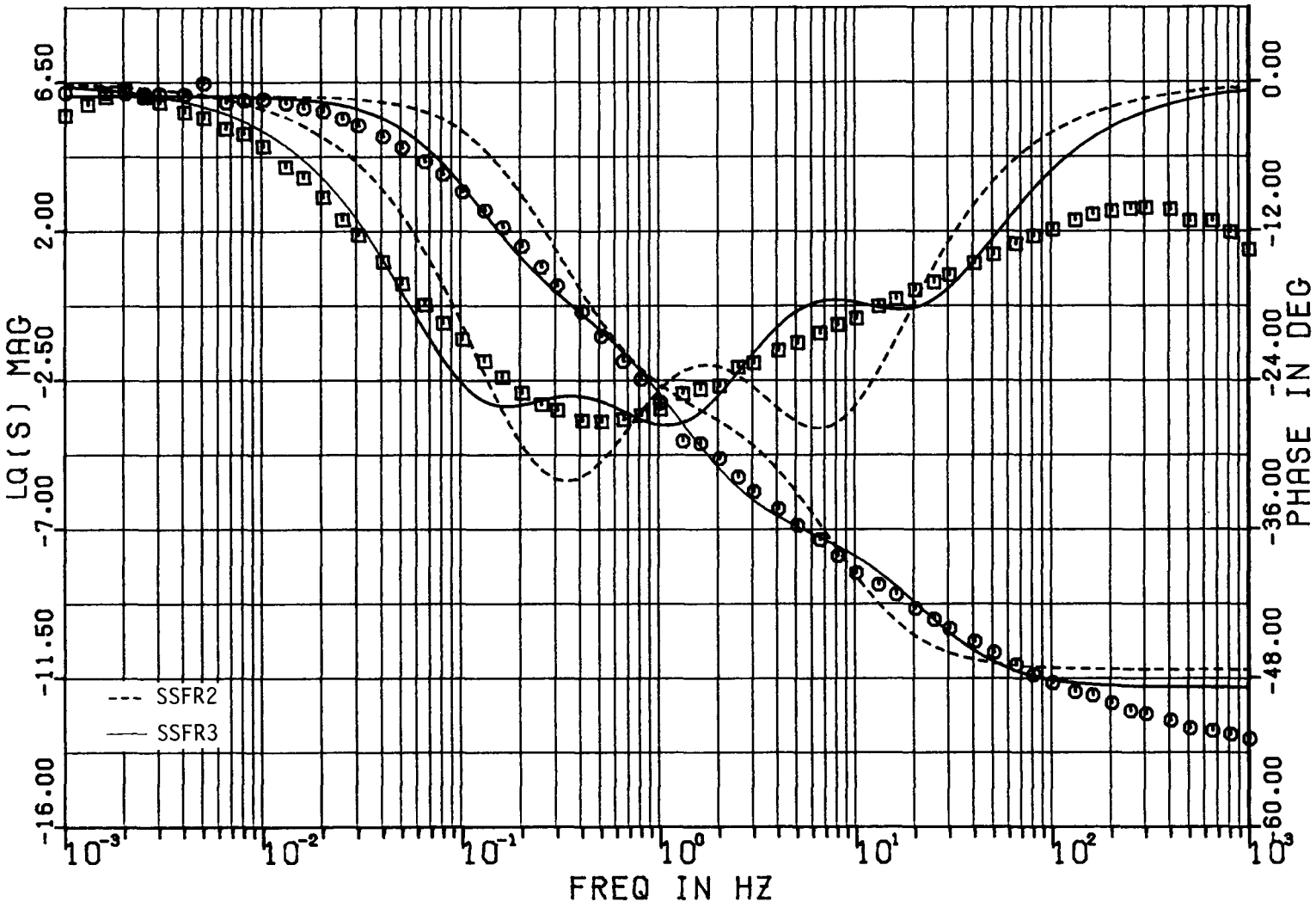

Figure 3-13. Two- and Three-Rotor-Winding Fits of Nanticoke $L_q(s)$.

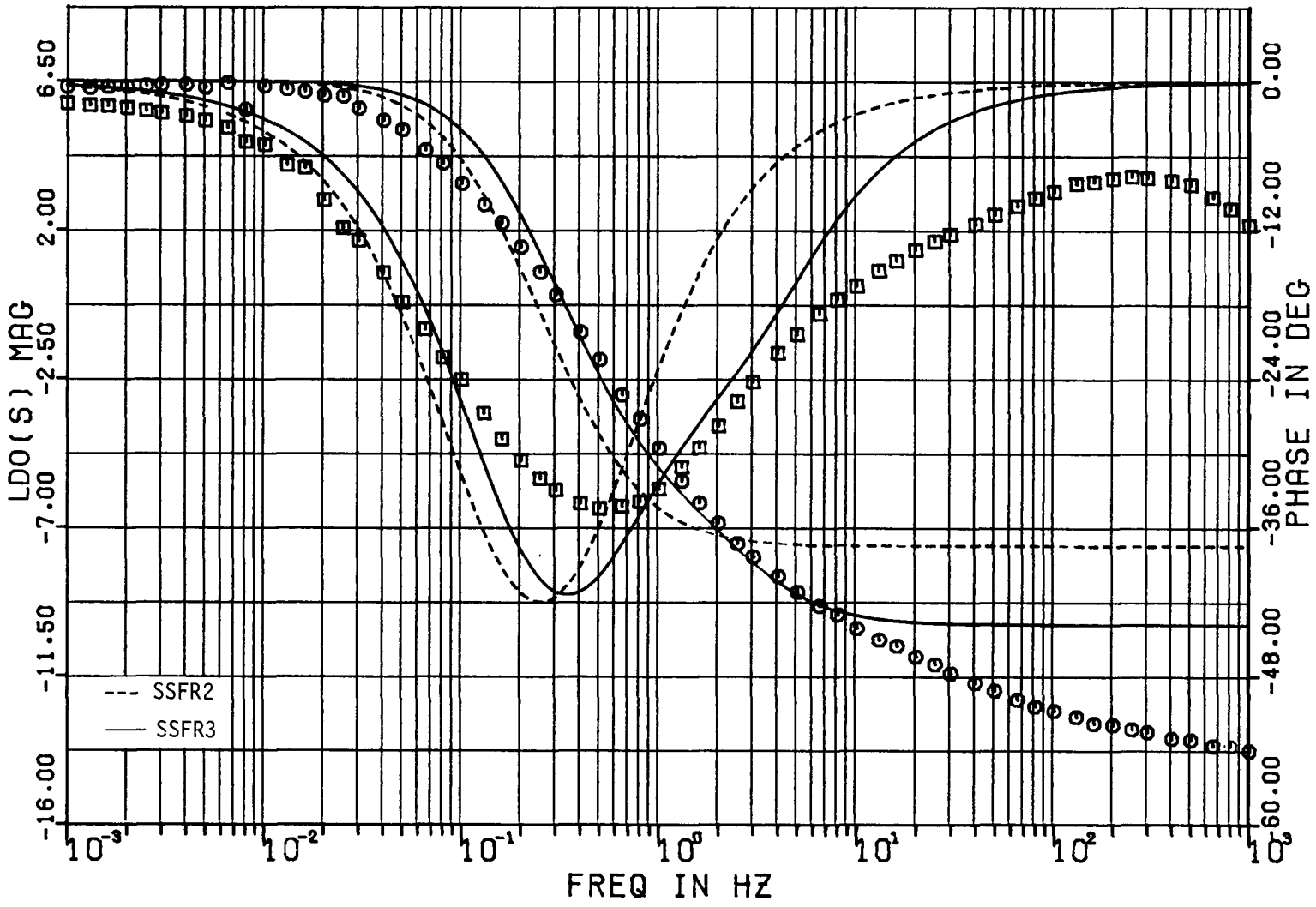

Figure 3-14. Two- and Three-Rotor-Winding Fits of Nanticoke $L_{do}(s)$.

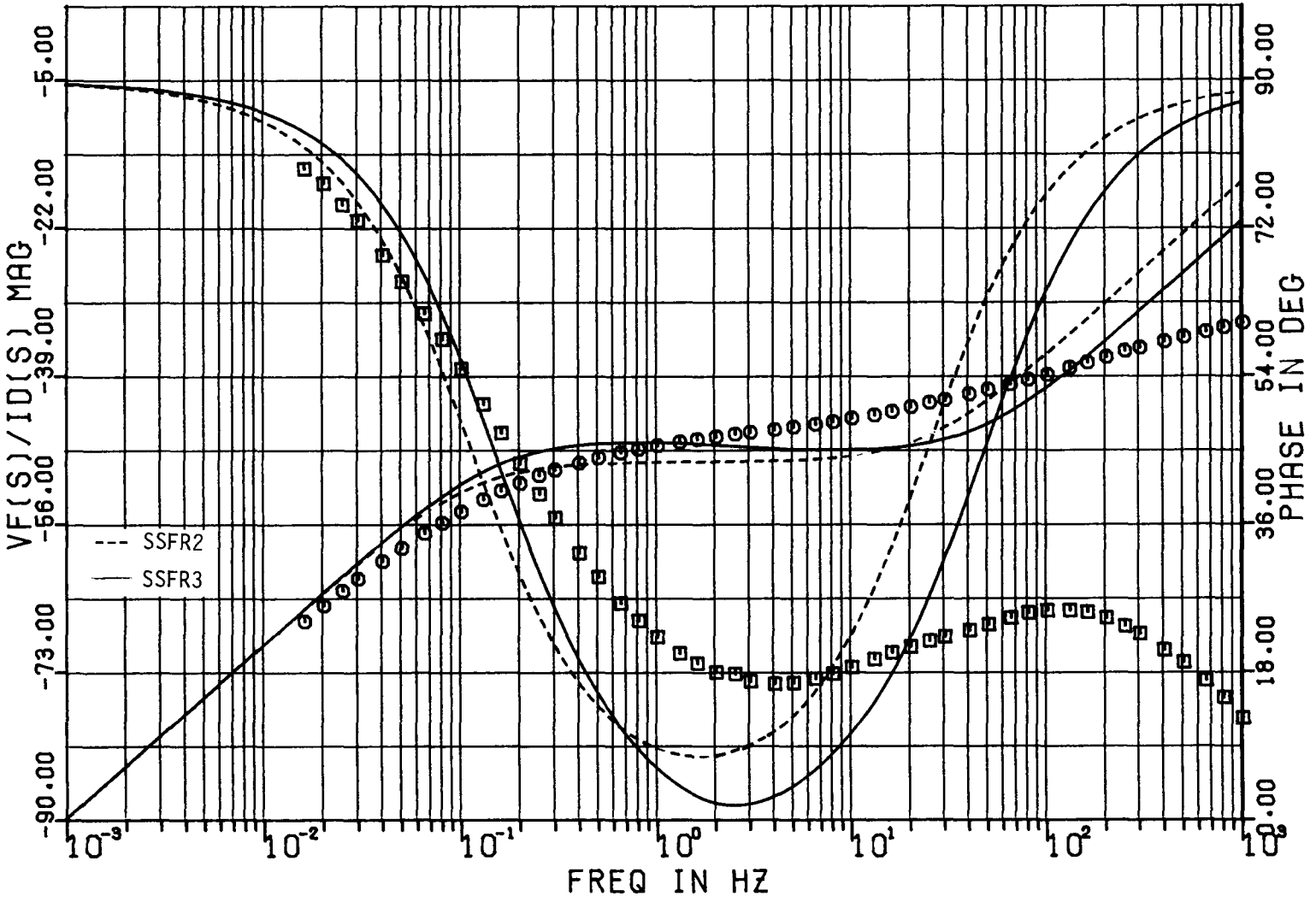

Figure 3-15. Two- and Three-Rotor-Winding Fits of Nanticoke Stator-To-Field Transfer Impedance.

MONTICELLO

Derivation of Models

Standstill frequency response tests were done on the Monticello machine by Westinghouse. Equivalent circuit models in the d- and q-axes were derived from this data, as before. In addition to these models, standard d- and q-axis models were obtained from the data provided by the manufacturer of this machine. This data is based on the quoted values of "transient" and "subtransient" parameters in Table 3-5.

As for the Nanticoke and Lambton generators, validation of the above models was performed by using the models to simulate the performance of the machine under standstill test conditions. Figures 3-16, 3-17 and 3-18 show the performance of second and third order models. It is evident that the d-axis data for this machine is well approximated by second order model, which implies a two rotor winding representation in the equivalent circuit; the q-axis data is best represented by a third order model which, in turn, implies a three rotor winding representation in the equivalent circuit.

The corresponding STANDARD model's parameters are shown in Table 3-6 along with those for SSFR2 and SSFR3. All parameter values are in per unit on the machine base.

Standstill frequency response data on the direct axis with the field open was not available, so the performance of the derived models could not be checked for this condition. However, the concordance among the SSFR models and the available data is very good (Figures 3-16 to 3-18).

Table 3-5

MANUFACTURER'S DATA FOR MONTICELLO

MVA	645
kV	18.0
L_d	1.90 pu
L'_d	0.355 pu
L''_d	0.289 pu
L_q	1.88 pu
L'_q	0.552 pu
L''_q	0.283 pu
T'_{do}	5.66 s
T''_{do}	0.041 s
T'_{qo}	0.62 s
T''_{qo}	0.065 s
L_l	0.209 pu

Table 3-6

MONTICELLO GENERATOR PARAMETERS

Parameter	SSFR3	SSFR2	STANDARD
L_{ad}	1.6910	1.6910	1.6910
L_{aq}	1.6270	1.6270	1.6710
L_{l}	0.2090	0.2090	0.2090
L_{fd}	0.0087	0.0171	0.1598
R_{fd}	0.000811	0.000811	0.000875
L_{kd1}	0.1144	0.0051	0.1770
R_{kd1}	0.0670	0.00727	0.0209
L_{fkd1}	0.0093	0.1258	-
L_{kq1}	1.9180	0.7202	0.0944
R_{kq1}	0.0106	0.0142	0.0720
L_{kq2}	0.1247	0.1314	0.4316
R_{kq2}	0.1293	0.0586	0.0090
L_{fkd2}	0.1287	-	-
L_{kd2}	0.0014	-	-
R_{kd2}	0.0091	-	-
L_{kq3}	0.3816	-	-
R_{kq3}	0.0210	-	-

Comparison of Different Models

Since only the STANDARD, SSFR2, and SSFR3 models were obtained for the Monticello machine, it is appropriate to compare them at this point in the report.

Table 3-7

MONTICELLO D- AND Q-AXIS TIME CONSTANTS

Model	T_{fd}	T_{kd1}	T_{kd2}	T_{kq1}	T_{kq2}	T_{kq3}
SSFR2	6.0	0.7	-	0.4	0.08	-
SSFR3	6.0	0.5	0.8	0.3	0.04	0.9
Standard	5.6	0.2	-	0.6	0.07	-

Table 3-7 lists the time constants of the rotor windings for each of the three models. The following salient points may be noted from examination of Tables 3-6 and 3-7.

- The d- and q-axis standstill models SSFR2 and SSFR3 show values of the mutual inductances L_{ad} and L_{aq} respectively which are about 17% higher than the corresponding values obtained from standstill tests. This difference is obtained by correcting the standstill value of L_{ad} to the design value (Table 3-5). This difference is quite substantial when compared with 11% and 7% respectively for the Nanticoke and Lambton units, and it suggests that the non-linearities at low excitation currents are much more pronounced for this Monticello unit.

- The q-axis time constants of the STANDARD and SSFR2 models are very similar, indicating that the q-axis performance of the two models should be very similar.

- There are substantial differences in the direct axis damper time constants between the STANDARD and the two SSFR models; the SSFR time constants show a stronger damper winding. It remains to be seen how the differences affect the model performance in the validation tests.

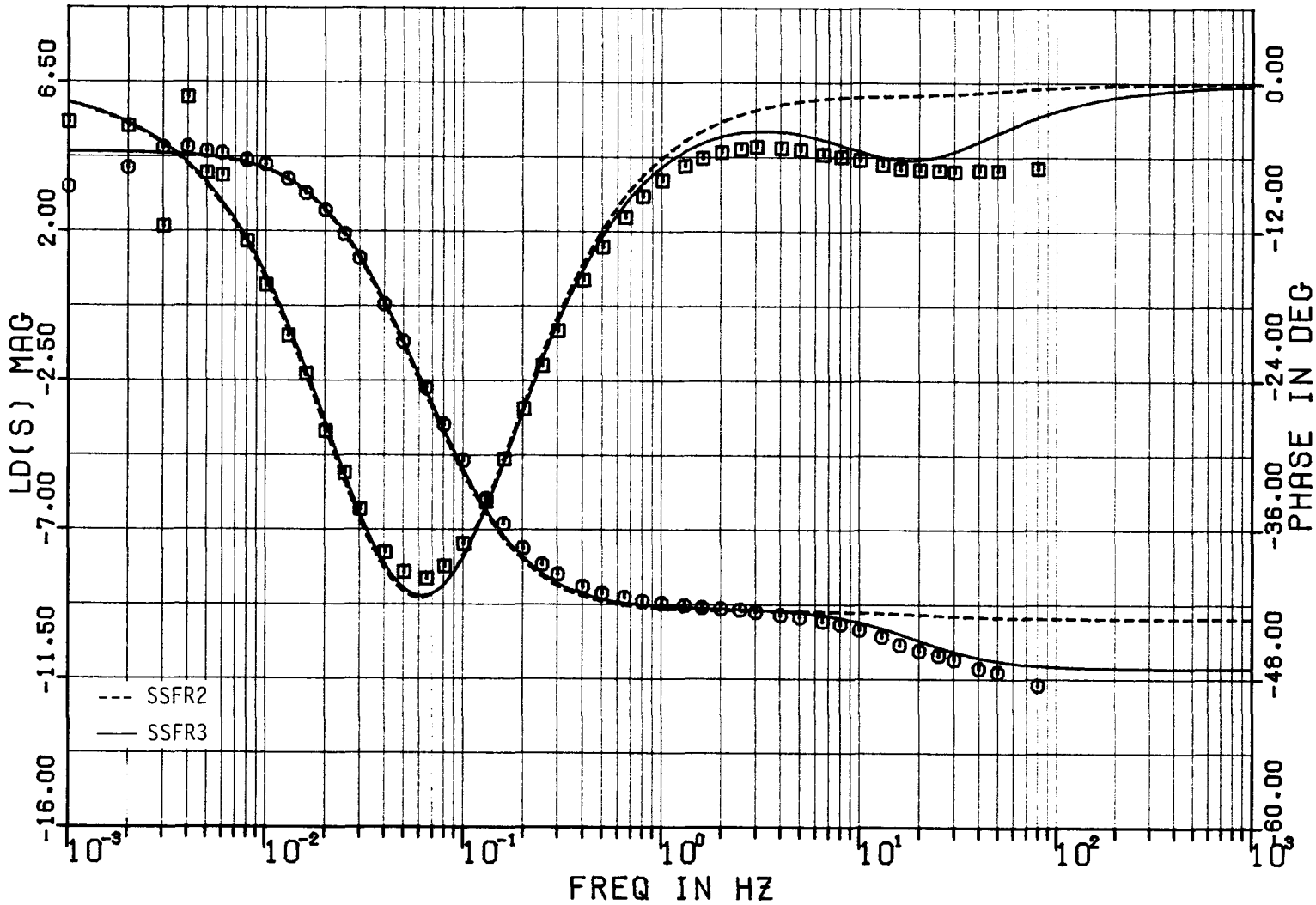

Figure 3-16. Two- and Three-Rotor-Winding Fits of Monticello $L_d(s)$.

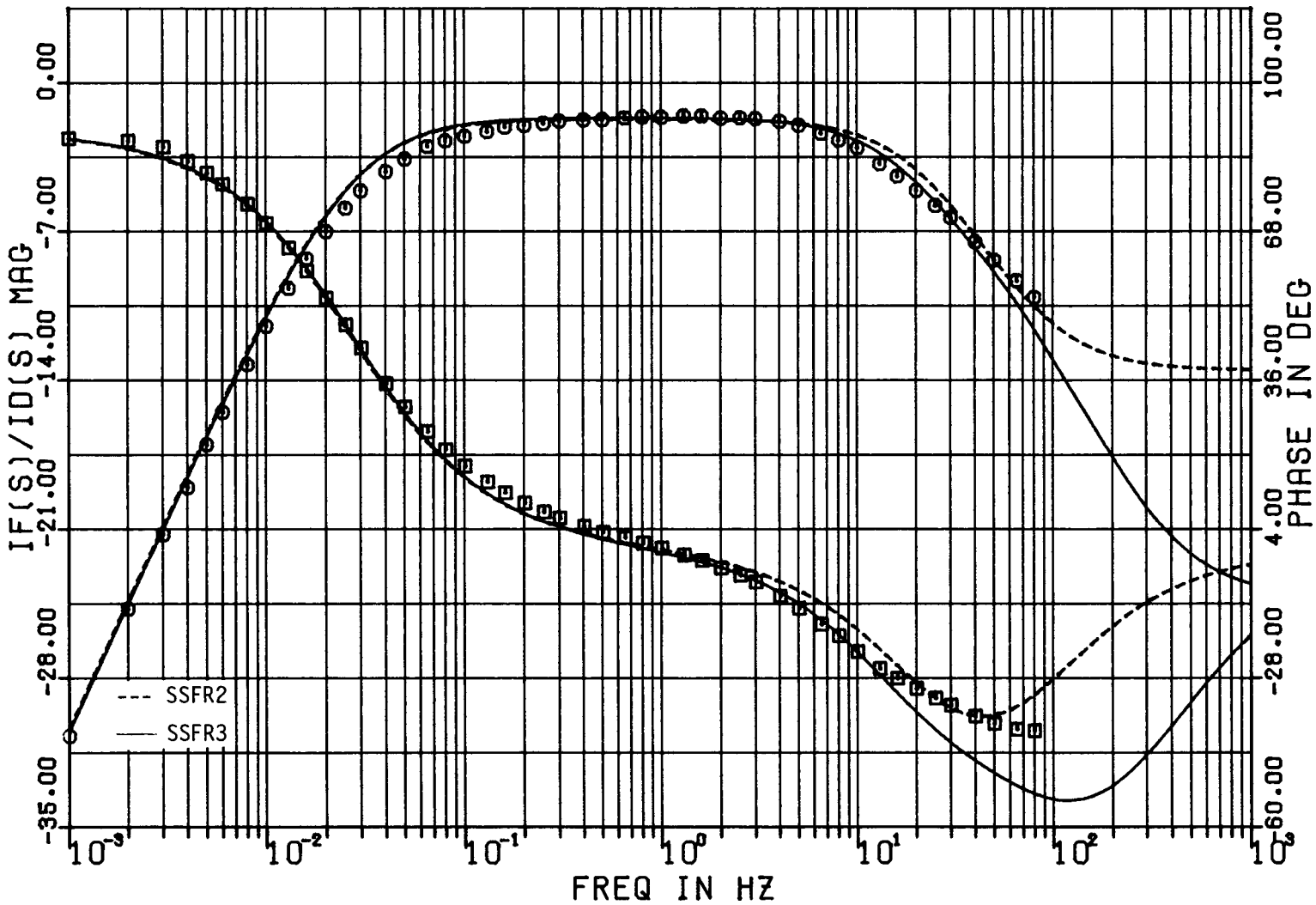

Figure 3-17. Two- and Three-Rotor-Winding Fits of Monticello sG(s).

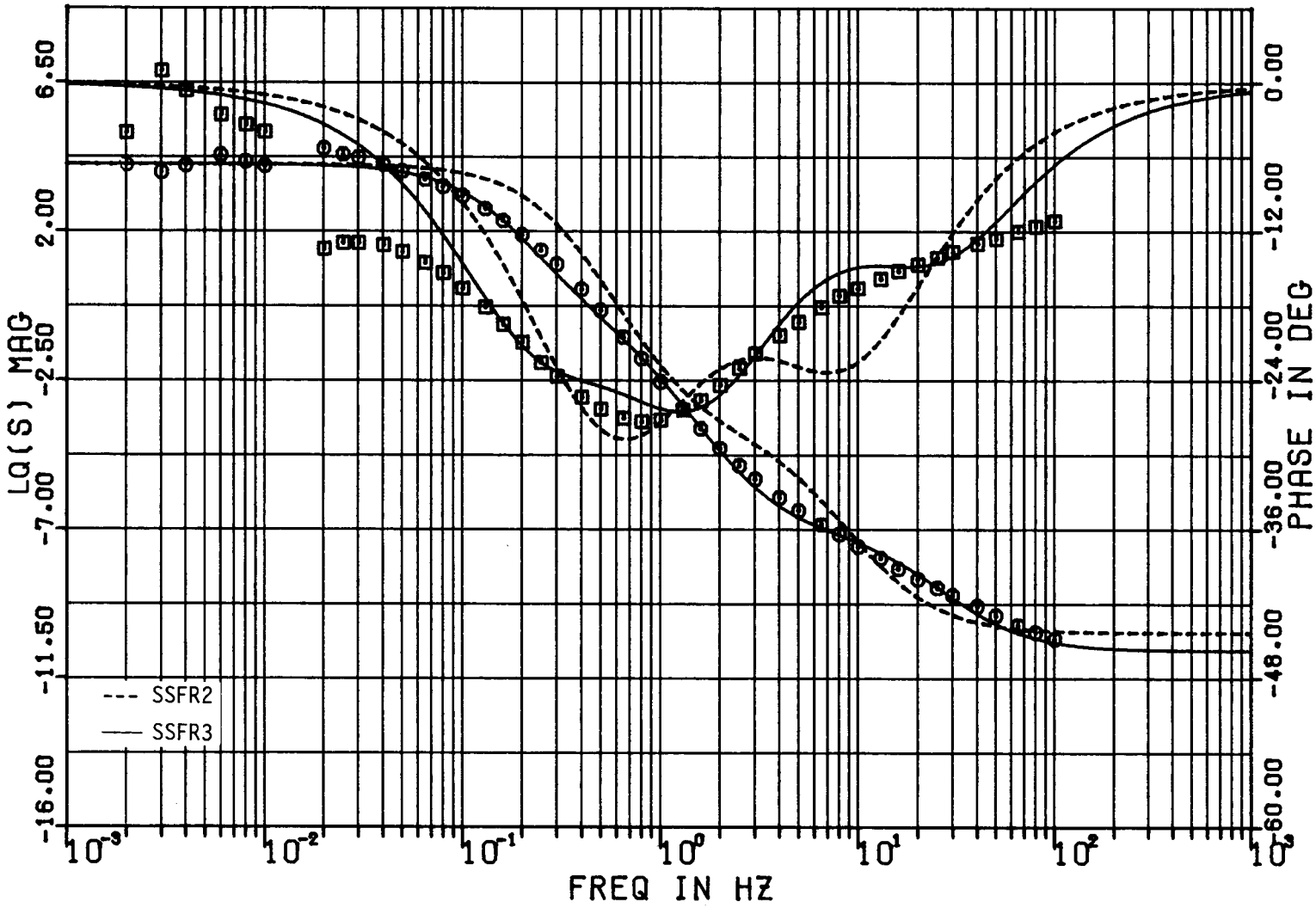

Figure 3-18. Two- and Three-Rotor-Winding Fits of Monticello $L_q(s)$.

REFERENCES

1. W. Watson and G. Manchur. Synchronous Machine Operational Impedance from Low Voltage Measurements at the Stator Terminals. IEEE Trans PAS-93, May/June 1974.

2. S.D. Umans, J.A. Mallick, G.L. Wilson. Modelling of Solid Rotor Turbogenerators (2 parts). IEEE Trans PAS-97, Jan/Feb 1977.

3. Supplementary Definitions and Associated Test Methods for Obtaining Parameters for Synchronous Machine Stability Study Simulations. IEEE Joint Working Group Paper F79-647-9. Presented at 1979 Summer Power Meeting.

4. I.M. Canay. Causes of Discrepancies in Calculation of Rotor Quantities and Exact Equivalent Diagrams of the Synchronous Machine. IEEE Trans PAS-88, July 1969.

Section 4

PERFORMANCE OF SSFR MODELS

THE CRITERION

The machine models were to be evaluated on their ability to reproduce a large disturbance. To this end, three sets of line switching transients were recorded, involving each of the three generators. The performance of each model was judged by its efficacy in simulating these measured transients, specifically the deviations of electrical power and field current on the test generator. It is our considered opinion that these quantities are sufficient to demonstrate the capabilities of each model in the simulations.

Half of the tests at Lambton and Nanticoke were done with a high gain (200) automatic voltage regulator in service; complete data from these tests is reported in Parts 4 and 5. However, in evaluating the models, only cases with constant field voltage on the test generator (AVR out of service) were considered. This was done to highlight the response of the generator itself by eliminating any action of supplementary controls such as the automatic voltage regulator and the power system stabilizer.

LAMBTON

Description of Line Switching Tests

With the system arrangements in Figures 4-1 and 4-2, open and close operations were done on the test line.

The External System

For the purpose of this investigation the system external to the test generator was represented by 799 busses, 1834 lines and 196 generators and included the remainder of the Ontario Hydro system and its interconnections with other utilities. All loads were represented as constant impedances. Of the 196 generators,

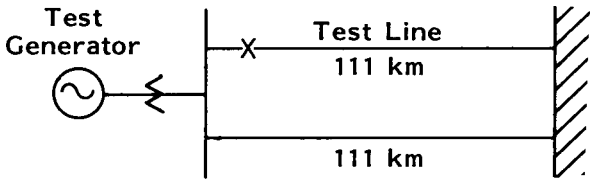

Figure 4-1. Balanced Arrangement for Lambton Line Switching Tests.

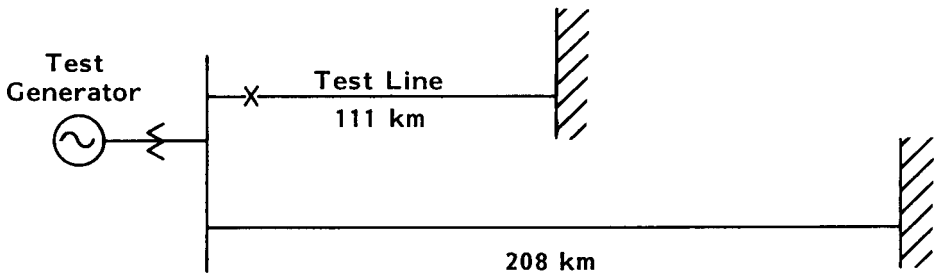

Figure 4-2. Unbalanced Arrangement For Lambton Line Switching Tests.

Table 4-1

SUMMARY OF LAMBTON LINE SWITCHING TEST CASES

Test No.	System Arrangement	Operation On Test Line	Test Generator Load
3	Balanced	Open	0.6 pu
4	Balanced	Close	0.6 pu
7	Unbalanced	Open	0.9 pu
8	Unbalanced	Close	0.9 pu

24 were modelled as detailed machines using Park's coordinates whilst the remainder were represented as classical machines, that is constant voltage behind transient reactance.

Ontario Hydro's ac load flow program was used in conjunction with steady-state measurements of system voltages, and active and reactive powers, to set up the correct system configuration and initial conditions for each test. Great care was taken to match, as closely as possible, the voltages, line flows and generator outputs to the system recordings. However, some difficulty was experienced in matching the voltages and line flows for Test 8; consequently, it is expected that some differences will arise between simulated and measured responses resulting from these discrepancies, over and above any inaccuracies introduced by the models.

Simulation of the Tests

Ontario Hydro's time domain program was used to carry out the simulations. Figures 4-3 through 4-14 show the comparisons for the three models considered herein (STANDARD, SSFR2, and SSFR3). In the context of this report the comparisons are restricted to generator active power and field current. In all cases machine excitation was on manual control (constant field voltage). The following points can be observed from the comparisons:

- It is clear that in all test operations the STANDARD model does not match the measured data. The frequency of rotor oscillations is seen to be greater than measured and the oscillations appear to be more damped than was actually the case.

- In general, both standstill frequency response models SSFR2 and SSFR3 give quite satisfactory performance in simulating the power and field current oscillations; ie, the frequency and damping of rotor oscillations is about right.

- The only exception is Test 8 (Figures 4-9 and 4-10) where it is seen that the frequency of rotor oscillations is quite different. As mentioned above we suspect the cause of this to be the inaccuracies in the load flow. In general, the model SSFR3 shows a slight improvement in the damping over model SSFR2, but the latter's performance is quite acceptable.

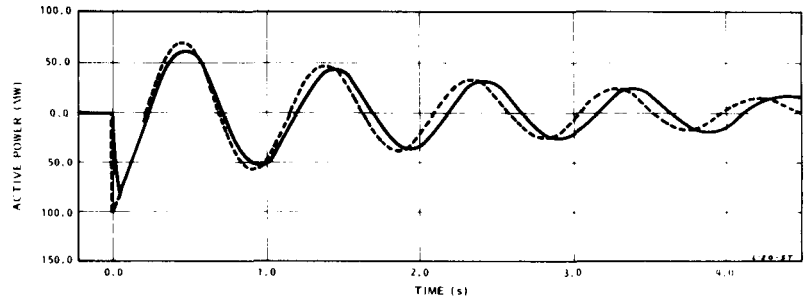

——— measured

- - - STANDARD

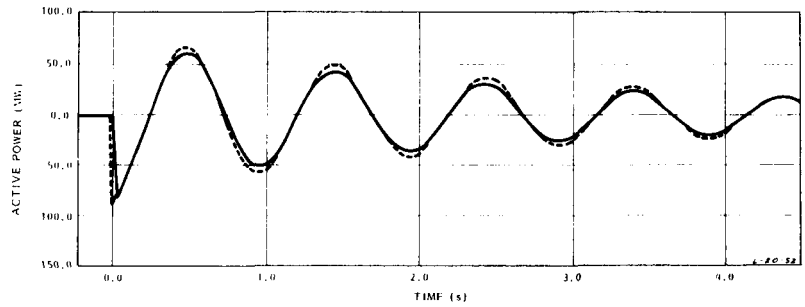

——— measured

- - - SSFR2

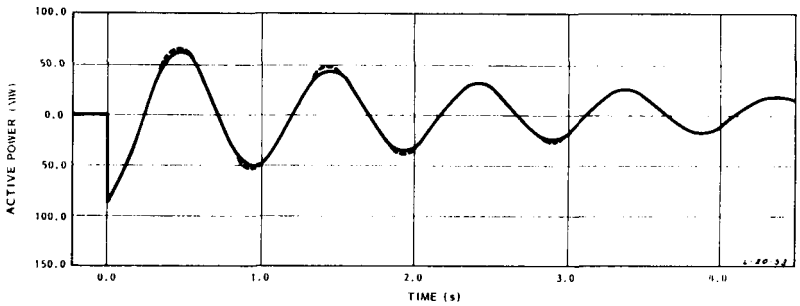

——— measured

- - - SSFR3

Figure 4-3. Lambton Line Switching Test Number 3. Open one line in balanced configuration, constant field voltage.

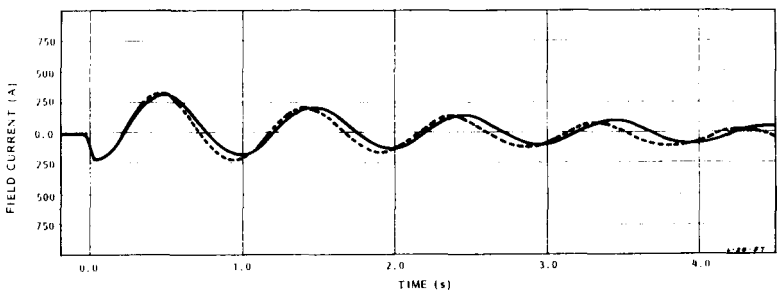

——— measured

- - - STANDARD

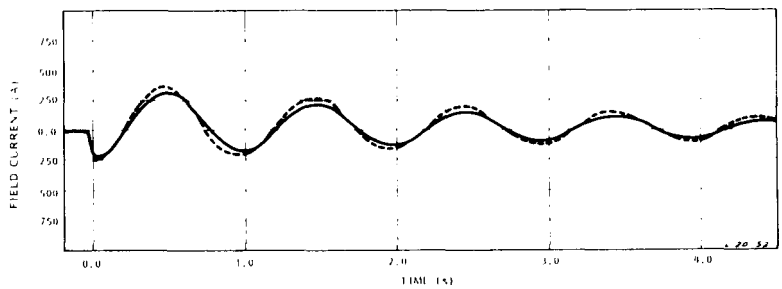

——— measured

- - - SSFR2

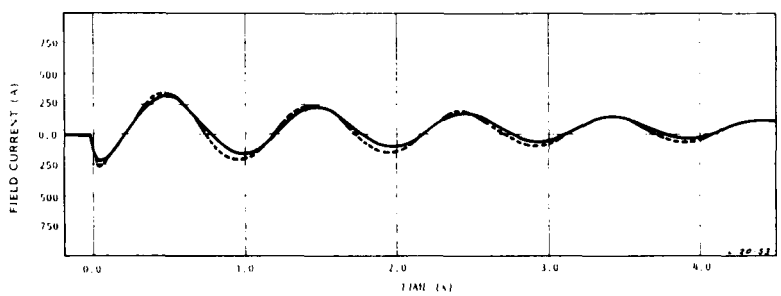

——— measured

- - - SSFR3

Figure 4-4. Lambton Line Switching Test Number 3. Open one line in balanced configuration, constant field voltage.

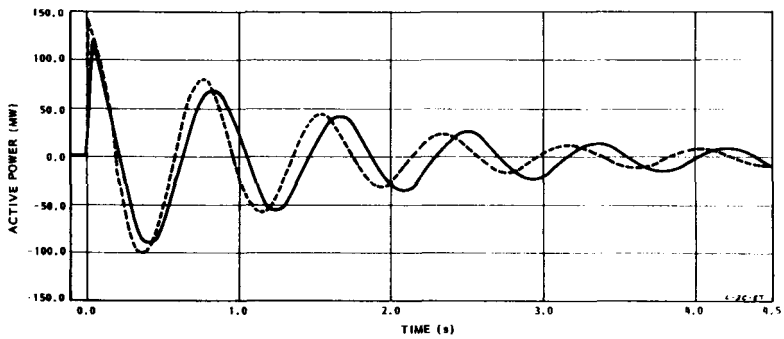

——— measured

- - - STANDARD

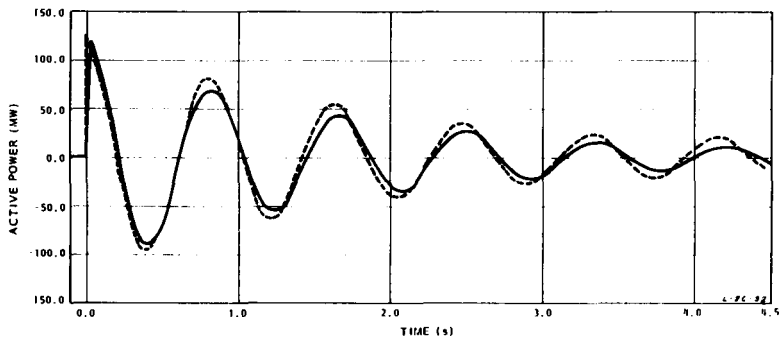

——— measured

- - - SSFR2

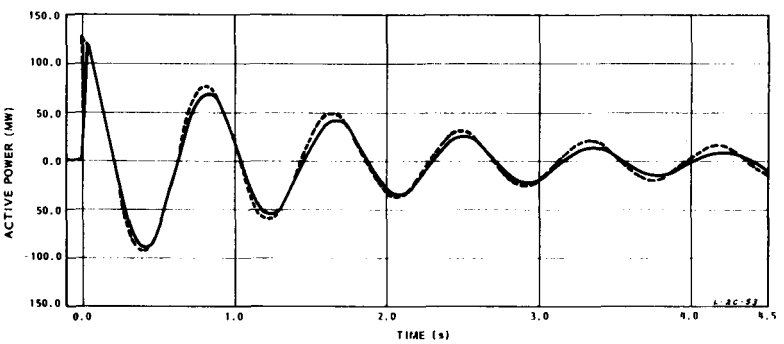

——— measured

- - - SSFR3

Figure 4-5. Lambton Line Switching Test Number 4. Close one line in balanced configuration, constant field voltage.

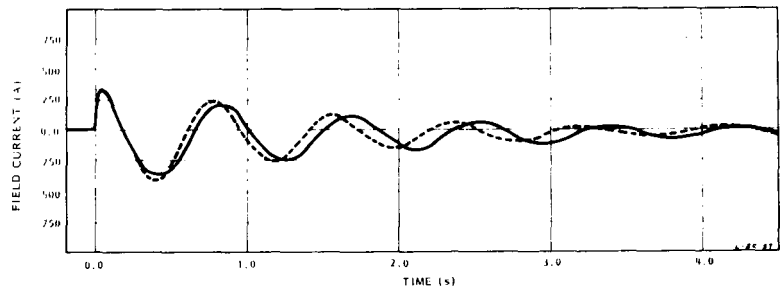

——— measured

- - - STANDARD

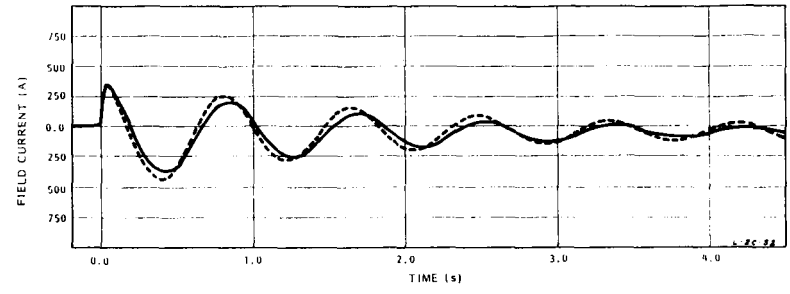

——— measured

- - - SSFR2

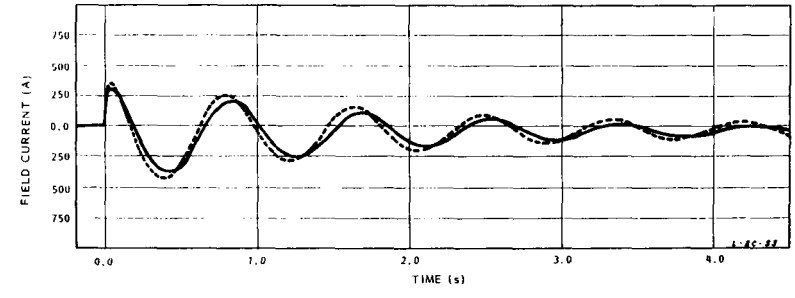

——— measured

- - - SSFR3

Figure 4-6. Lambton Line Switching Test Number 4. Close one line in balanced configuration, constant field voltage.

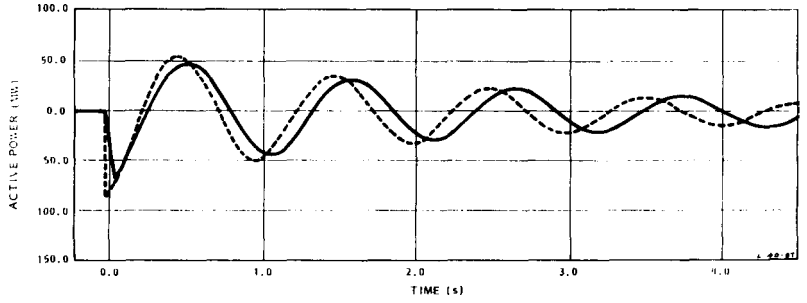

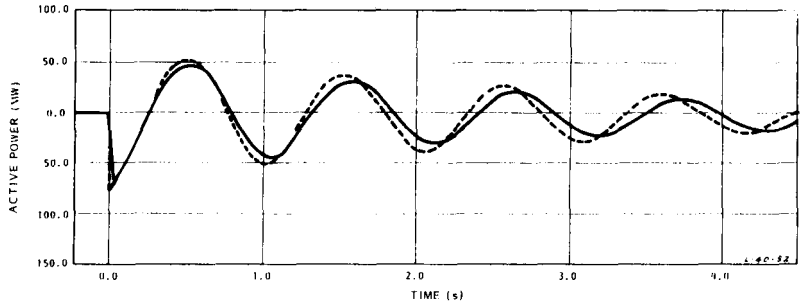

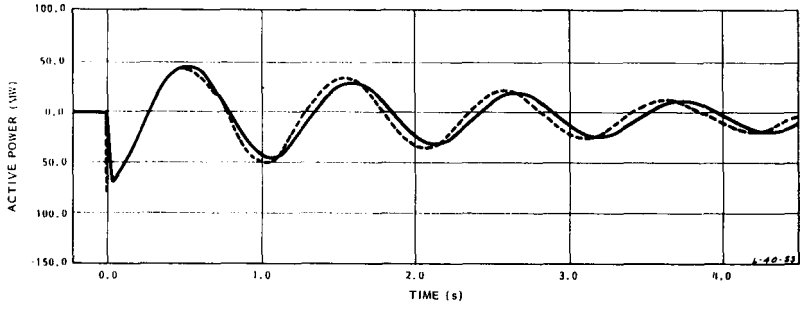

Figure 4-7. Lambton Line Switching Test Number 7. Open short line in unbalanced configuration, constant field voltage.

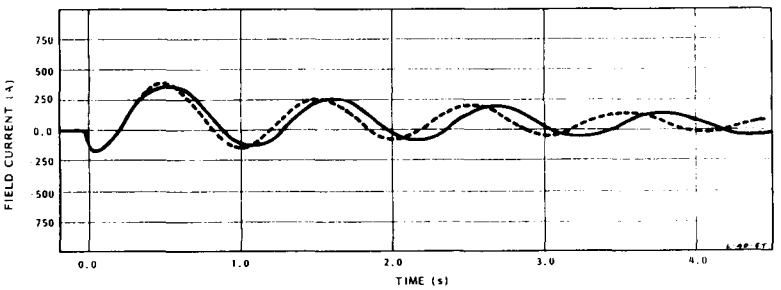

——— measured

- - - STANDARD

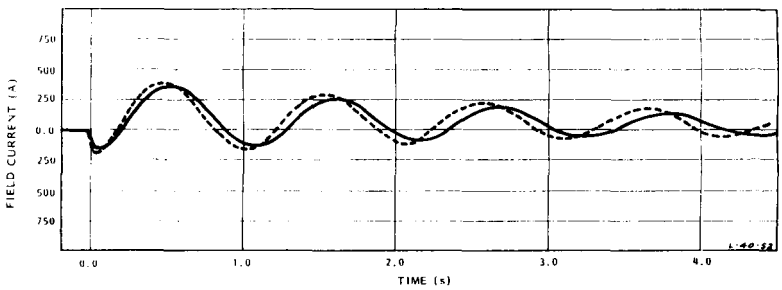

——— measured

- - - SSFR2

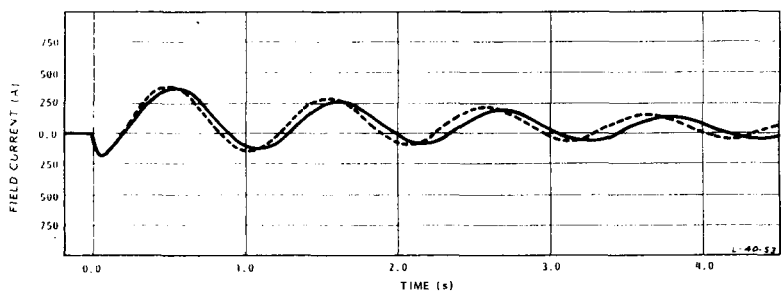

——— measured

- - - SSFR3

Figure 4-8. Lambton Line Switching Test Number 7. Open short line in unbalanced configuration, constant field voltage.

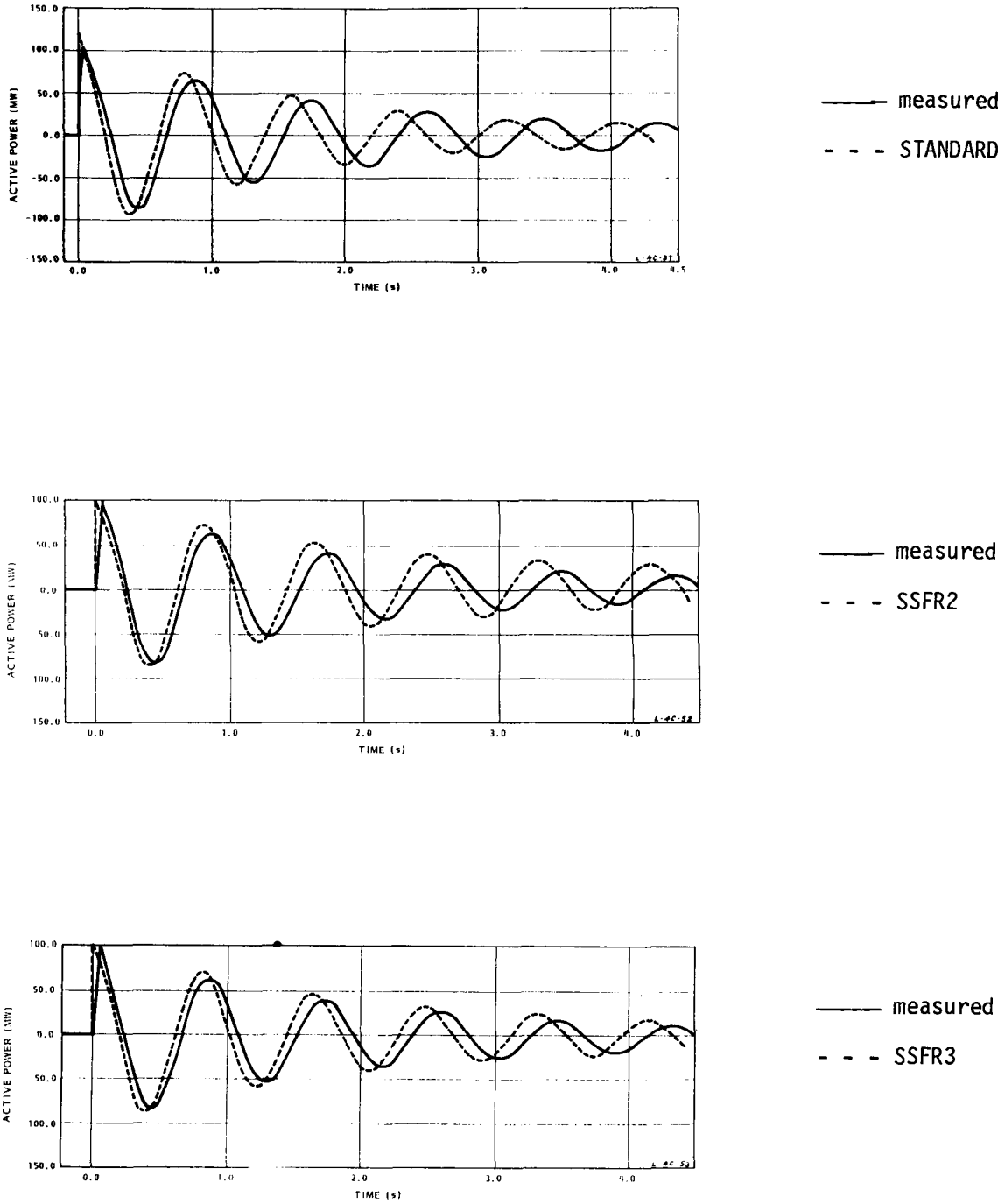

Figure 4-9. Lambton Line Switching Test Number 8. Close short line in unbalanced configuration, constant field voltage.

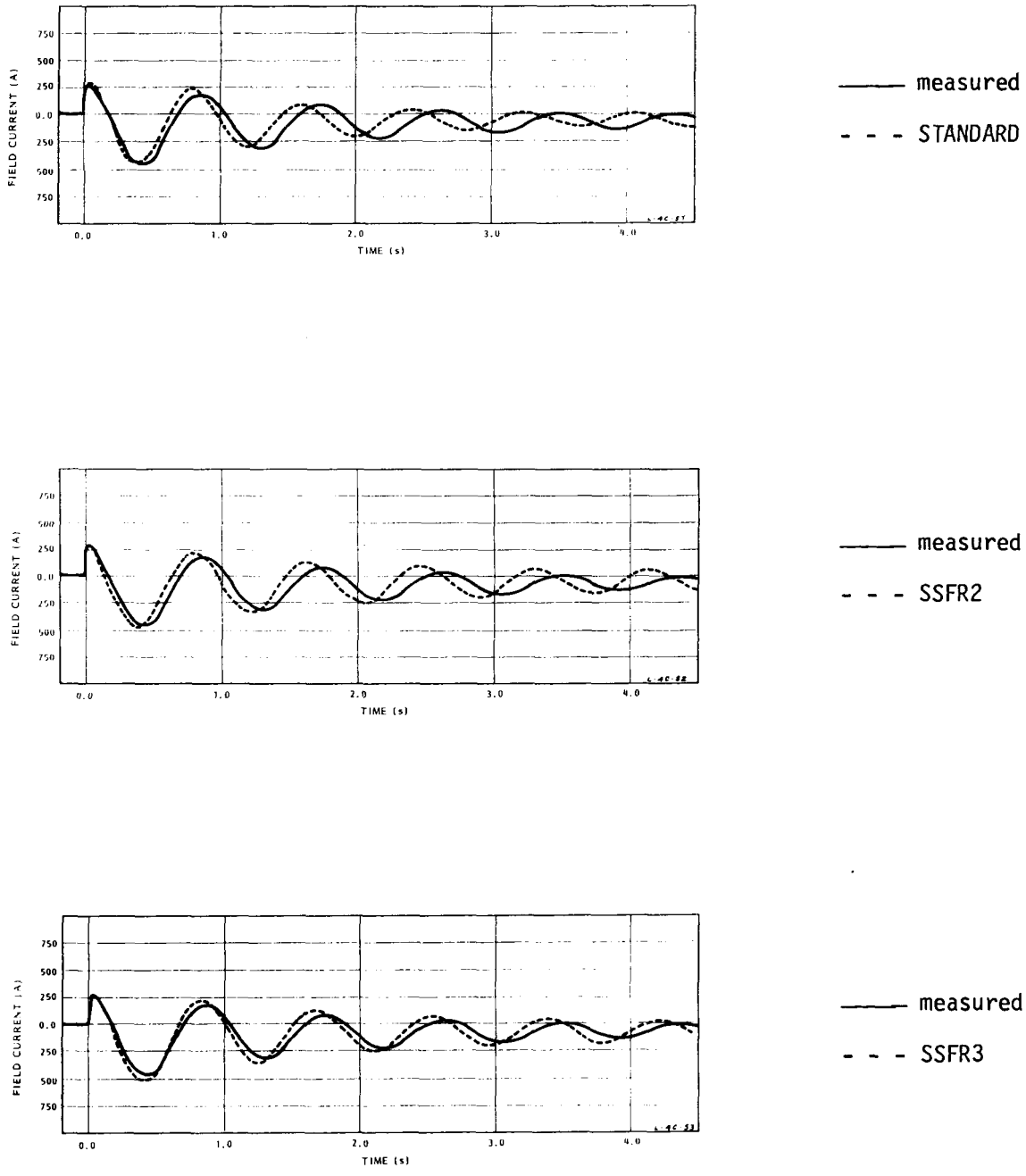

Figure 4-10. Lambton Line Switching Test Number 8. Close short line in unbalanced configuration, constant field voltage.

MONTICELLO

System Configuration and Representation

The system to which the test generator was connected is shown in Figure 4-11. This represents, in single-line form, the main transmission connections at 345 kV in the immediate vicinity of the Monticello station. For the purpose of this investigation, this system is shown connected to the remainder of the TUGCO 345 kV system (Infinite Bus) by a reactance of 2.5% on 100 MVA. The loads were represented as constant impedances. Thus, the system external to the test generator (Monticello Unit #2 located at Monticello-North bus) was represented by 4 generators, 25 lines and 23 buses. The disturbance to the test machine was caused by switching the line MONTICELLO North to PARIS. Base case load flows were established with the help of recorded steady-state measurements.

It should be noted that the loads and the voltage profile of the system in Figure 4-11 were measured only once throughout the test period and not, as would have been preferred, prior to each test. Consequently, there is some doubt about the validity of the initial conditions prior to each test, particularly since the tests stretched over a period of 3 hours during which time it was possible for the load pattern, and voltage profile to change. In addition, there were some problems matching the voltage profile to the load and generation pattern in our load flow studies; it is possible that this resulted in some errors in the simulation of the line switching tests.

Tests and Simulations

Table 4-2 shows the tests performed and the initial conditions of the test generator. The same digital computer program was used as previously and saturation was accounted for by varying L_{ad} and L_{aq} according to the operating point (excitation level).

For the purpose of this report, only simulations of recorded generator power (MW) were performed. It was not possible to obtain field current variations since this machine uses a rotating diode system. Figures 4-12 to 4-15 show the comparisons between the measured and calculated responses for each of the four tests. In all cases machine excitation was on manual control.

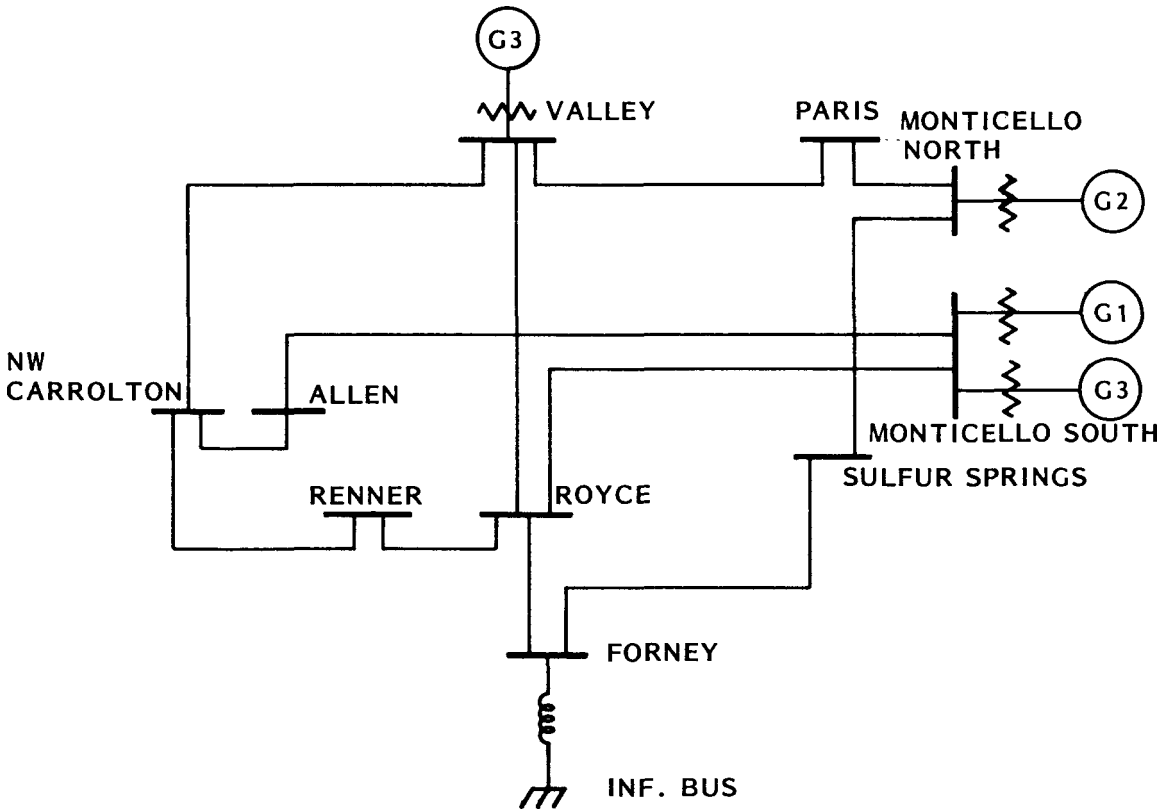

Figure 4-11. Monticello System Arrangement for Line Switching Tests.

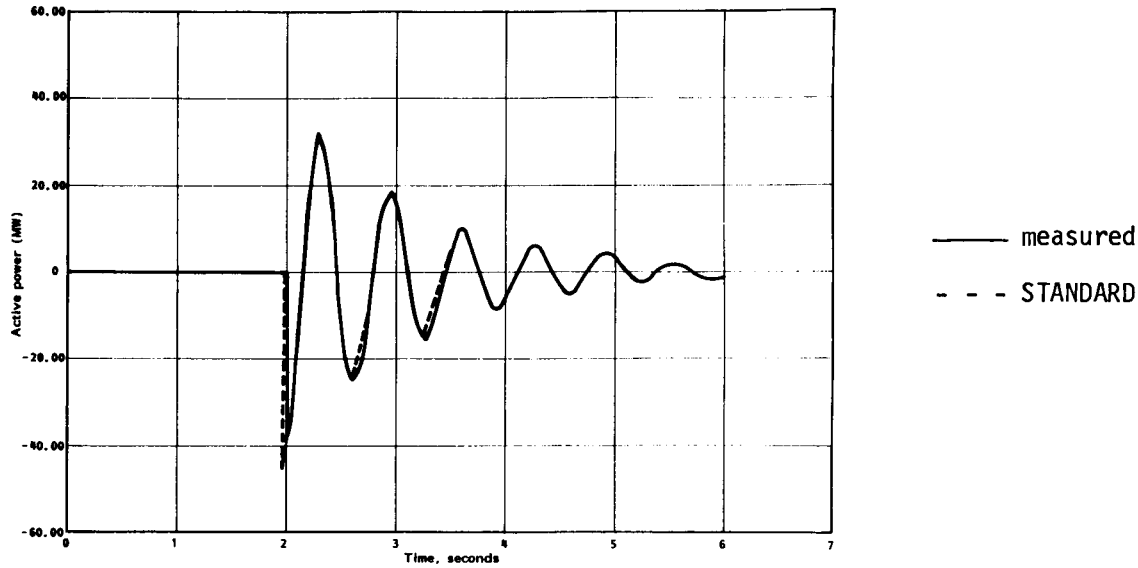

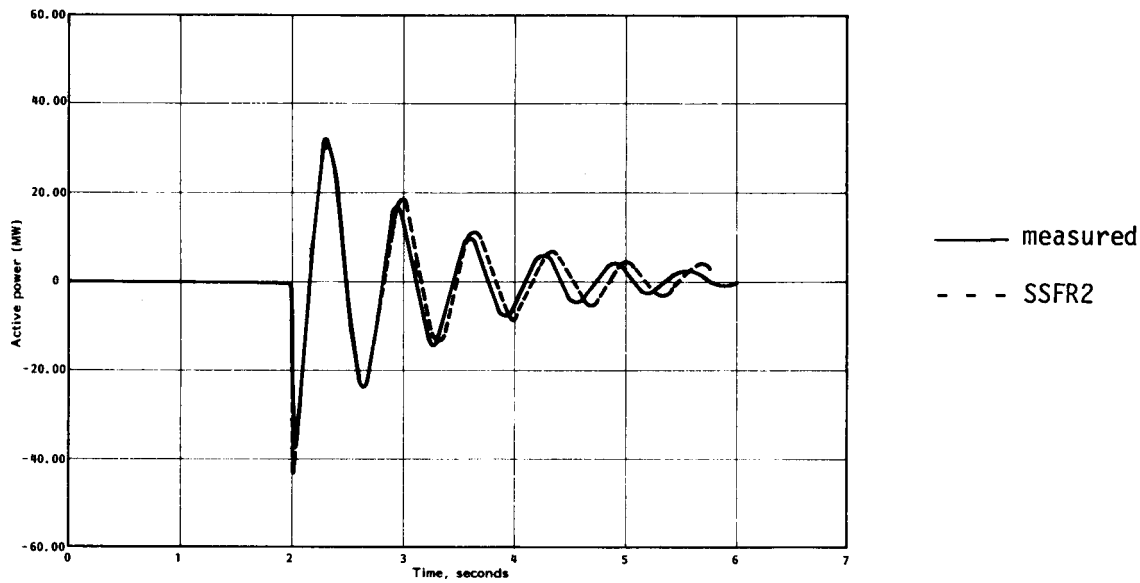

Figure 4-12. Monticello Line Switching Test Number 1. Open line between Paris and Monticello North, G2 at 350 MW, 50 MVAR lagging.

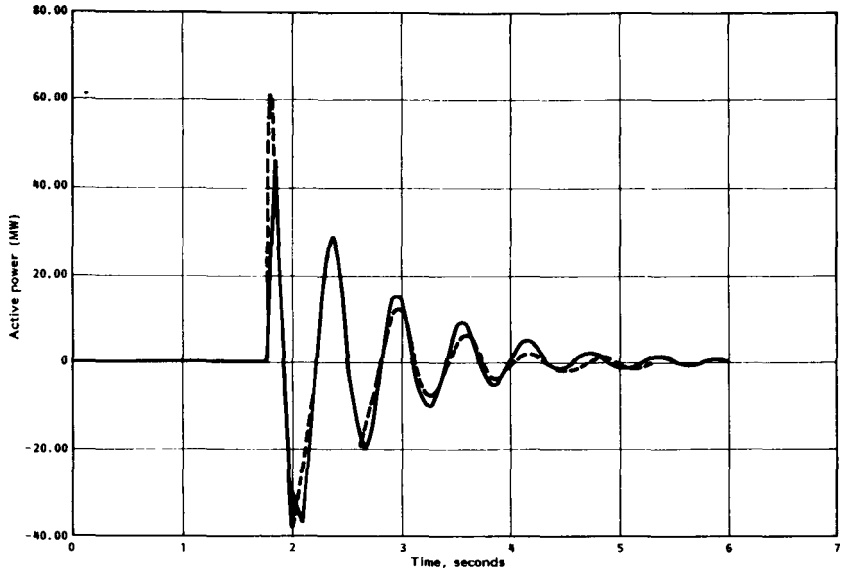

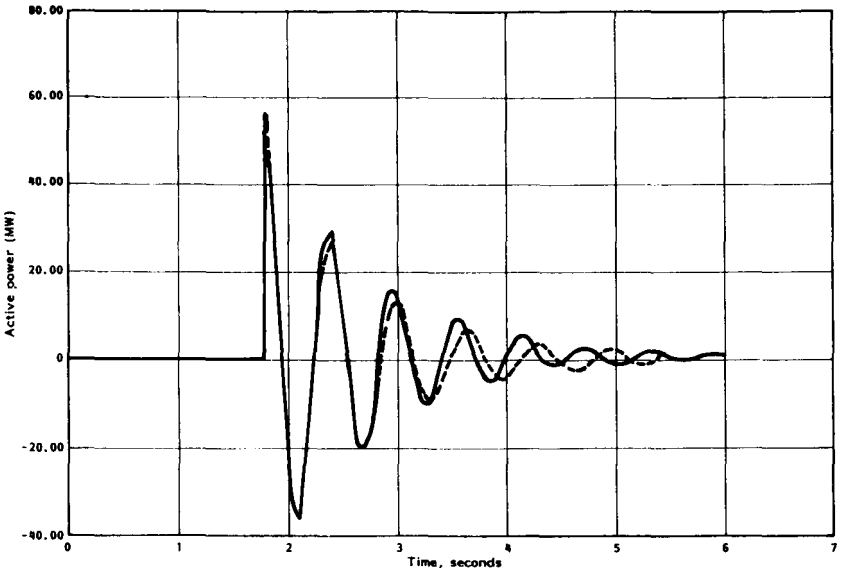

Figure 4-13. Monticello Line Switching Test Number 2. Close line between Paris and Monticello North, G2 at 350 mW, 50 MVAR lagging.

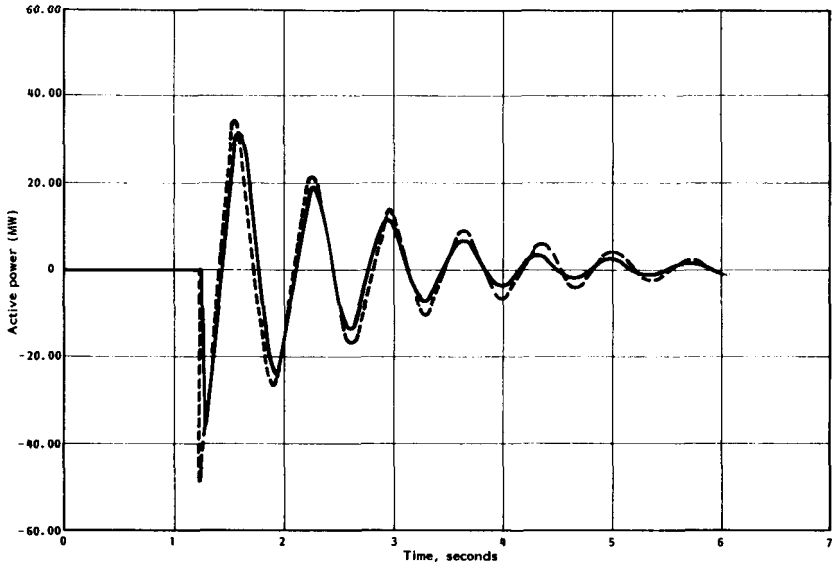

——— measured

- - - STANDARD

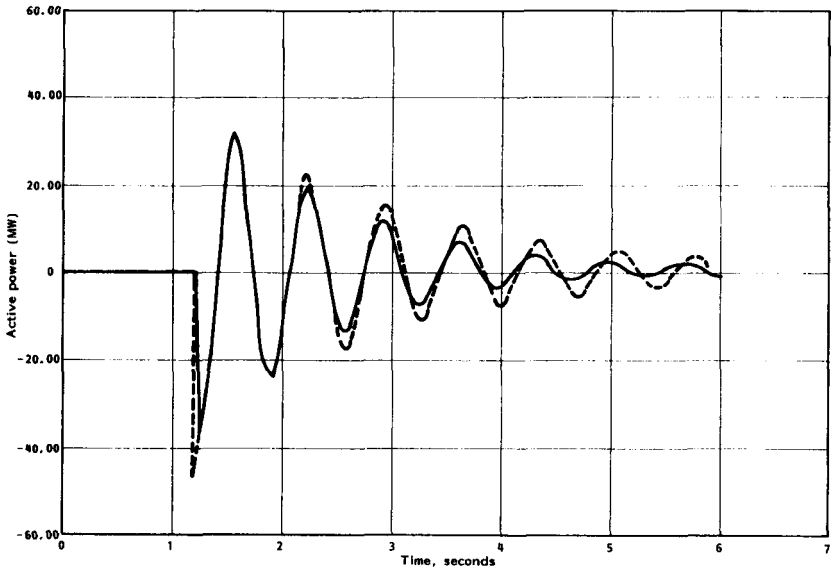

——— measured

- - - SSFR2

Figure 4-14. Monticello Line Switching Test Number 3. Open line between Paris and Monticello North, G2 at 350 MW, 50 MVAR leading.

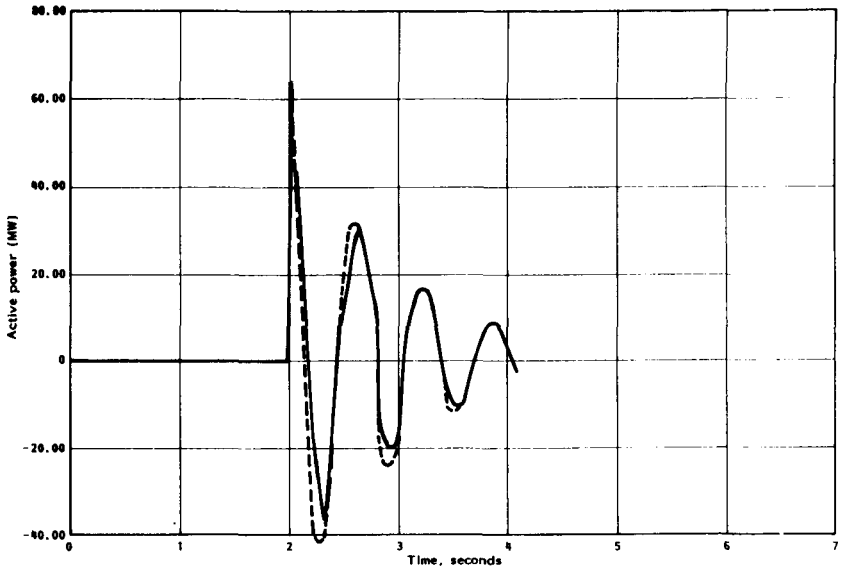

——— measured

- - - STANDARD

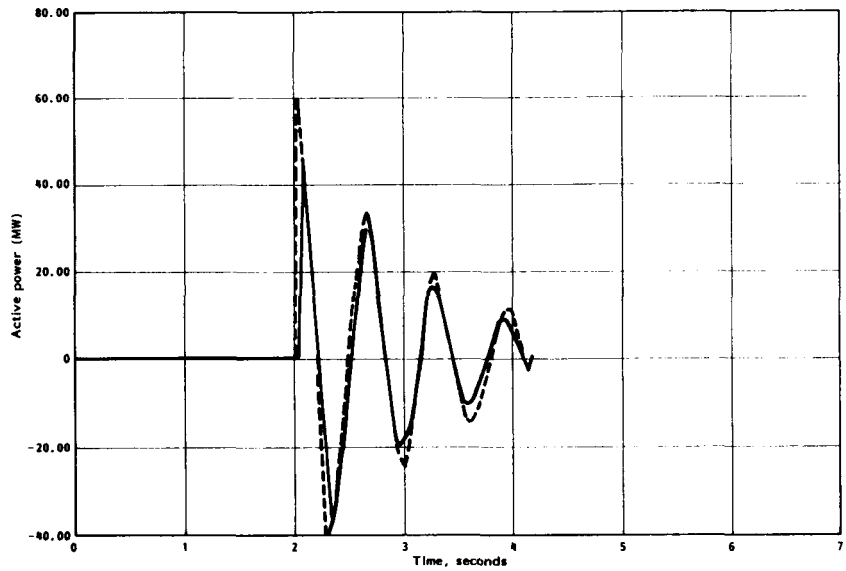

——— measured

- - - SSFR2

Figure 4-15. Monticello Line Switching Test Number 4. Close line between Paris and Monticello North, G2 at 350 MW, 50 MVAR leading.

Table 4-2

MONTICELLO LINE SWITCHING TESTS

Test No.	Operation	Test Generator Initial Conditions MW	MVAR	kV
1	Open line to Paris	350	50	18.0
2	Close line to Paris	350	50	18.0
3	Open line to Paris	350	-50	17.4
4	Close line to Paris	350	-50	17.3

In all cases the STANDARD and SSFR models give very similar responses, which match the measured results quite well. There is a tendency for all models to show a slight change in oscillation frequency after the first two or three swings. Also all models show the same tendancy to overdamping or underdamping of rotor oscillations for a given test. This would suggest that there is a common factor, other than the machine models, which causes this; we suspect that this is because the simulated initial conditions prior to each test are not true representations of the actual state. In all cases considered, a mechanical damping factor of 1 was used. Reducing this to zero resulted in greater mismatches between simulated and measured results for all models considered. Increasing this value to 2 did not show significant improvements over the case when it was 1. A sensitivity analysis with respect to the representation of the infinite bus was carried out and it was found that the effect of changing from a solid bus to a finite inertia produced little change. Consequently, we suspect that the main cause of the discrepancies is the uncertainty of the knowledge of the initial conditions prior to each test.

Evaluation

It was demonstrated that for this particular machine there was little to choose between STANDARD and standstill frequency response models. Both gave good results in simulating the standstill and on-line on-load performance of the ma-

chine. Although there were some discrepancies between simulated and measured results we feel that these may have been caused by the inaccuracies in the load flows rather than the models themselves. In any case the differences encountered appear acceptable.

Notwithstanding the above, we would suggest that, based on past experience with other generators, the close agreement obtained herein between the standstill frequency response and STANDARD models is an exception rather than the norm. It is gratifying that the manufacturer's data should be so reliable, since it means that a simpler representation for the machine model can be used with confidence. To many power system investigators this is a major constraint.

In general the results of these studies indicate that the standstill model represents the generator adequately over a wide range of operating conditions, although some discrepanices were noted to exist in the subtransient region. This suggests that, on the whole, the equivalent circuit model elements which pertain to the rotor circuits are relatively unaffected by rotor current levels and rotation. A similar conclusion was recorded for the Lambton machine.

NANTICOKE

System Arrangement

Line switching operations were done at Nanticoke with the test generator, G6, connected to the rest of the power system as shown in Figure 4-16.

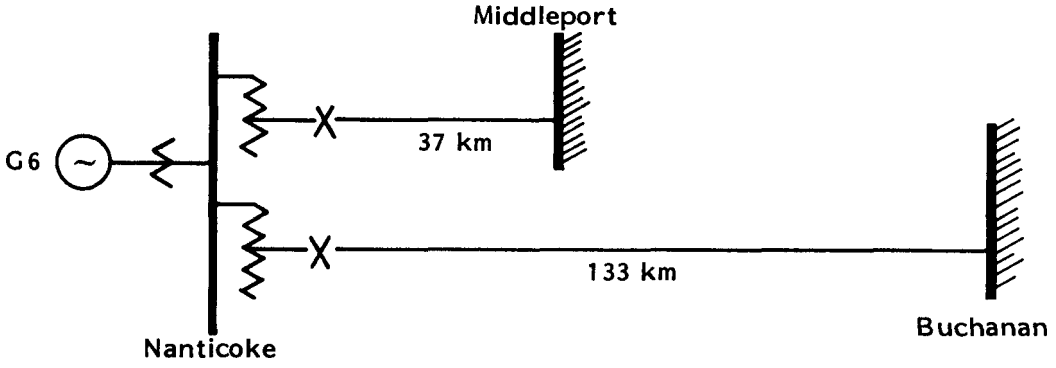

Figure 4-16. System Set-up For Nanticoke Line Switching Tests.

Table 4-3 is a summary of the test operations that were simulated to assess the performance of the models. All were done with constant field voltage on the test generator.

Table 4-3

SUMMARY OF NANTICOKE LINE SWITCHING TEST CASES

Test No.	Test Operation	G6 Operating Point MW	MVAR	kV
2-O	Open long line	300	108	22.0
2-C	Close long line	299	106	22.1
4-O	Open short line	302	112	22.1
4-C	Close short line	300	103	22.8

System Representation

The accuracy of the simulated results is dependent not only on the generator model but also to a great extent on the representation of the external system at the time of the test. The system external to the test generator was represented by 183 buses, 328 lines and 60 machines. For the purpose of this report, Ontario Hydro's ac load flow program was used in conjunction with recorded steady state measurements to set up the necessary system configuration to simulate each line switching test. Although considerable care was taken to obtain load flows with voltages, line flows and generator outputs close to system recordings taken just prior to each test, some difficulty was experienced in matching the line flows, particularly those on the outgoing transmission circuits from the test generator within the study area of the system. It is possible that the reason for this is the unsymmetrical configuration of these lines. The reason for using this unsymmetrical arrangement was that for a given switching operation a greater perturbation, to the test generator, could be obtained than would have been the case had a symmetrical system been used.

Results

The ability of the STANDARD, SSFR2 and SSFR3 models to simulate the line switching transients on a Nanticoke generator can be judged from Figures 4-17 to 4-24.

The STANDARD model gives rise to higher values of field current and generator power following the disturbance (first peak) compared to the measured data. The frequency of rotor oscillations is in most cases higher than the measured value. It is apparent that, in most cases, this model results in less damped oscillations compared to the measured response. These two facts indicate that the damper winding and rotor body affects are more pronounced in the actual machine than in the STANDARD model.

In view of past experience, the poor performance of the STANDARD model was not surprising. However, it is also apparent that the SSFR models are not satisfactory either. Both show a lower oscillation frequency than was measured, and neither has the correct amount of damping: SSFR2 has too little, and SSFR3 too much. This result is in sharp contrast to those from Lambton and Monticello where the SSFR models produced very good simulations of the measured line switching transients.

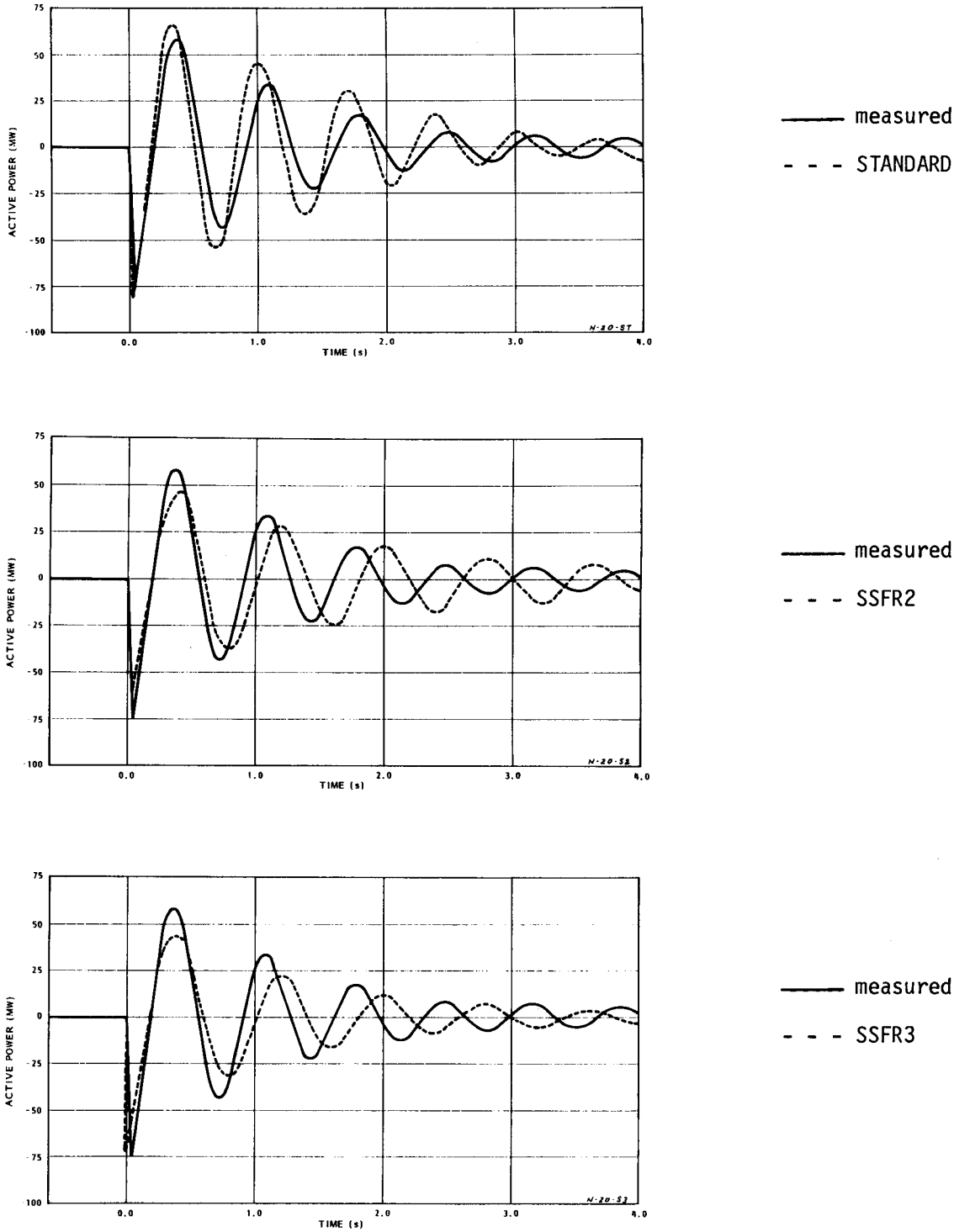

Figure 4-17. Nanticoke Line Switching Test Number 2-0, Open long line, constant field voltage.

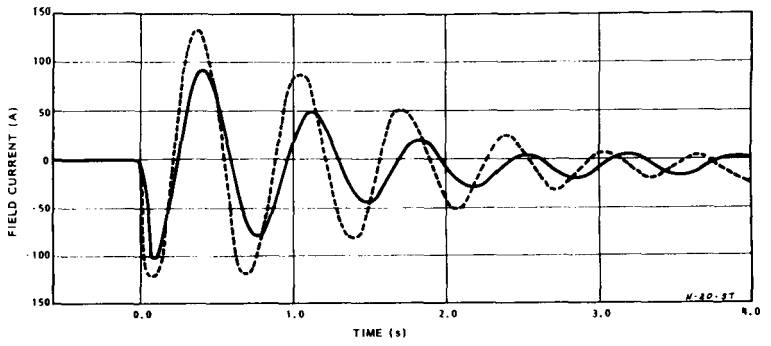

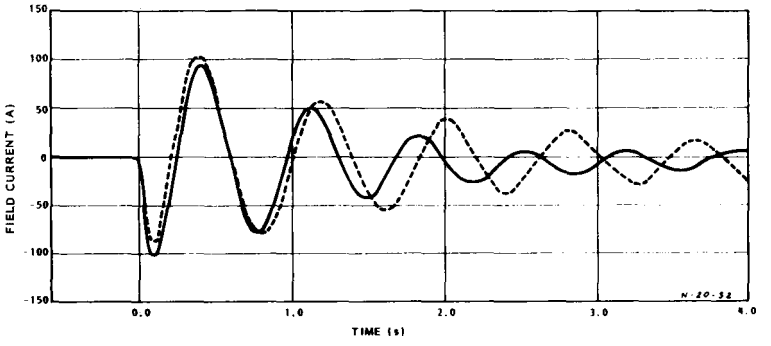

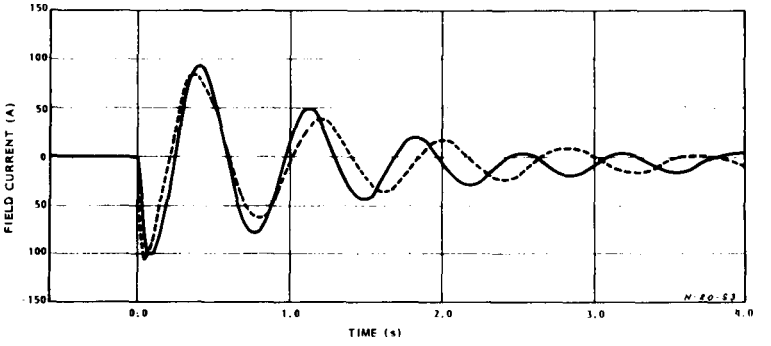

Figure 4-18. Nanticoke Line Switching Test Number 2-0. Open long line, constant field voltage.

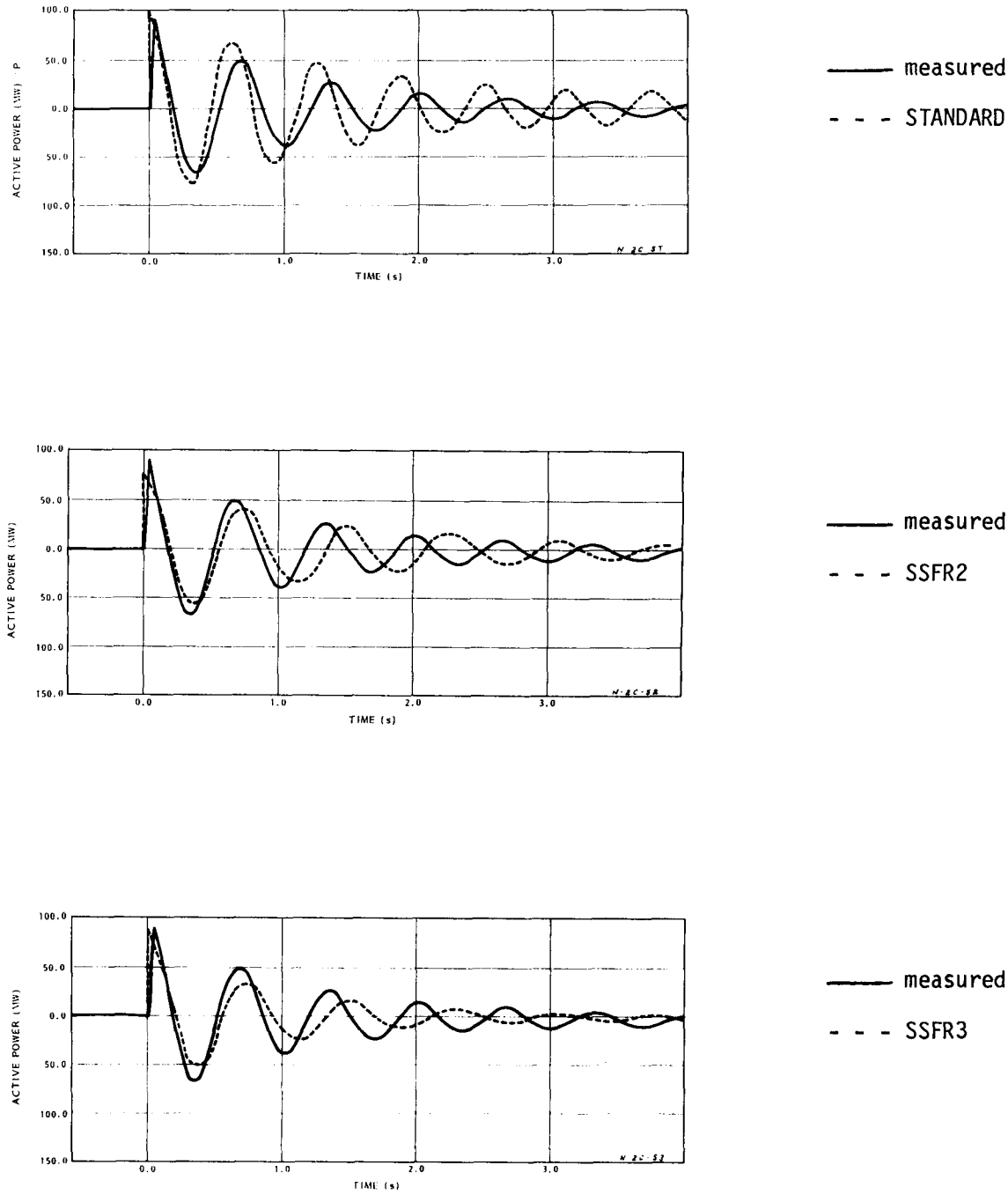

Figure 4-19. Nanticoke Line Switching Test Number 2-C. Close long line, constant field voltage.

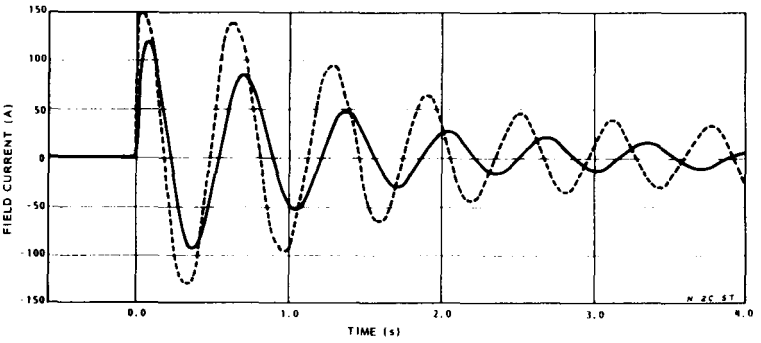

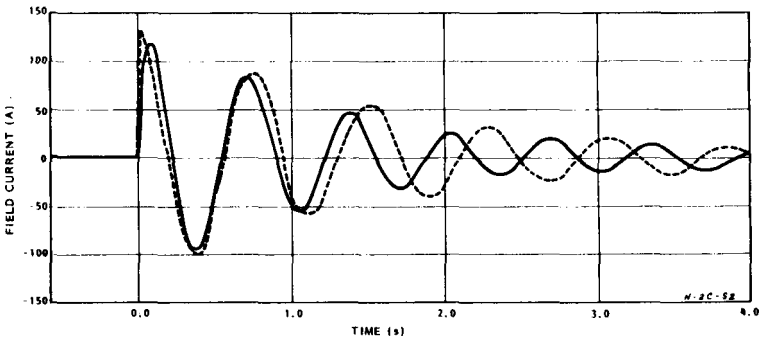

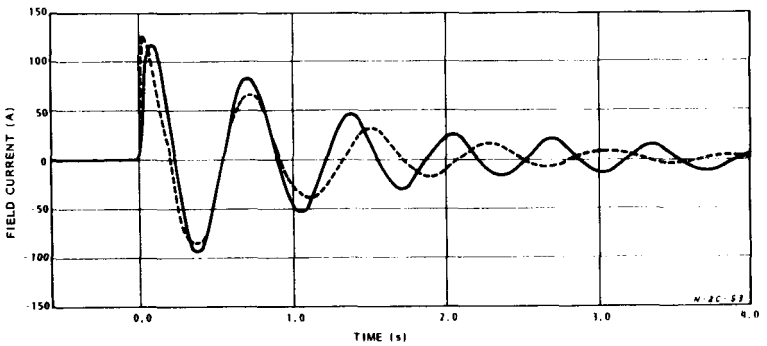

Figure 4-20. Nanticoke Line Switching Test Number 2-C. Close long line, constant field voltage.

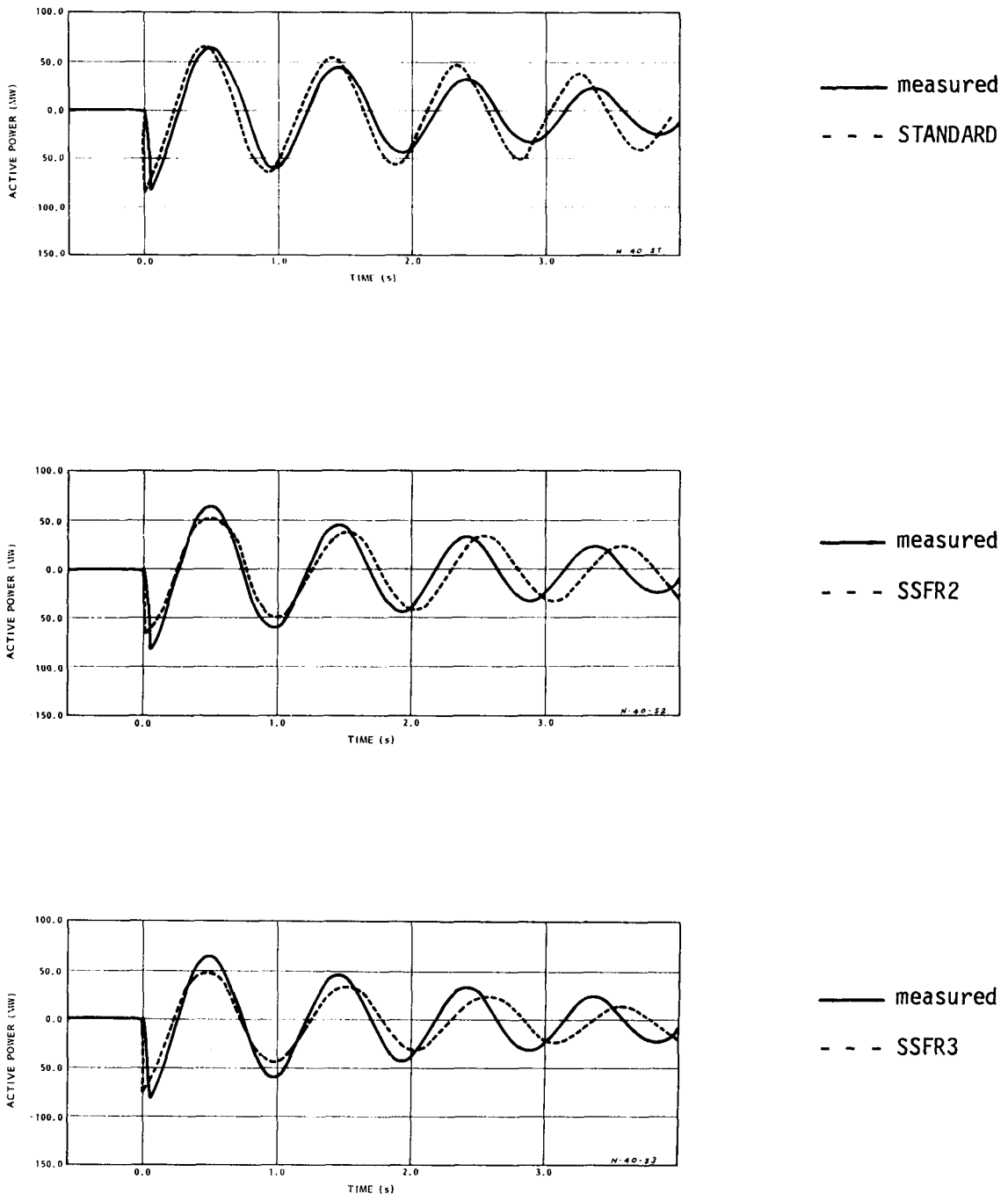

Figure 4-21. Nanticoke Line Switching Test Number 4-0. Open short line, constant field voltage.

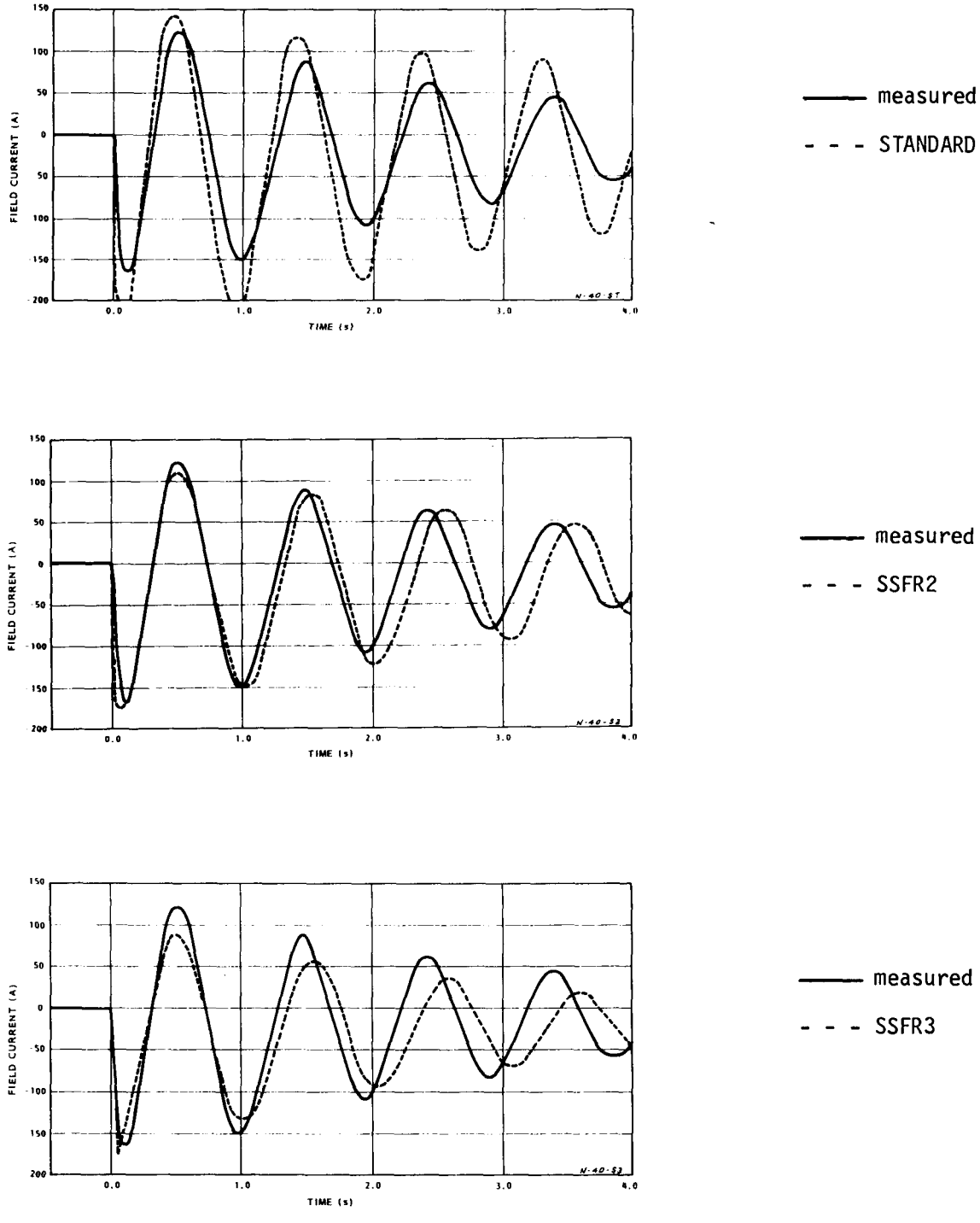

Figure 4-22. Nanticoke Line Switching Test Number 4-0. Open short line, constant field voltage.

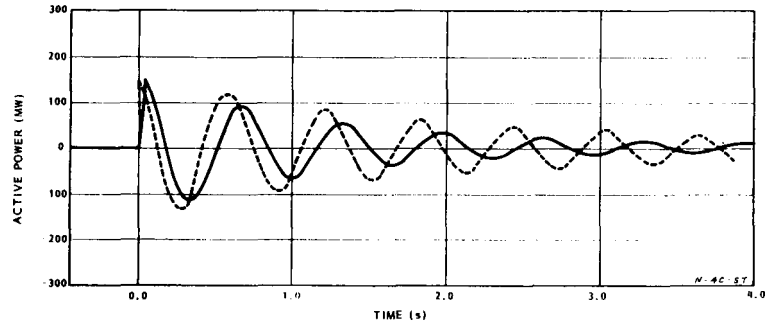

measured

- - - STANDARD

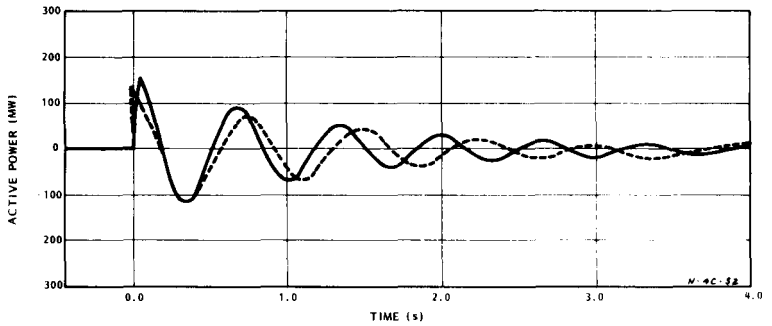

measured

- - - SSFR2

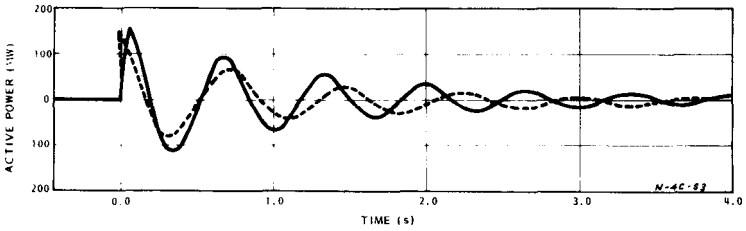

measured

- - - SSFR3

Figure 4-23. Nanticoke Line Switching Test Number 4-C. Close short line, constant field voltage.

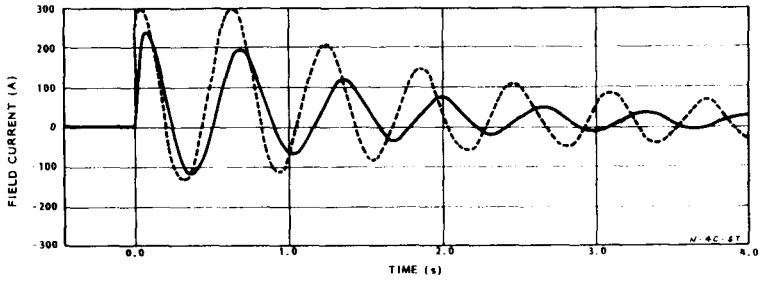

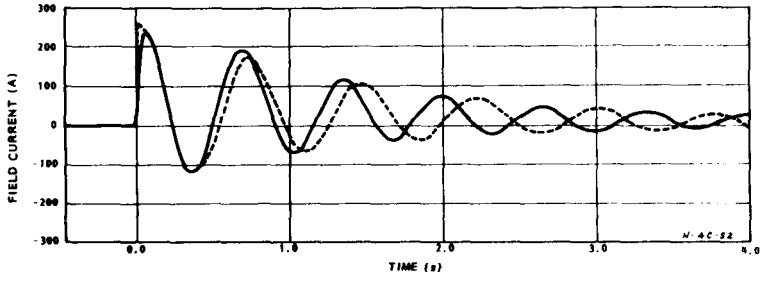

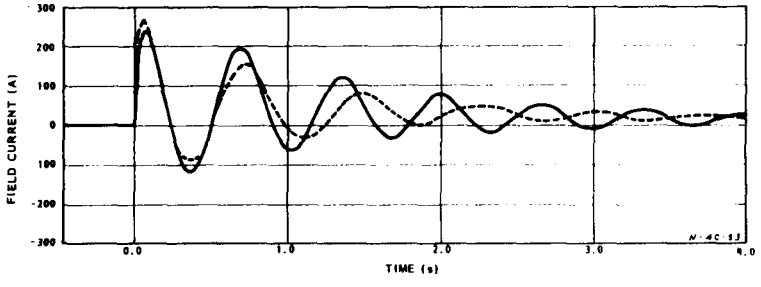

Figure 4-24. Nanticoke Line Switching Test Number 4-C. Close short line, constant field voltage.

INTERIM CONCLUSIONS

The failure of the SSFR models to simulate, adequately, the Nanticoke line switching transients necessitated a rethinking of the directions to be followed during the remainder of the project. It demonstrated that standstill frequency response tests and the associated model derivation methods that were used will not always result in an adequate representation of the generator, despite the fact that this approach was very successful at both Lambton and Monticello.

There was considerable speculation regarding the reasons for the problems with the Nanticoke machine model. The most prevalent opinion was that the contact resistances among the rotor body, the damper bars, the slot wedges, and the retaining rings were substantially different at standstill than at rated speed. With this in mind, a set of on-line frequency response tests was planned. The intent of these tests would be:

- To see how much discrepancy existed between the measured small signal performance of the machine on load, and that predicted by the standstill models.
- To obtain test data from which a satisfactory model could be developed.

Section 5

MODEL IMPROVEMENTS USING ON-LINE FREQUENCY RESPONSE DATA

THE MEASUREMENTS

On-line frequency response measurements were made at both Lambton and Nanticoke. These tests are documented in detail in Parts 4 and 5. Briefly, however, each test machine was operated at approximately 80% of full load, and connected to the power system through as much impedance as possible while maintaining adequate stability margins. The generator was perturbed, sinusoidally, by modulating the automatic voltage regulator reference. The transfer functions between field voltage and: field current, terminal voltage, active power, reactive power, and shaft speed were measured over the frequency range 0.01 Hz to 10 Hz.

THE METHOD

These transfer functions provide a suitable source of data by which modifications to the SSFR model parameter values can be made. The advantage over time-domain measurements is that all important modes are equally excited over a range of frequencies of interest to power system analysts. Hence by using this frequency response data to adjust the model parameters one would hope to make the model suitable for most power system disturbance studies.

In this approach, the derivation of a machine model requires the calculation of the on-line frequency response for the generator connected to the power system. Parameters derived from SSFR measurements serve as a good set of initial values. The computed response is used in an iterative technique which attempts to minimize the differences between the measured and computed responses at specified frequencies by adjusting the parameters of the machine model.

Calculation of the On-Line Frequency Response

In computing the on-line frequency response, the system steady-state flow conditions prevailing at the time of the test are first established using a load flow

program. The dynamic behaviour of the power system is simulated with different parts of the system represented by different degrees of modelling. The test unit and the units in the immediate vicinity are represented in detail. Other units electrically close to the test unit are represented by constant field flux linkage models with equivalent damping coefficients. Remote machines are modelled as infinite buses. The equations describing the dynamic performance of the power system are linearized about the operating point and arranged into the state-space form. The state-space coefficient matrices are then used to calculate the frequency response of the ratio between any two variables. In this case the variables which are relevant to the identification process are the machine terminal voltage, shaft speed, field voltage, and automatic voltage regulator reference.

The general method of formulating the state coefficient matrix of the power sysem is described in Reference 1. A significant feature of the method is that the relationship between the elements of the coefficient matrix and the machine parameters is directly known. This feature is particularly useful in the application of the identification technique.

Identification Technique

The developed identification technique adopts a Newton-Raphson method to minimize the error between the measured and the computed responses at a number of points in a specified frequency range. The program first calculates a Jacobian matrix which is formulated from the gradients of the error functions with respect to machine parameters which are to be varied. This Jacobian matrix, which is complex, is then transformed to a real form. The inverse of the real matrix multiplied by the real and complex elements of the error vector gives an estimate of the amount of the incremental change in the machine parameters which will result in reducing the error. Hence, the machine parameters are updated and the iteration is repeated. The iteration process is terminated when the sum of the squares of the errors ceases to decrease.

The flowchart in Figure 5-1 summarizes the identification process and Appendix B shows the relevant equations.

Generally, this process results in an equivalent circuit structure which is unchanged by the calculations, the only exception being the three rotor winding

d-axis model, where existing program limitations preclude the use of the second "mutual leakage" inductance term identified as L_{fkd2} in Figure 3-4. Since the relative current splits in the two branches of amortisseur circuits are not important, it is not considered essential to represent L_{fkd2}. However, it is important to represent L_{fkd1} to ensure accurate representation of the field circuit.

As the method of deriving the d-axis model from standstill frequency response data results in two "mutual leakage" terms (L_{fkd1} and L_{fkd2}) this model cannot be used directly to initialize the identification technique. To overcome this, the initial equivalent circuit obtained from standstill tests may be approximated by lumping the effect of the two inductances into one, L_{fkd1}; and setting L_{fkd2} to zero. This step is perfectly acceptable since the identification technique alters the mutual leakage term as well as rotor winding parameter values to minimize the error between simulated and measured responses, and in so doing, one of the mutual leakage inductances may be forced to zero. This results in a slightly less complex model.

It should be noted that the identification process considered herein can be used with models other than the standstill frequency response one, and that the choice of model parameters to be varied for minimizing the errors is dictated by the user. In general, however, it is our opinion that the rotor parameters are the ones which need to be chosen to be changed, in view of the expected variations in their values resulting from different test conditions, eg; temperature, rotation, and other effects.

Nomenclature

Models derived solely from standstill tests were identified as SSFR2, SSFR3 for two and three rotor winding models respectively. A new class of models, obtained by adjusting some parameters of the SSFR ones on the basis of on-line frequency response tests; ie, the technique just described, will be identified as OLFR2, OLFR3 for two or three rotor winding representations, respectively.

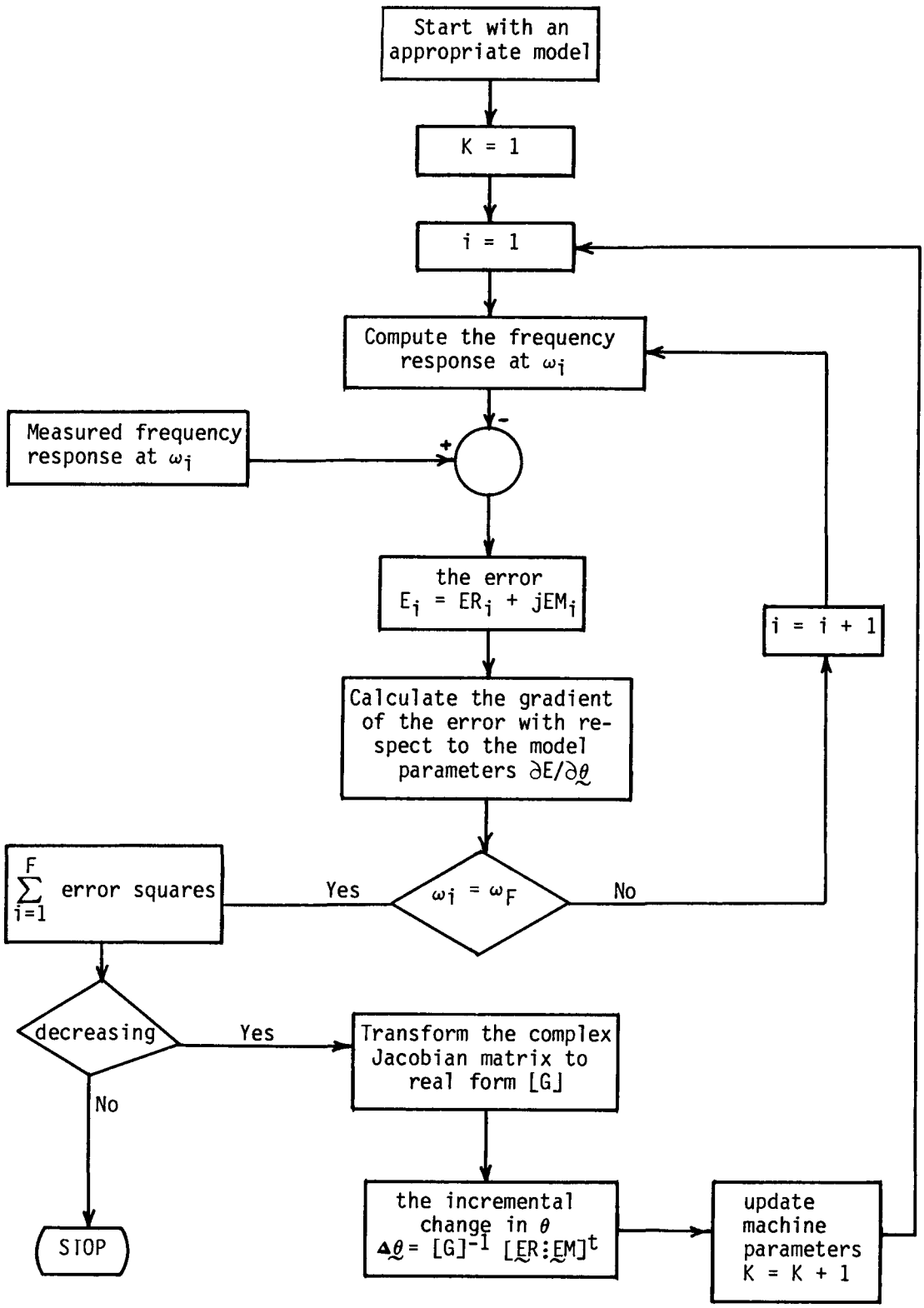

Figure 5-1. Computation of Direct and Quadrature Axis Models from On-Line Frequency Response Test Data.

APPLICATION TO LAMBTON AND NANTICOKE MODELS

Since there was little difference between the SSFR2 and SSFR3 models for Lambton, the simpler, SSFR2, was selected for subsequent use. For Nanticoke, the SSFR3 model was chosen because it was apparent that at least a third order model was needed to approximate this machine.

The equivalent circuit elements of these two models were adjusted, using on-line frequency response data and the modification technique just described. In this process, the frequency range 0.5 Hz to 5 Hz was most heavily weighted since the dynamic phenomena of most interest occur in this band of frequencies.

The change in equivalent circuit parameters produced by this process can be seen in Tables 5-1 and 5-2. Ontario Hydro's Eigenvalue and frequency domain programs were used to calculate the response of each of the models in Tables 5-1 and 5-2. These model responses for the transfer functions between field voltage and terminal voltage, and between field voltage and shaft speed are superimposed on the on-line frequency response test points in Figures 5-2 to 5-7 for Lambton and Figures 5-8 to 5-13 for Nanticoke. The ac load flow program was used in conjunction with recorded steady-state measurements to set up the proper system conditions for the calculation of each response. In other words, the response of each generator model was computed with it looking into the same external system that prevailed during the corresponding on-line frequency response test.

Table 5-1

LAMBTON EQUIVALENT CIRCUIT PARAMETERS

Parameter	Standard Model	SSFR2 Model	OLFR2 Model
L_{ad}	1.810	1.858	1.858
L_{aq}	1.707	1.762	1.845
L_{l}	0.160	0.155	0.142
L_{fd}	0.1171	0.01051	0.01119
R_{fd}	0.001189	0.001084	0.001084
L_{kd1}	0.01737	0.01136	0.01102
R_{kd1}	0.0109	0.01065	0.0100
L_{fkd1}	-	0.1328	0.1562
L_{kq1}	0.0638	0.5677	0.4502
R_{kq1}	0.0164	0.0147	0.0100
L_{kq2}	0.3833	0.1717	0.1983
R_{kq2}	0.0099	0.1765	0.1989

Table 5-2

NANTICOKE EQUIVALENT CIRCUIT PARAMETERS

Parameter	Standard Model	SSFR3 Model	OLFR3 Model
L_{ad}	2.165	2.152	2.152
L_{aq}	2.047	2.057	2.057
L_{el}	0.195	0.172	0.172
L_{fd}	0.0908	0.0155	0.2785
R_{fd}	0.00076	0.00094	0.00083
L_{kd1}	0.0457	2.732	5.182
R_{kd1}	0.00703	0.1142	0.0969
L_{fkd1}	-	-0.5215	-0.0403
L_{kq1}	0.1560	1.657	1.4475
R_{kq1}	0.00390	0.00538	0.00433
L_{kq2}	0.0378	0.1193	0.0560
R_{kq2}	0.00139	0.1081	0.0122
L_{fkd2}	-	0.8975	-
L_{kd2}	-	0.00753	0.0369
R_{kd2}	-	0.00592	0.0130
L_{kq3}	-	0.4513	0.4064
R_{kq3}	-	0.0188	0.0017

Lambton

In Figures 5-2 to 5-7, the solid curve is the magnitude and the dashed line is the phase of the particular model's response.

The first point to note is that there is practically no difference between the SSFR2 and OLFR2 responses. This is not surprising. Since the SSFR2 model performed quite well in simulating the line switching tests, it is reasonable to expect that corrections to the model parameters for running conditions would be minimal. Moreover, both the SSFR2 and OLFR2 models match the measured on-line frequency response test data quite well in the important range from 0.5 Hz to 5 Hz.

Examination of the phase characteristics of the STANDARD model transfer functions at 1 Hz and above shows errors between 10 and 20 degrees compared to the measured response. Hence, its poor performance in reproducing the line switching transients (~1 Hz) is understandable.

All models show two resonant peaks around 1 Hz; only one would be expected from a single-machine-infinite-bus arrangement. The second resonance is a result of interaction with another Lambton generator, which was separated from the test generator by an impedance of approximately 0.75 pu on the generator base.

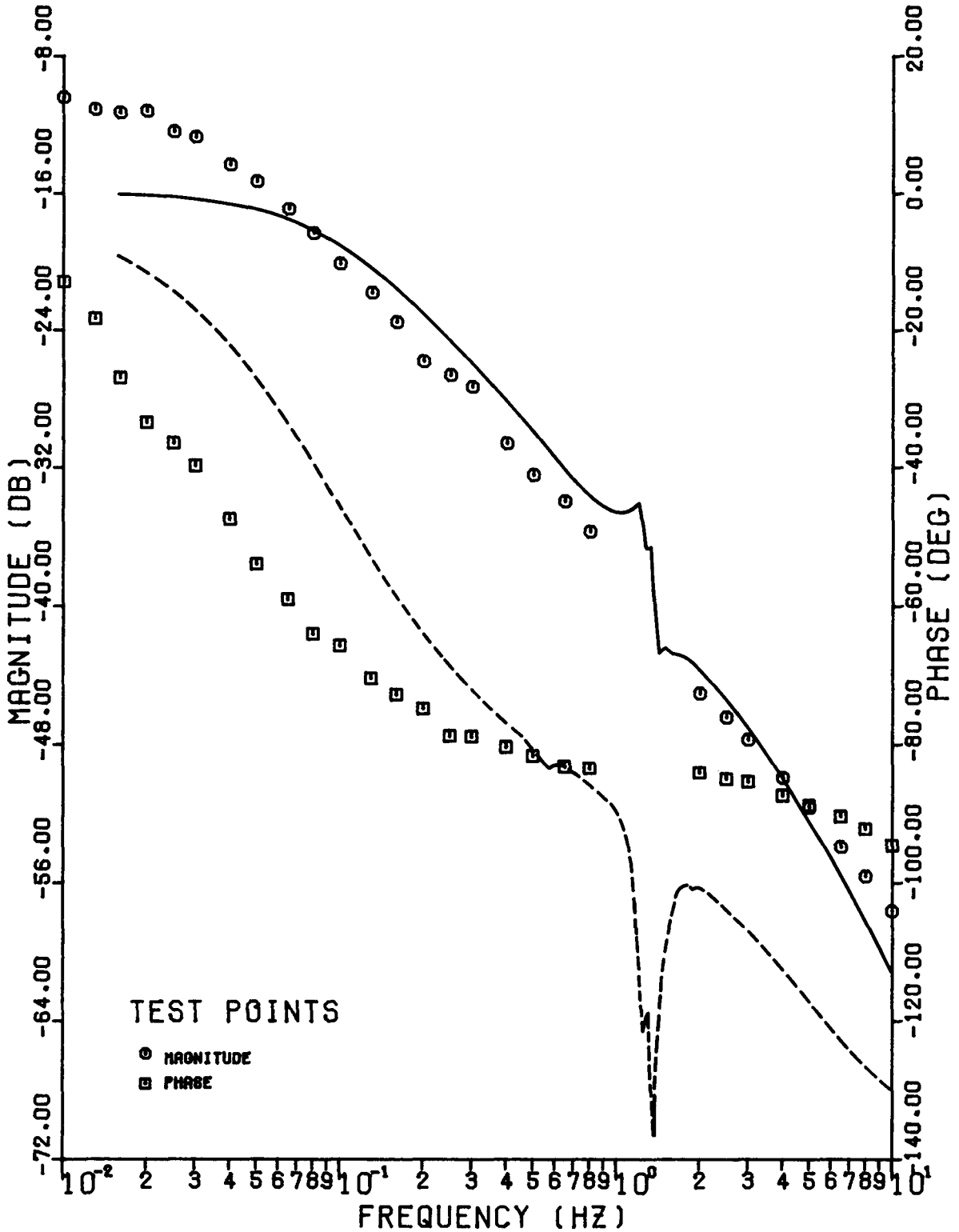

Figure 5-2. Lambton, On-Line Transfer Function From Field Voltage to Terminal Voltage, STANDARD Model.

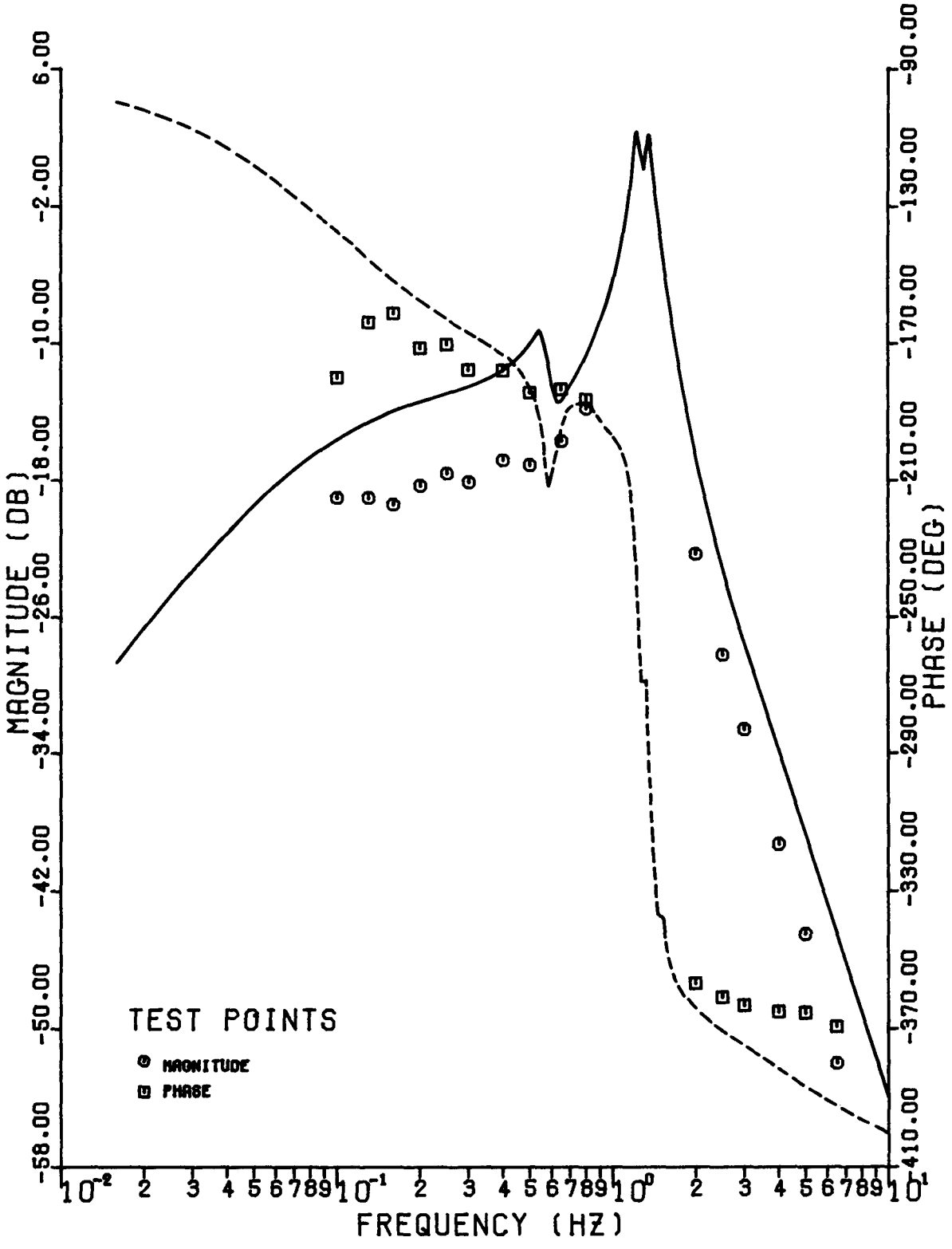

Figure 5-3. Lambton, On-Line Transfer Function From Field Voltage to Shaft Speed, STANDARD Model.

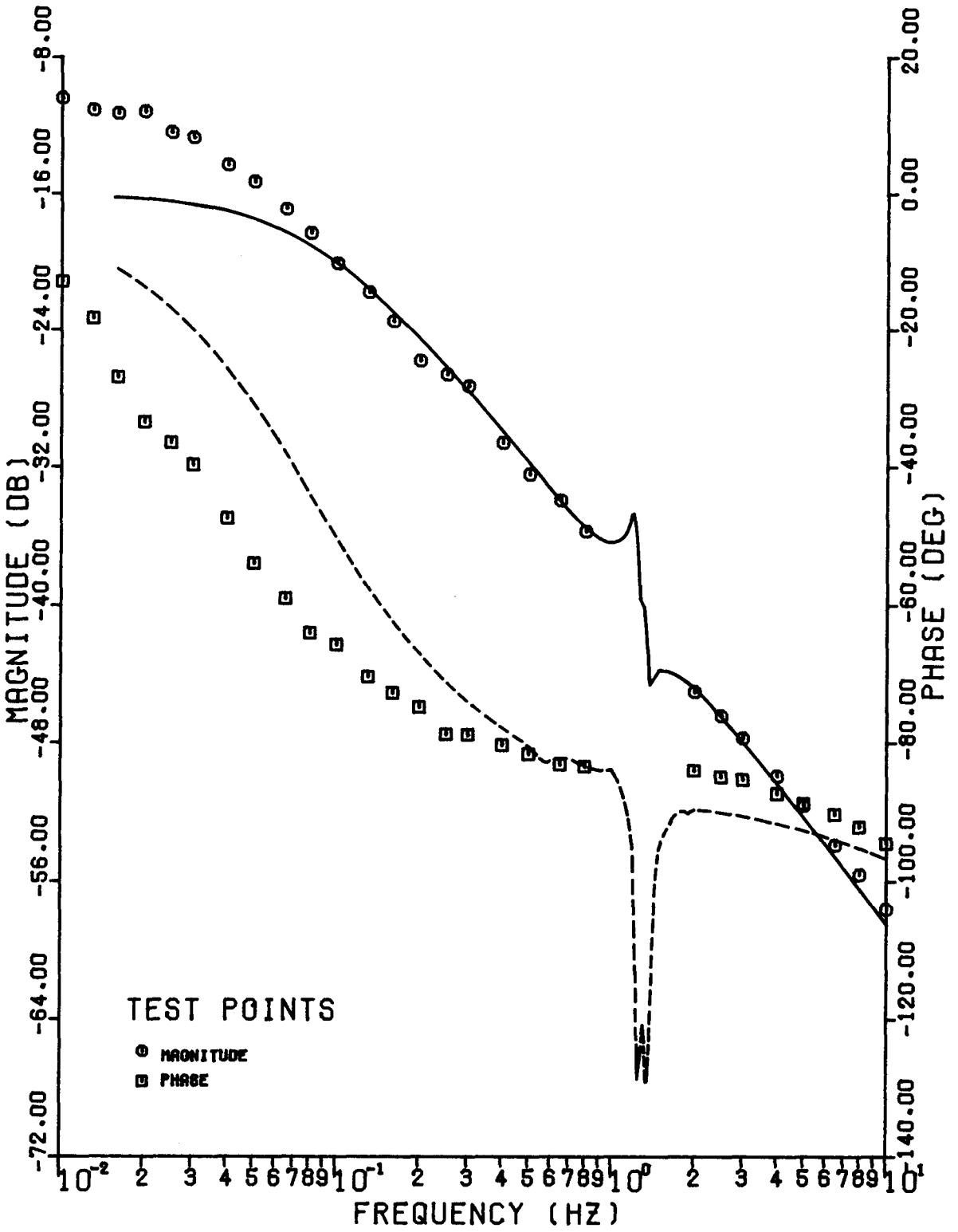

Figure 5-4. Lambton, On-Line Transfer Function From Field Voltage to Terminal Voltage, SSFR2 Model.

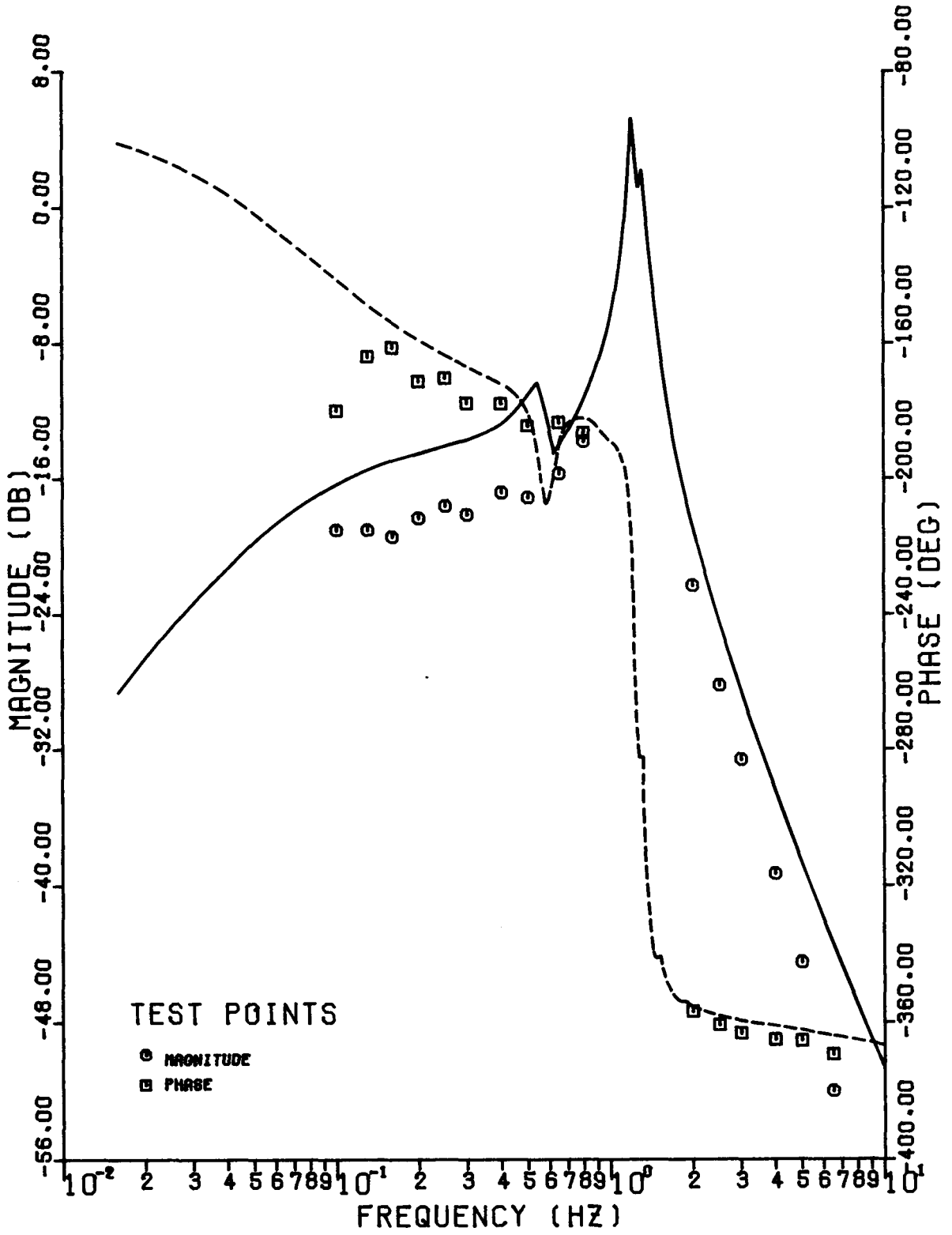

Figure 5-5. Lambton, On-Line Transfer Function From Field Voltage to Shaft Speed, SSFR2 Model.

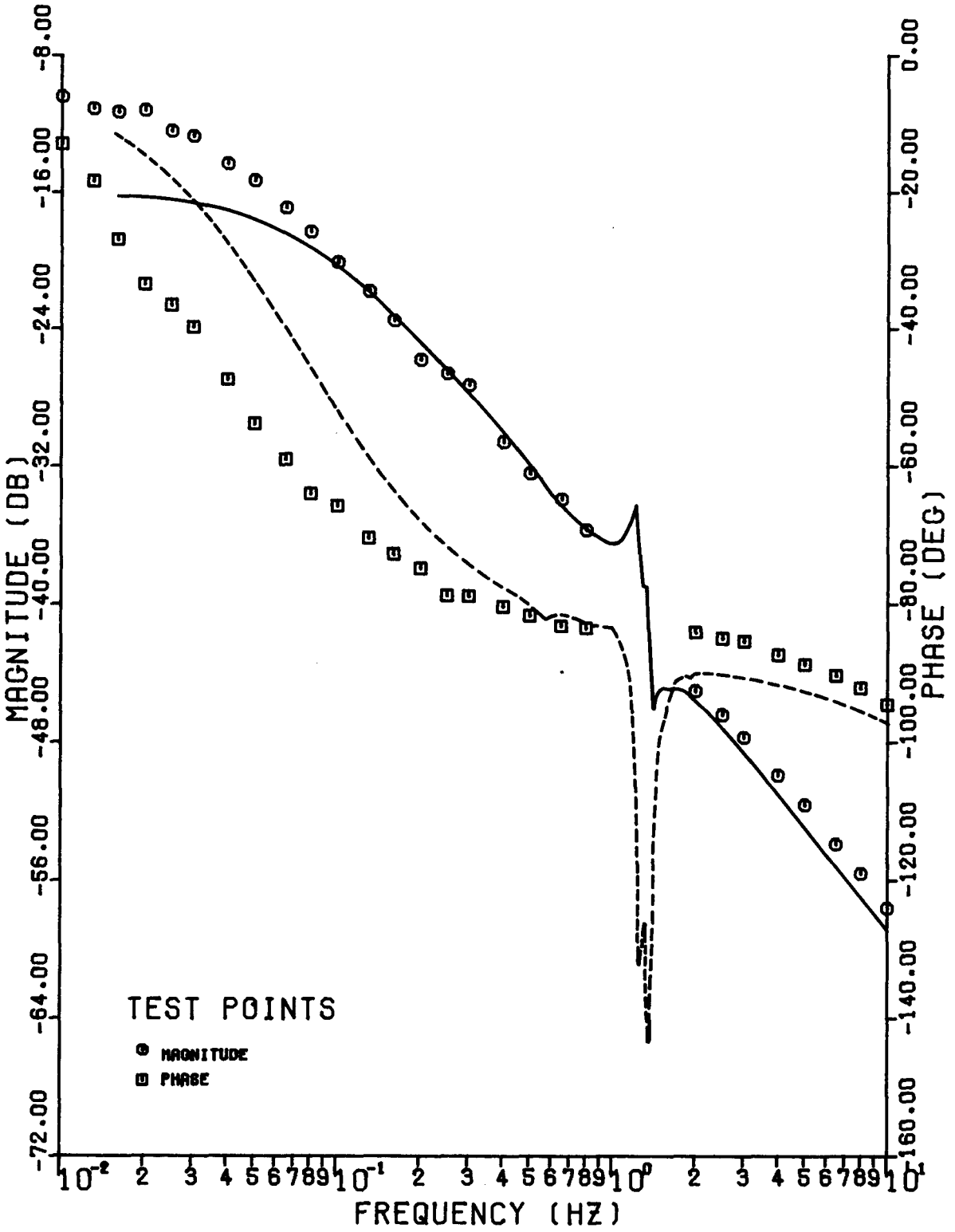

Figure 5-6. Lambton, On-Line Transfer Function From Field Voltage to Terminal Voltage, OLFR2 Model.

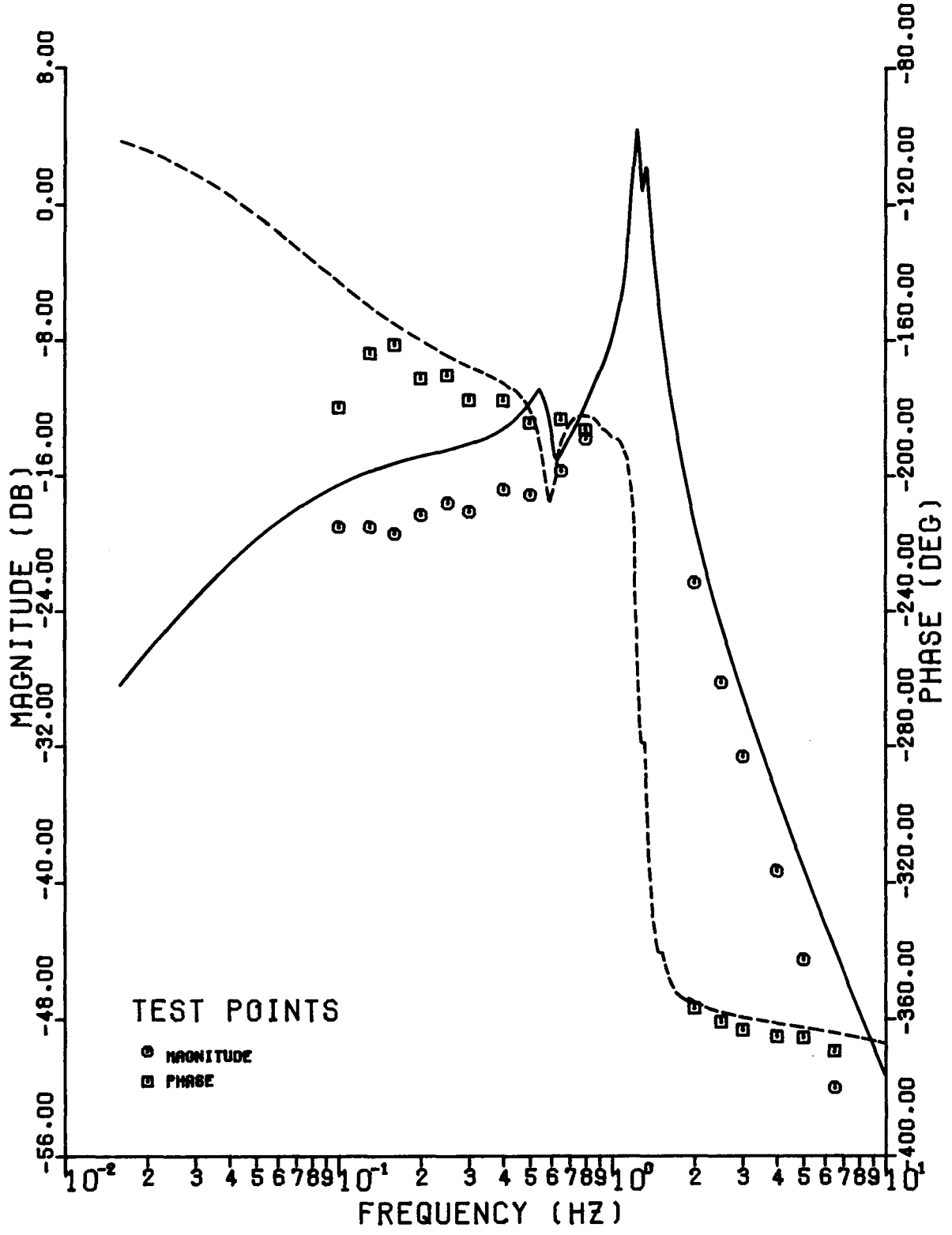

Figure 5-7. Lambton, On-Line Transfer Function From Field Voltage to Shaft Speed, OLFR2 Model.

Nanticoke

Figures 5-8 to 5-13 compare the measured Nanticoke on-line transfer functions to what is predicted by the STANDARD, SSFR3, and OLFR3 models. It should be noted that the test unit was isolated on one 230 kV line from Nanticoke to Middleport while 5 other units at Nanticoke were connected to Middleport via five 230 kV lines. Therefore, the test generator was relatively close (electrically) to other generators. It is therefore expected that inter-machine as well as machine-system modes will be apparent in the simulations.

It is clear from Figures 5-8 and 5-9 that the STANDARD model gives rise to large differences in gain and phase angle from those measured, and that, in the critical frequency range (1-2 Hz), a larger gain, and hence less damping, is predicted by this model. It is interesting to note that in this frequency range this model shows two successive peaks in the transfer functions which correspond to two lightly damped modes of response. These are the inter-machine and machine-system modes. The inter-machine mode (lower of the two peaks in the gain plots) is clearly seen because of the close coupling between the test unit and the remaining Nanticoke units.

Figures 5-10 and 5-11 show the results obtained using the standstill model SSFR3. In general the observed discrepancies manifest themselves as lower gain and higher phase angle compared to measured values. It is particularly noticeable that in the frequency range 1.0 to 2.0 Hz this model shows much more pronounced inter-machine and machine-system modes than was the case with the STANDARD model. This suggests that the corresponding damping and frequency of rotor oscillations will be much lower than actual values. It is also noticeable that significant phase angle differences are apparent at higher frequencies, above 2 Hz, which indicates, as was expected, that the subtransient effects are not modelled correctly.

In Figures 5-12 and 5-13 the on-line frequency response model OLFR3 is superimposed on the data from which it was derived. Both the gain and the phase angle of the two transfer functions are well matched but some discrepancies in the latter are apparent in frequencies above 3 Hz. The most important point to note is that the damping and frequency of rotor oscillations predicted by this model are in good agreement with the measured values. The inter-machine and machine-system modes are not as pronounced as with the other models.

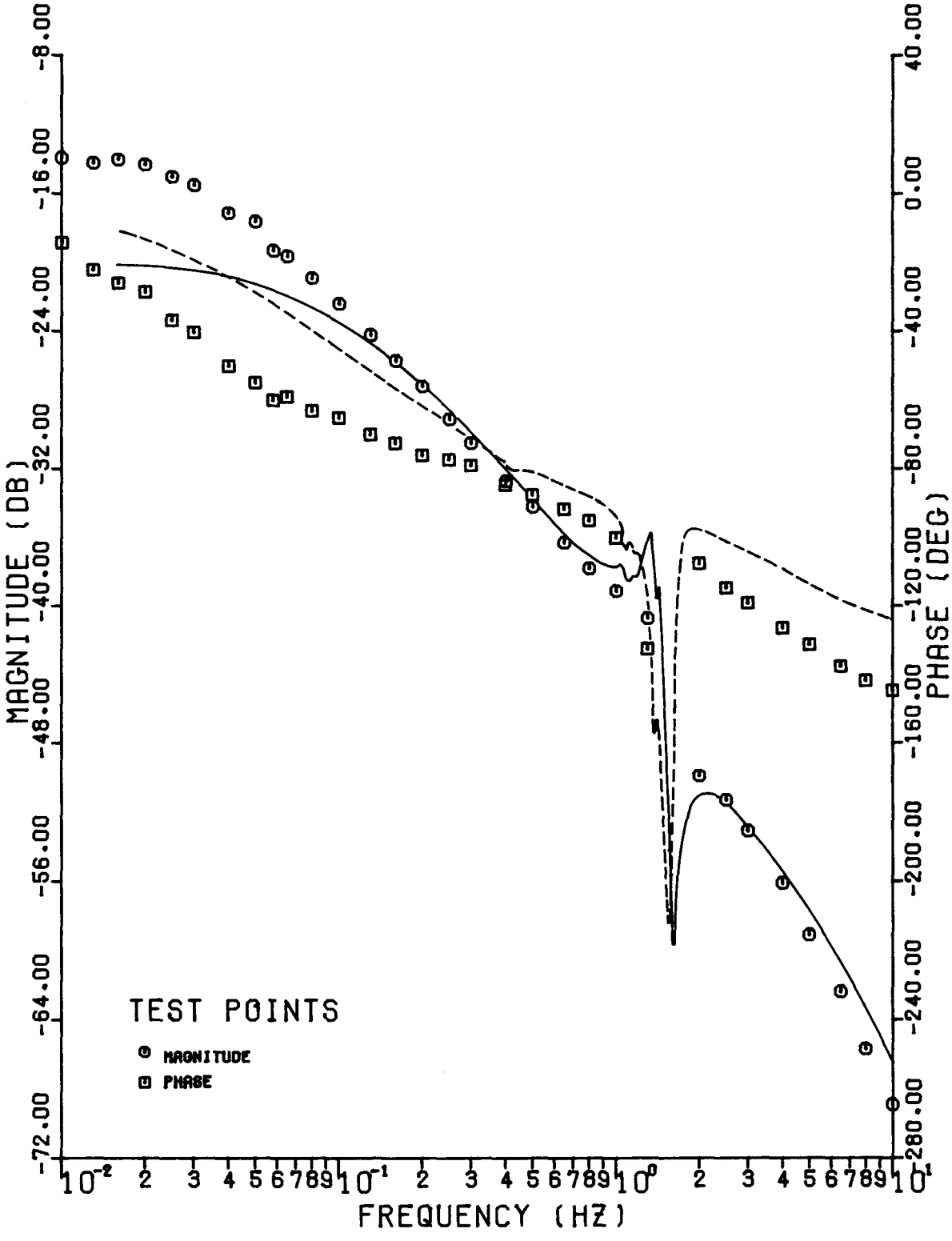

Figure 5-8. Nanticoke, On-Line Transfer Function From Field Voltage to Terminal Voltage, STANDARD Model.

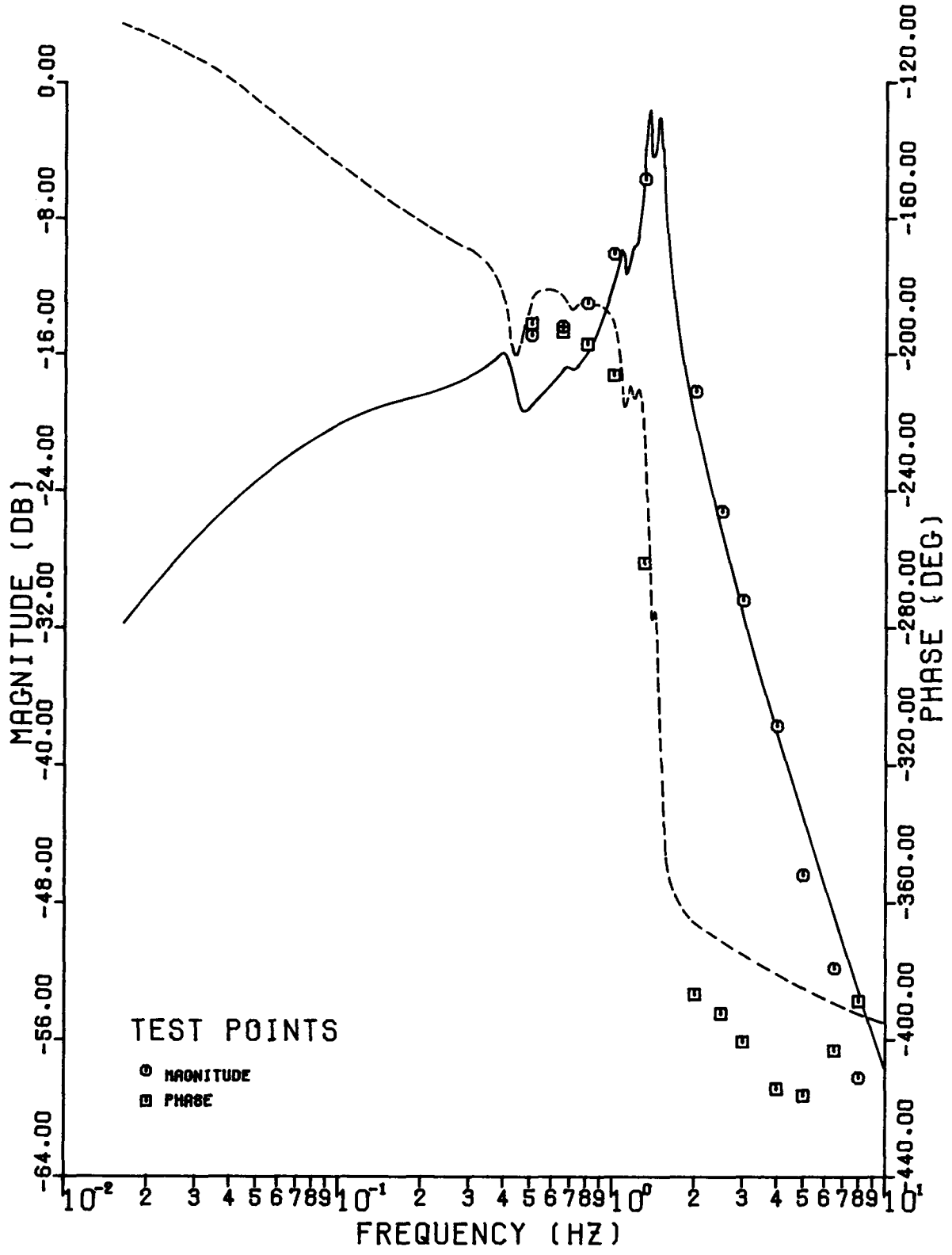

Figure 5-9. Nanticoke, On-Line Transfer Function From Field Voltage To Shaft Speed, STANDARD Model.

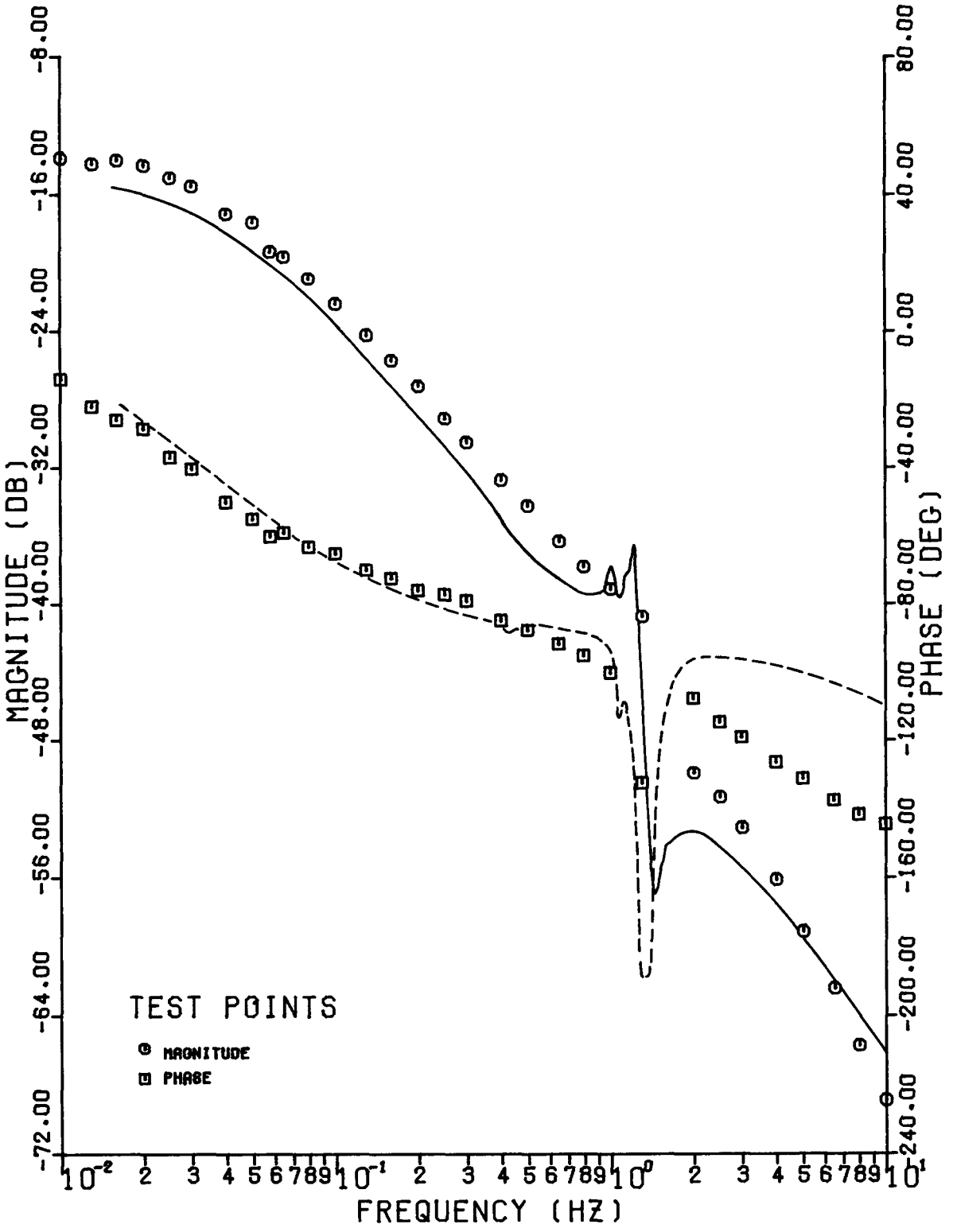

Figure 5-10. Nanticoke, On-Line Transfer Function From Field Voltage to Terminal Voltage, SSFR3 Model.

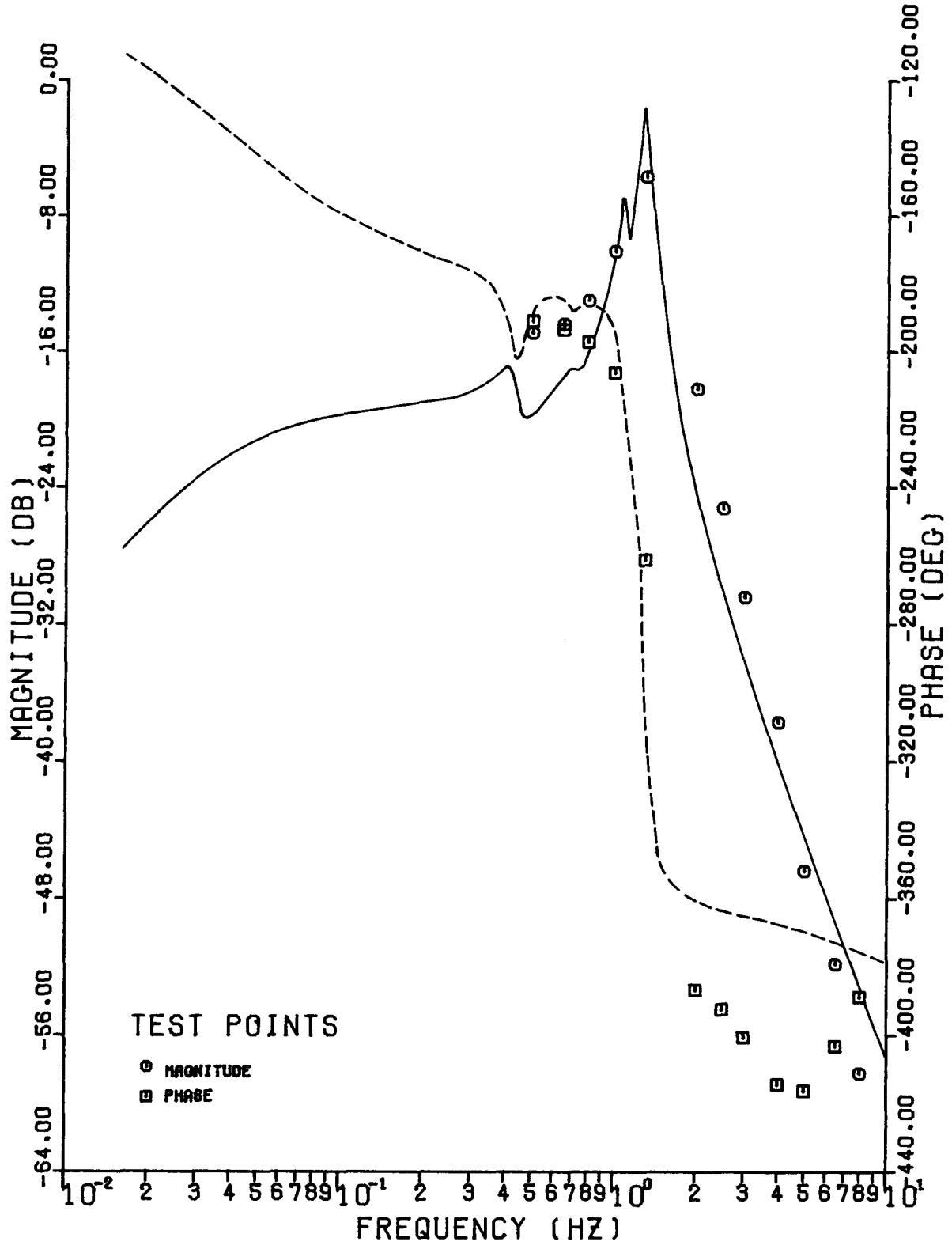

Figure 5-11. Nanticoke, On-Line Transfer Function From Field Voltage to Shaft Speed, SSFR3 Model.

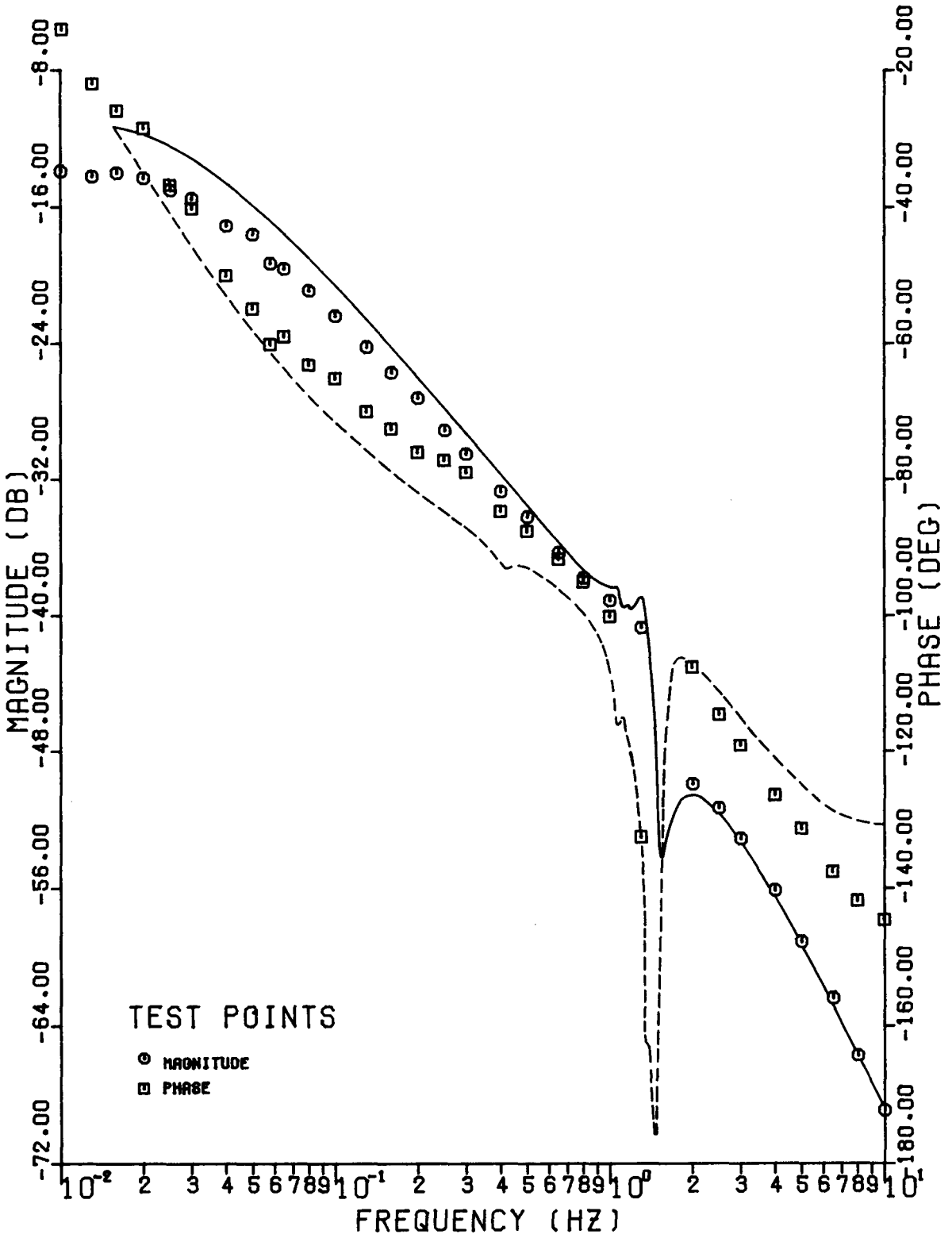

Figure 5-12. Nanticoke, On-Line Transfer Function From Field Voltage to Terminal Voltage, OLFR3 Model.

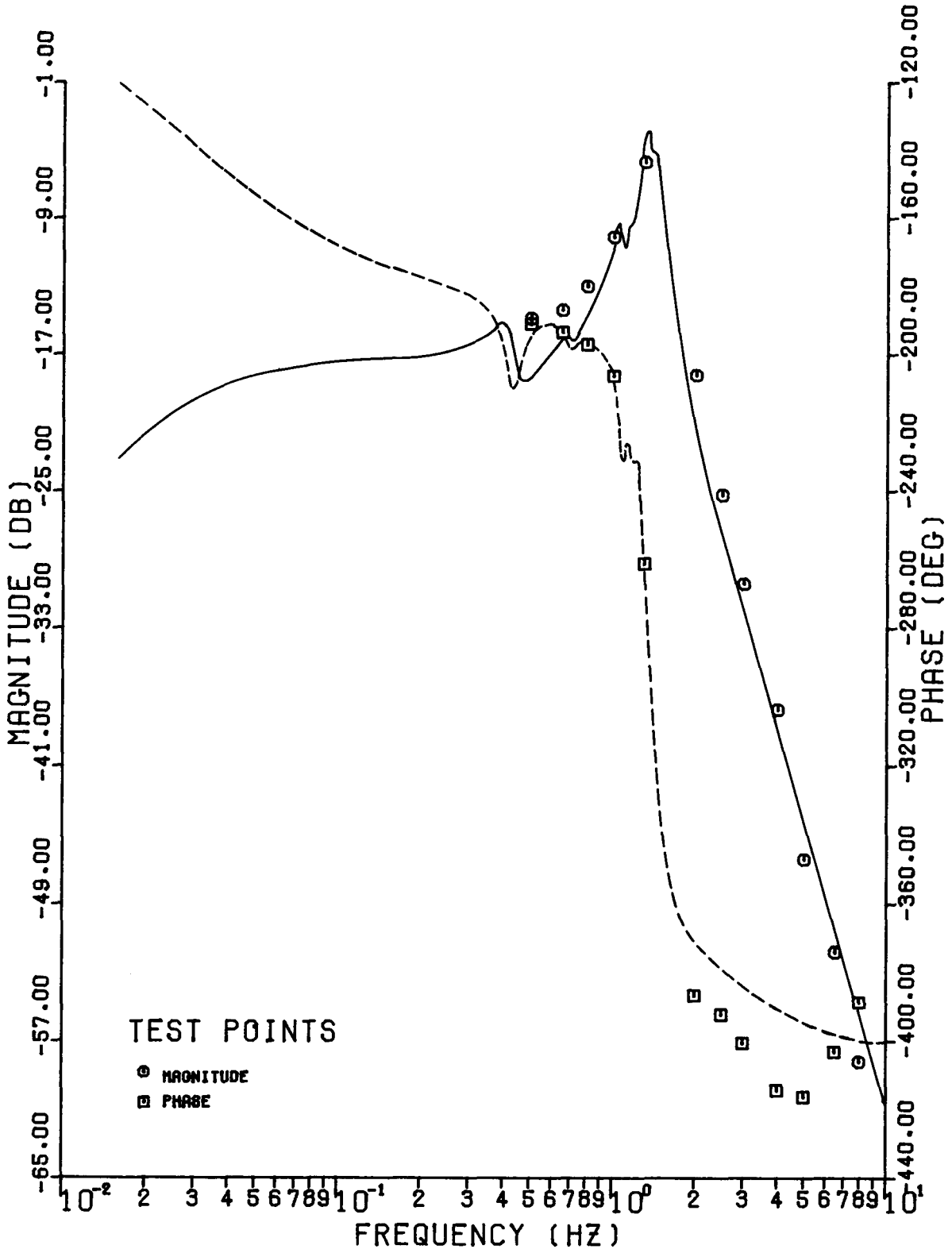

Figure 5-13. Nanticoke, On-Line Transfer Function From Field Voltage to Shaft Speed, OLFR3 Model.

PERFORMANCE OF OLFR MODELS

The OLFR models were then used to simulate the line switching tests at Lambton and Nanticoke.

As would be expected, the Lambton results (Figures 5-14 to 5-21) demonstrate that there is little to choose between the SSFR2 and OLFR2 models. Both produced quite satisfactory simulations of reality.

Nanticoke, of course, was the more interesting case. Would modifying the SSFR3 model on the basis of on-line frequency response test data result in a satisfactory generator model? The answer was yes, as is apparent from Figures 5-22 to 5-29. The OLFR3 model displays a dramatic improvement in performance over either the STANDARD or SSFR3 versions. Both the frequency and damping of the line switching transients are well matched.

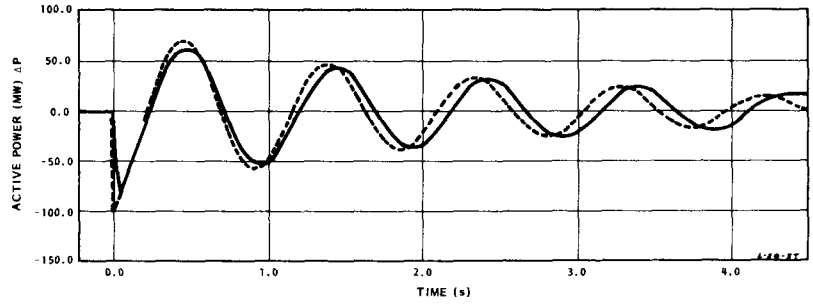

——— measured

- - - STANDARD

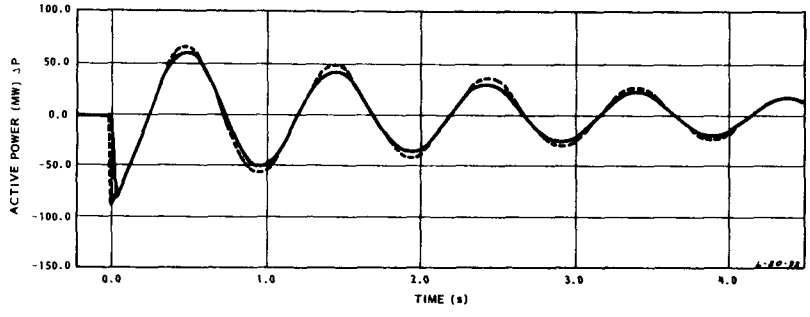

——— measured

- - - SSFR2

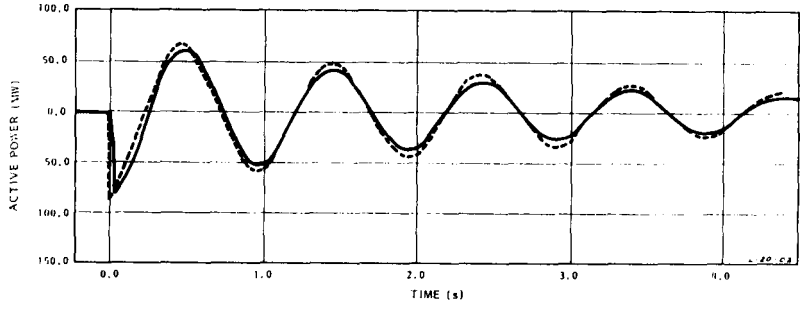

——— measured

- - - OLFR2

Figure 5-14. Lambton Line Switching Test Number 3, Active Power with STANDARD, SSFR2, and OLFR2 Models.

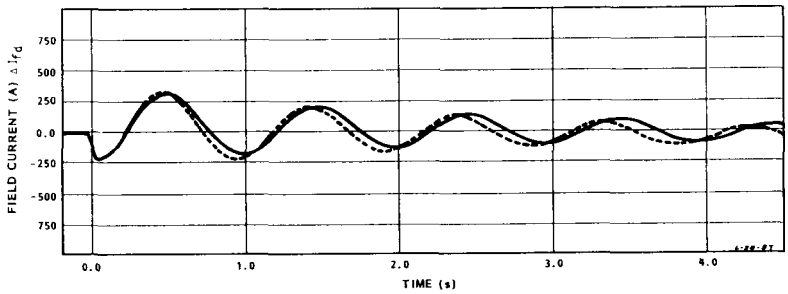

——— measured

- - - STANDARD

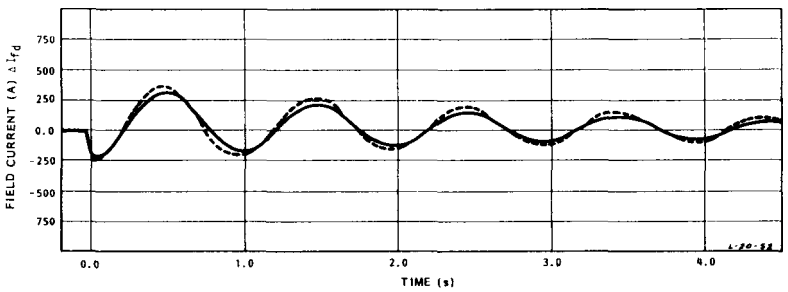

——— measured

- - - SSFR2

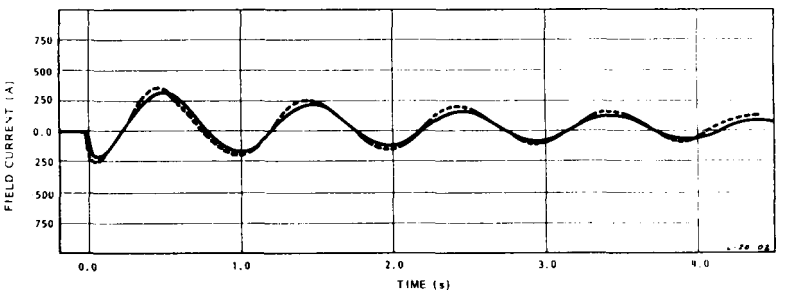

——— measured

- - - OLFR2

Figure 5-15. Lambton Line Switching Test Number 3, Field Current With STANDARD, SSFR2, and OLFR2 Models.

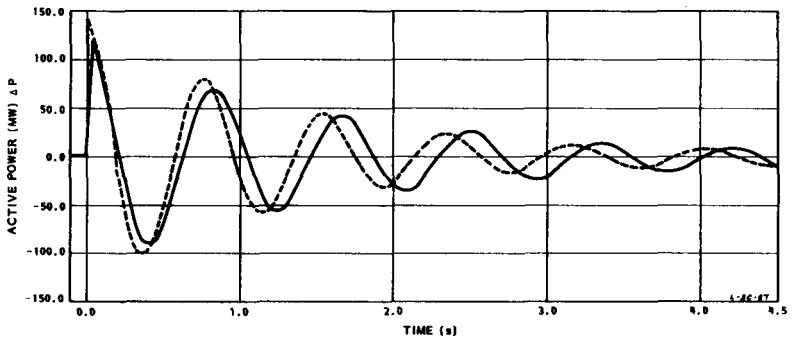

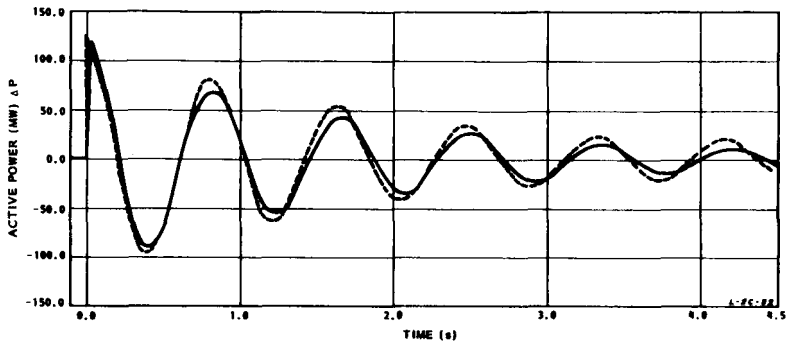

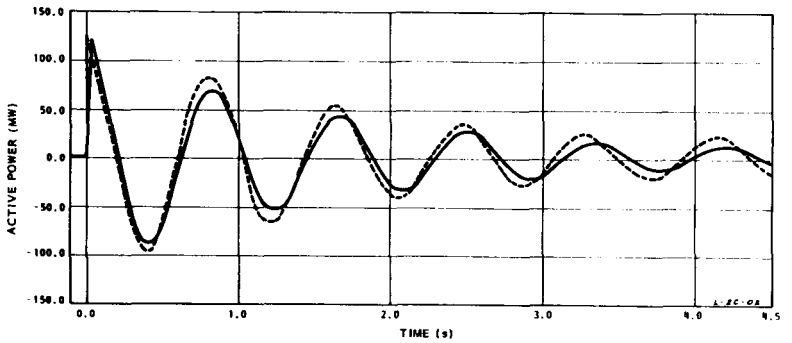

Figure 5-16. Lambton Line Switching Test Number 4, Active Power With STANDARD, SSFR2, and OLFR2 Models.

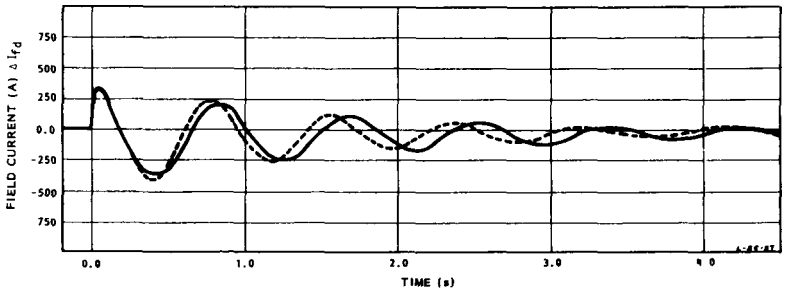

——— measured

- - - STANDARD

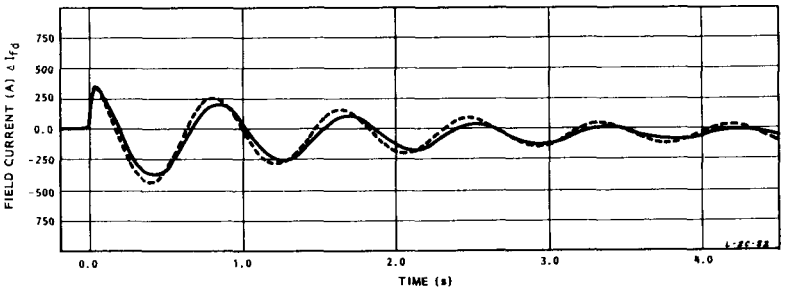

——— measured

- - - SSFR2

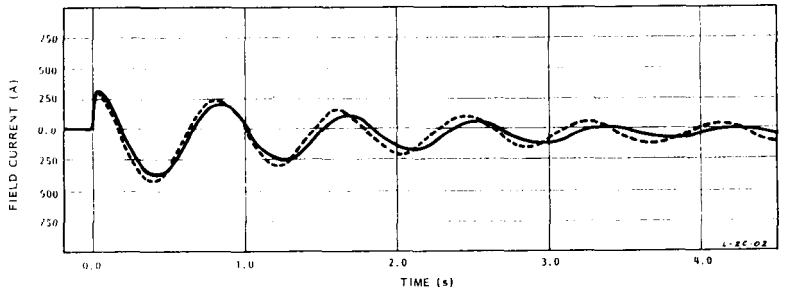

——— measured

- - - OLFR2

Figure 5-17. Lambton Line Switching Test Number 4, Field Current With STANDARD, SSFR2, and OLFR2 Models.

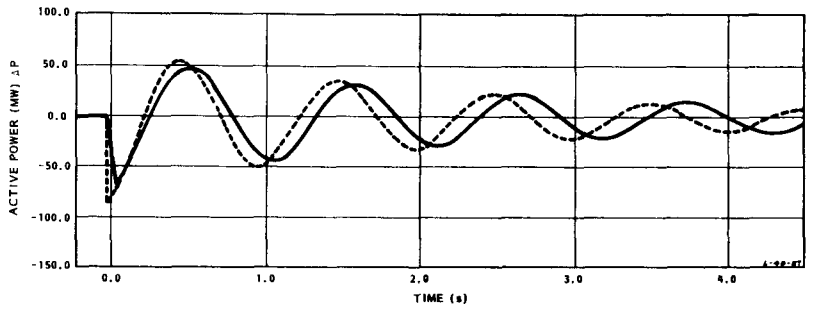

——— measured

- - - STANDARD

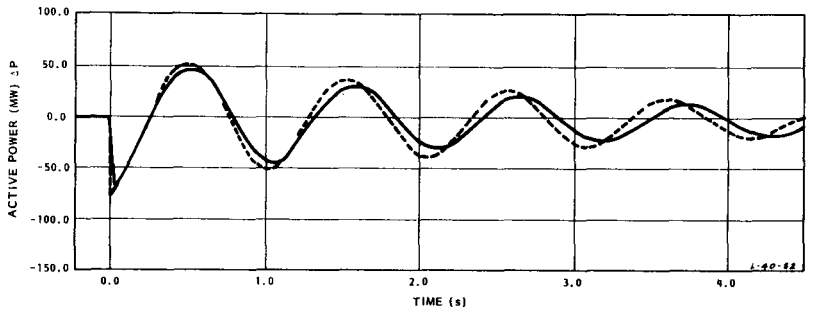

——— measured

- - - SSFR2

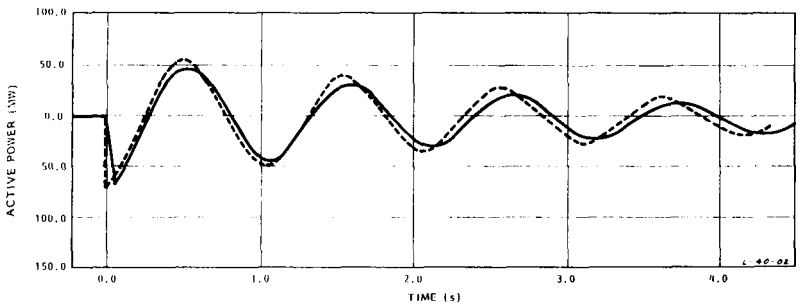

——— measured

- - - OLFR2

Figure 5-18. Lambton Line Switching Test Number 7, Active Power With STANDARD, SSFR2, and OLFR2 Models.

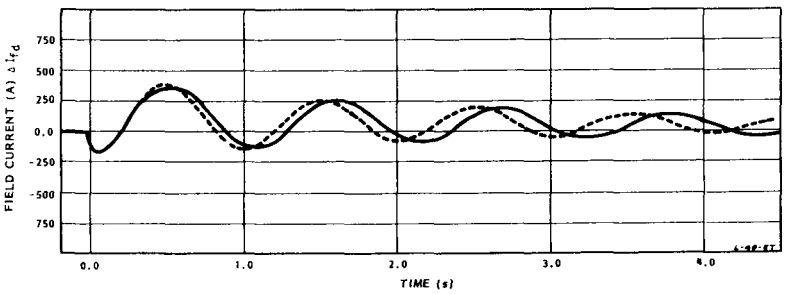

——— measured

- - - STANDARD

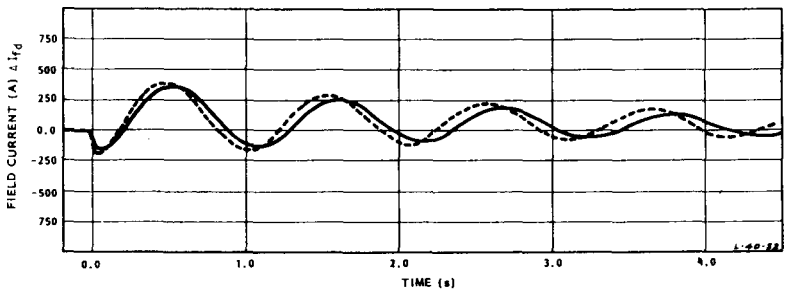

——— measured

- - - SSFR2

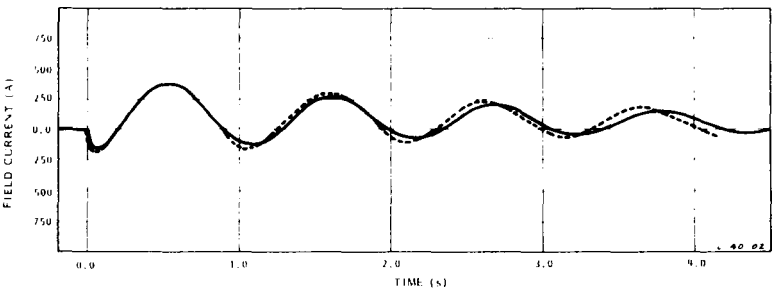

——— measured

- - - OLFR2

Figure 5-19. Lambton Line Switching Test Number 7, Field Current With STANDARD, SSFR2, and OLFR2 Models.

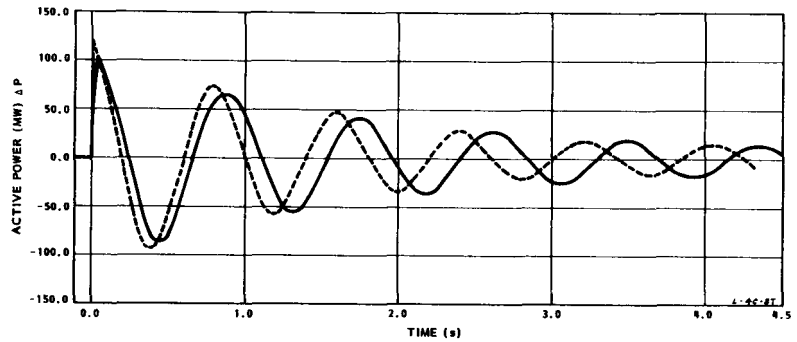

measured

- - - STANDARD

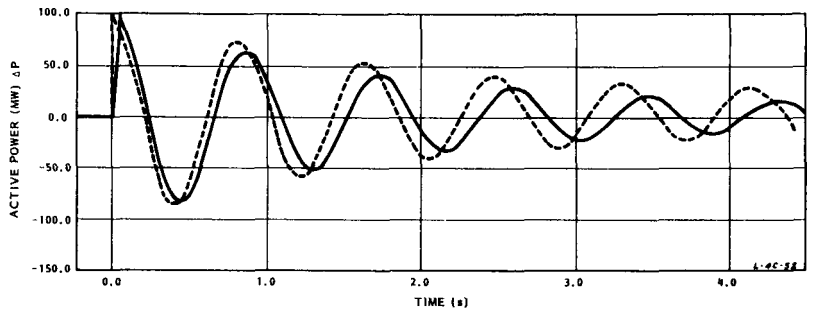

measured

- - - SSFR2

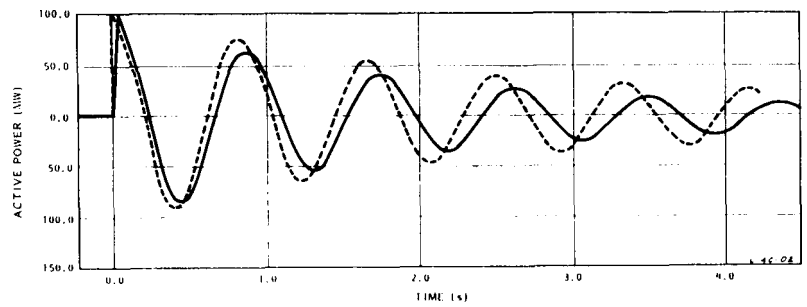

measured

- - - OLFR2

Figure 5-20. Lambton Line Switching Test Number 8, Active Power With Standard, SSFR2, and OLFR2 Models.

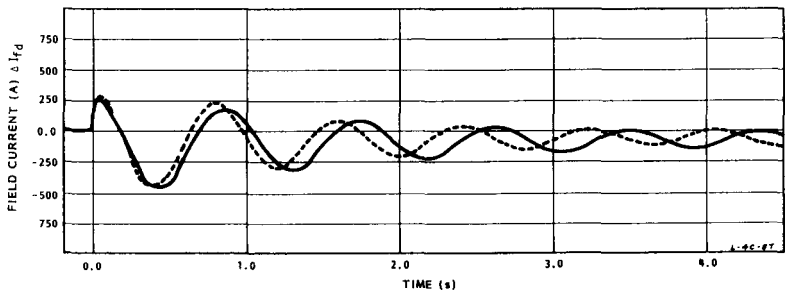

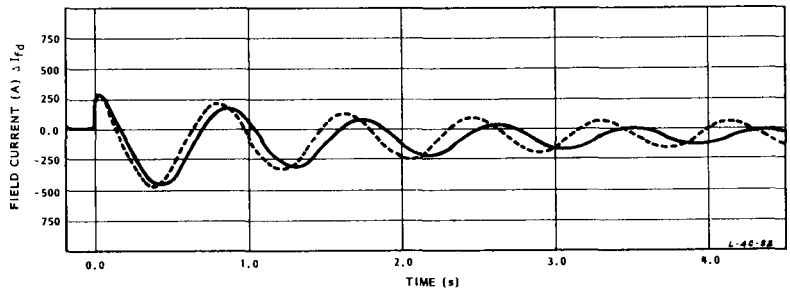

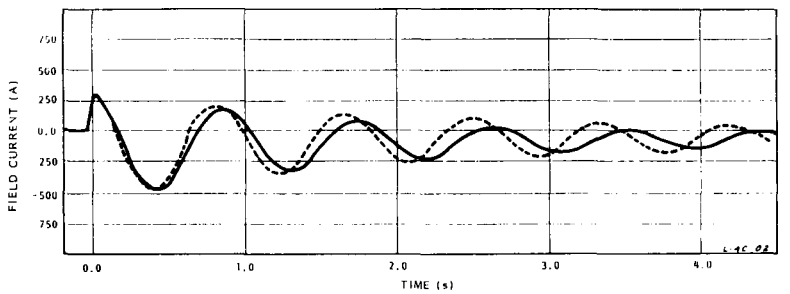

Figure 5-21. Lambton Line Switching Test Number 8, Field Current With STANDARD, SSFR2, and OLFR2 Models.

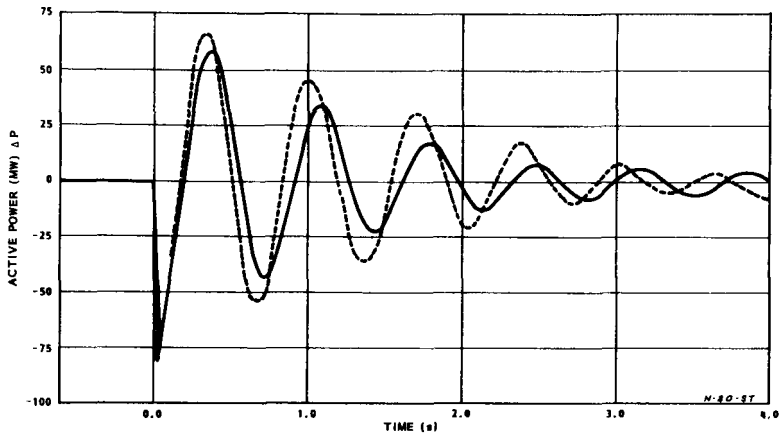

——— measured

- - - STANDARD

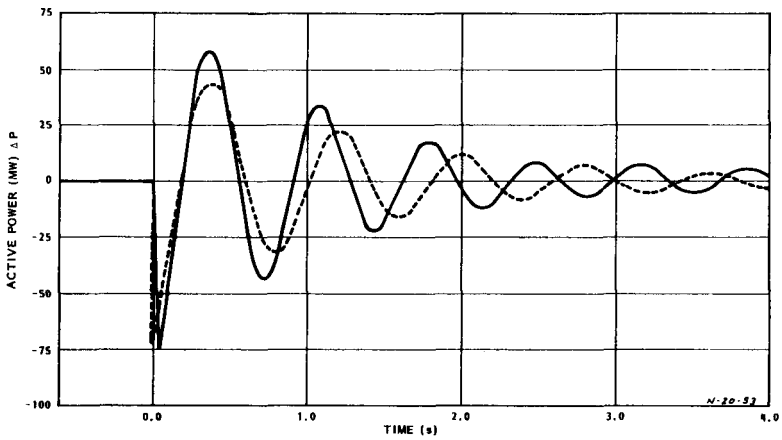

——— measured

- - - SSFR3

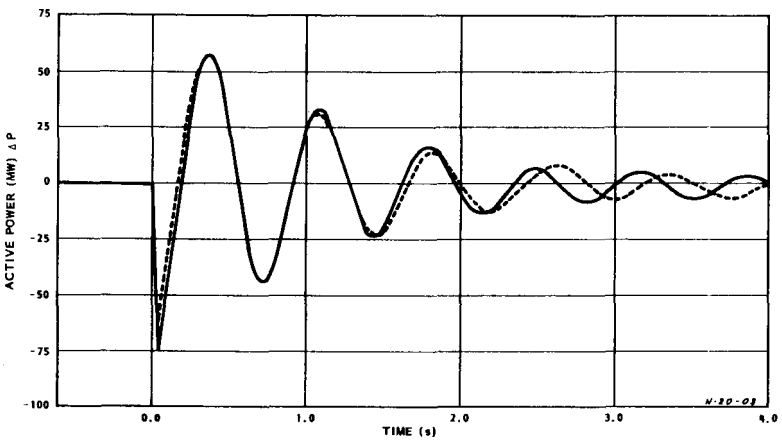

——— measured

- - - OLFR3

Figure 5-22. Nanticoke Line Switching Test Number 2-0, Active Power With STANDARD, SSFR3, and OLFR3 Models.

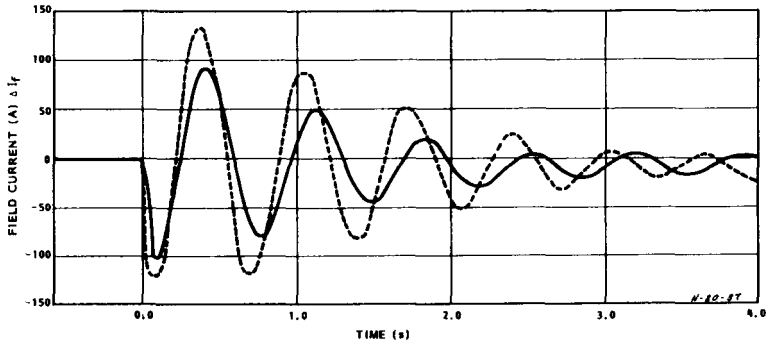

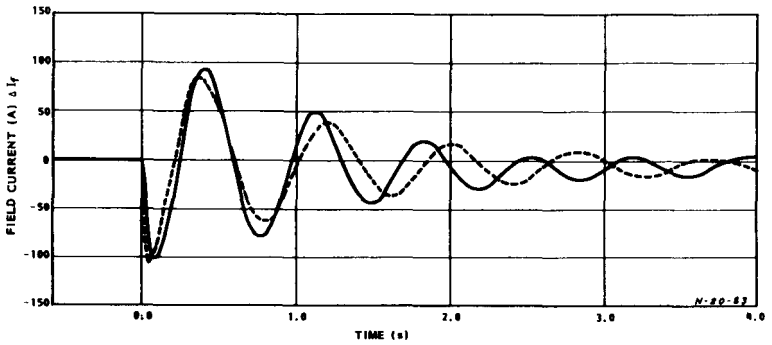

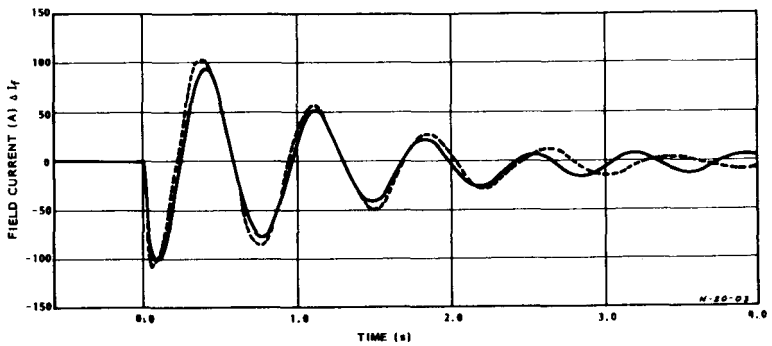

Figure 5-23. Nanticoke Line Switching Test Number 2-0, Field Current With STANDARD, SSFR3, and OLFR3 Models.

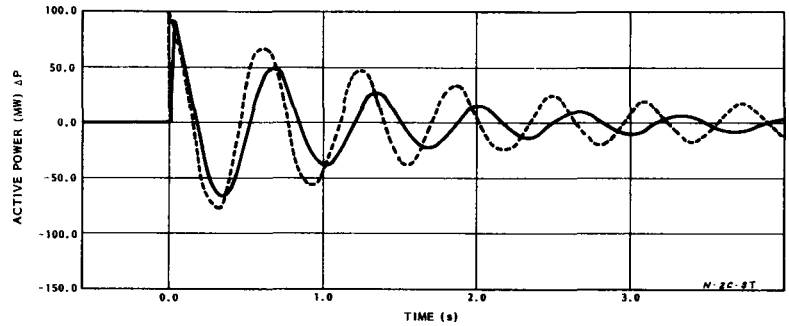

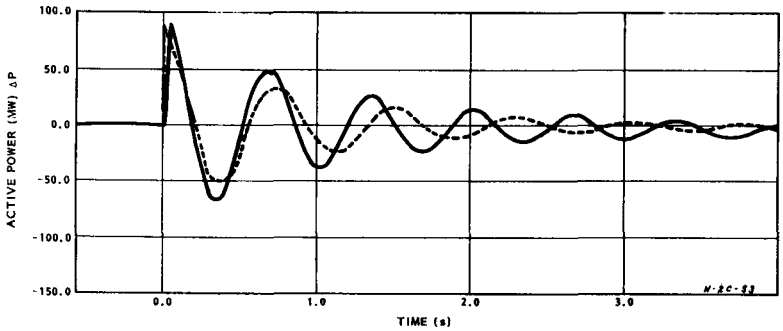

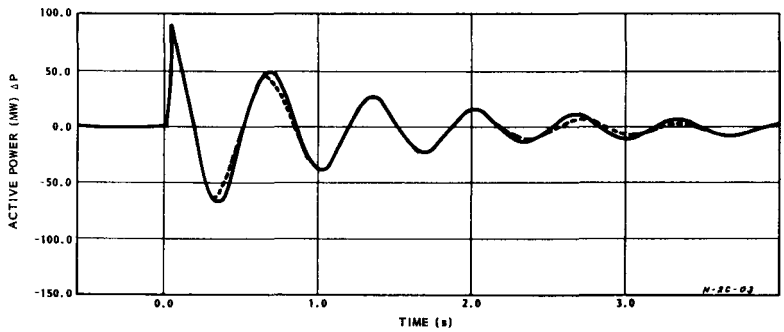

Figure 5-24. Nanticoke Line Switching Test Number 2-C, Active Power With STANDARD, SSFR3, and OLFR3 Models.

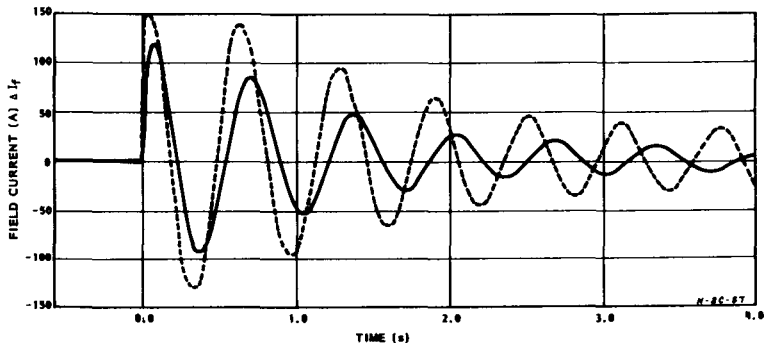

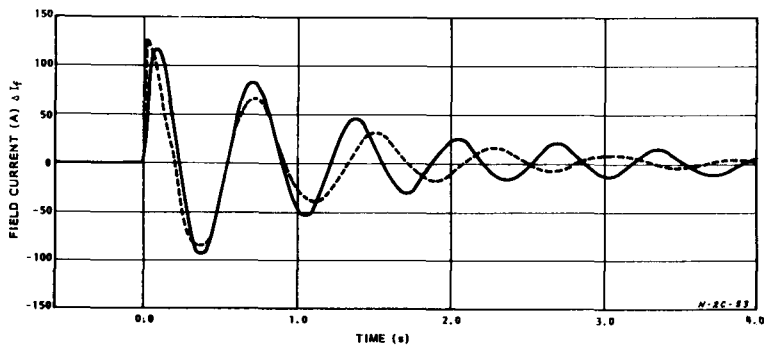

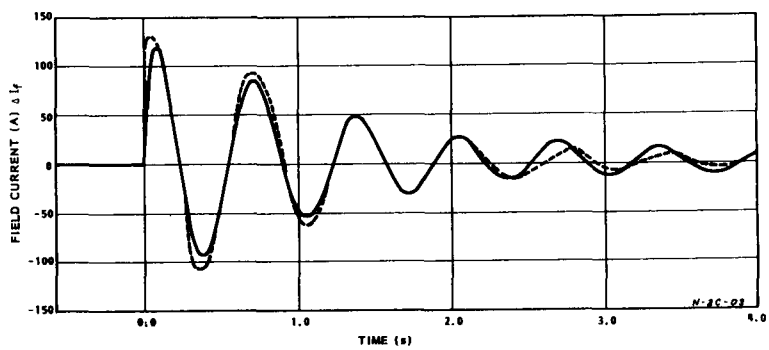

Figure 5-25. Nanticoke Line Switching Test Number 2-C, Field Current With STANDARD, SSFR3, and OLFR3 Models.

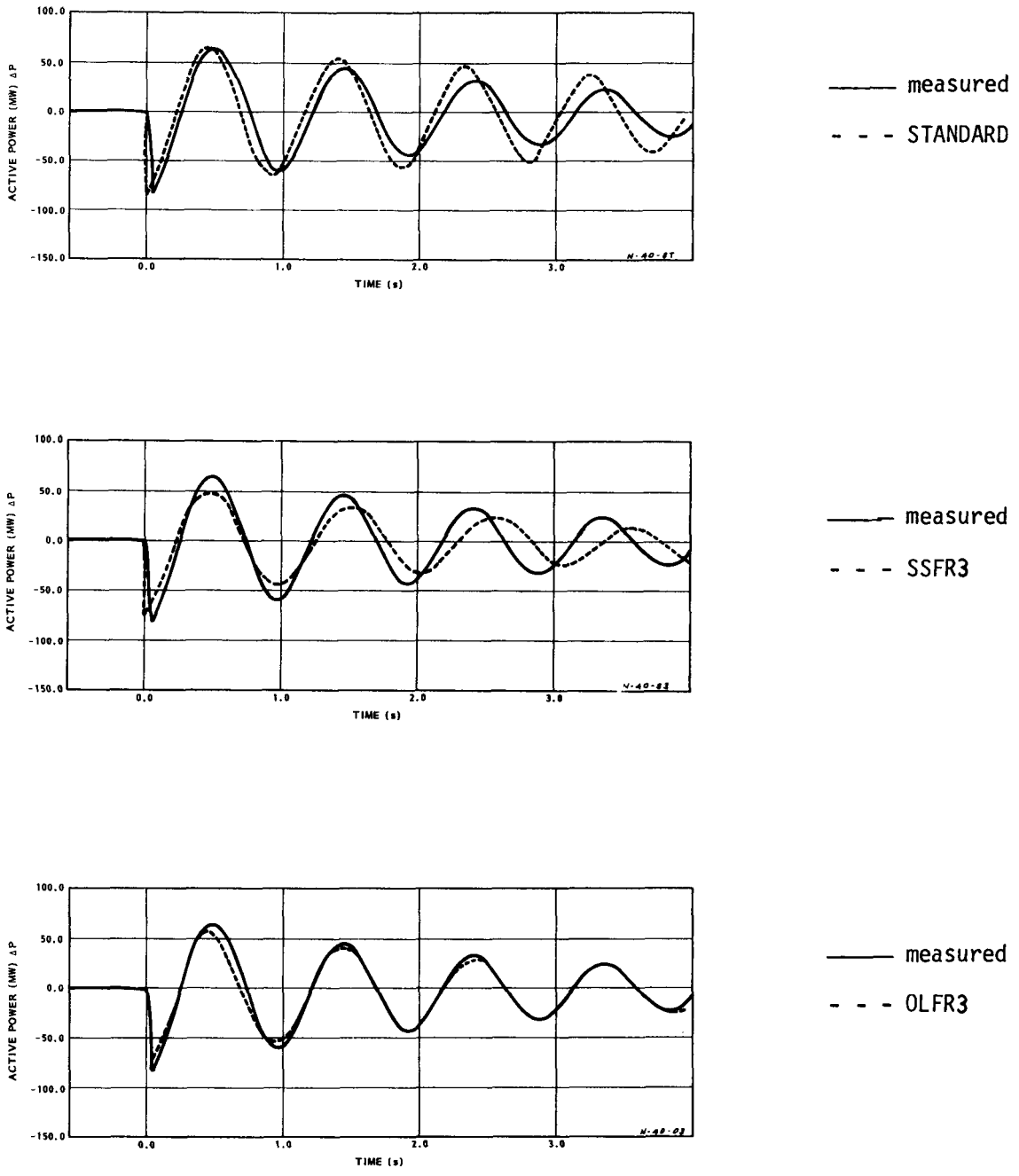

Figure 5-26. Nanticoke Line Switching Test Number 4-0, Active Power With STANDARD, SSFR3, and OLFR3 Models.

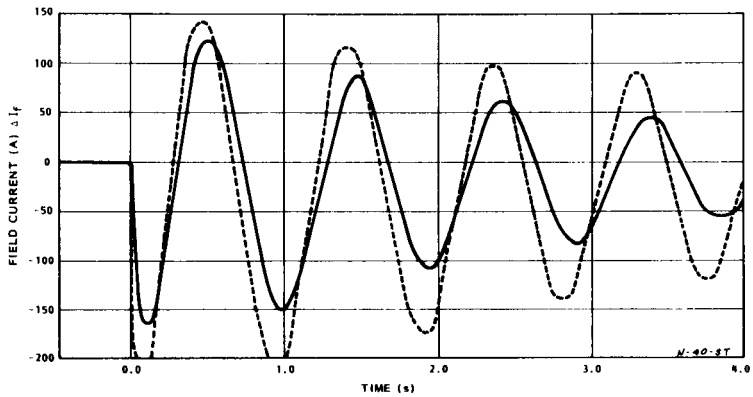

——— measured

- - - STANDARD

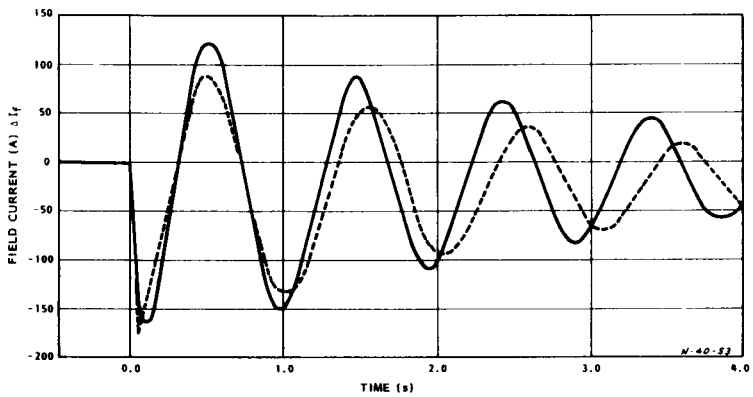

——— measured

- - - SSFR3

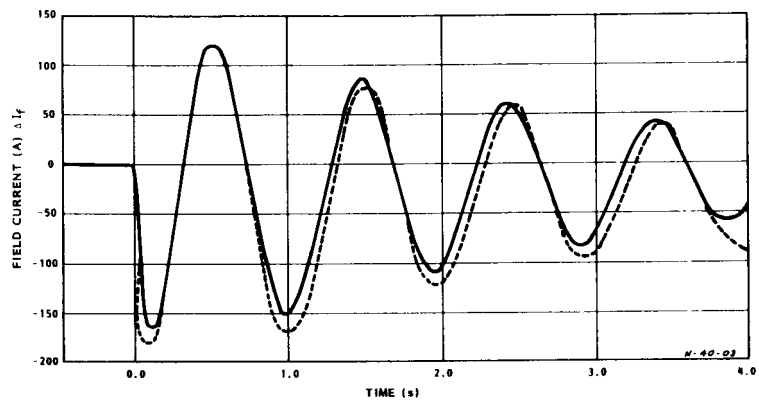

——— measured

- - - OLFR3

Figure 5-27. Nanticoke Line Switching Test Number 4-0, Field Current With STANDARD, SSFR3, and OLFR3 Models.

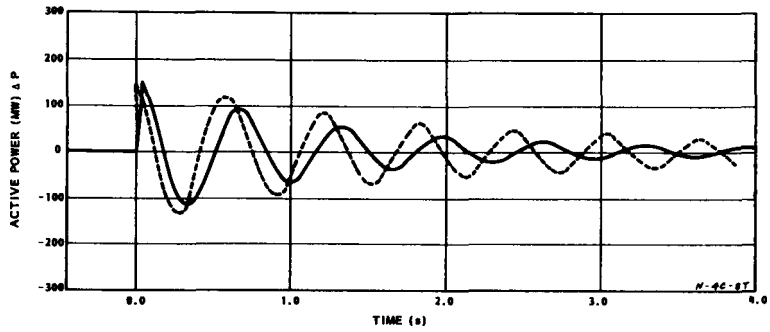

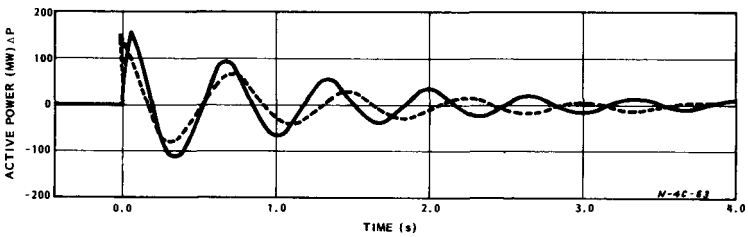

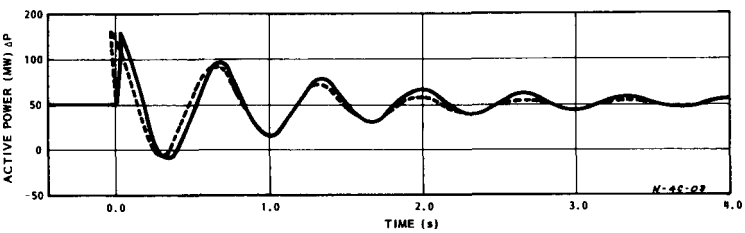

Figure 5-28. Nanticoke Line Switching Test Number 4-C, Active Power With STANDARD, SSFR3, and OLFR3 Models.

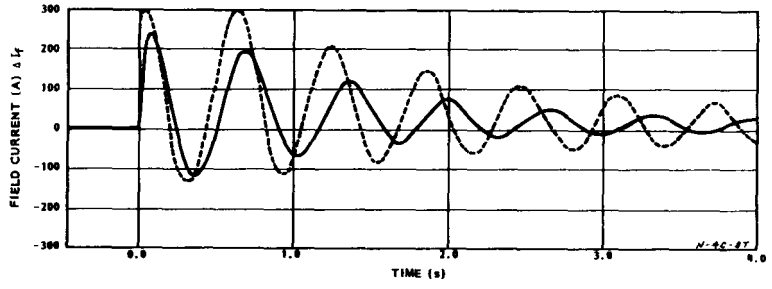

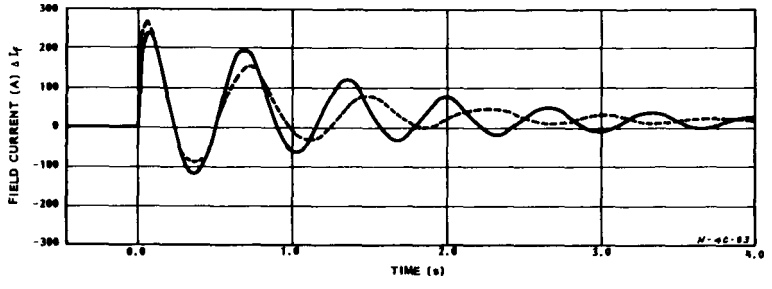

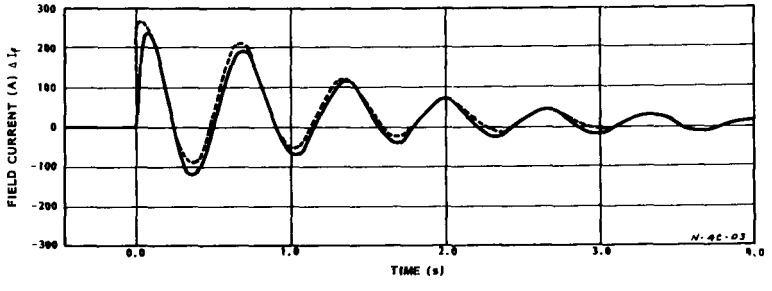

Figure 5-29. Nanticoke Line Switching Test Number 4-C, Field Current With STANDARD, SSFR3, and OLFR3 Models.

GENERAL COMMENTS

In summary, standstill frequency response models were satisfactory for two of the three machines. For the third case, the standstill models had to be adjusted on the basis of on-line frequency response test data, but once this was done, very good performance resulted.

It is also worth noting that even though test machines may be made as electrically distant from the rest of the power system as practical, the characteristics of that external system cannot be treated lightly. Great care must be exercised in setting up correct load flows and modelling nearby machines in sufficient detail. Otherwise, errors in the simulations may be as much a result of an inaccurate external system as a consequence of incorrect modelling of the test generator.

REFERENCES

1. P. Kundur and P.L. Dandeno. Practical Application of Eigenvalue Techniques in the Analysis of Power System Dynamic Stability Programs. Canadian Electrical Engineering Journal, Vol 1, No 1, Jan 1976.

Section 6

SATURATION

EXISTING METHOD

The usual practice within the industry is to model saturation in generators as follows. The manufacturer's open-circuit saturation curve in the d-axis is used to determine the saturation factor for any given operating condition (voltage behind armature leakage or Potier inductance is used). This factor is then applied equally to both the d- and q-axis mutual inductances L_{ad} and L_{aq} respectively. Hitherto this technique has not been validated by extensive testing, but some results (1), (2), (3), have indicated that it may not be adequate. These investigations have shown that the q-axis synchronous inductance has to be modified much more than the d-axis synchronous inductance, which suggests that the saturation characteristics in the two axes are not identical.

The steady-state measurements carried out over a wide range of loads on the Nanticoke and Lambton machines provided an opportunity to evaluate this approach. The two parameters which are indicative of how saturation affects the machine performance are internal angle and field current, the former is chiefly influenced by L_q whereas the latter is mainly dependent on L_d. Accordingly, field current and internal angle are examined here to see how well the existing method fits the measured results.

Comparisons between calculated and measured results were made at both Lambton and Nanticoke. The comparison between measured and calculated field current was made by determining the percentage error in the field current:

$$\text{error} = \frac{(\text{measured field current} - \text{calculated field current})}{\text{measured field current}} \times 100$$

whereas the comparison between the measured and calculated internal angle was done by obtaining the error = measured value - calculated value. The results are plotted against the per unit reactive loading of the machine in Figure 6-1 for Lambton and Figure 6-2 for Nanticoke.

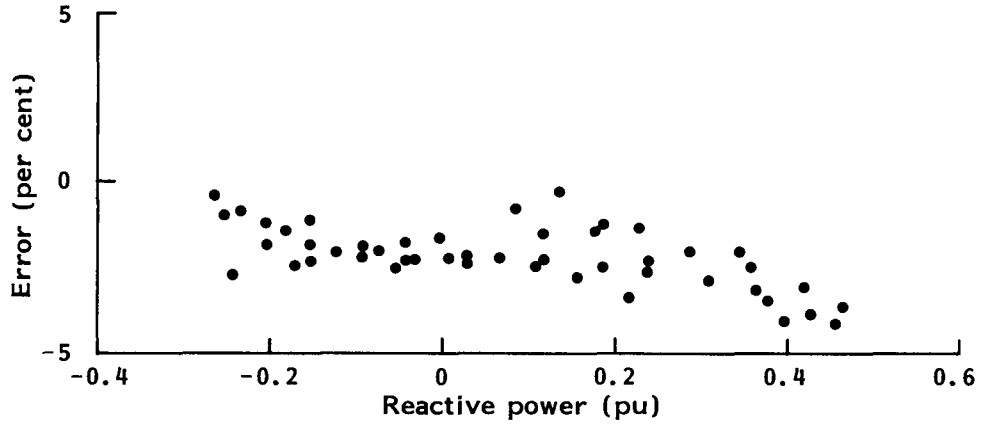

Field Current Error

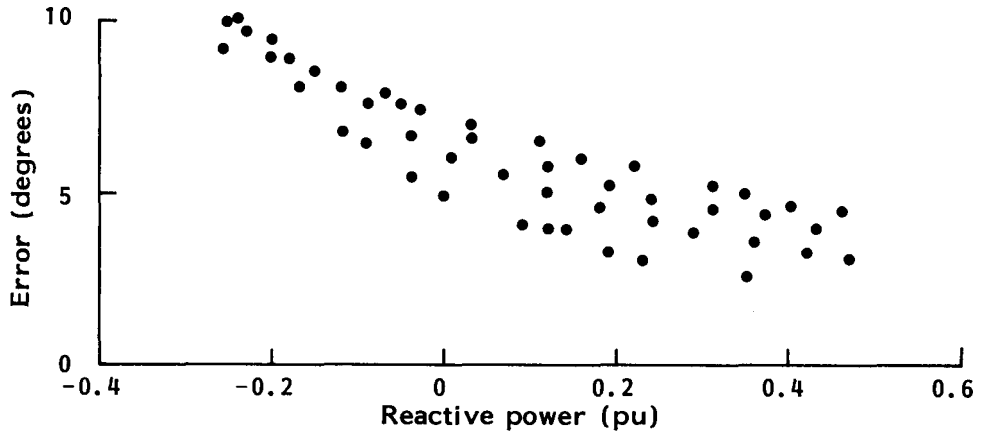

Internal Angle Error

Figure 6-1. Lambton, Field Current and Internal Angle Errors With Existing Saturation Model.

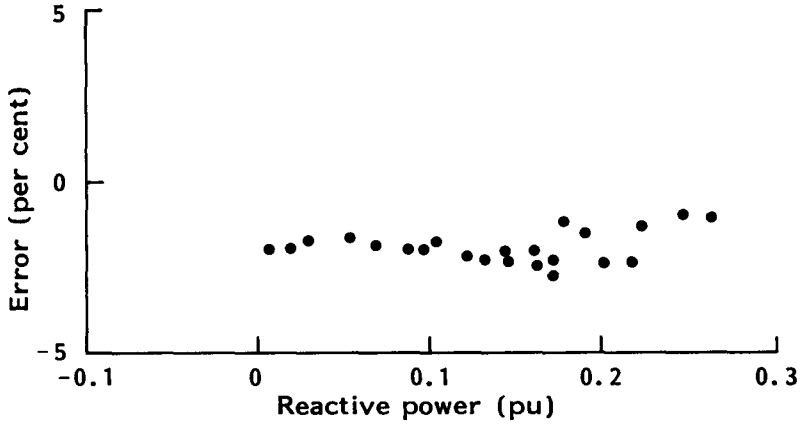

Field Current Error

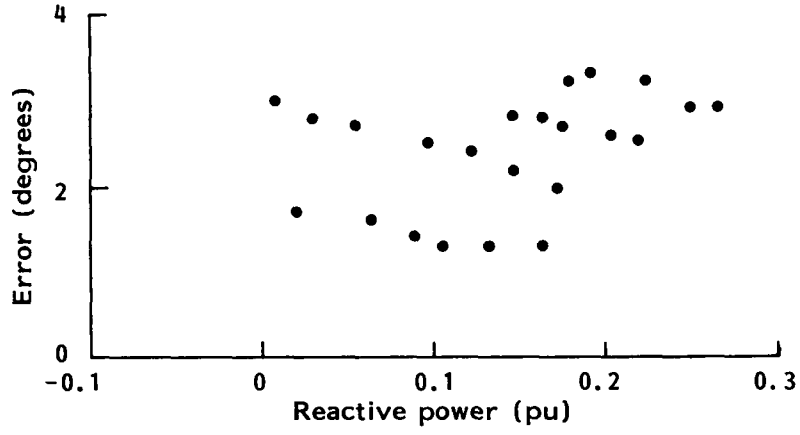

Internal Angle Error

Figure 6-2. Nanticoke, Field Current and Internal Angle Errors with Existing Saturation Model.

It is clear that significant errors appeared in the calculated values of field current and internal angle. At Lambton the field current errors were greater in the overexcited range and diminished towards the underexcited range, whereas the internal angle errors were higher at underexcited loads. By contrast, the Nanticoke results showed relatively constant errors in both field current and internal angle over the range of reactive loads covered. An interesting point was that the field current errors were, to a large extent, independent of the MW load, while the internal angle errors were quite dependent on both the MW and MVAR load, the larger error appearing at higher MW load. By analyzing the steady-state machine equations, it can be shown that this should indeed be so. The scatter of points associated with the Nanticoke machine is most probably due to measurement errors.

The large internal angle errors at Lambton, and the relatively poor field current predictions in the overexcited range, which is the normal operating point for most generators, was not encouraging. The existing technique was obviously not adequate and an alternative approach was required.

NEW TECHNIQUE FOR CALCULATING SATURATION

Results from tests on turbogenerators in the UK (1), (2), have indicated that the q-axis synchronous inductance saturates at a lower voltage than does that of the d-axis. Furthermore, the extent of this saturation is much greater in the q-axis than the d-axis. This suggests that the saturation characteristic in the quadrature axis is somewhat different from its direct axis counterpart. In most turbogenerators this is due to the presence of rotor teeth in the magnetic circuit of the q-axis. Thus, it is not surprising that the existing method of using the open-circuit d-axis characteristic to calculate saturation in the q-axis yielded such large errors in the rotor angle. It would seem that the problem could be easily resolved by using separate characteristics in each axis. But therein lies the crux of the matter; for although there is no difficulty in obtaining the d-axis characteristic, no such information has been forthcoming for the q-axis.

It has been shown (3) that steady-state, on-load measurements at the terminals of turbogenerators can be used to produce the q-axis saturation characteristic. The method proposed herein is much simpler, although based on the same concept.

Steady-state measurements over a range of MW and MVAR loads were used to calculate the corresponding values of L_{ad} and L_{aq}, based on the classical equations (4). Assuming that the correct approach to calculating the saturation factors is to apply the total air-gap voltage to each saturation characteristic, the equivalent excitation currents corresponding to each L_{ad} and L_{aq} value were obtained. These excitation currents were then plotted against air-gap voltage and the results are shown in Figures 6-3 (Lambton) and 6-4 (Nanticoke). Also shown is the manufacturer's open-circuit (d-axis) saturation characteristic for each machine. It is immediately obvious that the q-axis points lie on quite different characteristics compared with the d-axis, for both Nanticoke and Lambton machines. It is also interesting to note that for Lambton, and to a smaller extent Nanticoke, the open-circuit d-axis curve does not satisfactorily account for saturation when the machine is on load.

Thus, it would seem that in order to represent, adequately, saturation effects in a generator, one has not only to rely on separate saturation characteristics in each axis, but also to subdivide them into curves dependent on rotor angle. A proposed new saturation model (3), uses only one set of saturation characteristics, the usual, open-circuit d-axis curve ($\delta=0°$) and a measured q-axis curve ($\delta=90°$). In the calculation of the saturation factors, allowance is made to vary L_{ad} and L_{aq} with internal angle. The method proposed here is very much simpler, since we suggest that curves be drawn through the mean of the d- and q-axis load points using the shape of the open-circuit saturation curve. In this way, an average d- and q-axis saturation characteristic is obtained, which is more representative of the conditions in the machine supplying a load than is the open-circuit characteristic. These new characteristics are shown as dashed lines in Figures 6-3 and 6-4. For the Nanticoke machine, the new d-axis curve coincides with the original manufacturer's curve. As can be seen, particularly for Lambton, some errors are bound to result from this approach, but it is hoped that these errors can be shown to be acceptable for most practical cases. Further-

more, the simplicity of this technique enables it to be implemented readily in the existing time domain programs with negligible change to the computational efficiency. The important point to be made is that a q-axis saturation characteristic is now available which should enable more accurate estimation of internal angle. The new saturation characteristics derived here can be calculated readily from steady-state measurements similar to those reported in Parts 3 and 4 of this report. These measurements are very simple to do, with the possible exception of the internal angle, which, unfortunately, is an essential one.

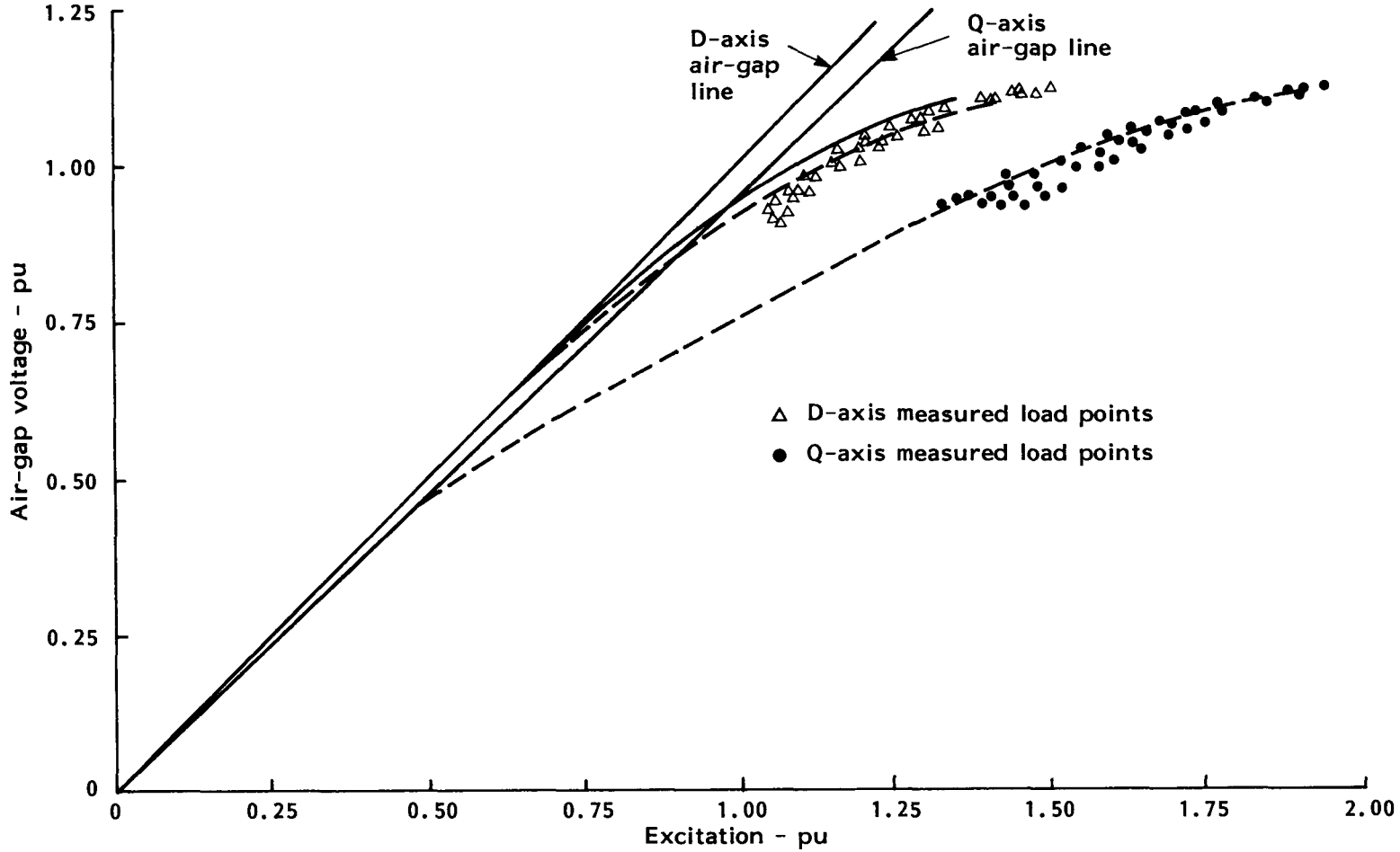

Figure 6-3. Lambton Saturation Curves.

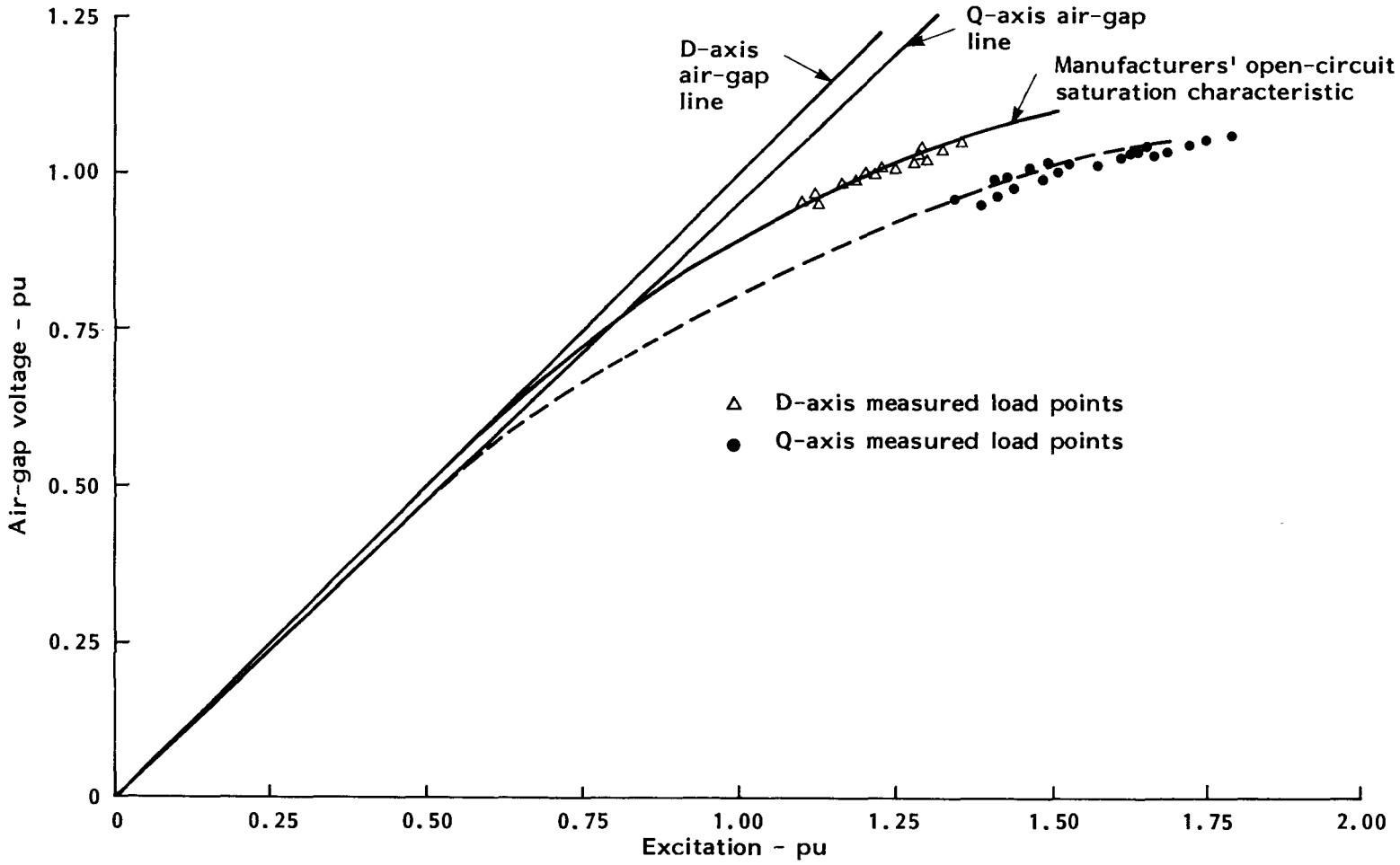

Figure 6-4. Nanticoke Saturation Curves.

Evaluation of New Method Using Steady-State Measurements

The results shown in Figures 6-5 and 6-6 were obtained by using the new d- and q-axis characteristics, for Lambton and Nanticoke, respectively, to calculate the field current and load angle over the same range of MW and MVAR loads as before. Comparing these results with those in Figures 6-1 and 6-2, it is obvious that, in most cases, a substantial improvement was obtained, particularly in the internal angle calculations. Using the new characteristics, the mean errors in field current and internal angle are -2.5% and -1.8 deg for Nanticoke, and +0.3% and -0.11 deg for Lambton. The scatter of errors in Figures 6-5 and 6-6 appears to be due to a bias in the field current in the underexcited load range. This is not surprising since the d-axis, and q-axis, saturation characteristics are only approximations to the real thing. However, in our opinion, the agreement between our results and those of (3) is sufficient justification for accepting the simplified technique. More accurate characteristics could possibly be obtained by adopting at least squares approach to the fitting of the data. However, the need for more accuracy is debatable.

REFERENCES

1. G. Shackshaft and R. Nielson. Results of Stability tests on an Underexcited 120 MW Generator. Proc IEE, vol 119, no 2, February 1972.

2. G. Shackshaft. Generator Parameters for Stability Studies. CIGRE, 1967, paper no 32-15.

3. G. Shackshaft and P.B. Henser. Model of Generator Saturation For Use In Power System Studies. Proc IEE, vol 126, no 8, August 1979.

4. C. Concordia. Synchronous Machines, Theory and Performance. Wiley, 1951, p 32.

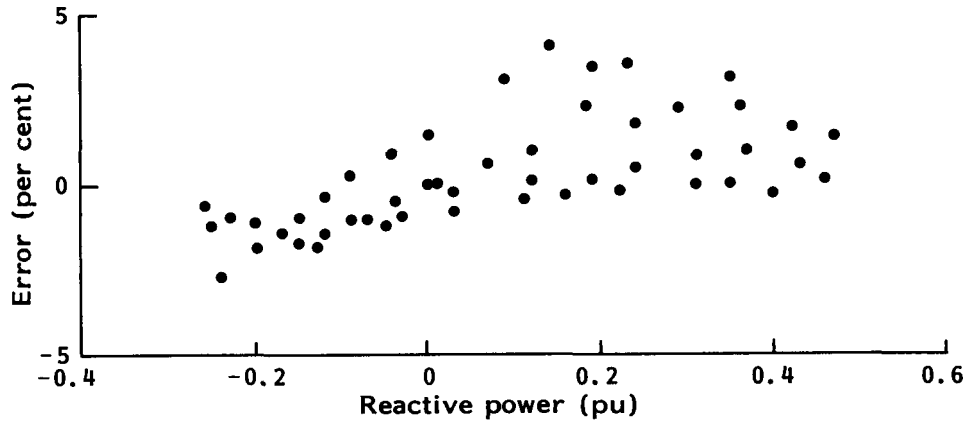

Field Current Error

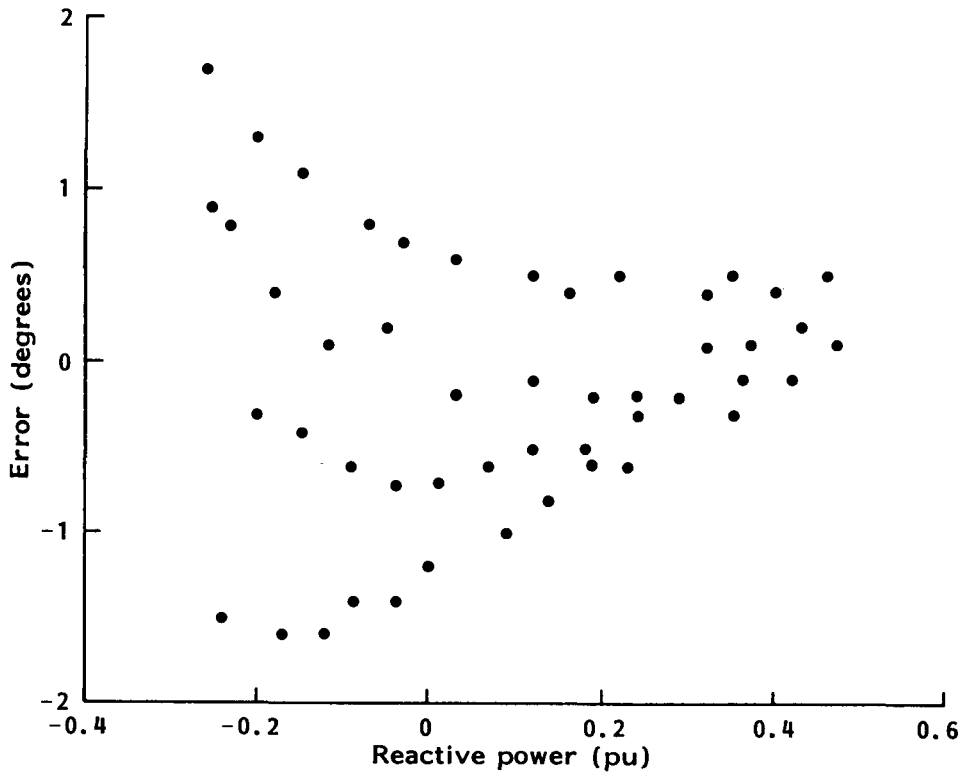

Internal Angle Error

Figure 6-5. Lambton, Field Current and Internal Angle Errors with New Saturation Model.

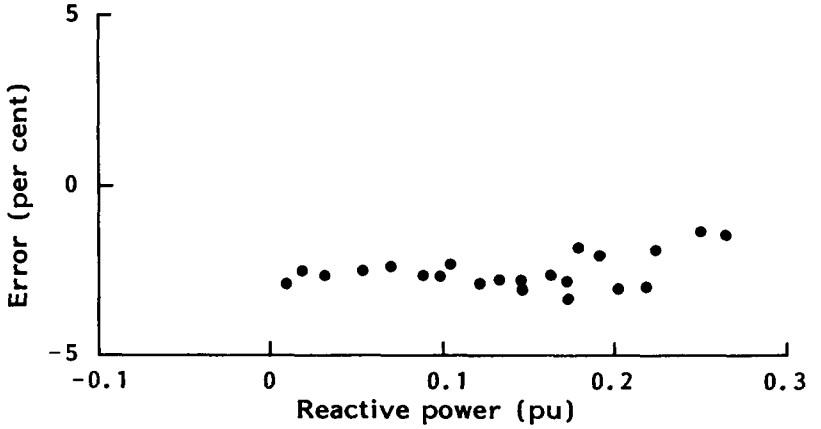

Field Current Error

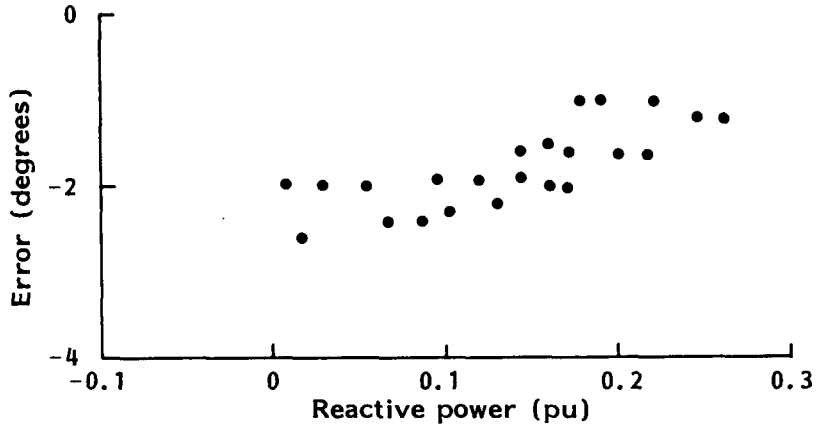

Internal Angle Error

Figure 6-6. Nanticoke, Field Current and Internal Angle with New Saturation Model.

Section 7

DISCUSSION

THE GENERATOR ROTOR

It is no surprise that the design and construction of a synchronous machine's rotor have a profound influence on its electrical characteristics. As an illustration, the direct axis operational inductance will be used to demonstrate the significance of different rotor designs to the present investigation.

Figure 7-1 shows the direct axis equivalent circuit and a plot of $L_d(s)$ for a very simple machine with a laminated rotor and only a field winding; ie, a single discrete winding on the rotor.

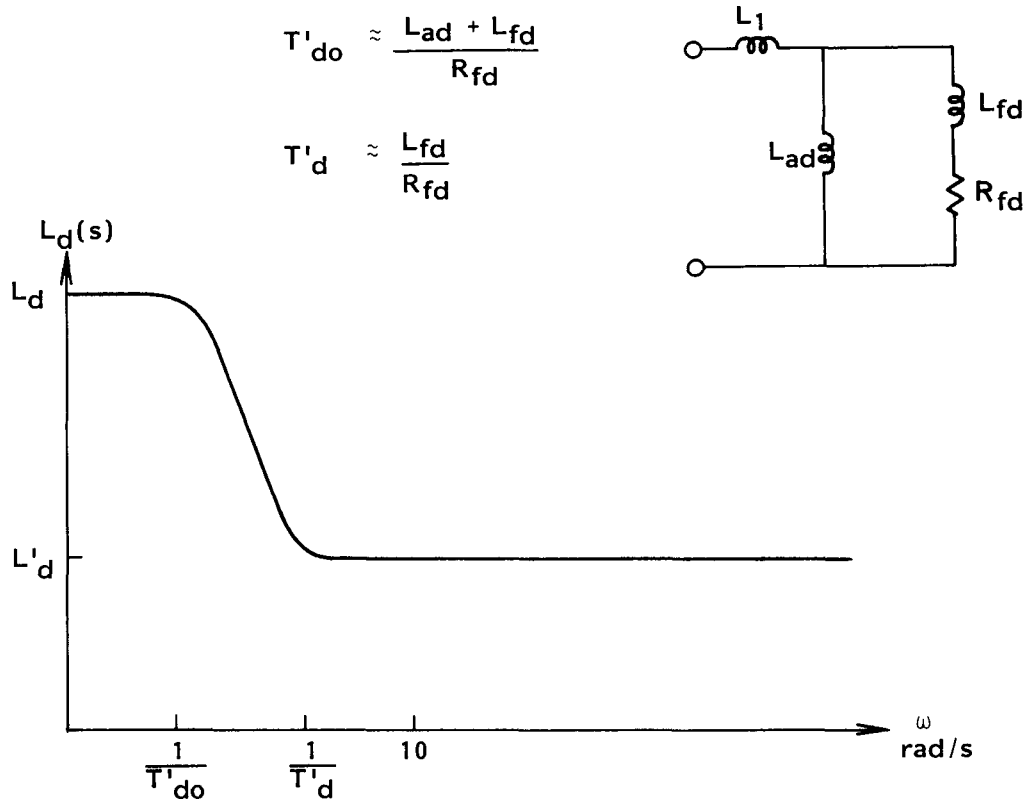

Figure 7-1. Direct Axis Operational Inductance and Equivalent Circuit for a Machine With a Laminated Rotor and No Damper Winding.

There are only two breakpoints in the curve. At very low frequencies, $L_d(s) = L_d = L_{ad} + L_l$, the synchronous inductance. The magnitude begins to drop off, governed by T'_{do}, which, in this case, is the time constant of the field winding, and levels off at L'_d, the transient inductance, which is the sum of L_l plus the parallel combination of L_{ad} and L_{fd}.

Figure 7-2 represents a machine with a laminated rotor, a field winding, and one discrete damper winding; the time constants of the field and damper are widely separated.

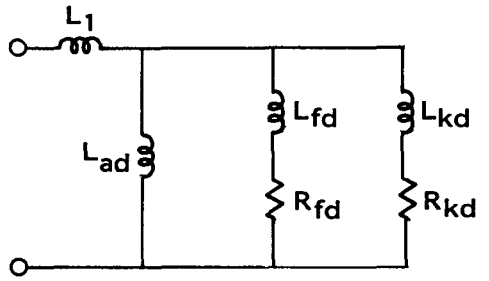

$$T'_{do} \approx \frac{L_{ad} + L_{fd}}{R_{fd}} \qquad T'_d \approx \frac{L_{fd}}{R_{fd}}$$

$$T''_{do} \approx \frac{L_{ad} + L_{kd}}{R_{kd}} \qquad T''_d \approx \frac{L_{kd}}{R_{kd}}$$

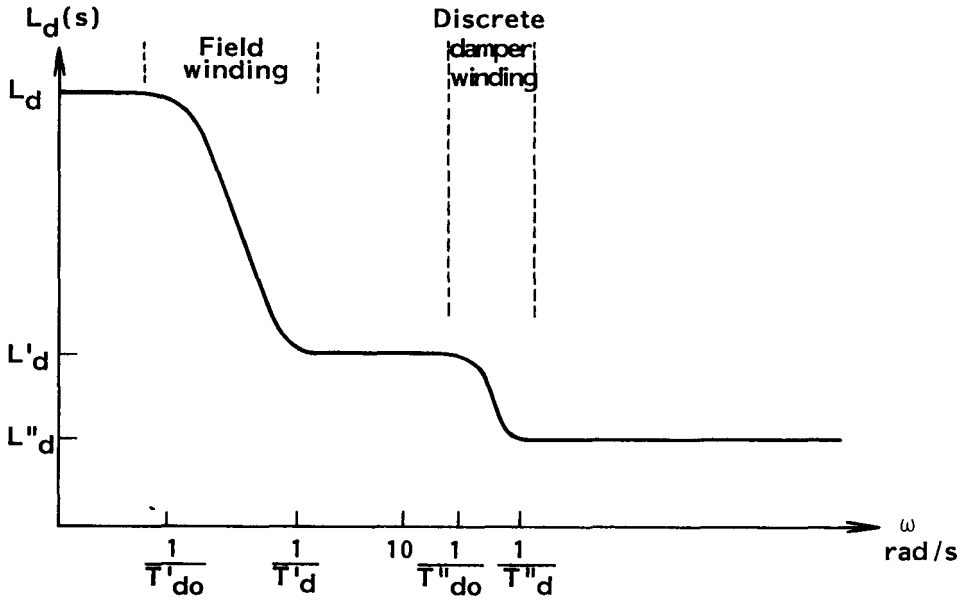

Figure 7-2. Direct Axis Operational Inductance and Equivalent Circuit for a Machine With a Laminated Rotor and One Discrete Damper Winding.

In this case, there are four breaks in the $L_d(s)$ curve, two produced by the field winding and two by the damper. As before, the magnitude starts out equal to the synchronous inductance at low frequencies and starts to decrease at 20 db/decade according to T'_{do}, the transient open circuit time constant. It levels off at the transient inductance $L'_d = L_l + L_{ad} \| L_{fd}$. Then, at even higher frequencies when the damper winding comes into play, the magnitude goes down again (at 20 db/decade) and levels off at the subtransient inductance, $L''_d = L_l + L_{ad} \| L_{fd} \| L_{kd}$. This is the lowest value that $L_d(s)$ will reach using the accompanying equivalent circuit, and is also realistic for machines of this type; eg, hydraulic generators with laminated pole pieces.

Note that the time constants associated with the damper winding, T''_{do} and T''_d are inversely proportional to the damper winding resistance. This means that the portion of the $L_d(s)$ curve which is dependent on the damper can move along the frequency axis with changes in the damper winding resistance.

Turbine generators imply a very different rotor design. There are no insulated laminations to block electric currents in the magnetic iron of the rotor body, and even more important, the field windings are held in slots in the rotor forging by metal wedges. This means that currents can be induced not only in the discrete conductors of the field winding, but also in the multitude of circuits formed by the rotor body and the slot wedges.

Any currents induced in this damper structure (rotor body plus slot wedges) will have a non-uniform radial distribution with the highest current density at the outer surface of the rotor (skin effect). To represent this damper structure rigorously, an equivalent circuit with an infinite number of rotor circuits would be required. Even to do it with sufficient accuracy for practical purposes, a large number of circuits would be necessary if the complete frequency spectrum were to be modelled.

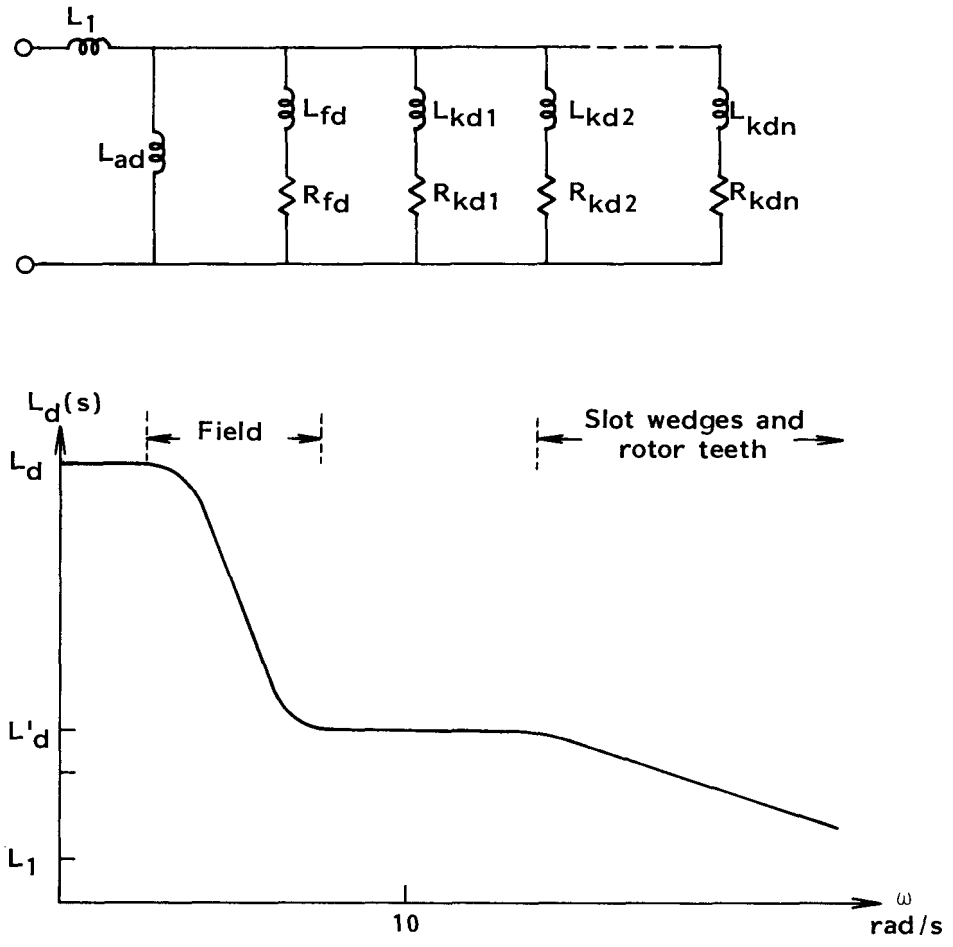

Figure 7-3. Direct Axis Operational Inductance and Equivalent Circuit For A Turbogenerator With a High Resistance Damper Structure.

Figure 7-3 illustrates how this complex damper influences the magnitude of the direct axis operational inductance. The field winding has the same effect as in the previous examples. However, the region of influence of the damper is distinguished by a slope considerably less than 20 db/decade which will ultimately bring the magnitude of the operational inductance down to the stator winding leakage inductance:

$$\lim_{s \to \infty} L_d(s) = L_l + L_{ad} \| L_{fd} \| L_{kd1} \| L_{kd2} \| \cdots \| L_{kdn}$$

$$= L_l$$

The less than 20 db/decade slope is a natural consequence of the distributed character of the damper structure.

Note that the region of influence of the damper in Figure 7-3 is well outside the range of frequencies important for stability studies (around 10 rad/s). A characteristic such as this is typical of modern turbogenerators with short, segmented slot wedges and no means for enhancing current transfer between adjacent wedges such as a copper backing strip. The Lambton generators are of this type.

An impression of the importance of the slot wedges to the dynamic performance of a turbogenerator can be gained by considering the distribution of transient currents in the damper structure. Even at frequencies as low as 10 rad/s, the depth of penetration of the induced current in the rotor teeth is typically only 2 to 3 cm, or about the depth of the slot wedges. In the wedge material itself, the depth of penetration is in the order of 6 cm at 10 rad/s. Thus, it is apparent that high conductivity, non-magnetic slot wedges are potentially capable of dominating the response of the damper structure in the important frequency range around 10 rad/s. The extent of this dominance depends on the resistance of the total series current path through the wedges. In the case of the Lambton machine, typified by Figure 7-3, this resistance is relatively high. Each slot contains many wedges and the wedge current has to transfer to and from a rotor tooth to get to the next wedge in the slot. This means that, in addition to the resistance of the current path around the ends of the rotor, there are also two contact resistances in series with each of the many wedges per slot.

The Nanticoke machine is quite different. Each slot containing field winding conductors has a single wedge running the full length of the rotor. This means that all of the wedge-to-wedge contact resistances present in a short wedge design are eliminated, leaving only the resistance of the current path around the ends of the rotor in addition to that of the wedges themselves.

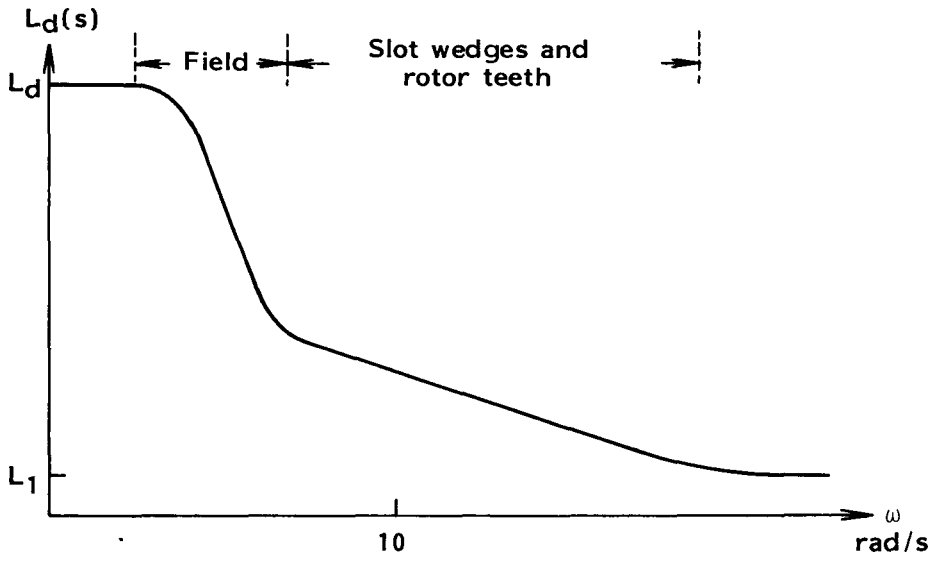

Figure 7-4. Direct Axis Operational Inductance For a Turbogenerator With a Low Resistance Damper Structure.

The effect of this design on the operational inductances can be seen in Figure 7-4. The lower resistance of the damper structure has moved its region of influence back along the frequency axis to the point where it is now right in the midst of the range of frequencies important to the performance of generators in stability studies.

The presence of a damper structure influence in this frequency range has at least two important consequences to the power system analyst. First, a more detailed generator model will be required to reproduce the gradual slope of $L_d(s)$ through the range of frequencies in which the machine must be accurately modelled. The second is that any change in the resistance of the damper structure will have a significant influence on the parameters of the model. This, of course, is not a problem in machines with high resistance dampers since even a 50% change in resistance would still leave the region of damper influence outside the important frequency range around 10 rad/s.

The first point is an action on authors and maintainers of stability programs to provide for the most complicated model structure that is likely to be required. The second is directed to those who produce the parameters for these generator models. They should ensure that the measurements and/or calculations used to obtain the equivalent damper parameters are realistic. In particular, due regard should be given to contact resistances in the damper structure since they can change significantly with contact pressure. The contacts among the slot wedges, copper liners, and retaining rings which are included in the current path around the end of the rotor can vary with the central forces produced by rotation; so, the resistance of this path is likely to be different at standstill than at rated speed. If these contact resistances are a significant portion of the total slot wedge circuit resistance, then standstill frequency response tests may yield a different effective damper resistance than exists at rated speed. In machines with short wedges, the interwedge resistances may very well swamp out any changes in the resistance of the path around the end of the rotor; and even if this is not the case, changes in the total damper resistance are likely to be unimportant since its domain of influence does not extend into the crucial range of frequencies around 10 rad/s. However, in machines with long wedges, the variable resistances may be very important, as implied by the experience with the Nanticoke machine, and both standstill and running tests may be necessary to obtain model parameters of sufficient accuracy.

SYNOPSIS

At the outset, the Lambton and Nanticoke generators were chosen for study because they seemed to be two machines with significant differences. The results from the project have confirmed this presumption. Not only is the rotor construction different, but also, the electrical parameters, and the complexity of the equivalent circuits required to simulate each machine's performance are notably dissimilar.

The relative simplicity of the Lambton generators and the apparent similarity of the Monticello unit is encouraging. The performance of both of these machines could be predicted accurately by a direct axis equivalent circuit with only two rotor windings (the field plus one damper). Furthermore, the parameters of the equivalent circuit could be measured from standstill tests alone. This means

that for generators of this type, there now exists a simple, safe test method which will allow manufacturers to deliver a dependable model verified by, or derived from tests before the machine is shipped to the customer.

The fly in the ointment, of course, is the Nanticoke machine. It needed a model with at least three rotor windings in each axis for accurate simulation of its performance; and perhaps worst of all, on-line frequency response tests were necessary to obtain the parameters for this model. The question that remains is, "How prevalent are generators of this type now, and what is likely to be the case in the near future?"

Until this question is answered, a recommendation that both complex models and on-line frequency response tests be adopted by the industry is difficult to justify. However, a defensible approach would be to make the standstill frequency response a standard test, and to provide for the more complex model structure in existing and future transient stability programs. The standstill tests have been shown to provide valuable data no matter what the machine's characteristics, and it is sound planning to have computer programs capable of handling the most detailed model structure likely to be encountered.

Section 8

CONCLUSIONS

The following conclusions have been drawn from the results reported in Parts 1 and 2 of this report:

1. A model structure incorporating three rotor circuits in each of the direct and quadrature axes plus rotor circuit mutual leakage elements in the direct axis was sufficiently detailed for all three generators studied. For two of the three machines, two rotor circuits per axis was enough.

2. Generator models with three rotor circuits per axis and rotor circuit mutual leakage elements have been successfully incorporated in both the Ontario Hydro (partitioned explicit structure) and the EPRI (simultaneous implicit structure) transient stability programs. The resulting increase in computation time was not significant in either program (Part 3).

3. For two of the three machines, the STANDARD model provided by the manufacturer was not satisfactory, judged on its ability to reproduce measured line switching transients.

4. A combination of standstill plus on-line frequency response tests yielded satisfactory models for all machines tested. Standstill tests alone were sufficient for two of the three machines.

5. Models from sudden short circuit tests and stator decrement tests (only available for Nanticoke) did not perform adequately (Part 2).

6. Calculating saturation in both the direct and quadrature axes on the basis of the direct axis open-circuit saturation curve produced substantial errors in internal angle because of inaccuracy in the q-axis synchronous reactance so obtained.

   Accurate saturation data was obtained for both the direct and quadrature axes from steady-state readings of various generator variables (including internal angle) over a broad range of loads.

7. The structure of a turbogenerator's rotor has a profound influence not only on its dynamic performance, but also on the amount of detail required to model it adequately. In particular, the Nanticoke machine with full length aluminum slot wedges backed by copper strips required the most detailed equivalent circuit structure and the largest amount of test data to produce a satisfactory model.

8. In simulations designed to check the accuracy of various generator models, careful representation of the external system was very important. Otherwise, errors due to inaccuracies in the model of the external system could mask the difference in performance between the generator models being compared.

9. Although standstill frequency response tests may not provide enough data for every generator (eg Nanticoke), the operational inductances so obtained enable one to decide whether or not on-line tests will be necessary.

10. The magnetic permeability of iron is lower for small flux changes than it is for larger excursions. This phenomenon was observed at both zero flux operating points (standstill frequency response tests) and at high flux density operating points (open-circuit linearity tests, Part 2).

    Models derived from standstill frequency response tests can be adjusted to "unsaturated" ones on the basis of direct current inductance measurements.

11. Rotor circuit leakage inductances are significantly influenced by magnetic non-linearities of the iron (60 Hz field impedance and open-circuit tests, Part 2).

Section 9

RECOMMENDATIONS

Based on the results of this project, and information generally available in the industry, we recommend:

1. That a generator model structure consisting of three rotor circuits on each of the direct and quadrature axes plus rotor circuit mutual leakage elements in the direct axis be adopted (Figure 9-1).

2. That standstill frequency response tests be incorporated in IEEE Standard No 115, "Test Procedures For Synchronous Machines", to provide model parameters directly and/or to verify manufacturers' calculated data.

3. That a test group consisting of a number of generators covering as broad a range of rotor constructions as possible be selected. Standstill frequency response tests should be done on each machine in the group, and the performance of the resulting models evaluated. The objectives of this work would be: to estimate the population of "Nanticoke type" machines, and to relate, quantitatively, the performance of standstill frequency response models to operational inductances measured by standstill tests.

4. That, until the results of recommendation 3 are available, any generator for which the direct axis operational inductance changes by more than 20% in the frequency range 1 Hz to 10 Hz be considered likely to require on-line frequency response tests for satisfactory modelling.

5. That manufacturers be encouraged to define the time constants and reactances that they supply as data for their machines.

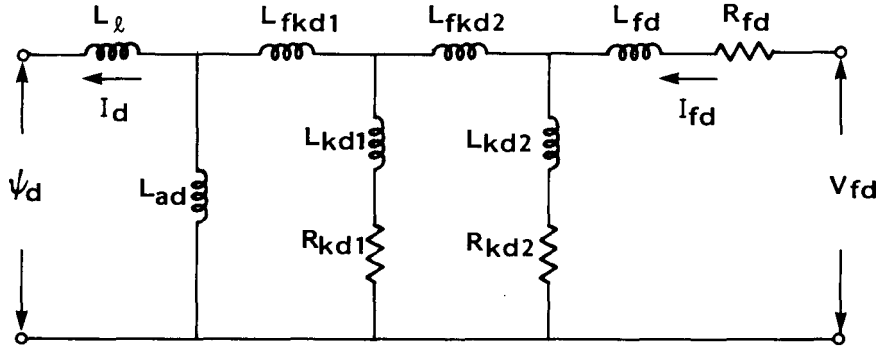

Direct Axis

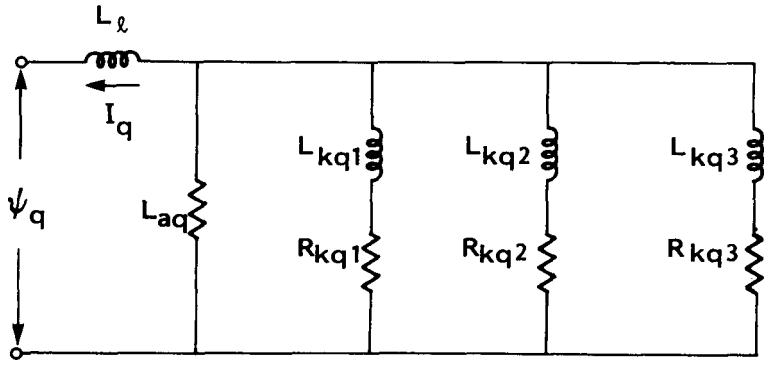

Quadrature Axis

Figure 9-1. Recommended Model Structure.

Appendix A

MATHEMATICS OF SSFR3 AND SSFR2 MODEL DERIVATION

SSFR3

Standstill frequency response tests in the d-axis, with field winding closed, yield the two functions $L_d(s)$ and $sG(s)$ which can be approximated by "curve fitting" procedures to transfer functions shown by equations 3-2 and 3-3 in the main text. In terms of the equivalent circuit elements shown in Figure 3-4 of the main text, the following relationships can be derived for the time constants of $L_d(s)$ and $sG(s)$,

$$T_1 + T_2 + T_3 = T_{kd1} + T_{kd2} + T_{ffd} - \frac{L_{ad}^2}{L_d R_o} = a_1 \tag{A-1}$$

$$T_1(T_2 + T_3) + T_2T_3 = (T_A + T_B + T_C)\left(M_1 - \frac{L_{ad}^2}{L_d}\right) + L_{fkd2}\left(T_A + \frac{L_{fkd1}}{R_p}\right) + \frac{L_{fd}}{R_{fd}}\left(T_{k1} + T_{k2}\right) + T_{k1}T_{k2} = a_2 \tag{A-2}$$

$$T_1T_2T_3 = \left(M_1 - \frac{L_{ad}^2}{L_d}\right)\left(T_AT_{k1} + T_A\frac{L_{fkd2}}{R_{kd1}} + \frac{T_{k1}T_{k2}}{R_{fd}}\right) + T_{k1}\left(T_AL_{fkd2} + \frac{L_{fd}}{R_{fd}}T_{k_2}\right) = a_3 \tag{A-3}$$

$$T_4 + T_5 + T_6 = T_{kd1} + T_{kd2} + T_{ffd} = b_1 \tag{A-4}$$

$$T_4(T_5 + T_6) + T_5T_6 = M_1(T_A + T_B + T_C)$$

$$+ \quad L_{fkd2}\left(T_A + \frac{L_{fkd1}}{R_p}\right)$$

$$+ \frac{L_{fd}}{R_{fd}}\left(T_{k1} + T_{k2}\right) + T_{k1}T_{k2} = b_2 \qquad \text{(A-5)}$$

$$T_4T_5T_6 = \left(M_1\ T_AT_{k1} + T_A\frac{L_{fkd2}}{R_{kd1}} + \frac{T_{k1}T_{k2}}{R_{fd}}\right)$$

$$+ \quad T_{k1}\left(T_A\ L_{fkd2} + \frac{L_{fd}}{R_{fd}}\ T_{k2}\right) = b_3 \qquad \text{(A-6)}$$

$$G_o = \frac{L_{ad}}{\omega_o R_{fd}} \qquad \text{(A-7)}$$

$$T_7 = \frac{L_{kd1}}{R_{kd1}} = T_{k1} \qquad \text{(A-8)}$$

$$T_8 = \frac{L_{kd2}}{R_{kd2}} = T_{k2} \qquad \text{(A-9)}$$

in which

$$\frac{1}{R_o} = \frac{1}{R_{kd1}} + \frac{1}{R_{kd2}} + \frac{1}{R_{fd}} \qquad \text{(A-10)}$$

$$M_1 = L_{ad} + L_{fkd1} \qquad \text{(A-11)}$$

$$T_{kd1} = T_{k1} + \frac{M_1}{R_{kd1}} \qquad \text{(A-12)}$$

$$T_{kd2} = T_{k2} + \frac{M_1 + L_{fkd2}}{R_{kd2}} \qquad \text{(A-13)}$$

$$T_{ffd} = \frac{L_{fd} + M_1 + L_{fkd2}}{R_{fd}} \qquad \text{(A-14)}$$

$$T_A = \frac{T_{ffd}}{R_{kd2}} + \frac{T_{kd2}}{R_{fd}} - \frac{2(M_1 + L_{fkd2})}{R_{kd2}R_{fd}} \qquad \text{(A-15)}$$

$$T_B = \frac{T_{ffd}}{R_{kd1}} + \frac{2M_{kd1}}{R_{fd}} - \frac{1}{R_{fd}R_{kd1}} \tag{A-16}$$

$$T_C = \frac{T_{kd1}}{R_{kd2}} + \frac{T_{kd2}}{R_{kd1}} - \frac{2M_1}{R_{kd1}R_{kd2}} \tag{A-17}$$

In the nine equations, A-1 to A-9 there are eight unknowns, namely, T_{kd1}, T_{kd2}, T_{ffd}, M_1, L_{fkd2}, R_{kd1}, R_{fd} and R_{kd2}. To assist in the solution equations A-1 and A-4, A-2 and A-5 and A-3 and A-6 can be combined thus:

$$\frac{1}{R_o} = \frac{L_d}{L_{ad}^2}(b_1 - a_1) \tag{A-18}$$

$$T_A + T_B + T_C = \frac{L_d}{L_{ad}^2}(b_2 - a_2) = K_1 \tag{A-19}$$

and

$$T_{k1}T_A + \frac{L_{fkd2}}{R_{kd1}}T_A + T_{k2}\frac{L_{fd}}{R_{kd1}R_{fd}} = \frac{L_d}{L_{ad}^2}(b_3 - a_3) = k_2 \tag{A-20}$$

By using equations A-4 to A-9 and A-18 to A-20 it is now possible to solve for these unknowns but the consequence of using equations A-18 to A-20 is that the individual equations of a_1 - a_3 and b_1 - b_3 will not be satisfied unless the input data and the equations form a consistent set. An iterative procedure was found necessary and the error was accepted in T_3.

Having solved the above equations it is now possible to obtain the parameters of the equivalent circuit in Figure 3-4, namely:

$$R_{fd} = \frac{L_{ad}}{\omega_o G_o} \tag{A-21}$$

$$L_{fkd1} = \frac{b_3 - T_7\,(b_2 - T_7\,(b_1 - T_7))}{k_2 - T_7\left(k_1 - \frac{T_7}{R_o}\right)} \tag{A-22}$$

$$R_{kd} = \frac{k_3}{(K_2 - T_7 T_A)} \tag{A-23}$$

$$L_{kd1} = T_7 R_{kd1} \tag{A-24}$$

$$\frac{1}{R_{kd2}} = \frac{1}{R_o} - \frac{1}{R_{fd}} - \frac{1}{R_{kd1}} \tag{A-25}$$

$$L_{kd2} = T_8 R_{kd2} \tag{A-26}$$

$$L_{fd} = R_{kd2} R_{fd} T_A - L_{kd2} \tag{A-27}$$

$$L_{fkd2} = R_{kd1}\left[\frac{1}{R_{fd}} + \frac{1}{R_{kd2}}\right]\left[k_1 - T_A - \frac{(L_{kd2} + L_{fd})}{R_{kd2} R_{fd}} - \frac{(L_{kd1} + L_{kd2})}{R_{kd1} R_{kd2}}\right] \tag{A-28}$$

in which

$$K_3 = b_2 - T_7(b_1 - T_7) - M_1\left(K_1 - \frac{T_7}{R_o}\right) \tag{A-29}$$

SSFR2

This model can be derived directly from equations A-1 to A-9 after first neglecting the second amortisseur winding, L_{kd2} and R_{kd2}, and the associated "mutual leakage" inductance L_{fkd2}. In effect this means that time constants T_3, T_6 and T_8 can be omitted from the $L_d(s)$ and $sG(s)$ transfer functions as well as equations A-1 to A-9. Precisely the same procedure is followed in deriving the two rotor winding model as was the case for the three rotor winding model. By making the above omissions, one obtains six equations in which there are five unknown quantities, namely L_{fkd1}, L_{kd1}, R_{kd1}, L_{fd} and R_{fd}. Because of this incompatability one is forced once again to adopt an iterative procedure, and in this case the error is taken up by T_2, the second numerator time constant in $L_d(s)$. The parameters of SSFR2 equivalent circuit are then governed by the following relationships,

$$R_{fd} = \frac{L_{ad}}{\omega_o G_o} \tag{A-30}$$

$$\frac{1}{R_{kd1}} = \frac{1}{R_o} - \frac{1}{R_{fd}} \tag{A-31}$$

$$L_{kd1} = T_7 R_{kd1} \tag{A-32}$$

$$L_{fd} = K_1 R_{kd1} R_{fd} - L_{kd1} \tag{A-33}$$

$$L_{fkd1} = R_o \left(b_1 - T_7 - \frac{L_{fd}}{R_{fd}}\right) - \frac{L^2_{ad}}{L_d R_o} \tag{A-34}$$

in which

$$\frac{1}{R_o} = \frac{(b_1 - a_1) L_d}{L^2_{ad}} \tag{A-35}$$

$$K_1 = \frac{(b_2 - a_2) L_d}{L^2_{ad}} \tag{A-36}$$

Appendix B

IDENTIFICATION OF SYNCHRONOUS MACHINE MODEL PARAMETER VALUES FROM ON-LINE FREQUENCY RESPONSE TEST RESULTS

MATHEMATICAL DEVELOPMENT

The differential equations describing the dynamics of a multi-machine power system can be arranged in the well known state-space form, namely:

$$\dot{\underline{x}} = [A]\underline{x} + \underline{b}\, e_{in} \tag{B-1}$$

taking the Laplace transform and rearranging the terms yields the following:

$$\underline{X}(s) = [sI-A]^{-1}\, \underline{b}\, \underline{E}_{in}(s) \tag{B-2}$$

Consequently, the calculated transfer functions, in the frequency domain, for the specified machine model can be obtained from

$$\begin{aligned} \Delta\omega/\Delta E_{in} &= G_1(j\ ) = \underline{C}_1^t\, [j\ I-A]^{-1}\, \underline{b} \\ \Delta E_t/\Delta E_{in} &= G_2(j\ ) = \underline{C}_2^t\, [j\ I-A]^{-1}\, \underline{b} \\ \Delta E_{fd}/\Delta E_{in} &= G_3(j\ ) = \underline{C}_3^t\, [j\ I-A]^{-1}\, \underline{b} \end{aligned} \tag{B-3}$$

in which ΔE_{in} is the change in AVR reference input

$\Delta\omega$ is the change in machine rotor speed

ΔE_t is the change in machine terminal voltage

ΔE_{fd} is the change in machine field voltage

$G(j\omega)$ is the appropriate transfer function

C^t is the output coefficient vector relating the particular $G(j\omega)$ to $\underline{X}(j\omega)$

I is the unit matrix

Let $H(j\ _i)$ be the measured transfer function at frequency $_i$(rad/sec). Thus, the error difference between the measured and calculated functions is:

$$E(j\omega_i) = H(j\omega_i) - G(j\omega_i)$$

and the normalized error difference is

$$E_n(j\omega_i) = 1 - \frac{G(j\omega_i)}{H(j\omega_i)} \tag{B-4}$$

The calculated transfer function $G(j\ _i)$ is a function of the model parameters (equivalent circuit resistances and inductances). Expanding the normalized error by using Taylor series, and considering only the first-order terms, one obtains an estimate for the change in error in terms of changes in model parameters. Thus,

$$\hat{E}_n(j\omega_i) = -\sum_{k=1}^{N} \frac{\partial E_n(j\omega_i)}{\partial \theta_k} \cdot \Delta\theta \tag{B-5}$$

where N is the total number of adjustable model parameters. Consequently, as a first approximation equations (B-4) and (B-5) can be considered equal, thus

$$1 - \frac{G(j\omega_i)}{H(j\omega_i)} = -\sum_{k=1}^{N} \frac{\partial E_n(j\omega_i)}{\partial \theta_k} \cdot \Delta\theta_k \tag{B-6}$$

Considering N/2 discrete frequencies in equation (B-6) the following relationship can be established between the normalized error vector $\underline{E}_n$ and the complex Jacobean matrix $[J_c]$, namely

$$\underline{E}_n \cong [J_c]\,\Delta\underline{\theta} \tag{B-7}$$

Equating the real and imaginary parts in equation (B-7)

$$\begin{bmatrix} \underline{E}_{n_R} \\ \underline{E}_{n_{im}} \end{bmatrix} \cong \begin{bmatrix} J_R \\ J_{im} \end{bmatrix} \cdot \Delta\underline{\theta} \tag{B-8}$$

and hence

$$\Delta\underline{\theta} \cong [J]^{-1}\, \underline{E}_n \tag{B-9}$$

The Jacobian matrix J is computed using as starting values the set of model parameters obtained from standstill (or other) models. The change in these parameters, $\Delta\underline{\theta}$, is then estimated using equation (B-9). The process is repeated until the error is minimized, ie, no successive improvement in the calculated transfer function compared to the measured transfer function is achieved.

COMPUTATION OF ERROR DERIVATIVES

The error derivatives $\partial E_n(j\omega_i)/\partial\theta_k$ in equation (B-5) are calculated as described below. Differentiating equation (B-4) with respect to the k^{th} parameter θ_k one obtains,

$$\frac{\partial E_n(j\omega_i)}{\partial\theta_k} = -\frac{1}{H(j\omega_i)} \cdot \frac{\partial G(j\omega_i)}{\partial\theta_k} \tag{B-10}$$

Now from (B-3)

$$\frac{\partial G}{\partial\theta_k}(j\omega_i) = C^t \frac{\partial}{\partial\theta_k} [j\omega_i I - A]^{-1} \cdot \underline{b} \tag{B-11}$$

Since

$$[I] = [j\omega_i I - A]^{-1}[j\omega_i I - A] \tag{B-12}$$

and denoting $Z(j\omega_i) = [j\omega_i I - A]^{-1}$

$$\frac{\partial}{\partial\theta_k} Z(j\omega_i) = -Z(j\omega_i)\left(\frac{\partial}{\partial\theta_k}[j\omega_i I - A]\right)Z(j\omega_i) \tag{B-13}$$

Since only the A matrix is a function of the variable parameters,

$$\frac{\partial E_n(j\omega_i)}{\partial \theta_k} = \frac{1}{H(j\omega_i)} \cdot \underline{C}^t \cdot Z(j\omega_i) \cdot \frac{\partial A}{\partial \theta_k} \cdot Z(j\omega_i) \cdot \underline{b} \qquad \text{(B-14)}$$

Appendix C

PROGRAM FOR MODIFYING SYNCHRONOUS MACHINE EQUIVALENT CIRCUIT PARAMETERS USING ON LINE FREQUENCY RESPONSE TEST DATA

GENERAL DESCRIPTION

The programs described here are mainly developed for identifying synchronous machine parameter values using on-line frequency response measurements. In the course of development, state-space coefficient matrices, describing power system dynamics, were required. The Ontario Hydro small signal stability program builds up these matrices in a very convenient form which can be appropriately used for the identification purpose.

In this program the synchronous machines can be represented either in detail or by a classical model (constant voltage behind transient reactance). The detailed model is used for machines close to the area of interest and the simple classical model is used for the rest of the machines. Provision is also made for representing infinite buses.

The network constraints are expressed as a set of algebraic equations relating perturbed values of generator voltages and currents. Loads can be modelled as constant impedances or as voltage dependent loads.

In the formulation of the coefficient matrix, the states ψ_d, ψ_q associated with the generator stator transients are retained.

To execute the program, data related to the following have to be provided:

1. Network and load flow data representing the system steady state operating condition about which the small signal stability has to be determined.

2. Constants of the generators and their controls representing the dynamic characteristics.

The network and load flow data is normally read from an output tape created by the Ontario Hydro Load Flow Program. However, an option is provided to read this data from cards.

The load flow data (read either from tape or cards) is processed by Conversion Program which converts it into a more convenient form for use by the Dynamic Stability Program. The conversion involves formation of the node admittance matrix relating the perturbed values of generator currents and voltages. The node admittance matrix is then transformed into a mixed matrix form.

PROGRAM STRUCTURE

Three separate programs are used to calculate changes in synchronous machine model parameters to give good matching of the measured on-line frequency responses. The first program (Load Flow Conversion) reads the Load Flow data, corresponding to the test conditions, which are determined using the Ontario Hydro A.C. Load Flow program. This data is processed and rearranged by this program to a format which can be appropriately used to formulate the state-space coefficient matrices. The converted output is stored on unit #8.

The load flow conversion data (from unit #8) and the system dynamic simulation data (machine and control parameters) are then used by the second program to compute the A matrix and its derivatives. This program is called STATE-SPACE COEFFICIENT MATRIX BUILD UP. The output of this program is stored on unit #19.

The last program (Model Identification) uses the information on unit #19 along with its input data to calculate the changes in the machine model parameters.

It should be noted that the Load Flow conversion program is used only once since only one operating condition is considered. However, the formulation of the A matrix and its derivatives, as well as the parameter change calculation, should be performed for each set of machine model parameter values.

Sample Run Stream

```
@ ASG,A     PROGFILE.
@ ASG,T     CONVX.
@ ASG,VT    LFTAPE.
@ USE 8.,   CONVX
```

```
@ USE 27.,  LFTAPE.
@ XQT       PROGFILE.  CONVERSION
```

CONVERSION DATA

```
@ ASG,T     SC.
@ ASG,T     TEMP.
@ ASG,A     MMDATA.

@ USE 1.,   SC.
@ USE 8.,   CONVX.
@ USE 12.,  TEMP.
@ USE 19.,  MMDATA.
@ XQT       PROGFILE.  SS-MATRIX
```

DYNAMIC SIMULATION DATA

```
@ USE 19.,  MMDATA.
@ XQT       PROGFILE.  IDENT
```

IDENTIFICATION DATA

DATA INPUT FOR LOAD FLOW CONVERSION PROGRAM
FOR STATE-SPACE COEFFICIENT MATRIX COMPUTATION

1. LFNO.,KEYLF - FORMAT (2I10)

   LFNO. = LF number
   KEYLF - If equal to zero, LF data from tape
           If not equal to zero, LF DATA FROM CARDS

2. BASE MVA - FORMAT (F10.5)

   BASE MVA - Must be same as in LF

3. NM,NFT,NINF,NLBS - FORMAT (4I10)

   NM = No. of generators modelled in <u>detail</u>
   NFT = No. of generators represented by classical model

NINF = No. of infinite buses. Normally read zero.
If desired, infinite buses can be represented separately in the dynamic stability program.
NLBS = No. of non-linear load buses

4. NGEND(I),I=1,NM - FORMAT (8I10)

NGEND = Bus no. in the LF for generators modelled in detail.

5. NINFB(I),I=1,NINF -FORMAT (8I10)

NINFB = Bus no. in the LF for infinite buses
(if NINF = 0, by-pass)

6. NGENC(I),X'_d(I),I-1,NFT -FORMAT (I10,F10.5)

NGENC = Bus no. in the LF for generators represented by classical model
X'_d = Transient reactance (or Thevenin's reactance)
Must be greater than zero (should be on MVA base).

One card providing above data for each generator.
Total of NFT cards.

7. NLOAD(I),PFRAC(I),OFRAC(I),NP(I),NO(I),I=1,NLBS
- FORMAT (I10,4F10.5)

One card for each non-linear load bus, if any.
NLOAD = Bus no in LF for the non-linear load
PFRAC = Fraction of the real component of load at the bus to be treated as non-linear load
QFRAC = Fraction of the imaginary component to be treated as non-linear load
NP,NQ = exponential power defined by:

$$P_{NL} \propto V^{NP}$$
$$Q_{NL} \propto V^{NQ}$$

Notes on LF Conversion

Generator Buses.

1. The program assigns internal bus numbers depending on the order in which the associated bus numbers are read. In other words, the order in which bus numbers NGEND(I), NGENC(I) and NINFB(I) and NINFB(1) are read determines the internal bus numbers.

2. The data should be read such that the generators which are intended to be treated as infinite buses appear last. Usually, it is better to read the bus numbers of generators electrically close to the area of interest first.

3. NOTE THAT NM CANNOT BE GREATER THAN 4 AND NFT CANNOT BE GREATER THAN 40.

4. If KEYLF = 0, the LF data is read from cards. This feature is useful when LF output tape created by Ontario Hydro LF program is not available.

Load Buses.

1. Any fraction of the real and/or imaginary component of load at any bus can be treated as a specified exponential power of the voltage at the bus.

2. Load at a generator bus can also be treated as a non-linear load.

DATA INPUT FOR
COMPUTING THE A-MATRIX AND ITS DERIVATIVES

1. Descriptive Data - Format (20 A4)
2. NM, MM, , BMVAC - Format (3I10, F10.5)
3. IRDT - Format (I10)

IRDT provides option for reading LF Conversion data from tape or cards (read from LF tape if IRDT = 1). If not equal to 1, LF conversion data from cards (Appendix 3).

4. Data for generators represented in detail

(a) Generator Data:

X_{ad}, X_{aq}, X_{a1}, X_{fd}, X_{kd1}, X_{kq1}, X_{kq2} - Format (7F10.5)

R_a, R_{fd}, R_{kd1}, R_{kq1}, R_{kq2}, BKVM, BMVAM, BKVC - Format (8F10.5)

X_{kd2}, X_{kq3}, X_{fkd}, R_{kd2}, R_{kq3} - Format (5F10.5)

H, KDAMP - Format (2F10.5)

ISAT, A_{SAT}, B_{SAT}, ψ_L, K_{SAT} (Limit) - Format (I10,4F10.5)

(b) Excitation System Data:

As appropriate to the exciter key selected (see attached models).

5. Data for generators represented by a classical model. One card for each of NFT machines specified in LF conversion - total of NFT cards.

H, KDAMP - Format (2F10.5)

Excitation System Models

Although the Ontario Hydro small signal stability program accommodates a wide variety of excitation system models, only two models are considered for the current purpose of parameter identification. The block diagram representation and the format of data input for these models are given below:

(1) Thyristor Exciter Without Delta-Omega Stabilizer - Key = 2

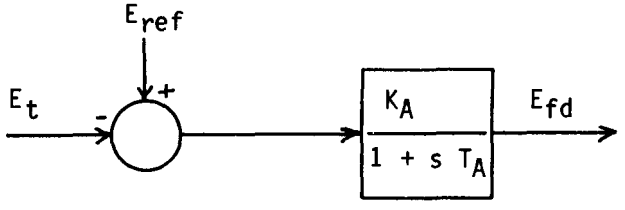

Parameters As Read By The Program (1 Card)

K_A, T_A, , Key No. - Format (2F10.5,40X,I10)

(2) Thyristor Exciter With Delta-Omega Stabilizer - Key = 7

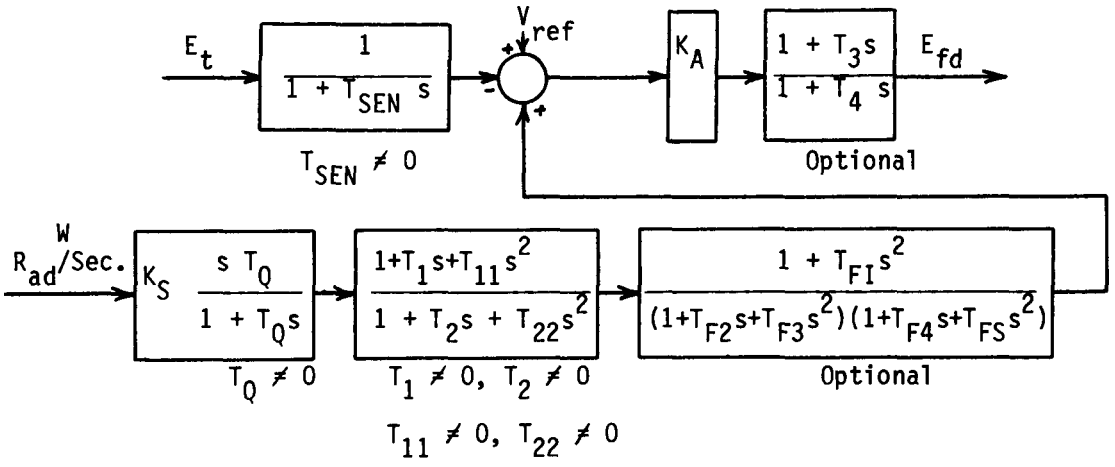

Paramaters as Read by the Program (2 Cards)

K_A, T_{SEN}, T_1, T_2, K_S, T_Q, Key No., IFLT - Format (6F10.5,2I10)

T_3, T_4, T_{11}, T_{22} - Format (4F10.5)

Torsional Filter Data (Only if IFLT = 1)

Torsional Filter Data

T_{F1}, T_{F2}, T_{F3}, T_{F4}, T_{F5} - Format (5F10.5)

Notes on Data Input

1. NM = No. of generators represented in detail. This should be same as that used for LF conversion and can not be greater than 4.

   MM = No. of generators represented by classical model. MM should be less than or equal to the corresponding value NFT used for LF conversion. It can not be greater than 40. If MM is less than NFT, the dynamics of the first MM of the classical generators are accounted for. The remaining generators will be treated as infinite buses, ie, the voltages behind their transient reactances will be fixed in magnitude and angle.

2. IRDT - If not equal to 1, LF conversion data is read from cards. This is used for very small systems for which creation of LF tape as well as LF dataconversion are unnecessary.

3. Generator Data

The order in which the generator data is read should correspond to the order in which the bus numbers NGEND(I) are read in the LF conversion.

Equivalent Circuit Parameters.

BKVM, BMVAM are the base kV and MVA on which the generator data is read. The program converts to reactances, resistances, inertia constant and damping factor to BKVC and BMVAC. If any one of BKVM, BMVAM, BMVAC is equal to zero, the generator constants read are assumed to be on common base MVA and kV and no conversion is performed.

The following points apply to all machines represented in detail:

1. X_{a1} can not be zero.

2. X_{Kd1}, X_{Kd2}, X_{Kq1}, X_{Kq3} or X_{FKd} can be negative.

3. If X_{Kd2} or X_{Kq3} equal to zero, the corresponding rotor circuit assumed to be absent.

Inertia Constant and Damping.

H = Inertia constant in MWSec/BMVAM
KDAMP - Damping factor in pu torque (on BMVAM base) per pu speed deviation.

Saturation.

A_{sat},B_{sat}, ψ_L are constants used to describe the non-linear portion of the open-circuit saturation characteristic, thus:

$$\psi_I = A_{sat}\exp(B_{sat}(\psi_a - \psi_L))$$

where:

ψ_I = change in flux linkages due to saturation at any given operating point (terminal voltage)

ψ_a = flux linkages corresponding to any given operating point (terminal voltage)

ψ_L = limiting value of flux linkages at which machine becomes saturated

The saturation factor K_{sat} is given by:

$$K_{SAT} = \frac{\psi_a}{\psi_a + \psi_I}$$

The incremental and total saturation factors satisfy the following constraints:

$$K_{SAT(abs)} \geq K_{SAT(incr)} \geq K_{SAT(Limit)}$$

If ISAT=0 - Round Rotor machine with $K_{SAT(incr)}=K_{SAT(abs)}$
ISAT-1 - Round Rotor machine with $K_{SAT(incr)}$ equal to incremental slope of the saturation curve
ISAT=2 - Salient Pole machine with $K_{SAT(incr)}=K_{SAT(abs)}$
ISAT=3 - Salient Pole machine with $K_{SAT(incr)}$ equal to incremental slope.

The program also provides the option of specifying the actual values of the saturation factors. This is achieved by reading ISAT=4, in which case the program assumes the following:

$K_{sat(abs)d} = A_{sat}$ $\qquad$ $K_{sat(incr)d} = B_{sat}$

$K_{sat(abs)q} = \psi_L$ $\qquad$ $K_{sat(incr)q} = K_{sat(LIMIT)}$

DATA INPUT FOR MODEL IDENTIFICATION PROGRAM

1. IORDER, NPT - FORMAT (2I10)

   IORDER - Order of the test machine model (2 or 3)
   NPT - Number of selected frequency points (note greater than 7)

2. E(I) - I=1,NPT - FORMAT (8F10.6)

   E(I) - The value of transfer function $\Delta\Omega/\Delta E_{in}$ at the ith frequency

3. ET(I) - I=1,NPT - FORMAT (8F10.6)

   ET(I) - The value of transfer function $\Delta E_t/\Delta E_{in}$ at the ith frequency

4. EFD(I) - I=1,NPT - FORMAT (8F10.6)

   EFD(I) - The value of transfer function $\Delta E_{fd}/\Delta E_{in}$ at the ith frequency

5. F(I) - I=1,NPT - FORMAT (7F10.6)

   F(I) - I=1,NPT - FORMAT (UF10.6)

Notes on the Identification Program

1. The program assumes that all the units represented in detail have identical generator models.

2. The test unit should be listed at the last generator of the units represented in detail.

3. IORDER could be chosen as 2 or 3 depending on machine model order. If equal to 2, the number of selected frequencies should be 5 and only ten parameters are subjected to change. In this case only one damper circuit is considered in the d-axis and two in the q-axis.

   If ORDER = 3, three rotor circuits are considered on both axis. The number of selected frequency points can be equal to 6 or 7. If equal to 6, the number of parameters subjected to change will be 12, and if equal to 7 the number of parameters will be 14.

4. The output of the program consists of an estimate of the error and the calculated changes in the model parameters at the step considered.

PROGRAM LISTING FOR COMPUTATION OF THE A-MATRIX AND DERIVATIVES

```
C      STATE-SPACE MODEL FOR MULTIMACHINE SYSTEM
C      BUILDS THE COEFFICIENT MATRIX A  AND  FINDS THE EIGEN VALUES
C
C      PRABHASHANKAR KUNDUR
C
C
C        MAX NO. OF GENERATORS REPRESENTED IN DETAIL=8
C        MAX NO. OF GENERATORS REPRESENTED BY X1D =40
C
C        PARAMETER SETTING
C
       PARAMETER MDIM=100
        PARAMETER MDIMEX=MDIM*MDIM
       DIMENSION  ITEXT(20)
       DIMENSION SND(10), CSD(10), AL1(10), AL2(10), AL3(10), AL4(10),
     1 AL5(10), R(10), AKTD(10),AKTQ(10), TC1(10), TC2(10), TV1(10),
     1 TV2(10),AL6(10),AL7(10),AL8(10)
       DIMENSION XXM(10,10),TIME(6,10),HMH(10),DAMPP(10),ISST(10),
     1 ASST(10),BSST(10), BSTL(10),SSTL(10),XXTR(11,10),GTQN(10)
       DIMENSION EMD(40),EMQ(40),HMM(40)
       DIMENSION              AKED(20),AKEQ(20)
       DIMENSION D1(40,8), D2(40,8), D3(40,8), D4(40,8)
      DIMENSION Z1(8,8), Z2(8,8), Z3(8,8),Z4(8,8),Z6( 8,40), Z5( 8,40),
     1 B1(8,8), B2(8,8), B3(8,8), B4(8,8), B5( 8,40), B6( 8,40)
       DIMENSION RN(8,8),XN(8,8),RG(8,40),XB(8,40), GN(40,40),BN(40,40)
       DIMENSION EMNEW(8), PWNEW(8),PXNEW(8),ANGNEW(8)
       DIMENSION INAME1(50), INAME2(50),NOLD(50)
       DIMENSION ITYPE(25), T1T2R(25), ITFLT(25), XTFL(5,10)
       DIMENSION EMN(40),ANG(40),PW(40),PX(40)
       DIMENSION A(MDIM,MDIM)
       COMMON /WORKFI/ DUM(MDIMEX)
        DIMENSION LDESC(13),X0(MDIM),NII(MDIM),LISTO(MDIM)
      DIMENSION IAE(MDIM,MDIM)
      EQUIVALENCE(IAE,A)
       DIMENSION HMCF(40),DAMPCF(40)
       DIMENSION WRFX(10)
       DIMENSION EFC(10)
      INTEGER EQUIL
      COMMON/INPUT/EQUIL,NPERM,N,NPRINT
       NDIM=MDIM
C
C
C       NM=NO. OF MACHINES REPRESENTED IN DETAIL
C       MM=NO. OF MACHINES REPRESENTED BY TRANSIENT REACTANCE
C       NM0=NO. MACHINES WITH CONST EFD
C       NM1=NO.OF MACHINES WITH STATIC EXTR & SPEED SIGNAL(INCLUDING THOSE
C       HAVING ANGLE SIGNAL AND/OR TGR)
C       NM2=NO. OF MACHINES WITH STATIC EXCTR ONLY
C       NM3=NO. OF MACHINES WITH CONVL EXCTR
C       NM4=NO. OF MACHINES WITH AMPLDN EXCTR
C       NM5=NO.OF MACHINES WITH STATIC(SPEED SIGNAL) HAVING ANGLESIG AND
C       /OR TGR
C       NM6=NO. OF MACHINES WITH STATIC EXTR & SPEED SIGNAL WITH SECOND  ORDER
C       PHASE LEAD &  TGR
C         NMFLT=NO.OF MACHINES WITH TORSIONAL FILTERS
C
C       ITYPE(N)=0--CONST EFD
C       ITYPE(N)=1---- STATIC WITH SPEED SIGNAL
C       ITYPE(N)=2-- ONLY STATIC
C       ITYPE(N)=3 --- CONVNL
C       ITYPE(N)=4 ---AMPLYDN
C       ITYPE(N)=5 --- STATIC WITH SPEED AND ANGLE SIGNAL
C       ITYPE(N)=6 --- STATIC WITH SPEED AND TGR
C       ITYPE(N)=7 - STATIC WITH SPEED SIGNAL,2ND ORDER PH LD,TGR
C         ITFLT(N)=1  - - - -  TORSIONAL FILTER (FOR ITYPE=1,5,6,7 ONLY )
C       ITPYE(N)=8 --- SELF EXCITED D.C. EXCITER
C
C         ISAT=0  ROUND ROTOR MACHINE WITH INCREMNTL SAT SAME AS TOTAL SAT
C         ISAT=1  ROUND ROTOR MACHINE WITH INCREMNTL SAT EQUAL TO INCRMNTL SLOPE
C         ISAT=2  SALIENTPOLE MACHINE WITH INCREMNTL SAT SAME AS TOTAL SAT
C         ISAT=3  SALIENTPOLE MACHINE WITH INCREMNTL SAT EQUAL TO INCRMNTL SLOPE
C
```

```
C        ISAT=4  EACH OF FOUR SATURATION FACTORS SPECIFIED
 1018 FORMAT(3I10,F10.5,I10,4I5)
  518 FORMAT(I10,5F10.5)
 1008 FORMAT(8I10)
 2357 FORMAT(           11H1STUDY NO.=   ,I3,10X ,20A4//2X,
     1  ' DATA FOR GENERATORS'  )
 5000 FORMAT(//4X, 'GENERATOR NO.=', I3,5X,2A6/)
 5100 FORMAT(4F10.5,2A6)
 1208 FORMAT (4F10.5)
 4098 FORMAT(I10,4F10.5)
 1207  FORMAT(7F10.5,I10)
 1209 FORMAT (8F10.5)
 1409 FORMAT(6F10.5,2I10)
 1410 FORMAT(/ 6X,'EXCITER DATA', 2X,'KEY=',I2)
 1411  FORMAT(/22X,'XAD=',F7.5,4X,'XAQ=',F7.5,4X,
     1     'XAL=',F7.5,4X,'XFL=',F7.5,4X,'XD1=',F7.5,
     2      4X,'XQ1=',F7.5,4X,'XQ2=',F7.5,/,
     3      22X,'RA=',F8.6,4X,'RF=',F8.6,4X,
     4      'RD1=',F7.6,4X,'RQ1=',F7.6,4X,
     5      'RQ2=',F7.6,/,
     6      22X,'XD2=',F7.5,4X,'XQ3=',F7.5,4X,
     7      'XC=',F8.5,4X,'RD2=',F7.6,4X,'RQ3=',F7.6)
 1412 FORMAT(/22X, 'ET=', F8.3,4X, 'ANG=',F7.3, 4X,'P =',F8.3, 4X,
     1 'Q=', F8.3, 4X, 'H=',F8.3,4X, 'DAMP=',F6.3)
 2410 FORMAT(6X,7F15.5)
C
       REWIND 19
        W0 =377.
       IKP1=1
       BIG=9999999.0
       RADIAN=57.29578
       HPII=3.14159256/2.0
       SMALL=1.E-6
        IOPT=1
        IOPTIN=0
        IOPTA=0
       IIREAD=12
 2348 FORMAT(2I10)
 9994 FORMAT(20A4)
C      ISTD=1   PRINT A MATRIX
C        IF IPSI=0 ELIMINATE STATOR TRANSIENTS AND SET W/W0=1
C
       READ(5,9994) (ITEXT(I),I=1,20)
CMMC2
       READ(5,1018) NM,MM,ISTD,BASPC,IPSI,IIOPT,IIOPTI,IIKEY
       IPSI=1
       IIOPT=61
       IIOPTI=5
       IIKEY=1
       IDIST=1
        IF(IIOPT.EQ.0)IIOPT=1
        IF(IIOPTI.EQ.0)IIOPTI=1
         IF(IIOPT.EQ.IOPT.AND.IIOPTI.EQ.IOPTIN.AND.IIKEY.EQ.0)GOTO 4700
        IOPT=IIOPT
        IPOTIN=IIOPTI
       IF(IOPT.LT.4)GOTO 4700
C                                  *****      RESPONSE PREDICTION
C
      DO 1301 I=1,N
 1301 X0(I)=0.
C     READ NON ZERO INITIAL CONDITIONS
C     IX0 IS THE NUMBER OF NON ZERO ENTRIES
      IF(IOPT.GT.50) GO TO 9
      READ(5,1302) IX0
      READ(5,1302) ((NII(I),X0(I)),I=1,IX0)
   9  CONTINUE
       MCNO=2
       NCHNL=1
       LISTO(1)=10
       TAU=.04
       TFIN=2.
C         *IOPT=1     EIGENVALUES ONLY
C         *IOPT=2     EIGENVECTORS
C         *IOPT=3     RECIPROCAL EIGENVECTORS
C         *IOPT=4     CLOSED FORM TIME RESPONSE
```

```
C         *IOPT=5     PLOTTED TIME RESPONSE
C          IOPT=6     CONTROLLABILITY AND OBSERVABILITY MATRICES
C          IOPT=7     MODAL INPUT-OUT DESCRIPTION
C          IOPT=8     MODAL INPUT-OUTPUT DESCRIPTION -EXPRESS
C          IOPT=9     FREQUENCY RESPONSE
C     IOPTIN=0        MATRICES ARE PASSED THRO COMMON BLOCKS
C     *IOPTIN=1        MATRICES ARE READ FROM UNIT12
C     *IOPTA=0         GENERALIZED NAMES FOR STATES,INPUTS AND OUTPUTS
C     IOPTA=1         NAMES FOR STATES,INPUTS AND OUTPUTS ARE INPUTTED
C
C
C
 4700   CONTINUE
 1313 FORMAT(2F10.5)
 1310 FORMAT(26I3,2X)
 1302 FORMAT(5(I5,F10.5))
 1937 FORMAT(13A6,2X)
C
C
       IERN=1
       IF(NM.GT.8) GO TO 181
       IF(MM.GT.40)GO TO 181
C
       NTT=NM+MM
C
       WRITE(6,9995)(ITEXT(I),I=1,20)
 9995 FORMAT(///1X,20A4)
       WRITE(6, 8000)
 8000 FORMAT(/// 2X, 26HPARAMETERS OF THE NETWORK    /)
C
C        IF IRDT=1  READ NETWORK DATA FROM TAPE
C
       READ(5,1008) IRDT
C
       IF(IRDT.EQ.1)GO TO 4099
C
C
       DO 8009 I=1,NM
       DO 8009 J=1,NM
       XN(I,J)=0.
 8009  RN(I,J)=0.
 9009 READ  (5,8008) IM,I,K,RN(I,K),XN(I,K)
       XN(K,I)=XN(I,K)
       RN(K,I)=RN(I,K)
      WRITE (6,8008) IM,I,K,RN(I,K),XN(I,K)
      IF(IM.NE.0) GOTO 9009
 8008 FORMAT(3I10,2F10.5)
       IF(MM.EQ.0)  GO TO 4089
       DO 8007 I=1,MM
       DO 8007 J=1,MM
       GN(I,J)=0.
 8007 BN(I,J)=0.
       DO 9008 I=1,NM
       DO 9008 J=1,MM
       XB(I,J)=0.
 9008 RG(I,J)=0.
 7009  READ (5,8008) IM,I,K,GN(I,K),BN(I,K)
       GN(K,I)=GN(I,K)
       BN(K,I)=BN(I,K)
       WRITE(6,8008) IM,I,K,GN(I,K),BN(I,K)
      IF(IM.NE.0) GOTO 7009
 6008  READ (5,8008) IM,I,K,RG(I,K),XB(I,K)
       WRITE(6,8008) IM,I,K,RG(I,K),XB(I,K)
      IF(IM.NE.0) GOTO 6008
       GO TO  4089
C
C
 4099 CONTINUE
C
       REWIND 8
       READ(8) LFNO,ND,NCT,NTK
       READ(8) (EMN(I),ANG(I),PW(I),PX(I),INAME1(I),
     1 INAME2(I),NOLD(I),I=1,NTK)
C      IF(NM.EQ.ND.AND.MM.EQ.NCT) GO TO 4198
C      WRITE(6,4298)
 4298 FORMAT(/2X,'NO.OF MACHINES SPECIFIED INCORRECT' )
```

```
 4198 CONTINUE
C
       IERN=2
       IF(ND.GT.5) GO TO 181
       IF(NCT.GT.40) GO TO 181
C
C
C      ZNN
       DO 251 I=1,ND
       DO 251 J=1,ND
  251  READ(8) RN(I,J),XN(I,J)
C
C   -ZY OR YZ
       IF(NCT.EQ.0) GO TO 4498
       DO 252 I=1,ND
       DO 252 J=1,NCT
  252  READ(8) RG(I,J),XB(I,J)
C
C    YMM
       DO 253 I=1,NCT
       DO 253 J=1,NCT
  253  READ(8) GN(I,J),BN(I,J)
C
C
 4498 CONTINUE
C
       WRITE(6,4598) LFNO,ND,NCT
 4598 FORMAT(///,2X,'DATA FROM LOAD FLOW NO.=',I7/2X,'NO.OF MACHINES REP
     1RSNTD IN DETAIL=',I4/2X,'NO.OF CONST FLUX LINKAGE MACHINES=',I4///
     1 4X, 'INITIAL VOLTAGE AND POWER' /)
       WRITE(6,4798)
 4798 FORMAT(////2X,'NETWORK DATA'///4X,'MATRIX ZNN'/)
       WRITE(6,4898)((I,K,RN(I,K),XN(I,K),K=1,ND),I=1,ND)
 4898 FORMAT(2X,2I5,2X,2F11.3,5X,2I5,2F11.3,5X,2I5,2F11.3)
       IF(MM.EQ.0)GO TO 4688
       WRITE(6,4188)
 4188 FORMAT(///2X,'MATRIX ZY'/)
       WRITE(6,4898)((I,K, RG(I,K),XB(I,K),K=1,NCT),I=1,ND)
       WRITE(6,4288)
 4288 FORMAT(///2X,'MATRIX YMM'/)
       WRITE(6,4898) ((I,K,GN(I,K),BN(I,K),K=1,NCT),I=1,NCT)
C
C
C
 4688 CONTINUE
C      SET IREDH=0 FOR READING INERTIA DATA FOR X1D MCHS FOR FIRST STUDY
       IREDH=0
       INXT=0
       NM0OLD=0
C                                                  *  *  *  *  *  *  *
C
 4089 CONTINUE
C
C                                                  *  *  *  *  *  *  *
       IREAD=0
       NMQ2=0
        NMD1=0
        NMQ1=0
        NMD2=0
        NMQ3=0
C
C                                                  *  *  *  *  *  *
C
 6987 CONTINUE
C
C                                                  *  *  *  *  *  *
C
C
       NM0=0
       NM1=0
       NM2=0
       NM3=0
       NM4=0
       NM5=0
       NM6=0
```

```
      NMFLT=0
C
C
      DO 1020 N=1,NM
      IF(IREAD.NE.0) GO TO 1026
C
       XXM(8,N)=0.0
       XXM(9,N)=0.0
       XXM(10,N)=0.0
      READ(5,1207) (XXM(I,N),I=1,7),IGEN
      IGEN=1
      READ(5,1209) R(N), (TIME(I,N),I=1,4),BASV,BASP,BASVC
       IF(IGEN.EQ.0)GOTO 1030
       READ(5,1209) (XXM(I,N),I=8,10),(TIME(I,N),I=5,6)
 1030   CONTINUE
      READ(5,1209) HMH(N),DAMPP(N)
      READ(5,518) ISST(N), ASST(N),BSST(N),BSTL(N),SSTL(N)
C
C       COMPUTE NMQ2=NO.OF MACHINES WITH 2CCTS IN Q-AXIS
      IF(ABS(XXM(7,N)).GE.SMALL) NMQ2=NMQ2+1
       IF(ABS(XXM(5,N)).GE.SMALL)NMD1=NMD1+1
       IF(ABS(XXM(6,N)).GE.SMALL)NMQ1=NMQ1+1
       IF(ABS(XXM(8,N)).GE.SMALL)NMD2=NMD2+1
       IF(ABS(XXM(9,N)).GE.SMALL)NMQ3=NMQ3+1
C
      IF(BASV.LT.SMALL) GO TO 1023
      IF(BASPC.LT.SMALL)GO TO 1023
      ZBAS=(BASV**2/BASVC**2)*(BASPC/BASP)
C
C
C   CONVERTING INERTIA AND DAMPING CONSTANTS
C
      HMH(N)=HMH(N)*BASP/BASPC
      DAMPP(N)=DAMPP(N)*BASP/BASPC
C
      DO 1025 I=1,7
 1025 XXM(I,N)=XXM(I,N)*ZBAS
      R(N)=R(N)*ZBAS
       IF(IGEN.EQ.0)GOTO 1023
       XXM(8,N)=XXM(8,N)*ZBAS
       XXM(9,N)=XXM(9,N)*ZBAS
       XXM(10,N)=XXM(10,N)*ZBAS
       DO 1035 I=1,6
 1035   TIME(I,N)=TIME(I,N)*ZBAS
C
 1023 CONTINUE
C
C       READ GENERATOR OUTPUT IF IRDT.NE.1 (LF DATA FROM CARDS)
C
      IF(IRDT.EQ.1) GO TO 1026
      READ(5,5100) EMN(N),ANG(N),PW(N),PX(N), INAME1(N),INAME2(N)
 1026 CONTINUE
C
      READ(5,1409) (XXTR(I,N),I=1,6), ITYPE(N),ITFLT(N)
      IF(ITYPE(N).LE.2.OR.ITYPE(N).EQ.4) GO TO 1021
      READ(5,1209) (XXTR(I,N),I=7,11)
 1021 CONTINUE
C       READ TORSIONAL FILTER TIME CONSTANTS
      IF(ITFLT(N).NE.1) GO TO 1027
      READ(5,1209) (XTFL(I,N),I=1,5)
 1027 CONTINUE
C
C
      IF(ITYPE(N).EQ.0) NM0=NM0+1
      IF(ITYPE(N).EQ.1) NM1=NM1+1
      IF(ITYPE(N).EQ.2) NM2=NM2+1
      IF(ITYPE(N).EQ.3) NM3=NM3+1
      IF(ITYPE(N).EQ.8) NM3=NM3+1
      IF(ITYPE(N).EQ.4) NM4=NM4+1
      IF(ITYPE(N).EQ.7.AND.XXTR(8,N).GT.SMALL) NM6=NM6+1
      IF(ITYPE(N).GE.5.AND.ITYPE(N).LE.7)NM1=NM1+1
      IF(ITYPE(N).GE.5.AND.ITYPE(N).LE.7)NM5=NM5+1
      IF(ITYPE(N).EQ.6.AND.XXTR(8,N).LE.SMALL)NM5=NM5-1
C
C       FILTER
```

```
       IF(ITFLT(N).NE.1) GO TO 1028
       IF(ITYPE(N).EQ.1) NMFLT=NMFLT+1
       IF(ITYPE(N).GE.5.AND.ITYPE(N).LE.7) NMFLT=NMFLT+1
 1028 CONTINUE
C
 1020 CONTINUE
C
C
C    DATA FOR CLASSICAL MACHINES READ FOR FIRST CASE ONLY)
        IF(NCT.EQ.0)GOTO 1051
        IF(IREDH.NE.0)GOTO 1051
        DO 1050 J=1,NCT
        IF(IRDT.EQ.1)GOTO 1050
        JNM=NM+J
       READ(5,5100) EMN(JNM), ANG(JNM),PW(JNM),PX(JNM),INAME1(JNM),
     1 INAME2(JNM)
 1050   READ(5,1209) HMCF(J),DAMPCF(J)
 1051   CONTINUE
C
C
C
C
C         IF INXT=2 SET IREAD=0 TO RECOMPUTE ALL ELEMENTS OF A MATRIX
C
       IF(INXT.EQ.2)IREAD=0
       IF(INXT.GT.2.AND.NM0OLD.NE.NM0)IREAD=0
C
C
       IF(IREAD.NE.0)GO TO 1007
C
C
C                                                  *  *  *  *  *
 1019 CONTINUE
C                                                  *  *  *  *  *
C
       DO 1009 I=1,NDIM
       DO 1009 J=1,NDIM
 1009  A(I,J)=0.
C
 1007 CONTINUE
C
C
C
       IEFD=0
       ISV3=0
       ISPED=0
       ISV4=0
       ISV5=0
       INKQ2=0
        INKD1=0
       INKQ1=0
        INKD2=0
        INKQ3=0
       INFLT=0
C
C        TOTAL SIZE OF A-MATRIX
        NMRF=NMD1+NMD2+NMQ1+NMQ2+NMQ3
        NZ=6*NM+2*MM+NMRF+2*(NM1+NM3)+NM4+NM5+NM6-NM0
C
C        TORSIONAL FILTER
       NZWFL=NZ
       NZ=NZ+4*NMFLT
C
        JJ8=5*NM+NMD1+NMQ1+NM-NM0+2*MM
        JJ11=JJ8+NMQ2+NMD2+NMQ3
C
C
       WRITE(6,2357)IKP1, (ITEXT(I),I=1,20)
C
C
       IERN=3
       IF((NZ+2).GT.NDIM) GO TO 183
C
C
C                                                  *  *  *  *  *  *  *
```

```
C
      DO 8999 N=1,NM
C
C                                                  *  *  *  *  *  *  *
      IF(INXT.LT.0) GO TO 2009
C
      ET=EMN(N)
      PD=PW(N)
      PQ=PX(N)
      ANGLE=ANG(N)/RADIAN
      ANGDG=ANG(N)
      GO TO 2010
C
 2009 CONTINUE
      ET=EMNEW(N)
      PD=PWNEW(N)
       PQ=PXNEW(N)
      ANGLE=ANGNEW(N)/RADIAN
      ANGDG=ANGNEW(N)
C
 2010 CONTINUE
      WRITE(6,5000) N,INAME1(N),INAME2(N)
C
      GE=  XXTR(1,N)
      TE=  XXTR(2,N)
      T1=  XXTR(3,N)
      T2=  XXTR(4,N)
      GD=  XXTR(5,N)
      TQ=  XXTR(6,N)
      AEX3=XXTR(7,N)
      BEX3=XXTR(8,N)
      T11= XXTR(9,N)
      T22= XXTR(10,N)
C                                                  *   *   *   *   *
      IF(IREAD.NE.0) GO TO 6605
C                                                  *   *   *   *   *
C
       IF(IGEN.EQ.0)GOTO 1995
C  DATA IN TERMS OF INDUCTANCES AND RESISTANCES
       XAD=XXM(1,N)
       XAQ=XXM(2,N)
       XAL=XXM(3,N)
       XFL=XXM(4,N)
       XKDL=XXM(5,N)
       XKQL=XXM(6,N)
       XKQ2=XXM(7,N)
       XKD2=XXM(8,N)
       XKQ3=XXM(9,N)
       XRC=XXM(10,N)
C XXM(5,N) TO XXM(9,M) IS DEFINED IN ABSLUTE VALUE TO REST OF THE PROGRAM
      XXM(5,N)=ABS(XXM(5,N))
      XXM(6,N)=ABS(XXM(6,N))
      XXM(7,N)=ABS(XXM(7,N))
      XXM(8,N)=ABS(XXM(8,N))
      XXM(9,N)=ABS(XXM(9,N))
       RF=TIME(1,N)
       RKD=TIME(2,N)
       RKQ=TIME(3,N)
      RKQ2=TIME(4,N)
       RKD2=TIME(5,N)
       RKQ3=TIME(6,N)
       IF(ABS(XKDL).LT.SMALL)XKDL=BIG
       IF(ABS(XKQL).LT.SMALL)XKQL=BIG
       IF(ABS(XKQ2).LT.SMALL)XKQ2=BIG
       IF(ABS(XKQ3).LT.SMALL)XKQ3=BIG
       IF(ABS(XKD2).LT.SMALL)XKD2=BIG
       GOTO 1996
C
 1995   CONTINUE
C
      XD=  XXM(1,N)
      XQ=  XXM(2,N)
      XAL= XXM(3,N)
      X1D= XXM(4,N)
```

```
      X11D=XXM(5,N)
      X1Q= XXM(6,N)
      X11Q=XXM(7,N)
      T1D =TIME(1,N)
      T11D=TIME(2,N)
      T1Q =TIME(3,N)
      T11Q=TIME(4,N)
C
      XAD=XD-XAL
      XAQ=XQ-XAL
      XFL= (( X1D-XAL)*XAD ) / (XD-X1D )
      RF= (XFL+XAD) / (W0*T1D)
      IF(X11D.LE.SMALL) GO TO 2001
      XKDL= (( X11D-XAL )* (X1D-XAL)) / (X1D-X11D)
      RKD= (XKDL+ ((XFL*XAD) /(XFL+XAD))) / (W0*T11D)
      GO TO 2002
 2001   XKDL=BIG
        RKD=0.
 2002  IF(X1Q.LE.SMALL)GOTO 2004
      XKQL= (( X1Q-XAL) *XAQ)/(XQ-X1Q)
      RKQ= (XAQ+XKQL)/(W0*T1Q)
      GO TO 2005
 2004  XKQL=BIG
        RKQ=0.0
 2005 CONTINUE
      IF(X11Q.LE.SMALL)GOTO 2007
      XKQ2=((X11Q-XAL)*(X1Q-XAL))/(X1Q-X11Q)
      RKQ2=(XKQ2+((XKQL*XAQ)/(XKQL+XAQ)))/(W0*T11Q)
      GO TO 2008
 2007     XKQ2=BIG
      RKQ2=0.
 2008 CONTINUE
       XKD2=BIG
       XKQ3=BIG
       XRC=0.
C
      XAFA= (XAD*XFL)/(XAD+XFL)
      XPD=XAL+XAFA
      XPPD=XAL+(XAFA*XKDL)/(XAFA+XKDL)
      XAFQ= (XAQ*XKQL) /(XAQ+XKQL)
      XPQ= XAL+XAFQ
      TPDO= (XFL+XAD)/(RF*W0)
      TPPDO=(XFL*XAD)/(XFL+XAD)
      TPPDO=(XKDL+TPPDO)/(RKD*W0)
      TQPO= (XKQL+XAQ) /(RKQ*W0)
      XD=XAD+XAL
      XQ=XAQ+XAL
      XPPQ=XAL+(XAFQ*XKQ2)/(XAFQ+XKQ2)
      TPPQO=(XAFQ+XKQ2)/(RKQ2*W0)
      WRITE(6,2006) XD,XQ,XPD,XPPD,XPQ,XPPQ,TPDO,TPPDO,TQPO, TPPQO
 2006 FORMAT(22X, 'XD=',F8.3, 4X, 'XQ=',F8.3,4X, 'X1D=',F7.3,4X, 'X11D='
     1 ,F6.3,4X, 'X1Q=', F7.3,4X,'X11Q=',F6.3/
     2 22X,'T1DO=',F6.3,4X, 'T11DO=',F6.3,3X, 'T1QO=',F6.3,4X,'T11QO=',
     3 F6.3)
C
C
 1996   CONTINUE
C
      WRITE (6,1411) XAD, XAQ,XAL,XFL,XKDL,XKQL,
     1  XKQ2, R(N), RF, RKD, RKQ,RKQ2,XKD2,XKQ3,XRC,RKD2,RKQ3
C
      WRITE(6,1412) ET,ANGDG,PD,PQ,HMH(N),DAMPP(N)
C                                                    *   *   *   *   *
 6605 CONTINUE
C                                                    *   *   *   *   *
      WRITE(6,1410)ITYPE(N)
C
C
      VAMX=0.
      IF(ITYPE(N).EQ.0)GO TO 1588
      IF(ITYPE(N).EQ.1)GO TO 1600
      IF(ITYPE(N).EQ.2)GO TO 1601
      IF(ITYPE(N).EQ.3)GO TO 1602
      IF(ITYPE(N).EQ.8)GO TO 1602
      IF(ITYPE(N).EQ.4)GO TO 1604
```

```
      IF(ITYPE(N).EQ.5)GO TO 1605
      IF(ITYPE(N).EQ.6)GO TO 1606
      IF(ITYPE(N).EQ.7) GO TO 1608
C
      WRITE(6,1589)
 1589 FORMAT(//8X, '****** ITYPE(N).GT 7 *******'/
     1 8X, '******** CHECK DATA *******' ////)
 1588 CONTINUE
      WRITE(6,1591)
 1591 FORMAT(   22X, 'CONST. EFD')
      GO TO 1607
 1600 CONTINUE
      WRITE(6,1610)GE,TE,T1,T2,GD,TQ
 1610 FORMAT(22X,'THYRSTR WITH SPEED SIGNAL'/
     1 22X,'KA=',F8.3,4X,'TA=', F8.3,4X,'T1=', F8.3,4X, 'T2=',F8.3,4X,
     1 'KD=',F8.3,4X,'TQ=',F8.3 )
      GO TO 1609
 1601 CONTINUE
      VAMX=XXTR(3,N)
      WRITE(6,1611)GE,TE
 1611 FORMAT(22X,'THYRSTR WITH NO SPEED SIGNAL'/
     1 22X,'KA=',F8.3,4X,'TA=', F8.3 )
      GO TO 1607
 1602 CONTINUE
      WRITE(6,1612)GE,TE,T1,T2,GD,TQ,AEX3,BEX3
 1612 FORMAT(22X,'ROTATING EXCITER'/
     1 22X,'KA=',F8.3,4X,'TA=', F8.3 ,4X, 'KE=', F8.3,4X, 'TE=', F8.3,
     1 4X,'KF= ',F8.3,4X,'TF=', F8.3 /
     1 22X,'AEX=',F7.3,4X,'BEX=',F7.3)
      GO TO 1607
 1604 CONTINUE
      VAMX=XXTR(5,N)
      WRITE(6,1614)GE,TE,T1,T2
 1614 FORMAT(22X,'AMPLYDNE(TEMP STABLZN)'/
     1 22X,'KA=',F8.3,4X,'TA=', F8.3,4X,'T1=', F8.3,4X, 'T2=',F8.3 )
      GO TO 1607
 1605 CONTINUE
      WRITE(6,1615)GE,TE,T1,T2,GD,TQ,AEX3,BEX3
 1615 FORMAT(22X,'THYRSTR WITH SPEED SIGNAL AND ANGLE SIGNAL'/
     1 22X,'KA=',F8.3,4X,'TA=', F8.3,4X,'T1=', F8.3,4X, 'T2=',F8.3,4X,
     1 'KD=',F8.3,4X,'TQ=',F8.3 /
     1 22X, 'KANG=',F6.3, 4X, 'TANG=',F6.3)
      GO TO 1609
 1606 CONTINUE
      VAMX=XXTR(9,N)
      WRITE(6,1616)GE,TE,T1,T2,GD,TQ,AEX3,BEX3
 1616 FORMAT(22X,'THYRSTR WITH SPEED SIGNAL AND TGR'/
     1 22X,'KA=',F8.3,4X,'TA=', F8.3,4X,'T1=', F8.3,4X, 'T2=',F8.3,4X,
     1 'KD=',F8.3,4X,'TQ=',F8.3 /
     1 22X, 'T3=',F8.3, 4X,'T4=',F8.3 )
      GO TO 1609
 1608 CONTINUE
      VAMX=XXTR(11,N)
      WRITE(6,1617) GE,TE,GD,TQ,T1, T11,T2,T22,AEX3,BEX3
 1617 FORMAT(22X, 'THYRSTR WITH SPEED SIGNAL,2ND ORDER PH.LD. & TGR'/
     1 22X,'KA=',F8.3, 4X, 'TA=', F8.3,4X,'GD=',F8.3,4X, 'TQ=',F8.3/
     2 22X, 'T1=',F8.3, 4X, 'T11=',F7.3, 4X,'T2=',F8.3,4X,'T22=',F7.3/
     3 22X,'T3=',F8.3,4X,'T4=',F8.3)
C
 1609 CONTINUE
      IF(ITFLT(N).NE.1) GO TO 1607
      WRITE(6,1618) (XTFL(I,N),I=1,5)
 1618 FORMAT(22X, 'TORSIONAL FILTER'/22X, 'TF1=',F7.6,4X, 'TF2=',F7.6,
     1 4X, 'TF3=',F7.6,4X, 'TF4=',F7.6,4X, 'TF5=', F7.6 )
C
 1607 CONTINUE
C
C
      N1MN=NM+N
      N2MN =2*NM+N
C  STATE VARIABLE NO. FOR FLUX XKD,FLUX XKQ
       IF(XXM(5,N).GE.SMALL)INKD1=INKD1+1
       IF(XXM(6,N).GE.SMALL)INKQ1=INKQ1+1
       N3MN=3*NM+INKD1
       N4MN=3*NM+NMD1+INKQ1
```

```
        N6MN=3*NM+NMD1+NMQ1+NM-NM0+N
       N7MN= N6MN+NM
C        STATE VARIABLE NO. FOR FLUXKQ2,D2,Q3
       IF(XXM(7,N).GE.SMALL) INKQ2=INKQ2+1
       N11NEW=JJ8+INKQ2
        IF(XXM(8,N).GE.SMALL)INKD2=INKD2+1
        IF(XXM(9,N).GE.SMALL)INKQ3=INKQ3+1
        N11KD2=JJ8+NMQ2+INKD2
        N11KQ3=JJ8+NMQ2+NMD2+INKQ3
C
C                                                    *   *   *   *   *
C   KEY=8 IF IREAD.NE.0-COMPUTE RX,KE USING EFC(N)
        IF(IREAD.NE.0.AND.ITYPE(N).EQ.8)GOTO 6603
C
       IF(IREAD.NE.0) GO TO 6602
C                                                    *   *   *   *   *
       XADU=XAD
       XAQU=XAQ
C
C
       ISAT=ISST(N)
       ASAT=ASST(N)
       BSAT=BSST(N)
       BATL=BSTL(N)
       SATL=SSTL(N)
C
C      ISAT=1  SALIENT POLE
C      ISAT=2  ROND ROTOR
       CT= (PD*PD+PQ*PQ)/(ET*ET)
       CT= SQRT(CT)
       PHI= ATAN2(PQ,PD)
       CTR=CT*COS(PHI)
       CTI=-CT*SIN(PHI)
       BAR=ET+R(N)*CTR-XAL*CTI
       BAI=CTR*XAL+CTI*R(N)
       BAT=SQRT(BAR**2+BAI**2)
        IF(ISAT.EQ.4)GOTO 502
       IF(BAT.LE.BATL) GO TO 500
       XSAT=BAT-BATL
       XSATI=ASAT*(EXP(BSAT*XSAT))
       SD=BAT/(BAT+XSATI)
       IF(SD.LT.SATL)SD=SATL
       SINCR=1./(1.+XSATI*BSAT)
       IF(SINCR.LT.SATL)SINCR=SATL
       IF(ISAT.EQ.0)SINCR=SD
       GO TO 501
  500 SD=1.
       SINCR=1.
  501 CONTINUE
       SQ=SD
       IF(ISAT.GE.2)SQ=1.
       SDINCR=SINCR
       SQINCR=SINCR
       IF(ISAT.GE.2)SQINCR=1.
       IF(ISAT.EQ.3)SDINCR=SD
        GOTO 503
  502  SD=ASAT
        SQ=BATL
        SDINCR=BSAT
        SQINCR=SATL
  503   CONTINUE
C      ACTUAL SATURATED VALUE OF XAD,XAQ FOR INITIAL CODTNS
       XAD=XADU*SD
       XAQ=XAQU*SQ
      XD=XAD+XAL
       XQ=XAQ+XAL
       THEN=PD*XQ-PQ*R(N)
       THED=ET*ET+(PD*R(N)+PQ*XQ)
      DEM=ATAN2(THEN,THED)
      ED= ET*SIN(DEM)
      EQ=ET* COS(DEM)
      EDEM=ED/(ET*ET)
      EQEM=EQ/(ET*ET)
      CD=PD*EDEM +PQ*EQEM
```

```
      CQ=PD*EQEM - PQ*EDEM
      PFD= EQ +R(N)*CQ
      PFQ= -ED -R(N)* CD
      CFD=(EQ+R(N)*CQ+XD*CD)/XAD
      EF=(RF*CFD)*(XADU/RF)
      EFC(N)=EF
C   AIR GAP FLUX
      FLXAD=XAD*(CFD-CD)
      FLXAQ=-XAQ*CQ
      DEMDG=DEM*RADIAN
C
C   KEY=8
 6603   CONTINUE
      IF(ITYPE(N).NE.8)GOTO 510
      EF=EFC(N)
      SEX=AEX3*EXP(BEX3*EF)
      RX=1./(1.+(SEX/EF))
      T1=RX-1.
      AEX3=RX*AEX3
      WRITE(6,511)RX,T1,AEX3
  511  FORMAT(22X,'CONSTANTS DETERMINED BY PROGRAM INTERNALLY',
     1 3X,'RX=',F8.3,4X,'KE=',F8.3,4X,'AEX=',F7.3)
C   SET KEY=8 TO KEY=3
      ITYPE(N)=3
      IF(IREAD.NE.0)GOTO 6602
C
  510   CONTINUE
      WRITE(6,508)ASAT,BSAT,BATL,SD,SQ,SDINCR,SQINCR
  508 FORMAT(/22X,
     1                'ASAT=',F6.3, 4X, 'BSAT=',F6.3,4X, 'BATL=', F6.3,4X,
     1 'SD =' ,F7.3, 4X,  'SQ =',F7.3, 4X, 'SDINC=',F5.3,4X,'SQINC=',
     2 F5.3)
       WRITE(6,509) EF,CFD,DEMDG,FLXAD,FLXAQ,BAT
 509  FORMAT(22X,'EFD=',F7.3,4X,'IFD=',F7.3,4X,
     1   'DEM=',F7.3,4X,'FLXAD=',F6.3,3X,'FLXAQ=',F6.3,3X,'FLXAT=',F6.3)
C
C
      HM=2.*HMH(N)/W0
C
      IF(N.EQ.1)HM1=HM
C
      DAMP=DAMPP(N)/W0
C
      DEL=DEM+ANGLE-HPII
      SND(N)=SIN(DEL)
      CSD(N)=COS(DEL)
C     INCREMENTAL REACTANCES
      XAD=XADU*SDINCR
      XAQ=XAQU*SQINCR
      XD=XAD+XAL
      XQ= XAQ+XAL
       AK11=1./XAD+1./XAL
       AK12=1./XFL+1./XKDL+1./XKD2
      AK1=AK11+AK12
      AK2=1./XAQ+1./XAL+ 1./XKQL
       AK2=AK2+(1./XKQ2)+(1./XKQ3)
       AKRC=AK1+(XRC*AK11*AK12)
       A1L=1./(AKRC*XAL)
      RFFL=(W0*RF)/(AKRC*XFL)
       RKDL=(W0*RKD)/(AKRC*XKDL)
      RKQL=(W0*RKQ)/ (AK2*XKQL)
      RKQL2=(W0*RKQ2)/(AK2*XKQ2)
       AL1RC=XRC*AK12*(1.-(AK11*XAL))
       AL1(N)=(A1L/XAL)*(1.-AK1*XAL+AL1RC)
      AL2(N)=A1L/XFL
      AL3(N) =A1L/XKDL
      AL7(N)=A1L/XKD2
      A2L=1./(AK2*XAL)
      AL4(N)=(A2L*(1.-AK2*XAL))/XAL
      AL5(N)=A2L/XKQL
      AL6(N)=A2L/XKQ2
           AL8(N)=A2L/XKQ3
       AKRC1=1.+XRC*AK11
C
C     FIELD FLUXLINKAGE
```

```
C      COMPUTE A(3,1) TO A(3,3)
        A(N2MN,N) =RFFL/XAL
       AKRCD1 = (1./(AKRC**2))*(1.+XRC*AK12)/(XAL**2)
       AKRCD2 = -AK11*AK12/(AKRC**2)
       AKRCD3 = (1./(AKRC**2))*(1.+XRC*AK11)/(XKDL**2)
       AKRCD4 = (1./(AKRC**2))*(1.+XRC*AK11)/(XKD2**2)
       AKRCD7 = (1./(AKRC**2))*(1.+XRC*AK11)/(XFL**2)
       RFFL1=RFFL*AKRC*AKRCD1
       RFFL2=RFFL*AKRC*AKRCD2
       RFFL3=RFFL*AKRC*AKRCD3
       RFFL4=RFFL*AKRC*AKRCD4
       RFFL7=RFFL*(AKRC*AKRCD7-1./XFL)
       A1L1=-1/(AKRC*XAL**2)+AKRCD1/XAL
       A1L2=AKRCD2/XAL
       A1L3=AKRCD3/XAL
       A1L4=AKRCD4/XAL
       A1L7=AKRCD7/XAL
       A2L1=A2L/XAL*(A2L-1.0)
       A2L8=A2L/(AK2*(XAQ**2))
       A2L9=A2L/(AK2*(XKQL**2))
       A2L10=A2L/(AK2*(XKQ2**2))
       A2L11=A2L/(AK2*(XKQ3**2))
       AL21 = A1L1/XFL
       AL22 = A1L2/XFL
       AL23 = A1L3/XFL
       AL24 = A1L4/XFL
       AL27 = A1L7/XFL  -A1L /(XFL**2)
       AL31 = A1L1/XKDL
       AL32 = A1L2/XKDL
       AL33 = A1L3/XKDL -A1L /(XKDL**2)
       AL34 = A1L4/XKDL
       AL37 = A1L7/XKDL
       AL71 = A1L1/XKD2

       AL72 = A1L2/XKD2
       AL73 = A1L3/XKD2
       AL74 = A1L4/XKD2 -A1L /(XKD2**2)
       AL77 = A1L7/XKD2
       AL51 = A2L1/XKQL
       AL58 = A2L8/XKQL
       AL59 = A2L9/XKQL -A2L /(XKQL**2)
       AL510= A2L10/XKQL
       AL511= A2L11/XKQL
       AL61 = A2L1 /XKQ2
       AL68 = A2L8 /XKQ2
       AL69 = A2L9 /XKQ2
       AL610= A2L10/XKQ2-A2L /(XKQ2**2)
       AL611= A2L11/XKQ2
       AL81 = A2L1 /XKQ3
       AL88 = A2L8 /XKQ3
       AL89 = A2L9 /XKQ3
       AL810= A2L10/XKQ3
       AL811= A2L11/XKQ3-A2L /(XKQ3**2)
       AL41 = A2L1 /XAL - A2L/(XAL**2)+1.0/(XAL**2)
       AL48 = A2L8 /XAL + 1.0/(XAQ **2)
       AL49 = A2L9 /XAL + 1.0/(XKQL**2)
       AL410= A2L10/XAL + 1.0/(XKQ2**2)
       AL411= A2L11/XAL + 1.0/(XKQ3**2)
       AL11=A1L1 *(1.0/XAL-AK1+(XRC*AK12/XAL)-AK12*AK11*XRC)
       AL12=A1L2 *(1.0/XAL-AK1+(XRC*AK12/XAL)-AK12*AK11*XRC)
       AL12=AL12+A1L*(AK12/XAL-AK12*AK11)
       AL13=A1L3 *(1.0/XAL-AK1+(XRC*AK12/XAL)-AK12*AK11*XRC)
       AL13=AL13+A1L*((1.0/XKDL**2)-XRC/(XAL*XKDL**2)+XRC*AK11/XKDL**2)
       AL14=A1L4 *(1.0/XAL-AK1+(XRC*AK12/XAL)-AK12*AK11*XRC)
       AL14=AL14+A1L*((1.0/XKD2**2)-XRC/(XAL*XKD2**2)+XRC*AK11/XKD2**2)
       AL17=A1L7 *(1.0/XAL-AK1+(XRC*AK12/XAL)-AK12*AK11*XRC)
       AL17=AL17+A1L*((1.0/XFL **2)-XRC/(XAL*XFL **2)+XRC*AK11/XFL **2)
       IMAG = 1
       ADER = (RFFL1*XAL-RFFL)/(XAL**2)
       WRITE(19) IMAG,N2MN,N,ADER
       IMAG = 2
       ADER = RFFL2/XAL
       WRITE(19) IMAG,N2MN,N,ADER
       IMAG = 3
       ADER = RFFL3/XAL
```

```
      WRITE(19) IMAG,N2MN,N,ADER
      IMAG = 4
      ADER = RFFL4/XAL
      WRITE(19) IMAG,N2MN,N,ADER
      IMAG = 7
      ADER = RFFL7/XAL
      WRITE(19) IMAG,N2MN,N,ADER
        AL2RC=XRC*AK11*(1.-AK12*XFL)
        A(N2MN,N2MN)=(RFFL*(1.-AK1*XFL+AL2RC))/XFL
      IMAG = 1
      ADER = RFFL1/XFL+1./(XAL**2)-XRC/(XFL*XAL**2)+XRC*AK12/(XAL**2)
      WRITE(19) IMAG,N2MN,N2MN,ADER
      IMAG = 2
      ADER = RFFL2/XFL+AK11/XFL-AK11*AK12
      WRITE(19) IMAG,N2MN,N2MN,ADER
      IMAG = 3
      ADER = RFFL3/XFL+1./(XKDL**2)+XRC*AK11/(XKDL**2)
      WRITE(19) IMAG,N2MN,N2MN,ADER
      IMAG = 4
      ADER = RFFL4/XFL+1./(XKD2**2)+XRC*AK11/(XKD2**2)
      WRITE(19) IMAG,N2MN,N2MN,ADER
      IMAG = 7
      ADER = (RFFL7*XFL-RFFL7)/(XFL**2)+1./(XFL**2)-XRC*AK11/(XFL**2)+
     1 XRC*AK11/(XFL**2)
      WRITE(19) IMAG,N2MN,N2MN,ADER
       WRFX(N)=(W0*RF)/XADU
C
C       D-AXIS DAMPER
C     COMPUTE A(3,4) A(4,1),A(4,3),A(4,4)
        IF(XXM(5,N).LT.SMALL)GOTO 820
        A(N2MN,N3MN)=(RFFL/XKDL)*AKRC1
      IMAG = 1
      ADER = RFFL1/XKDL+(XRC/XKDL)*(AK11*RFFL1-RFFL/(XAL**2))
      WRITE(19) IMAG,N2MN,N3MN,ADER
      IMAG = 2
      ADER = RFFL2/XKDL+(AK11/XKDL)*(XRC*RFFL2+RFFL)
      WRITE(19) IMAG,N2MN,N3MN,ADER
      IMAG = 3
      ADER = (XKDL*RFFL3*(1.+XRC*AK11)-RFFL*(1.+XRC*AK11))/(XKDL**2)
      WRITE(19) IMAG,N2MN,N3MN,ADER
      IMAG = 4
      ADER = RFFL4/XKDL+RFFL4*XRC*AK11/XKDL
      WRITE(19) IMAG,N2MN,N3MN,ADER
      IMAG = 7
       ADER = RFFL7/XKDL+RFFL7*XRC*AK11/XKDL
      WRITE(19) IMAG,N2MN,N3MN,ADER
       A(N3MN,N) = RKDL/XAL
       IMAG=1
      ADER=A(N3MN,N)*(AKRC*AKRCD1-1./XAL)
      WRITE(19) IMAG,N3MN,N,ADER
      IMAG=2
      ADER=A(N3MN,N)*AKRC*AKRCD2
      WRITE(19) IMAG,N3MN,N,ADER
      IMAG=3
      ADER=A(N3MN,N)*(AKRC*AKRCD3-1./XKDL)
      WRITE(19) IMAG,N3MN,N,ADER
      IMAG=4
      ADER=A(N3MN,N)*AKRC*AKRCD4
      WRITE(19) IMAG,N3MN,N,ADER
      IMAG=5
      ADER=A(N3MN,N)/RKD
      WRITE(19) IMAG,N3MN,N,ADER
      IMAG=7
      ADER=A(N3MN,N)*AKRC*AKRCD7
      WRITE(19) IMAG,N3MN,N,ADER
        A(N3MN,N2MN)=(RKDL/XFL)*AKRC1
      IMAG=1
      ADER=A(N3MN,N2MN)*AKRC*AKRCD1
      ADER=ADER-XRC*A(N3MN,N2MN)/(AKRC1*XAL**2)
      WRITE(19) IMAG,N3MN,N2MN,ADER
      IMAG=2
      ADER=A(N3MN,N2MN)*(AKRC*AKRCD2+AK11/AKRC1)
      WRITE(19) IMAG,N3MN,N2MN,ADER
      IMAG=3
      ADER=A(N3MN,N2MN)*(AKRC*AKRCD3-1./XKDL)
```

```
      WRITE(19) IMAG,N3MN,N2MN,ADER
      IMAG=4
      ADER=A(N3MN,N2MN)*AKRC*AKRCD4
      WRITE(19) IMAG,N3MN,N2MN,ADER
      IMAG=5
      ADER=A(N3MN,N2MN)/RKD
      WRITE(19) IMAG,N3MN,N2MN,ADER
      IMAG=7
      ADER=A(N3MN,N2MN)*(AKRC*AKRCD7-1./XFL)
      WRITE(19) IMAG,N3MN,N2MN,ADER
        AL3RC=XRC*AK11*(1.-AK12*XKDL)
         A(N3MN,N3MN)=(RKDL*(1.-AK1*XKDL+AL3RC))/XKDL
      IMAG=1
      ADER=A(N3MN,N3MN)*AKRC*AKRCD1
      ADER=ADER+RKDL*(1.-XRC/XKDL+XRC*AK12)/(XAL**2)
      WRITE(19) IMAG,N3MN,N3MN,ADER
      IMAG=2
      ADER=A(N3MN,N3MN)*AKRC*AKRCD2
      ADER=ADER+RKDL*(AK11/XKDL-AK11*AK12)
      WRITE(19) IMAG,N3MN,N3MN,ADER
      IMAG=3
      ADER=A(N3MN,N3MN)*AKRC*AKRCD3
      ADER=ADER+(RKDL/XKDL)*(-1./XKDL+AK1-2.*XRC*AK11/XKDL+XRC*AK11*
     1(1./XKDL+AK12))
      WRITE(19) IMAG,N3MN,N3MN,ADER
      IMAG=4
      ADER=A(N3MN,N3MN)*AKRC*AKRCD4
      ADER=ADER+RKDL*(1.+XRC*AK11)/(XKD2**2)
      WRITE(19) IMAG,N3MN,N3MN,ADER
      IMAG=5
      ADER=A(N3MN,N3MN)/RKD
      WRITE(19) IMAG,N3MN,N3MN,ADER
      IMAG=7
      ADER=A(N3MN,N3MN)*AKRC*AKRCD7
      ADER=ADER+RKDL*(1.+XRC*AK11)/(XFL**2)
      WRITE(19) IMAG,N3MN,N3MN,ADER
        IF(XXM(8,N).LT.SMALL)GOTO 820
C     D-AXIS 2ND DAMPER
        A(N2MN,N11KD2)=(RFFL/XKD2)*AKRC1
      IMAG = 1
      ADER = (RFFL/XKD2)*(-XRC/(XAL**2))+RFFL1*A(N2MN,N11KD2)/RFFL
      WRITE(19) IMAG,N2MN,N11KD2,ADER
      IMAG = 2
      ADER = RFFL*AK11/XKD2+RFFL2*A(N2MN,N11KD2)/RFFL
      WRITE(19) IMAG,N2MN,N11KD2,ADER
      IMAG = 3
      ADER = RFFL3*A(N2MN,N11KD2)/RFFL
      WRITE(19) IMAG,N2MN,N11KD2,ADER
      IMAG = 4
       ADER=A(N2MN,N11KD2)*(RFFL4/RFFL-1./XKD2)
      WRITE(19) IMAG,N2MN,N11KD2,ADER
      IMAG = 7
      ADER = RFFL7*A(N2MN,N11KD2)/RFFL
      WRITE(19) IMAG,N2MN,N11KD2,ADER
        A(N3MN,N11KD2)=(RKDL/XKD2)*AKRC1
      IMAG=1
      ADER=A(N3MN,N11KD2)*AKRC*AKRCD1
      ADER=ADER-XRC*A(N3MN,N11KD2)/(AKRC1*XAL**2)
      WRITE(19) IMAG,N3MN,N11KD2,ADER
      IMAG=2
      ADER=A(N3MN,N11KD2)*AKRC*AKRCD2
      ADER=ADER+AK11*A(N3MN,N11KD2)/AKRC1
      WRITE(19) IMAG,N3MN,N11KD2,ADER
      IMAG=3
      ADER=A(N3MN,N11KD2)*(AKRC*AKRCD3-1./XKDL)
      WRITE(19) IMAG,N3MN,N11KD2,ADER
      IMAG=4
      ADER=A(N3MN,N11KD2)*(AKRC*AKRCD4-1./XKD2)
      WRITE(19) IMAG,N3MN,N11KD2,ADER
      IMAG=5
      ADER=A(N3MN,N11KD2)*(1./RKD)
      WRITE(19) IMAG,N3MN,N11KD2,ADER
      IMAG=7
      ADER=A(N3MN,N11KD2)*AKRC*AKRCD7
      WRITE(19) IMAG,N3MN,N11KD2,ADER
```

```
  RKDL2=(W0*RKD2)/(AKRC*XKD2)
  A(N11KD2,N)=RKDL2/XAL
IMAG = 1
ADER = A(N11KD2,N)*(AKRCD1*AKRC-1./XAL)
WRITE(19) IMAG,N11KD2,N,ADER
IMAG = 2
ADER = A(N11KD2,N)*(AKRCD2*AKRC)
WRITE(19) IMAG,N11KD2,N,ADER
IMAG = 3
ADER = A(N11KD2,N)*(AKRCD3*AKRC)
WRITE(19) IMAG,N11KD2,N,ADER
IMAG = 4
ADER = A(N11KD2,N)*(AKRC*AKRCD4-1./XKD2)
WRITE(19) IMAG,N11KD2,N,ADER
IMAG = 6
ADER = A(N11KD2,N)/RKD2
WRITE(19) IMAG,N11KD2,N,ADER
IMAG = 7
ADER = A(N11KD2,N)*AKRC*AKRCD7
WRITE(19) IMAG,N11KD2,N,ADER
  A(N11KD2,N2MN)=(RKDL2/XFL)*AKRC1
IMAG = 1
ADER = A(N11KD2,N2MN)*(-(XRC/XAL**2)/(1.+XRC*AK11)+AKRC*AKRCD1)
WRITE(19) IMAG,N11KD2,N2MN,ADER
IMAG = 2
ADER = A(N11KD2,N2MN)*(-AK11/(1.+XRC*AK11)+AKRC*AKRCD2)
WRITE(19) IMAG,N11KD2,N2MN,ADER
IMAG = 3
ADER = A(N11KD2,N2MN)*AKRC*AKRCD3
WRITE(19) IMAG,N11KD2,N2MN,ADER
IMAG = 4
ADER = A(N11KD2,N2MN)*(AKRC*AKRCD4-1./XKD2)
WRITE(19) IMAG,N11KD2,N2MN,ADER
IMAG = 6
ADER = A(N11KD2,N2MN)/RKD2
WRITE(19) IMAG,N11KD2,N2MN,ADER
IMAG = 7
ADER = A(N11KD2,N2MN)*(AKRC*AKRCD7-1./XFL)
WRITE(19) IMAG,N11KD2,N2MN,ADER
   A(N11KD2,N3MN)=(RKDL2/XKDL)*AKRC1
IMAG = 1
ADER = A(N11KD2,N3MN)*(-(XRC/XAL**2)/(1.+XRC*AK11)+AKRC*AKRCD1)
WRITE(19) IMAG,N11KD2,N3MN,ADER
IMAG = 2
ADER = A(N11KD2,N3MN)*(AK11/(1.+XRC*AK11)+AKRC*AKRCD2)
WRITE(19) IMAG,N11KD2,N3MN,ADER
IMAG = 3
ADER = A(N11KD2,N3MN)*(AKRC*AKRCD3-1./XKDL)
WRITE(19) IMAG,N11KD2,N3MN,ADER
IMAG = 4
ADER = A(N11KD2,N3MN)*(AKRC*AKRCD4-1./XKD2)
WRITE(19) IMAG,N11KD2,N3MN,ADER
IMAG = 6
ADER = A(N11KD2,N3MN)/RKD2
WRITE(19) IMAG,N11KD2,N3MN,ADER
IMAG = 7
ADER = A(N11KD2,N3MN)*AKRC*AKRCD7
WRITE(19) IMAG,N11KD2,N3MN,ADER
  AL4RC=XRC*AK11*(1.-AK12*XKD2)
  A(N11KD2,N11KD2)=(RKDL2*(1.-AK1*XKD2+AL4RC))/XKD2
IMAG = 1
ADER = A(N11KD2,N11KD2)*AKRC*AKRCD1
ADER = ADER+RKDL2*(XKD2-XRC+XRC*AK12*XKD2)/((XAL**2)*XKD2)
WRITE(19) IMAG,N11KD2,N11KD2,ADER
IMAG = 2
ADER = A(N11KD2,N11KD2)*AKRC*AKRCD2
ADER = ADER+RKDL2*(AK11+AK11*AK12*XKD2)/XKD2
WRITE(19) IMAG,N11KD2,N11KD2,ADER
IMAG = 3
ADER = A(N11KD2,N11KD2)*AKRC*AKRCD3
ADER = ADER+RKDL2*(1.+XRC*AK11)/XKD2
WRITE(19) IMAG,N11KD2,N11KD2,ADER
IMAG = 4
ADER = RKDL2*AKRC*(1.+XRC*AK11)*AKRCD4/XKD2
ADER = ADER-2.*RKDL2*(1.+XRC*AK11)/(XKD2**2)
```

```
      ADER = ADER+RKDL2*AKRC/XKD2
      WRITE(19) IMAG,N11KD2,N11KD2,ADER
      IMAG = 6
      ADER = A(N11KD2,N11KD2)/RKD2
      WRITE(19) IMAG,N11KD2,N11KD2,ADER
      IMAG = 7
      ADER = A(N11KD2,N11KD2)*AKRC*AKRCD7
      ADER = ADER+(1.+XRC*AK11)*(RKDL2/XFL**2)
      WRITE(19) IMAG,N11KD2,N11KD2,ADER
  820   CONTINUE
C
C       Q-AXIS DAMPER
C      COMPUTE A(5,2) AND A(5,5)
       IF(XXM(6,N).LT.SMALL)GOTO 840
       A(N4MN,N1MN) = RKQL/XAL
      AK2D1 = 1./(XAL*AK2)**2
      AK2D8 = 1./(XAQ*AK2)**2
      AK2D9 = 1./(XKQL*AK2)**2
      AK2D10 = 1./(XKQ2*AK2)**2
      AK2D11 = 1./(XKQ3*AK2)**2
      IMAG = 1
       ADER=A(N4MN,N1MN)*(AK2*AK2D1-1./XAL)
       WRITE(19) IMAG,N4MN,N1MN,ADER
       IMAG=8
       ADER=A(N4MN,N1MN)*AK2*AK2D8
       WRITE(19) IMAG,N4MN,N1MN,ADER
       IMAG=9
       ADER=A(N4MN,N1MN)*(AK2*AK2D9-1./XKQL)
       WRITE(19) IMAG,N4MN,N1MN,ADER
       IMAG=10
       ADER=A(N4MN,N1MN)*AK2*AK2D10
       WRITE(19) IMAG,N4MN,N1MN,ADER
       IMAG=11
       ADER=ADER*AK2D11/AK2D10
       WRITE(19) IMAG,N4MN,N1MN,ADER
       IMAG=12
       ADER=A(N4MN,N1MN)/RKQ
       WRITE(19) IMAG,N4MN,N1MN,ADER
       A(N4MN,N4MN) = (RKQL* (1.-AK2*XKQL)) /XKQL
      IMAG=1
      ADER=(W0*RKQ/(XKQL**2))*AK2*AK2D1
      WRITE(19) IMAG,N4MN,N4MN,ADER
      IMAG=8
      ADER=ADER*AK2D8/AK2D1
      WRITE(19) IMAG,N4MN,N4MN,ADER
      IMAG=10
      ADER=ADER*AK2D10/AK2D8
      WRITE(19) IMAG,N4MN,N4MN,ADER
      IMAG=11
      ADER=ADER*AK2D11/AK2D10
      WRITE(19) IMAG,N4MN,N4MN,ADER
      IMAG=9
      ADER=ADER*AK2D9/AK2D11
      ADER=ADER-2.*RKQL/(XKQL**2)
      ADER=ADER+W0*RKQ/(XKQL**2)
      WRITE(19) IMAG,N4MN,N4MN,ADER
       IMAG=12
      ADER=A(N4MN,N4MN)/RKQ
      WRITE(19) IMAG,N4MN,N4MN,ADER
       IF(XXM(7,N).LT.SMALL) GO TO 840
C      COMPUTE A(5,11)
        A(N4MN,N11NEW)=RKQL/XKQ2
      IMAG=1
      ADER=A(N4MN,N11NEW)*AK2*AK2D1
      WRITE(19) IMAG,N4MN,N11NEW,ADER
      IMAG=8
      ADER=ADER*AK2D8/AK2D1
      WRITE(19) IMAG,N4MN,N11NEW,ADER
      IMAG=11
      ADER=ADER*AK2D11/AK2D8
      WRITE(19) IMAG,N4MN,N11NEW,ADER
      IMAG=9
      ADER=A(N4MN,N11NEW)*(AK2*AK2D9-1./XKQL)
      WRITE(19) IMAG,N4MN,N11NEW,ADER
      IMAG=10
```

```
      ADER=A(N4MN,N11NEW)*(AK2*AK2D10-1./XKQ2)
      WRITE(19) IMAG,N4MN,N11NEW,ADER
      IMAG=12
      ADER=A(N4MN,N11NEW)/RKQ
      WRITE(19) IMAG,N4MN,N11NEW,ADER
C
C       Q AXIS 2ND ROTOR
C       COMPUTE(A(11,2),A(11,5),A(11,11)
C
       A(N11NEW,N1MN  )=RKQL2/XAL
      IMAG = 1
      ADER = A(N11NEW,N1MN)*(AK2*AK2D1-1./XAL)
      WRITE(19) IMAG,N11NEW,N1MN,ADER
      IMAG = 8
      ADER = A(N11NEW,N1MN)*AK2*AK2D8
      WRITE(19) IMAG,N11NEW,N1MN,ADER
       IMAG=9
       ADER=ADER*AK2D9/AK2D8
      WRITE(19) IMAG,N11NEW,N1MN,ADER
       IMAG = 10
      ADER = A(N11NEW,N1MN)*(AK2*AK2D10-1./XKQ2)
      WRITE(19) IMAG,N11NEW,N1MN,ADER
      IMAG = 11
      ADER = A(N11NEW,N1MN)*AK2*AK2D11
      WRITE(19) IMAG,N11NEW,N1MN,ADER
      IMAG = 13
      ADER = A(N11NEW,N1MN)/RKQ2
      WRITE(19) IMAG,N11NEW,N1MN,ADER
       A(N11NEW,N4MN  )=RKQL2/XKQL
       IMAG = 1
      ADER = A(N11NEW,N4MN)*AK2*AK2D1
      WRITE(19) IMAG,N11NEW,N4MN,ADER
      IMAG = 8
      ADER = A(N11NEW,N4MN)*AK2*AK2D8
      WRITE(19) IMAG,N11NEW,N4MN,ADER
      IMAG = 9
      ADER = A(N11NEW,N4MN)*(AK2*AK2D9-1./XKQL)
      WRITE(19) IMAG,N11NEW,N4MN,ADER
      IMAG = 10
      ADER = A(N11NEW,N4MN)*(AK2*AK2D10-1./XKQ2)
      WRITE(19) IMAG,N11NEW,N4MN,ADER
      IMAG = 11
      ADER = A(N11NEW,N4MN)*AK2*AK2D11
      WRITE(19) IMAG,N11NEW,N4MN,ADER
      IMAG = 13
      ADER = A(N11NEW,N4MN)/RKQ2
      WRITE(19) IMAG,N11NEW,N4MN,ADER
       A(N11NEW,N11NEW)= (RKQL2*(1.-AK2*XKQ2))/XKQ2
      IMAG = 1
      ADER = (RKQL2*AK2D1/XKQ2)*AK2
      WRITE(19) IMAG,N11NEW,N11NEW,ADER
      IMAG = 8
      ADER = (RKQL2*AK2D8/XKQ2)*AK2
      WRITE(19) IMAG, N11NEW,N11NEW,ADER
      IMAG = 9
      ADER = (RKQL2*AK2D9/XKQ2)*AK2
      WRITE(19) IMAG,N11NEW,N11NEW,ADER
      IMAG = 10
       ADER = RKQL2*AK2*AK2D10/XKQ2
       ADER = ADER-2.*RKQL2/XKQ2**2
       ADER = ADER+RKQL2*AK2/XKQ2
        WRITE(19) IMAG,N11NEW,N11NEW,ADER
       IMAG = 11
       ADER = RKQL2*AK2*AK2D11/XKQ2
       WRITE(19) IMAG,N11NEW,N11NEW,ADER
        IMAG = 13
       ADER = A(N11NEW,N11NEW)/RKQ2
       WRITE(19) IMAG,N11NEW,N11NEW,ADER
C   Q-AXIS 3RD ROTOR
          IF(XXM(9,N).LT.SMALL)GOTO 840
          RKQL3=(W0*RKQ3)/(AK2*XKQ3)
          A(N4MN,N11KQ3)=RKQL/XKQ3
         IMAG=1
         ADER=A(N4MN,N11KQ3)*AK2*AK2D1
         WRITE(19) IMAG,N4MN,N11KQ3,ADER
```

```
 IMAG=8
 ADER=ADER*AK2D8/AK2D1
 WRITE(19) IMAG,N4MN,N11KQ3,ADER
 IMAG=9
 ADER=A(N4MN,N11KQ3)*(AK2*AK2D9-1./XKQL)
 WRITE(19) IMAG,N4MN,N11KQ3,ADER
 IMAG=10
 ADER=A(N4MN,N11KQ3)*AK2*AK2D10
 WRITE(19) IMAG,N4MN,N11KQ3,ADER
 IMAG=11
 ADER=A(N4MN,N11KQ3)*(AK2*AK2D11-1./XKQ3)
 WRITE(19) IMAG,N4MN,N11KQ3,ADER
 IMAG=12
 ADER=A(N4MN,N11KQ3)/RKQ
 WRITE(19) IMAG,N4MN,N11KQ3,ADER
  A(N11NEW,N11KQ3)=RKQL2/XKQ3
IMAG = 1
ADER = A(N11NEW,N11KQ3)*AK2*AK2D1
WRITE(19) IMAG,N11NEW,N11KQ3,ADER
IMAG = 8
ADER = ADER*AK2D8/AK2D1
WRITE(19) IMAG,N11NEW,N11KQ3,ADER
 IMAG = 9
ADER = ADER*AK2D9/AK2D8
 WRITE(19) IMAG,N11NEW,N11KQ3,ADER
IMAG = 10
ADER = A(N11NEW,N11KQ3)*(AK2*AK2D10-1./XKQ2)
WRITE(19) IMAG,N11NEW,N11KQ3,ADER
IMAG = 11
ADER = A(N11NEW,N11KQ3)*(AK2*AK2D11-1./XKQ3)
WRITE(19) IMAG,N11NEW,N11KQ3,ADER
IMAG = 13
ADER = A(N11NEW,N11KQ3)/RKQ2
WRITE(19) IMAG,N11NEW,N11KQ3,ADER
  A(N11KQ3,N11KQ3)=(RKQL3*(1.-AK2*XKQ3))/XKQ3
IMAG = 1
ADER = W0*RKQ3*AK2D1/(XKQ3**2)
WRITE(19)  IMAG,N11KQ3,N11KQ3,ADER
IMAG = 8
ADER = ADER*AK2D8/AK2D1
WRITE(19) IMAG,N11KQ3,N11KQ3,ADER
IMAG = 9
ADER = ADER*AK2D9/AK2D8
WRITE(19) IMAG,N11KQ3,N11KQ3,ADER
IMAG = 10
ADER = ADER*AK2D10/AK2D9
WRITE(19)  IMAG,N11KQ3,N11KQ3,ADER
IMAG = 11
ADER = ADER*AK2D11/AK2D10
 ADER=ADER-(2.*W0*RKQ3)/(AK2*XKQ3**3)
ADER = ADER+W0*RKQ3/(XKQ3**2)
WRITE(19) IMAG,N11KQ3,N11KQ3,ADER
IMAG = 14
ADER = A(N11KQ3,N11KQ3)/RKQ3
WRITE(19) IMAG,N11KQ3,N11KQ3,ADER
  A(N11KQ3,N1MN)=RKQL3/XAL
IMAG = 1
ADER = A(N11KQ3,N1MN)*(AK2*AK2D1-1./XAL)
WRITE(19) IMAG,N11KQ3,N1MN,ADER
IMAG = 8
ADER = A(N11KQ3,N1MN)*AK2*AK2D8
WRITE(19) IMAG,N11KQ3,N1MN,ADER
IMAG = 9
ADER = ADER*AK2D9/AK2D8
WRITE(19) IMAG,N11KQ3,N1MN,ADER
IMAG = 10
ADER = ADER*AK2D10/AK2D9
WRITE(19) IMAG,N11KQ3,N1MN,ADER
IMAG = 11
ADER = A(N11KQ3,N1MN)*(AK2*AK2D11-1./XKQ3)
WRITE(19) IMAG,N11KQ3,N1MN,ADER
IMAG = 14
ADER = A(N11KQ3,N1MN)/RKQ3
WRITE(19) IMAG,N11KQ3,N1MN,ADER
  A(N11KQ3,N4MN)=RKQL3/XKQL
```

```
       IMAG = 1
      ADER = A(N11KQ3,N4MN)*AK2*AK2D1
      WRITE(19) IMAG,N11KQ3,N4MN,ADER
      IMAG = 9
      ADER = A(N11KQ3,N4MN)*(AK2*AK2D9-1./XKQL)
      WRITE(19)  IMAG,N11KQ3,N4MN,ADER
      IMAG = 8
      ADER = A(N11KQ3,N4MN)*AK2*AK2D8
      WRITE(19) IMAG,N11KQ3,N4MN,ADER
      IMAG = 10
      ADER = ADER*AK2D10/AK2D8
      WRITE(19)  IMAG,N11KQ3,N4MN,ADER
       IMAG = 11
      ADER = A(N11KQ3,N4MN)*(AK2*AK2D11-1./XKQ3)
      WRITE(19) IMAG,N11KQ3,N4MN,ADER
      IMAG = 14
      ADER = A(N11KQ3,N4MN)/RKQ3
      WRITE(19) IMAG,N11KQ3,N4MN,ADER
        A(N11KQ3,N11NEW)=RKQL3/XKQ2
      IMAG = 1
      ADER = A(N11KQ3,N11NEW)*AK2*AK2D1
      WRITE(19) IMAG,N11KQ3,N11NEW,ADER
       IMAG = 8
       ADER = ADER*AK2D8/AK2D1
       WRITE(19) IMAG,N11KQ3,N11NEW,ADER
       IMAG = 9
       ADER = ADER*AK2D9/AK2D8
       WRITE(19) IMAG,N11KQ3,N11NEW,ADER
       IMAG = 10
        ADER = A(N11KQ3,N11NEW)*(AK2*AK2D10-1./XKQ2)
       WRITE(19) IMAG,N11KQ3,N11NEW,ADER
       IMAG = 11
       ADER = A(N11KQ3,N11NEW)*(AK2*AK2D11-1./XKQ3)
       WRITE(19) IMAG,N11KQ3,N11NEW,ADER
       IMAG = 14
       ADER = A(N11KQ3,N11NEW)/RKQ3
       WRITE(19) IMAG,N11KQ3,N11NEW,ADER
  840 CONTINUE
C
C       COUPLING BETWEEN STATOR FLUX AND SPEED
C       COMPUTE A(1,7) AND A(2,7)
C         IF IPSI=0  SET  W/W0=1
C
       IF(IPSI.EQ.0) GO TO 6601
       A( N    ,N6MN)=PFQ
       A(N1MN ,N6MN)= -PFD
 6601 CONTINUE
C
C       ROTOR ANGLE AND SPEED
C       COMPUTE A(7,1) TO A(7,5) AND A(7,7), A( 8,7)
       A(N6MN ,N     )= (PFQ*AL1(N) -CQ)/HM
      IMAG = 1
      ALLOW = A(N6MN,N)+CQ/HM
      ADER = (XRC*AK12-1.)/(XAL**3)
      ADER = ADER+(XRC*AK12-AK1-XRC*AK12*AK11)/(XAL**2)
      ADER = ADER*PFQ/(HM*AKRC)
      ADER = ADER+ALLOW*AKRC*AKRCD1
      WRITE(19) IMAG,N6MN,N,ADER
      IMAG = 2
      ADER = (AK12-AK12*AK11)*PFQ/(AKRC*HM*XAL)
      ADER = ADER+ALLOW*AKRC*AKRCD2
      WRITE(19) IMAG,N6MN,N,ADER
      IMAG = 3
      ADER = (XRC*AK11-XRC+1.)*PFQ/(XAL*AKRC*HM*XKDL*XKDL)
      ADER = ADER+ALLOW*AKRC*AKRCD3
      WRITE(19) IMAG,N6MN,N,ADER
      IMAG = 4
      ADER = (XRC*AK11-XRC+1.)/(XAL*AKRC*HM*XKD2*XKD2)
      ADER = ADER*PFQ+ALLOW*AKRC*AKRCD4
      WRITE(19) IMAG,N6MN,N,ADER
      IMAG = 7
      ADER = (XRC*AK11-XRC+1.)/(XAL*AKRC*HM*XFL*XFL)
      ADER = ADER*PFQ+ALLOW*AKRC*AKRCD7
      WRITE(19) IMAG,N6MN,N,ADER
C**     ILCT=1
```

```
C**     WRITE(6,930) ILCT,A(1,1),A(2,1),A(6,1),A(7,1)
  930   FORMAT(4X,'ILCT=',I2,2X,4F9.3)
        A(N6MN ,N1MN)= (CD-PFD*AL4(N))/HM
       IMAG = 1
        ADER = (-PFD/HM)*(AK2D1+1.-2./(XAL*AK2))/XAL**2
        WRITE(19) IMAG,N6MN,N1MN,ADER
        IMAG = 8
        ADER = (-PFD/HM)*AK2D8/XAL**2
        WRITE(19) IMAG,N6MN,N1MN,ADER
        IMAG = 9
        ADER = (-PFD/HM)*AK2D9/XAL**2
        WRITE(19) IMAG,N6MN,N1MN,ADER
        IMAG = 10
        ADER = ADER*AK2D10/AK2D9
        WRITE(19) IMAG,N6MN,N1MN,ADER
        IMAG = 11
        ADER = ADER*AK2D11/AK2D10
        WRITE(19) IMAG,N6MN,N1MN,ADER
         A(N6MN ,N2MN)= ( PFQ*AL2(N))/HM
        IMAG = 1
        ADER = A(N6MN,N2MN)*(AKRC*AKRCD1-1./XAL)
        WRITE(19) IMAG,N6MN,N2MN,ADER
        IMAG = 2
        ADER = AKRC*AKRCD2*A(N6MN,N2MN)
        WRITE(19) IMAG,N6MN,N2MN,ADER
        IMAG = 3
        ADER = ADER*AKRCD3/AKRCD2
        WRITE(19) IMAG,N6MN,N2MN,ADER
        IMAG = 4
        ADER = ADER*AKRCD4/AKRCD3
        WRITE(19) IMAG,N6MN,N2MN,ADER
        IMAG = 7
        ADER = A(N6MN,N2MN)*(AKRC*AKRCD7-1./XFL)
        WRITE(19) IMAG,N6MN,N2MN,ADER
          IF(XXM(5,N).LT.SMALL)GOTO 830
         A(N6MN ,N3MN)= ( PFQ*AL3(N))/HM
        IMAG = 1
        ADER = A(N6MN,N3MN)*(AKRC*AKRCD1-1./XAL)
        WRITE(19) IMAG,N6MN,N3MN,ADER
        IMAG = 2
        ADER = A(N6MN,N3MN)*AKRC*AKRCD2
        WRITE(19) IMAG,N6MN,N3MN,ADER
        IMAG = 3
        ADER = A(N6MN,N3MN)*(AKRC*AKRCD3-1./XKDL)
        WRITE(19) IMAG,N6MN,N3MN,ADER
        IMAG = 4
        ADER = A(N6MN,N3MN)*AKRC*AKRCD4
        WRITE(19) IMAG,N6MN,N3MN,ADER
        IMAG = 7
        ADER = ADER*AKRCD7/AKRCD4
        WRITE(19) IMAG,N6MN,N3MN,ADER
          IF(XXM(8,N).LT.SMALL)GOTO 830
          A(N6MN,N11KD2)=(PFQ*AL7(N))/HM
        IMAG = 1
        ADER = A(N6MN,N11KD2)*(AKRC*AKRCD1-1./XAL)
        WRITE(19) IMAG,N6MN,N11KD2,ADER
        IMAG = 2
        ADER = A(N6MN,N11KD2)*AKRC*AKRCD2
        WRITE(19) IMAG,N6MN,N11KD2,ADER
        IMAG = 3
        ADER = ADER*AKRCD3/AKRCD2
        WRITE(19) IMAG,N6MN,N11KD2,ADER
        IMAG = 4
        ADER = A(N6MN,N11KD2)*(AKRC*AKRCD4-1./XKD2)
        WRITE(19) IMAG,N6MN,N11KD2,ADER
        IMAG = 7
        ADER = A(N6MN,N11KD2)*AKRC*AKRCD7
        WRITE(19) IMAG,N6MN,N11KD2,ADER
  830     CONTINUE
          IF(XXM(6,N).LT.SMALL)GOTO 841
         A(N6MN ,N4MN)= ( -PFD*AL5(N))/HM
        IMAG = 1
        ADER = A(N6MN,N4MN)*(AK2*AK2D1-1./XAL)
        WRITE(19) IMAG,N6MN,N4MN,ADER
        IMAG = 8
```

```
      ADER = A(N6MN,N4MN)*AK2*AK2D8
      WRITE(19) IMAG,N6MN,N4MN,ADER
       IMAG = 9
      ADER = A(N6MN,N4MN)*(AK2*AK2D9-1./XKQL)
      WRITE(19) IMAG,N6MN,N4MN,ADER
      IMAG = 10
      ADER = A(N6MN,N4MN)*AK2*AK2D10
      WRITE(19) IMAG,N6MN,N4MN,ADER
      IMAG = 11
      ADER = ADER*AK2D11/AK2D10
      WRITE(19) IMAG,N6MN,N4MN,ADER
C      COMPUTE A(7,11)
       IF(XXM(7,N).LT.SMALL) GO TO 841
       A(N6MN,N11NEW)= (-PFD*AL6(N))/HM
      IMAG = 1
      ADER = A(N6MN,N11NEW)*(AK2*AK2D1-1./XAL)
      WRITE(19) IMAG,N6MN,N11NEW,ADER
      IMAG = 8
      ADER = A(N6MN,N11NEW)*AK2*AK2D8
      WRITE(19) IMAG,N6MN,N11NEW,ADER
      IMAG = 9
      ADER = ADER*AK2D9/AK2D8
      WRITE(19) IMAG,N6MN,N11NEW,ADER
      IMAG = 10
      ADER = A(N6MN,N11NEW)*(AK2*AK2D10-1./XKQ2)
      WRITE(19) IMAG,N6MN,N11NEW,ADER
      IMAG = 11
      ADER = A(N6MN,N11NEW)*AK2*AK2D11
      WRITE(19) IMAG,N6MN,N11NEW,ADER
        IF(XXM(9,N).LT.SMALL)GOTO 841
        A(N6MN,N11KQ3)=-(PFD*AL8(N))/HM
      IMAG = 1
      ADER = A(N6MN,N11KQ3)*(AK2*AK2D1-1./XAL)
      WRITE(19) IMAG,N6MN,N11KQ3,ADER
      IMAG = 8
      ADER = A(N6MN,N11KQ3)*AK2*AK2D8
      WRITE(19) IMAG,N6MN,N11KQ3,ADER
      IMAG = 9
      ADER = ADER*AK2D9/AK2D8
      WRITE(19) IMAG,N6MN,N11KQ3,ADER
      IMAG = 10
      ADER = ADER*AK2D10/AK2D9
      WRITE(19) IMAG,N6MN,N11KQ3,ADER

       IMAG = 11
       ADER = A(N6MN,N11KQ3)*(AK2*AK2D11-1./XKQ3)
       WRITE(19) IMAG,N6MN,N11KQ3,ADER
  841 CONTINUE
       A(N6MN ,N6MN)=  -DAMP/HM
       A(N7MN ,N6MN)=1.
C
C
C
C
C

       TV1(N)=EQ
       TV2(N)=-ED
       TC1 (N)=-CD*SND(N) -CQ*CSD(N)
       TC2 (N) = CD*CSD(N) -CQ*SND(N)
       AKED(N)=ED/ET
       AKEQ(N)=EQ/ET
C
C                                                    *   *   *   *   *
 6602 CONTINUE
C                                                    *   *   *   *   *
C
C
C
C   MULTIPLIER FOR VARIABLE KA FOR KEYS=2,4,6,7
       IF(VAMX.LT.SMALL)GOTO 515
       SINPH=EFC(N)/(ET*VAMX)
       ANGPH=ASIN(SINPH)
       GMULT=ET*COS(ANGPH)
       GEFF=GE*GMULT
       WRITE(6,1621) VAMX,GEFF
 1621  FORMAT(22X,'VAMX=',F6.2,4X,'*KA VARIES WITH DELAY ANGLE *',
```

```
     1 5X,'KEFF=',F6.2)
 515   CONTINUE
C
C
       IF(ITYPE(N).EQ.0)GO TO 8999
       IEFD=IEFD+1
        N5MN=3*NM+NMD1+NMQ1+IEFD
       A(N2MN,N5MN)=WRFX(N)
C
       AKTD(N)= (-GE/TE)*AKED(N)
       AKTQ(N)= (-GE/TE)*AKEQ(N)
C
C   VARIABLE KA FOR KEYS=2,4,6,7
        IF(VAMX.LT.SMALL)GOTO 7730
        GMULT=ET*COS(ANGPH)
        AKTD(N)=AKTD(N)*GMULT
        AKTQ(N)=AKTQ(N)*GMULT
 7730   CONTINUE
C
       IF(ITYPE(N).EQ.3) GO TO 2898
       IF(ITYPE(N).EQ.4) GO TO 2897
C
C      STATIC EXCITER WITH OR WITHOUT SPEED SIGNAL
C      ITYPE(N)=1,2,5,6,7
C
C      COMPUTE A(6,6),A(6,13)
       A(N5MN,N5MN)= -1./TE
       IF(ITYPE(N).EQ.2) GO TO 8999
       ISPED=ISPED+1
       ISV3=ISV3+1
        N10MN=JJ11+ISPED
        N11MN=JJ11+(NM1+NM3+NM4)+ISV3
C
       IF(ITFLT(N).NE.1) GO TO 6666
C        TORSIONAL FILTER
C
         INFLT=INFLT+1
       NFL1=NZWFL+INFLT
       NFL2= NFL1+NMFLT
       NFL3= NFL2+NMFLT
       NFL4= NFL3+NMFLT
       NINPUT=N10MN
 6666 CONTINUE
C
       A(N5MN,N11MN)=GE/TE
       GQ=(GD/GE)*TQ
       GTQ=GQ/TQ
       GTQN(N)=GTQ
C
C      COMPUTE A(12,1) TO A(12,5)  AND A(12,12),A(12,7)
      A(N10MN, N    ) =GTQ*A(N6MN, N    )
      IMAG = 1
      ADER = (XRC*AK12-1.)/(XAL**3)
      ADER = ADER+(XRC*AK12-AK1-XRC*AK12*AK11)/(XAL**2)
      ADER = ADER*PFQ/(HM*AKRC)
      ADER = ADER+ALLOW*AKRC*AKRCD1
       ADER=ADER*GTQ
      WRITE(19) IMAG,N10MN,N,ADER
      IMAG = 2
      ADER = (AK12-AK12*AK11)*PFQ/(AKRC*HM*XAL)
      ADER = ADER+ALLOW*AKRC*AKRCD2
       ADER=ADER*GTQ
      WRITE(19) IMAG,N10MN,N,ADER
      IMAG = 3
      ADER = (XRC*AK11-XRC+1.)*PFQ/(XAL*AKRC*HM*XKDL*XKDL)
      ADER = ADER+ALLOW*AKRC*AKRCD3
       ADER=ADER*GTQ
      WRITE(19) IMAG,N10MN,N,ADER
      IMAG = 4
      ADER = (XRC*AK11-XRC+1.)/(XAL*AKRC*HM*XKD2*XKD2)
      ADER = ADER*PFQ+ALLOW*AKRC*AKRCD4
       ADER=ADER*GTQ
      WRITE(19) IMAG,N10MN,N,ADER
      IMAG = 7
      ADER = (XRC*AK11-XRC+1.)/(XAL*AKRC*HM*XFL*XFL)
```

```
      ADER = ADER*PFQ+ALLOW*AKRC*AKRCD7
       ADER=ADER*GTQ
      WRITE(19) IMAG,N10MN,N,ADER
C
       A(N10MN,N1MN) =GTQ*A(N6MN,N1MN )
      IMAG = 1
      ADER = (-PFD/HM)*(AK2D1+1.-2./(XAL*AK2))/XAL**2
       ADER=ADER*GTQ
      WRITE(19) IMAG,N10MN,N1MN,ADER
      IMAG = 8
      ADER = (-PFD/HM)*AK2D8/XAL**2
       ADER=ADER*GTQ
      WRITE(19) IMAG,N10MN,N1MN,ADER
      IMAG = 9
      ADER = (-PFD/HM)*AK2D9/XAL**2
       ADER=ADER*GTQ
      WRITE(19) IMAG,N10MN,N1MN,ADER
      IMAG = 10
      ADER = ADER*AK2D10/AK2D9
       ADER=ADER*GTQ
      WRITE(19) IMAG,N10MN,N1MN,ADER
      IMAG = 11
      ADER = ADER*AK2D11/AK2D10
       ADER=ADER*GTQ
      WRITE(19) IMAG,N10MN,N1MN,ADER
      A(N10MN,N2MN ) =GTQ*A(N6MN,N2MN )
      IMAG = 1
      ADER = A(N6MN,N2MN)*(AKRC*AKRCD1-1./XAL)
       ADER=ADER*GTQ
      WRITE(19) IMAG,N10MN,N2MN,ADER
      IMAG = 2
      ADER = AKRC*AKRCD2*A(N6MN,N2MN)
       ADER=ADER*GTQ
      WRITE(19) IMAG,N10MN,N2MN,ADER
      IMAG = 3
      ADER = ADER*AKRCD3/AKRCD2
       ADER=ADER*GTQ
      WRITE(19) IMAG,N10MN,N2MN,ADER
      IMAG = 4
      ADER = ADER*AKRCD4/AKRCD3
       ADER=ADER*GTQ
      WRITE(19) IMAG,N10MN,N2MN,ADER
      IMAG = 7
      ADER = A(N6MN,N2MN)*(AKRC*AKRCD7-1./XFL)
       ADER=ADER*GTQ
      WRITE(19) IMAG,N10MN,N2MN,ADER
        IF(XXM(5,N).LT.SMALL)GOTO 831
      A(N10MN,N3MN ) =GTQ*A(N6MN,N3MN )
      IMAG = 1
      ADER = A(N6MN,N3MN)*(AKRC*AKRCD1-1./XAL)
       ADER=ADER*GTQ
      WRITE(19) IMAG,N10MN,N3MN,ADER
      IMAG = 2
      ADER = A(N6MN,N3MN)*AKRC*AKRCD2
       ADER=ADER*GTQ
      WRITE(19) IMAG,N10MN,N3MN,ADER
      IMAG = 3
      ADER = A(N6MN,N3MN)*(AKRC*AKRCD3-1./XKDL)
       ADER=ADER*GTQ
      WRITE(19) IMAG,N10MN,N3MN,ADER
      IMAG = 4
      ADER = A(N6MN,N3MN)*AKRC*AKRCD4
       ADER=ADER*GTQ
      WRITE(19) IMAG,N10MN,N3MN,ADER
      IMAG = 7
       ADER = ADER*AKRCD7/AKRCD4
        ADER=ADER*GTQ
       WRITE(19) IMAG,N10MN,N3MN,ADER
         IF(XXM(8,N).LT.SMALL)GOTO 831
         A(N10MN,N11KD2)=GTQ*A(N6MN,N11KD2)
       IMAG = 1
       ADER = A(N6MN,N11KD2)*(AKRC*AKRCD1-1./XAL)
        ADER=ADER*GTQ
       WRITE(19) IMAG,N10MN,N11KD2,ADER
       IMAG = 2
```

```
      ADER = A(N6MN,N11KD2)*AKRC*AKRCD2
       ADER=ADER*GTQ
      WRITE(19) IMAG,N10MN,N11KD2,ADER
      IMAG = 3
      ADER = ADER*AKRCD3/AKRCD2
       ADER=ADER*GTQ
      WRITE(19) IMAG,N10MN,N11KD2,ADER
      IMAG = 4
      ADER = A(N6MN,N11KD2)*(AKRC*AKRCD4-1./XKD2)
       ADER=ADER*GTQ
      WRITE(19) IMAG,N10MN,N11KD2,ADER
      IMAG = 7
      ADER = A(N6MN,N11KD2)*AKRC*AKRCD7
       ADER=ADER*GTQ
      WRITE(19) IMAG,N10MN,N11KD2,ADER
  831   CONTINUE
      A(N10MN,N6MN ) =GTQ*A(N6MN,N6MN )
       A(N10MN,N10MN ) =-1./TQ
        IF(XXM(6,N).LT.SMALL)GOTO 842
        A(N10MN,N4MN)=GTQ*A(N6MN,N4MN)
      IMAG = 1
      ADER = A(N6MN,N4MN)*(AK2*AK2D1-1./XAL)
       ADER=ADER*GTQ
       WRITE(19) IMAG,N10MN,N4MN,ADER
      IMAG = 8
      ADER = A(N6MN,N4MN)*AK2*AK2D8
       ADER=ADER*GTQ
       WRITE(19) IMAG,N10MN,N4MN,ADER
       IMAG = 9
      ADER = A(N6MN,N4MN)*(AK2*AK2D9-1./XKQL)
       ADER=ADER*GTQ
       WRITE(19) IMAG,N10MN,N4MN,ADER
      IMAG = 10
      ADER = A(N6MN,N4MN)*AK2*AK2D10
       ADER=ADER*GTQ
       WRITE(19) IMAG,N10MN,N4MN,ADER
      IMAG = 11
      ADER = ADER*AK2D11/AK2D10
       ADER=ADER*GTQ
       WRITE(19) IMAG,N10MN,N4MN,ADER
C       COMPUTE A(12,11)
       IF(XXM(7,N).LT.SMALL) GO TO 842
       A(N10MN,N11NEW)=GTQ*A(N6MN,N11NEW)
      IMAG = 1
      ADER = A(N6MN,N11NEW)*(AK2*AK2D1-1./XAL)
       ADER=ADER*GTQ
      WRITE(19) IMAG,N10MN,N11NEW,ADER
      IMAG = 8
      ADER = A(N6MN,N11NEW)*AK2*AK2D8
       ADER=ADER*GTQ
      WRITE(19) IMAG,N10MN,N11NEW,ADER
      IMAG = 9
      ADER = ADER*AK2D9/AK2D8
       ADER=ADER*GTQ
      WRITE(19) IMAG,N10MN,N11NEW,ADER
      IMAG = 10
      ADER = A(N6MN,N11NEW)*(AK2*AK2D10-1./XKQ2)
       ADER=ADER*GTQ
      WRITE(19) IMAG,N10MN,N11NEW,ADER
      IMAG = 11
      ADER = A(N6MN,N11NEW)*AK2*AK2D11
       ADER=ADER*GTQ
      WRITE(19) IMAG,N10MN,N11NEW,ADER
        IF(XXM(9,N).LT.SMALL)GOTO 842
        A(N10MN,N11KQ3)=GTQ*A(N6MN,N11KQ3)
      IMAG = 1
      ADER = A(N6MN,N11KQ3)*(AK2*AK2D1-1./XAL)
       ADER=ADER*GTQ
      WRITE(19) IMAG,N10MN,N11NEW,ADER
      IMAG = 8
      ADER = A(N6MN,N11KQ3)*AK2*AK2D8
       ADER=ADER*GTQ
       WRITE(19) IMAG,N10MN,N11KQ3,ADER
      IMAG = 9
      ADER = ADER*AK2D9/AK2D8
```

```
       ADER=ADER*GTQ
       WRITE(19) IMAG,N10MN,N11KQ3,ADER
      IMAG = 10
      ADER = ADER*AK2D10/AK2D9
       ADER=ADER*GTQ
       WRITE(19) IMAG,N10MN,N11KQ3,ADER
      IMAG = 11
      ADER = A(N6MN,N11KQ3)*(AK2*AK2D11-1./XKQ3)
       ADER=ADER*GTQ
       WRITE(19) IMAG,N10MN,N11KQ3,ADER
  842 CONTINUE
C
C
       IF(ITYPE(N).EQ.7) GO TO 8977
C
C        KEYS=1,5,6
       TT2=T1/T2
       A(N11MN,N11MN)=-1./T2
       IF(ITFLT(N).EQ.1) GO TO 850
       A(N11MN,N   )= TT2* A(N10MN,N  )
       A(N11MN,N1MN )=TT2 *A(N10MN,N1MN)
       A(N11MN,N2MN )=TT2 *A(N10MN,N2MN)
        IF(XXM(5,N).LT.SMALL)GOTO 832
       A(N11MN,N3MN )=TT2 *A(N10MN,N3MN)
        IF(XXM(8,N).LT.SMALL)GOTO 832
        A(N11MN,N11KD2)=TT2*A(N10MN,N11KD2)
  832   CONTINUE
       A(N11MN,N6MN )=TT2 *A(N10MN,N6MN)
       A(N11MN,N10MN)=TT2 *A(N10MN,N10MN ) +1./T2
C
        IF(XXM(6,N).LT.SMALL)GOTO 843
        A(N11MN,N4MN)=TT2*A(N10MN,N4MN)
       IF(XXM(7,N).LT.SMALL) GO TO 843
       A(N11MN,N11NEW)=TT2*A(N10MN,N11NEW)
        IF(XXM(9,N).LT.SMALL)GOTO 843
        A(N11MN,N11KQ3)=TT2*A(N10MN,N11KQ3)
  843 CONTINUE
C
       IF(ITYPE(N).EQ.1)GO TO 8999
       GO TO 8977
  850 CONTINUE
C        TORSIONAL FILTER(FOR KEYS=1,5,6)
C
       A(N11MN,NFL3) =TT2
       A(N11MN,NFL4) =1./T2
C
       IF(ITYPE(N).EQ.1) GO TO 4567
C
 8977 CONTINUE
C
C      KEYS=5,6,7
       ISV4=ISV4+1
       IF(ITYPE(N).EQ.6.AND.BEX3.LT.SMALL)ISV4=ISV4-1
        N12MN=JJ11+2*(NM1+NM3)+NM4+ISV4
C
       IF(ITYPE(N).EQ.6)GO TO 8988
       IF(ITYPE(N).EQ.7) GO TO 8978
C
C        KEY=5
C      STATIC EXTR WITH ANGLE SIGNAL
C       COMPUTE A(6,14),A(14,7),A(14,14)
C      KANG=AEX3    TANG=BEX3
       A(N5MN,N12MN)=GE/TE
       A(N12MN,N12MN)= -1./BEX3
       A(N12MN,N6MN)= AEX3/BEX3
       IF(ITFLT(N).EQ.1) GO TO 4567
       GO TO 8999
 8988 CONTINUE
C
C      KEY=6
C      STATIC EXTR WITH SPEED SIGNAL AND TGR
C      NOTE   X6=V1   AND NOT EF
C       SET A(6,13) TO 0.  FOR  KEY=6
       A(N5MN,N11MN)=0.
C
```

```
C        COMPUTE A(14,6),A(14,13),A(14,14)
C       AEX3=T3       BEX3=T4
C
        IF(BEX3.LE.SMALL)GOTO 7736
        A(N12MN,N5MN)=1./BEX3
        A(N12MN,N11MN)=GE/BEX3
        A(N12MN,N12MN)=-1./BEX3
C        FIELD CIRCUIT  COEFFTS
C        COMPUTE A(3,6),A(3,13),A(3,14)
C
        AEBX=AEX3/BEX3
        A(N2MN,N5MN)=AEBX*WRFX(N)
        A(N2MN,N11MN)=(AEBX*WRFX(N))*GE
        A(N2MN,N12MN)=(1.-AEBX)*WRFX(N)
C
C   EFFECT OF VARIABLE KA
         IF(VAMX.LT.SMALL)GOTO 7731
         A(N12MN,N11MN)=A(N12MN,N11MN)*GMULT
         A(N2MN,N11MN)=A(N2MN,N11MN)*GMULT
 7731    CONTINUE
C
         GOTO 7738
C   T4=0. FOR KEY=6
 7736    CONTINUE
         A(N2MN,N5MN)=WRFX(N)
         GEGM=GE
         IF(VAMX.GT.SMALL)GEGM=GE*GMULT
         A(N2MN,N11MN)=GEGM*WRFX(N)
 7738    CONTINUE
C
        IF(ITFLT(N).EQ.1) GO TO 4567
        GOTO 8999
C
 8978 CONTINUE
C
C       KEY=7(STATIC,SPEED SIGNAL,TGR, 2ND ORDR PH LD)
C
        IF(BEX3.GT.SMALL)ISV5=ISV5+1
         N13MN=JJ11+2*(NM1+NM3)+NM4+NM5+ISV5
C          NOTE X6=V1 AND NOT EF
C          SET A(6,13)=0. FOR KEY=7
        A(N5MN,N11MN)=0.
C
C
C          COMPUTE A(13,12),A(13,13),A(13,14)
C
        A(N11MN,N10MN) = 1./T22
        A(N11MN,N11MN) = -T2/T22
        A(N11MN,N12MN) = -1./T22
C          COMPUTE A(14,13)
        A(N12MN,N11MN) = 1.
C
C          COMPUTE A(15,14),A(15,13),A(15,12),A(15,6),A(15,15)
C
        IF(BEX3.GT.SMALL)GT4=GE/BEX3
C
C   VARIABLE KA
         IF(VAMX.LT.SMALL)GOTO 7732
         GT4=GT4*GMULT
 7732    CONTINUE
        T12T=T11/T22
        IF(BEX3.LE.SMALL)GOTO 7734
        A(N13MN,N12MN)= GT4*(1.-T12T)
        A(N13MN,N13MN)= -1./BEX3
        A(N13MN,N11MN)= GT4*(T1-(T12T*T2))
        A(N13MN,N10MN)= GT4*T12T
        A(N13MN,N5MN) =1./BEX3
C
C          COMPUTE A(3,6)A(3,12),A(3,13),A(3,14),A(3,15)  FOR KEY=7
C
        AEWN= AEX3*WRFX(N)
        A(N2MN,N5MN)= AEWN*A(N13MN,N5MN)
        A(N2MN,N10MN)=AEWN*A(N13MN,N10MN)
        A(N2MN,N11MN)=AEWN*A(N13MN,N11MN)
```

```
      A(N2MN,N12MN)=AEWN*A(N13MN,N12MN)
      A(N2MN,N13MN)=AEWN*A(N13MN,N13MN)+WRFX(N)
C
       GOTO 7735
C   T4=0. FOR KEY=7
 7734   CONTINUE
       GEWN=GE*WRFX(N)
       A(N2MN,N12MN)=GEWN*(1.-T12T)
       A(N2MN,N11MN)=GEWN*(T1-(T12T*T2))
      A(N2MN,N10MN)=GEWN*T12T
       A(N2MN,N5MN)=WRFX(N)
 7735   CONTINUE
      IF(ITFLT(N).NE.1) GO TO 8999
C
C       KEY=7 WITH TORSIONAL FILTER
      A(N11MN,NFL4) = A(N11MN,N10MN)
      A( N2MN,NFL4) = A( N2MN,N10MN)
      A(N11MN,N10MN)=0.
      A( N2MN,N10MN)=0.
      IF(BEX3.LE.SMALL)GOTO 4567
      A(N13MN,NFL4) = A(N13MN,N10MN)
      A(N13MN,N10MN)=0.
C
      GO TO 4567
C
C
C
C
C     CONVENTIONAL EXCITER
 2898 CONTINUE
      ISPED=ISPED+1
      ISV3=ISV3+1
       N10MN=JJ11+ISPED
       N11MN=JJ11+(NM1+NM3+NM4)+ISV3
C
C      COMPUTE A(6,6),A6,12),A(12,12),A(12,13),A(13,6),A(13,12 ),A(13,13)
      A(N5MN,N10MN)=1./T2
      A66C=-T1-((AEX3*BEX3 ) *EXP(BEX3*EFC(N)) )
      A(N5MN,N5MN)=A66C/T2
      A(N10MN,N10MN) = -1./TE
      A(N10MN,N11MN )= -GE/TE
      A(N11MN,N11MN)=-1./TQ
      A(N11MN,N10MN)=GD*A(N5MN,N10MN)
      A(N11MN,N5MN) =GD*A(N5MN,N5MN)
C
      GO TO 8999
C     AMPLYDINE EXCITER
 2897 CONTINUE
      ISPED=ISPED+1
       N10MN=JJ11+ISPED
C
C     COMPUTE A(6,6),A(6,11),A(11,11)
      A(N5MN,N5MN)=-1./T2
      A(N5MN,N10MN)=(1./T2)*(1.-T1/TE)
      A(N10MN,N10MN)=-1./TE
C     COMPUTE RATIO T1/T2 FOR LATER USE TO COMPUTE A(6,I)
      T1T2R(N)=T1/T2
C
      GO TO 8999
C
C                                          *  *  *  *
 4567 CONTINUE
C                                          *  *  *  *
C
C       TORSIONAL FILTER(KEYS=1,5,6,7 WITH ITFLT(N)=1)
C
      A(NFL1,NFL2)=1.
      A(NFL2,NINPUT)=1./XTFL(3,N)
      A(NFL2,NFL2)=-XTFL(2,N)/XTFL(3,N)
      A(NFL2,NFL1) =-1./XTFL(3,N)
        XTFLL= XTFL(1,N)/(XTFL(3,N)*XTFL(5,N))
      A(NFL3,NFL1)= (1./XTFL(5,N))-XTFLL
      A(NFL3,NFL2)=-XTFLL*XTFL(2,N)
      A(NFL3,NFL3)=-XTFL(4,N)/XTFL(5,N)
      A(NFL3,NFL4)=-1./XTFL(5,N)
```

```
      A(NFL3,NINPUT)=XTFLL
      A(NFL4,NFL3)=1.
C
C
C
C
C                                        *  *  *  *  *  *  *
C
 8999 CONTINUE
C
C                                        *  *  *  *  *  *  *
C
C***     ILCT=2
C***    WRITE(6,930) ILCT,A(1,1),A(2,1),A(6,1),A(7,1)
C
C
      WRITE(6,1675) NM,MM,NM0, NM1, NM2,NM3,NM4, NM5,NM6
     1   ,NMQ1,NMD1,NMQ2,NMD2,NMQ3
 1675 FORMAT(//22X, 'NM=',I3,4X, 'MM=',I3, 4X,    'NM0=',I3, 4X,
     1 'NM1=', I3,4X, 'NM2=', I3, 4X, 'NM3=',I3, 4X, 'NM4=',I3,  4X,
     2  'NM5=',I3,3X,'NM6=',I3,/,
     3   22X,'NMQ1=',I2,3X,'NMD1=',I2,3X,'NMQ2=',I2,4X,
     4  'NMD2=',I2,4X,'NMQ3=',I2)
C
      NEF=NM-IEFD
      NV2=NM1+NM3+NM4
      NV3=NM1+NM3
      NV4=NM5
      NV5=NM6
      NISV= (8*NM+IEFD)+ 2 *MM+ISPED+ISV3+ISV4+ISV5
       NISV=NISV-(NM-INKQ1)-(NM-INKD1)+INKD2+INKQ3
      NISV=NISV-(NM-INKQ2)
      NISV=NISV+4*INFLT
      WRITE(6,1676) NM0, NEF, NV2, ISPED, NV3,ISV3, NV4,ISV4, NV5,ISV5,
     1 NZ,NISV,INXT,IREAD
 1676 FORMAT(22X, '(NM0=' ,I3,1X,'NEF=',I3,')',4X,
     1 '(NV2=', I3, 1X,'ISPED=',I3,')', 4X,
     1 '(NV3=', I3, 1X,'ISV3=' ,I3,')', 4X,
     1 '(NV4=', I3, 1X,'ISV4=' ,I3,')', 4X,
     1 '(NV5=', I3, 1X,'ISV5=' ,I3,')', /
     1 22X, '(NZ=', I5, 2X,'NISV=', I5, ')', 10X, 'INXT=',I3,2X, 'IREAD=
     2',I3)
C
      IF(NZ.EQ.NISV) GO TO 1677
      WRITE(6,1679)
 1679 FORMAT(///6X, '***** NZ.NE.NISV **** CHECK DATA *****' //)
 1677 CONTINUE
C
C
C
C
C                                                 *   *   *   *   *
      IF(IREAD.NE.0) GO TO 6604
C                                                 *   *   *   *   *
      DO 6009 I=1,NM
      DO 6009 N=1,NM
      Z1(I,N)=  RN(I,N) *CSD(N) - XN(I,N)* SND(N)
      Z2(I,N)=  RN(I,N) *SND(N) + XN(I,N)* CSD(N)
      Z3(I,N)=  RN(I,N) *TC1(N) - XN(I,N)* TC2(N)
 6009 Z4(I,N)=  RN(I,N) *TC2(N) + XN(I,N)* TC1(N)
      DO 6099 N=1,NM
      DO 6099 J=1,NM
      B1(N,J)= CSD(N)*Z1(N,J) + SND(N)*Z2(N,J)
      B2(N,J)= SND(N)*Z1(N,J) - CSD(N)*Z2(N,J)
      B3(N,J)= CSD(N)*Z3(N,J) + SND(N)*Z4(N,J)
      B4(N,J)= CSD(N)*Z4(N,J) - SND(N)*Z3(N,J)
      IF(N.NE.J) GOTO 6099
      B3(N,J)= B3(N,J)+TV1(N)
      B4(N,J)= B4(N,J)+TV2(N)
 6099 CONTINUE
C
C     COMPUTE  A(1,1) TO A(1,5) AND A(1,8 )
C
      INKQ2=0
       INKD1=0
```

```
        INKQ1=0
        INKD2=0
        INKQ3=0
C
       DO 6188 J=1,NM
         J1= NM+J
         J2= 2*NM+J
        IF(XXM(5,J).GE.SMALL)INKD1=INKD1+1
        J3=3*NM+INKD1
        IF(XXM(8,J).GE.SMALL)INKD2=INKD2+1
        J11KD2=JJ8+NMQ2+INKD2
        IF(XXM(6,J).GE.SMALL)INKQ1=INKQ1+1
        J4=3*NM+NMD1+INKQ1
        J7=5*NM-NM0+NMD1+NMQ1+J
       IF(XXM(7,J).GE.SMALL) INKQ2=INKQ2+1
       J11NEW=JJ8+INKQ2
        IF(XXM(9,J).GE.SMALL)INKQ3=INKQ3+1
        J11KQ3=JJ8+NMQ2+NMD2+INKQ3
C
       DO 6188 I=1,NM
         I1= NM+I
       A(I,J)= W0*B1(I,J)*AL1(J)
      IMAG=1
      ADER=A(I,J)*AL11/AL1(J)
      WRITE(19) IMAG,I,J,ADER
      IMAG=2
      ADER=A(I,J)*AL12/AL1(J)
      WRITE(19) IMAG,I,J,ADER
      IMAG=3
      ADER=A(I,J)*AL13/AL1(J)
      WRITE(19) IMAG,I,J,ADER
      IMAG=4
      ADER=A(I,J)*AL14/AL1(J)
      WRITE(19) IMAG,I,J,ADER
      IMAG=7
      ADER=A(I,J)*AL17/AL1(J)
      WRITE(19) IMAG,I,J,ADER
C**     ILCT=3
C**    WRITE(6,930) ILCT,A(1,1),A(2,1),A(6,1),A(7,1)
       A(I, J1) =W0*B2(I,J) * AL4(J)
      IMAG=1
      ADER=A(I,J1)*AL41/AL4(J)
      WRITE(19) IMAG,I,J1,ADER
      IMAG=8
      ADER=A(I,J1)*AL48/AL4(J)
      WRITE(19) IMAG,I,J1,ADER
      IMAG=9
      ADER=A(I,J1)*AL49/AL4(J)
      WRITE(19) IMAG,I,J1,ADER
      IMAG=10
      ADER=A(I,J1)*AL410/AL4(J)
      WRITE(19) IMAG,I,J1,ADER
      IMAG=11
      ADER=A(I,J1)*AL411/AL4(J)
      WRITE(19) IMAG,I,J1,ADER
       A(I, J2) =W0*B1(I,J) * AL2(J)
      IMAG=1
      ADER=A(I,J2)*AL21/AL2(J)
      WRITE(19) IMAG,I,J2,ADER
      IMAG=2
      ADER=A(I,J2)*AL22/AL2(J)
      WRITE(19) IMAG,I,J2,ADER
      IMAG=3
      ADER=A(I,J2)*AL23/AL2(J)
      WRITE(19) IMAG,I,J2,ADER
      IMAG=4
      ADER=A(I,J2)*AL24/AL2(J)
      WRITE(19) IMAG,I,J2,ADER
      IMAG=7
      ADER=A(I,J2)*AL27/AL2(J)
      WRITE(19) IMAG,I,J2,ADER
        IF(XXM(5,J).LT.SMALL) GOTO 835
       A(I, J3) =W0*B1(I,J) * AL3(J)
      IMAG=1
      ADER=A(I,J3)*AL31/AL3(J)
```

```
      WRITE(19) IMAG,I,J3,ADER
      IMAG=2
      ADER=A(I,J3)*AL32/AL3(J)
      WRITE(19) IMAG,I,J3,ADER
      IMAG=3
      ADER=A(I,J3)*AL33/AL3(J)
      WRITE(19) IMAG,I,J3,ADER
      IMAG=4
      ADER=A(I,J3)*AL34/AL3(J)
      WRITE(19) IMAG,I,J3,ADER
      IMAG=7
      ADER=A(I,J3)*AL37/AL3(J)
      WRITE(19) IMAG,I,J3,ADER
       A(I1,J3)= -W0*B2(I,J) *AL3(J)
      IMAG=1
      ADER=A(I1,J3)*AL31/AL3(J)
      WRITE(19) IMAG,I1,J3,ADER
      IMAG=2
      ADER=A(I1,J3)*AL32/AL3(J)
      WRITE(19) IMAG,I1,J3,ADER
      IMAG=3
      ADER=A(I1,J3)*AL33/AL3(J)
      WRITE(19) IMAG,I1,J3,ADER
      IMAG=4
      ADER=A(I1,J3)*AL34/AL3(J)
      WRITE(19) IMAG,I1,J3,ADER
      IMAG=7
      ADER=A(I1,J3)*AL37/AL3(J)
      WRITE(19) IMAG,I1,J3,ADER
        IF(XXM(8,J).LT.SMALL)GOTO 835
        A(I,J11KD2)=W0*B1(I,J)*AL7(J)
      IMAG=1
      ADER=A(I,J11KD2)*AL71/AL7(J)
      WRITE(19) IMAG,I,J11KD2,ADER
      IMAG=2
      ADER=A(I,J11KD2)*AL72/AL7(J)
      WRITE(19) IMAG,I,J11KD2,ADER
      IMAG=3
      ADER=A(I,J11KD2)*AL73/AL7(J)
      WRITE(19) IMAG,I,J11KD2,ADER
      IMAG=4
      ADER=A(I,J11KD2)*AL74/AL7(J)
      WRITE(19) IMAG,I,J11KD2,ADER
      IMAG=7
      ADER=A(I,J11KD2)*AL77/AL7(J)
      WRITE(19) IMAG,I,J11KD2,ADER
        A(I1,J11KD2)=-W0*B2(I,J)*AL7(J)
      IMAG=1
      ADER=A(I1,J11KD2)*AL71/AL7(J)
      WRITE(19) IMAG,I1,J11KD2,ADER
      IMAG=2
      ADER=A(I1,J11KD2)*AL72/AL7(J)
      WRITE(19) IMAG,I1,J11KD2,ADER
      IMAG=3
      ADER=A(I1,J11KD2)*AL73/AL7(J)
      WRITE(19) IMAG,I1,J11KD2,ADER
      IMAG=4
      ADER=A(I1,J11KD2)*AL74/AL7(J)
      WRITE(19) IMAG,I1,J11KD2,ADER
      IMAG=7
      ADER=A(I1,J11KD2)*AL77/AL7(J)
      WRITE(19) IMAG,I1,J11KD2,ADER
 835   CONTINUE
       A(I, J7) =W0*B3(I,J)
C
C      COMPUTE A(2,1) TO A(2,5) AND A(2,8 )
       A(I1,J )= -W0*B2(I,J) *AL1(J)
      IMAG=1
      ADER=A(I1,J)*AL11/AL1(J)
      WRITE(19) IMAG,I1,J,ADER
      IMAG=2
      ADER=A(I1,J)*AL12/AL1(J)
      WRITE(19) IMAG,I1,J,ADER
      IMAG=3
      ADER=A(I1,J)*AL13/AL1(J)
```

```
      WRITE(19) IMAG,I1,J,ADER
      IMAG=4
      ADER=A(I1,J)*AL14/AL1(J)
      WRITE(19) IMAG,I1,J,ADER
      IMAG=7
      ADER=A(I1,J)*AL17/AL1(J)
      WRITE(19) IMAG,I1,J,ADER
       A(I1,J2)= -W0*B2(I,J) *AL2(J)
      IMAG=1
      ADER=A(I1,J2)*AL21/AL2(J)
      WRITE(19) IMAG,I1,J2,ADER
      IMAG=2
      ADER=A(I1,J2)*AL22/AL2(J)
      WRITE(19) IMAG,I1,J2,ADER
      IMAG=3
      ADER=A(I1,J2)*AL23/AL2(J)
      WRITE(19) IMAG,I1,J2,ADER
      IMAG=4
      ADER=A(I1,J2)*AL24/AL2(J)
      WRITE(19) IMAG,I1,J2,ADER
      IMAG=7
      ADER=A(I1,J2)*AL27/AL2(J)
      WRITE(19) IMAG,I1,J2,ADER
       A(I1,J1)=  W0*B1(I,J) *AL4(J)
      IMAG=1
      ADER=A(I1,J1)*AL41/AL4(J)
      WRITE(19) IMAG,I1,J1,ADER
      IMAG=8
      ADER=A(I1,J1)*AL48/AL4(J)
      WRITE(19) IMAG,I1,J1,ADER
      IMAG=9
      ADER=A(I1,J1)*AL49/AL4(J)
      WRITE(19) IMAG,I1,J1,ADER
      IMAG=10
      ADER=A(I1,J1)*AL410/AL4(J)
      WRITE(19) IMAG,I1,J1,ADER
      IMAG=11
      ADER=A(I1,J1)*AL411/AL4(J)
      WRITE(19) IMAG,I1,J1,ADER
       A(I1,J7)=  W0*B4(I,J)
C
        IF(XXM(6,J).LT.SMALL)GOTO 845
        A(I,J4)=W0*B2(I,J)*AL5(J)
      IMAG=1
      ADER=A(I,J4)*AL51/AL5(J)
      WRITE(19) IMAG,I,J4,ADER
      IMAG=8
      ADER=A(I,J4)*AL58/AL5(J)
      WRITE(19) IMAG,I,J4,ADER
      IMAG=9
      ADER=A(I,J4)*AL59/AL5(J)
      WRITE(19) IMAG,I,J4,ADER
      IMAG=10
      ADER=A(I,J4)*AL510/AL5(J)
      WRITE(19) IMAG,I,J4,ADER
      IMAG=11
      ADER=A(I,J4)*AL511/AL5(J)
      WRITE(19) IMAG,I,J4,ADER
       A(I1,J4)=W0*B1(I,J)*AL5(J)
      IMAG=1
      ADER=A(I1,J4)*AL51/AL5(J)
      WRITE(19) IMAG,I1,J4,ADER
      IMAG=8
      ADER=A(I1,J4)*AL58/AL5(J)
      WRITE(19) IMAG,I1,J4,ADER
      IMAG=9
      ADER=A(I1,J4)*AL59/AL5(J)
      WRITE(19) IMAG,I1,J4,ADER
      IMAG=10
      ADER=A(I1,J4)*AL510/AL5(J)
      WRITE(19) IMAG,I1,J4,ADER
      IMAG=11
      ADER=A(I1,J4)*AL511/AL5(J)
      WRITE(19) IMAG,I1,J4,ADER
       IF(XXM(7,J).LT.SMALL) GO TO 845
```

```
C
C        COMPUTE A(1,11),A(2,11)
       A(I,J11NEW)=W0*B2(I,J)*AL6(J)
      IMAG=1
      ADER=A(I,J11NEW)*AL61/AL6(J)
      WRITE(19) IMAG,I,J11NEW,ADER
      IMAG=8
      ADER=A(I,J11NEW)*AL68/AL6(J)
      WRITE(19) IMAG,I,J11NEW,ADER
      IMAG=9
      ADER=A(I,J11NEW)*AL69/AL6(J)
      WRITE(19) IMAG,I,J11NEW,ADER
      IMAG=10
      ADER=A(I,J11NEW)*AL610/AL6(J)
      WRITE(19) IMAG,I,J11NEW,ADER
      IMAG=11
      ADER=A(I,J11NEW)*AL611/AL6(J)
      WRITE(19) IMAG,I,J11NEW,ADER
      A(I1,J11NEW)=W0*B1(I,J)*AL6(J)
      IMAG=1
      ADER=A(I1,J11NEW)*AL61/AL6(J)
      WRITE(19) IMAG,I1,J11NEW,ADER
      IMAG=8
      ADER=A(I1,J11NEW)*AL68/AL6(J)
      WRITE(19) IMAG,I1,J11NEW,ADER
      IMAG=9
      ADER=A(I1,J11NEW)*AL69/AL6(J)
      WRITE(19) IMAG,I1,J11NEW,ADER
      IMAG=10
      ADER=A(I1,J11NEW)*AL610/AL6(J)
      WRITE(19) IMAG,I1,J11NEW,ADER
      IMAG=11
      ADER=A(I1,J11NEW)*AL611/AL6(J)
      WRITE(19) IMAG,I1,J11NEW,ADER
        IF(XXM(9,J).LT.SMALL)GOTO 845
        A(I,J11KQ3)=W0*B2(I,J)*AL8(J)
      IMAG=1
      ADER=A(I,J11KQ3)*AL81/AL8(J)
      WRITE(19) IMAG,I,J11KQ3,ADER
      IMAG=8
      ADER=A(I,J11KQ3)*AL88/AL8(J)
      WRITE(19) IMAG,I,J11KQ3,ADER
      IMAG=9
      ADER=A(I,J11KQ3)*AL89/AL8(J)
      WRITE(19) IMAG,I,J11KQ3,ADER
      IMAG=10
      ADER=A(I,J11KQ3)*AL810/AL8(J)
      WRITE(19) IMAG,I,J11KQ3,ADER
      IMAG=11
      ADER=A(I,J11KQ3)*AL811/AL8(J)
      WRITE(19) IMAG,I,J11KQ3,ADER
        A(I1,J11KQ3)=W0*B1(I,J)*AL8(J)
      IMAG=1
      ADER=A(I1,J11KQ3)*AL81/AL8(J)
      WRITE(19) IMAG,I1,J11KQ3,ADER
      IMAG=8
      ADER=A(I1,J11KQ3)*AL88/AL8(J)
      WRITE(19) IMAG,I1,J11KQ3,ADER
      IMAG=9
      ADER=A(I1,J11KQ3)*AL89/AL8(J)
      WRITE(19) IMAG,I1,J11KQ3,ADER
      IMAG=10
      ADER=A(I1,J11KQ3)*AL810/AL8(J)
      WRITE(19) IMAG,I1,J11KQ3,ADER
      IMAG=11
      ADER=A(I1,J11KQ3)*AL811/AL8(J)
      WRITE(19) IMAG,I1,J11KQ3,ADER
C
  845 CONTINUE
         IF(I.NE.J) GOTO 6188
       A(I,J)= A(I,J)+W0*R(J)*AL1(J)
       A(I,J1)= A(I,J1)+W0
       A(I,J2)= A(I,J2)+W0 *R(J) *AL2(J)
        IF(XXM(5,J).LT.SMALL)GOTO 836
       A(I,J3)= A(I,J3)+W0 *R(J) *AL3(J)
```

```
        IF(XXM(8,J).LT.SMALL)GOTO 836
        A(I,J11KD2)=A(I,J11KD2)+W0*R(J)*AL7(J)
  836   CONTINUE
       A(I1,J)= A(I1,J) -W0
       A(I1,J1)= A(I1,J1)+W0*R(J) *AL4(J)
        IF(XXM(6,J).LT.SMALL)GOTO 6188
       A(I1,J4)= A(I1,J4)+W0*R(J)*AL5(J)
       IF(XXM(7,J).LT.SMALL) GO TO 6188
       A(I1,J11NEW)=A(I1,J11NEW)+ W0*R(J)*AL6(J)
        IF(XXM(9,J).LT.SMALL)GOTO 6188
        A(I1,J11KQ3)=A(I1,J11KQ3)+W0*R(J)*AL8(J)
 6188 CONTINUE
C                                                    *   *   *   *   *
 6604 CONTINUE
C                                                    *   *   *   *   *
C**     ILCT=4
C**    WRITE(6,930) ILCT,A(1,1),A(2,1),A(6,1),A(7,1)
C
C      COMPUTE A(6,1) TO A(6,5) AND A(6,8 )  FOR STATIC OR AMPLDN EXCTR
C      OR A(12,1) TO A(12,5) AND A(12,8) FOR CONVNL OR AMPLDN EXCTR
C
       INKQ2=0
        INKD2=0
        INKD1=0
        INKQ1=0
        INKQ3=0
C
       DO 7969 J=1,NM
          J1=  NM+J
          J2=2*NM+J
        IF(XXM(5,J).GE.SMALL)INKD1=INKD1+1
        IF(XXM(8,J).GE.SMALL)INKD2=INKD2+1
        IF(XXM(6,J).GE.SMALL)INKQ1=INKQ1+1
        J3=3*NM+INKD1
        J11KD2=JJ8+NMQ2+INKD2
        J4=3*NM+NMD1+INKQ1
        J7=5*NM-NM0+NMD1+NMQ1+J
       IF(XXM(7,J).GE.SMALL) INKQ2=INKQ2+1
        IF(XXM(9,J).GE.SMALL)INKQ3=INKQ3+1
       J11NEW=JJ8+INKQ2
        J11KQ3=JJ8+NMQ2+NMD2+INKQ3
       IEFD=0
       IS11=0
       DO 7969 I=1,NM
       IF(ITYPE(I).EQ.0)GO TO 7969
       IEFD=IEFD+1
C
       IF(ITYPE(I).NE.2) IS11=IS11+1
C      CONVNL OR AMPLDN EXCTR
        I1=JJ11+IS11
C
C      STATIC EXCITER
       IF(ITYPE(I).EQ.3) GO TO 7968
       IF(ITYPE(I).EQ.4) GO TO 7968
C      ITYPE(N)=1,2,5,6,7
        I1=3*NM+NMD1+NMQ1+IEFD
 7968 CONTINUE
C
      IF(IOPT.LT.50) GO TO 3
      IF(I.NE.MCNO) GO TO  3
       IF(J.NE.MCNO) GO TO 3
       IF(IDIST.EQ.2) GO TO 2
      IF(ITYPE(I).LE.4) X0(I1)=-1./XXTR(2,I)
      IF(ITYPE(I).EQ.6.OR.ITYPE(I).EQ.7) X0(I1)=-1./XXTR(2,I)
      IX0=I1
      IF(IPSI.NE.0) GO TO 3
      IX0=IX0-2*NM
      X0(IX0)=X0(I1)
      X0(I1)=.0
       WRITE(6,1008) IX0
   2  CONTINUE
      IF(IDIST.NE.2) GO TO 3
      IX0=6*NM+MCNO
       IF(IPSI.EQ.0) IX0=IX0-2*NM
```

```
      X0(IX0)=W0/(2.*HMH(MCNO))
      WRITE(6,1008) IX0
 3    CONTINUE
      XX= AKTD(I)*B1(I,J) - AKTQ(I)*B2(I,J)
      XY= AKTD(I)*B2(I,J)+AKTQ(I)*B1(I,J)
     A(I1,J)=XX*AL1(J)
     IMAG=1
     ADER=XX*AL11
     WRITE(19) IMAG,I1,J,ADER
     IMAG=2
     ADER=XX*AL12
     WRITE(19) IMAG,I1,J,ADER
     IMAG=3
     ADER=XX*AL13
     WRITE(19) IMAG,I1,J,ADER
     IMAG=4
     ADER=XX*AL14
     WRITE(19) IMAG,I1,J,ADER
     IMAG=7
     ADER=XX*AL17
     WRITE(19) IMAG,I1,J,ADER
      A(I1,J2)= XX*AL2(J)
     IMAG=1
     ADER=XX*AL21
     WRITE(19) IMAG,I1,J2,ADER
     IMAG=2
     ADER=XX*AL22
     WRITE(19) IMAG,I1,J2,ADER
     IMAG=3
     ADER=XX*AL23
     WRITE(19) IMAG,I1,J2,ADER
     IMAG=4
     ADER=XX*AL24
     WRITE(19) IMAG,I1,J2,ADER
     IMAG=7
     ADER=XX*AL27
     WRITE(19) IMAG,I1,J2,ADER
       IF(XXM(5,J).LT.SMALL)GOTO 837
      A(I1,J3)= XX*AL3(J)
     IMAG=1
     ADER=XX*AL31
     WRITE(19) IMAG,I1,J3,ADER
     IMAG=2
     ADER=XX*AL32
     WRITE(19) IMAG,I1,J3,ADER
     IMAG=3
     ADER=XX*AL33
     WRITE(19) IMAG,I1,J3,ADER
     IMAG=4
     ADER=XX*AL34
     WRITE(19) IMAG,I1,J3,ADER
     IMAG=7
     ADER=XX*AL37
     WRITE(19) IMAG,I1,J3,ADER
       IF(XXM(8,J).LT.SMALL)GOTO 837
       A(I1,J11KD2)=XX*AL7(J)
     IMAG=1
     ADER=XX*AL71
     WRITE(19) IMAG,I1,J11KD2,ADER
     IMAG=2
     ADER=XX*AL72
     WRITE(19) IMAG,I1,J11KD2,ADER
     IMAG=3
     ADER=XX*AL73
     WRITE(19) IMAG,I1,J11KD2,ADER
     IMAG=4
     ADER=XX*AL74
     WRITE(19) IMAG,I1,J11KD2,ADER
     IMAG=7
     ADER=XX*AL77
     WRITE(19) IMAG,I1,J11KD2,ADER
837    CONTINUE
      A(I1,J1)= XY*AL4(J)
     IMAG=1
     ADER=XY*AL41
```

```
      WRITE(19) IMAG,I1,J1,ADER
      IMAG=8
      ADER=XY*AL48
      WRITE(19) IMAG,I1,J1,ADER
      IMAG=9
      ADER=XY*AL49
      WRITE(19) IMAG,I1,J1,ADER
      IMAG=10
      ADER=XY*AL410
      WRITE(19) IMAG,I1,J1,ADER
      IMAG=11
      ADER=XY*AL411
      WRITE(19) IMAG,I1,J1,ADER
       A(I1,J7)=AKTD(I)*B3(I,J)+AKTQ(I)*B4(I,J)
        IF(XXM(6,J).LT.SMALL)GOTO 846
        A(I1,J4)=XY*AL5(J)
      IMAG=1
      ADER=XY*AL51
      WRITE(19) IMAG,I1,J4,ADER
      IMAG=8
      ADER=XY*AL58
      WRITE(19) IMAG,I1,J4,ADER
      IMAG=9
       ADER=XY*AL59
      WRITE(19) IMAG,I1,J4,ADER
      IMAG=10
      ADER=XY*AL510
      WRITE(19) IMAG,I1,J4,ADER
      IMAG=11
      ADER=XY*AL511
      WRITE(19) IMAG,I1,J4,ADER
       IF(XXM(7,J).LT.SMALL) GO TO 846
       A(I1,J11NEW)=XY*AL6(J)
      IMAG=1
      ADER=XY*AL61
      WRITE(19) IMAG,I1,J11NEW,ADER
      IMAG=8
      ADER=XY*AL68
      WRITE(19) IMAG,I1,J11NEW,ADER
      IMAG=9
      ADER=XY*AL69
      WRITE(19) IMAG,I1,J11NEW,ADER
      IMAG=10
      ADER=XY*AL610
      WRITE(19) IMAG,I1,J11NEW,ADER
      IMAG=11
      ADER=XY*AL611
      WRITE(19) IMAG,I1,J11NEW,ADER
        IF(XXM(9,J).LT.SMALL)GOTO 846
        A(I1,J11KQ3)=XY*AL8(J)
      IMAG=1
      ADER=XY*AL81
      WRITE(19) IMAG,I1,J11KQ3,ADER
      IMAG=8
      ADER=XY*AL88
      WRITE(19) IMAG,I1,J11KQ3,ADER
      IMAG=9
      ADER=XY*AL89
      WRITE(19) IMAG,I1,J11KQ3,ADER
      IMAG=10
      ADER=XY*AL810
      WRITE(19) IMAG,I1,J11KQ3,ADER
      IMAG=11
      ADER=XY*AL811
      WRITE(19) IMAG,I1,J11KQ3,ADER
  846 CONTINUE
       IF(ITYPE(I).NE.4) GO TO 7969
C      AMPLYDINE EXCITER
C
       II1=3*NM+NMD1+NMQ1+IEFD
      A(II1,J )= T1T2R(I)*A(I1,J )
      A(II1,J1)= T1T2R(I)*A(I1,J1)
      A(II1,J2)= T1T2R(I)*A(I1,J2)
       IF(XXM(5,J).LT.SMALL)GOTO 838
      A(II1,J3)= T1T2R(I)*A(I1,J3)
```

```
        IF(XXM(8,J).LT.SMALL)GOTO 838
        A(II1,J11KD2)=T1T2R(I)*A(I1,J11KD2)
 838    CONTINUE
        IF(XXM(6,J).LT.SMALL)GOTO 847

        A(II1,J4)= T1T2R(I)*A(I1,J4)
        IF(XXM(7,J).LT.SMALL) GO TO 847
        A(II1,J11NEW)=T1T2R(I)*A(I1,J11NEW)
        IF(XXM(9,J).LT.SMALL)GOTO 847
        A(II1,J11KQ3)=T1T2R(I)*A(I1,J11KQ3)
  847 CONTINUE
        A(II1,J7)= T1T2R(I)*A(I1,J7)
 7969 CONTINUE
C
C**     ILCT=5
C**     WRITE(6,930) ILCT,A(1,1),A(2,1),A(6,1),A(7,1)
C
        IF(MM.EQ.0) GOTO 7008                                          *******
C                                          *   *   *   *   *
        IF(IREAD.NE.0) GO TO 6608
C                                          *   *   *   *   *
        WRITE(6,1415)
 1415 FORMAT( /// ' CONSTANT FLUX MACHINES'/)
C
C
        DO 6809 J=1,MM
        JNM=J+NM
        EM=EMN(JNM)
        ANGLE= ANG(JNM)/ RADIAN
C         ANGLE IN DEGREES FOR PRINTING ONLY
        ANGLD=ANG(JNM)
        PD=PW(JNM)
        PQ=PX(JNM)
 6912 CONTINUE
        HM=HMCF(J)
        DAMP=DAMPCF(J)
        WRITE(6,1416) EM,ANGLD,PD,PQ,HM,DAMP,JNM
     1 ,INAME1(JNM),INAME2(JNM)
 1416 FORMAT(/10X, 'ET=', F8.3,4X, 'ANG=',F7.3, 4X,'P =',F8.3, 4X,
     1 'Q=',F7.2,4X, 'H=',F7.2,3X, 'DAMP=',F7.2,4X, 'GEN NO.=',I3,2X,
     2 2A6)
          EMD(J)= EM*COS(ANGLE)
          EMQ(J)= EM*SIN(ANGLE)
        HMM(J)= (2.*HM)/W0
        DAMP=DAMP/W0
        DO 7809 I=1,NM
        Z5(I,J)= RG(I,J)*EMQ(J)+XB(I,J)*EMD(J)
        Z6(I,J)= XB(I,J)*EMQ(J)-RG(I,J)*EMD(J)
 7809 CONTINUE
        EDEM= EMD(J)/(EM*EM)
        EQEM= EMQ(J)/(EM*EM)
        CMD= PD*EDEM+PQ*EQEM
        CMQ= PD*EQEM-PQ*EDEM
C
C       COMPUTE  A(9,9)
        NM0J=6*NM+NMD1+NMQ1-NM0+J
        N11J=NM0J+MM
C
        A(NM0J,NM0J)= -DAMP/HMM(J)
C
C       COMPUTE PART OF A(9,10)
        A(NM0J,N11J)=(EMQ(J)*CMD-EMD(J)*CMQ)/HMM(J)

 6809 CONTINUE
C
        DO 1109 I=1,MM
        DO 1109 J=1,NM
        D1(I,J)= RG(J,I)*CSD(J) - XB(J,I)*SND(J)
        D2(I,J)= RG(J,I)*SND(J) + XB(J,I)*CSD(J)
        D3(I,J)= RG(J,I)*TC1(J) - XB(J,I)*TC2(J)
        D4(I,J)= RG(J,I)*TC2(J) + XB(J,I)*TC1(J)
 1109 CONTINUE
        DO 8208 I=1,NM
        DO 8208 J=1,MM
        B5(I,J)= CSD(I)*Z5(I,J) + SND(I)*Z6(I,J)
 8208   B6(I,J)= CSD(I)*Z6(I,J) - SND(I)*Z5(I,J)
```

```
C
C       COMPUTE A(1,10), AND A(2,10)
        DO 8218 J=1,MM
         J1=6*NM+NMD1+NMQ1-NM0+MM+J
        DO 8218 I=1,NM
        I1=NM+I
        A(I ,J1)= W0*B5(I,J)
 8218   A(I1,J1)= W0* B6(I,J)
C
C       COMPUTE A( 9,1) TO A( 9,5) AND A(9,8)
        INKQ2=0
         INKD1=0
         INKQ1=0
         INKD2=0
         INKQ3=0
C
        DO 8989 J=1,NM
          J1=  NM +J
          J2=2*NM +J
         IF(XXM(5,J).GE.SMALL)INKD1=INKD1+1
         IF(XXM(8,J).GE.SMALL)INKD2=INKD2+1
         IF(XXM(6,J).GE.SMALL)INKQ1=INKQ1+1
         IF(XXM(9,J).GE.SMALL)INKQ3=INKQ3+1
        IF(XXM(7,J).GE.SMALL) INKQ2=INKQ2+1
         J3=3*NM+INKD1
         J4=3*NM+NMD1+INKQ1
        J11NEW=JJ8+INKQ2
         J11KD2=JJ8+NMQ2+INKD2
         J11KQ3=JJ8+NMQ2+NMD2+INKQ3
         J7=5*NM+NMD1+NMQ1-NM0+J
        DO 8989 I=1,MM
         I1=6*NM+NMD1+NMQ1-NM0+I
        XX= -(EMD(I)*D1(I,J)+EMQ(I)*D2(I,J))/HMM(I)
        XY=  (EMD(I)*D2(I,J)-EMQ(I)*D1(I,J))/HMM(I)
        A(I1,J )= XX*AL1(J)
       IMAG=1
       ADER=XX*AL11
       WRITE(19) IMAG,I1,J,ADER
       IMAG=2
       ADER=XX*AL12
       WRITE(19) IMAG,I1,J,ADER
       IMAG=3
       ADER=XX*AL13
       WRITE(19) IMAG,I1,J,ADER
       IMAG=4
       ADER=XX*AL14
       WRITE(19) IMAG,I1,J,ADER
       IMAG=7
       ADER=XX*AL17
       WRITE(19) IMAG,I1,J,ADER
        A(I1,J1)= XY*AL4(J)
       IMAG=1
       ADER=XY*AL41
       WRITE(19) IMAG,I1,J1,ADER
       IMAG=8
       ADER=XY*AL48
       WRITE(19) IMAG,I1,J1,ADER
       IMAG=9
       ADER=XY*AL49
       WRITE(19) IMAG,I1,J1,ADER
       IMAG=10
       ADER=XY*AL410
       WRITE(19) IMAG,I1,J1,ADER
       IMAG=11
       ADER=XY*AL411
       WRITE(19) IMAG,I1,J1,ADER
        A(I1,J2)= XX*AL2(J)
       IMAG=1
       ADER=XX*AL21
       WRITE(19) IMAG,I1,J2,ADER
       IMAG=2
       ADER=XX*AL22
       WRITE(19) IMAG,I1,J2,ADER
       IMAG=3
       ADER=XX*AL23
```

```
      WRITE(19) IMAG,I1,J2,ADER
      IMAG=4
      ADER=XX*AL24
      WRITE(19) IMAG,I1,J2,ADER
      IMAG=7
      ADER=XX*AL27
      WRITE(19) IMAG,I1,J2,ADER
        IF(XXM(5,J).LT.SMALL)GOTO 839
       A(I1,J3)= XX*AL3(J)
      IMAG=1
      ADER=XX*AL31
      WRITE(19) IMAG,I1,J3,ADER
      IMAG=2
      ADER=XX*AL32
      WRITE(19) IMAG,I1,J3,ADER
      IMAG=3
      ADER=XX*AL33
      WRITE(19) IMAG,I1,J3,ADER
      IMAG=4
      ADER=XX*AL34
      WRITE(19) IMAG,I1,J3,ADER
      IMAG=7
      ADER=XX*AL37
      WRITE(19) IMAG,I1,J3,ADER
        IF(XXM(8,J).LT.SMALL)GOTO 839
        A(I1,J11KD2)=XX*AL7(J)
      IMAG=1
      ADER=XX*AL71
      WRITE(19) IMAG,I1,J11KD2,ADER
      IMAG=2
      ADER=XX*AL72
      WRITE(19) IMAG,I1,J11KD2,ADER
      IMAG=3
      ADER=XX*AL73
      WRITE(19) IMAG,I1,J11KD2,ADER
      IMAG=4
      ADER=XX*AL74
      WRITE(19) IMAG,I1,J11KD2,ADER
      IMAG=7
      ADER=XX*AL77
      WRITE(19) IMAG,I1,J11KD2,ADER
  839   CONTINUE
       A(I1,J7)= -(EMD(I)*D3(I,J)+EMQ(I)*D4(I,J))/HMM(I)
        IF(XXM(6,J).LT.SMALL)GOTO 8989
        A(I1,J4)=XY*AL5(J)
      IMAG=1
      ADER=XY*AL51
      WRITE(19) IMAG,I1,J4,ADER
      IMAG=8
      ADER=XY*AL58
      WRITE(19) IMAG,I1,J4,ADER
      IMAG=9
      ADER=XY*AL59
      WRITE(19) IMAG,I1,J4,ADER
      IMAG=10
      ADER=XY*AL510
      WRITE(19) IMAG,I1,J4,ADER
      IMAG=11
      ADER=XY*AL511
      WRITE(19) IMAG,I1,J4,ADER
       IF(XXM(7,J).LT.SMALL) GO TO 8989
C        COMPUTE A(9,11)
       A(I1,J11NEW)=XY*AL6(J)
      IMAG=1
      ADER=XY*AL61
      WRITE(19) IMAG,I1,J11NEW,ADER
      IMAG=8
      ADER=XY*AL68
      WRITE(19) IMAG,I1,J11NEW,ADER
      IMAG=9
      ADER=XY*AL69
      WRITE(19) IMAG,I1,J11NEW,ADER
      IMAG=10
      ADER=XY*AL610
      WRITE(19) IMAG,I1,J11NEW,ADER
```

```
      IMAG=11
      ADER=XY*AL611
      WRITE(19) IMAG,I1,J11NEW,ADER
        IF(XXM(9,J).LT.SMALL)GOTO 8989
        A(I1,J11KQ3)=XY*AL8(J)
      IMAG=1
      ADER=XY*AL81
      WRITE(19) IMAG,I1,J11KQ3,ADER
      IMAG=8
      ADER=XY*AL88
      WRITE(19) IMAG,I1,J11KQ3,ADER
      IMAG=9
      ADER=XY*AL89
      WRITE(19) IMAG,I1,J11KQ3,ADER
      IMAG=10
      ADER=XY*AL810
      WRITE(19) IMAG,I1,J11KQ3,ADER
      IMAG=11
      ADER=XY*AL811
      WRITE(19) IMAG,I1,J11KQ3,ADER
 8989 CONTINUE
C
C      COMPUTE A(9,10), AND A(10,9)
       DO 6989 I=1,MM
        I1=6*NM+NMD1+NMQ1-NM0+I
        I2=I1+MM
       DO   6989 J=1,MM
        J1=6*NM+NMD1+NMQ1-NM0+J
        J2=J1+MM
       A(I1,J2)= (EMD(I)*(GN(I,J)*EMQ(J) + BN(I,J)*EMD(J))+EMQ(I)*
     1  (BN(I,J)*EMQ(J)-GN(I,J)*EMD(J)))/HMM(I)  +A(I1,J2)
       IF(I.NE.J) GOTO 6989
       A(I2,J1)= 1.
 6989 CONTINUE
C                                                    *   *   *   *   *
 6608 CONTINUE
C                                                    *   *   *   *   *
C
C   COMPUTE A(6,10) FOR STATIC AND AMPLYDINE EXCITER
C        COMPUTE A(12,10) FOR CONVL AND AMPLDN EXCITER
       IEFD=0
       IV2=0
       DO 6898 I=1,NM
       IF(ITYPE(I).EQ.0)GO TO 6898
       IEFD=IEFD+1
       IF(ITYPE(I).NE.2)IV2=IV2+1
        I1=JJ11+IV2
       IF(ITYPE(I).EQ.3) GO TO 7964
       IF(ITYPE(I).EQ.4) GO TO 7964
C      ITYPE(N)=1,2,5,6,7
        I1=3*NM+NMD1+NMQ1+IEFD
 7964 CONTINUE
       DO 6899 J=1,MM
         J1=6*NM+NMD1+NMQ1-NM0+MM+J
      A(I1,J1)= AKTD(I)*B5(I,J) + AKTQ(I)*B6(I,J)
       IF(ITYPE(I).NE.4)GO TO 6899
        II1=3*NM+NMD1+NMQ1+IEFD
       A(II1,J1)=T1T2R(I)*A(I1,J1)
 6899 CONTINUE
 6898 CONTINUE
C
 7008 CONTINUE                                                    * * * *
C
        NZZ=JJ11
C
       REWIND 1
       WRITE(1) ((A(I,J),J=1,NZZ),I=1,NZZ)
C**     ILCT=6
C**    WRITE(6,930) ILCT,A(1,1),A(2,1),A(6,1),A(7,1)
C
C
       N=NZ
C
C
```

```
      IMAG=0
      WRITE(19) IMAG,I,J,ADER
C                                        *  *  *  *  *  *  *  *
C
       IERN=4
       IF((N+2).GT.NDIM) GO TO 183
C
C
C                                        *  *  *  *  *  *  *  *
C
       IF(ISTD.NE.1) GO TO 2349
       DO 11 I=1,N
       WRITE(6,908) I
       WRITE(6,909) (A(I,J),J=1,N)
   11 CONTINUE
  909 FORMAT(3X,10F9.3)
  908 FORMAT(//3X,5HROW =,I5/)
 2349 CONTINUE
C
C      SET IREDH=1 FOR BYPASSING INERTIA READ CARDS FOR X1D MCHS
       IREDH=1
        EQUIL=1
        NPERM=1
       NPRINT=0
      IF(N.EQ.0)STOP
      SPURA=0.
      DO 55 J=1,N
   55 SPURA=SPURA+A(J,J)
C
C
CMMC2
C
       REWIND IIREAD
C       WRITE(IIREAD) N
C       WRITE(IIREAD) ((A(I,J),I=1,N),J=1,N)
        WRITE(IIREAD) (LDESC(I),I=1,13)
       WRITE(IIREAD) IX0,IDIST,MCNO
      IF(IOPT.GT.50) GO TO 4
        WRITE(IIREAD)(NII(I),X0(I),I=1,IX0)
    4  CONTINUE
      IF(IOPT.GT.50) WRITE(IIREAD) X0
        WRITE(IIREAD)NCHNL
        WRITE(IIREAD) (LISTO(I),I=1,NCHNL)
        WRITE(IIREAD) TAU,TFIN
C
  110 CONTINUE
C
C
      WRITE(19) N,NM,TIME(1,NM),XXM(1,NM),XXTR(1,NM),XXTR(2,NM)
      DO 707 I=1,N
      DO 707 J=1,N
  707  WRITE(19) A(I,J)
      IF(IIOPT.GT.60) STOP
C
C
CMMC2.END
C
       NM0OLD=NM0
C
       INXT=0
C
       IF(INXT.EQ.0)STOP
C
  181   CONTINUE
       WRITE(6,182) IERN,NM,MM,ND,NCT
       STOP
  183   CONTINUE
       WRITE(6,184) IERN,NZ,N
       STOP
  182 FORMAT(///10X, ' * * *  ERROR  * * *  ' / 10X, ' *  CHECK DATA a
     1IERN=',I2,/
     2 10X, 'NM=', I4,3X, 'MM=', I5, 4X, 'ND=',I4,3X,'NCT=',I5 )
  184 FORMAT(///10X, ' * * *  ERROR  * * *  ' / 10X, ' *  CHECK DATA a
     1IERN=',I2,/
     2 10X, 'NZ=',I5, 4X,'N=',I5)
```

```
C
 1000 FORMAT (I6)
 2000 FORMAT (4E16.8)
 3000 FORMAT (50X,13H INPUT MATRIX//)
 4000 FORMAT (1H07E17.8)
 7000 FORMAT (/22H1TRACE OF THE MATRIX =E17.9/21H SUM OF EIGENVALUES =E1
     17.9/21H ITS PER EIGENVALUE = F6.2/
     27H NORM = E17.9)
       END
```

LISTING OF THE IDENTIFICATION PROGRAM

```
      DIMENSION IRAY1(500,2),IRAY2(300,2),IRAY3(300,2),IRAY4(300,2),
     1IRAY5(40,2),IRAY6(40,2),IRAY7(300,2),IRAY8(300,2),IRAY9(300,2),
     1IRAY10(300,2),IRAY11(300,2),IRAY12(300,2),IRAY13(40,2)
      DIMENSION IRAY14(40,2),RAY1(500),RAY2(300),RAY3(300),RAY4(300),
     1RAY5(40),RAY6(40),RAY7(300),RAY8(300),RAY9(300),RAY10(300),
     1RAY11(300),RAY12(300),RAY13(40),RAY14(40)
      DIMENSION B(100),GACR(14,14),W(7)
       double precision gacr
      COMPLEX Z(100),ZRAY(100),GAC(7,14),E(7)
        DOUBLE PRECISION XX(196)
       COMPLEX*16 AC(85,85),XY(7225)
       EQUIVALENCE(XY,AC)
       COMPLEX EP(7),CTEMP,EPP(7)
       READ(5,996) IORDER,MG1
996     FORMAT(2I10)
       MG2=2*MG1
      I1=1
      I2=1
      I3=1
      I4=1
      I5=1
      I6=1
      I7=1
       I8=1
      I9=1
      I10=1
      I11=1
      I12=1
      I13=1
      I14=1
       D1=2.
       D2=2.
      READ(5,4) (E(I),I=1,7)
       READ(5,4) (EP(I),I=1,7)
       READ(5,4) (EPP(I),I=1,7)
      DO 8 I=1,100
  8   B(I)=0.0
      B(NINPUT)=((377.0*RF)/XAF)*AKE
      READ(5,4) (W(I),I=1,7)
      WRITE(6,400)(W(I),I=1,MG1)
400    FORMAT(1X,'FREQS CONSIDERED IN HZ',7F10.5)
  4   FORMAT(8F10.6)
      REWIND 19
  1   CONTINUE
      READ(19) IMAG,N1,N2,ADER
      IF(IMAG.EQ.0) GO TO 3
      IF(IMAG.EQ.1) GO TO 5
      IF(IMAG.EQ.2) GO TO 7
      IF(IMAG.EQ.3) GO TO 9
      IF(IMAG.EQ.4) GO TO 11
      IF(IMAG.EQ.5) GO TO 13
      IF(IMAG.EQ.6) GO TO 15
      IF(IMAG.EQ.7) GO TO 17
      IF(IMAG.EQ.8) GO TO 19
      IF(IMAG.EQ.9) GO TO 21
      IF(IMAG.EQ.10) GO TO 23
      IF(IMAG.EQ.11) GO TO 25
      IF(IMAG.EQ.12) GO TO 27
      IF(IMAG.EQ.13) GO TO 29
      IF(IMAG.EQ.14) GO TO 31
  5   CONTINUE
      IRAY1(I1,1)=N1
      IRAY1(I1,2)=N2
      RAY1(I1)=ADER
      I1=I1+1
      GO TO 33
  7   CONTINUE
      IRAY2(I2,1)=N1
      IRAY2(I2,2)=N2
      RAY2(I2)=ADER
      I2=I2+1
      GO TO 33
  9   CONTINUE
```

```
      IRAY3(I3,1)=N1
      IRAY3(I3,2)=N2
      RAY3(I3)=ADER
      I3=I3+1
      GO TO 33
   11 CONTINUE
      IRAY4(I4,1)=N1
      IRAY4(I4,2)=N2
      RAY4(I4)=ADER
      I4=I4+1
      GO TO 33
   13 CONTINUE
      IRAY5(I5,1)=N1
      IRAY5(I5,2)=N2
      RAY5(I5)=ADER
      I5=I5+1
      GO TO 33
   15 CONTINUE
      IRAY6(I6,1)=N1
      IRAY6(I6,2)=N2
      RAY6(I6)=ADER
      I6=I6+1
      GO TO 33
   17 CONTINUE
      IRAY7(I7,1)=N1
      IRAY7(I7,2)=N2
      RAY7(I7)=ADER
      I7=I7+1
      GO TO 33
   19 CONTINUE
      IRAY8(I8,1)=N1
      IRAY8(I8,2)=N2
      RAY8(I8)=ADER
      I8=I8+1
      GO TO 33
   21 CONTINUE
      IRAY9(I9,1)=N1
      IRAY9(I9,2)=N2
      RAY9(I9)=ADER
      I9=I9+1
      GO TO 33
   23 CONTINUE
      IRAY10(I10,1)=N1
      IRAY10(I10,2)=N2
      RAY10(I10)=ADER
      I10=I10+1
      GO TO 33
   25 CONTINUE
      IRAY11(I11,1)=N1
      IRAY11(I11,2)=N2
      RAY11(I11)=ADER
      I11=I11+1
      GO TO 33
   27 CONTINUE
      IRAY12(I12,1)=N1
      IRAY12(I12,2)=N2
      RAY12(I12)=ADER
      I12=I12+1
      GO TO 33
   29 CONTINUE
      IRAY13(I13,1)=N1
      IRAY13(I13,2)=N2
      RAY13(I13)=ADER
      I13=I13+1
      GO TO 33
   31 CONTINUE
      IRAY14(I14,1)=N1
      IRAY14(I14,2)=N2
      RAY14(I14)=ADER
      I14=I14+1
   33 CONTINUE
      GO TO 1
    3 CONTINUE
   16 FORMAT('1',5X,14I5)
       IF(MG1.EQ.7) IER=1
       IF(IER.EQ.1) GO TO 305
```

```
      DO 301 I=1,I4
      TREP=RAY4(I)
      N1=IRAY4(I,1)
      N2=IRAY4(I,2)
      RAY4(I)=RAY12(I)
      RAY12(I)=TREP
      IRAY4(I,1)=IRAY12(I,1)
      IRAY4(I,2)=IRAY12(I,2)
      IRAY12(I,1)=N1
      IRAY12(I,2)=N2
301   CONTINUE
      IREP=I4
      I4=I12
      I12=IREP
      DO 303 I=1,I6
      TREP=RAY6(I)
      N1=IRAY6(I,1)
      N2=IRAY6(I,2)
      RAY6(I)=RAY13(I)
      RAY13(I)=TREP
      IRAY6(I,1)=IRAY13(I,1)
      IRAY6(I,2)=IRAY13(I,2)
      IRAY13(I,1)=N1
      IRAY13(I,2)=N2
303   CONTINUE
      IREP=I6
      I6=I13
      I13=IREP
305   CONTINUE
     II=1
         DO 36 I=1,7
     DO 36 J=1,14
 36  GAC(I,J)=CMPLX(0.,0.)
     KKK=I1+I2+I3+I4+I5+I6+I7+I8+I9+I10+I11+I12+I13+I14-13
      READ(19) NC,NM,RF,XAF,AKE,TR
      NINPUT=3*NM
      NC1=7*NM
      NC2=6*NM
      B(NINPUT)=((377.*RF)/XAF)*AKE
 37   WI=W(II)*(44./7.)
     REWIND 19
     DO 38 KK=1,KKK
     READ(19) IMAG,N1,N2,ADER
 38   CONTINUE
401  FORMAT(5X,3I5,E14.6)
      READ(19) NC,NM,RF,XAF,AKE,TR
     DO 40 I=1,NC
     DO 40 J=1,NC
     READ(19) T
     AC(I,J)=CMPLX(-T,.0)
 40  CONTINUE
     DO 39 I=1,NC
 39  AC(I,I)=AC(I,I)+CMPLX(0.0,WI)
      KI=0
      DO 500 J=1,NC
      DO 500 I=1,NC
      KI=KI+1
500   XY(KI)=AC(I,J)
      CALL REDUCT(XY,NC,0)
      KI=0
      DO 502 J=1,NC
      DO 502 I=1,NC
      KI=KI+1
502   AC(I,J)=XY(KI)
      IER=0
 42   FORMAT('0',5X,'IER=',I5)
     DO 41 I=1,NC
 41  Z(I)=AC(I,NINPUT)*B(NINPUT)
      TEMP=CABS(E(II))
      TEMP=20.*ALOG10(TEMP)
      THET=ATAN2(AIMAG(E(II)),REAL(E(II)))*57.2
      TEMP=CABS(Z(NC1))
      TEMP=20.*ALOG10(TEMP)
      THET=ATAN2(AIMAG(Z(NC1)),REAL(Z(NC1)))*57.2
 405   FORMAT(5X,2F10.5)
     TEMP=WI*TR
```

```
      CTEMP=CMPLX(1.,TEMP)
      CTEMP=-CTEMP/AKE
      E(II)=E(II)+EP(II)+EPP(II)
      EP(II)=E(II)
      E(II)=E(II)-Z(NC1)-Z(NC2)*CTEMP-Z(NC2)-AKE
      A1=1.
     DO 45 I=1,NC
45   ZRAY(I)=CMPLX(.0,.0)
      I1=I1-1
     DO 47 I=1,I1
     K1=IRAY1(I,1)
     K2=IRAY1(I,2)
47   ZRAY(K1)=RAY1(I)*Z(K2)+ZRAY(K1)
     DO 49 J=1,NC
49   GAC(II,1)=GAC(II,1)+(AC(NC1,J)+AC(NC2,J)*(A1+CTEMP)+AKE)*ZRAY(J)
      DO 51 I=1,NC
51   ZRAY(I)=CMPLX(.0,.0)
     I2=I2-1
     DO 53 I=1,I2
     K1=IRAY2(I,1)
     K2=IRAY2(I,2)
53   ZRAY(K1)=RAY2(I)*Z(K2)+ZRAY(K1)
     DO 55 J=1,NC
55   GAC(II,2)=GAC(II,2)+(AC(NC1,J)+AC(NC2,J)*(A1+CTEMP)+AKE)*ZRAY(J)
     DO 57 I=1,NC
57   ZRAY(I)=CMPLX(.0,.0)
     I3=I3-1
     DO 59 I=1,I3
     K1=IRAY3(I,1)
     K2=IRAY3(I,2)
59   ZRAY(K1)=RAY3(I)*Z(K2)+ZRAY(K1)
     DO 61 J=1,NC
61   GAC(II,3)=GAC(II,3)+(AC(NC1,J)+AC(NC2,J)*(A1+CTEMP)+AKE)*ZRAY(J)
     DO 63 I=1,NC
63   ZRAY(I)=CMPLX(.0,.0)
     I4=I4-1
     DO 65 I=1,I4
     K1=IRAY4(I,1)
     K2=IRAY4(I,2)
65   ZRAY(K1)=RAY4(I)*Z(K2)+ZRAY(K1)
     DO 67 J=1,NC
67   GAC(II,4)=GAC(II,4)+(AC(NC1,J)+AC(NC2,J)*(A1+CTEMP)+AKE)*ZRAY(J)
     DO 69 I=1,NC
69   ZRAY(I)=CMPLX(.0,.0)
     I5=I5-1
     DO 71 I=1,I5
     K1=IRAY5(I,1)
     K2=IRAY5(I,2)
71   ZRAY(K1)=RAY5(I)*Z(K2)+ZRAY(K1)
     DO 73 J=1,NC
73   GAC(II,5)=GAC(II,5)+(AC(NC1,J)+AC(NC2,J)*(A1+CTEMP)+AKE)*ZRAY(J)
     DO 75 I=1,NC
75   ZRAY(I)=CMPLX(.0,.0)
     I6=I6-1
     DO 77 I=1,I6
     K1=IRAY6(I,1)
     K2=IRAY6(I,2)
77   ZRAY(K1)=RAY6(I)*Z(K2)+ZRAY(K1)
     DO 79 J=1,NC
79   GAC(II,6)=GAC(II,6)+(AC(NC1,J)+AC(NC2,J)*(A1+CTEMP)+AKE)*ZRAY(J)
     DO 81 I=1,NC
81   ZRAY(I)=CMPLX(.0,.0)
     I7=I7-1
     DO 83 I=1,I7
     K1=IRAY7(I,1)
     K2=IRAY7(I,2)
83   ZRAY(K1)=RAY7(I)*Z(K2)+ZRAY(K1)
     DO 85 J=1,NC
85   GAC(II,7)=GAC(II,7)+(AC(NC1,J)+AC(NC2,J)*(A1+CTEMP)+AKE)*ZRAY(J)
     DO 87 I=1,NC
87   ZRAY(I)=CMPLX(.0,.0)
     I8=I8-1
     DO 89 I=1,I8
     K1=IRAY8(I,1)
     K2=IRAY8(I,2)
89   ZRAY(K1)=RAY8(I)*Z(K2)+ZRAY(K1)
```

```
      DO 91 J=1,NC
 91   GAC(II,8)=GAC(II,8)+(AC(NC1,J)+AC(NC2,J)*(A1+CTEMP)+AKE)*ZRAY(J)
      DO 93 I=1,NC
 93   ZRAY(I)=CMPLX(.0,.0)
      I9=I9-1
      DO 95 I=1,I9
      K1=IRAY9(I,1)
      K2=IRAY9(I,2)
 95   ZRAY(K1)=RAY9(I)*Z(K2)+ZRAY(K1)
      DO 97 J=1,NC
 97   GAC(II,9)=GAC(II,9)+(AC(NC1,J)+AC(NC2,J)*(A1+CTEMP)+AKE)*ZRAY(J)
      DO 99 I=1,NC
 99   ZRAY(I)=CMPLX(.0,.0)
      I10=I10-1
      DO 101 I=1,I10
      K1=IRAY10(I,1)
      K2=IRAY10(I,2)
101   ZRAY(K1)=RAY10(I)*Z(K2)+ZRAY(K1)
      DO 103 J=1,NC
103   GAC(II,10)=GAC(II,10)+(AC(NC1,J)+AC(NC2,J)*(A1+CTEMP)+AKE)*ZRAY(J)
      DO 105 I=1,NC
105   ZRAY(I)=CMPLX(.0,.0)
       IF(IORDER.LT.3) GO TO 307
      I11=I11-1
      DO 107 I=1,I11
      K1=IRAY11(I,1)
      K2=IRAY11(I,2)
107   ZRAY(K1)=RAY11(I)*Z(K2)+ZRAY(K1)
      DO 109 J=1,NC
109   GAC(II,11)=GAC(II,11)+(AC(NC1,J)+AC(NC2,J)*(A1+CTEMP)+AKE)*ZRAY(J)
      DO 111 I=1,NC
111   ZRAY(I)=CMPLX(.0,.0)
      I12=I12-1
      DO 113 I=1,I12
      K1=IRAY12(I,1)
      K2=IRAY12(I,2)
113   ZRAY(K1)=RAY12(I)*Z(K2)+ZRAY(K1)
      DO 115 J=1,NC
115   GAC(II,12)=GAC(II,12)+(AC(NC1,J)+AC(NC2,J)*(A1+CTEMP)+AKE)*ZRAY(J)
      DO 117 I=1,NC
117   ZRAY(I)=CMPLX(.0,.0)
      I13=I13-1
      DO 119 I=1,I13
      K1=IRAY13(I,1)
      K2=IRAY13(I,2)
119   ZRAY(K1)=RAY13(I)*Z(K2)+ZRAY(K1)
      DO 120 J=1,NC
120   GAC(II,13)=GAC(II,13)+(AC(NC1,J)+AC(NC2,J)*(A1+CTEMP)+AKE)*ZRAY(J)
      DO 121 I=1,NC
121   ZRAY(I)=CMPLX(.0,.0)
      I14=I14-1
      DO 123 I=1,I14
      K1=IRAY14(I,1)
      K2=IRAY14(I,2)
123   ZRAY(K1)=RAY14(I)*Z(K2)+ZRAY(K1)
      DO 125 J=1,NC
125   GAC(II,14)=GAC(II,14)+(AC(NC1,J)+AC(NC2,J)*(A1+CTEMP)+AKE)*ZRAY(J)
307    CONTINUE
      IF(II.GE.MG1) GO TO 127
      II=II+1
      GO TO 37
127   CONTINUE
       IF(MG1.EQ.7) GO TO 410
       IF(MG1.LT.6) GO TO 410
       DO 195 I=1,MG1
       DO 195 J=9,14
195    GAC(I,J-1)=GAC(I,J)
       DO 197 I=1,MG1
       DO 197 J=12,13
197    GAC(I,J-1)=GAC(I,J)
410    CONTINUE
      DO 129 I=1,MG1
      B(I)=REAL(E(I))
129   B(I+MG1)=AIMAG(E(I))
      DO 131 I=1,MG1
      DO 131 J=1,MG2
```

```
      GACR(I,J)=REAL(GAC(I,J))
  131 GACR(I+MG1,J)=AIMAG(GAC(I,J))
       KI=0
       DO 201 J=1,MG2
       DO 201 I=1,MG2
       KI=KI+1
  201  XX(KI)=GACR(I,J)
       call reduce(xx,mg2,0)
       KI=0
       DO 203 J=1,MG2
       DO 203 I=1,MG2
       KI=KI+1
  203  GACR(I,J)=XX(KI)
  155  FORMAT(1X,10E11.4)
       TEMP=0.0
       CTEMP=CMPLX(0.0,0.0)
       DO 209 I=1,MG1
       T1=REAL(E(I))
       T2=AIMAG(E(I))
       T2=-T2
       V1=REAL(EP(I))
       V2=-AIMAG(EP(I))
       TEMP=TEMP+EP(I)*CMPLX(V1,V2)
  209  CTEMP=CTEMP+E(I)*CMPLX(T1,T2)
       CTEMP=CTEMP/TEMP
      WRITE(6,169) CTEMP
  169 FORMAT(1X,'SQUARE OF ERRORS = ',2E11.4)
      WRITE(6,660)
  660 FORMAT(20X,'SEQUENCE OF PARAMETER NUMBERING')
      IF (MG1.EQ.5) WRITE(6,661)
      IF (MG1.EQ.6) WRITE(6,662)
      IF (MG1.EQ.7) WRITE(6,663)
  661 FORMAT('  XAL  XFKD  XKD1  RKQ1  RKD1  RKQ2  XFL  XAQ  XKQ1  XKQ2'
     &)
  662 FORMAT('  XAL  XFKD  XKD1  XKD2  RKD1  RKD2  XFL  XKQ1  XKQ2  XKQ3
     &  RKQ2  RKQ3')
  663 FORMAT('  XAL  XFKD  XKD1  XKD2  RKD1  RKD2  XFL  XAQ  XKQ1  XKQ2
     & XKQ3  RKQ1  RKQ2  RKQ3')
  133  CONTINUE
       DO 135 I=1,MG2
       T=.0
       DO 137 J=1,MG2
  137  T=T+GACR(I,J)*B(J)
       WRITE(6,139) I,T
  135  CONTINUE
  139  FORMAT('0',5X,'PARM NO',I3,5X,'PARM VALUE',E14.6)
       STOP
       END
```

Appendix D

NOMENCLATURE AND DEFINITIONS

SYMBOLS

B	magentic flux density
f	frequency (Hz)
f_o	rated frequency
$G(s)$	stator-to-field transfer function
H	magnetic intensity
$I_{a,b,c}$	stator phase currents
I_{ao}	base stator current
I_d	direct axis stator current
I_{fd}	field current
I_{fo}	field current required to produce rated stator terminal voltage on the air-gap line of the open-circuit saturation curve
I_{kd}	direct axis damper winding current
I_{kq}	quadrature axis damper winding current
I_q	quadrature axis stator current
I_s	stator winding current
L_{ad}	direct axis stator to rotor mutual inductance
L_{afd}	mutual inductance between the field winding and one phase of the stator winding with the magnetic axes of the two aligned
L_{afdss}	L_{afd} obtained from standstill frequency response test data
L_{afdu}	unsaturated value of L_{afd} such as would be calculated from the air-gap line of the d-axis open-circuit saturation curve
L_{aq}	quadrature axis stator to rotor mutual inductance
L_{aqu}	unsaturated value of L_{aq}
L_d	direct axis synchronous inductance

L'_d direct axis transient inductance

L''_d direct axis subtransient inductance

$L_d(s)$ direct axis operational inductance

$L_{do}(s)$ open-circuit stator driving point operational inductance

L_{fd} field leakage inductance

L_{ffd} field winding self inductance

L_{fkd} rotor circuit mutual leakage inductance representing flux which links the field and damper windings but not the stator winding

L_l stator winding leakage inductance

L_{kd} direct axis damper winding leakage inductance

L_{kkd} direct axis damper winding self inductance

L_{kq} quadrature axis damper winding leakage inductance

L_q quadrature axis synchronous inductance

$L_q(s)$ quadrature axis operational inductance

R_a stator winding resistance per phase

R_{fd} field winding resistance

R_{kd} direct axis damper winding resistance

R_{kq} quadrature axis damper winding resistance

s Laplace operator

T'_d direct axis transient short circuit time constant

T''_d direct axis subtransient short circuit time constant

T'_{do} direct axis transient open circuit time constant

T''_{do} direct axis subtransient open circuit time constant

$T_{1,2,\ldots}$ time constants

$V_{a,b,c}$ stator phase-to-neutral voltages

V_d direct axis stator voltage

V_{fd} field voltage

V_s	stator voltage
V_q	quadrature axis stator voltage
$Y_{af}(s)$	stator-to-field transfer admittance
$Z_{afo}(s)$	stator-to-field transfer impedance
$Z_d(s)$	direct axis operational impedance
$Z_{do}(s)$	open-circuit stator driving point impedance
$Z_{fdo}(s)$	open-circuit field driving point impedance
$Z_q(s)$	quadrature axis operational impedance
Δ	small change
δ	internal angle, the angle between the quadrature axis and the terminal voltage vector
θ	the angle between the magnetic axes of phase a of the stator winding and thefield winding
Ω	ohm
ω	angular frequency (radians/s)
ω_o	rated angular frequency

MODEL DESIGNATION

Each of the various generator models is identified with letters followed by a number; eg, SSFR2. The letters indicate the source of the data from which the model was derived, and the numeral, the number of rotor circuits on the direct axis, including the field winding. For example, SSFR2 means a model derived from standstill frequency response test data, and one that has one damper winding plus the field on the direct axis. Unless stated otherwise, the number of q-axis rotor circuits is equal to the total number of d-axis rotor circuits.

SSFR2	two rotor windings in d- and q-axes, derived from standstill frequency response tests
SSFR3	three rotor windings in d- and q-axes, derived from standstill frequency response tests
OLFR2	two rotor windings in d- and q-axes, derived from on-line frequency response tests
OLFR3	three rotor windings in d- and q-axes, derived from on-line frequency response tests
SC2	two rotor windings in d- and q-axes, d-axis model derived from three phase sudden short circuit test, q-axis model same as for SSFR2
SD3	three rotor windings in d-axis, two rotor windings in q-axis; derived from stator decrement tests
STANDARD	two rotor windings in d- and q-axes, derived from manufacturer's data

Part 2

SECONDARY MODELS AND ANCILLARY TESTS

CONTENTS

ILLUSTRATIONS

ILLUSTRATIONS (Cont'd)

TABLES

Section 1

INTRODUCTION

The function of this part is to document the results of work which is considered less significant than that reported in Part 1. Some of these results have considerable individual merit, but they are not fundamental to the main conclusions and recommendations of the report.

Section 2

NANTICOKE MODELS FROM MEASUREMENT OF LARGE TRANSIENTS

TYPE OF TEST

The generator models in Part 1 obtained from standstill and on-line frequency response tests were based on small signal measurements. This section deals with two sets of large signal tests: three phase sudden short circuit and stator decrement tests. These measurements are quite different from the prior ones in that they involve significant excursions of the generator quantities relative to their initial values.

THREE PHASE SUDDEN SHORT CIRCUIT

It is fortunate that a complete set of test data (stator and field current decrements) from the manufacturer's three phase sudden short circuit test was available for the Nanticoke machine. This enabled us to derive a two-rotor-winding d-axis model for comparison with other models obtained under significantly different test conditions.

This test data was analysed using a method (1,2) which is somewhat more comprehensive than the standard procedure (3). The stator current decrements are analyzed together with the field current decrement. It has been shown (1,2) that the rotor current transient contains unique information which, together with that obtained from the stator currents, enables one to derive a unique equivalent circuit model for that set of conditions. This is analogous to using $sG(s)$ and $L_d(s)$ together when developing standstill models. The results of the analysis of the sudden short circuit test data are shown in Table 2-1 and the corresponding equivalent circuit parameters in Table 2-2. The parameters A_1 and A_2 in Table 2-1 pertain to the transient and sub-transient components of rotor current as indicated in Figure 1 of Reference 2.

Table 2-1

NANTICOKE REACTANCES AND TIME CONSTANTS

	STANDARD Data	Sudden Short Circuit Test
L_{du}	2.36 pu	2.35 pu
L'_d	0.287 pu	0.287 pu
L''_d	0.211 pu	0.211 pu
T'_{do}	7.606 s	7.861 s
T''_{do}	0.052 s	0.052 s
A_1	-	5.00
A_2	-	0.100

Note: All normalized parameters are on the generator base of 588 MVA, 22 kV, 60 Hz.

Table 2-2

NANTICOKE EQUIVALENT CIRCUIT PARAMETERS
FOR DIFFERENT MODELS

Parameter	STANDARD Model	SSFR2 Model	SSFR3 Model	OLFR3 Model	SC2 Model	SD3 Model
L_{ad}	2.165	2.152	2.152	2.152	2.170	2.305
L_{aq}	2.047	2.057	2.057	2.057	2.056	1.875
L_{l}	0.195	0.172	0.172	0.172	0.180	0.225
L_{fd}	0.0908	0.0231	0.0155	0.2785	0.0495	0.225
R_{fd}	0.00076	0.00094	0.00094	0.00083	0.00115	0.0009
L_{kd1}	0.0457	0.0101	2.732	5.182	0.00062	0.8457
R_{kd1}	0.00703	0.00416	0.1142	0.0969	0.00207	0.00279
L_{fkd1}	-	0.2728	-0.5215	-0.0403	0.0805	-
L_{kq1}	0.1560	0.8006	1.657	1.4475	-	0.0679
R_{kq1}	0.00390	0.00842	0.00538	0.00433	-	0.0128
L_{kq2}	0.0378	0.1243	0.1193	0.0560	-	0.8845
R_{kq2}	0.00139	0.04893	0.1081	0.0122	-	0.00427
L_{fkd2}	-	-	0.8975	-	-	-
L_{kd2}	-	-	0.00753	0.0369	-	0.05634
R_{kd2}	-	-	0.00592	0.0130	-	0.00734
L_{kq3}	-	-	0.4513	0.4064	-	-
R_{kq3}	-	-	0.0188	0.0017	-	-

Note: All parameters are normalized to the machine base of 588 MVA, 22 kV, 60 Hz.

STATOR DECREMENT

Stator decrement tests were conducted at Nanticoke by Ontario Hydro for Power Technologies Incorporated (PTI). For details of the background theory and the actual measurements, refer to the final report from PTI to EPRI on RP997.

Ontario Hydro's responsibilities did, however, include evaluation of the generator models resulting from these tests. PTI derived a three-rotor-winding direct axis equivalent circuit and a two winding quadrature axis equivalent circuit. The parameters for this model (SD3) are given in Table 2-2.

PERFORMANCE OF MODELS

First, the sudden short circuit (SC2) and stator decrement (SD3) models were used to try to reproduce the field current transients during the tests from which they were derived. Each model did quite well at simulating its respective test. The SC2 model was also respectable in attempts to duplicate the stator decrement test, but the SD3 model left a bit to be desired in reproducing the field current transient following a three phase sudden short circuit. These results are demonstrated in Figures 2-1 and 2-2 where, as a matter of interest, the SSFR3, OLFR3 and STANDARD models' responses are also shown.

Next, the SC2 and SD3 models were used to simulate the line switching tests at Nanticoke, this being the standard by which all models were to be judged. Since the three phase sudden short circuit test does not provide any q-axis information, it was necessary to form a composite model (SC2) consisting of the d-axis circuit from the sudden short circuit test and the q-axis one from the standstill frequency response test for these simulations. Figures 2-3 to 2-10 compare the performance of the SC2 and SD3 models to that of OLFR3 in reproducing the line switching transients.

The SC2 and SD3 models were somewhat similar in behaviour, with SC2 marginally better than SD3 at predicting the frequency and damping of the rotor oscillations. However, on the whole, the OLFR3 model is still clearly the best.

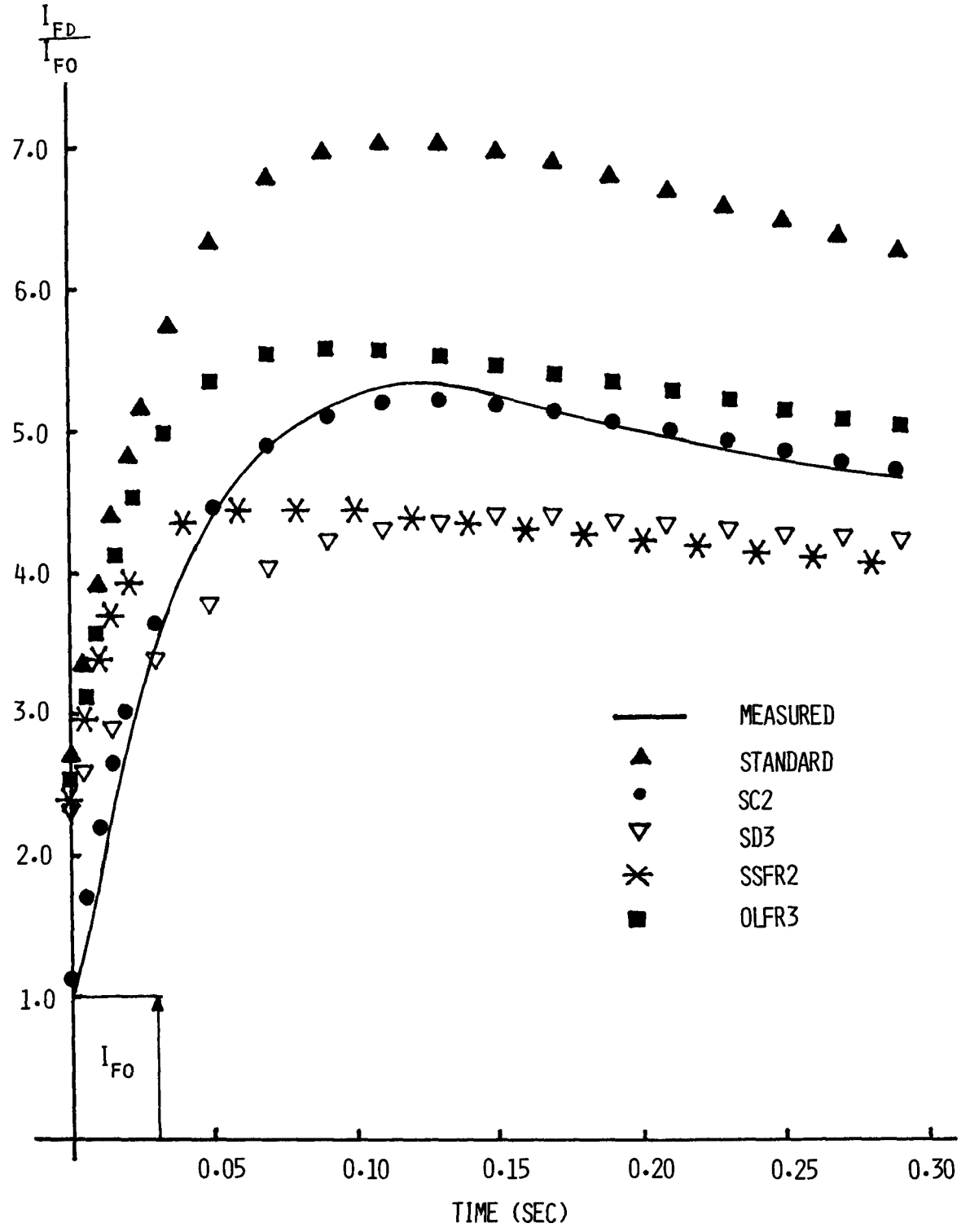

Figure 2-1. Field Current Transient from Nanticoke Three Phase Sudden Short Circuit Test.

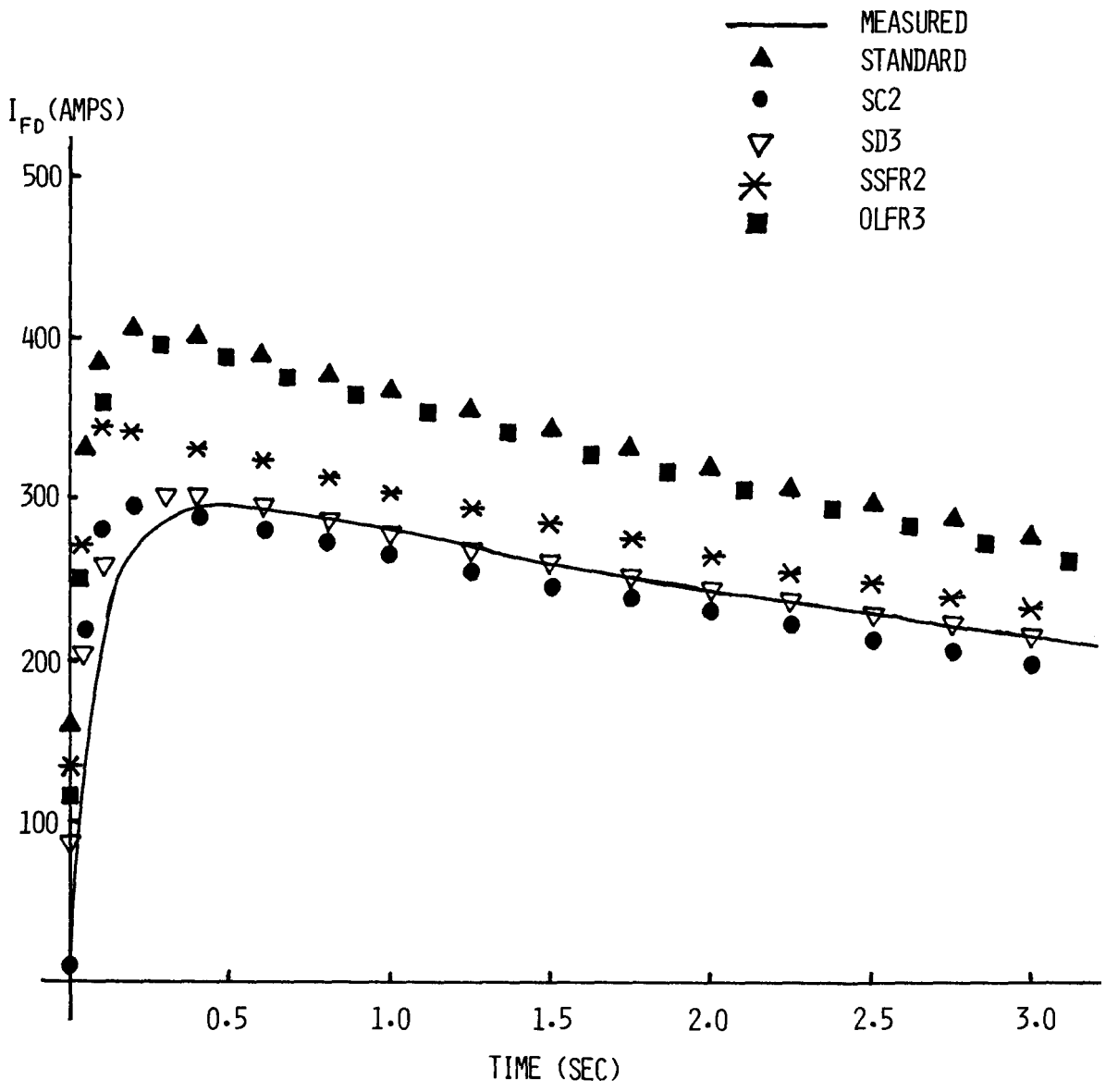

Figure 2-2. Field Current Transient from Nanticoke Stator Decrement Test.

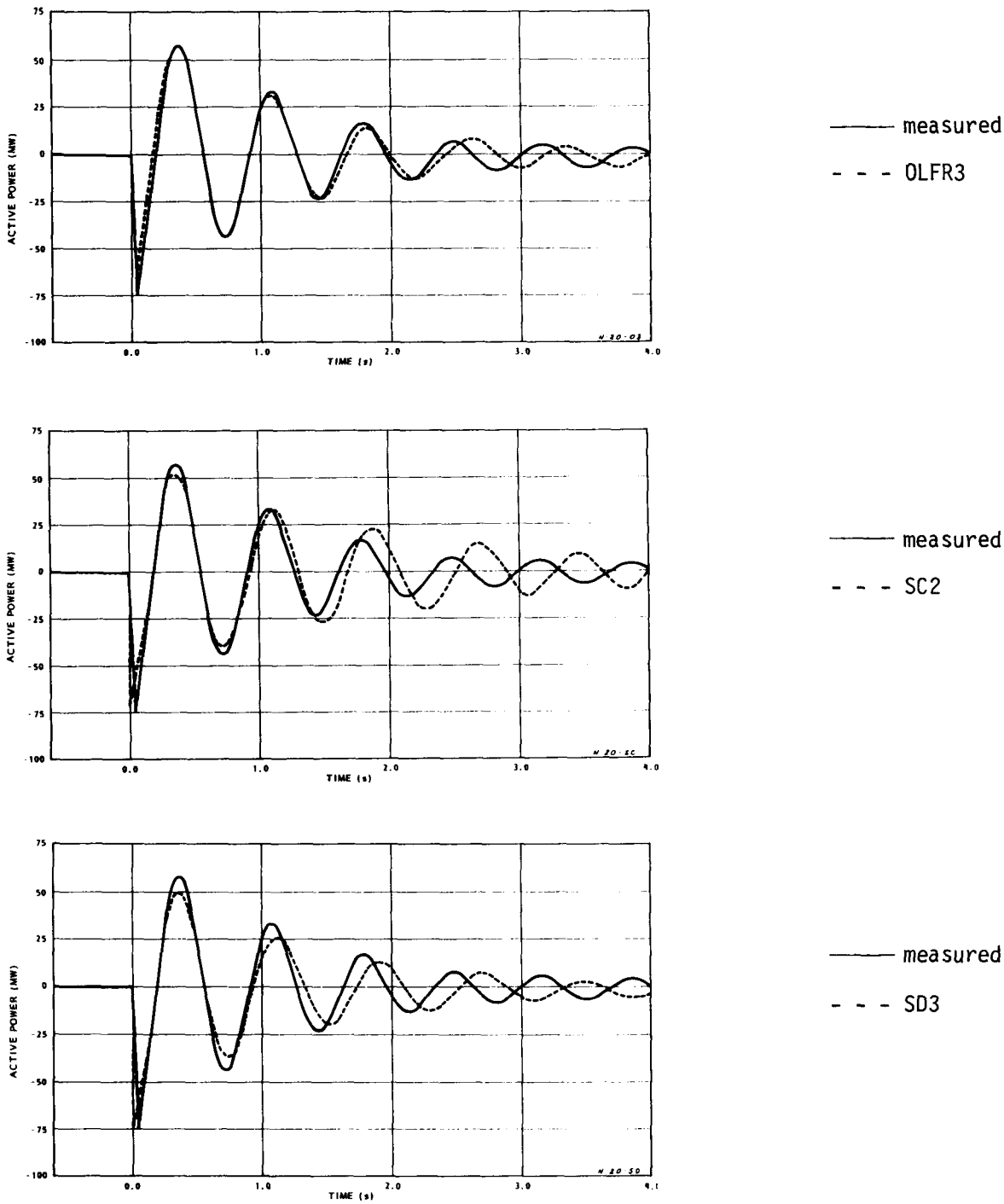

Figure 2-3. Nanticoke Line Switching Test 2-0. Active Power with OLFR3, SC2, and SD3 Models.

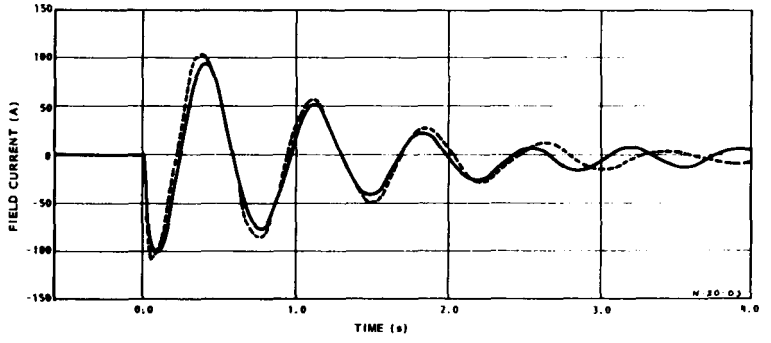

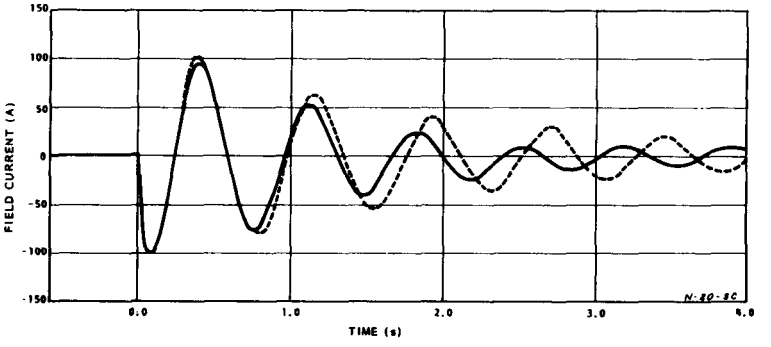

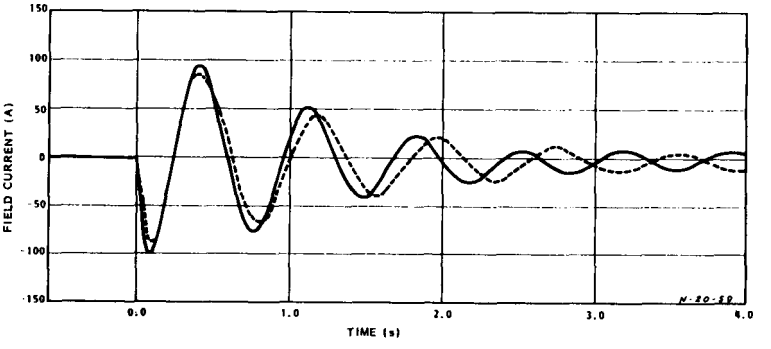

Figure 2-4. Nanticoke Line Switching Test 2-0. Field Current with OLFR3, SC2, and SD3 Models.

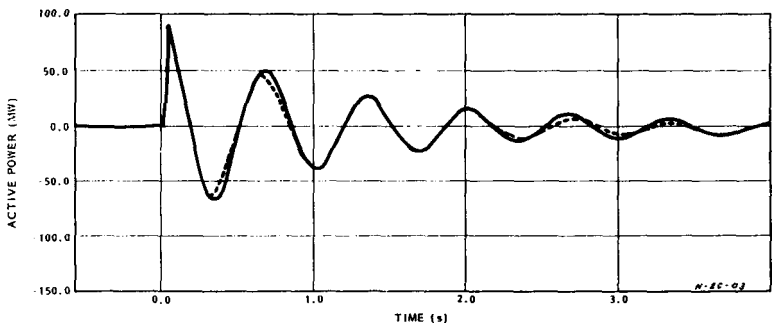

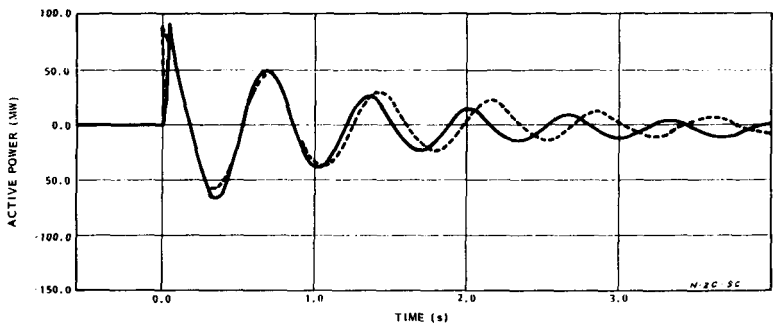

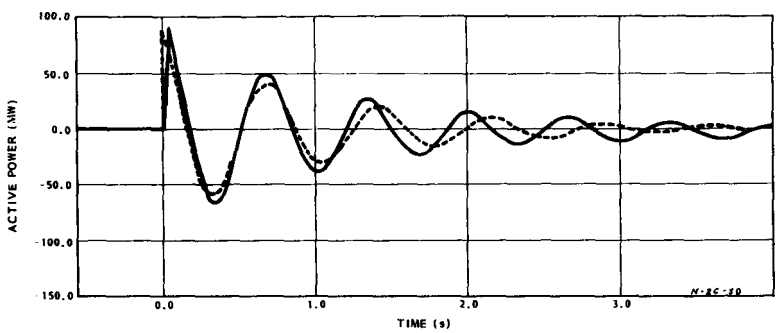

Figure 2-5. Nanticoke Line Switching Test 2-C. Active Power with OLFR3, SC2, and SD3 Models.

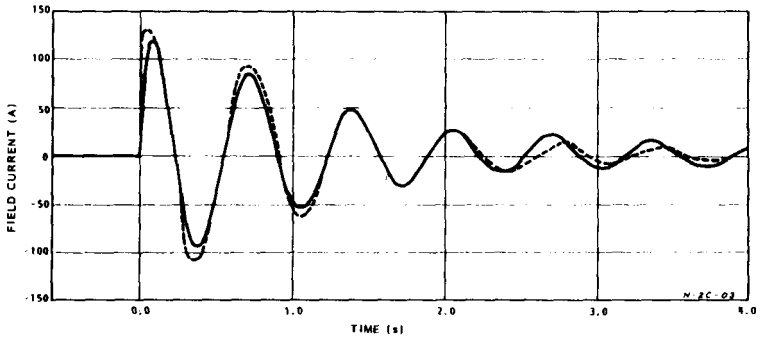

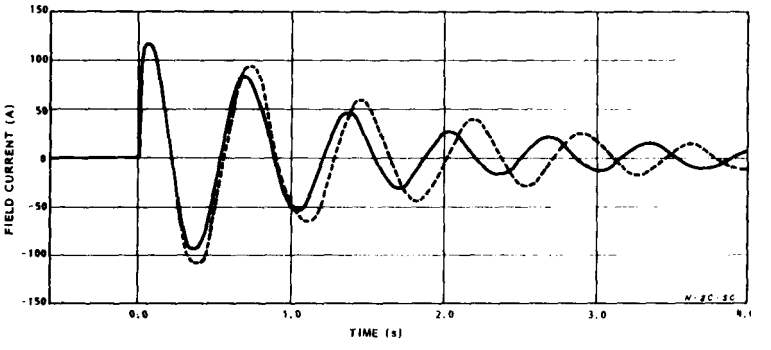

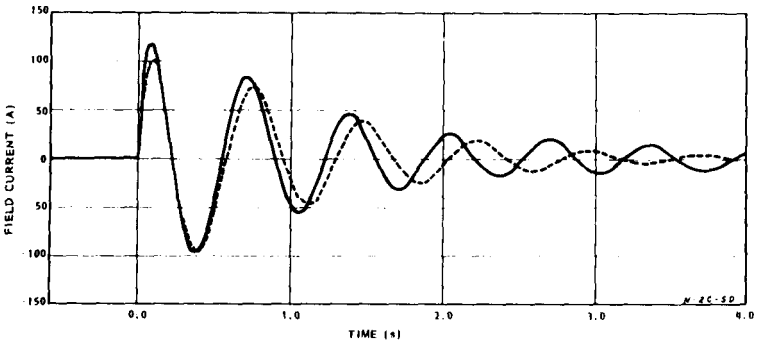

Figure 2-6. Nanticoke Line Switching Test 2-C. Field Current with OLFR3, SC2, and SD3 Models.

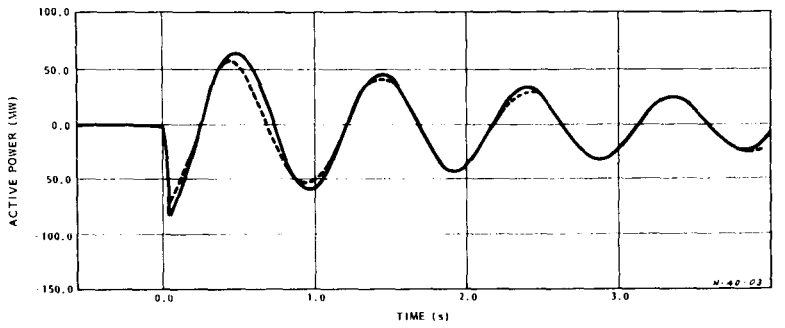

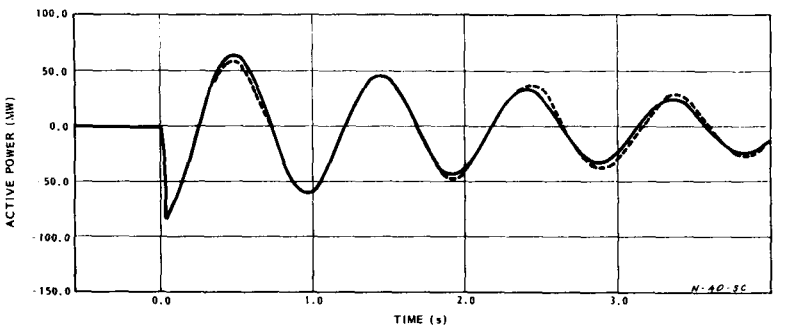

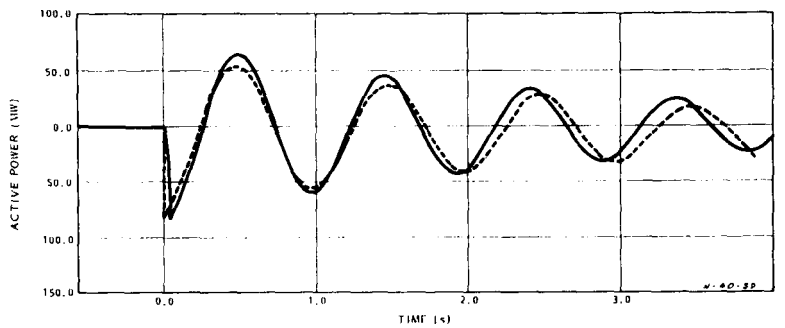

Figure 2-7. Nanticoke Line Switching Test 4-0. Active Power with OLFR3, SC2, and SD3 Models.

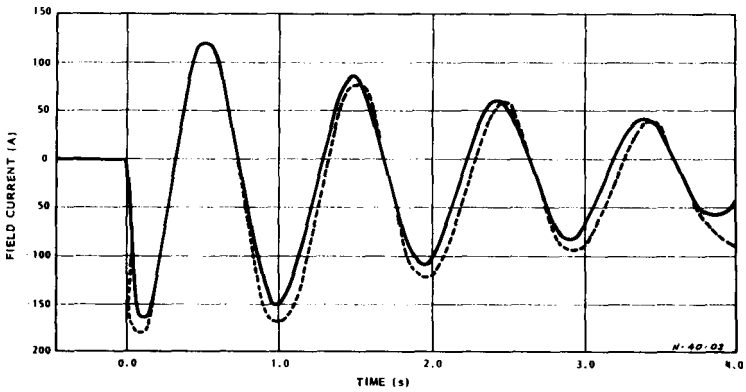

——— measured

- - - OLFR3

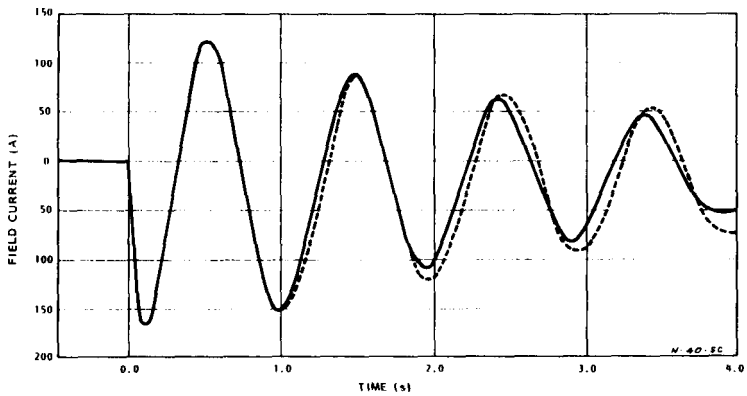

——— measured

- - - SC2

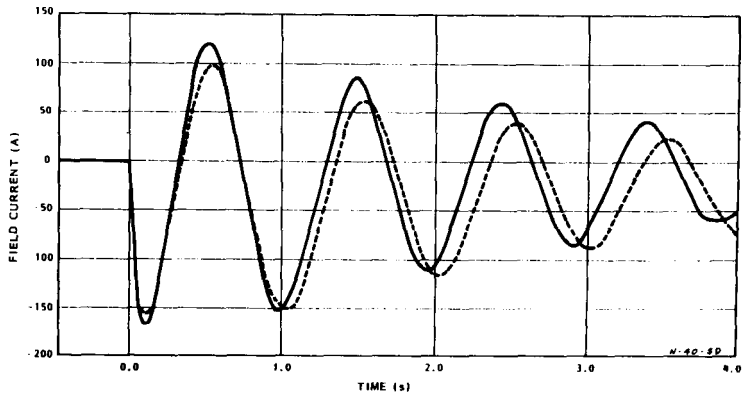

——— measured

- - - SD3

Figure 2-8. Nanticoke Line Switching Test 4-0. Field Current with OLFR3, SC2, and SD3 Models.

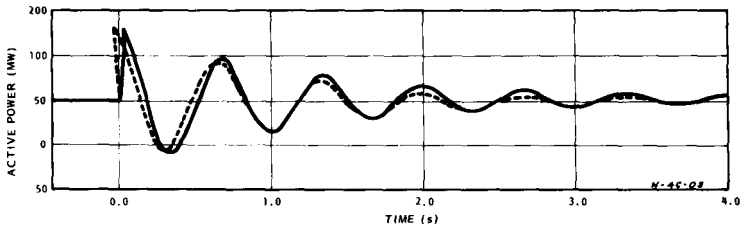

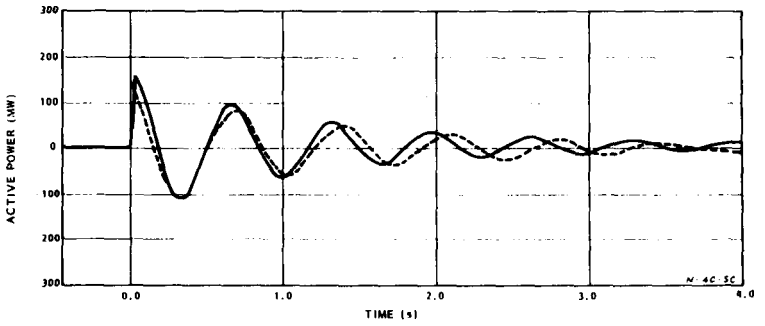

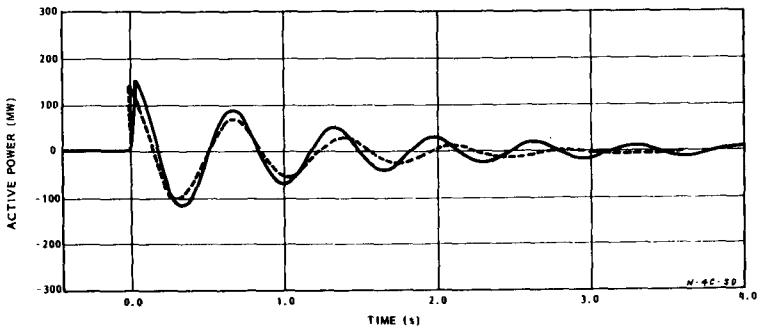

Figure 2-9. Nanticoke Line Switching Test 4-C. Active Power with OLFR3, SC2, and SD3 Models.

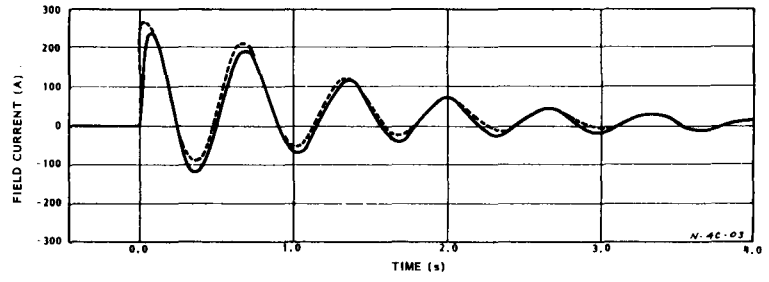

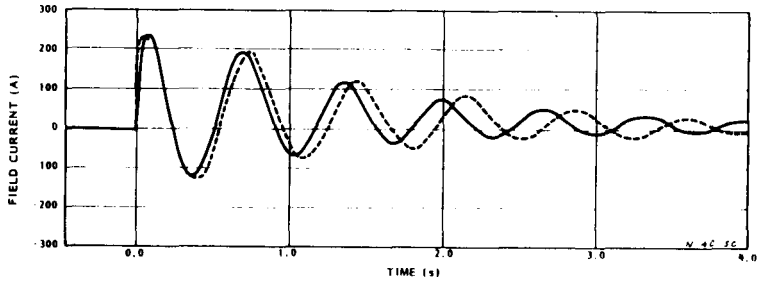

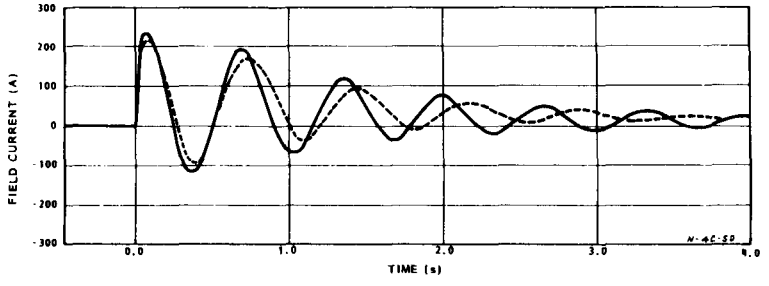

Figure 2-10. Nanticoke Line Switching Test 4-C. Field Current with OLFR3, SC2, and SD3 Models.

REFERENCES

1. G. Shackshaft. New Approach to the Determination of Synchronous Machine Parameters From Tests. Proc IEE, Vol 121, no 11, November 1974.

2. G. Shackshaft and A.T. Poray. Implementation of New Approach to Determination of Synchronous Machine Parameters from Tests. Proc IEE, vol 124, no 12, December 1977.

3. Test Procedures for Synchronous Machines. IEEE Standard No 115, March 1965.

Section 3

60 Hz FIELD IMPEDANCE

BACKGROUND

The magnitude of the non-linearity in L_{afd} was measured at zero frequency by the inductance tests done with the dc welding set and the electronic version of the ballistic galvanometer (Part 1, Section 2). A necessary condition for making such a measurement is the existence of a power supply with sufficient capacity to produce a broad range of flux densities in the generator. This meant that, in addition to the dc tests already discussed, some kind of 60 Hz measurement was also feasible. The field winding was chosen because its greater number of turns will produce more mmf for a given current than any other winding on the generator.

THE MEASUREMENTS

Voltage, current, and active power to the field winding were measured with the rotor stationary and the stator winding open. The power measurement made it possible to separate the real and imaginary parts of the field winding impedance. Readings were taken from zero to approximately 33 A rms on both the Lambton and Nanticoke machines. The resistive and reactive parts of the field impedance as well as their corresponding polar components are plotted in Figures 3-1 and 3-2.

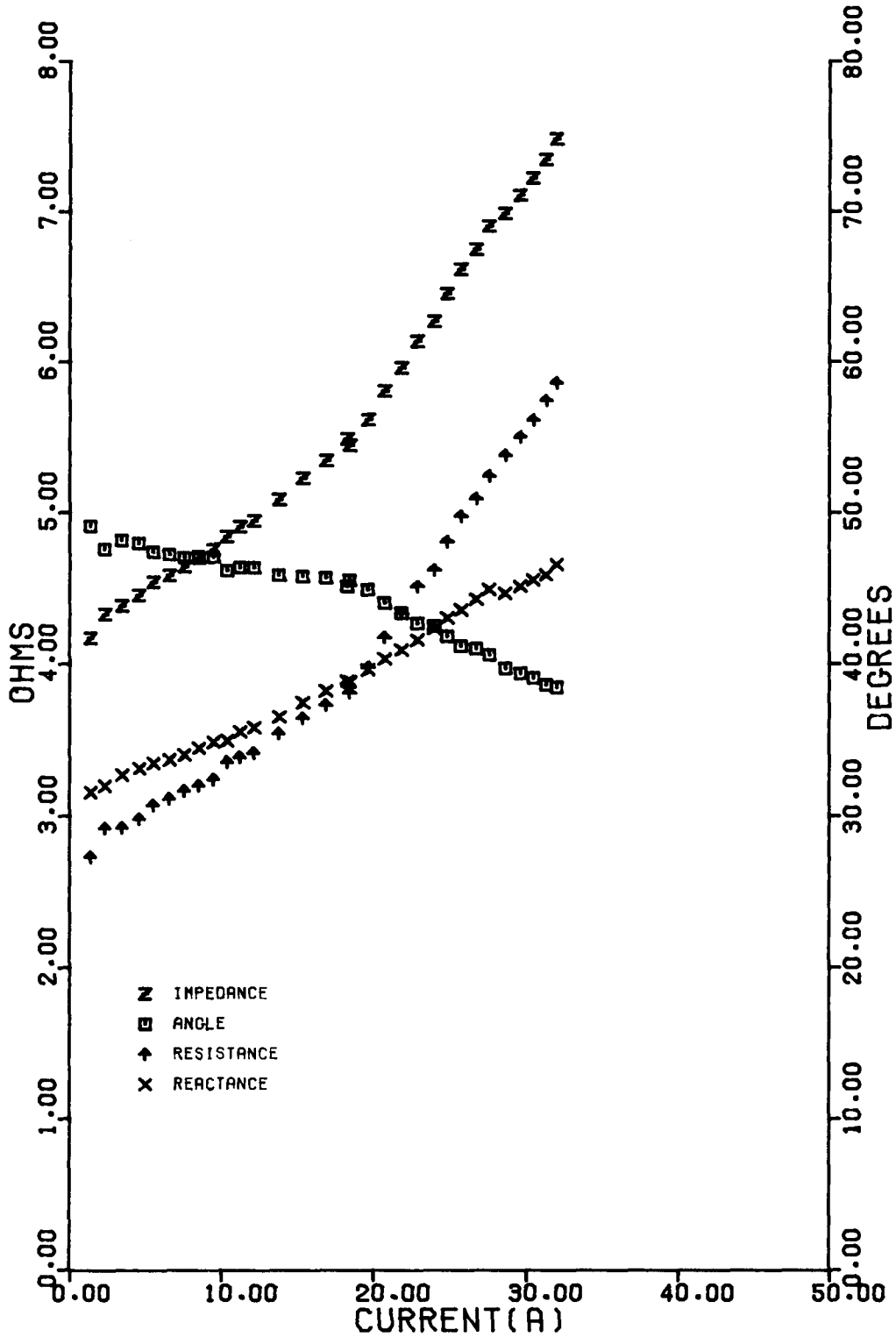

Figure 3-1. Lambton Open-Circuit Field Driving Point Impedance at 60 Hz.

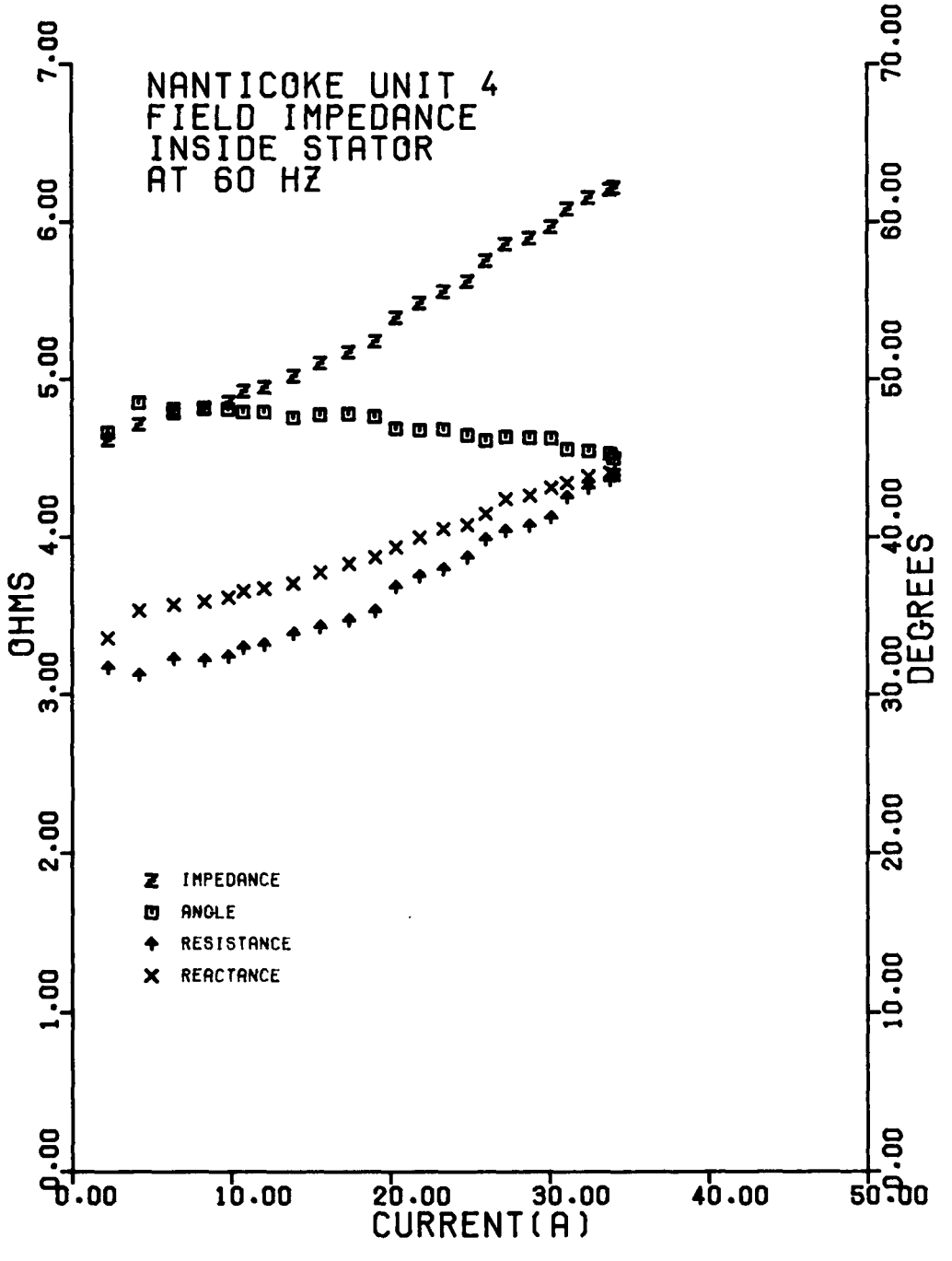

Figure 3-2. Nanticoke Open-Circuit Field Driving Point Impedance at 60 Hz.

DISCUSSION

It is apparent that, in both cases, the impedance viewed from the field terminals is non-linear and increases as the test current gets higher. This trend is what one would anticipate in view of the iron non-linearities and dc inductance measurements described in Part 1. However, beyond this, the behaviour of the field impedance is not entirely what might be expected.

It is not uncommon to regard leakage inductances in the equivalent circuit for a generator as air-core elements. As such, they are linear elements, unaffected by the magnetic properties of the iron. Following this line of reasoning, the 60 HZ impedance of the field winding, which is dominated by the leakage inductances of the field and damper windings, should be largely independent of flux density. However, it is clear from the test results in Figures 3-1 and 3-2 that this is not so. Not only does the inductive component of the impedance rise with the test current level, but its proportional change is greater than that of L_{afd} measured at dc. Although this result is at odds with the concept of air-core leakage inductances, it is consistant with another set of tests at Nanticoke. In this instance, the 60 Hz field impedance measurement was done with the rotor both inside and outside the stator bore; there was little or no difference in the two sets of data. This confirmed that, at least for the Nanticoke machine, 60 Hz field current does not produce any signficant amount of air-gap flux; i.e., the field impedance is governed by the field and damper leakage inductances. Otherwise, the impedance inside the stator would have been higher because of the lower-reluctance flux path through the stator iron.

Since the flux produced by 60 Hz field current is mostly confined to the rotor body, it is reasonable that the field impedance at this frequency is significantly influenced by the magnetic properties of the rotor iron. The corollary, of course, is that it is not strictly correct to regard the rotor leakage inductances as air-core elements. However, the importance of their non-linearity is yet to be evaluated. This will depend on its size relative to other equivalent circuit parameters, and this, in turn, will be affected by the extent to which saturaion of the leakage flux paths swamps out any other magnetic non-linearities.

RESULTS

Figures 3-4 to 3-11 are the oscillograms of the recorded transients from each of the eight test operations.

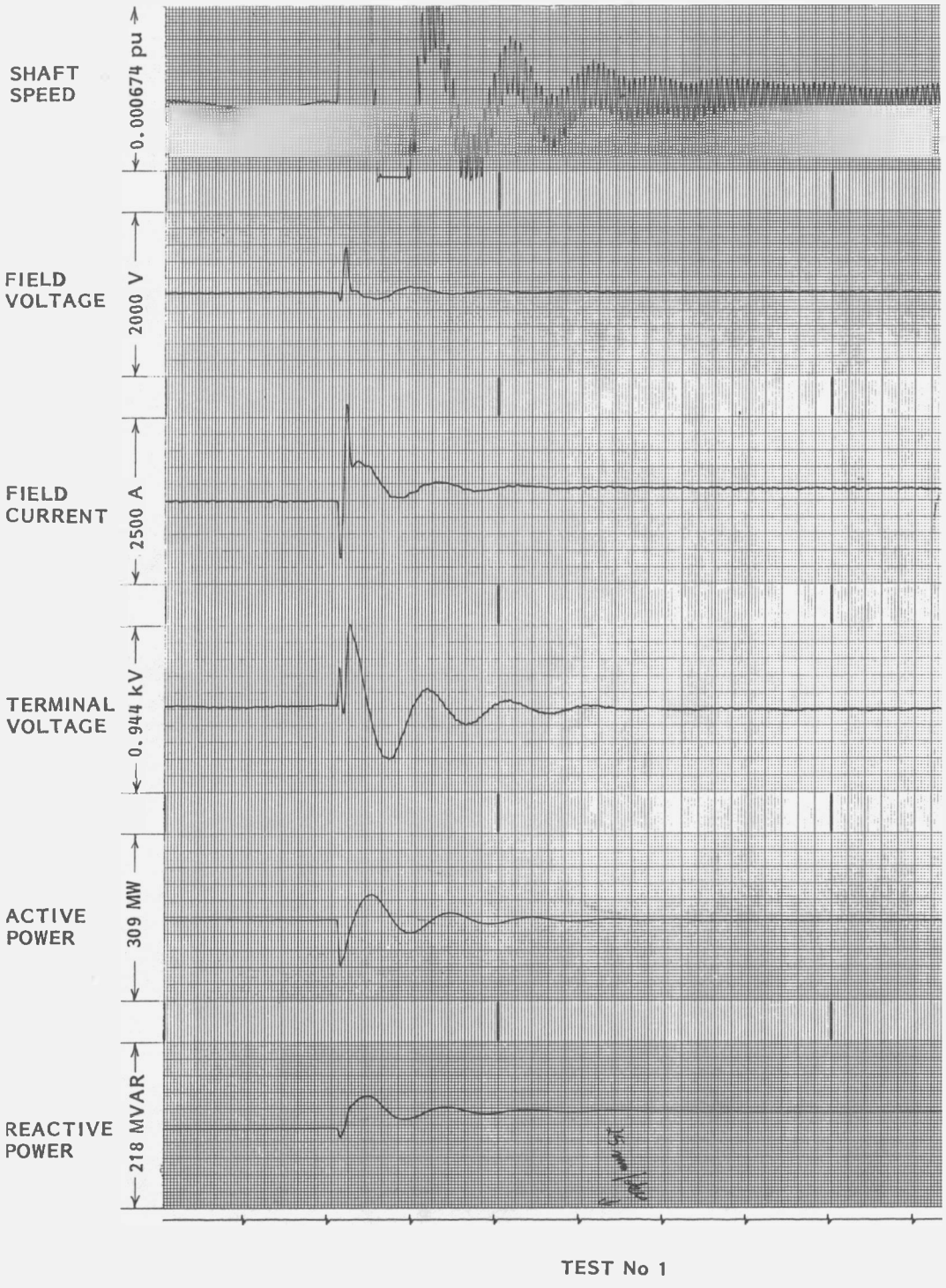

Figure 3-4. Oscillogram of Lambton Line Switching Test Number 1. Open One Line in Balanced Configuration with Voltage Regulator on Automatic.

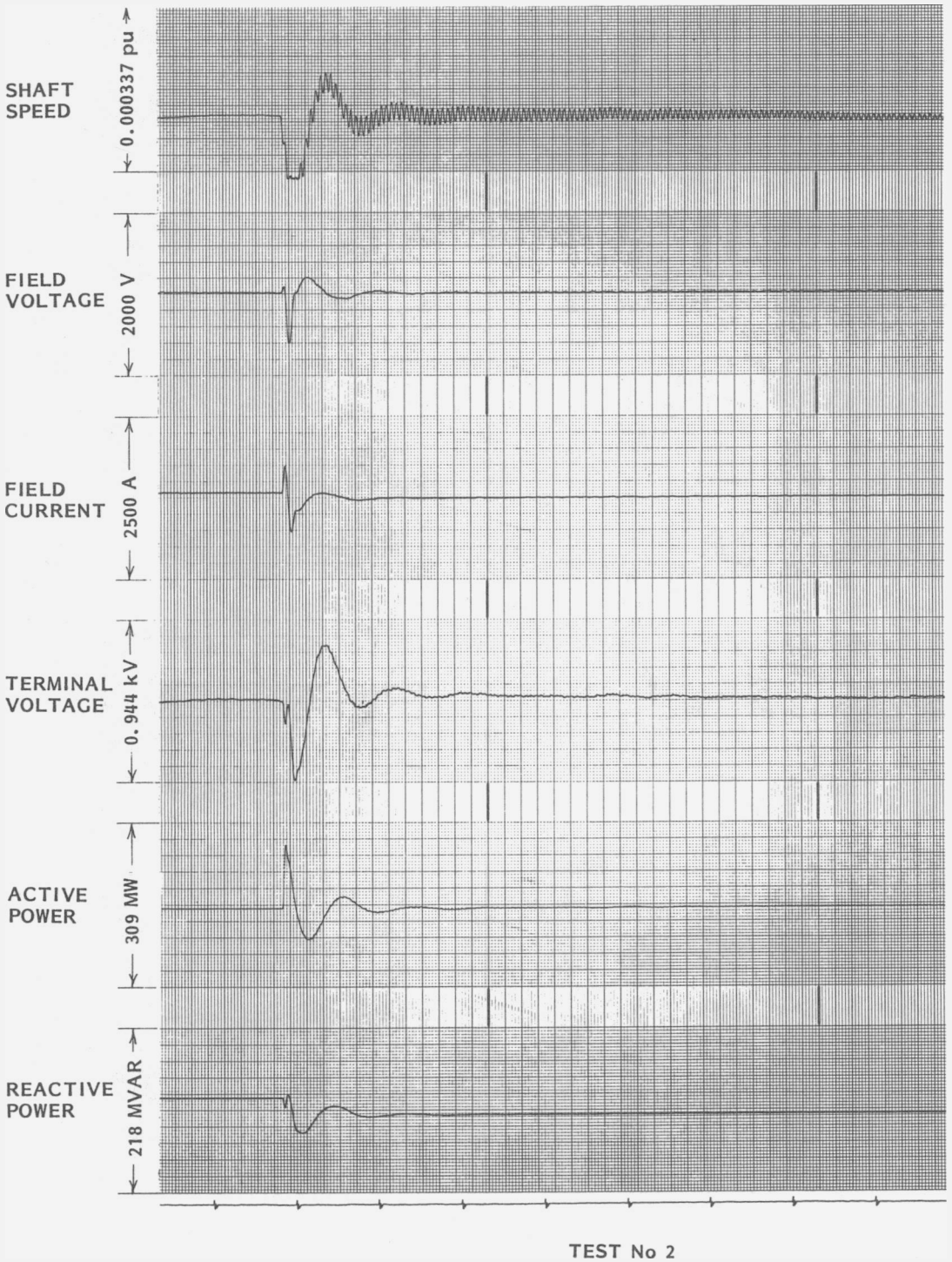

Figure 3-5. Oscillogram of Lambton Line Switching Test Number 2. Close One Line in Balanced Configuration with Voltage Regulator on Automatic.

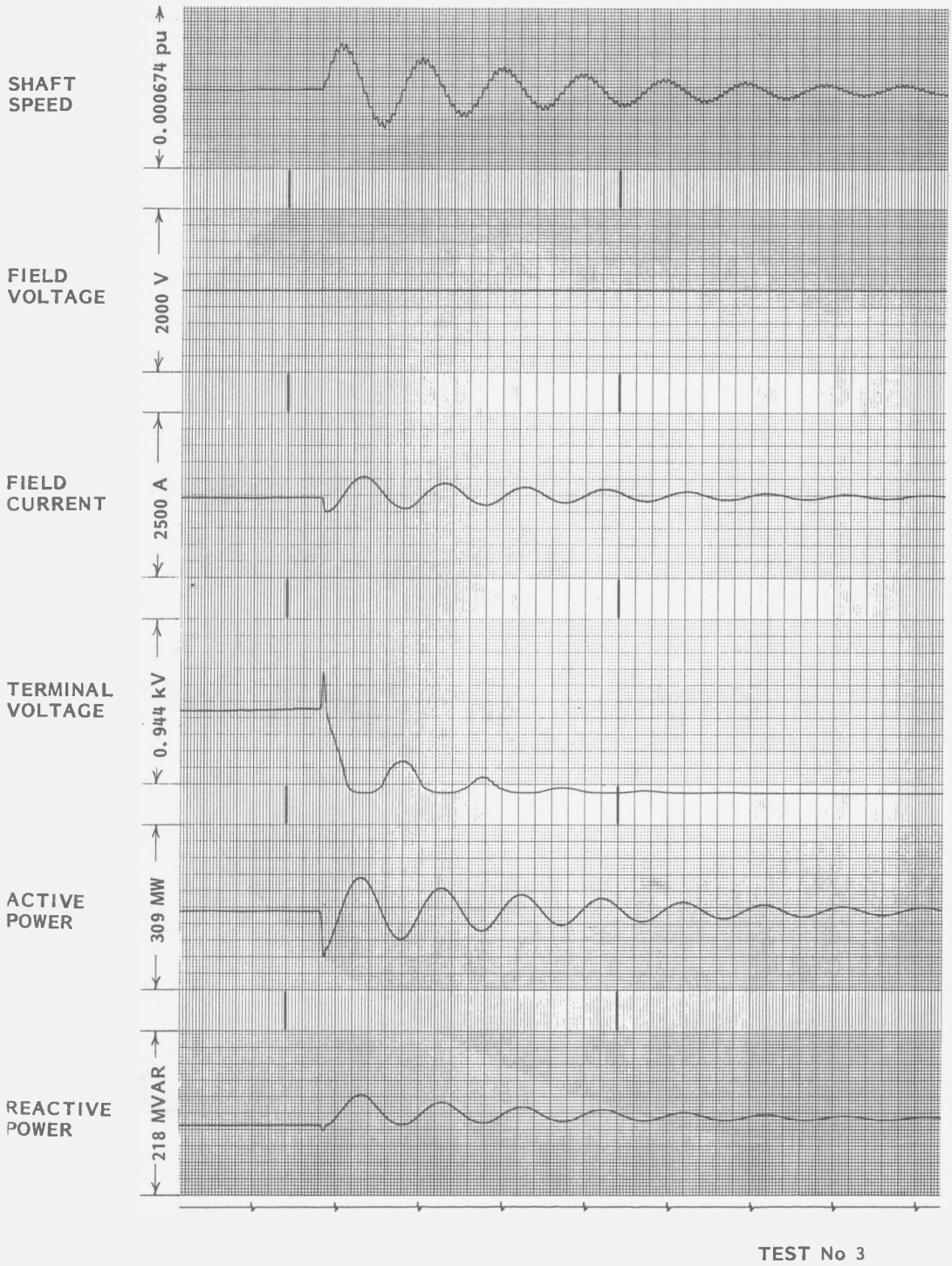

Figure 3-6. Oscillogram of Lambton Line Switching Test Number 3. Open One Line in Balanced Configuration with Voltage Regulator on Manual.

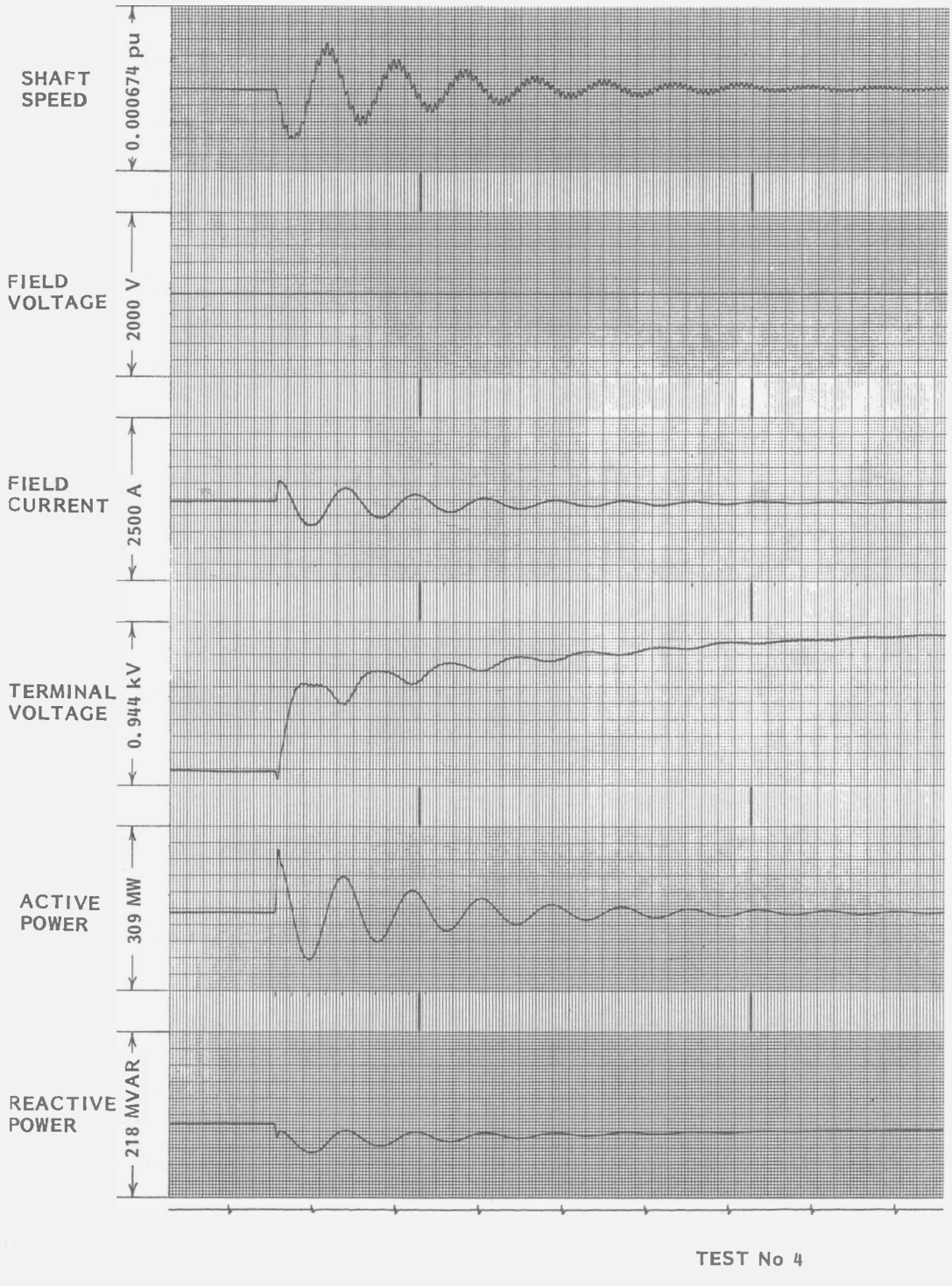

Figure 3-7. Oscillogram of Lambton Line Switching Test Number 4. Close One Line in Balanced Configuration with Voltage Regulator on Manual.

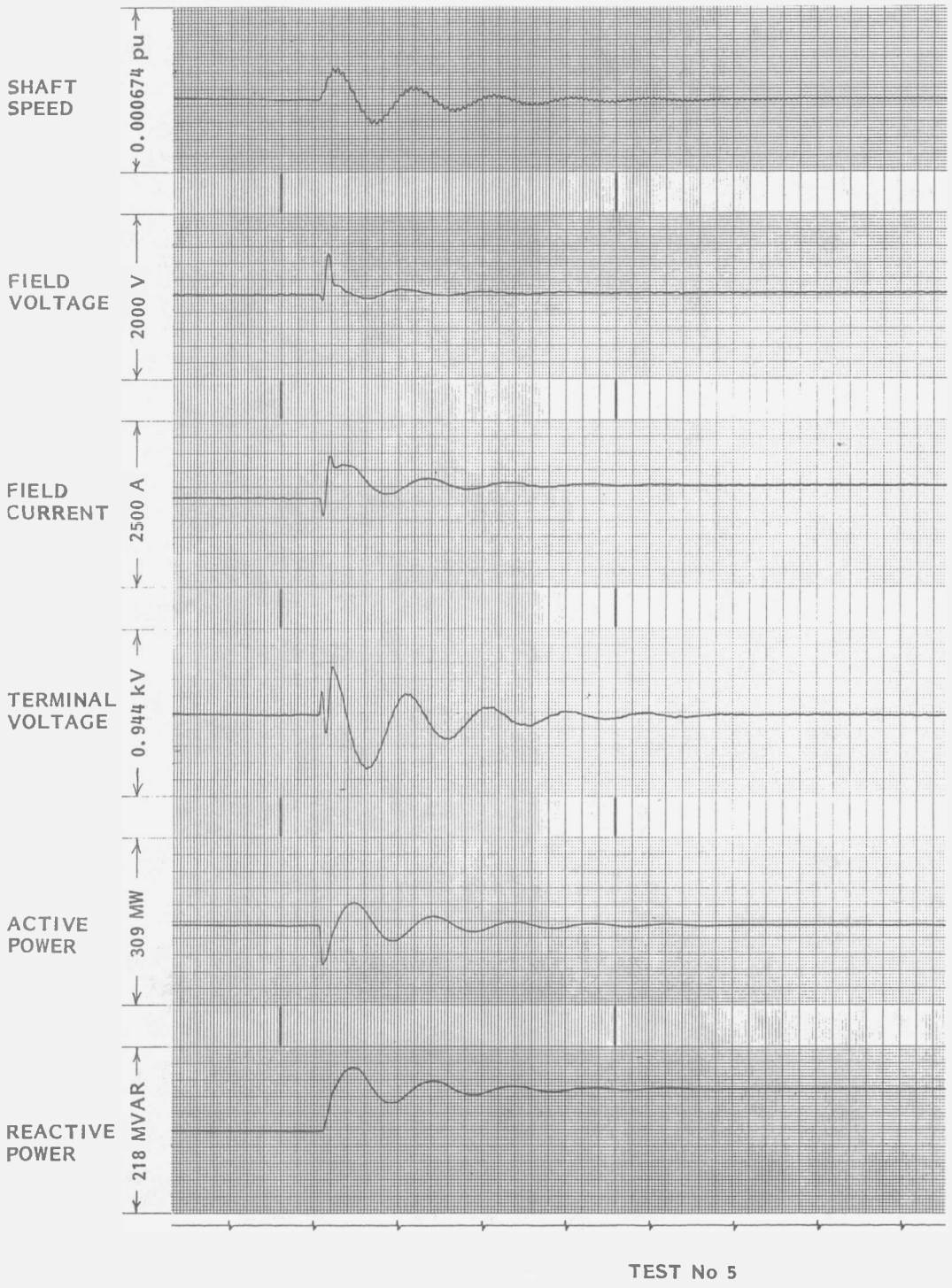

Figure 3-8. Oscillogram of Lambton Line Switching Test Number 5. Open Short Line in Unbalanced Configuration with Voltage Regulator on Automatic.

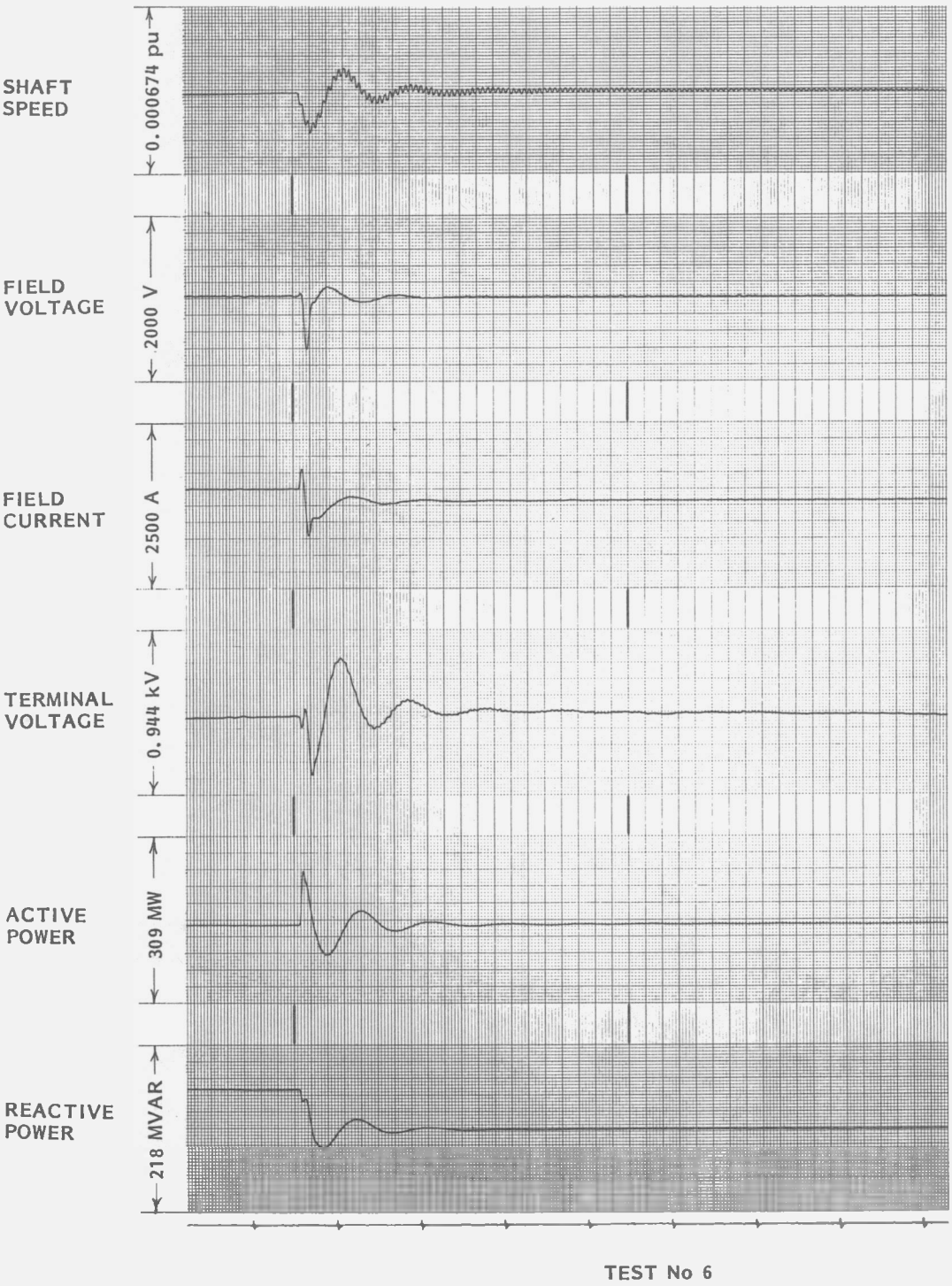

Figure 3-9. Oscillogram of Lambton Line Switching Test Number 6. Close Short Line in Unbalanced Configuration with Voltage Regulator on Automatic.

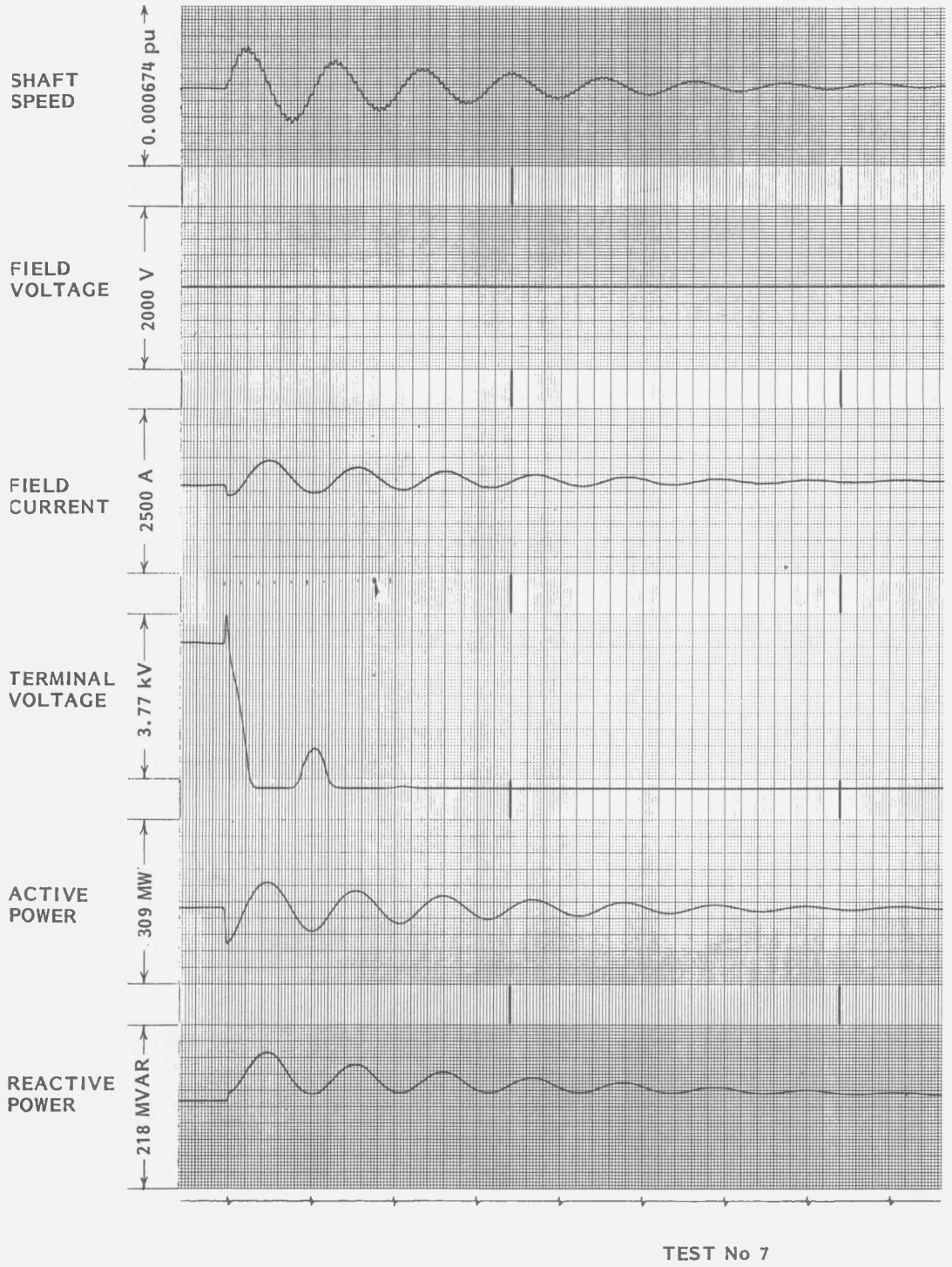

Figure 3-10. Oscillogram of Lambton Line Switching Test Number 7. Open Short Line in Unbalanced Configuration with Voltage Regulator on Manual.

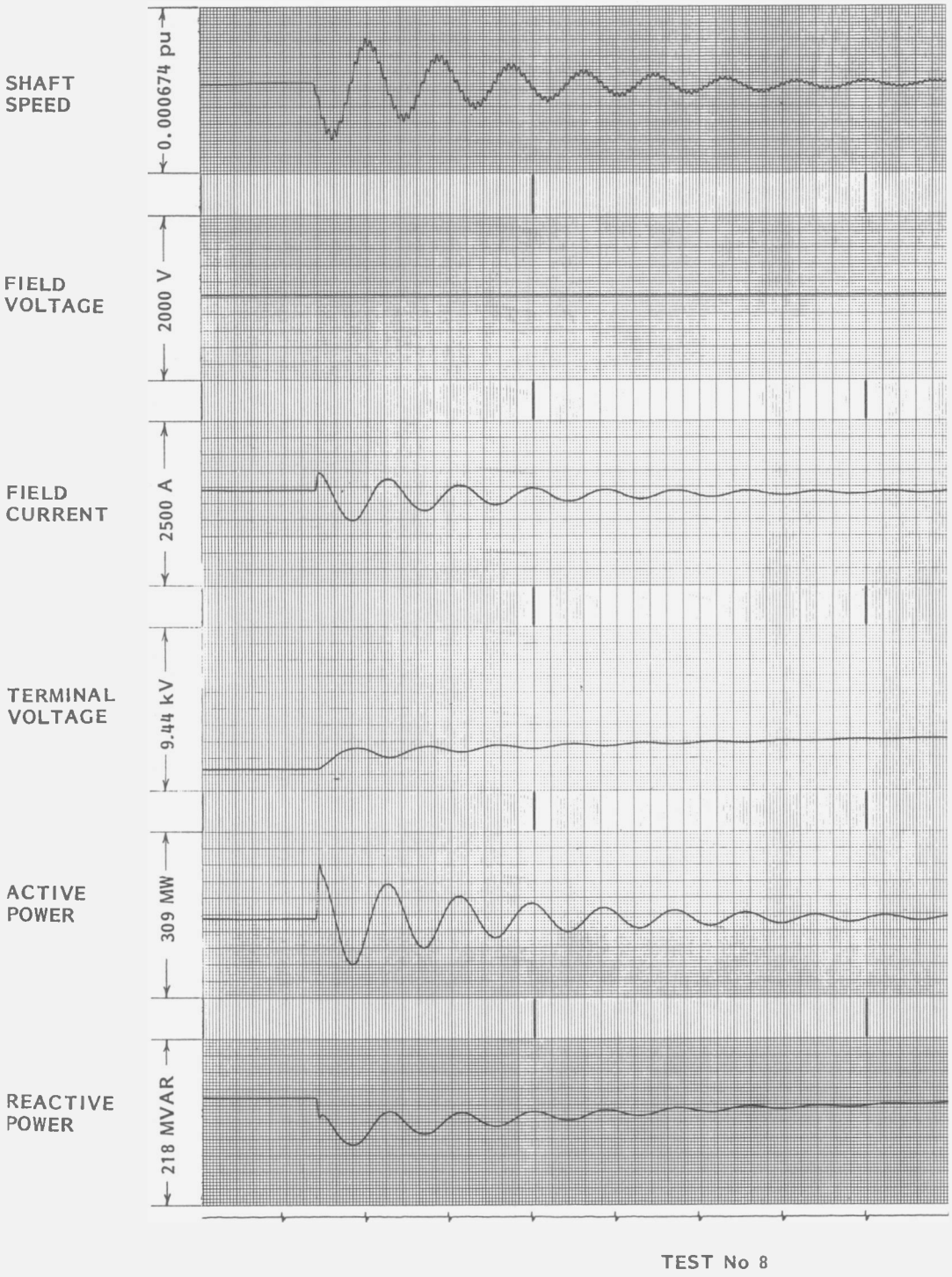

Figure 3-11. Oscillogram of Lambton Line Switching Test Number 8. Close Short Line in Unbalanced Configuration with Voltage Regulator on Manual.

Section 4

OPEN-CIRCUIT FREQUENCY RESPONSE

PURPOSE

The open-circuit tests at Lambton and Nanticoke (documented in Parts 3 and 4 respectively) were motivated primarily by the experiences with the Nanticoke generator. There, satisfactory models were obtained only when some elements of the d- and q-axis equivalent circuits in the SSFR3 model were adjusted to match the measured on line frequency response of the machine. Given the complexity of on-line frequency response tests and the system security risks associated with them, a decision was made to experiment with the simpler, safer, open-circuit frequency response test as an alternative method for computing the adjustments to the SSFR models.

A secondary objective was to see if the iron non-linearities observed with low signal levels and low flux density operating points during the standstill frequency response tests were also present with small signals at high operating flux densities.

MODEL ADJUSTMENT USING OPEN-CIRCUIT TEST DATA

In their primary mission, the open circuit frequency response tests were not successful. Since they are exclusively direct axis tests, they provide no firm basis on which to adjust the q-axis parameters. As it turned out, the q-axis model was quite important, so the open-circuit frequency response was not sufficient to account for all of the "rotational" effects in the rotor parameters.

COMPARISON WITH OTHER TESTS

Nevertheless, the open-circuit test data contains much useful information. Figures 4-1 and 4-2 compare the SSFR, and OLFR models with respect to the open-

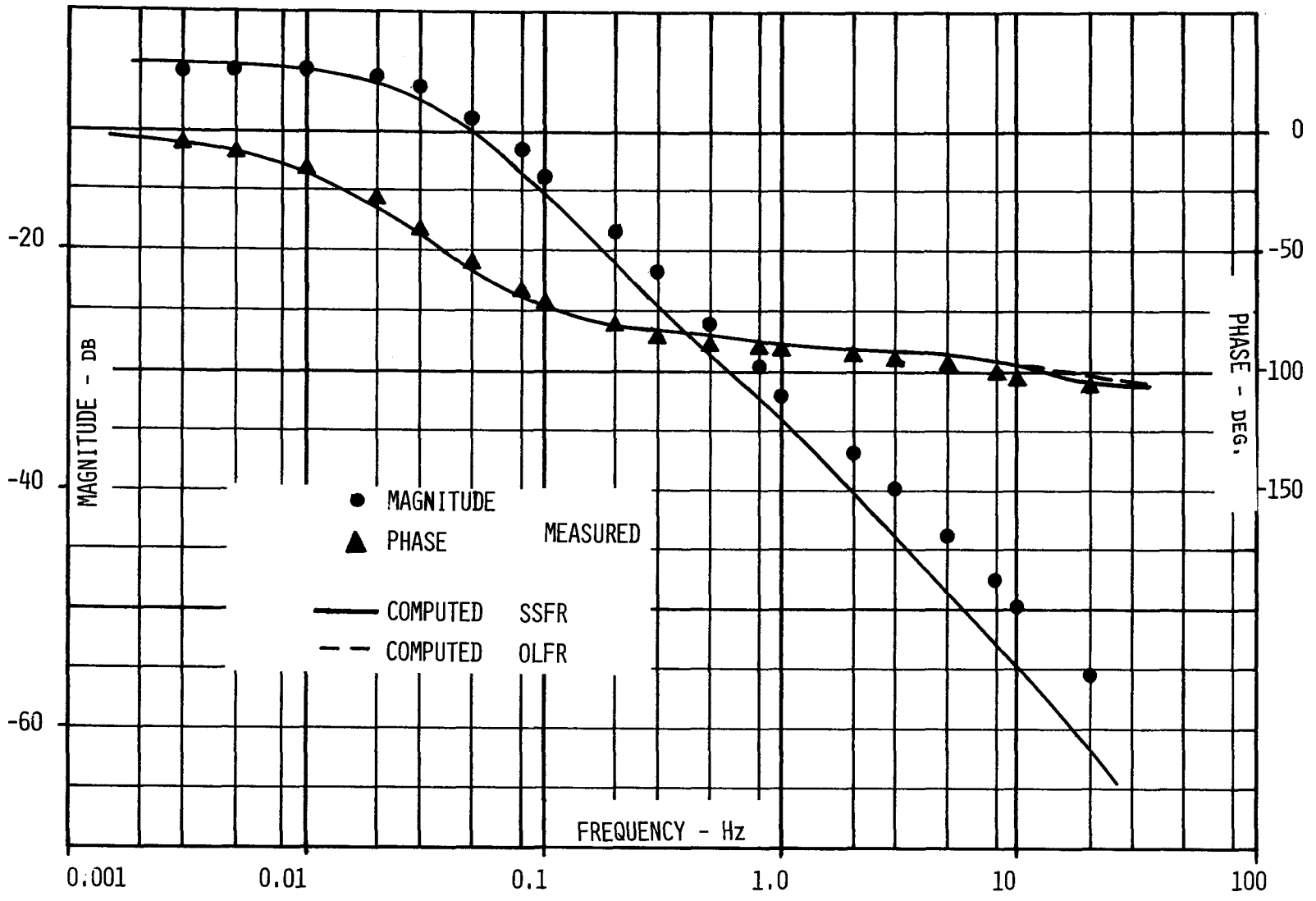

Figure 4-1. Simulation of Lambton Open-Circuit Transfer Function From Field Voltage to Terminal Voltage by SSFR2 and OLFR2 Models.

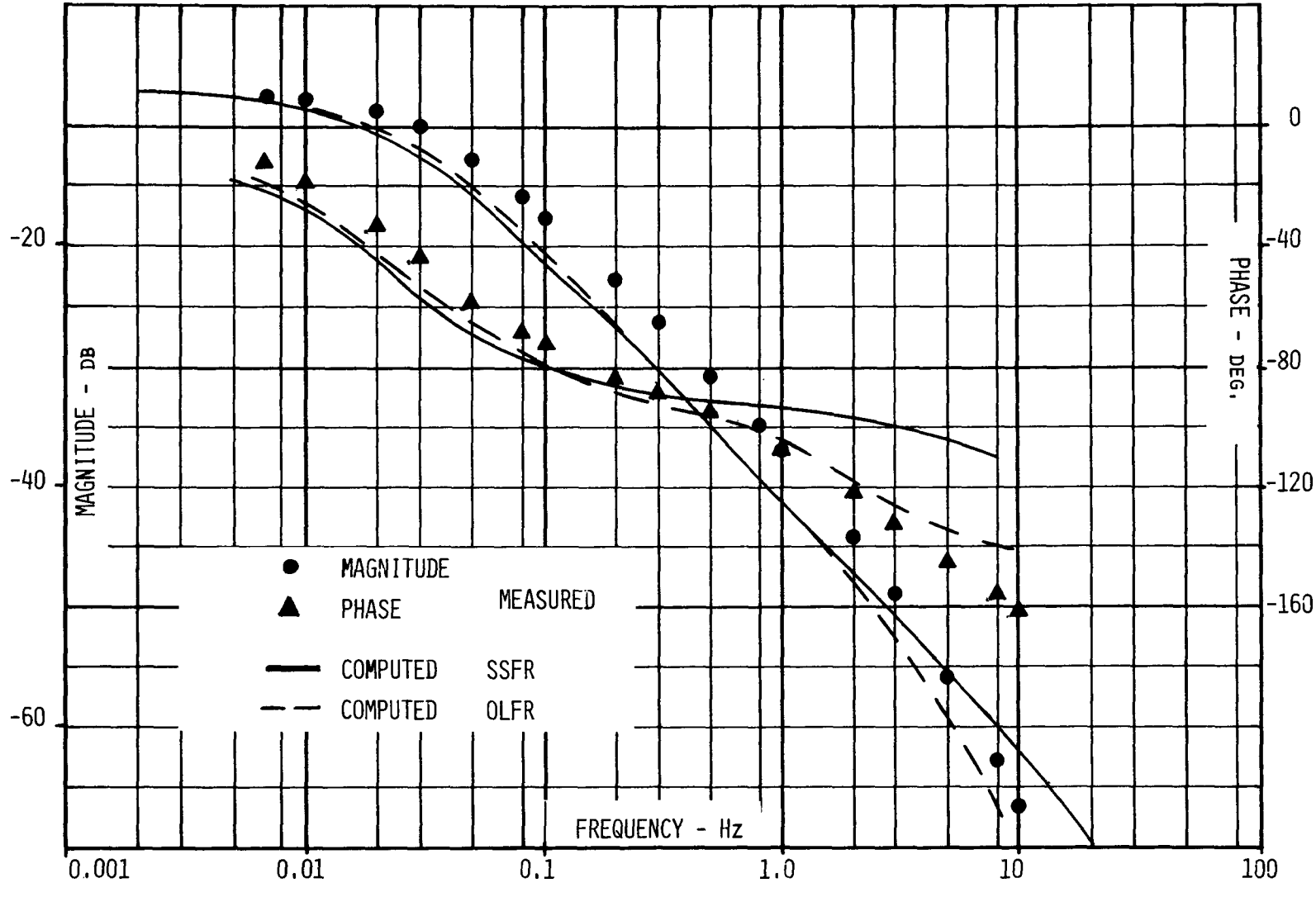

Figure 4-2. Simulation of Nanticoke Open-Circuit Transfer Function From Field Voltage to Terminal Voltage by SSFR3 and OLFR3 Models.

circuit transfer functions between field voltage and terminal voltage for the Lambton and Nanticoke generators. It is interesting to note the correlation between the phase accuracy of each model between 1 Hz and 2 Hz in the open-circuit tests and its ability to simulate the line switching transients: the Lambton SSFR2 and OLFR2 and Nanticoke OLFR3 do well in both categories while the Nanticoke SSFR3 does poorly in both. This corroborates the validity of the method used to adjust the standstill models since the so-adjusted Nanticoke model (OLFR3) has now been verified by a separate, different running test. It also adds credence to the thesis that what really matters in generator modelling is having the machine accurately represented at the frequencies of the dominant modes of oscillation.

EFFECT OF SATURATION ON OPEN-CIRCUIT PERFORMANCE

Theory

A generator having a single damper winding will be used to illustrate the effect that saturation would be expected to have on the open-circuit transfer functions at constant speed.

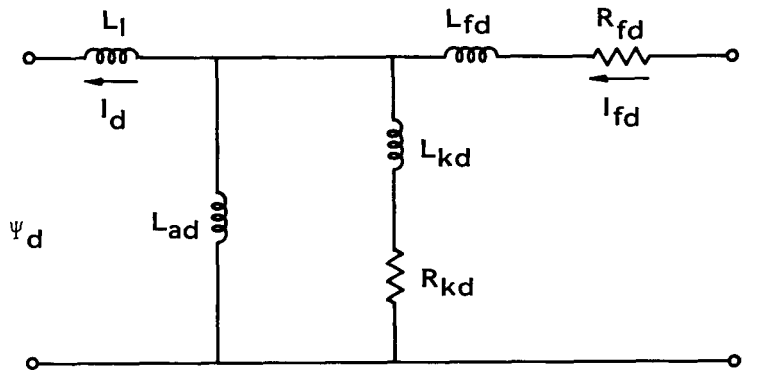

Figure 4-3. Direct Axis Equivalent Circuit for a Generator With One Damper Winding.

These transfer functions are:

$$\frac{\Delta I_{fd}}{\Delta V_{fd}} = \frac{\frac{1}{R_{fd}}\left(1 + s\,\frac{L_{ad}+L_{kd}}{R_{kd}}\right)}{1 + s\left(\frac{L_{ad}+L_{fd}}{R_{fd}} + \frac{L_{ad}+L_{kd}}{R_{kd}}\right) + s^2\left(\frac{L_{ad}L_{fd}+L_{ad}L_{kd}+L_{fd}L_{kd}}{R_{fd}R_{kd}}\right)} \tag{4-1}$$

$$\frac{\Delta V_t}{\Delta I_{fd}} = \frac{L_{ad}\left(1 + s\,\frac{L_{kd}}{R_{kd}}\right)}{1 + s\left(\frac{L_{ad}+L_{kd}}{R_{kd}}\right)} \tag{4-2}$$

$$\frac{\Delta V_t}{\Delta V_{fd}} = \frac{L_{ad}\left(1 + s\,\frac{L_{kd}}{R_{kd}}\right)}{1 + s\left(\frac{L_{ad}+L_{kd}}{R_{fd}} + \frac{L_{ad}+L_{kd}}{R_{kd}}\right) + s^2\left(\frac{L_{ad}L_{fd}+L_{ad}L_{kd}+L_{fd}L_{kd}}{R_{fd}R_{kd}}\right)} \tag{4-3}$$

At very low frequencies, Equations 4-1 to 4-3 reduce to:

$$\lim_{s \to o} \frac{\Delta I_{fd}}{\Delta V_{fd}} = \frac{1}{R_{fd}} \tag{4-4}$$

$$\lim_{s \to o} \frac{\Delta V_t}{\Delta I_{fd}} = L_{ad} \tag{4-5}$$

$$\lim_{s \to o} \frac{\Delta V_t}{\Delta V_{fd}} = \frac{L_{ad}}{R_{fd}} \tag{4-6}$$

At very high frequencies, the open-circuit transfer function become:

$$\lim_{s\to\infty} \frac{\Delta I_{fd}}{\Delta V_{fd}} = \frac{1}{s\left[\dfrac{L_{kd}}{1 + \dfrac{L_{kd}}{L_{ad}}} + L_{fd}\right]} \approx \frac{1}{s(L_{fd} + L_{kd})} \tag{4-7}$$

$$\lim_{s\to\infty} \frac{\Delta V_t}{\Delta I_{fd}} = \frac{L_{kd}}{1 + \dfrac{L_{kd}}{L_{ad}}} \approx L_{kd} \tag{4-8}$$

$$\lim_{s\to\infty} \frac{\Delta V_t}{\Delta V_{fd}} = \frac{L_{kd}}{s\left(L_{fd} + L_{kd} + \dfrac{L_{fd}L_{kd}}{L_{ad}}\right)} \approx \frac{1}{s\left(1 + \dfrac{L_{fd}}{L_{kd}}\right)} \tag{4-9}$$

If L_{ad} is assumed to be the only equivalent circuit element affected by iron non-linearity, the sensitivity of the limiting values of the transfer functions can be seen in Table 4-1. Here, the limits have been calculated for $L_{ad} = 1$ and $L_{ad} = 2$, with the other parameters fixed at:

$R_{fd} = 1.0$
$R_{kd} = 2.0$
$L_{fd} = 0.2$
$L_{kd} = 0.1$

Table 4-1

SENSITIVITY OF OPEN-CIRCUIT TRANSFER FUNCTIONS TO CHANGES IN L_{ad}

	$\lim \frac{\Delta I_{fd}}{\Delta V_{fd}}$		$\lim \frac{\Delta V_t}{\Delta I_{fd}}$		$\lim \frac{\Delta V_t}{\Delta V_{fd}}$	
L_{ad}	$s \to 0$	$s \to \infty$	$s \to 0$	$s \to \infty$	$s \to 0$	$s \to \infty$
1.00	1.00	3.44s	1.00	0.0909	1.00	0.313s
2.00	1.00	3.39s	2.00	0.0952	2.00	0.323s

At low frequencies, $\frac{\Delta I_{fd}}{\Delta V_{fd}}$ is not influenced by saturation while $\frac{\Delta V_t}{\Delta I_{fd}}$ and $\frac{\Delta V_t}{\Delta V_{fd}}$ vary directly with L_{ad}. It is also evident that, at high frequencies, with typical parameters, none of the transfer functions is much influenced by changes in L_{ad}.

Both the Lambton and Nanticoke machines behaved predictably with regard to saturation at very low frequencies. As is evident in Figures 4-4 and 4-7, the low frequency limit of the magnitude of the transfer function between field voltage and terminal voltage goes down as the terminal voltage and consequent iron saturation increase. In fact, this magnitude is approximately equal to the slope of the open-circuit saturation curve at the corresponding voltage level.

The high frequency data, however, is not consistent with the theory that only L_{ad} is affected by saturation. This is particularly evident in the Lambton data (Figure 4-5 and 4-6) where there are substantial differences, at high frequencies, in the magnitudes of the $\frac{\Delta I_{fd}}{\Delta V_{fd}}$ and $\frac{\Delta V_t}{\Delta I_{fd}}$ transfer functions at the three different operating points. The same is true for Nanticoke (Figures 4-8 and 4-9), although less pronounced. This behaviour can be explained quite well by allowing the rotor leakage inductances, L_{fd} and L_{kd} to saturate with L_{ad} (Equations 4-7 and 4-8).

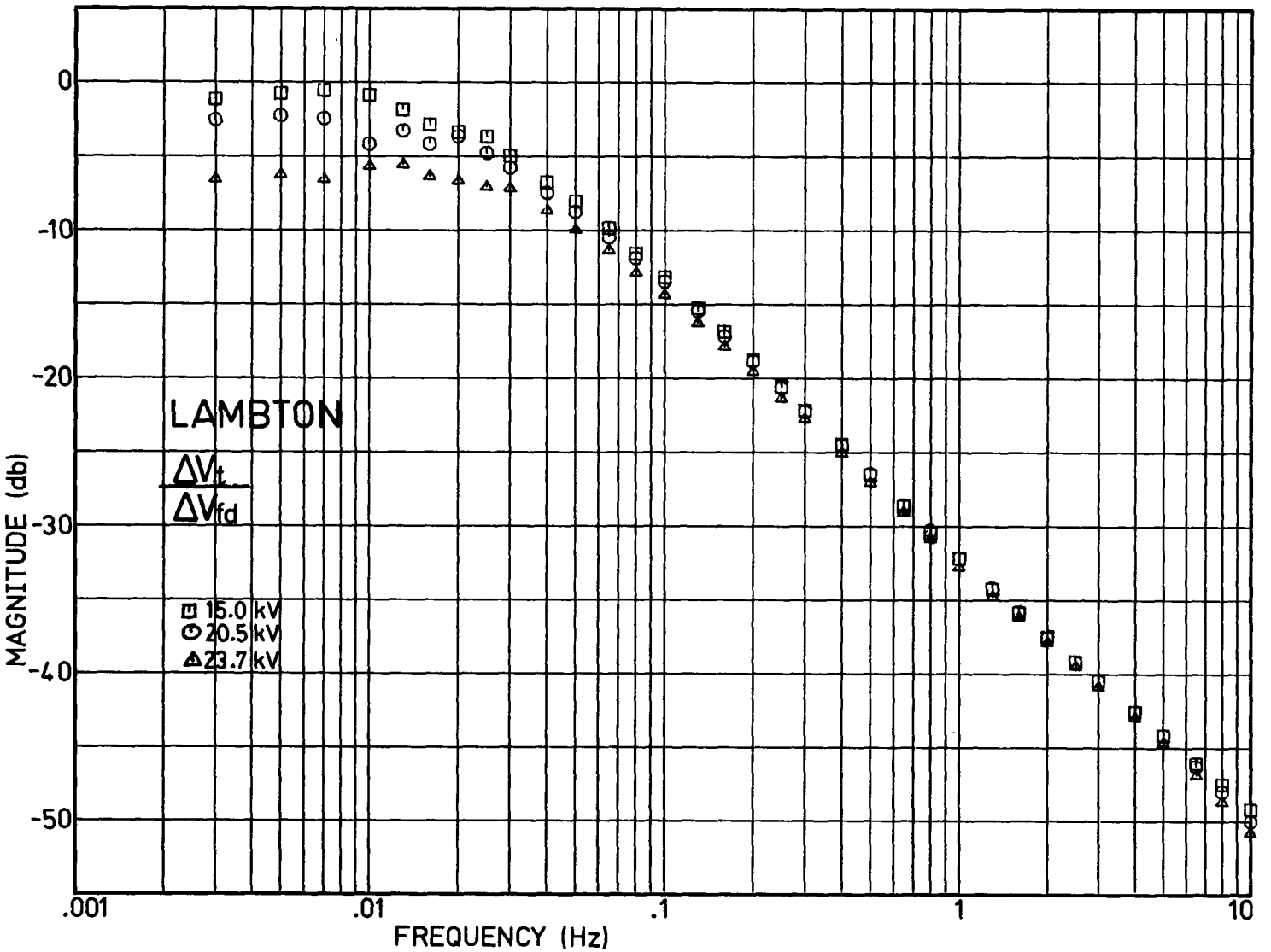

Figure 4-4. Lambton Open-Circuit Transfer Function From Field Voltage to Terminal Voltage.

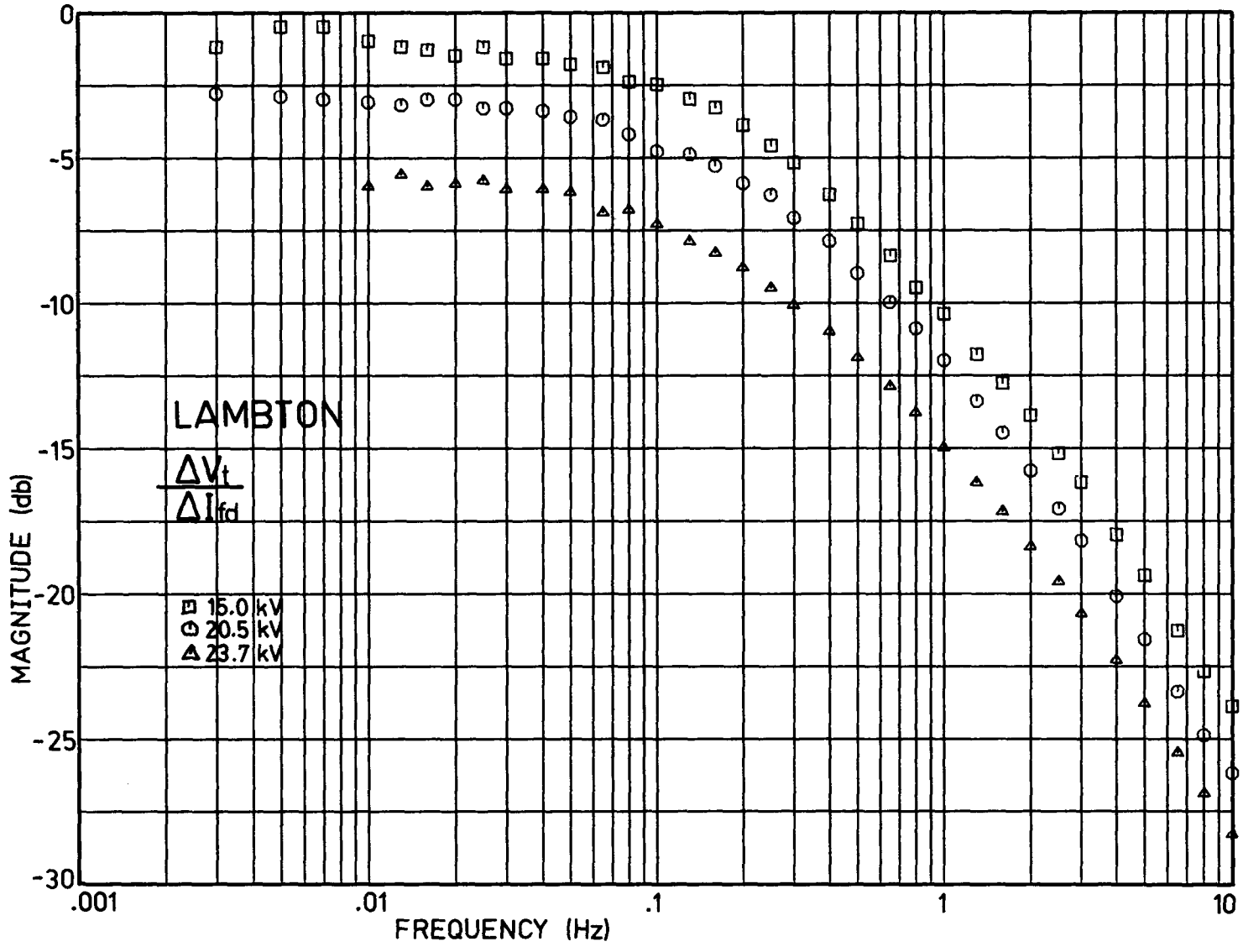

Figure 4-5. Lambton Open-Circuit Transfer Function From Field Current to Terminal Voltage.

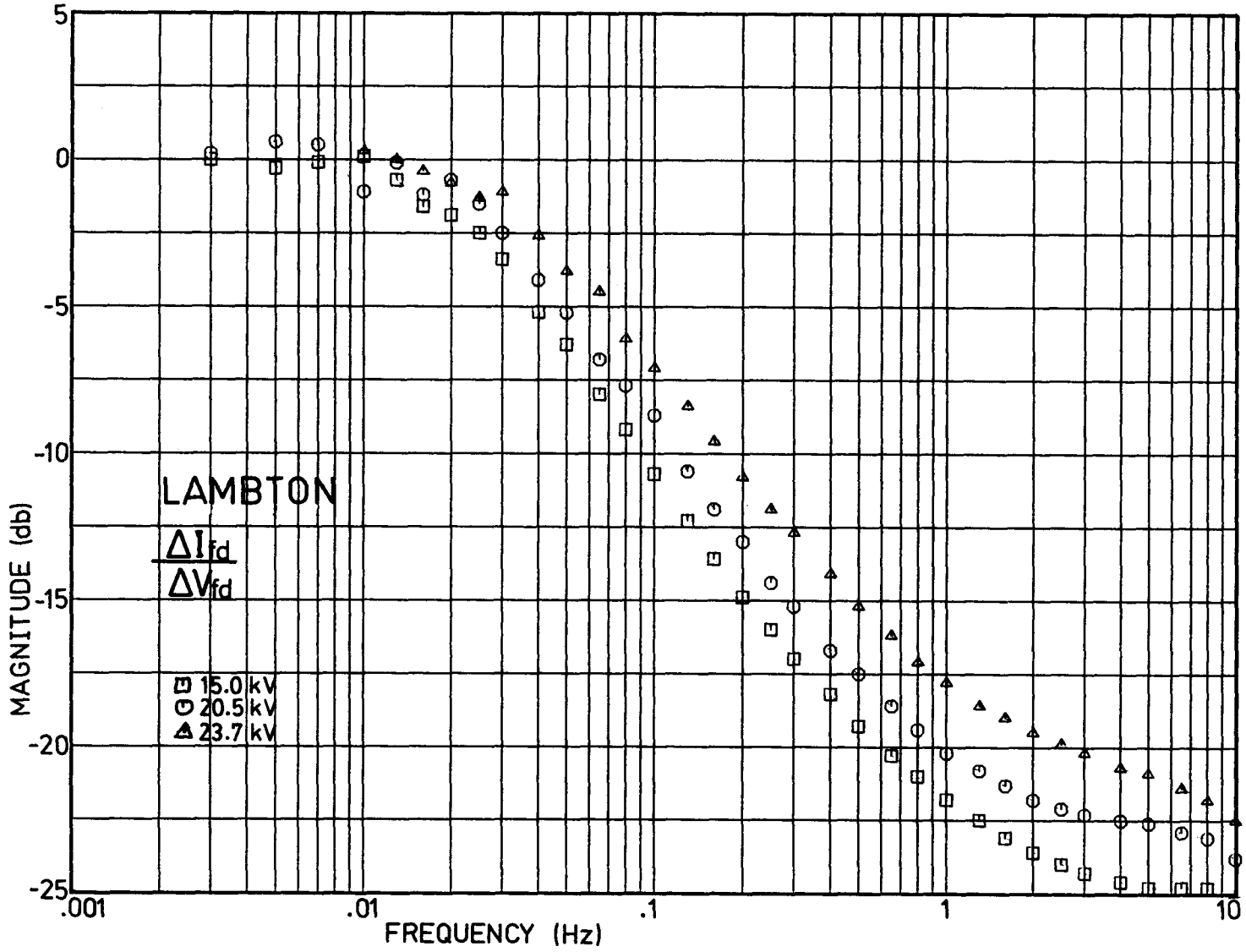

Figure 4-6. Lambton Open-Circuit Transfer Function From Field Voltage to Field Current.

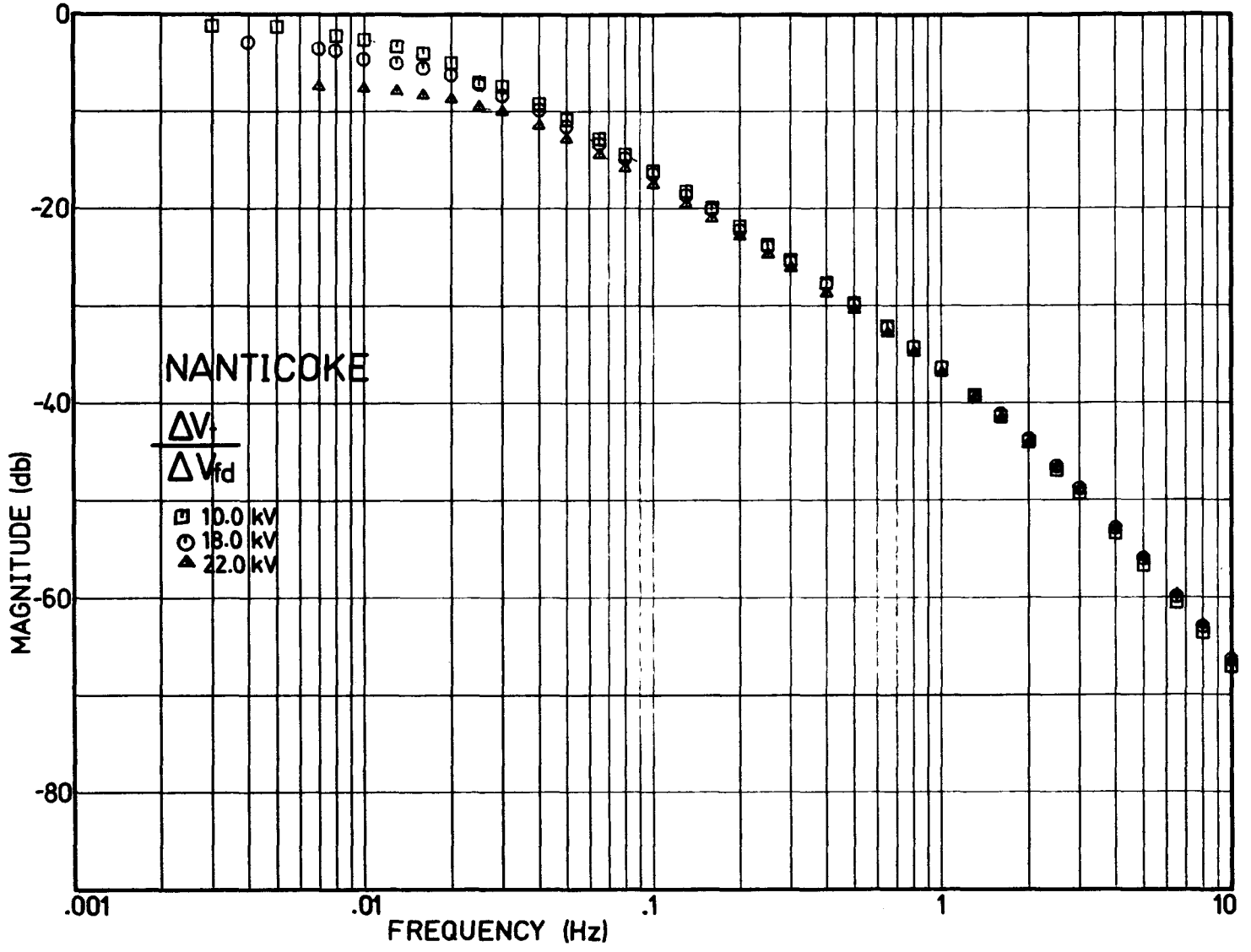

Figure 4-7. Nanticoke Open-Circuit Transfer Function From Field Voltage to Terminal Voltage.

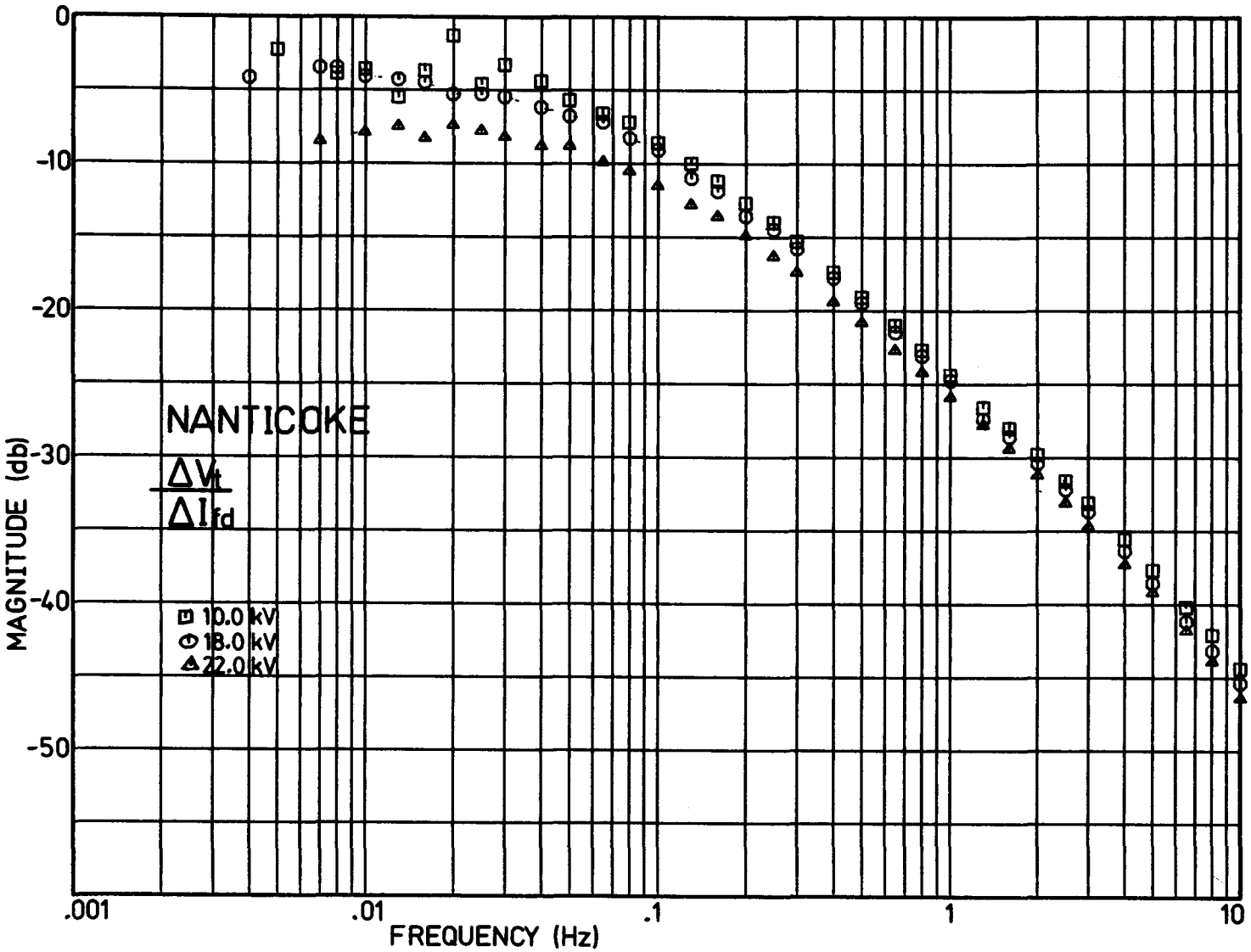

Figure 4-8. Nanticoke Open-Circuit Transfer Function From Field Current to Terminal Voltage.

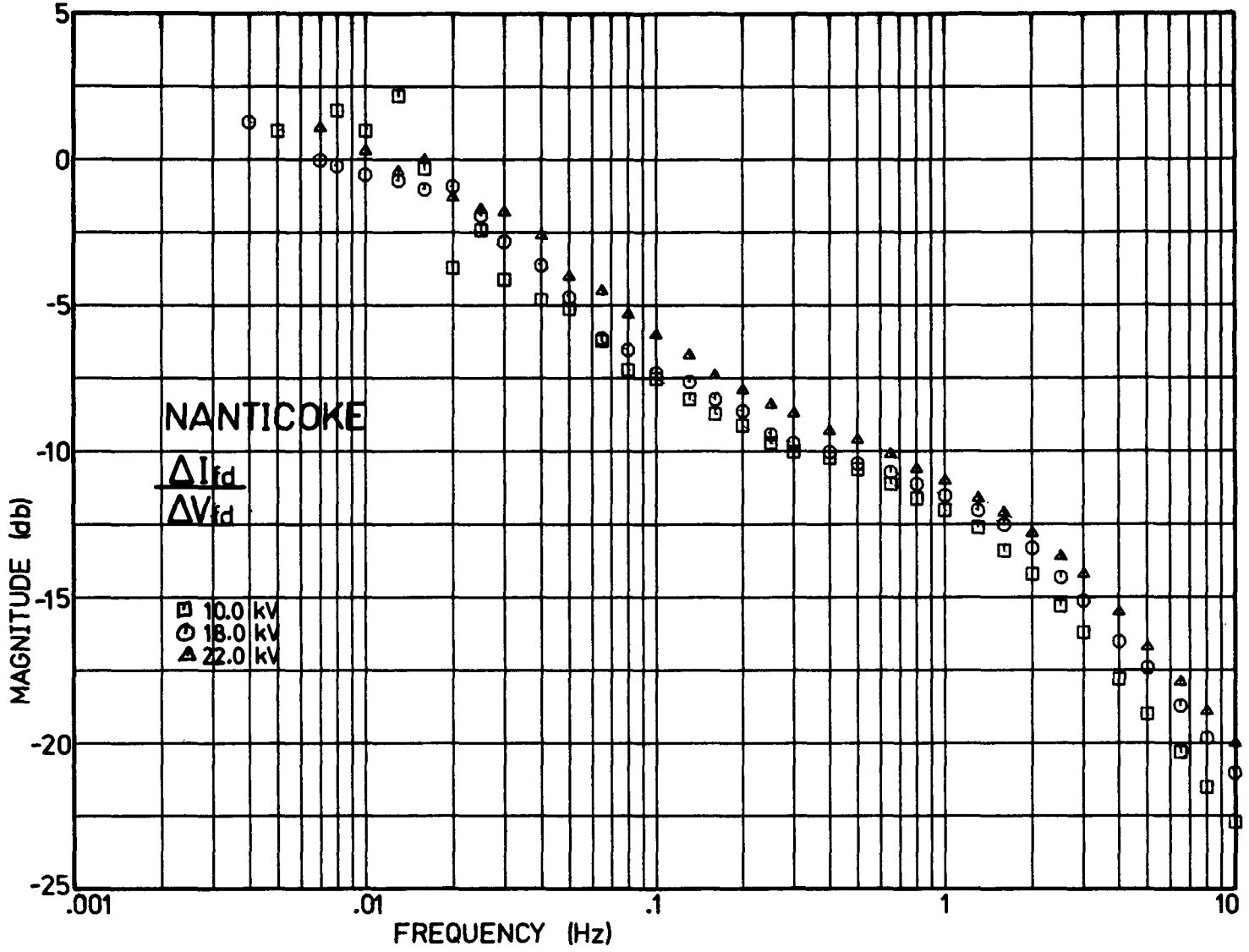

Figure 4-9. Nanticoke Open-Circuit Transfer Function From Field Voltage to Field Current.

LINEARITY TESTS

Open-circuit linearity checks were done at both Lambton and Nanticoke. The generators were operated off-line at rated speed, with the excitation adjusted to a point in the linear part of the open-circuit saturation curve (8.5 kV for Lambton and 10 kV for Nanticoke). Then, the field voltage was modulated sinusoidally at three different frequencies. At each frequency, the magnitude of the oscillations was varied over as wide a range as possible, from the smallest measurable to the largest permitted by the limits of exciter ceiling voltage and zero field current.

Three transfer functions were measured: field voltage to field current, field current to terminal voltage, and field voltage to terminal voltage. The Lambton results are plotted in Figures 4-10 to 4-12, those for Nanticoke in Figures 4-13 to 4-15. In each case, the circles are the magnitude, and the squares the phase angle of the measured transfer functions.

The following observations can be made from these plots:

- There are measureable non-linearities in all three transfer functions for both machines.
- the lowest frequency (0.1 Hz for Lambton and 0.2 Hz for Nanticoke non-linearities are in the direction, and of the order that would be expected from previously measured changed in L_{ad} from the direct current tests.

These two points are confirmation of the hypothesis that the small signal performance of an iron-core device is independent of the operating point. In other words, whether the starting point is zero or a more typical operating flux density, the iron-dependent inductances that govern a small change around that point will be lower than they would be for a larger change.

If L_{ad} and L_{aq} were the only elements in the d- and q-axis equivalent circuits involved in this phenomenon, evidence of it would be most apparent at lower frequencies (Table 4-1). However, it is very obvious in the Lambton results, and to a lesser degree the Nanticoke ones, that the reverse is true---the effect is more pronounced at the higher frequencies.

It is too soon to draw any firm conclusions from these results. However, it is in order to postulate a mechanism. When a generator is running, the stator iron is constantly describing relatively large B-H loops due to the rotating magnetic field. Consequently, the small signal effects, previously discussed, apply only to the rotor iron. L_{ad} is associated with a flux path which has the stator iron, the rotor iron and the air gap as its main components. The rotor leakage reactances, on the other hand, are not influenced by the stator iron. Accordingly, it is entirely plausible that a rotor leakage inductance associated with a flux path around the slot through the rotor iron, and across the gap between two rotor teeth could have a considerably greater small signal non-linearity than L_{ad}. Then, as the dominanting influence on the open-circuit transfer functions (Equations 4-1 to 4-3) shifts from L_{ad} at low frequencies to the rotor leakage inductances at high frequencies, the non-linearity of the transfer functions could be expected to increase with frequency.

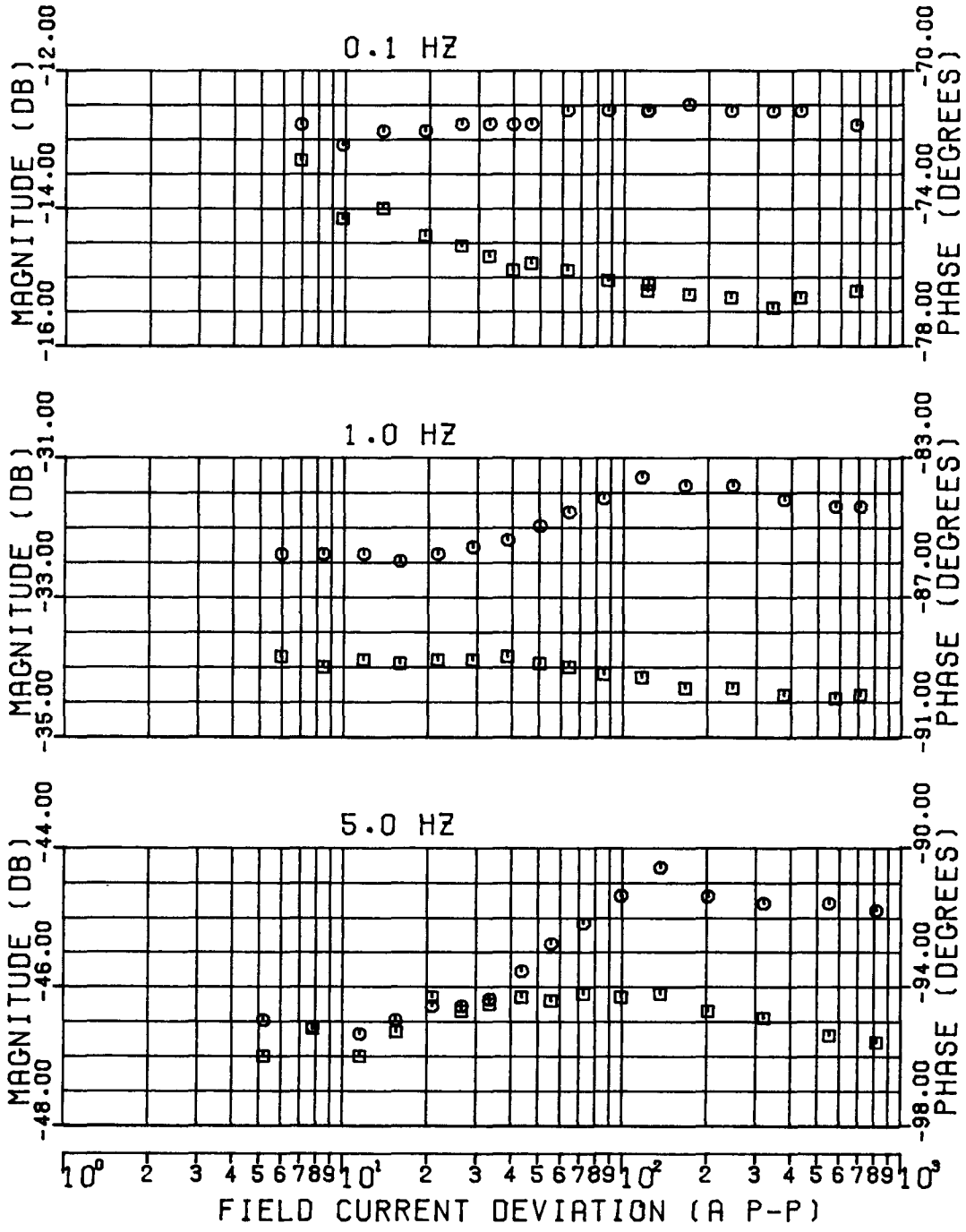

Figure 4-10. Lambton Open-Circuit Transfer Function From Field Voltage to Field Current as a Function of Field Current Deviation.

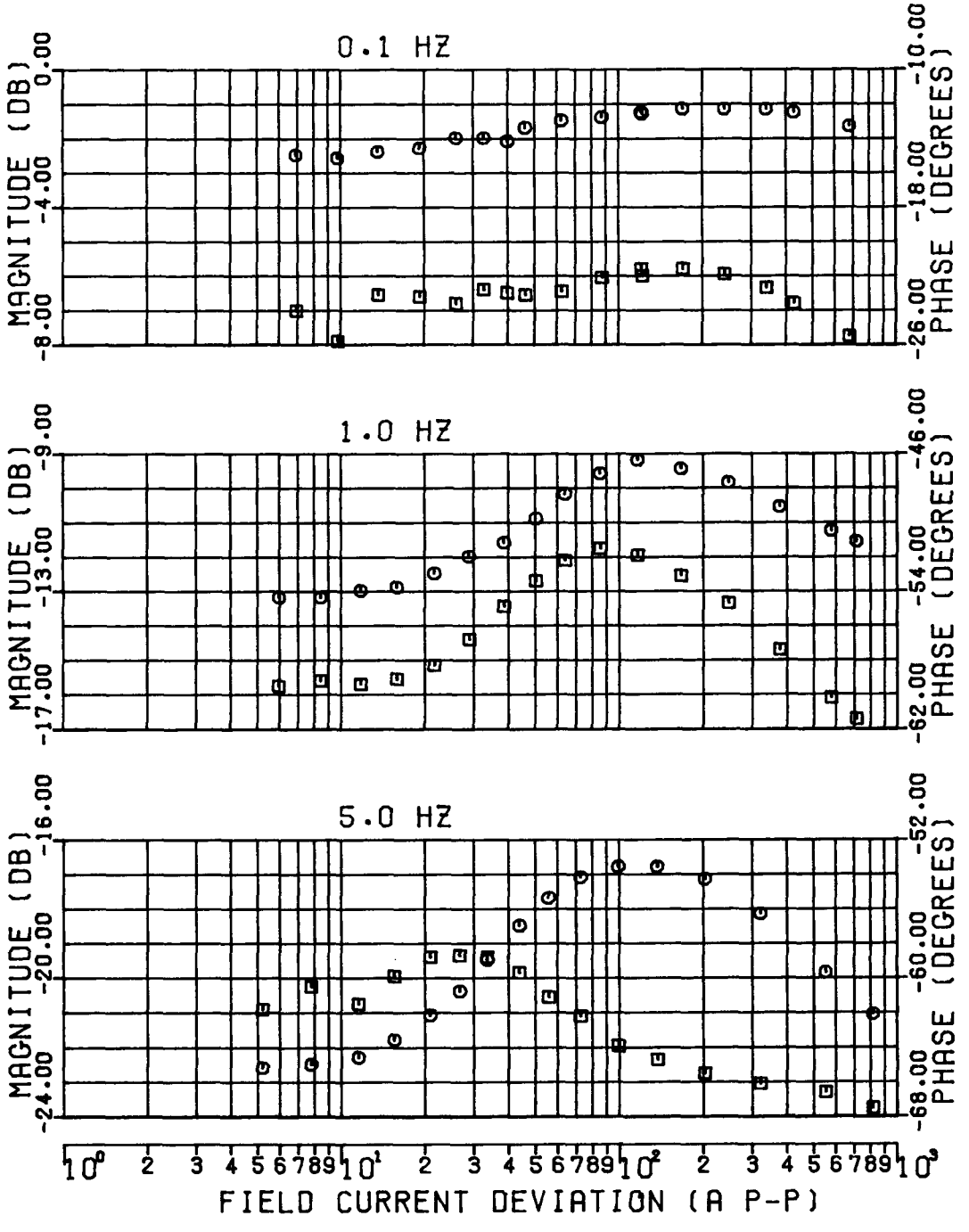

Figure 4-11. Lambton Open-Circuit Transfer Function From Field Current to Terminal Voltage as a Function of Field Current Deviation.

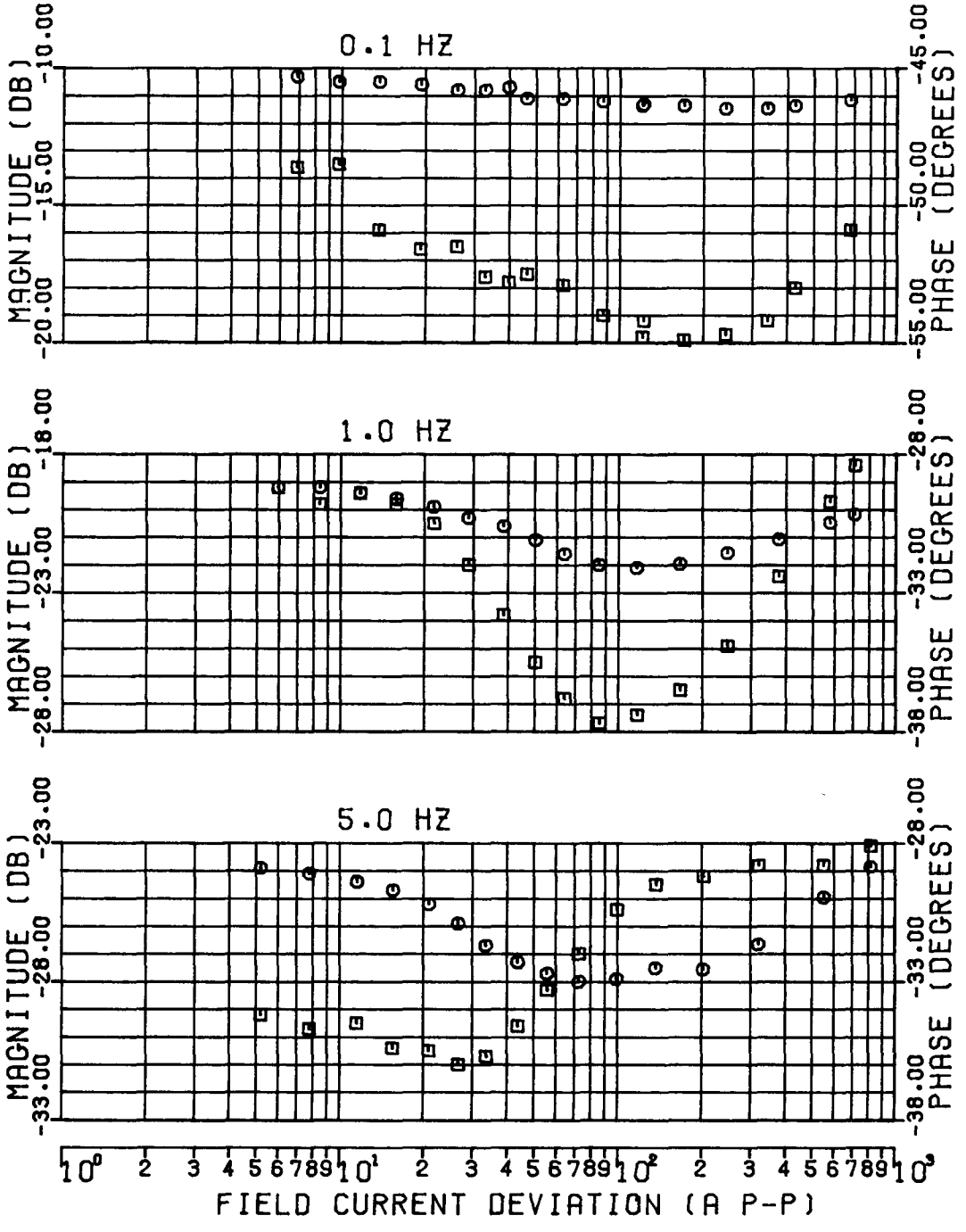

Figure 4-12. Lambton Open-Circuit Transfer Function From Field Voltage to Terminal Voltage as a Function of Field Current Deviation.

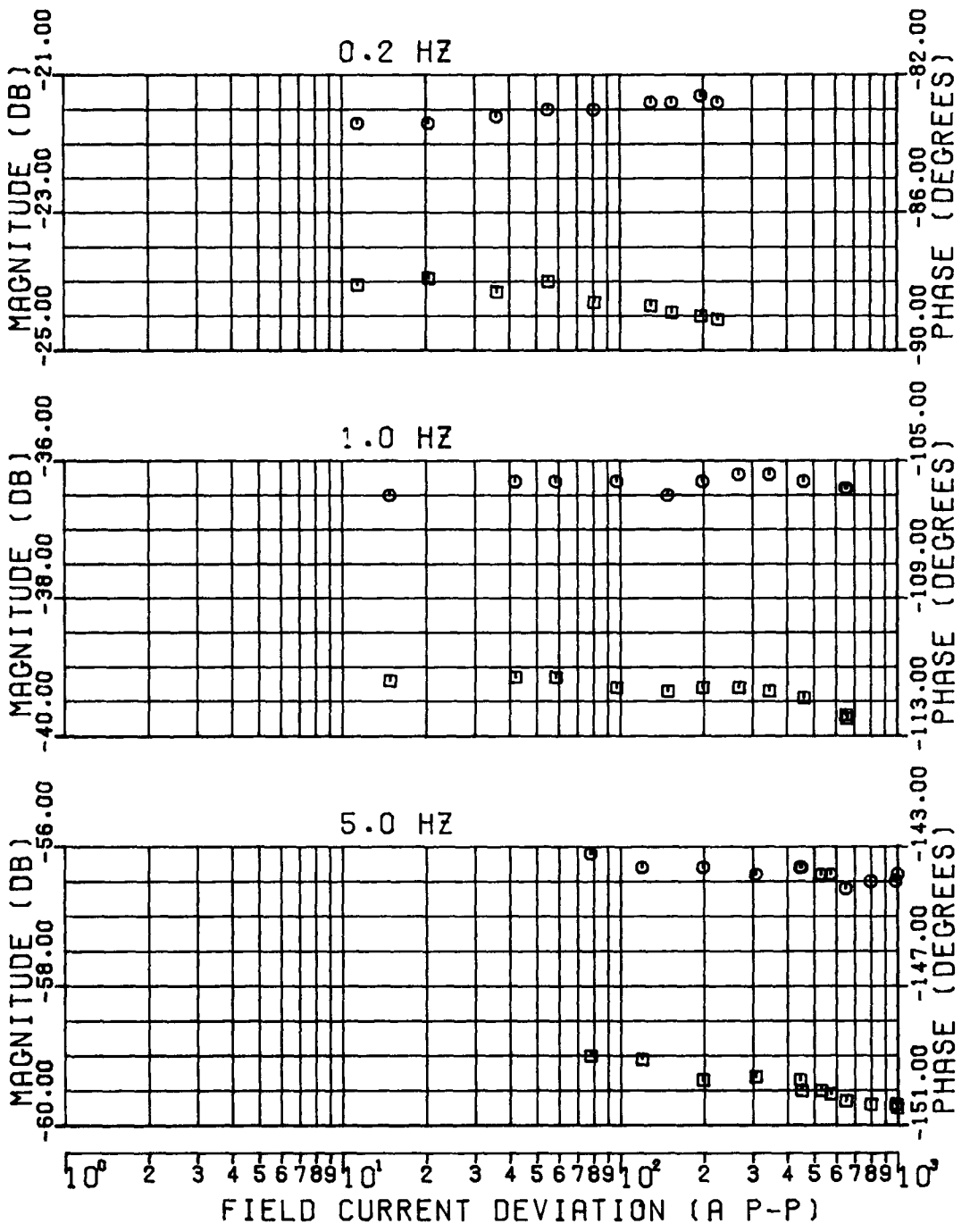

Figure 4-13. Nanticoke Open-Circuit Transfer Function From Field Voltage to Field Current as a Function of Field Current Deviation.

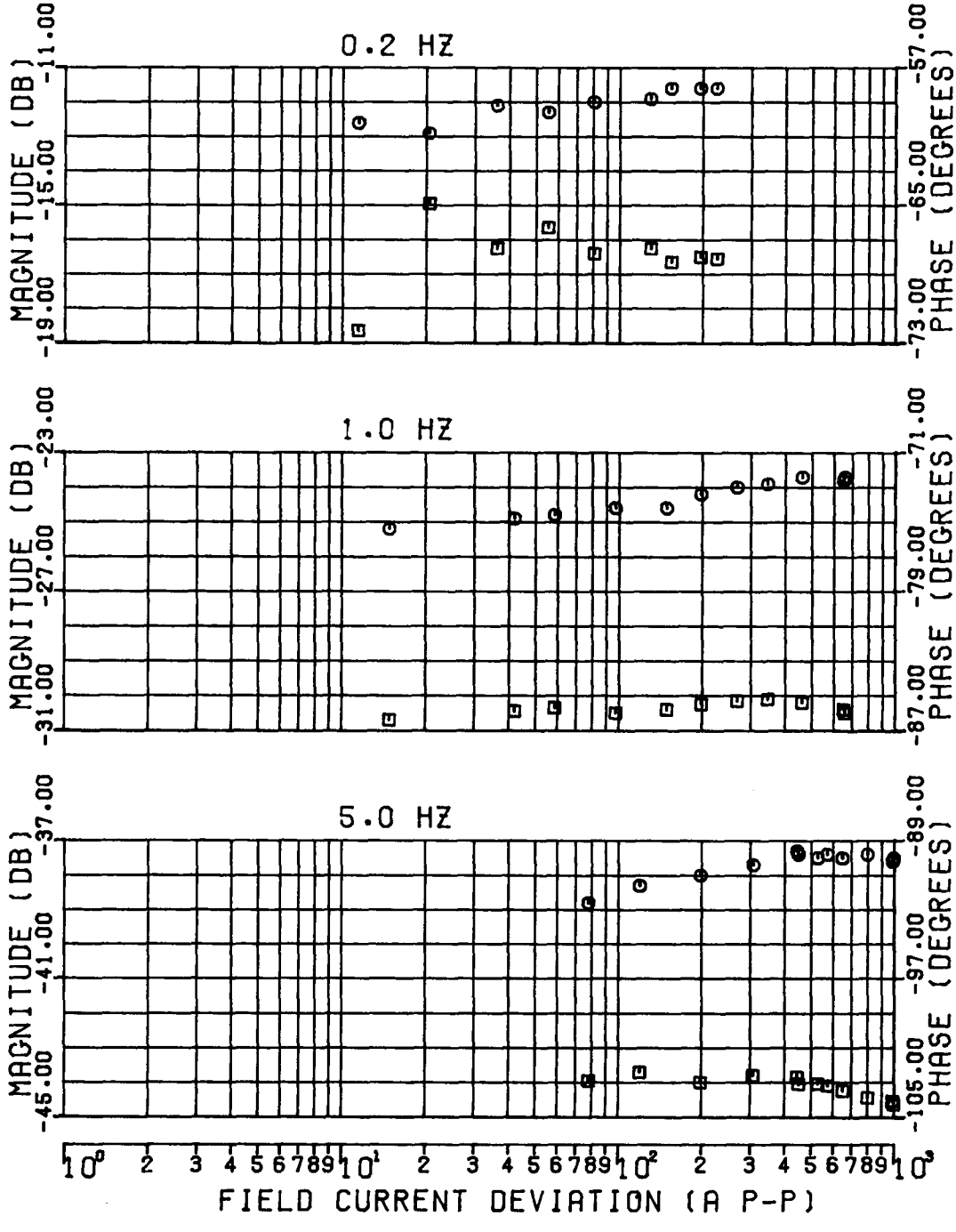

Figure 4-14. Nanticoke Open-Circuit Transfer Function From Field Current to Terminal Voltage as a Function of Field Current Deviation.

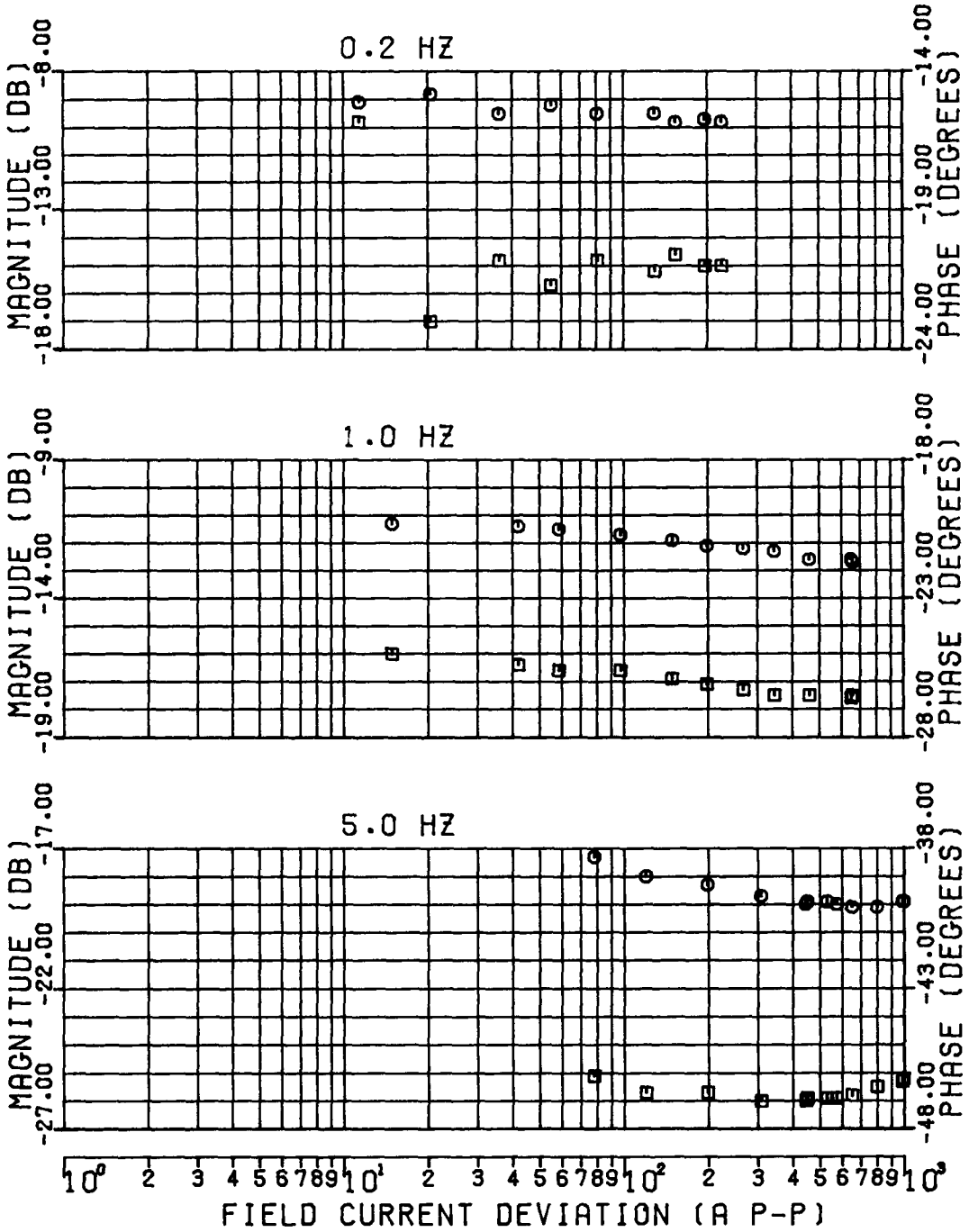

Figure 4-15. Nanticoke Open-Circuit Transfer Function From Field Voltage to Terminal Voltage as a Function of Field Current Deviation.

COMMENTS

Although the investigations are still at an early stage, there is considerable evidence from the 60 Hz field impedance measurements and the various open-circuit running tests that all of the inductors in the d- and q-axis equivalent circuits are non-linear devices whose values depend on both the operating point and the size of the disturbance. However, the importance of these effects; namely, the sensitivity of the performance of the generator model to them, needs to be studied before a recommendation can be made on whether or not they should be embodied in the synchronous machine model.

Part 3

IMPLEMENTATION OF RECOMMENDED MODELS IN THE EPRI TRANSIENT AND MIDTERM STABILITY PROGRAM

CONTENTS

ILLUSTRATIONS

TABLES

Section 1

DEFINITION OF SYNCHRONOUS MACHINE MODELS AND IMPLEMENTATION OF THE MODELS INTO THE TRANSIENT AND MIDTERM STABILITY PROGRAM

MODEL DEFINITION

The synchronous machine models considered for implementation are based on the well known concept of representing the machine in terms of the direct (d) and quadrature (q) axes equivalent circuits. The structure of the most complex synchronous machine model recommended is shown in Figure 1-1. It has a field winding and two amortisseur circuits in the d-axis, and three amortisseur circuits in the q-axis. The d-axis equivalent circuit accounts for unequal mutual inductances between stator and rotor circuits.

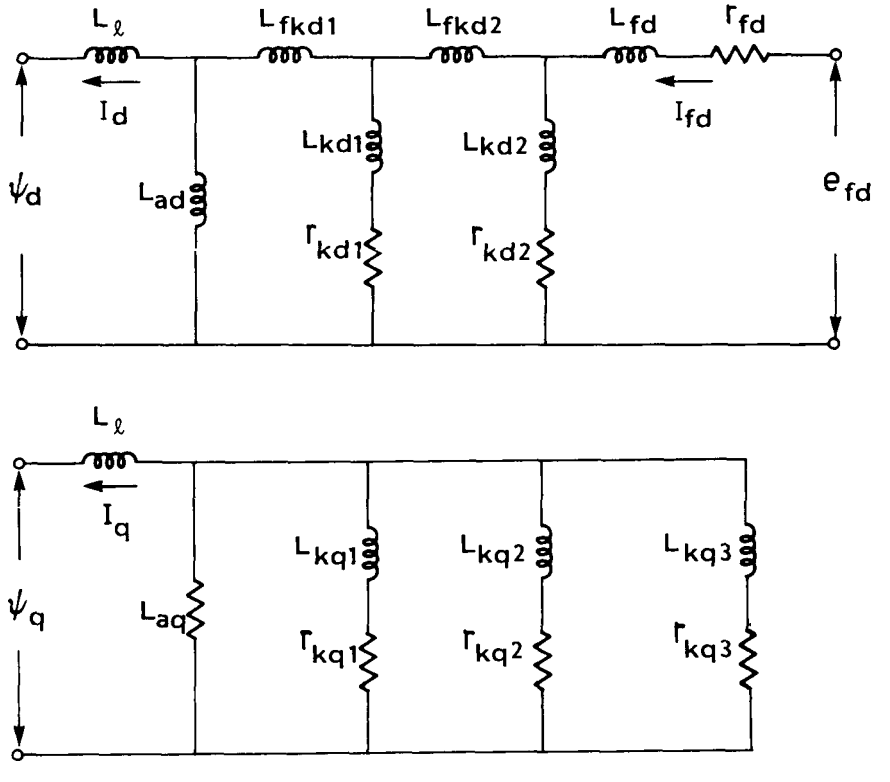

Figure 1-1. Structure of the Most Complex Model for Representing Synchronous Machines.

Designation of the different models of varying degrees of rotor representation are summarized in Table 1-1. The models are identified by two numbers with a period between them. The first number represents the number of rotor circuits in the d-axis including the field winding. The second number represents the number of q-axis rotor circuits.

Table 1-1

DEFINITION OF SYNCHRONOUS MACHINE MODEL STRUCTURES

	Q - Axis Order			
D-Axis Order	No Amortisseurs	One Amortisseur	Two Amortisseurs	Three Amortisseurs
Field Only	Model 1.0	Model 1.1	Model 1.2	Model 1.3
Field & One Amortisseur	Model 2.0	Model 2.1	Model 2.2	Model 2.3
Field & Two Amortisseurs	Model 3.0	Model 3.1	Model 3.2	Model 3.3
Constant Flux Linkages (Classical)	Model 0.0	-	-	-

IMPLEMENTATION OF THE SYNCHRONOUS MACHINE MODELS

A method of incorporating the most complex model is developed first and then the simplifications associated with the less complex models are discussed.

The EPRI transient and mid-term stability program has a Simultaneous-Implicit structure and uses the trapezoidal rule to integrate the differential equations. This is taken into consideration in developing the method of implementing the new models.

The existing synchronous machine model in the EPRI stability program accounts for one rotor winding in each axis (Model 1.1). A brief description of the manner in which this model has been implemented in the program is given in the EPRI report on

"Midterm Simulation of Electric Power Systems", EL-596, RP-745, June 1979. To facilitate incorporation of the new models, the general approach currently used in the program is followed and wherever possible the same symbols and notations used in the EPRI report are retained.

Equations of the Most Complex Model Proposed

The following equations, based on Park's transformation, describe the non-linear dynamic performance of a synchronous machine in a d-q reference frame. It is assumed that the q-axis leads the d-axis by 90°. This is consistent with the reference frame used for the existing model in the EPRI stability program. A per-unit system in which the mutual inductances are reciprocal is used (1). The nomenclature used is summarized in the Appendix. Unless otherwise specified, all the variables and parameters are in per unit.

D-Axis Flux Linkage - Current Relationship

The relationship between the d-axis flux linkages and currents, identified in Figure 1-1, is given by Equation 1-1:

$$\begin{bmatrix} \psi_d \\ \psi_{fd} \\ \psi_{kd1} \\ \psi_{kd2} \end{bmatrix} = \begin{bmatrix} (L_{ad} + L_1) & L_{ad} & L_{ad} & L_{ad} \\ L_{ad} & (L_{ad} + L_{fd} + L_{fkd1} + L_{fkd2}) & (L_{ad} + L_{fkd1}) & (L_{ad} + L_{fkd1} + L_{fkd2}) \\ L_{ad} & (L_{ad} + L_{fkd1}) & (L_{ad} + L_{kd1} + L_{fkd1}) & (L_{ad} + L_{fkd1}) \\ L_{ad} & (L_{ad} + L_{fkd1} + L_{fkd2}) & (L_{ad} + L_{fkd1}) & (L_{ad} + L_{kd2} + L_{fkd1} + L_{fkd2}) \end{bmatrix} \begin{bmatrix} -I_d \\ i_{fd} \\ i_{kd1} \\ i_{kd2} \end{bmatrix} \quad (1\text{-}1)$$

D-Axis Rotor Circuit Dynamic Equations

$$p(\psi_{fd}) = w_o(e_{fd} - r_{fd} i_{fd}) \quad (1\text{-}2)$$

$$p(\psi_{kd1}) = -w_o r_{kd1} i_{kd1} \quad (1\text{-}3)$$

$$p(\psi_{kd2}) = -w_o r_{kd2} i_{kd2} \quad (1\text{-}4)$$

In the above equations, p is the differential operator d/dt, with time t in seconds, and w_0 is the rated speed in electrical radians per second. The per unit field voltage e_{fd} is related to the per unit exciter output voltage (air-gap line excitation voltage) V_f by:

$$e_{fd} = \frac{r_{fd}}{L_{adu}} \cdot V_f \tag{1-5}$$

Where L_{adu} is the unsaturated value of L_{ad}.

Q-Axis Flux Linkage - Current Relationship

The relationship between the q-axis flux linkages and currents, identified in Figure 1-1, is given by:

$$\begin{bmatrix} \psi_q \\ \psi_{kq1} \\ \psi_{kq2} \\ \psi_{kq3} \end{bmatrix} = \begin{bmatrix} (L_{aq} + L_1) & L_{aq} & L_{aq} & L_{aq} \\ L_{aq} & (L_{aq} + L_{kq1}) & L_{aq} & L_{aq} \\ L_{aq} & L_{aq} & (L_{aq} + L_{kq2}) & L_{aq} \\ L_{aq} & L_{aq} & L_{aq} & (L_{aq} + L_{kq3}) \end{bmatrix} \begin{bmatrix} -I_q \\ i_{kq1} \\ i_{kq2} \\ i_{kq3} \end{bmatrix} \tag{1-6}$$

Q-Axis Rotor Dynamic Equations

$$p(\psi_{kq1}) = -w_o r_{kq1} i_{kq1} \tag{1-7}$$

$$p(\psi_{kq2}) = -w_o r_{kq2} i_{kq2} \tag{1-8}$$

$$p(\psi_{kq3}) = -w_o r_{kq3} i_{kq3} \tag{1-9}$$

Saturation

It is assumed that the effect of saturation is to vary only the mutual inductances L_{ad} and L_{aq}. Experience has shown that the saturation of the q-axis is appreciably more than that of the d-axis. It is recommended that different saturation characteristics be used for the two axes, with L_{ad} and L_{aq} varying as a function of the total air-gap flux linkage. It can be readily shown that the total air-gap flux linkage is equal to the voltage behind the stator resistance and the leakage inductance.

Stator Equations

$$p(\psi_d) = w_o(V_d + w/w_o\ \psi_q + R_a I_d)$$

$$p(\psi_q) = w_o(V_q - w/w_o\ \psi_d + R_a I_q)$$

For large scale stability studies, the stator transients represented by $p\psi_d$ and $p\psi_q$ terms are neglected (2). This is consistent with the representation used for the transmission system in which the electromagnetic transients are neglected. When $p\psi_d$ and $p\psi_q$ terms are neglected, it is also usual to assume $w=w_o$, in the stator equations. It can be shown that the two assumptions have counter balancing effects, so far as the low frequency rotor oscillations are concerned.

As a result of the above assumptions, the stator equations are given by the following algebraic equations:

$$V_d = -\psi_q - R_a I_d \tag{1-10}$$

$$V_q = \psi_d - R_a I_q \tag{1-11}$$

Axis Transformation

The reference axes (d,q) of each machine rotate with its rotor. For the purpose of solving the interconnecting network equations, synchronously rotating real and imaginary axes (R,I) are used. The following equations are used to transform variables from one reference frame to the other:

$$I_R = I_d \sin\delta + I_q \cos\delta$$

$$I_I = -I_d \cos\delta + I_q \sin\delta \tag{1-12}$$

$$V_d = V_R \sin\delta - V_I \cos\delta$$

$$V_q = V_R \cos\delta + V_I \sin\delta \tag{1-13}$$

In the above equations, δ represents the angle by which the q-axis leads the real axis of the common reference frame as shown in Figure 1-2. Since the q-axis rotates with the rotor, the angle δ is also used to identify rotor position with respect to the real axis.

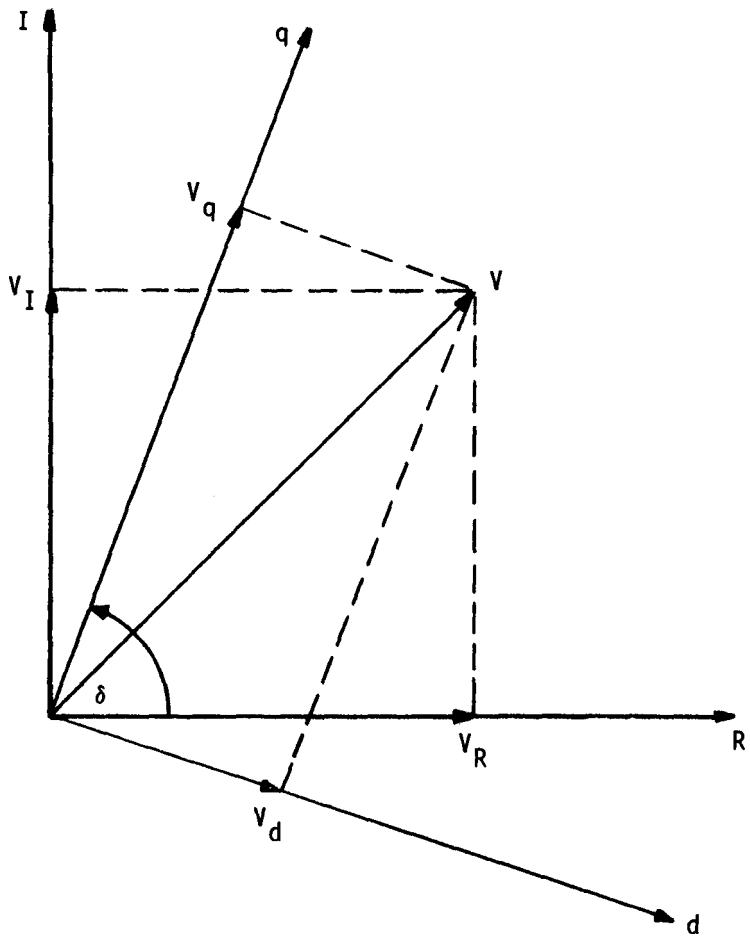

Figure 1-2. Relationship Between d, q axes and R, I axes.

Equations of Motion

$$p(\Delta w) = \frac{w_o}{2H}(T_i - T_g - K_D \Delta w) \qquad (1\text{-}14)$$

$$p(\delta) = \Delta w \qquad (1\text{-}15)$$

in which

T_i is the mechanical torque input
T_g is the air-gap torque
H is the inertia constant in MW s/MVA
K_D is the damping coefficient
δ is the angle of the q-axis in radians
Δw is the speed deviation equal to $(w-w_o)$ rads/sec.

The air-gap torque T_g is given by,

$$T_g = \psi_d I_q - \psi_q I_d$$

$$= (P_e + I_t^2 R_a) \frac{w_o}{w} \qquad (1\text{-}16)$$

The term $I_t^2 R_a$ represents the stator resistance loss and P_e is the terminal real power.

Elimination of Rotor Currents and Stator Flux Linkages

The state variables chosen to describe the dynamics of the synchronous machine are the rotor flux linkages, the rotor angle, and speed deviation. The values of the state variables are obtained by solving the corresponding differential equations as a function of the field voltage and the stator current components I_d and I_q. The field voltage is determined by the excitation system models and the stator current components are determined from the interconnecting network relations.

In order to solve the synchronous machine equations, it is necessary to express the stator flux linkages and rotor currents in terms of the rotor flux linkages and stator current components.

For the d-axis, Equation 1-1 can be rearranged in terms of the partial inverse of the d-axis inductance matrix as follows:

$$\begin{bmatrix} \psi_d \\ i_{fd} \\ i_{kd1} \\ i_{kd2} \end{bmatrix} = \begin{bmatrix} L_{dd} & C_{df} & C_{dk1} & C_{dk2} \\ -C_{df} & M_{ff} & M_{fk1} & M_{fk2} \\ -C_{dk1} & M_{fk1} & M_{k1k1} & M_{k1k2} \\ -C_{dk2} & M_{fk2} & M_{k1k2} & M_{k2k2} \end{bmatrix} \begin{bmatrix} -I_d \\ \psi_{fd} \\ \psi_{kd1} \\ \psi_{kd2} \end{bmatrix} \tag{1-17}$$

The above equation gives the d-axis stator flux and rotor currents in terms of the rotor flux linkages and stator current. It should be noted that the inductance matrix in Equation 1-1 is symmetrical and this is reflected in the mixed matrix of Equation 1-17.

For the q-axis, in view of the simpler structure of the equivalent circuit, the partial inverse of the inductance matrix of Equation 1-6 can be written directly in terms of the elements of the equivalent circuit:

$$\begin{bmatrix} \psi_q \\ i_{kq1} \\ i_{kq2} \\ i_{kq3} \end{bmatrix} = \begin{bmatrix} L_{qq} & \frac{L_{pq}}{L_{kq1}} & \frac{L_{pq}}{L_{kq2}} & \frac{L_{pq}}{L_{kq3}} \\ -\frac{L_{pq}}{L_{kq1}} & \frac{1}{L_{kq1}}\left(1-\frac{L_{pq}}{L_{kq1}}\right) & -\frac{L_{pq}}{L_{kq1}L_{kq2}} & -\frac{L_{pq}}{L_{kq1}L_{kq3}} \\ -\frac{L_{pq}}{L_{kq2}} & -\frac{L_{pq}}{L_{kq1}L_{kq2}} & \frac{1}{L_{kq2}}\left(1-\frac{L_{pq}}{L_{kq2}}\right) & -\frac{L_{pq}}{L_{kq2}L_{kq3}} \\ -\frac{L_{pq}}{L_{kq3}} & -\frac{L_{pq}}{L_{kq1}L_{kq3}} & -\frac{L_{pq}}{L_{kq2}L_{kq3}} & \frac{1}{L_{kq3}}\left(1-\frac{L_{pq}}{L_{kq3}}\right) \end{bmatrix} \begin{bmatrix} -I_q \\ \psi_{kq1} \\ \psi_{kq2} \\ \psi_{kq3} \end{bmatrix} \tag{1-18}$$

In the above equation L_{pq} represents the parallel combination of the mutual inductance and the leakage inductances of the three rotor circuits.

$$L_{pq} = \frac{1}{1/L_{aq} + 1/L_{kq1} + 1/L_{kq2} + 1/L_{kq3}} \tag{1-19}$$

and

$$L_{qq} = L_{pq} + L_l \tag{1-20}$$

INCORPORATION IN THE EPRI STABILITY PROGRAM

The rotor currents and the stator flux linkages are first eliminated from the synchronous machine equations. Then, the trapezoidal rule is applied to the resulting equations.

D-Axis Rotor Circuit Equations

Equations 1-2 to 1-5, representing the dynamics of the d-axis rotor circuits, can be combined and written in the following matrix form:

$$p(\underline{\psi}_{rd}) = -w_o \underline{R}_d \underline{I}_{rd} + \underline{b} V_f \tag{1-21}$$

where

$$\underline{\psi}_{rd} = \begin{bmatrix} \psi_{fd} \\ \psi_{kd1} \\ \psi_{kd2} \end{bmatrix} \qquad \underline{I}_{rd} = \begin{bmatrix} i_{fd} \\ i_{kd1} \\ i_{kd2} \end{bmatrix}$$

$$\underline{R}_d = \begin{bmatrix} r_{fd} & 0 & 0 \\ 0 & r_{kd1} & 0 \\ 0 & 0 & r_{kd2} \end{bmatrix} \qquad \underline{b} = \begin{bmatrix} w_o\left(\frac{r_{fd}}{L_{adu}}\right) \\ 0 \\ 0 \end{bmatrix}$$

Equation 1-17, giving the relationship between the d-axis flux linkages and currents may be written in the following form:

$$\begin{bmatrix} \psi_d \\ \underline{I}_{rd} \end{bmatrix} = \begin{bmatrix} L_{dd} & \underline{C}_{dr} \\ \underline{C}_{rd} & \underline{M}_d \end{bmatrix} \begin{bmatrix} -I_d \\ \underline{\psi}_{rd} \end{bmatrix} \tag{1-22}$$

Where $\underline{C}_{dr}$, $\underline{C}_{rd}$, and $\underline{M}_d$ are submatrices associated with the mixed matrix of Equation 1-17.

Substituting for $\underline{I}_{rd}$ from Equation 1-22 in Equation 1-21.

$$p(\underline{\psi}_{rd}) = -w_o \underline{R}_d (\underline{M}_d \underline{\psi}_{rd} - \underline{C}_{rd} I_d) + \underline{b} V_f$$

$$= \underline{A}_d \underline{\psi}_{rd} + \underline{B}_d \begin{bmatrix} I_d \\ V_f \end{bmatrix} \tag{1-23}$$

where

$$\underline{A}_d = -w_o \underline{R}_d \underline{M}_d$$

$$\underline{B}_d = [(w_o \underline{R}_d \underline{C}_{rd}), \underline{b}]$$

Q-Axis Rotor Circuit Equations

Similarly, writing Equations 1-7 to 1-9, representing the dynamics of the q-axis rotor circuits, in matrix form:

$$p(\underline{\psi}_{rq}) = -w_o \underline{R}_q \underline{I}_{rq} \tag{1-24}$$

with

$$\underline{\psi}_{rq} = \begin{bmatrix} \psi_{kq1} \\ \psi_{kq2} \\ \psi_{kq3} \end{bmatrix}, \qquad \underline{I}_{rq} = \begin{bmatrix} i_{kq1} \\ i_{kq2} \\ i_{kq3} \end{bmatrix}$$

$$\underline{R}_q = \begin{bmatrix} r_{kq1} & 0 & 0 \\ 0 & r_{kq2} & 0 \\ 0 & 0 & r_{kq3} \end{bmatrix}$$

Rewriting Equation 1-18 in a form similar to that of Equation 1-22,

$$\begin{bmatrix} \psi_q \\ \underline{I}_{rq} \end{bmatrix} = \begin{bmatrix} L_{qq} & \underline{C}_{qr} \\ \underline{C}_{rq} & \underline{M}_q \end{bmatrix} \begin{bmatrix} -I_q \\ \underline{\psi}_{rq} \end{bmatrix} \tag{1-25}$$

Substituting for $\underline{I}_{rq}$ from Equation 1-25 in Equation 1-24,

$$p(\underline{\psi}_{rq}) = \underline{A}_q \underline{\psi}_{rq} + \underline{B}_q I_q \tag{1-26}$$

where

$$\underline{A}_q = -w_o \underline{R}_q \underline{M}_q$$

$$\underline{B}_q = w_o \underline{R}_q \underline{C}_{rq}$$

Stator Equations

Substituting in the stator voltage equations 1-10 and 1-11, the expressions for ψ_d and ψ_q from Equation 1-22 and Equation 1-25,

$$V_d = -\psi_q - R_a I_d$$

$$= L_{qq} I_q - \underline{C}_{qr} \underline{\psi}_{rq} - R_a I_d \tag{1-27}$$

$$V_q = \psi_d - R_a I_q \tag{1-28}$$

$$= -L_{dd} I_d + \underline{C}_{dr} \underline{\psi}_{rd} - R_a I_q$$

The inductances L_{dd} and L_{qq} are the d-and q-axis sub-subtransient inductances.

Equations 1-23 and 1-26 represent the d-and q-axis rotor circuit dynamic equations in the desired form. The stator equations are given by 1-27 and 1-28.

Application of the Trapezoidal Rule

Following the procedure described in Section 4 of the EPRI report on RP-745 for applying the trapezoidal rule, Equations 1-23 and 1-26 can be replaced by the following difference equations,

$$\underline{\psi}_{rd}(t) = \underline{P}_d \underline{\psi}_{rd}(t_o) + \underline{Q}_d \begin{bmatrix} I_d(t_o) \\ V_f(t_o) \end{bmatrix} + [Q_{dI} Q_{dF}] \begin{bmatrix} I_d(t) \\ V_f(t) \end{bmatrix} \tag{1-29}$$

$$\underline{\psi}_{rq}(t) = \underline{P}_q \underline{\psi}_{rq}(t_o) + \underline{Q}_q I_q(t_o) + \underline{Q}_q I_q(t) \tag{1-30}$$

where

$$\underline{P}_d = [I - \underline{A}_d \tfrac{h}{2}]^{-1} [I + \underline{A}_d \tfrac{h}{2}]$$

$$\underline{Q}_d = [\underline{Q}_{dI} \; \underline{Q}_{dF}]$$

$$= [I - \underline{A}_d \tfrac{h}{2}]^{-1} \underline{B}_d \tfrac{h}{2}$$

$$\underline{P}_q = [I - \underline{A}_q \frac{h}{2}]^{-1} [I + \underline{A}_q \frac{h}{2}]$$

$$\underline{Q}_q = [I - \underline{A}_q \frac{h}{2}]^{-1} \underline{B}_q \frac{h}{2}$$

$$h = t - t_o = \text{time step}$$

Substituting for $\underline{\psi}_{rd}$ and $\underline{\psi}_{rq}$ given by Equations 1-29 and 1-30 in Equations 1-27 and 1-28 results in:

$$\begin{bmatrix} V_d \\ V_q \end{bmatrix} = \begin{bmatrix} -R_a & X_{qm} \\ -X_{dm} & -R_a \end{bmatrix} \cdot \begin{bmatrix} I_d \\ I_q \end{bmatrix} + \begin{bmatrix} o \\ g_1 \end{bmatrix} V_f + \begin{bmatrix} g_2 \\ g_3 \end{bmatrix} \qquad (1\text{-}31)$$

where

$$X_{dm} = L_{dd} - \underline{C}_{dr} \underline{Q}_{dI}$$

$$X_{qm} = L_{qq} - \underline{C}_{qr} \underline{Q}_q$$

$$g_1 = \underline{C}_{dr} \underline{Q}_{dF}$$

$$g_2 = - \underline{C}_{qr}[\underline{P}_q \underline{\psi}_{rq}(t_o) + \underline{Q}_q I_q(t_o)]$$

$$g_3 = \underline{C}_{dr}[\underline{P}_d \underline{\psi}_{rd}(t_o) + \underline{Q}_{dI} I_d(t_o) + \underline{Q}_{dF} V_f(t_o)]$$

and solving Equation 1-31 for I_d and I_q yields:

$$\begin{bmatrix} I_d \\ I_q \end{bmatrix} = \begin{bmatrix} C_{od} \\ C_{oq} \end{bmatrix} + \begin{bmatrix} C_{V1} & C_{V2} \\ C_{V3} & C_{V4} \end{bmatrix} \begin{bmatrix} V_d \\ V_q \end{bmatrix} + \begin{bmatrix} C_{F1} \\ C_{F2} \end{bmatrix} V_f \qquad (1\text{-}32)$$

where:

$$C_{od} = (X_{qm} g_3 + R_a g_2)/Det$$

$$C_{oq} = (R_a g_3 - X_{dm} g_2)/Det$$

$$C_{V1} = C_{V4} = -R_a/Det$$

$$C_{V2} = -X_{qm}/Det$$

$$C_{V3} = X_{dm}/Det$$

$$C_{F1} = X_{qm}g_1/Det$$

$$C_{F2} = R_a g_1/Det$$

$$Det = R_a^2 + X_{dm} X_{qm}$$

Using the axes transformation Equations 1-12 and 1-13 to express Equation 1-32 in terms of real and imaginary components of stator voltage and current,

$$\begin{bmatrix} b \\ a \end{bmatrix} = \begin{bmatrix} GC2 \\ GC1 \end{bmatrix} + \begin{bmatrix} GC4 & GC6 \\ GC3 & -GC5 \end{bmatrix} \begin{bmatrix} e \\ f \end{bmatrix} + \begin{bmatrix} GC8 \\ GC7 \end{bmatrix} V_f \qquad (1\text{-}33)$$

where

b = imaginary component of stator current
a = real component of stator current
e = real component of stator voltage
f = imaginary component of stator voltage

$$GC1 = [Sin\delta(R_a g_2 + X_{qm} g_3) + Cos\delta(R_a g_3 - X_{dm} g_2)]/Det$$

$$GC2 = [Sin\delta(R_a g_3 - X_{dm} g_2) - Cos\delta(R_a g_2 + X_{qm} g_3)]/Det$$

$$GC3 = (X_{dm} Sin\delta Cos\delta - X_{qm} Sin\delta Cos\delta - R_a)/Det$$

$$GC4 = (X_{dm} Sin^2\delta + X_{qm} Cos^2\delta)/Det$$

$$GC5 = (X_{dm} Cos^2\delta + X_{qm} Sin^2\delta)/Det$$

$$GC6 = (X_{qm} Sin\delta Cos\delta - X_{dm} Sin\delta Cos\delta - R_a)/Det$$

$$GC7 = (sin\delta X_{qm} g_1 + cos\delta R_a g_1)/Det$$

$$GC8 = (sin\delta R_a g_1 - cos\delta X_{qm} g_1)/Det$$

The equations of motion 1-14 to 1-16 are not affected by the complexity of the d- and q-axis equivalent circuits. With the possible exception of the w/w_0 term in the expression for the air-gap torque, these equations should be equivalent to the equations of motion currently used in the EPRI stability program.

Summarizing: Equations 1-29 and 1-30 give the solution of the rotor flux linkages and correspond to Equations 4-21 and 4-22 of the EPRI report on RP-745. Equation 1-33 gives the relationship between stator current and voltage components in a form suitable for inclusion in the network solution. It corresponds to Equation 4-24 of the EPRI report.

Initial Values of the State Variables

For the purpose of finding the initial values of the state variables, it is first necessary to compute the saturated values of L_{ad} and L_{aq} as a function of the air-gap flux linkage (voltage behind stator resistance and leakage inductance). Then the rotor angle δ, and the d- and q-axis components of the stator current and voltage are determined as for the existing model in the EPRI stability program.

The steady-state value of the field current is given by,

$$i_{fd} = (V_q + I_q R_a + I_d L_l + I_d L_{ad})/L_{ad}$$

Under steady-state, all other rotor currents are zero and the rotor flux linkages are given by,

$$\psi_{fd} = -L_{ad} I_d + (L_{ad} + L_{fd} + L_{fkd1} + L_{fkd2}) i_{fd}$$

$$\psi_{kd1} = -L_{ad} I_d + (L_{ad} + L_{fkd1}) i_{fd}$$

$$\psi_{kd2} = \psi_{kd1} + L_{fkd2} i_{fd}$$

$$\psi_{kq1} = \psi_{kq2} = \psi_{kq3} = -L_{aq} I_q$$

Per-Unit Value of the Field Current

It should be noted that in the "reciprocal" per-unit system used for the synchronous machine equations, the field current required to produce one per unit generator terminal voltage on the air-gap line is equal to $1/L_{adu}$ per unit. It is often convenient to use the "non-reciprocal" per-unit system for the field current (3). In this sytem, one per unit field current is that current required to

produce rated generator terminal voltage on the air-gap line. The relationship between the per unit values of field current in the two systems is given by,

$$I_{fd} = L_{adu} i_{fd}$$

where

I_{fd} = field current in the non-reciprocal per unit system.

i_{fd} = field current in the reciprocal per unit system.

L_{adu} = unsaturated value of L_{ad}

Implementation of Simpler Models

The method developed above is quite general and is applicable to any of the generator models. For simpler models the order of the different vectors and matrices have to be reduced appropriately. To illustrate how the simpler models can be treated, two cases, one with 2 rotor circuits in the d-axis and the other with one rotor circuit in the q-axis, are considered here.

Model With Two D-Axis Rotor Circuits

For this model, ψ_{kd2}, i_{kd2} and the related elements do not exist. In the inductance matrix of Equation 1-1, the last row and column disappears and L_{fkd2} is zero. The following are various vectors and matrices associated with the d-axis equations:

$$\underline{\psi}_{rd} = \begin{bmatrix} \psi_{fd} \\ \psi_{kd1} \end{bmatrix} \qquad \underline{R}_d = \begin{bmatrix} r_{fd} & 0 \\ 0 & r_{kd1} \end{bmatrix}$$

$$\underline{b} = \begin{bmatrix} (w_o r_{fd}/L_{adu}) \\ o \end{bmatrix} \qquad \underline{M}_d = \begin{bmatrix} M_{ff} & M_{fk1} \\ M_{fk1} & M_{k1k1} \end{bmatrix}$$

$$\underline{C}_{dr} = [C_{df} \; C_{dk1}] \qquad \underline{C}_{rd} = -\underline{C}_{dr}^t$$

The size of the matrices A_d, B_d, P_d and Q_d is now reduced to 2x2.
If it is found to be computationally advantageous, the elements of these matrices can be expressed directly in terms of the parameters of the equivalent circuits.

Model With One Q-Axis Rotor Circuit

In this case the elements related to ψ_{kq2} and ψ_{kq3} disappear resulting in the following simplifications:

$$\underline{\psi}_{rq} = \psi_{kq1}, \quad \underline{R}_q = r_{kq1},$$

$$L_{pq} = L_{aq} L_{kq1}/(L_{aq} + L_{kq1}), \quad L_{qq} = L_{pq} + L_l$$

$$\underline{M}_q = 1/(L_{aq} + L_{kq1}), \quad \underline{C}_{qr} = -\underline{C}_{rq} = L_{aq}/(L_{aq} + L_{kq1})$$

The matrices A_q, B_q, P_q, Q_q have one element each and are given by

$$\underline{A}_q = -w_o\, r_{kq1}/(L_{aq} + L_{kq1})$$

$$\underline{B}_q = -w_o\, r_{kq1}\, L_{aq}/(L_{aq} + L_{kq1})$$

$$\underline{P}_q = \frac{2(L_{aq} + L_{kq1}) - w_o\, r_{kq1}\, h}{2(L_{aq} + L_{kq1}) + w_o\, r_{kq1}\, h}$$

$$\underline{Q}_q = \frac{-w_o\, r_{kq1}\, L_{aq}\, h}{2(L_{aq} + L_{kq1}) + w_o\, r_{kq1}\, h}$$

INPUT DATA FOR MACHINE CONSTANTS

In general the input data required to evaluate the equivalent circuit parameters of a synchronous machine is in the form of transient and subtransient inductances and time constants. These are normally available as data from manufacturers design calculations or actual test measurements. The relationship between such data and the more fundamental parameters of the equivalent circuits in Figure 1-1 are shown below for the most complex model considered; viz, Model 3.3.

D-Axis Relationships

$$L_d' = L_{ad} + L_l - L_{ad}^2 \left(\frac{1}{r_{fd}} + \frac{1}{r_{kd1}} + \frac{1}{r_{kd2}} \right) \left(\frac{1}{T_{ffd} + T_{kd1} + T_{kd2}} \right) \frac{1}{w_o}$$

$$L_d'' = L_{ad} + L_l - L_{ad}^2\; L_{dfk}''\; L_{dfk}'^{-1}$$

$$L_d''' = L_{ad} + L_l - L_{ad}^2 \left(L'_{fkd2} + L''_{fkd2} \left(L_{kd1} - L_{ad} - L_{fkd1}\right)\right) L_{dfk}'''^{-1} \qquad (1\text{-}34)$$

$$T'_{do} + T''_{do} + T'''_{do} = T_{ffd} + T_{kd1} + T_{kd2} \cong T'_{do}$$

$$T''_{do} + T'''_{do} + T''_{do}\, T'''_{do}\, T'^{-1}_{do} = L'_{dfk}\, T'^{-1}_{do} \cong T''_{do}$$

$$T'''_{do} = L'''_{dfk} \left(r_{kd1}\, r_{kd2}\, r_{fd}\, L'_{dfk}\right)^{-1}$$

where

$$T_{ffd} = \frac{L_{fd} + L_{ad} + L_{fkd1} + L_{fkd2}}{w_o\, r_{fd}} = \frac{L_{ffd}}{w_o r_{fd}}$$

$$T_{kd1} = \frac{L_{kd1} + L_{ad} + L_{fkd1}}{w_o\, r_{kd1}} = \frac{L_{dd1}}{w_o r_{kd1}}$$

$$T_{kd2} = \frac{L_{kd2} + L_{ad} + L_{fkd1} + L_{fkd2}}{w_o\, r_{kd2}} = \frac{L_{dd2}}{w_o r_{kd2}}$$

$$L'_{fkd1} = L_{ffd}\, L_{dd1} - \left(L_{ad} + L_{fkd1}\right)^2$$

$$L'_{fkd2} = L_{ffd}\, L_{dd2} - \left(L_{ad} + L_{fkd1} + L_{fkd2}\right)^2$$

$$L'_{dkd} = L_{dd1}\, L_{dd2} - \left(L_{ad} + L_{fkd1}\right)^2$$

$$L''_{fkd1} = L_{ffd} + L_{dd1} - 2\left(L_{ad} + L_{fkd1}\right)$$

$$L''_{fkd2} = L_{ffd} + L_{dd2} - 2\left(L_{ad} + L_{fkd1} + L_{fkd2}\right)$$

$$L''_{dkd} = L_{dd1} + L_{dd2} - 2\left(L_{ad} + L_{fkd1}\right)$$

$$L'_{dfk} = \left(\frac{L'_{dkd}}{r_{kd1}\, r_{kd1}} + \frac{L'_{fkd1}}{r_{kd1}\, r_{fd}} + \frac{L'_{fkd2}}{r_{kd2}\, r_{fd}}\right) \frac{1}{w_o^2}$$

$$L''_{dfk} = \left(\frac{L''_{dkd}}{r_{kd1} r_{kd2}} + \frac{L''_{fkd1}}{r_{kd1} r_{fd}} + \frac{L''_{fkd2}}{r_{kd2} r_{fd}} \right) \frac{1}{w_o^2}$$

$$L'''_{dfk} = L_{dd1} L'_{fkd2} - L''_{fkd2} (L_{ad} + L_{fkd1})^2$$

Q-Axis Relationships

$$L'_q = L_{aq} + L_l - L_{aq}^2 \left(\frac{1}{r_{kq1}} + \frac{1}{r_{kq2}} + \frac{1}{r_{kq3}} \right) \left(\frac{1}{T_{kq1} + T_{kq2} + T_{kq3}} \right) \frac{1}{w_o}$$

$$L''_q = L_{aq} + L_l - L_{aq}^2 L''_{qq} L'^{-1}_{qq} \qquad (1\text{-}35)$$

$$L'''_q = L_{aq} + L_l - L_{aq}^2 (L'_{q2q3} + L'''_{q2q3} (L_{kq1} - L_{aq})) L'''^{-1}_{qq}$$

$$T'_{qo} + T''_{qo} + T'''_{qo} = T_{kq1} + T_{kq2} + T_{kq3} \cong T'_{qo}$$

$$T''_{qo} + T'''_{qo} + T''_{qo} T'''_{qo} T'^{-1}_{qo} = L'_{qq} T'^{-1}_{qo} \cong T''_{qo}$$

$$T'''_{qo} = L'''_{qq} (r_{kq1} r_{kq2} r_{kq3} L'_{qq})^{-1}$$

where

$$T_{kq1} = \frac{L_{kq1} + L_{aq}}{w_o r_{kq1}} = \frac{L_{qq1}}{w_o r_{kq1}}$$

$$T_{kq2} = \frac{L_{kq2} + L_{aq}}{w_o r_{kq2}} = \frac{L_{qq2}}{w_o r_{kq2}}$$

$$T_{kq3} = \frac{L_{kq3} + L_{aq}}{w_o r_{kq3}} = \frac{L_{qq3}}{w_o r_{kq3}}$$

$$L'_{q1q2} = L_{qq1} L_{qq2} - L_{aq}^2$$

$$L'_{q2q3} = L_{qq2} L_{qq3} - L_{aq}^2$$

$$L'_{q3q1} = L_{qq3}\, L_{qq1} - L_{aq}^2$$

$$L''_{q1q2} = L_{qq1} + L_{qq2} - 2\, L_{aq}$$

$$L''_{q2q3} = L_{qq2} + L_{qq3} - 2\, L_{aq}$$

$$L''_{q3q1} = L_{qq3} + L_{qq1} - 2\, L_{aq}$$

$$L'_{qq} = \left(\frac{L'_{q1q2}}{r_{kq1} r_{kq2}} + \frac{L'_{q2q3}}{r_{kq2}\, r_{kq3}} + \frac{L'_{q3q1}}{r_{kq3}\, r_{kq1}} \right) \frac{1}{w_o^2}$$

$$L''_{qq} = \left(\frac{L''_{q1q2}}{r_{kq1}\, r_{kq2}} + \frac{L''_{q2q3}}{r_{kq2}\, r_{kq3}} + \frac{L''_{q3q1}}{r_{kq3}\, r_{kq1}} \right) \frac{1}{w_o^2}$$

$$L'''_{qq} = L_{qq1}\, L'_{q2q3} - L_{aq}^2\, L''_{q2q3}$$

Corresponding relationships for equivalent circuits with less complex rotor representations can be obtained directly from Equations 1-34 and 1-35 by making the correct assumptions about the state of the relevant rotor windings. Thus for the simpler Model 2.2, the above equations can be reduced to yield L_d, L''_d, T'_{do}, T''_{do}, L_q, L'_q, T''_{qo} and T'_{qo}, by removing the elements L_{kd2}, r_{kd2}, L_{kq3}, r_{kq3} and setting L_{fkd2} to zero.

As can be seen, the relationships in Equations 1-34 and 1-35 are not the same as the classical relationships defined by Concordia (4) and Adkins (5), and which are widely used by industry in their digital computer models. The assumptions which are at the basis of these classical relationships are discussed elsewhere (6) and are outside the scope of the present report. However, they do significantly simplify the relationships in Equation 1-34 and 1-35, although these are likely to lead to some loss of accuracy when used with actual test data (7), but because of their extensive usage they are reproduced herein. The assumptions necessary for reducing Equations 1-34 and 1-35 into their more common forms are; in the sub-sub-transient period $r_{kd1} = r_{fd} = r_{kq1} = r_{kq2} = 0$, in the sub-transient period $r_{fd} = r_{kq1} = 0$ and $r_{kd2} = r_{kq3} = \infty$, and in the transient period $r_{kd1} = r_{kd2} = r_{kq2} = r_{kq3} = \infty$. Thus the new relationships are as follows:

D-Axis Relationships

$$L_d = L_{ad} + L_l$$

$$L_d' = L_{ad} + L_l - \frac{L_{ad}^2}{L_{ffd}}$$

$$L_d'' = L_{ad} + L_l - \frac{L_{ad}^2 L_{fkd1}''}{L_{fkd1}'}$$

$$L_d''' = \text{Same as in Equation 1-34} \qquad (1\text{-}36)$$

$$T_{do}' = T_{ffd}$$

$$T_{do}'' = \frac{L_{fkd1}'}{r_{kd1} L_{ffd}} \frac{1}{w_o}$$

$$T_{do}''' = \frac{L_{dfk}'''}{r_{kd2} L_{fkd1}'} \frac{1}{w_o}$$

Q-Axis Relationship

$$L_q = L_{aq} + L_l$$

$$L_q' = L_{aq} + L_l - \frac{L_{aq}^2}{L_{qq1}}$$

$$L_q'' = L_{aq} + L_l - \frac{L_{aq}^2 L_{q1q2}''}{L_{q1q2}'}$$

$$L_q''' = \text{same as in Equation 1-35} \qquad (1\text{-}37)$$

$$T_{qo}' = T_{kq1}$$

$$T_{qo}'' = \frac{L_{q1q2}'}{r_{kq2} L_{qq1}} \frac{1}{w_o}$$

$$T'''_{qo} = \frac{L'_{qq}}{r_{kq3} L'_{q1q2}} \frac{1}{w_o}$$

Attention is drawn to the different definitions of T'_{do} in Equations 1-34 and 1-36 respectively, as a result of the simplifications in classical theory. It is our experience that most turbogenerator manufacturers tend to quote values for this parameter based on the classical definition (Equation 1-36), but this is by no means a standard. The same is true of the remaining parameters in the d- and q-axes, and care should be taken to ascertain the basis of assumption before processing the data to obtain the models.

The relationships in Equations 1-34 and 1-35 are quite cumbersome, particularly since the d-axis equivalent circuit accounts for unequal mutual effects between the different rotor circuits and rotor and stator circuits, ie, L_{fkd1} and L_{fkd2} do not equal zero. Consequently no attempt is made here to show the inverse transformations, that is expressions showing the fundamental circuit parameters in terms of the measured parameters L_d, L'_d, L''_d, T'_{do} etc. It is our opinion that in most cases where such complex models need to be considered, the data will be available in the form of equivalent circuit parameters, either as a result of manufacturers design calculations or from special measurements. With respect to the latter, one method of calculating such parameters is detailed in this report and is based on measurements made at the generator terminals with the rotor at standstill (Part 1). Other methods may also be formulated. Thus it is recommended that in the instance of Model 3.3 and Model 2.2, in which unequal mutual effects are accounted for, the data be entered in the form of inductances and resistances. In all other cases (without unequal mutual effects) the standard approach of using the transient, sub-transient and sub-sub-transient (when required) inductances and time constants should be retained. Thus for Model 3.3 with L_{fkd1} and L_{fkd2} equal to zero, the inverse relationships are as follows:

D-Axis

$$L_{fd} = \frac{L_{ad}(L'_d - L_1)}{(L_d - L'_d)}$$

$$L_{kd1} = \frac{(L'_d - L_1)(L''_d - L_1)}{(L'_d - L''_d)}$$

$$L_{kd2} = \frac{(L_d'' - L_l)\ (L_d''' - L_l)}{(L_d'' - L_d''')} \qquad (1\text{-}38)$$

$$r_{fd} = \frac{L_{ad} + L_{fd}}{w_o\ T_{do}'}$$

$$r_{kd1} = \frac{L_{kd1} + L_d' - L_l}{w_o\ T_{do}''}$$

$$r_{kd2} = \frac{L_{kd2} + L_d'' - L_l}{w_o\ T_{do}'''}$$

Q-Axis

$$L_{kq1} = \frac{L_{aq}\ (L_q' - L_l)}{(L_q' - L_q'')}$$

$$L_{kq2} = \frac{(L_q' - L_l)\ (L_q'' - L_l)}{(L_q'' - L_q''')} \qquad (1\text{-}39)$$

$$L_{kq3} = \frac{(L_q'' - L_l)\ (L_q''' - L_l)}{(L_q''' - L_q'''')}$$

$$r_{kq1} = \frac{L_{aq} + L_{kq1}}{w_o\ T_{qo}'}$$

$$r_{kq2} = \frac{L_{kq2} + L_q' - L_l}{w_o\ T_{qo}''}$$

$$r_{kq3} = \frac{L_{kq3} + L_q'' - L_l}{w_o\ T_{qo}'''}$$

Equations 1-38 and 1-39 are the inverse transformations of Equations 1-36 and 1-37. They can be readily adapted for models of less complex structure. For example in the case of Model 2.2, the sub sub-transient parameters need not be considered and hence L_{kd2}, L_{kq3}, r_{kd2} and r_{kq3} would be eliminated.

REFERENCES

1. A.W. Rankin. Per-Unit Impedances of Synchronous Machines. AIEE trans., Vol. 64, Part I, pp. 569-573, Aug. 1945; Part II, pp. 839-841, Dec. 1945.

2. P.L. Dandeno, P. Kundur, R.P. Shultz. Recent Trends and Progress in Synchronous Machine Modelling in the Electric Utility Industry. Proceedings of the IEEE, Vo. 62, No. 7, July 1974.

3. Excitation System Models for Power System Stability Studies. IEEE Committee report, paper no. F80 250-4, presented at the PES Winter Meeting, New York, N.Y., Feb. 3-8, 1980.

4. C. Concordia. Synchronous Machines. Wiley, 1951.

5. B. Adkins. The General Theory of Electrical Machines. Chapman and Hall, 1957.

6. Supplementary Definitions and Associated Test Methods for Obtaining Parameters for Synchronous Machine Stability Study Simulations. Joint Working Group Paper F79647-9 (P.L. Dandeno, Chairman) presented at the PES Summer Meeting, Vancouver, B.C., July, 1979.

7. G. Shackshaft. New Approach to Determination of Synchronous Machine Parameters From Tests. Proceedings IEE, Vol. 121, Nov. 1974, pp. 1385-1392.

Section 2

PROGRAM TESTS

METHOD

The Ontario Hydro time domain program was used for simulating the performance of the different synchronous machine models. These results will provide a check on the results of the EPRI mid term stability program into which it is proposed to implement these advanced models. For this purpose two test systems were used: the WSCC 9-bus system and the New England 39-bus system. The former system was used in the EPRI mid term stability program studies, whilst the latter was used in the NPCC Working Group #10 study. In both cases the results were checked using the Ontario Hydro stability program to establish that they were compatible with the original studies, prior to implementation of the advanced machine models. The following describe in more detail the studies carried out.

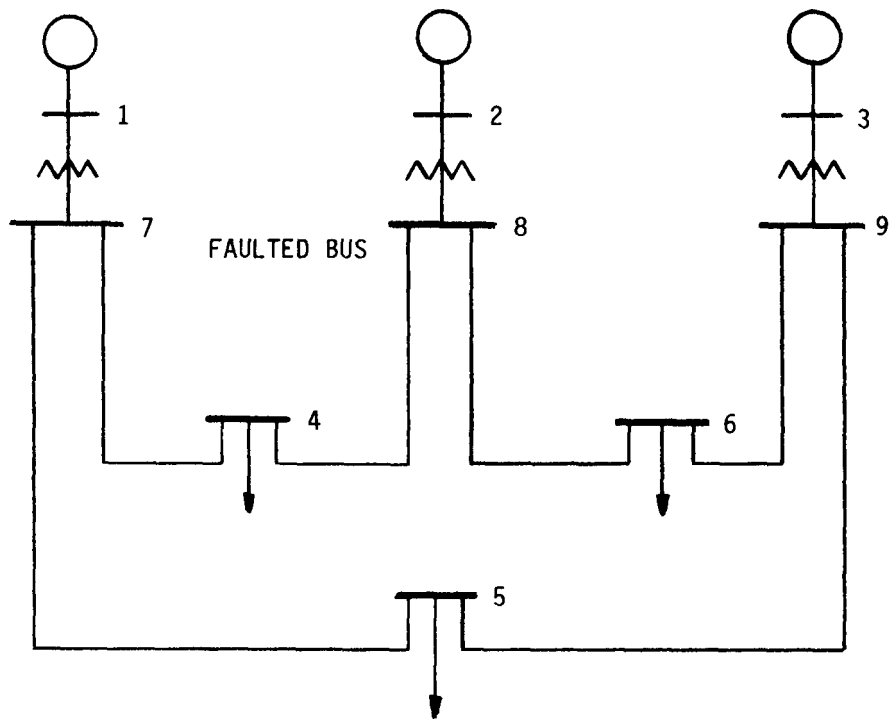

Figure 2-1. WSCC System Line Diagram.

WSCC 9-BUS SYSTEM STUDIES

The system simulated here is made up of 9-buses, 6 lines and three generators (with associated generator transformers) and is shown in Figure 2-1. The generator connected to bus #2 was used as the test unit, and consequently was represented by the various synchronous machine models with constant field voltage. The remaining generators were treated as classical machines; ie, constant voltage behind transient inductance. The disturbance to the network was created by applying a 3-phase-ground fault on the line from bus #8 to bus #4, close to bus #8; the fault was cleared in 0.083 seconds by removing this line. Figures 2-2 to 2-5 show the variation in rotor angle of unit #2 following the fault clearance, using the different models. It should be noted that this angle is relative to unit #1. The solid lines indicate the simulated results in which saturation was not represented.

In Figure 2-4, results are shown for two additional cases where saturation was accounted for by (a) using the open-circuit saturation curve to modify the d- and q-axis synchronous mutual inductances L_{ad} and L_{aq}, and (b) using separate saturation characteristics in the d- and q-axes to modify these inductances. Table 2-1 summarizes the input data for the different synchronous machine models, and Figure 6-3 in Part I of this report shows the saturation characteristics used in the above simulations. All parameters are shown in per unit on 100 MVA base.

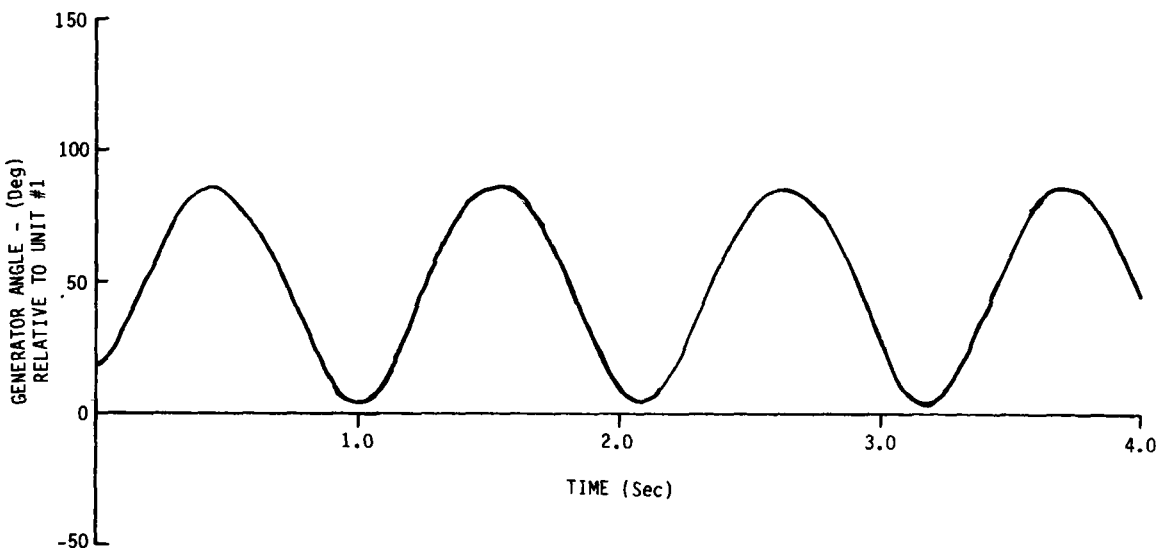

Figure 2-2. Variation in Rotor Angle of Unit #2 WSCC System Classical Model (Model 0.0).

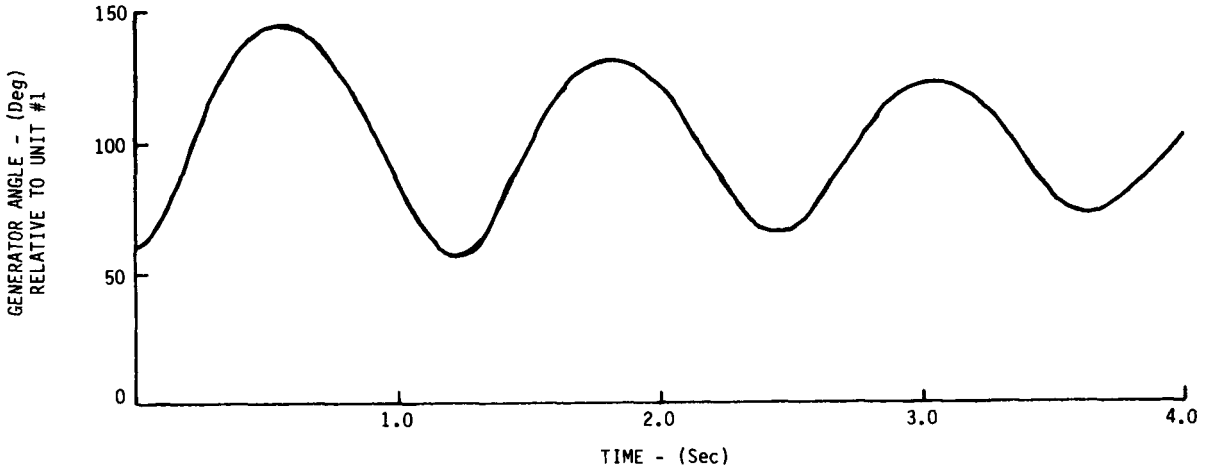

Figure 2-3. Variation in Rotor Angle of Unit #2 WSCC System Standard Model (Model 1.1).

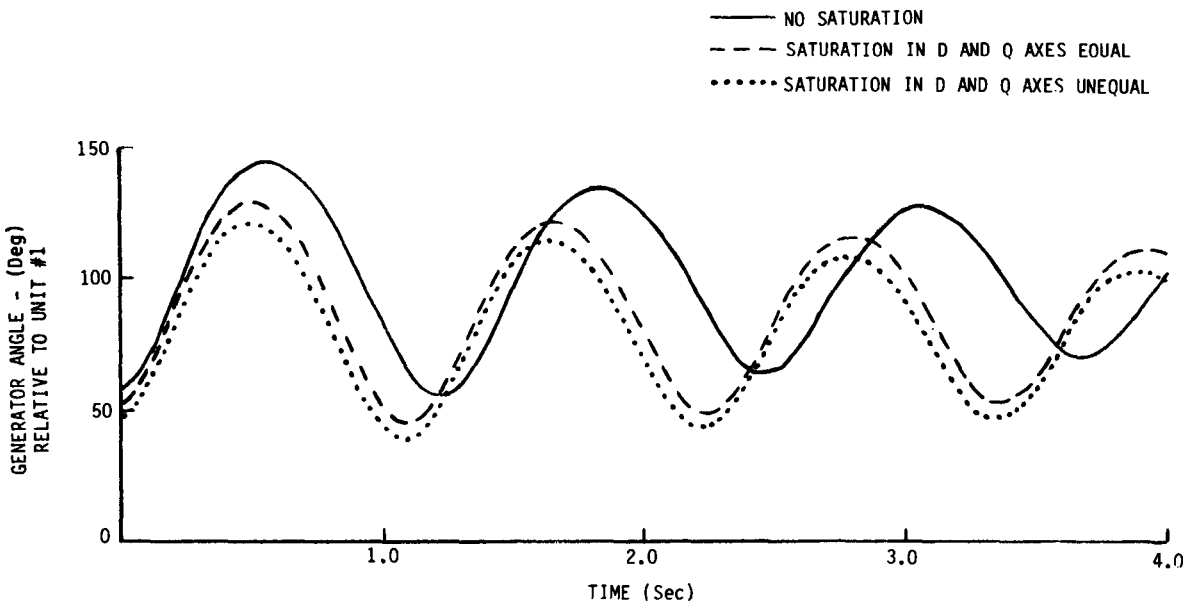

Figure 2-4. Variation in Rotor Angle of Unit #2 WSCC System Improved Model (Model 2.2).

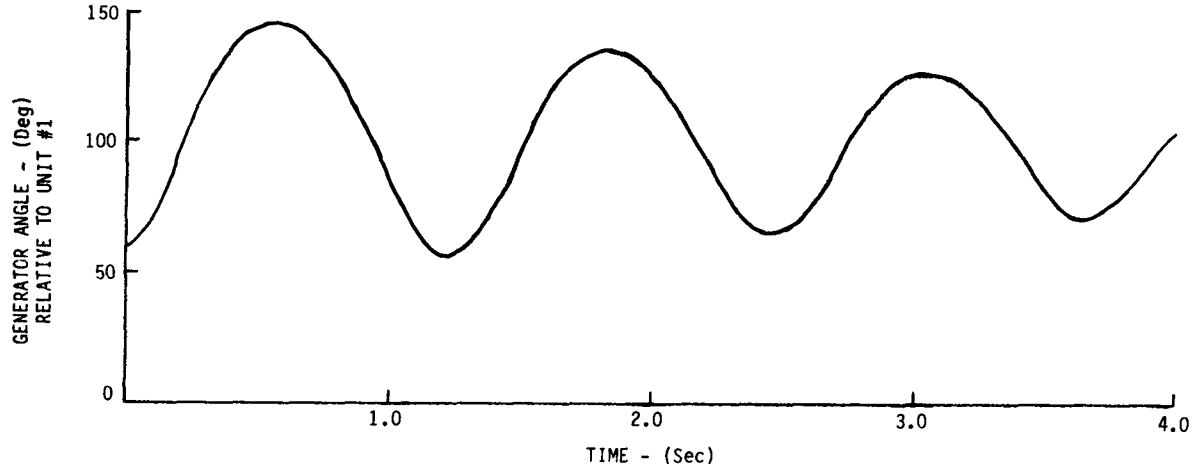

Figure 2-5. Variation in Rotor Angle of Unit #2 WSCC System Improved Model (Model 3.3).

The results in Figures 2-2 to 2-5 show that the classical model 0.0 gives rise to undamped rotor oscillations compared to the other models, ie, 1.1, 2.2 and 3.3, which show some damping. This damping is, of course, attributed to the presence of rotor windings in the latter models.

The initial starting angle predicted by the classical model is lower compared to the other models because of the lower steady-state inductance in this model, ie, transient inductance as compared to synchronous inductance in models 1.1, 2.2 and 3.3 (see Table 2-1). The effect of saturation (Figure 2-4) is obvious in that the initial steady-state angle is lower when saturation effects are included; a slight reduction in rotor angle is also obtained when different saturation characteristics are used in the d- and q- axes as compared to using the same characteristic in both axes.

For this particular machine (Unit #2) there are insignificant differences between the standard, 1.1, and detailed, 2.2 and 3.3, models. This is because data for the advanced models was derived on the premise that the transient parameters, L'_d, T'_{do}, L'_q and T'_{qo}, in these models should be the same as in the standard model, in the absence of any test or manufacturers design information.

These parameters mostly influence the transient behaviour of the machine in the post-fault recovery period and hence one would expect the models to behave similarly. However, based on our experience, this is an exception rather than the rule and in most cases we would expect significant differences to be observed between the performance of the standard and more detailed models.

Table 2-1

INPUT DATA FOR GENERATOR MODELS USED IN WSCC STUDY

	Unit #2				Unit #1	Unit #3
Parameter	Model 3.3	Model 2.2	Model 1.1	Model 0.0	Model 0.0	Model 0.0
L_d	0.8773	0.8773	0.8958	-	-	-
L_q	0.8500	0.8500	0.8645	-	-	-
L_l	0.0705	0.0705	-	-	-	-
L_{fkd1}	0.4759	0.0604	-	-	-	-
L_{kd1}	9.2955	0.0052	-	-	-	-
R_{kd1}	0.0553	0.00417	-	-	-	-
L_{kq1}	0.9550	0.2580	-	-	-	-
R_{kq1}	0.00482	0.00668	-	-	-	-
L_{kq2}	0.2047	0.0780	-	-	-	-
R_{kq2}	0.01368	0.08023	-	-	-	-
L_{fkd2}	-0.3994	-	-	-	-	-
L_{kd2}	0.0045	-	-	-	-	-
R_{kd2}	0.00400	-	-	-	-	-
L_{kq3}	0.0514	-	-	-	-	-
R_{kq3}	0.1186	-	-	-	-	-
L_{fd}	0.0045	0.0048	-	-	-	-
R_{fd}	0.000425	0.000425	-	-	-	-
L'_d	-	-	0.1198	0.0608	0.0608	0.1813
T'_{do}	-	-	6.00	-	-	-
L'_q	-	-	0.1969	-	-	-
T'_{qo}	-	-	0.540	-	-	-

NPCC WORKING GROUP #10 SYSTEM STUDIES

The New England 39 bus, 43 branch and 10 generator system has been used in the past by a number of investigators in several different projects (1, 2, 3) and hence it is a well-tried and familiar system. For the purpose of this report the system used in NPCC-10 (Phase 1) investigation was given due consideration. A line diagram of this system is shown in Figure 2-6 and the input data for the generators is given in Table 2-2. It is to be noted that the test unit, #1, was represented by two models, Model 2.2 and Model 2.2 Alt, the difference being in the relative values of the time constants T'_{do}, T''_{do} and T'_{qo}. For the non test units 2-10, constant rotor flux linkages were used, ie, they were held constant at their initial values. In the test unit, the rotor flux linkages were allowed to vary and the machine was under automatic voltage control. The unit exciter is a Type 1 IEEE model with parameter values as shown in Figure 2-7. A three phase fault was applied to bus #9 for a period of 0.12 sec. No lines were tripped when the fault was cleared.

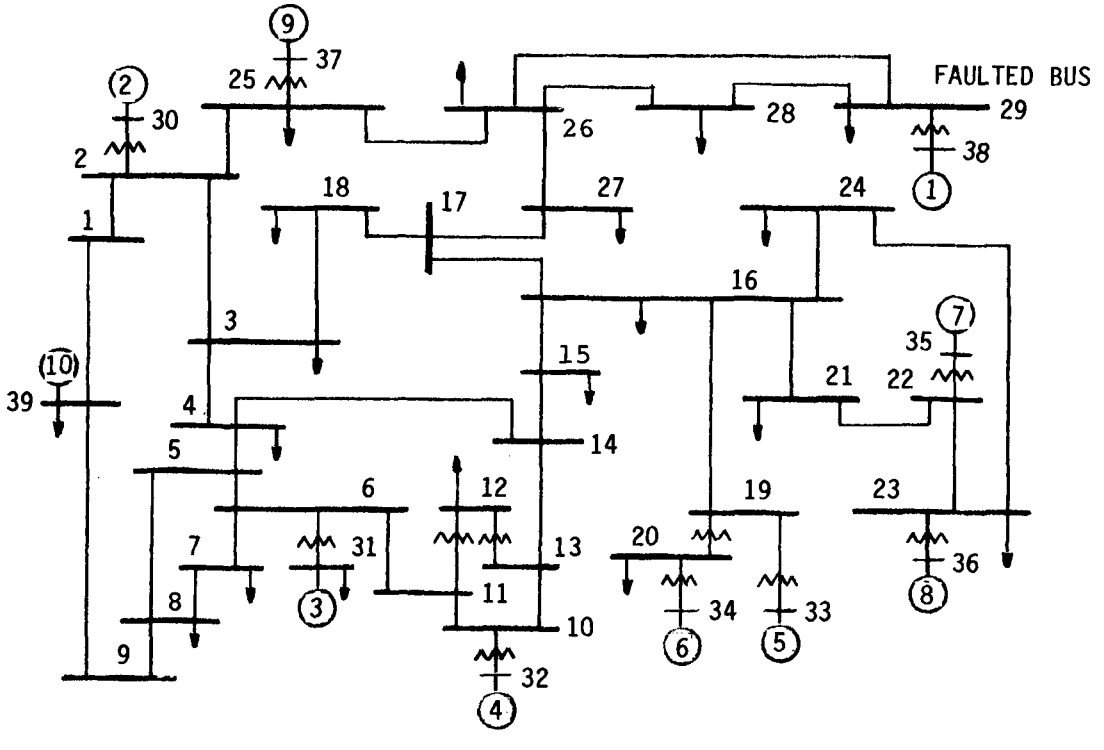

Figure 2-6. New England System Line Diagram.

Table 2-2

INPUT DATA FOR GENERATOR MODELS USED IN NPCC - 10 STUDY

Parameter	Unit 1 Model 2.2	Unit 1 Model 2.2A	Unit 2	Unit 3	Unit 4	Unit 5	Unit 6	Unit 7	Unit 8	Unit 9	Unit 10
L_d	0.2188	0.2188	0.100	0.295	0.2495	0.2620	0.3350	0.2540	0.2950	0.2900	0.0200
L_q	0.2100	0.2100	0.069	0.282	0.237	0.2580	0.3100	0.2410	0.2920	0.2800	0.0190
L_d'	0.0356	0.0356	0.031	0.0697	0.0531	0.0436	0.0660	0.0500	0.0490	0.0570	0.0060
L_d''	0.0300	0.0300	0.020	0.0480	0.0375	0.0374	0.0425	0.0339	0.0405	0.0359	0.0040
L_q'	0.0587	0.0587	0.020	0.1700	0.0876	0.1660	0.0840	0.0814	0.1860	0.0911	0.0080
L_q''	0.0356	0.0300	0.0125	0.0480	0.0375	0.0374	0.0425	0.0339	0.0405	0.0359	0.0040
T_{do}'	4.000	5.200	-	-	-	-	-	-	-	-	-
T_{do}''	0.0290	0.0107	-	-	-	-	-	-	-	-	-
T_{qo}'	0.540	1.965	-	-	-	-	-	-	-	-	-
T_{qo}''	0.0530	0.0530	-	-	-	-	-	-	-	-	-
L_l	0.0235	0.0235	0.0125	0.0350	0.0304	0.0295	0.0270	0.0224	0.0322	0.0280	0.0030
R_a	0.0005	0.0005	0.0001	0.0003	0.0004	0.0002	0.0001	0.0006	0.0003	0.0007	0.0001

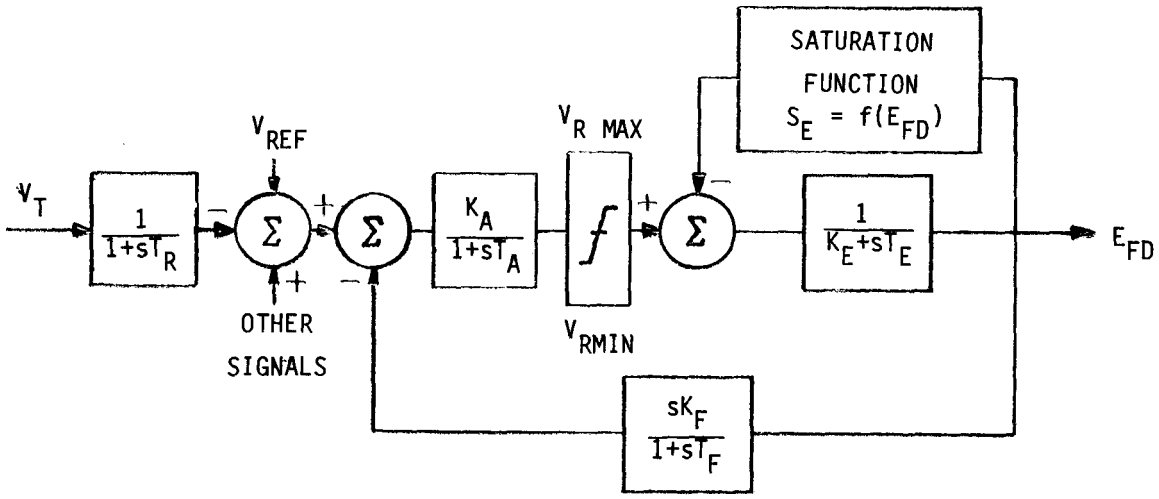

$K_A = 25$ $K_F = .16$ $K_E = -.0445$

$S_E = .0016e^{1.465E_{FD}}$

$T_A = .06$ $T_F = 1.0$ $T_E = .5$ $V_{RMAX} = 1\ PU$

$T_R = 0$

$V_{RMIN} = -1\ PU$

Figure 2-7. Model of Excitation System (Type 1 IEEE Model) for Unit #1.

Figures 2-8 and 2-9 show the results of the two simulations. In these, the rotor angle variations of the test unit are shown relative to unit #10. As can be seen, the main difference between the two models is a lower rotor angular swing predicted by the alternative model 2.2A. This is to be expected as a result of the increased value in the time constant T'_{do} (and T'_{qo}) as shown in Table 2-2, which has the effect of maintaining the air-gap flux at a higher value during the fault period. This in turn results in a higher synchronizing torque after the fault is cleared, and hence a lower rotor angular swing.

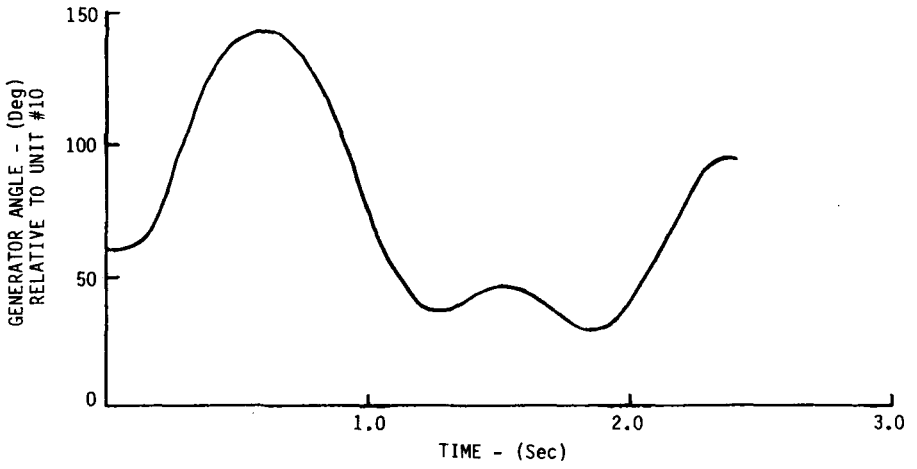

Figure 2-8. Variation in Rotor Angle of Unit #1 NPCC-10 System - Model 2.2.

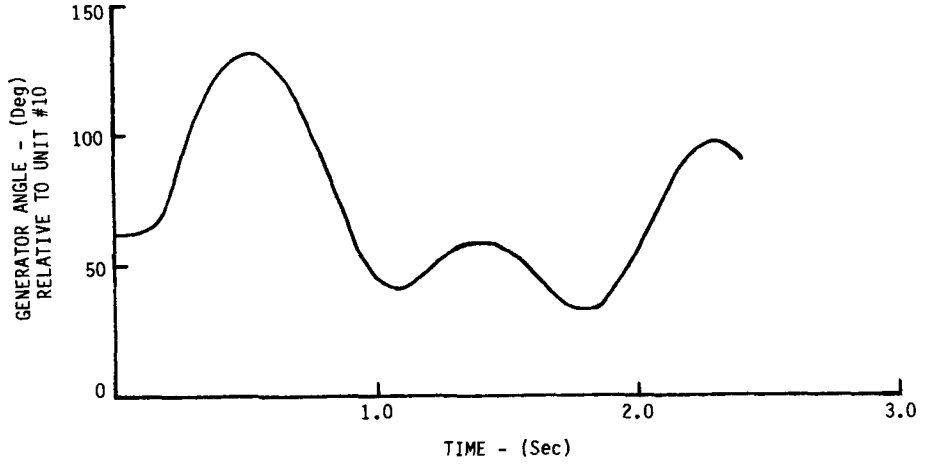

Figure 2-9. Variation in Rotor Angle of Unit #1 NPCC-10 System - Model 2.2 Alternative.

REFERENCES

1. J.M. Undrill et al. Power System Equivalents. Final report on Electric Research Council Project RP90-4, Jan. 1971.

2. P.L. Dandeno, R.L. Hauth, R.P. Schultz. Effects of Synchronous Machine Modelling in Large Scale Stability Studies. IEEE Trans. Vol. PAS-92, pp. 574-582, Mar/April 1973.

3. R. Podmore, A. Germond. Development of Dynamic Equivalents for Transient Stability Studies. Final report on EPRI project RP-763, April 1977.

Section 3

CONCLUSIONS

Techniques have been developed for implementing advanced turbogenerator models into the existing EPRI mid-term stability program. The models considered range from the classical model (constant voltage behind transient inductance) to a detailed model in which the rotor is represented by three windings in each axis. Expressions have been developed to relate the fundamental inductances and resistances of the generator equivalent circuits to the commonly used transient and subtransient inductances and time constants, such that data pertaining to the models can be entered in the established manner. However, due to the complexity of the equivalent circuit models in which unequal mutual effects are considered, it is suggested that in such an instant the data should be entered using the fundamental inductances and resistances of the model structure. In all other cases the established format may be used.

Digital computer simulations were carried out, using the different turbogenerator models in the Ontario Hydro time domain program, with the aim of providing comparative basis for checking the results of the EPRI mid-term stability program. For this purpose two well-tried systems were used; WSCC 9-bus system and NPCC 39-bus system.

Appendix

NOMENCLATURE

e_{fd}	Field voltage
H	Inertia constant MWsec/MVA
I_d, I_q	d- and q-axis components of armature current
i_{fd}	Field current (in reciprocal per unit system)
I_{fd}	Field current (in non-reciprocal per unit system)
i_{kd1}, i_{kd2}	d-axis amortisseur currents
i_{kq1}, i_{kq2}	q-axis amortisseur currents
L_{ad}, L_{aq}	d- and q-axis mutual inductances
L_{adu}	unsaturated value of L_{ad}
L_{fkd1}, L_{fkd2}	mutual leakage inductances
L_{fd}	Field leakage inductance
L_{kd1}, L_{kd2}	d-axis amortisseur leakage inductances
$L_{kq1}, L_{kq2}, L_{kq3}$	q-axis amortisseur leakage inductances
L_d, L_q	d- and q-axis synchronous inductance
L'_d, L'_q	d- and q-axis transient inductance
L''_d, L''_q	d- and q-axis subtransient inductance
L'''_d, L'''_q	d- and q-axis sub-subtransient inductance
T'_{do}, T'_{qo}	d- and q-axis transient open circuit time constants in seconds
T''_{do}, T''_{qo}	d- and q-axis subtransient open circuit time constant in seconds
T'''_{do}, T'''_{qo}	d- and q-axis sub-subtransient open circuit time constant in seconds
p	Differential operator d/dt
R_a	Armature resistance
r_{fd}	Field resistance
r_{kd1}, r_{kd2}	d-axis amortisseur resistances
$r_{kq1}, r_{kq2}, r_{kq3}$	q-axis amortisseur resistances

t	Time in seconds
V_d, V_q	d- and q-axis components of armature voltage
V_f	Exciter output voltage = $(L_{adu}/r_{fd})\ e_{fd}$
δ	Angle by which q-axis leads the real axis (radians)
ψ_d, ψ_q	d- and q-axis armature flux linkage
ψ_{fd}	Field flux linkage
ψ_{kd1}, ψ_{kd2}	d-axis amortisseur flux linkage
$\psi_{kq1}, \psi_{kq2}, \psi_{kq3}$	q-axis amortisseur flux linkage
w_o, w	Synchronous and instantaneous angular frequencies rads/s

Part 4

LAMBTON TEST DATA

CONTENTS

ILLUSTRATIONS

ILLUSTRATIONS (Cont'd)

ILLUSTRATIONS (Cont'd)

TABLES

Section 1

DESCRIPTION OF GENERATOR AND STATION

THE STATION

Lambton Generating Station is located on the St. Clair River, approximately 20 km below the southern tip of Lake Huron. Sarnia, Ontario and Port Huron, Michigan are about 15 km north of the station.

The Lambton installation has a total capacity of 2000 MW, made up of four identical 500 MW units. The fuel is either standard or low-sulphur, U.S. bituminous coal, depending upon the prevailing emission requirements.

THE GENERATOR

The generators are 2-pole, 3600 rpm machines with water-cooled stator windings and hydrogen-cooled rotors. They are rated: 500 MW, 0.90 power factor, 24 kV line-to-line stator voltage.

The rotor is machined from a single forging and has transverse flexibility slits in the pole faces. The field winding conductors are held in place by short, aluminum alloy slot wedges. There is a single steel wedge in each end of each slot. The rotor does not have a full length damper winding.

Section 2

STATIONARY TESTS

STANDSTILL FREQUENCY RESPONSE

Measurements of stator impedance and stator to rotor transfer functions were made and analyzed according to the description in Part 1, Section 2. The following functions were measured:

$\left.\begin{array}{l} Z_d(s) \\ \dfrac{\Delta I_{fd}}{\Delta I_d} \end{array}\right\}$ On the direct axis with the field winding shorted through a metering shunt.

$\left.\begin{array}{l} Z_{do}(s) \\ \dfrac{\Delta V_{fd}}{\Delta I_d} \end{array}\right\}$ On the direct axis with the field winding open.

$Z_q(s)$ } On the quadrature axis.

From each of the three operational impedances, an operational inductance was calculated as explained in Part 1. The results of the tests and analysis are detailed in the following tables and Bode plots (Tables 2-1 to 2-4 and Figures 2-1 to 2-22). To satisfy the preferences of individual readers, each function is plotted twice, once directly, with the magnitude on a logarithmic scale, and once with the magnitude converted to db. With the exception of the operational inductance, the magnitudes are in SI units (ohms, volts, etc.) and, in the case of the db plots, are normalized to 1 ohm, 1 volt, etc. The operational inductance magnitudes are in p.u. on the generator base and db above 1.0 p.u.

Magnitude and phase test points are identified on the Bode plots as follows:

- ⊙ magnitude
- ◙ phase

TABLE 2-1

STANDSTILL FREQUENCY RESPONSE TEST DATA ON THE DIRECT AXIS WITH THE FIELD SHORTED

FREQUENCY (HZ)	D-AXIS STATOR CURRENT (A)	FIELD CURRENT (A)	DIRECT AXIS STATOR IMPEDANCE (OHM)	(DEG)	DIRECT AXIS OPERATIONAL INDUCTANCE (PU)	(DB)	(DEG)	STATOR TO FIELD TRANSFER FUNCTION (A/A)	(DB)	(DEG)
.0010	46.3	.143	.00197	.94	1.877	5.47	-4.9	.0031	-50.2	87.4
.0013	46.3	.186	.00198	1.22	1.882	5.49	-6.7	.0040	-47.9	86.6
.0016	46.3	.229	.00198	1.50	1.890	5.53	-8.1	.0050	-46.1	86.0
.0020	46.3	.282	.00198	1.87	1.895	5.55	-9.2	.0061	-44.3	83.8
.0025	46.3	.355	.00199	2.33	1.898	5.57	-9.7	.0077	-42.3	84.5
.0030	46.3	.427	.00199	2.79	1.898	5.57	-9.8	.0092	-40.7	83.5
.0040	46.3	.563	.00200	3.68	1.887	5.52	-10.2	.0122	-38.3	81.6
.0050	46.3	.700	.00201	4.51	1.867	5.42	-11.3	.0151	-36.4	79.6
.0065	46.3	.902	.00203	5.64	1.822	5.21	-13.3	.0195	-34.2	76.5
.0080	46.3	1.085	.00205	6.74	1.798	5.10	-14.7	.0234	-32.6	74.0
.0100	46.3	1.334	.00208	8.02	1.768	4.95	-17.8	.0288	-30.8	70.4
.0130	46.3	1.661	.00213	9.57	1.680	4.51	-20.2	.0359	-28.9	65.6
.0160	46.3	1.951	.00219	10.64	1.608	4.13	-24.4	.0422	-27.5	61.2
.0200	46.3	2.266	.00227	11.81	1.524	3.66	-28.2	.0490	-26.2	56.1
.0250	46.3	2.602	.00235	12.63	1.404	2.95	-32.1	.0562	-25.0	50.7
.0300	46.3	2.853	.00240	13.40	1.288	2.20	-33.5	.0616	-24.2	46.2
.0400	45.7	3.238	.00252	13.90	1.111	.92	-38.0	.0708	-23.0	39.1
.0500	46.3	3.550	.00261	13.90	.972	-.25	-41.8	.0767	-22.3	33.9
.0650	45.7	3.760	.00270	14.90	.838	-1.53	-42.5	.0822	-21.7	28.2
.0800	45.7	3.938	.00276	15.50	.731	-2.73	-43.1	.0861	-21.3	24.2
.1000	45.7	4.076	.00283	16.60	.632	-3.98	-42.4	.0891	-21.0	20.4
.1300	45.7	4.219	.00289	18.50	.533	-5.46	-40.0	.0922	-20.7	16.7
.1600	45.7	4.318	.00299	20.60	.485	-6.29	-38.3	.0944	-20.5	14.0
.2000	46.3	4.418	.00306	23.50	.428	-7.36	-34.4	.0955	-20.4	11.7
.2500	46.3	4.469	.00317	27.10	.388	-8.22	-30.5	.0966	-20.3	9.6
.3000	45.7	4.469	.00332	30.60	.368	-8.68	-27.7	.0977	-20.2	8.2
.4000	45.7	4.521	.00364	37.00	.345	-9.25	-23.1	.0988	-20.1	6.3
.5000	46.3	4.626	.00395	42.30	.326	-9.73	-19.6	.1000	-20.0	5.0
.6500	46.3	4.626	.00453	48.90	.317	-9.98	-16.4	.1000	-20.0	3.7
.8000	46.3	4.626	.00514	54.00	.310	-10.16	-14.2	.1000	-20.0	2.6
1.0000	46.3	4.680	.00597	59.10	.303	-10.37	-12.1	.1011	-19.9	1.6
1.3000	45.7	4.626	.00726	64.40	.296	-10.57	-10.1	.1011	-19.9	.4
1.6000	46.3	4.680	.00873	68.10	.297	-10.55	-9.0	.1011	-19.9	-.5
2.0000	46.3	4.680	.01050	71.30	.291	-10.74	-8.0	.1011	-19.9	-1.6
2.5000	46.3	4.626	.01291	74.00	.290	-10.76	-7.3	.1000	-20.0	-2.6
3.0000	45.7	4.573	.01517	76.00	.286	-10.88	-6.6	.1000	-20.0	-3.6
4.0000	45.7	4.521	.02000	78.20	.285	-10.91	-6.2	.0988	-20.1	-5.0
5.0000	46.3	4.521	.02433	79.60	.278	-11.11	-5.8	.0977	-20.2	-6.1
6.5000	46.3	4.418	.03134	80.80	.277	-11.16	-5.6	.0955	-20.4	-7.3
8.0000	46.3	4.318	.03811	81.50	.274	-11.25	-5.5	.0933	-20.6	-8.3
10.0000	53.8	4.900	.04743	82.00	.273	-11.27	-5.6	.0912	-20.8	-9.1
13.0000	43.7	3.893	.06040	82.60	.268	-11.44	-5.5	.0891	-21.0	-10.3
16.0000	44.2	3.848	.07346	82.80	.265	-11.54	-5.7	.0871	-21.2	-11.1
20.0000	42.7	3.591	.09038	83.10	.261	-11.67	-5.7	.0841	-21.5	-12.0
25.0000	46.3	3.804	.11248	83.10	.260	-11.71	-5.9	.0822	-21.7	-12.8
30.0000	42.7	3.390	.13215	83.10	.254	-11.89	-6.1	.0794	-22.0	-13.6
40.0000	36.3	2.756	.17420	82.90	.252	-11.98	-6.5	.0758	-22.4	-14.7
50.0000	31.3	2.266	.21187	82.80	.245	-12.22	-6.7	.0724	-22.8	-15.5
65.0000	25.7	1.759	.26981	82.70	.240	-12.40	-6.9	.0684	-23.3	-15.9
80.0000	21.9	1.430	.32814	82.60	.237	-12.50	-7.1	.0653	-23.7	-16.0
100.0000	18.4	1.136	.39908	82.50	.231	-12.74	-7.2	.0616	-24.2	-15.8
130.0000	14.6	.861	.50823	82.40	.226	-12.91	-7.4	.0589	-24.6	-15.4
160.0000	12.0	.676	.61810	82.40	.223	-13.02	-7.4	.0562	-25.0	-15.1
200.0000	9.8	.531	.75173	82.40	.217	-13.25	-7.5	.0543	-25.3	-14.8
250.0000	7.8	.408	.92483	82.30	.214	-13.39	-7.6	.0525	-25.6	-14.8
300.0000	6.4	.328	1.08658	82.20	.210	-13.57	-7.7	.0513	-25.8	-15.1
400.0000	4.6	.227	1.41599	81.90	.205	-13.77	-8.0	.0490	-26.2	-16.2
500.0000	3.5	.164	1.72211	81.70	.199	-14.01	-8.2	.0468	-26.6	-17.5
650.0000	3.9	.172	2.14319	81.00	.191	-14.39	-8.9	.0441	-27.1	-19.1
800.0000	3.0	.125	2.54719	80.60	.184	-14.69	-9.4	.0417	-27.6	-20.5
1000.0000	2.3	.087	2.95842	80.60	.171	-15.33	-9.4	.0376	-28.5	-21.6

TABLE 2-2

STANDSTILL FREQUENCY RESPONSE TEST DATA ON THE DIRECT AXIS WITH THE FIELD OPEN

	D-AXIS STATOR		FIELD-OPEN D-AXIS STATOR IMPEDANCE		FIELD-OPEN D-AXIS OPERATIONAL INDUCTANCE			STATOR TO FIELD TRANSFER IMPEDANCE		
FREQUENCY (HZ)	CURRENT (A)	FIELD VOLTAGE (V)	(OHM)	(DEG)	(PU)	(DB)	(DEG)	(V/A)	(DB)	(DEG)
.0010	46.3	.016	.00198	.93	1.871	5.44	-1.9	.0003	-69.2	88.9
.0013	46.3	.021	.00198	1.21	1.871	5.44	-2.1	.0005	-66.8	88.8
.0016	46.3	.026	.00198	1.49	1.873	5.45	-2.4	.0006	-65.0	88.6
.0020	46.3	.032	.00199	1.87	1.872	5.45	-2.6	.0007	-63.1	88.2
.0025	46.3	.040	.00199	2.33	1.874	5.45	-2.9	.0009	-61.2	88.2
.0030	46.3	.048	.00199	2.79	1.873	5.45	-3.2	.0010	-59.6	88.0
.0040	46.3	.064	.00199	3.72	1.874	5.46	-3.7	.0014	-57.2	87.5
.0050	46.3	.079	.00200	4.63	1.876	5.46	-4.3	.0017	-55.3	87.0
.0065	46.3	.102	.00201	6.01	1.885	5.51	-5.6	.0022	-53.1	86.3
.0080	46.3	.126	.00203	7.33	1.882	5.49	-6.3	.0027	-51.3	85.6
.0100	46.3	.157	.00205	9.03	1.873	5.45	-6.9	.0034	-49.4	84.7
.0130	46.3	.202	.00208	11.41	1.846	5.33	-7.6	.0044	-47.2	83.5
.0160	46.3	.248	.00211	13.69	1.824	5.22	-7.9	.0054	-45.4	82.4
.0200	46.3	.305	.00216	16.48	1.795	5.08	-8.5	.0066	-43.6	81.1
.0250	46.3	.376	.00223	19.78	1.772	4.97	-9.0	.0081	-41.8	79.6
.0300	46.3	.442	.00231	22.69	1.745	4.84	-9.6	.0095	-40.4	78.2
.0400	46.3	.575	.00250	27.58	1.709	4.65	-11.4	.0124	-38.1	75.9
.0500	46.3	.708	.00270	31.21	1.666	4.43	-13.3	.0153	-36.3	73.8
.0650	46.3	.881	.00302	35.12	1.609	4.13	-15.8	.0190	-34.4	71.1
.0800	46.3	1.047	.00334	37.97	1.560	3.86	-17.6	.0226	-32.9	68.7
.1000	46.3	1.245	.00372	40.50	1.484	3.43	-19.4	.0269	-31.4	65.7
.1300	46.8	1.531	.00428	42.50	1.388	2.85	-22.1	.0327	-29.7	61.9
.1600	46.8	1.778	.00485	43.40	1.329	2.47	-24.9	.0380	-28.4	58.4
.2000	46.8	2.065	.00557	43.70	1.262	2.02	-28.0	.0441	-27.1	54.5
.2500	46.8	2.371	.00625	43.70	1.160	1.29	-30.4	.0507	-25.9	50.6
.3000	46.8	2.600	.00686	43.50	1.078	.65	-32.4	.0555	-25.1	47.4
.4000	46.8	2.985	.00787	43.10	.950	-.45	-35.0	.0638	-23.9	42.5
.5000	46.3	3.236	.00863	43.00	.846	-1.45	-36.3	.0699	-23.1	39.0
.6500	46.3	3.589	.00968	43.30	.744	-2.57	-37.3	.0776	-22.2	35.2
.8000	46.3	3.802	.01050	44.00	.664	-3.56	-37.4	.0822	-21.7	32.6
1.0000	45.7	3.981	.01151	45.40	.591	-4.57	-36.7	.0870	-21.2	30.2
1.3000	45.7	4.266	.01306	47.70	.526	-5.58	-35.2	.0932	-20.6	28.1
1.6000	45.2	4.416	.01432	50.00	.475	-6.46	-33.4	.0976	-20.2	26.9
2.0000	45.2	4.624	.01607	52.90	.433	-7.27	-31.0	.1022	-19.8	26.0
2.5000	45.7	4.898	.01824	56.10	.398	-7.99	-28.4	.1071	-19.4	25.7
3.0000	45.2	5.070	.02047	58.80	.376	-8.49	-26.2	.1121	-19.0	25.7
4.0000	46.3	5.559	.02518	63.00	.352	-9.06	-22.8	.1201	-18.4	26.5
5.0000	45.7	5.821	.02993	65.90	.338	-9.43	-20.5	.1272	-17.9	27.4
6.5000	45.2	6.237	.03682	69.00	.322	-9.85	-18.1	.1379	-17.2	28.9
8.0000	44.7	6.607	.04376	71.00	.312	-10.11	-16.5	.1478	-16.6	30.1
10.0000	36.8	5.754	.05261	72.90	.301	-10.42	-15.0	.1565	-16.1	31.0
13.0000	35.1	6.095	.06623	74.80	.293	-10.67	-13.5	.1736	-15.2	32.2
16.0000	33.1	6.237	.07963	75.90	.286	-10.86	-12.7	.1882	-14.5	32.9
20.0000	30.9	6.383	.09684	76.90	.279	-11.09	-12.0	.2064	-13.7	33.1
25.0000	28.5	6.383	.11778	77.70	.272	-11.32	-11.4	.2237	-13.0	33.1
30.0000	26.3	6.310	.13838	78.20	.266	-11.50	-11.0	.2397	-12.4	32.9
40.0000	22.4	5.957	.17826	79.10	.257	-11.79	-10.3	.2658	-11.5	32.4
50.0000	19.5	5.559	.21931	79.60	.253	-11.92	-9.9	.2849	-10.9	32.2
65.0000	16.4	5.070	.27610	80.00	.246	-12.20	-9.6	.3088	-10.2	32.1
80.0000	14.0	4.571	.33194	80.40	.240	-12.40	-9.3	.3271	-9.7	32.4
100.0000	11.8	4.121	.40838	80.80	.236	-12.54	-8.9	.3504	-9.1	32.8
130.0000	9.6	3.631	.51412	81.10	.229	-12.81	-8.7	.3799	-8.4	33.4
160.0000	8.0	3.311	.61810	81.20	.223	-13.02	-8.6	.4117	-7.7	33.9
200.0000	6.6	2.951	.76043	81.40	.220	-13.15	-8.5	.4463	-7.0	34.3
250.0000	5.4	2.661	.93554	81.50	.216	-13.29	-8.4	.4894	-6.2	34.4
300.0000	4.6	2.427	1.09916	81.50	.212	-13.47	-8.4	.5243	-5.6	34.3
400.0000	3.6	2.138	1.41599	81.30	.205	-13.77	-8.6	.5883	-4.6	33.6
500.0000	3.0	1.905	1.72211	81.20	.199	-14.01	-8.7	.6377	-3.9	32.7
650.0000	2.4	1.660	2.16801	80.70	.193	-14.29	-9.2	.6912	-3.2	31.5
800.0000	2.0	1.479	2.54719	80.50	.184	-14.69	-9.5	.7238	-2.8	30.5
1000.0000	1.7	1.288	2.99268	80.30	.173	-15.23	-9.7	.7492	-2.5	29.7

TABLE 2-3

QUADRATURE AXIS STANDSTILL FREQUENCY RESPONSE TEST DATA

FREQUENCY (HZ)	Q-AXIS STATOR CURRENT (A)	QUADRATURE AXIS STATOR IMPEDANCE (OHM)	(DEG)	QUADRATURE AXIS OPERATIONAL INDUCTANCE (PU)	(DB)	(DEG)
.0010	46.3	.00197	.90	1.797	5.09	-.1
.0013	46.3	.00197	1.18	1.796	5.09	-.1
.0016	46.3	.00197	1.45	1.798	5.10	-.1
.0020	46.3	.00197	1.81	1.797	5.09	-.2
.0025	46.3	.00197	2.26	1.798	5.10	-.5
.0030	46.3	.00197	2.71	1.797	5.09	-.7
.0040	46.3	.00197	3.61	1.798	5.09	-1.1
.0050	46.3	.00198	4.50	1.798	5.10	-1.6
.0065	46.3	.00199	5.83	1.799	5.10	-2.6
.0080	46.3	.00200	7.11	1.792	5.07	-3.5
.0100	46.8	.00200	9.00	1.811	5.16	-1.6
.0130	46.3	.00205	11.10	1.764	4.93	-6.0
.0160	46.3	.00208	14.30	1.872	5.45	-5.9
.0200	46.8	.00212	16.10	1.712	4.67	-6.7
.0250	46.3	.00219	19.40	1.703	4.62	-7.9
.0300	46.3	.00224	22.40	1.663	4.42	-7.2
.0400	46.3	.00240	27.60	1.629	4.24	-8.4
.0500	45.7	.00261	31.60	1.608	4.12	-10.5
.0650	46.3	.00286	36.10	1.530	3.69	-11.5
.0800	46.3	.00317	40.00	1.511	3.59	-12.8
.1000	46.3	.00356	43.40	1.459	3.28	-14.2
.1300	46.3	.00418	46.90	1.415	3.01	-16.2
.1600	45.7	.00474	49.10	1.360	2.67	-17.6
.2000	45.7	.00551	51.20	1.314	2.37	-19.1
.2500	45.2	.00640	52.40	1.256	1.98	-20.9
.3000	44.7	.00726	53.20	1.212	1.67	-22.3
.4000	45.2	.00863	53.80	1.105	.87	-24.2
.5000	45.2	.01002	54.10	1.043	.37	-25.7
.6500	45.7	.01178	54.60	.958	-.37	-26.8
.8000	46.3	.01321	55.00	.882	-1.09	-27.4
1.0000	46.8	.01517	55.60	.819	-1.73	-27.8
1.3000	47.4	.01762	56.80	.740	-2.61	-27.5
1.6000	46.8	.02000	57.80	.688	-3.25	-27.2
2.0000	45.7	.02323	59.00	.645	-3.81	-26.7
2.5000	45.7	.02667	60.90	.597	-4.49	-25.3
3.0000	45.7	.03027	62.20	.567	-4.92	-24.4
4.0000	45.2	.03768	64.10	.533	-5.46	-23.1
5.0000	45.7	.04427	65.50	.503	-5.96	-22.1
6.5000	44.7	.05446	66.80	.478	-6.41	-21.3
8.0000	45.7	.06398	67.80	.458	-6.79	-20.6
10.0000	44.7	.07692	68.60	.441	-7.11	-20.0
13.0000	43.2	.09464	69.30	.418	-7.57	-19.6
16.0000	41.2	.11248	69.80	.404	-7.86	-19.3
20.0000	38.5	.13368	70.20	.385	-8.29	-19.0
25.0000	34.7	.15888	70.60	.366	-8.72	-18.7
30.0000	31.7	.18453	70.90	.355	-9.00	-18.5
40.0000	26.9	.23231	71.40	.335	-9.49	-18.1
50.0000	23.2	.27929	71.60	.323	-9.83	-18.0
65.0000	19.5	.34758	71.80	.309	-10.20	-17.9
80.0000	16.8	.41789	71.80	.302	-10.40	-17.9
100.0000	12.7	.51412	71.50	.297	-10.54	-18.3
130.0000	9.9	.66998	70.50	.298	-10.52	-19.3
160.0000	7.9	.84345	69.10	.305	-10.32	-20.8
200.0000	5.8	1.13779	66.20	.329	-9.66	-23.7
250.0000	4.0	1.62578	60.20	.376	-8.49	-29.7
300.0000	2.7	2.37717	49.70	.458	-6.78	-40.3
350.0000	1.9	3.55681	29.60	.588	-4.62	-60.4
400.0000	1.4	4.32574	-3.10	.626	-4.07	-93.1
410.0000	1.6	4.37583	-10.50	.617	-4.19	-100.5
420.0000	1.6	4.37583	-17.30	.603	-4.40	-107.3
450.0000	1.8	3.85532	-35.60	.496	-6.10	-125.6
500.0000	2.0	2.89108	-53.50	.334	-9.51	-143.5
570.0000	3.3	2.09440	-67.10	.213	-13.45	-157.1
650.0000	3.3	1.57058	-73.60	.140	-17.09	-163.7
800.0000	6.9	1.08658	-80.60	.079	-22.09	-170.7
1000.0000	9.7	.77815	-84.50	.045	-26.93	-174.6

TABLE 2-4

FIELD IMPEDANCE WITH THE STATOR WINDING OPEN

FREQUENCY (HZ)	FIELD VOLTAGE (V)	FIELD CURRENT (A)	FIELD IMPEDANCE (OHM)	(DB)	(DEG)
.0010	2.11	29.30	.072	-22.84	2.6
.0013	2.11	29.30	.072	-22.84	3.3
.0016	2.11	29.30	.072	-22.84	4.2
.0020	2.11	29.30	.072	-22.84	5.1
.0025	2.14	29.30	.073	-22.74	6.4
.0030	2.14	29.30	.073	-22.74	7.5
.0040	2.16	29.30	.074	-22.64	9.9
.0050	2.19	29.30	.075	-22.54	12.3
.0065	2.21	29.30	.076	-22.44	15.5
.0080	2.26	28.97	.078	-22.14	18.7
.0100	2.37	28.97	.082	-21.74	22.4
.0130	2.51	28.97	.087	-21.24	27.4
.0160	2.66	28.63	.093	-20.64	31.7
.0200	2.88	28.31	.102	-19.84	36.3
.0250	3.16	27.66	.114	-18.84	40.9
.0300	3.43	27.03	.127	-17.94	44.1
.0400	3.94	25.82	.152	-16.34	48.6
.0500	4.42	24.94	.177	-15.04	51.0
.0650	4.95	23.27	.213	-13.44	52.7
.0800	5.43	21.47	.253	-11.94	53.1
.1000	5.89	20.04	.294	-10.64	52.9
.1300	6.31	17.86	.353	-9.04	51.3
.1600	6.61	16.48	.401	-7.94	49.4
.2000	6.92	15.20	.455	-6.84	47.2
.2500	7.08	13.71	.517	-5.74	44.8
.3000	7.24	12.79	.566	-4.94	42.4
.4000	7.50	11.66	.643	-3.84	39.0
.5000	7.59	10.89	.697	-3.14	36.7
.6500	7.67	10.16	.755	-2.44	33.4
.8000	7.76	9.70	.800	-1.94	31.7
1.0000	7.85	9.27	.847	-1.44	30.2
1.3000	8.04	8.85	.908	-.84	29.1
1.6000	11.22	11.53	.973	-.24	29.3
2.0000	11.35	10.89	1.043	.36	29.3
2.5000	11.89	11.01	1.079	.66	30.1
3.0000	11.61	10.16	1.143	1.16	30.9
4.0000	12.16	9.81	1.239	1.86	32.8
5.0000	12.45	9.27	1.343	2.56	34.7
6.5000	12.59	8.55	1.473	3.36	37.2
8.0000	12.88	8.07	1.596	4.06	39.0
10.0000	13.03	7.36	1.771	4.96	40.9
13.0000	13.18	6.64	1.987	5.96	42.9
16.0000	13.34	6.05	2.204	6.86	44.1
20.0000	13.49	5.46	2.472	7.86	45.2
25.0000	13.65	4.86	2.806	8.96	46.0
30.0000	13.65	4.43	3.077	9.76	46.5
40.0000	13.80	3.91	3.533	10.96	46.8
50.0000	13.80	3.44	4.010	12.06	47.3
65.0000	13.96	3.03	4.604	13.26	47.4
80.0000	13.96	2.70	5.166	14.26	47.4
100.0000	13.96	2.38	5.863	15.36	47.3
130.0000	13.80	2.05	6.732	16.56	46.9
160.0000	13.65	1.81	7.553	17.56	46.4
200.0000	13.34	1.56	8.573	18.66	45.6
250.0000	13.03	1.34	9.730	19.76	44.6
300.0000	12.59	1.17	10.792	20.66	43.5
400.0000	11.61	.91	12.827	22.16	41.2
500.0000	10.72	.71	15.070	23.56	38.1
650.0000	9.33	.53	17.706	24.96	32.9
800.0000	8.22	.40	20.329	26.16	26.2
1000.0000	7.08	.30	23.341	27.36	15.1

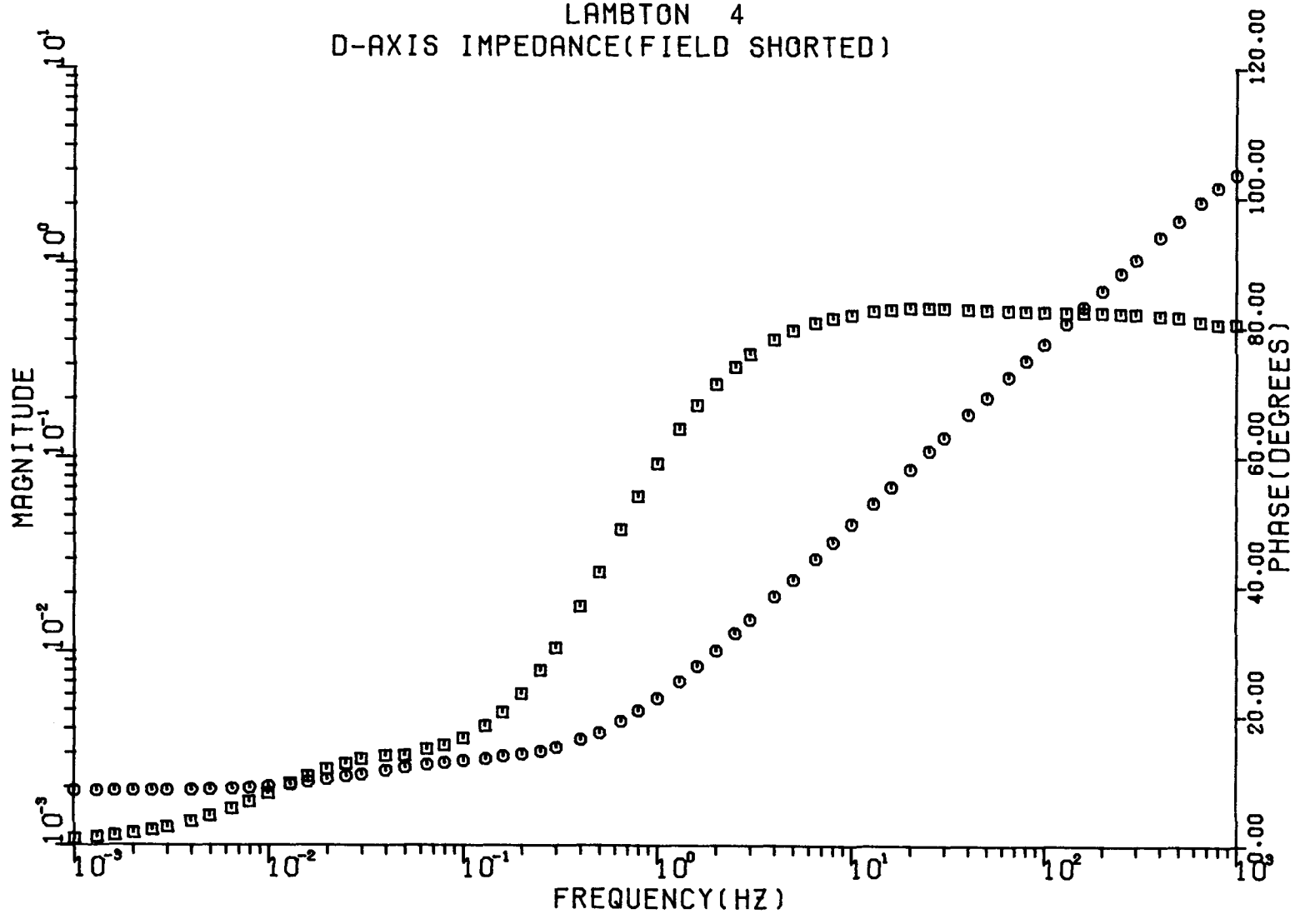

Figure 2-1. Lambton Direct Axis Operational Impedance, Magnitude in pu.

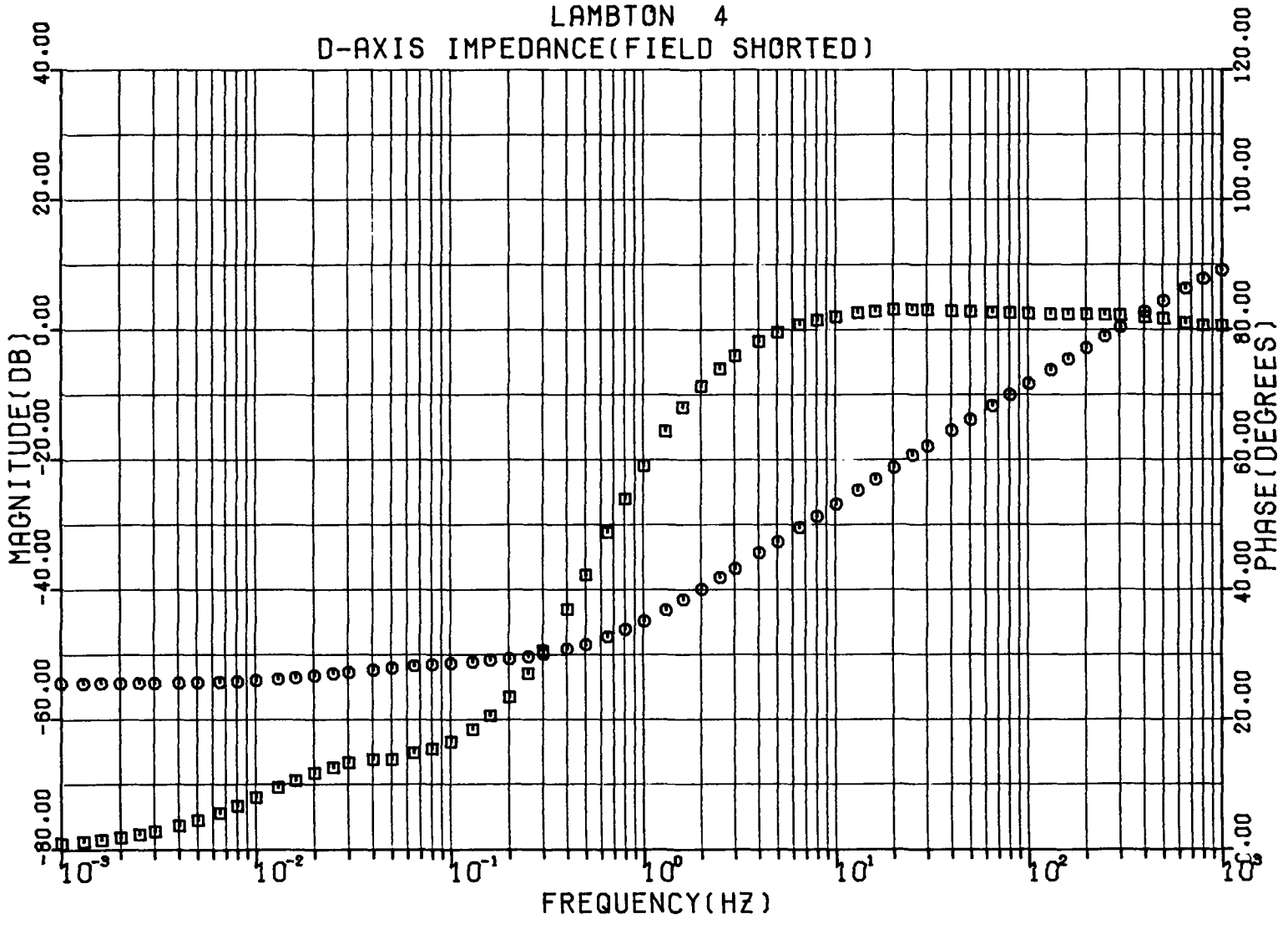

Figure 2-2. Lambton Direct Axis Operational Impedance, Magnitude in dB Above 1 pu.

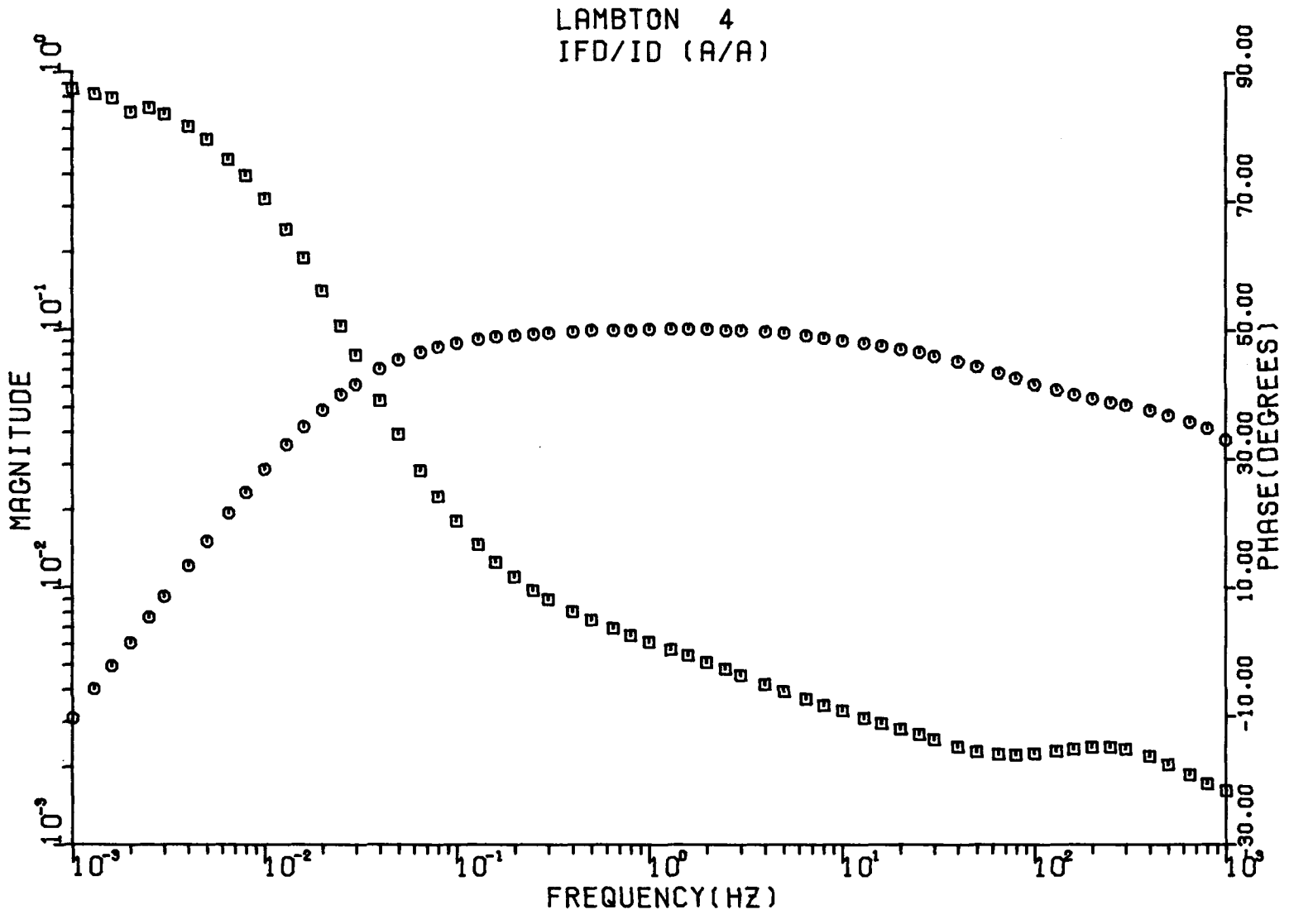

Figure 2-3. Lambton Stationary Stator-To-Field Transfer Function, Magnitude in A/A.

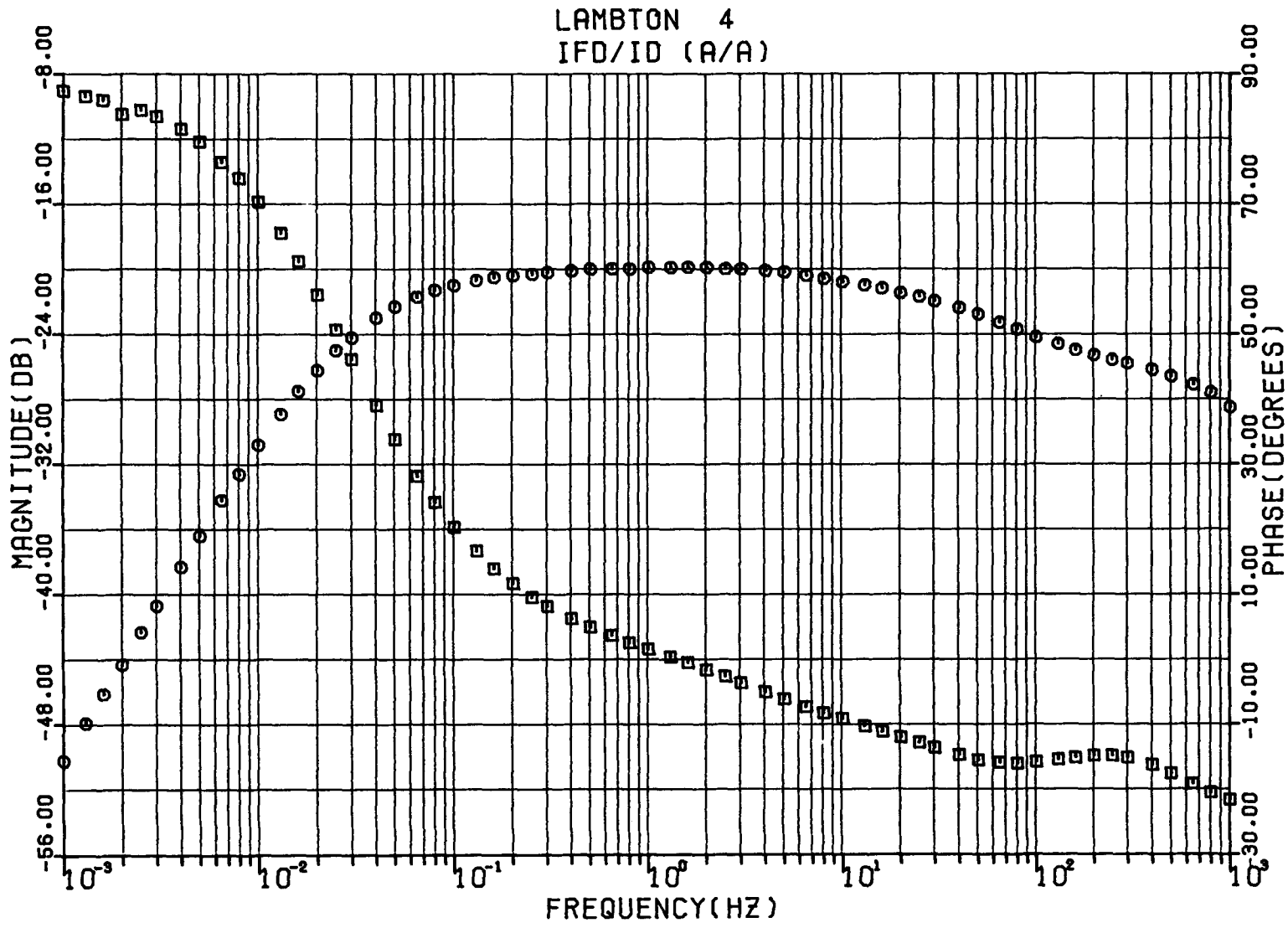

Figure 2-4. Lambton Stationary Stator-To Field Transfer Function, Magnitude in dB Above 1 A/A.

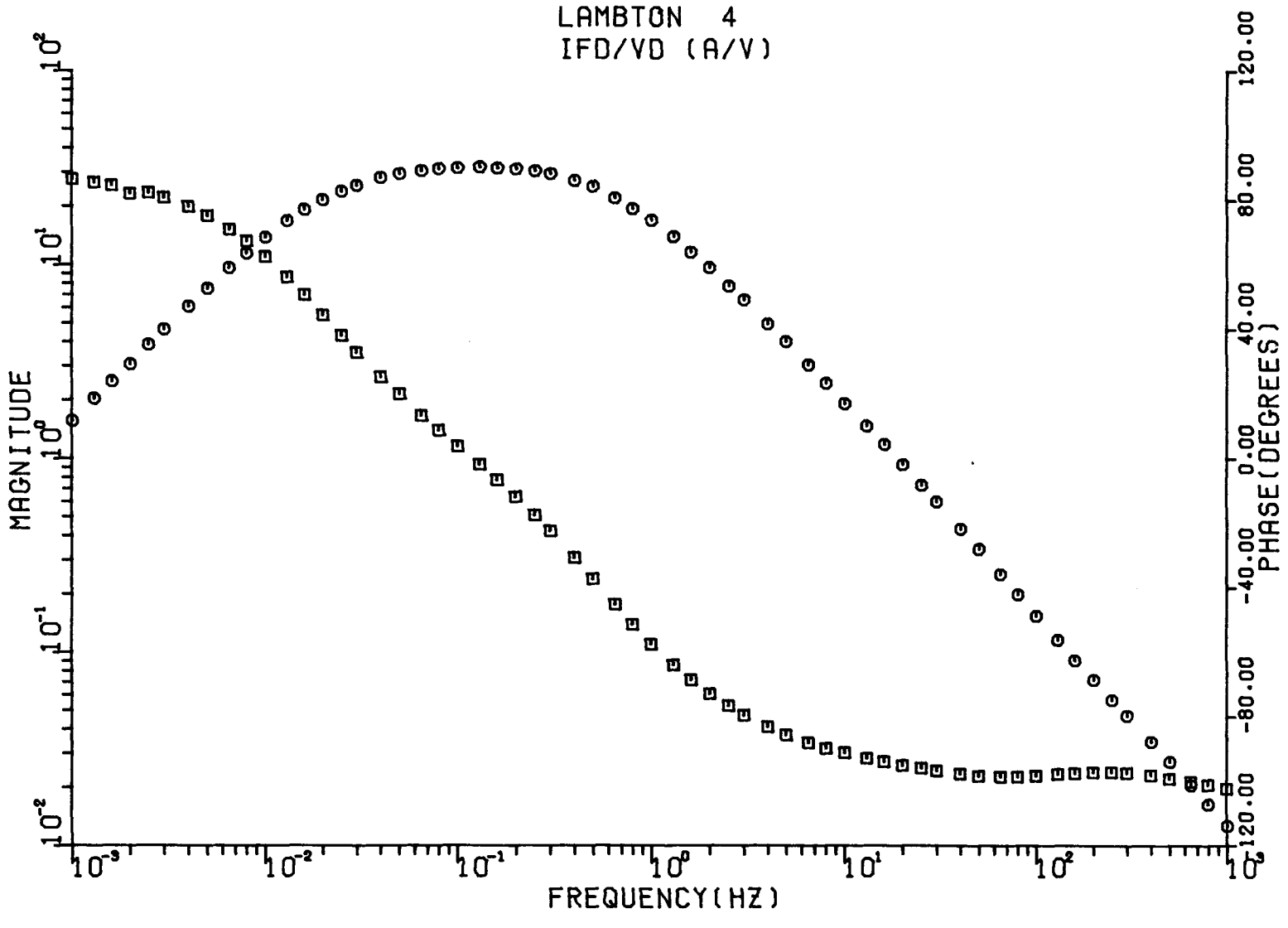

Figure 2-5. Lambton Stator-To-Field Transfer Admittance, Magnitude in A/V.

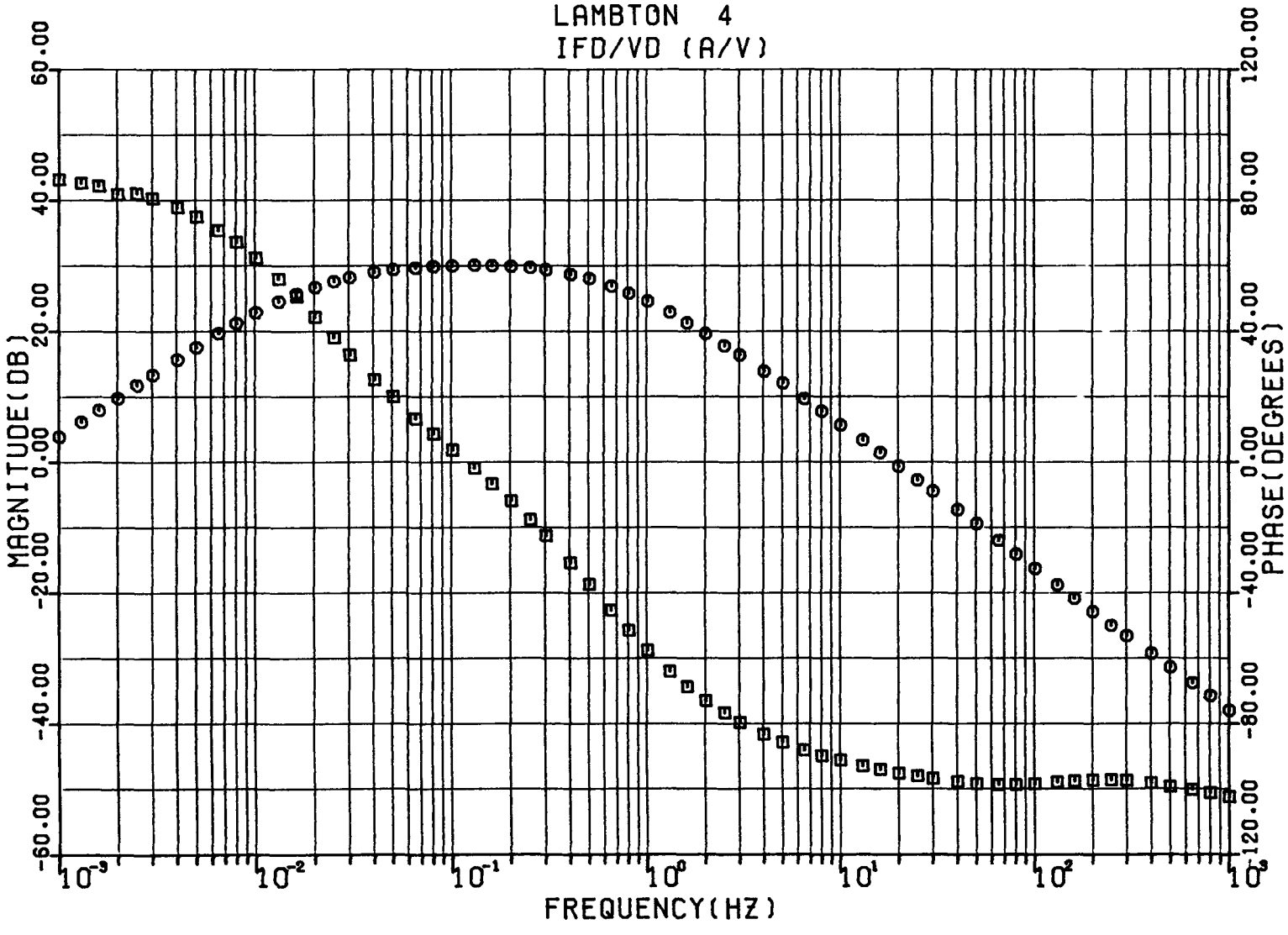

Figure 2-6. Lambton Stator-To-Field Transfer Admittance, Magnitude in dB Above 1 A/V.

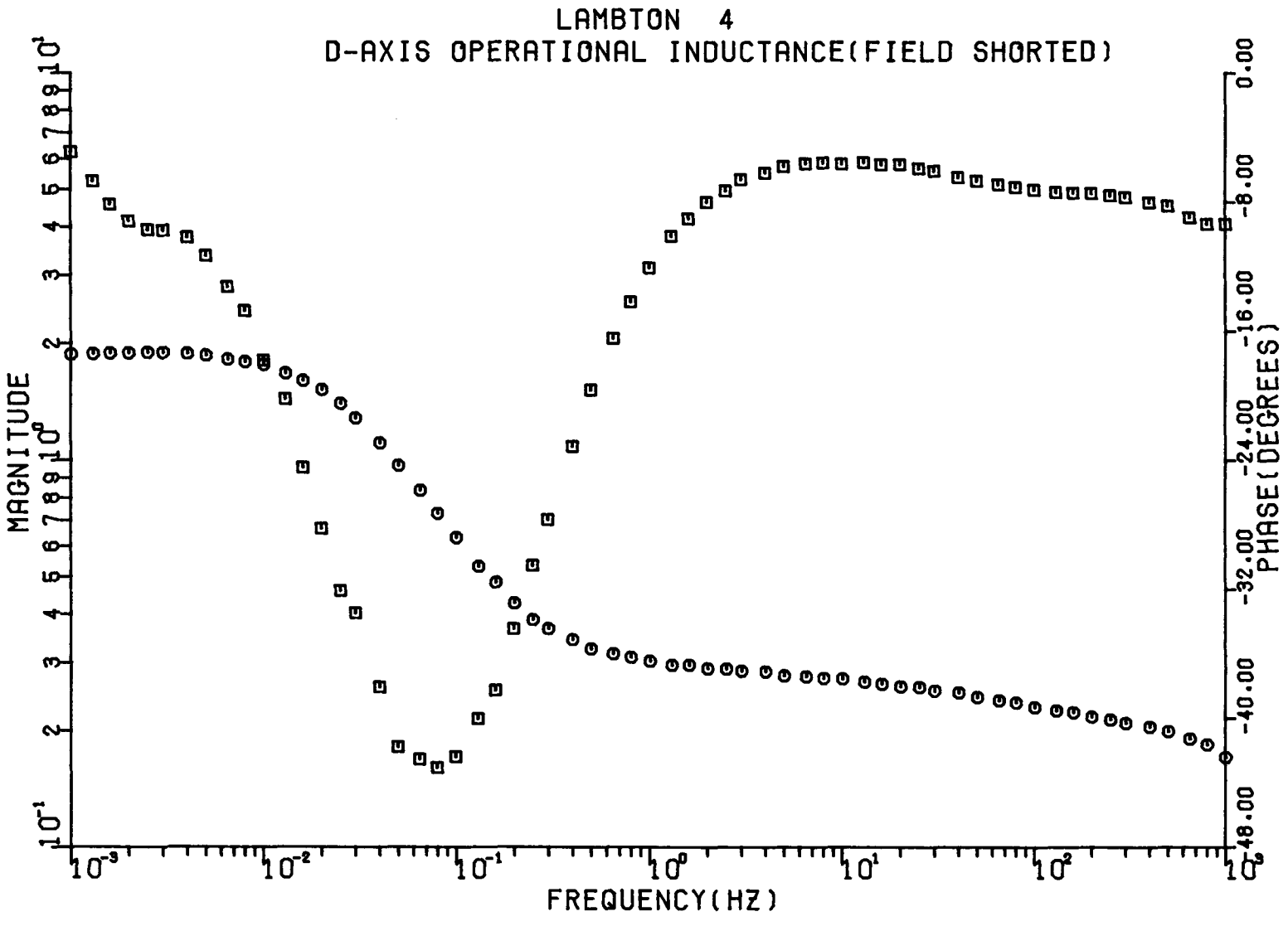

Figure 2-7. Lambton Direct Axis Operational Inductance, Magnitude in pu.

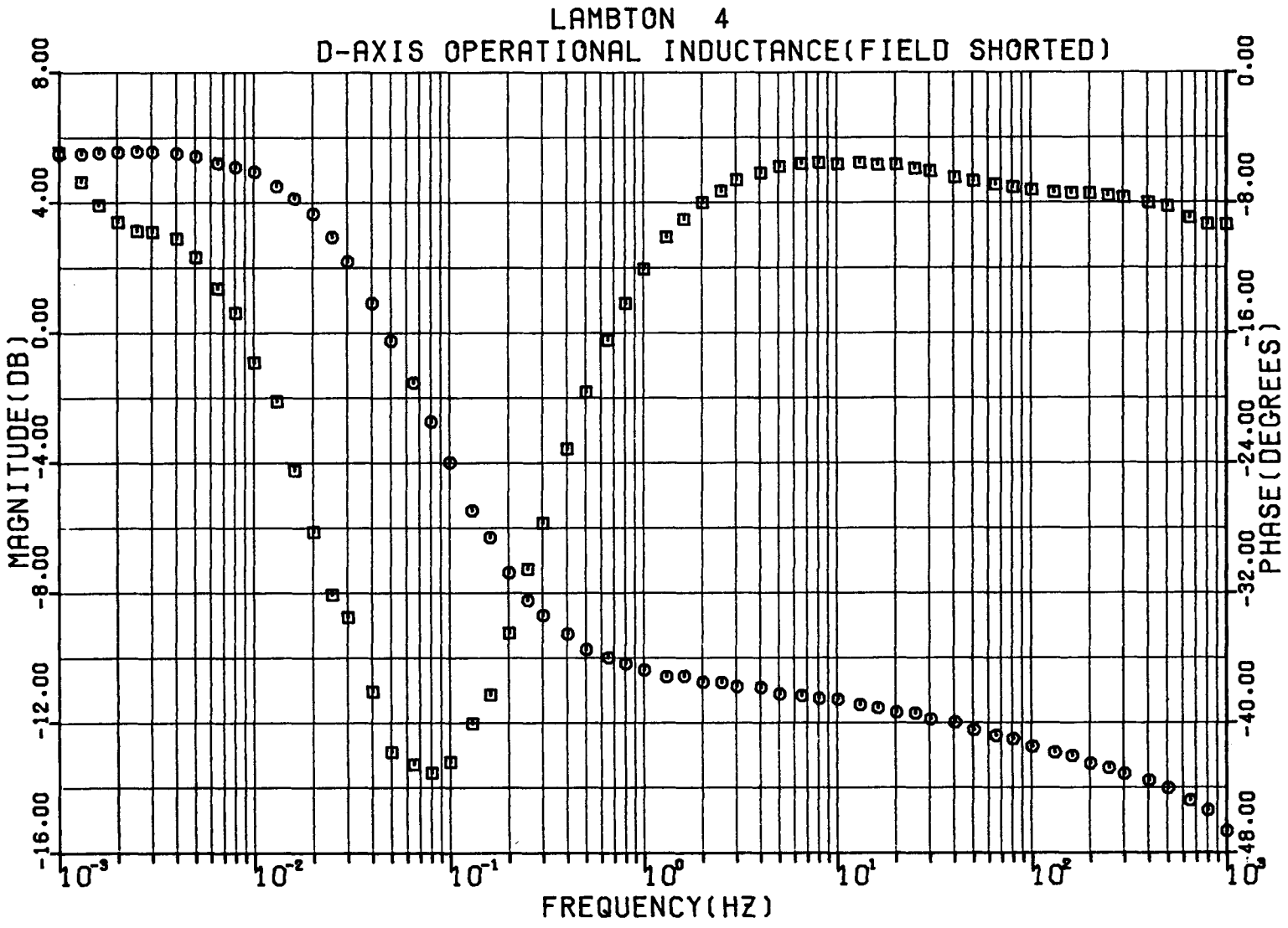

Figure 2-8. Lambton Direct Axis Operational Inductance, Magnitude in dB Above 1 pu.

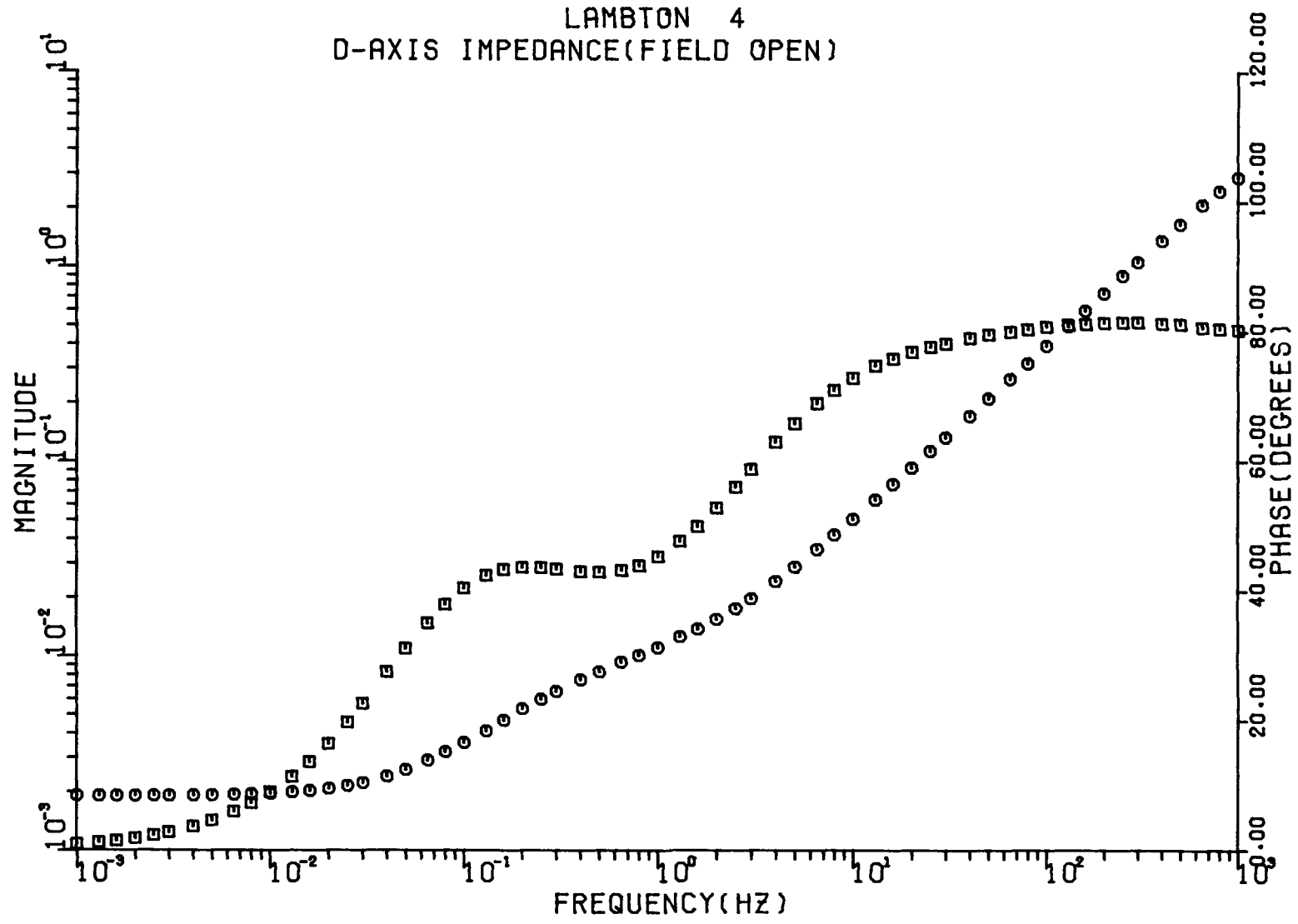

Figure 2-9. Lambton Open-Circuit Stator Driving Point Impedance, Magnitude in pu.

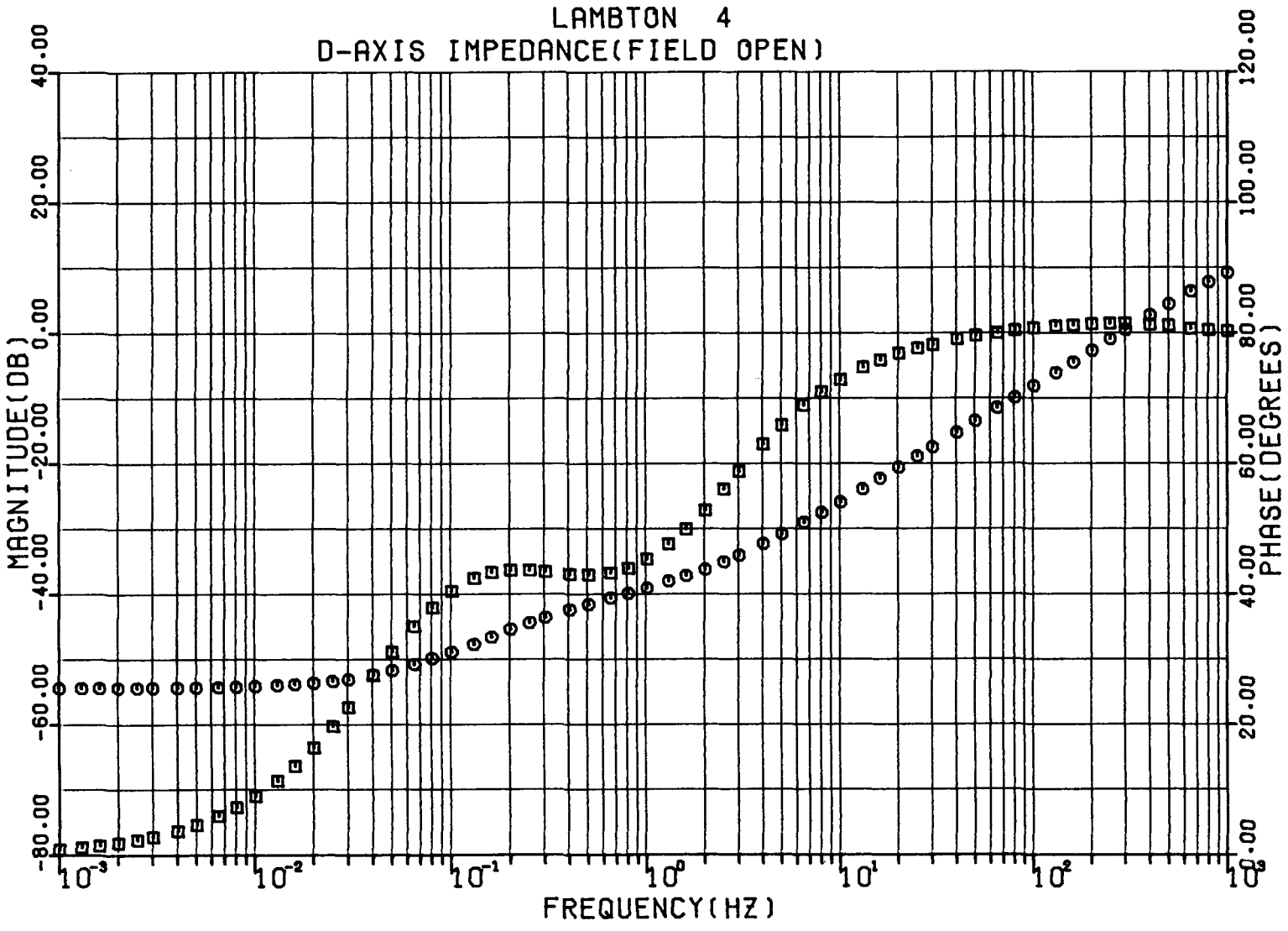

Figure 2-10. Lambton Open-Circuit Stator Driving Point Impedance, Magnitude in dB Above 1 pu.

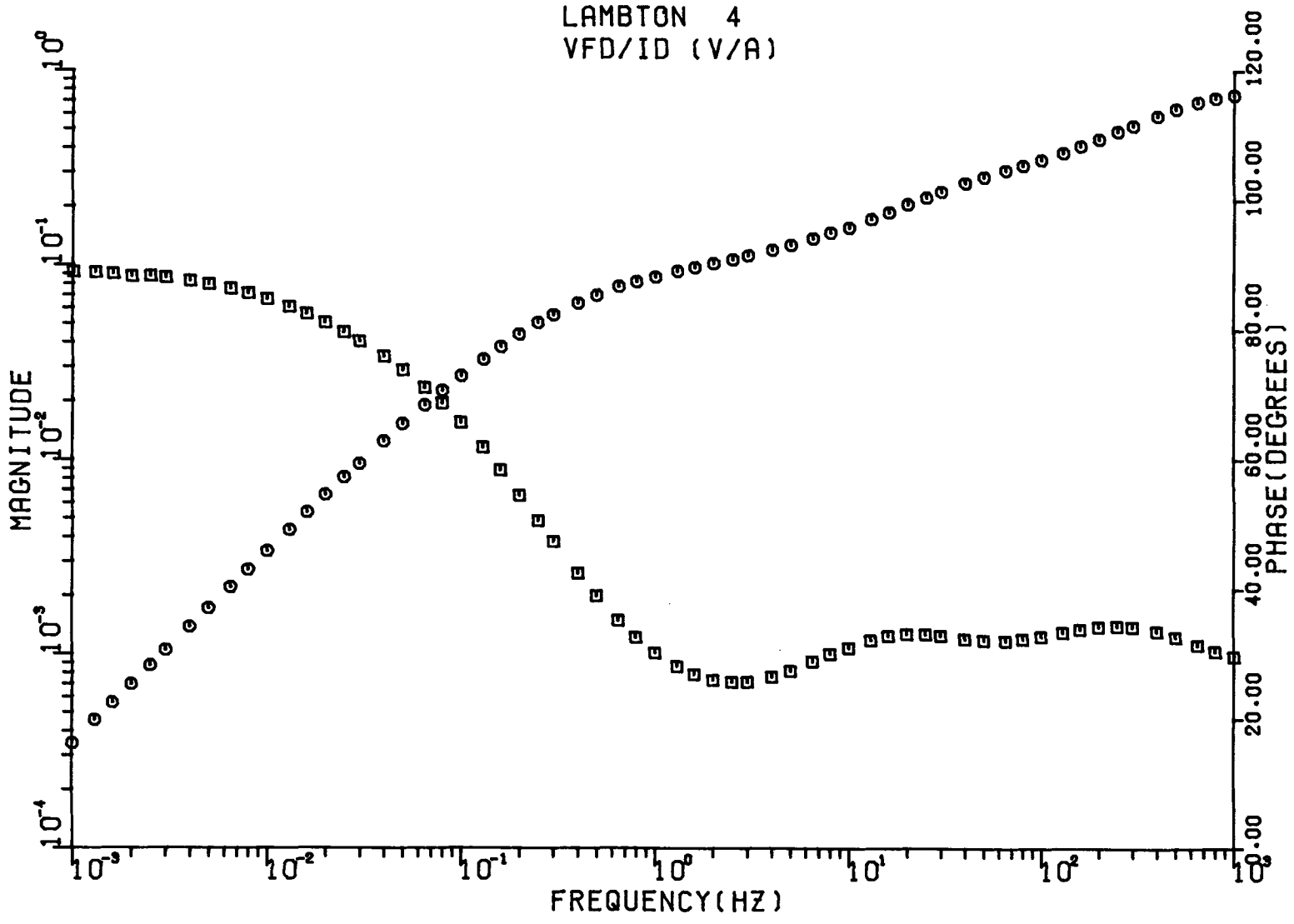

Figure 2-11. Lambton Stator-To-Field Transfer Impedance, Magnitude in V/A.

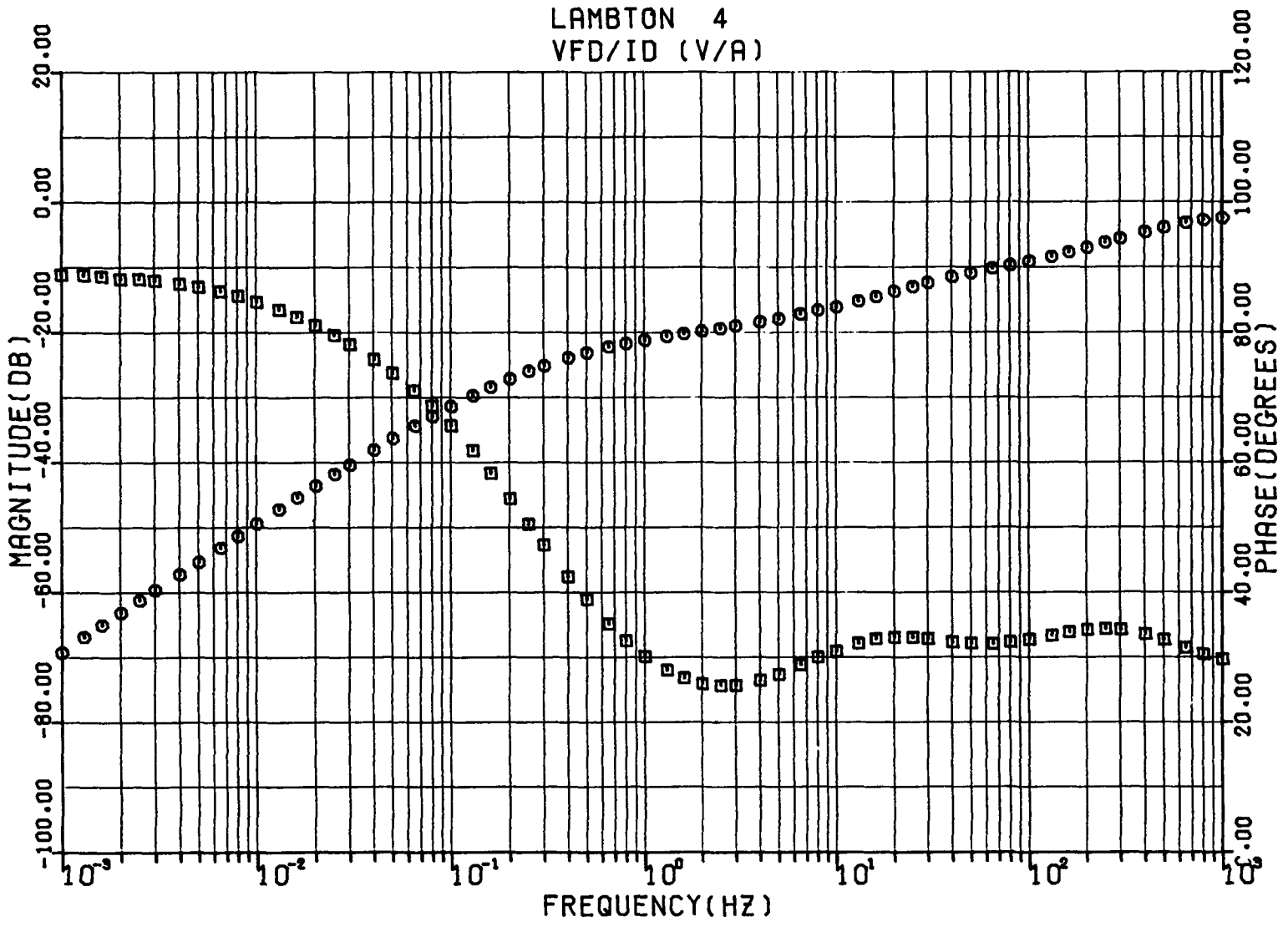

Figure 2-12. Lambton Stator-To-Field Transfer Impedance, Magnitude in dB Above 1 V/A.

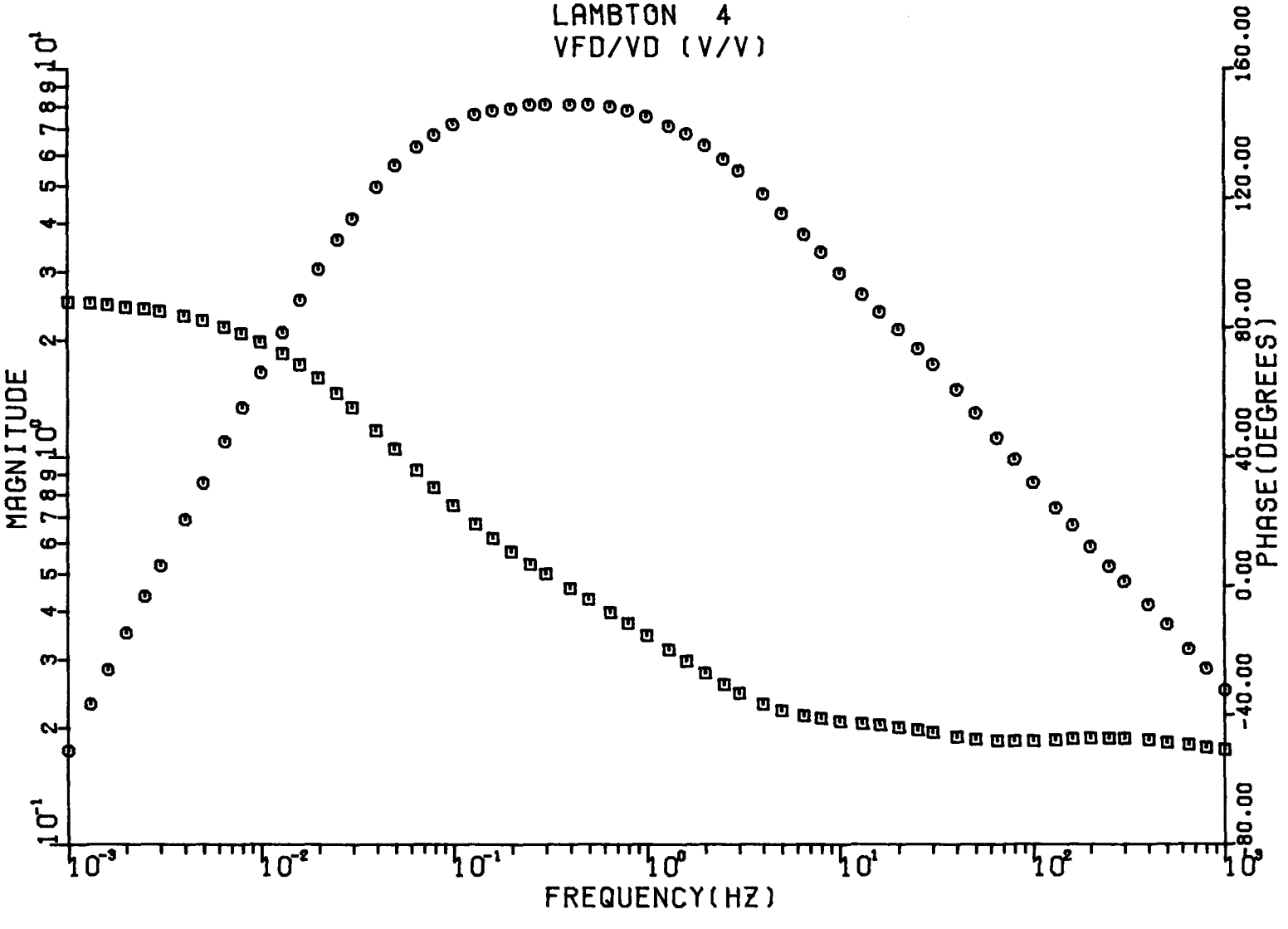

Figure 2-13. Lambton Open-Circuit Stator-To-Field Transfer Function, Magnitude in V/V.

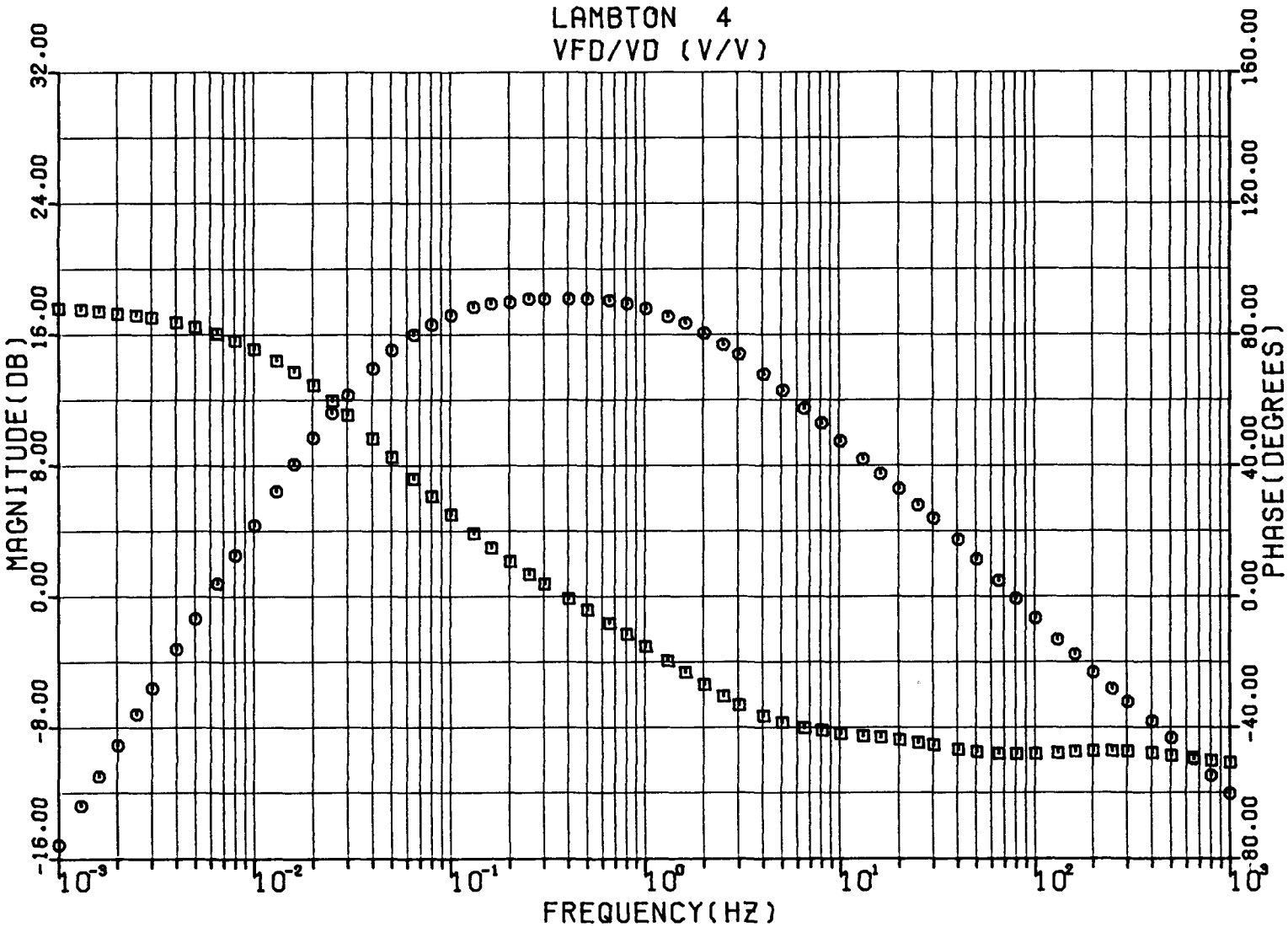

Figure 2-14. Lambton Open-Circuit Stator-To-Field Transfer Function, Magnitude in dB Above 1 V/V.

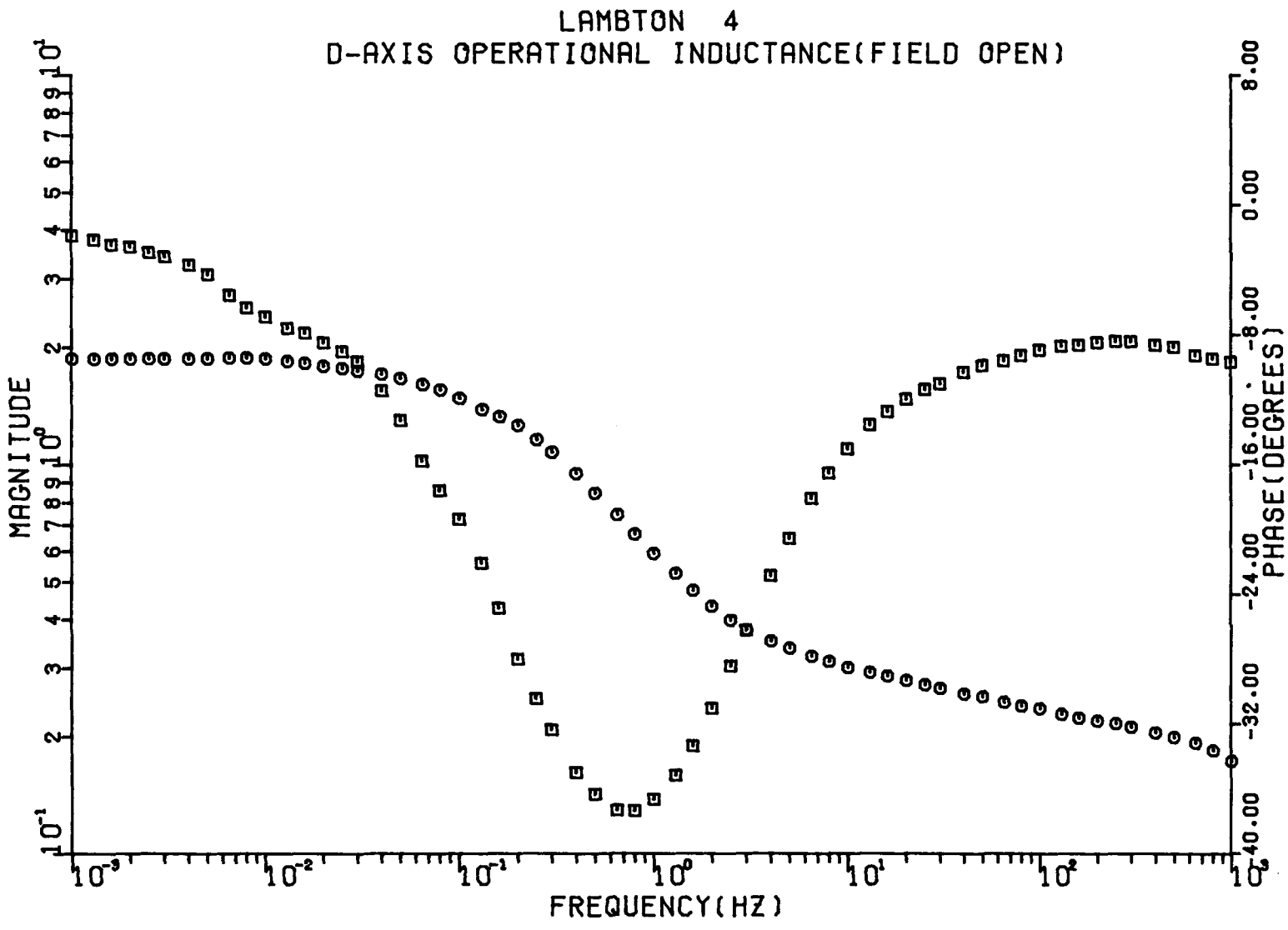

Figure 2-15. Lambton Open-Circuit Stator Driving Point Operational Inductance, Magnitude in pu.

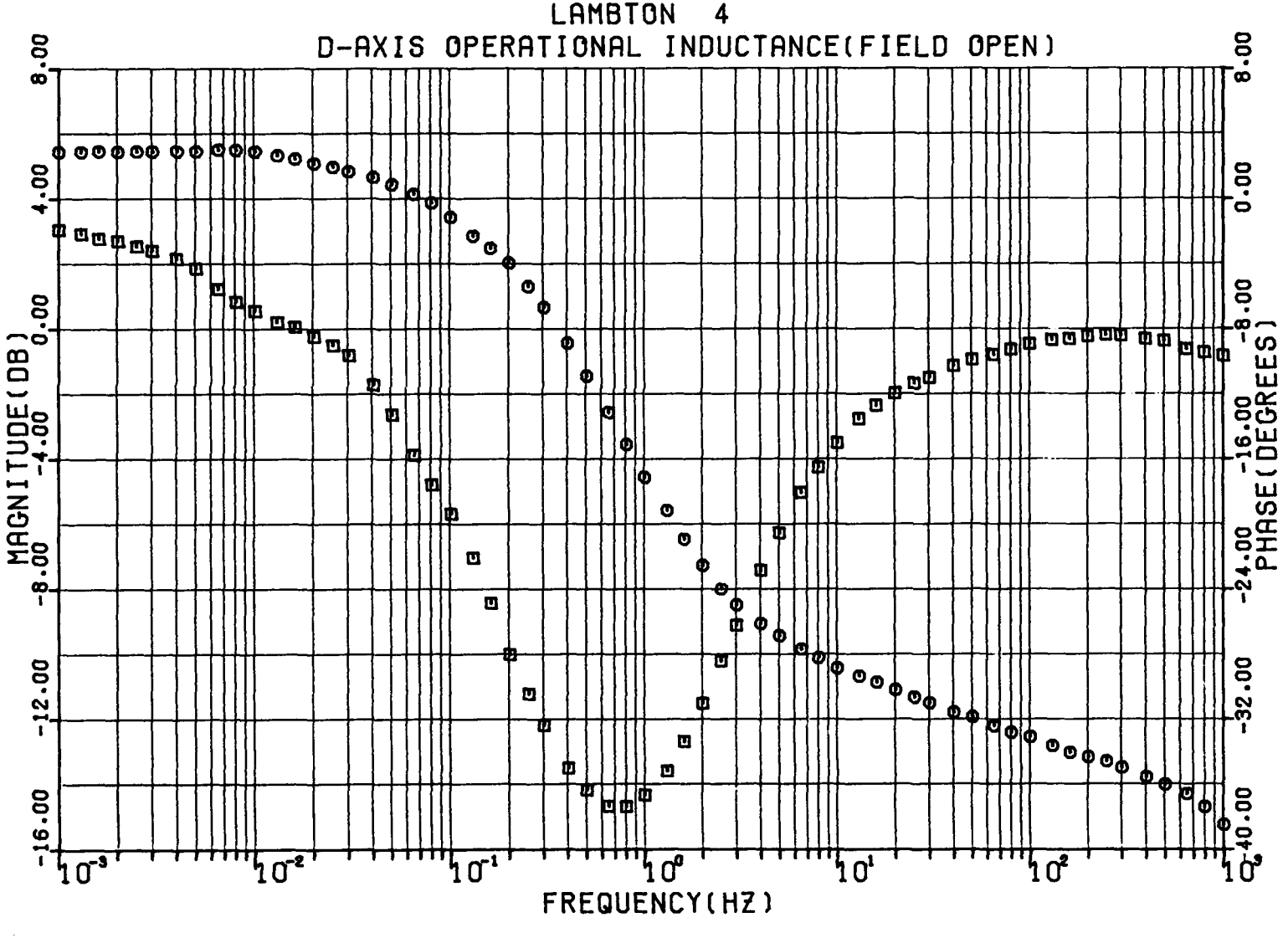

Figure 2-16. Lambton Open-Circuit Stator Driving Point Operational Inductance, Magnitude in dB Above 1 pu.

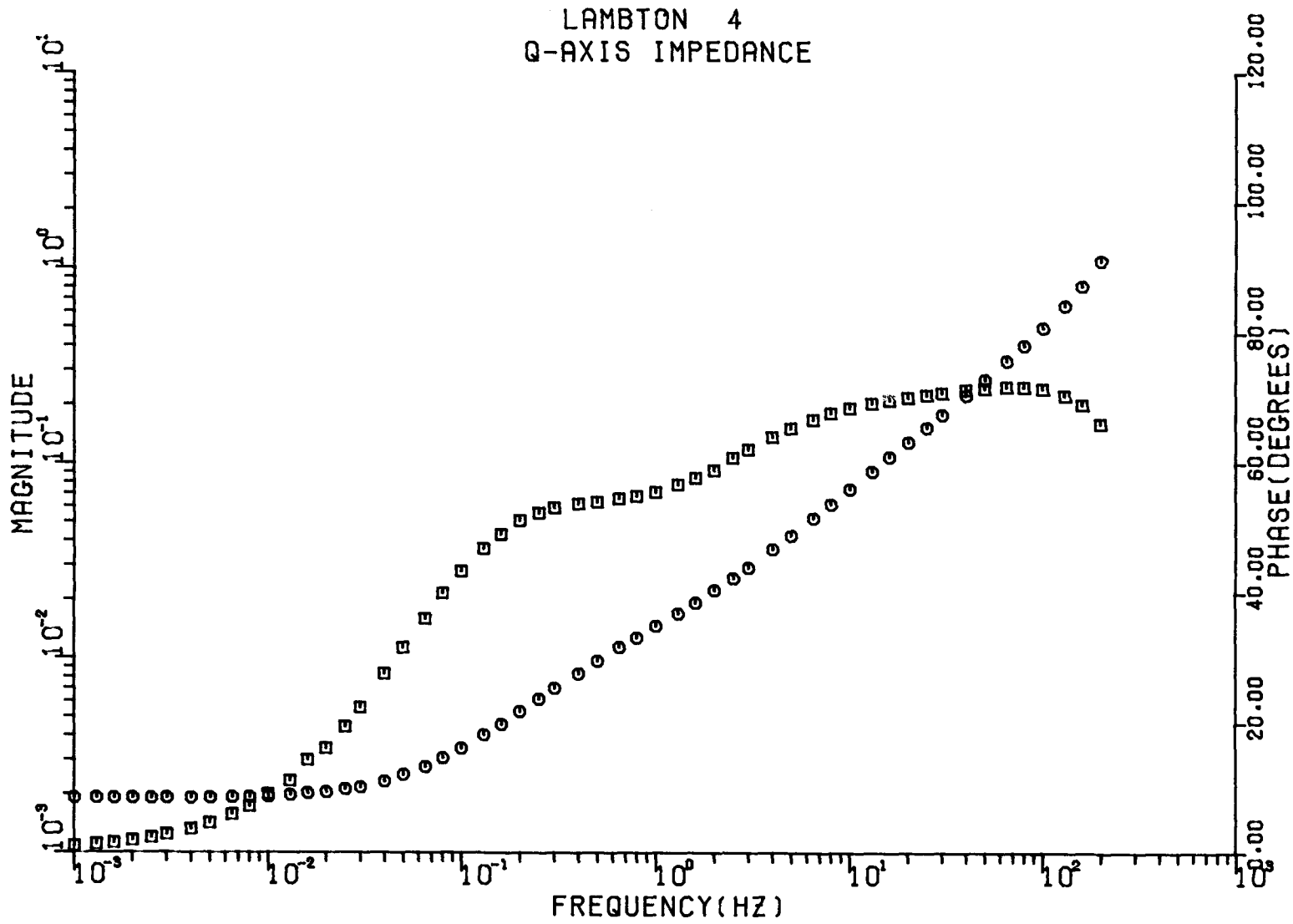

Figure 2-17. Lambton Quadrature Axis Operational Impedance, Magnitude in pu.

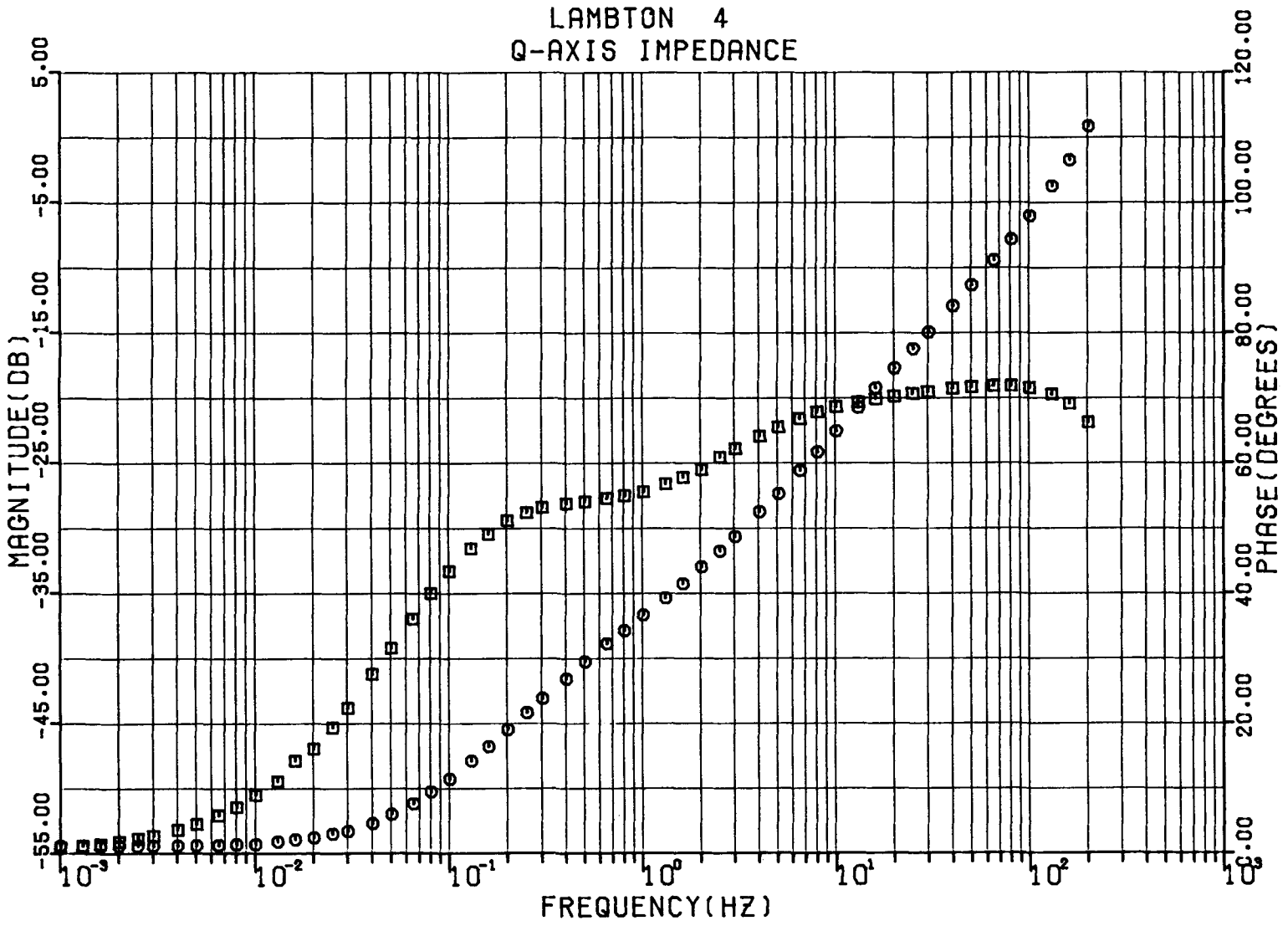

Figure 2-18. Lambton Quadrature Axis Operational Impedance, Magnitude in dB Above 1 pu.

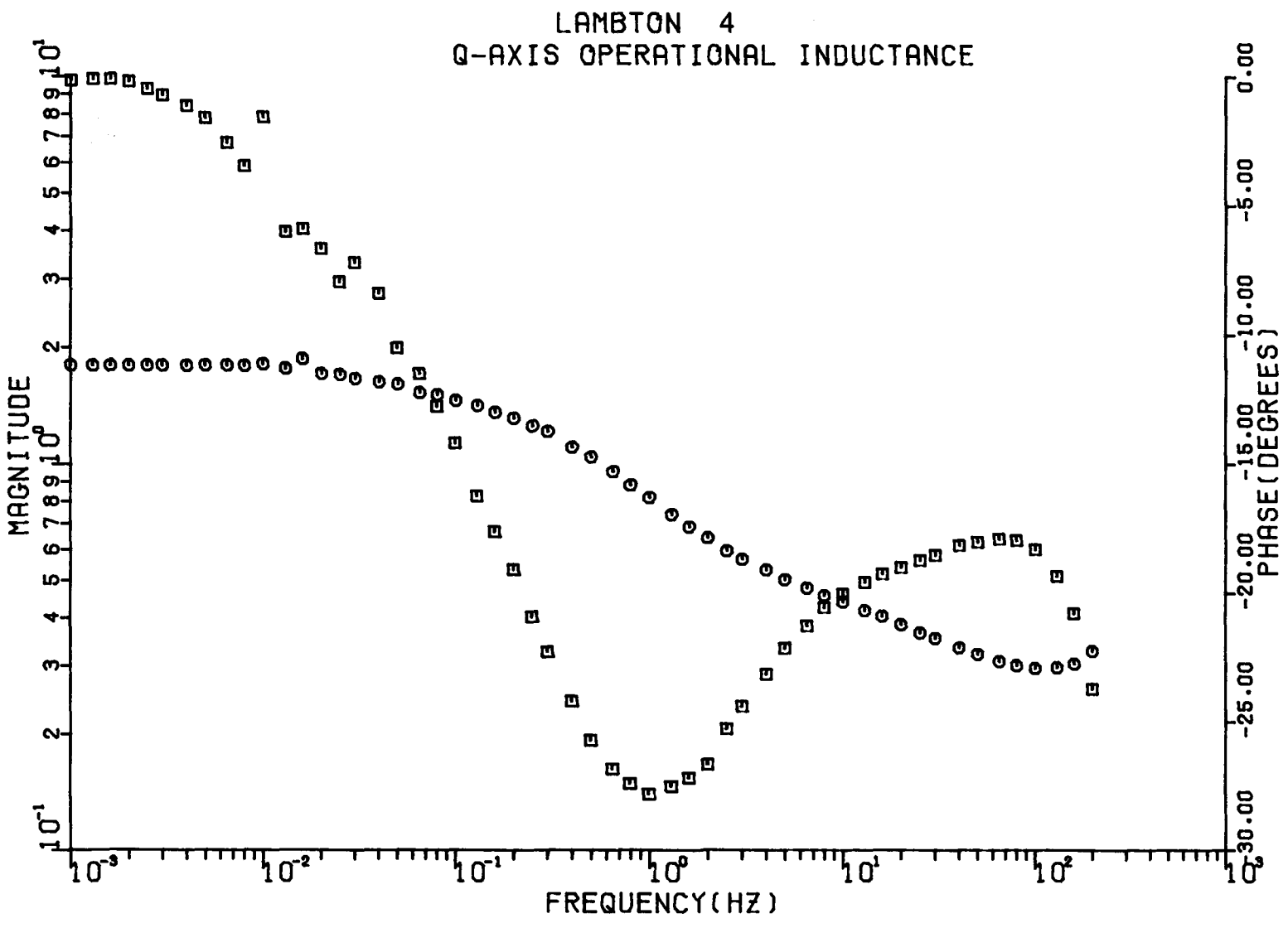

Figure 2-19. Lambton Quadrature Axis Operational Inductance, Magnitude in pu.

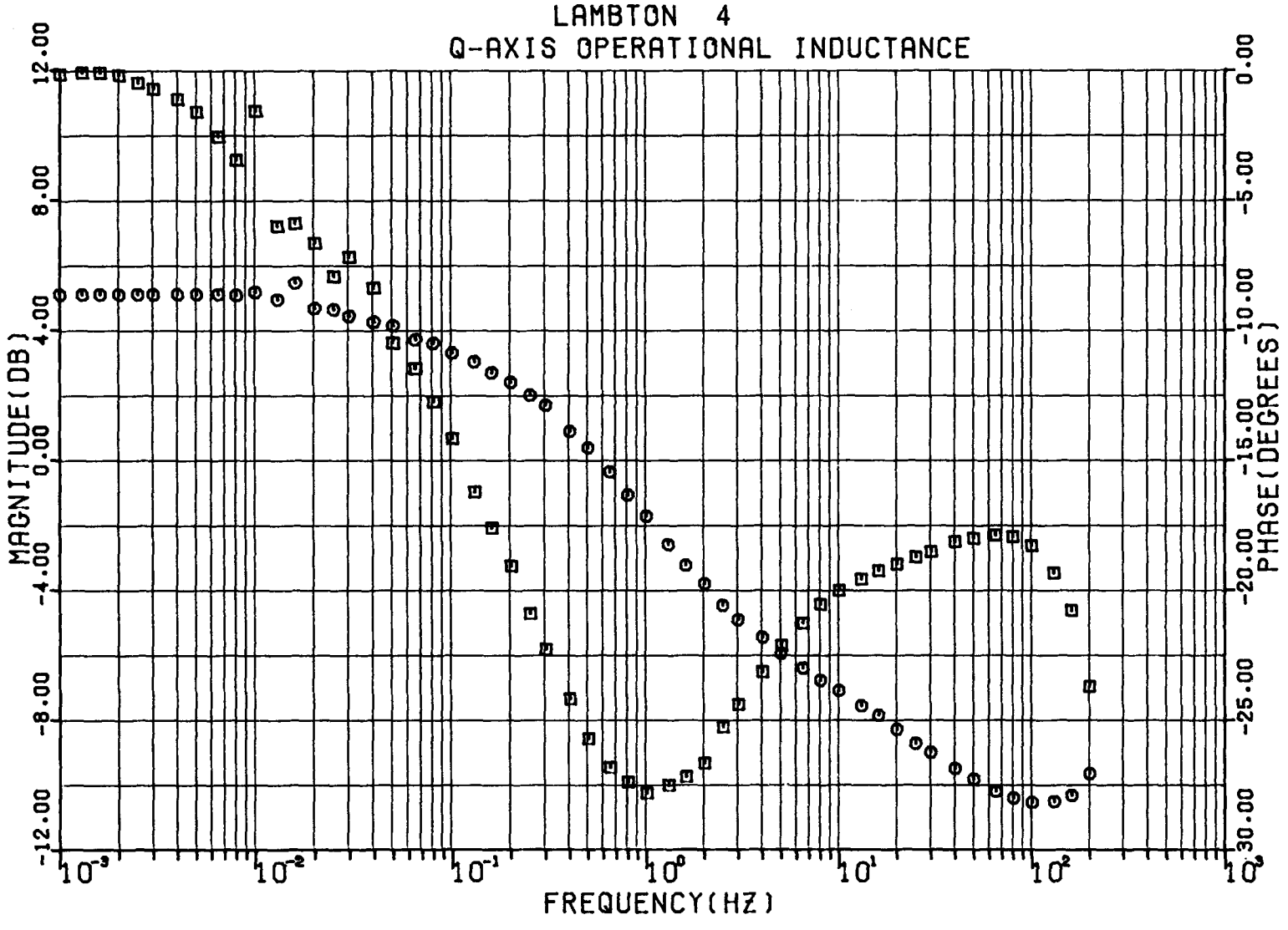

Figure 2-20. Lambton Quadrature Axis Operational Inductance, Magnitude in dB Above 1 pu.

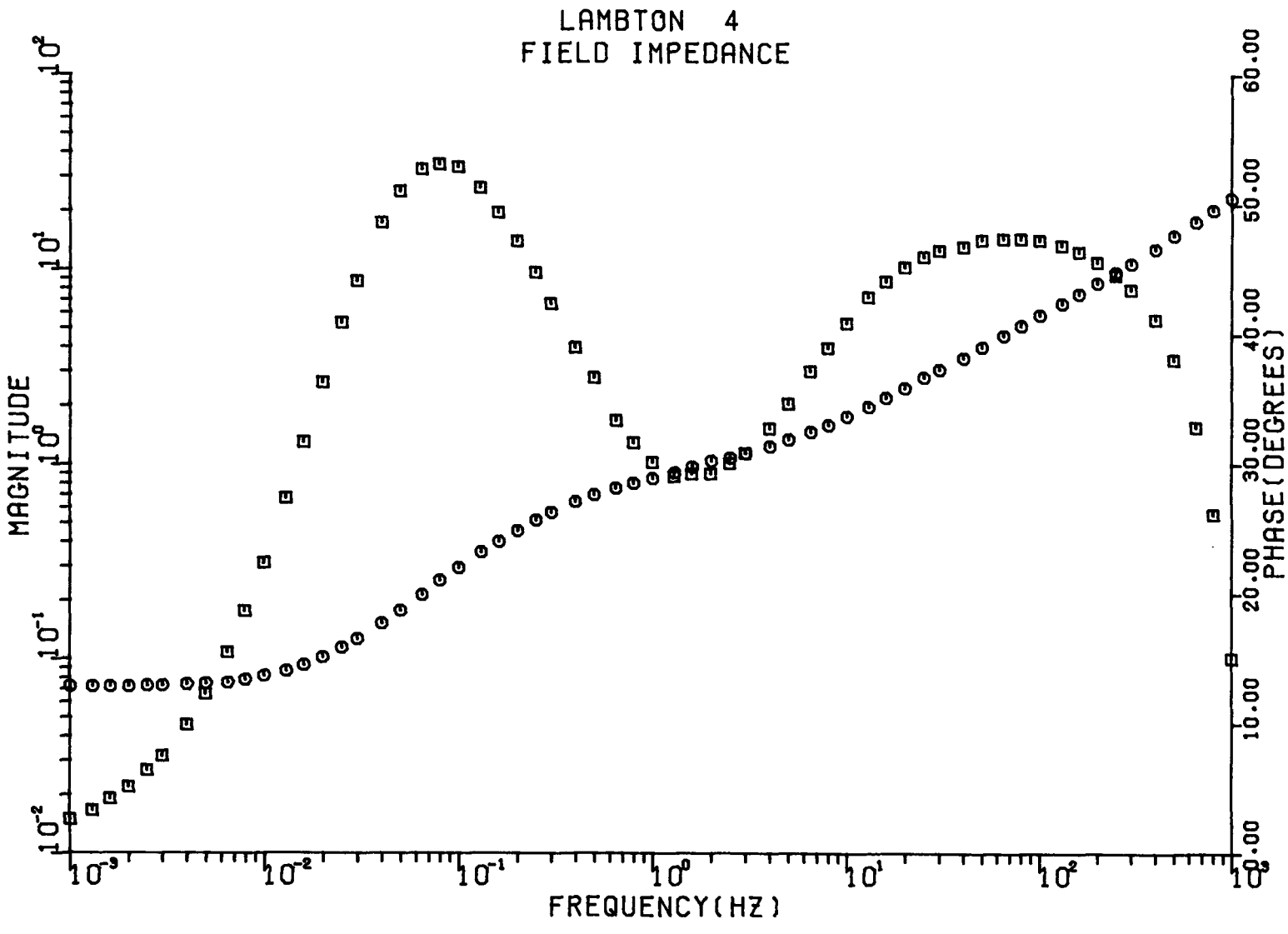

Figure 2-21. Lambton Open-Circuit Field Driving Point Impedance, Magnitude in Ohms.

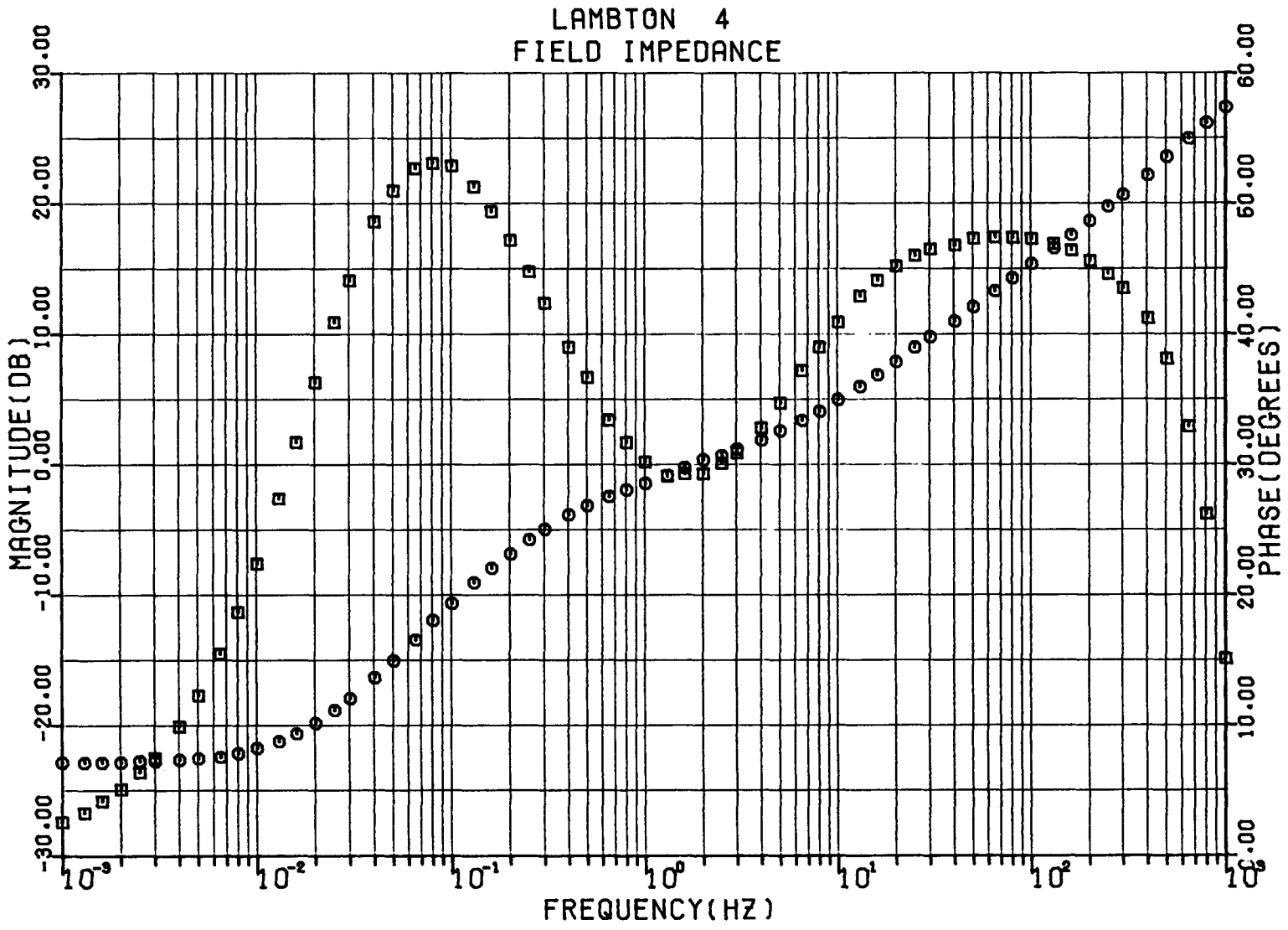

Figure 2-22. Lambton Open-Circuit Field Driving Point Impedance, Magnitude in dB Above 1 Ohm.

INDUCTANCE OF GENERATOR WINDINGS

The self and mutual inductances of various generator windings were measured with the rotor in two positions, using the direct current method described in Part 1, Section 2. All of the inductances quoted in Table 2-5 were measured by changing the level of direct current in the appropriate winding by approximately 100 A; i.e., alternating between ±50 A dc. In addition to these measurements of self and mutual inductances at essentially one level of flux density, the mutual inductance between the field winding and one phase of the stator winding was measured over a wide range of flux densities by using a motor-generator welding set to supply direct current to the field. Figure 2-23 is a plot of this mutual inductance as a function of field current. The peak-to-peak change in field current used to make each measurement was twice the value on the horizontal axis.

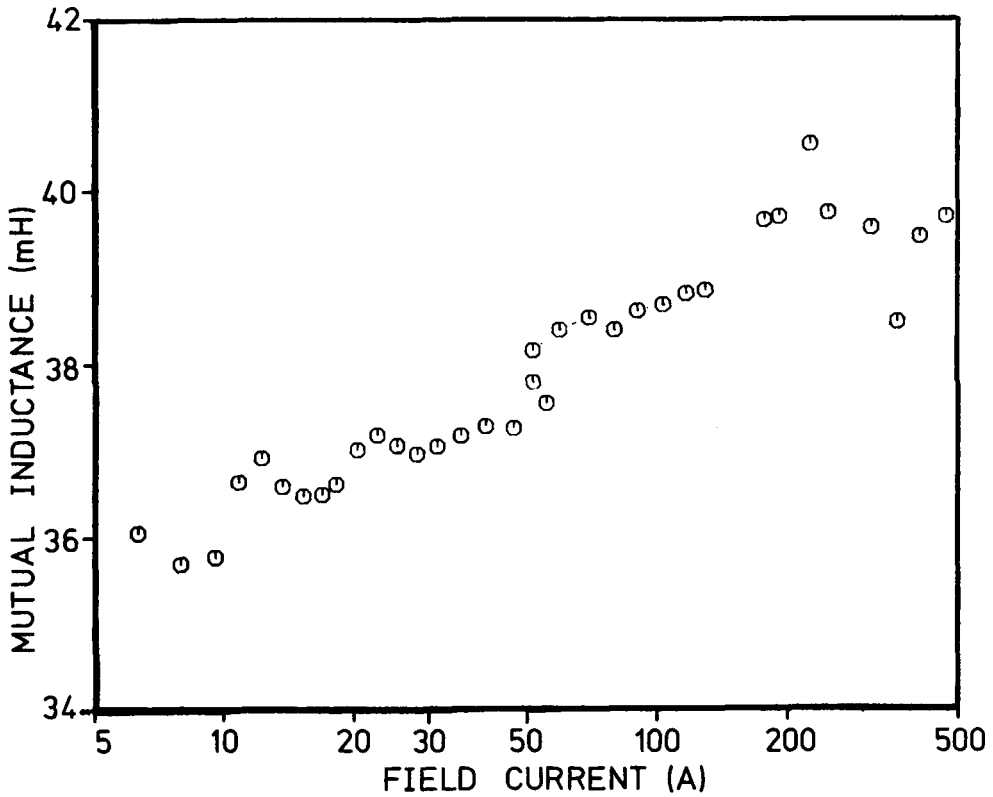

Figure 2-23. Lambton Mutual Inductance Between Field and Stator Windings.

Table 2-5

LAMBTON GENERATOR WINDING INDUCTANCES

Angle Between Phase a and Field	Flux Change Measured On	Winding Energized	Current Excursion (A)	Inductance Identification	Inductance (mH)
90	Phase b	Field	±40.0	L_{bf}	32.17
90	Phase c	Field	±40.0	L_{cf}	32.08
0	Field	Phase c	±58.0	L_{cf}	18.46
0	Field	Phase a	±57.5	L_{af}	36.33
0	Phase a	Field	±55.5	L_{af}	37.17
0	Phase b	Field	±55.5	L_{bf}	18.50
0	Phase b	Phase c	±58.5	L_{bc}	1.383
90	Phase b	Phase a	±59.0	L_{ab}	1.413
0	Phase a	Phase c	±58.5	L_{ac}	1.504
90	Phase b	Phase c	±59.0	L_{bc}	1.521
0	Phase a	Phase a	±59.0	L_{aa}	3.533
90	Phase a	Phase a	±33.5	L_{aa}	3.375
0	Phase c	Phase c	±58.5	L_{cc}	3.500
90	Phase c	Phase c	±33.5	L_{cc}	3.471
90	b to c	Phases b&c	±57.0	$2L_d$	10.058
0	b to c	Phases b&c	±59.5	$2L_q$	9.667
90	Field	Phases b&c	±56.5	1.73 L_{afd}	62.63
90	b to c	Field	±40.0	1.73 L_{afd}	64.17

60 HZ FIELD IMPEDANCE

The impedance at the terminals of the field winding was measured by the voltmeter-ammeter method with the rotor inside the stator bore, and the stator winding open. A range of 60 Hz currents between 0 and 32 A rms was supplied to the field from a variable autotransformer connected to the 208 V ac mains. Voltage, current, and active power input to the field winding were measured with portable standard meters (Table 2-6).

The non-linearity of this impedance is apparent from the V-A plot in Figure 2-24.

The input power measurements made it possible to separate the real and imaginary components of the impedance; these, as well as their polar counterparts are plotted against current in Figure 2-25.

Table 2-6

LAMBTON 60 HZ FIELD IMPEDANCE INSIDE STATOR

Voltage (V)	Current (A)	Power Active (W)	Power Reactive (VAR)	Impedance R (Ω)	Impedance X (Ω)	Impedance Z (Ω)	Angle (deg)
5.76	1.38	5.20	6.01	2.73	3.16	4.17	49.14
10.05	2.32	15.72	17.22	2.92	3.20	4.33	47.61
15.09	3.44	34.60	38.60	2.92	3.27	4.39	48.20
20.32	4.56	62.00	68.86	2.98	3.31	4.46	48.00
24.99	5.50	92.96	101.2	3.07	3.35	4.54	47.44
30.10	6.56	134.0	145.0	3.11	3.37	4.59	47.26
35.04	7.54	180.0	193.4	3.17	3.40	4.65	47.05
39.98	8.50	231.2	249.1	3.20	3.45	4.70	47.13
45.03	9.46	290.0	312.0	3.24	3.49	4.76	47.10
50.19	10.36	360.0	375.2	3.35	3.50	4.84	46.18
55.00	11.20	424.8	446.1	3.39	3.56	4.91	46.40
60.00	12.12	501.6	526.5	3.41	3.58	4.95	46.39
70.03	13.76	670.8	691.8	3.54	3.65	5.09	45.88
80.11	15.32	855.6	879.8	3.65	3.75	5.23	45.80
89.99	16.84	1058.	1085.	3.73	3.82	5.34	45.70
100.08	18.24	1288.	1294.	3.87	3.89	5.49	45.12
100.18	18.40	1291.	1316.	3.81	3.89	5.44	45.54
110.05	19.60	1528.	1522.	3.98	3.96	5.61	44.90
120.18	20.70	1789.	1729.	4.18	4.03	5.81	44.02
129.96	21.80	2060.	1945.	4.33	4.09	5.96	43.36
140.17	22.85	2355.	2171.	4.51	4.16	6.13	42.67
150.09	23.95	2650.	2429.	4.62	4.23	6.27	42.51
160.07	24.80	2958.	2647.	4.81	4.30	6.45	41.83
170.02	25.70	3288.	2878.	4.98	4.36	6.62	41.19
180.15	26.70	3630.	3156.	5.09	4.43	6.75	41.00
190.17	27.55	3978.	3409.	5.24	4.49	6.90	40.60
199.9	28.60	4398.	3653.	5.38	4.47	6.99	39.71
210.5	29.60	4816.	3953.	5.50	4.51	7.11	39.38
220.0	30.45	5201.	4222.	5.61	4.55	7.22	39.07
230.0	31.30	5624.	4494.	5.74	4.59	7.35	38.63
239.5	32.00	6000.	4768.	5.86	4.66	7.48	38.47

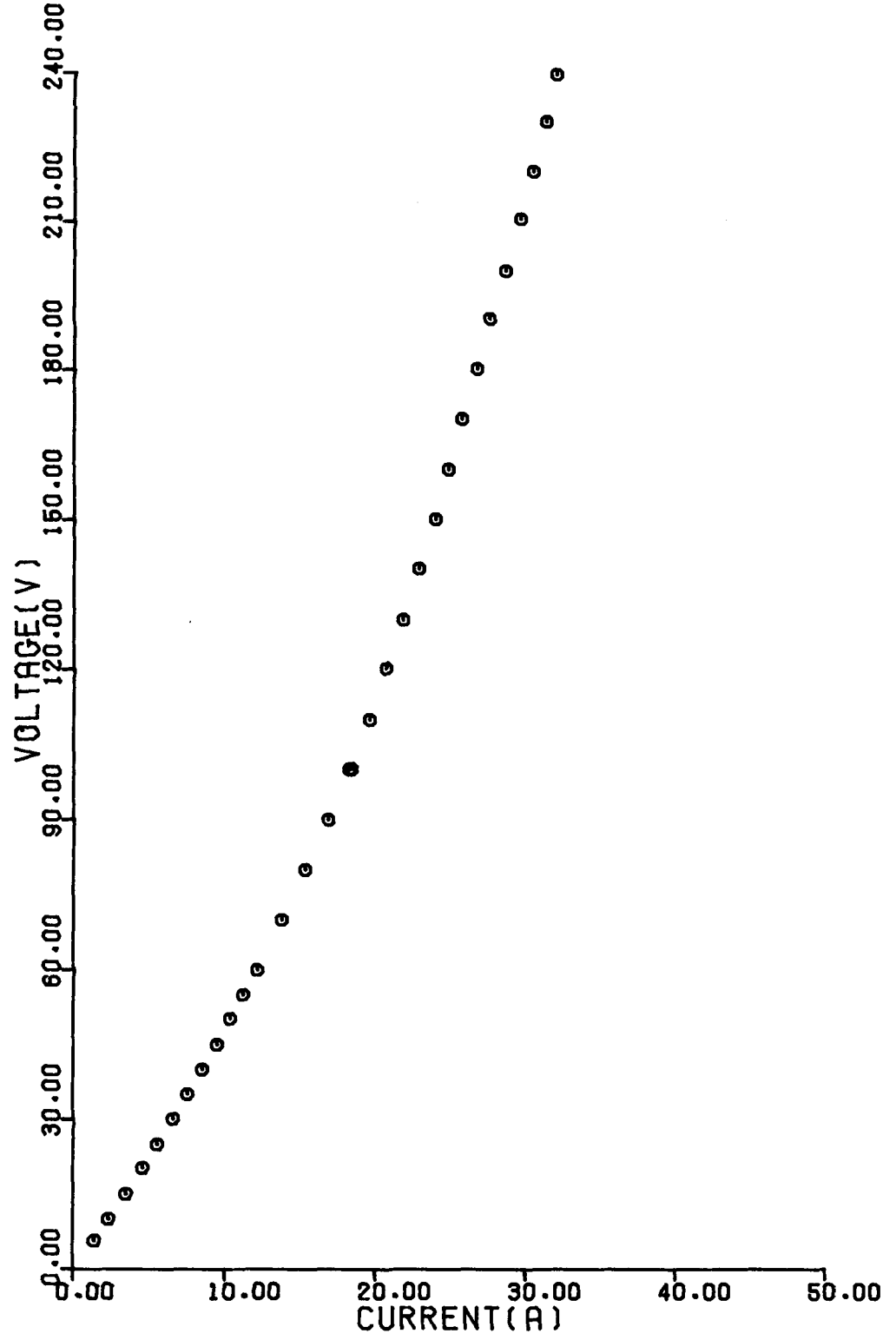

Figure 2-24. V-A Characteristic of Lambton 60 Hz Field Impedance.

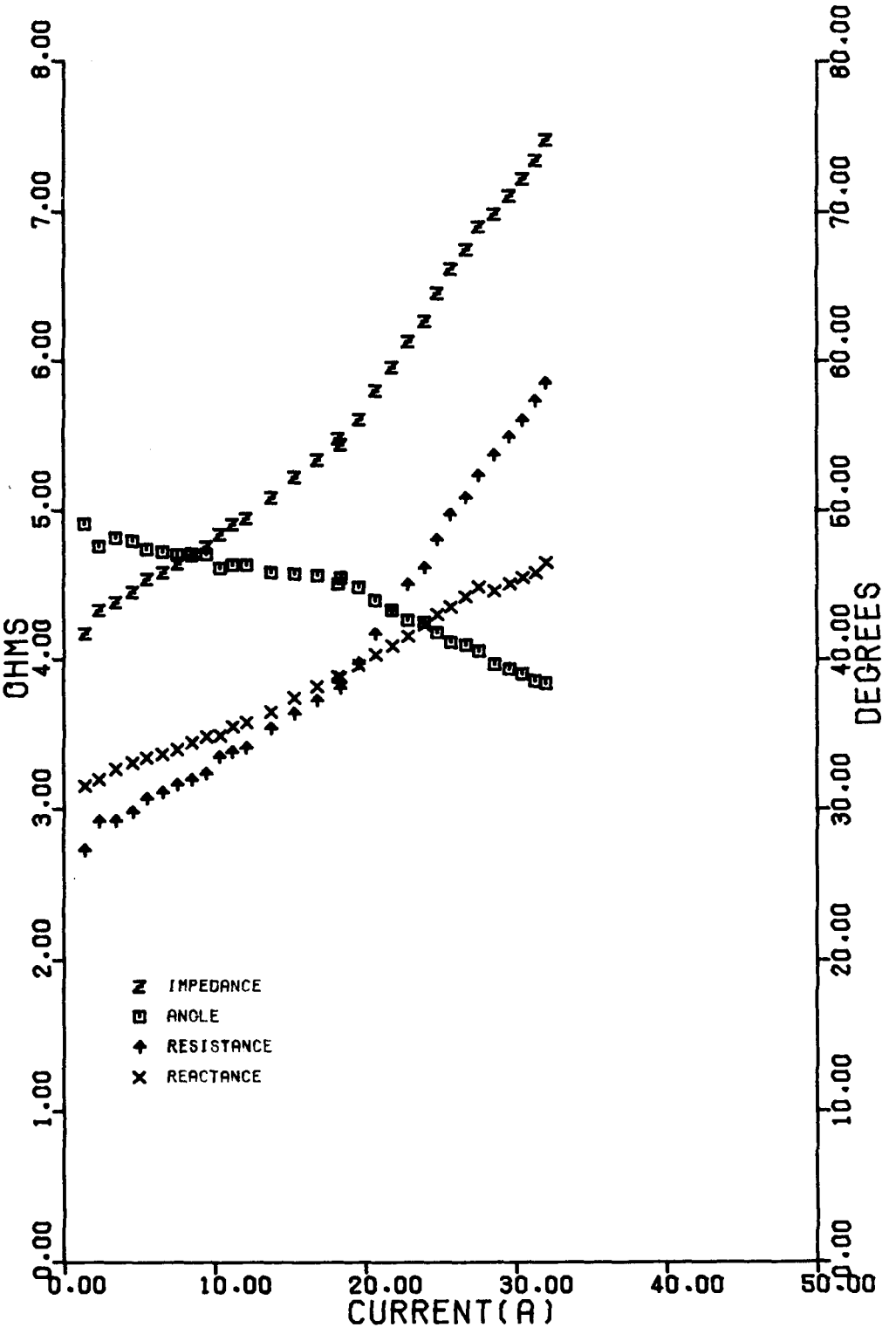

Figure 2-25. Components of Lambton 60 Hz Field Impedance.

Section 3

LINE SWITCHING TESTS

INTRODUCTION

On October 1, 1978, a series of line switching tests was done on Unit 1 at the Lambton Generating Station. The purpose of these tests was to measure the response of a Lambton generator to a large transient; these records formed the standard by which the performance of generator models derived from other tests was judged.

SYSTEM ARRANGEMENT

The first set of tests was done with a balanced arrangement. The G1 generator was connected radially to the rest of the power system via two identical lines (Figure 3-1). Transients were produced by opening one of these lines and closing it one minute later.

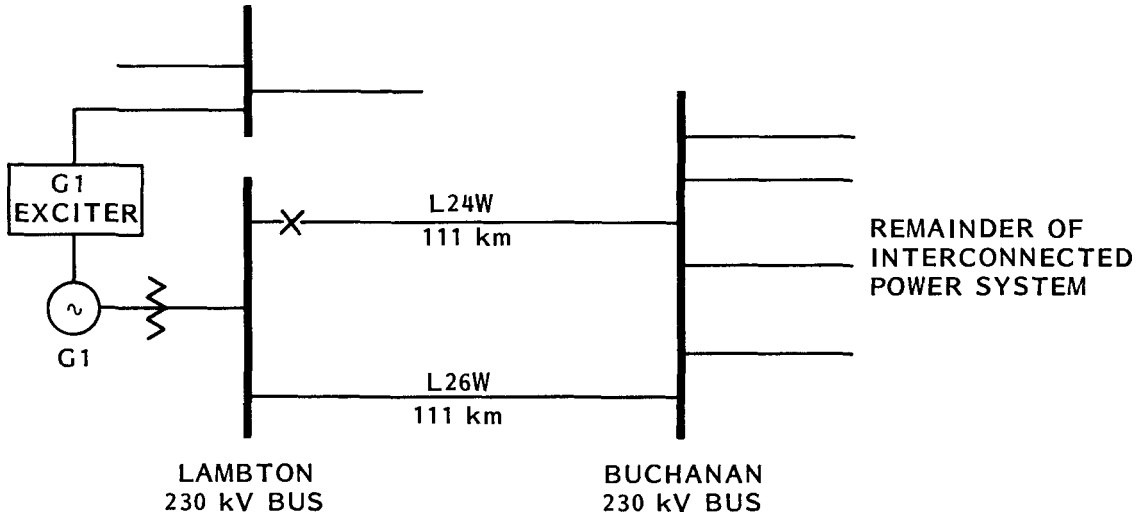

Figure 3-1. Balanced System Set-Up.

A second group of tests was done from an unbalanced set-up. This time, G1 was connected to the rest of the power system by two lines of different length (Figure 3-2). The test operations consisted of opening and closing the shorter line.

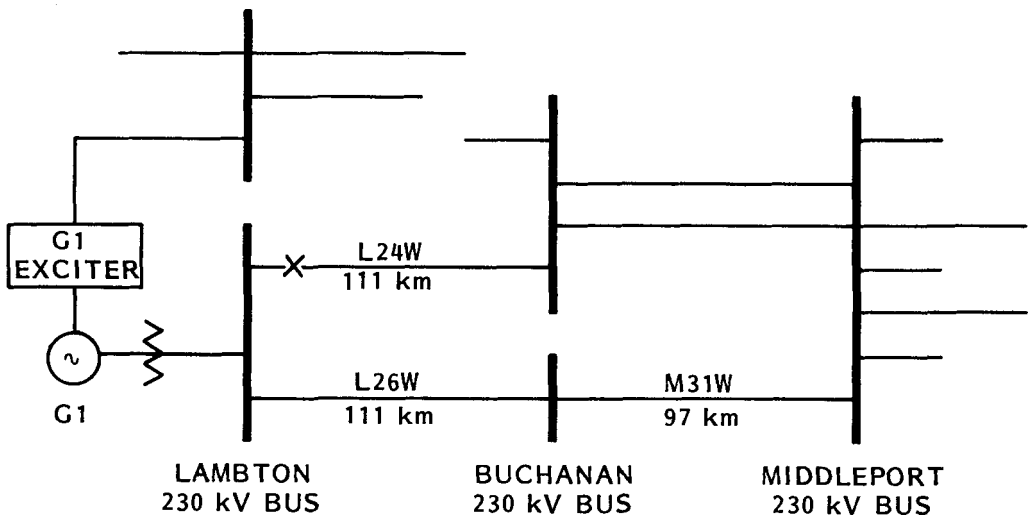

Figure 3-2. Unbalanced System Set-Up.

For all tests, the G1 exciter was supplied from the 230 kV station bus, as electrically remote from the G1 terminals as possible. Any governor action during the tests was precluded by an appropriate setting of the generator load limiter.

TEST OPERATIONS

Table 3-1 is a summary of the switching operations and the respective system conditions.

Table 3-1

LAMBTON LINE SWITCHING TESTS

Test No	Transmission Lines From G1 To System	G1 Generator Conditions Voltage Regulator	Load MW	MVAR	kV	Operation On L24W
1	Balanced	Automatic	350	36	23.9	Open
2	Balanced	Automatic	350	58	23.9	Close
3	Balanced	Manual	351	26	23.7	Open
4	Balanced	Manual	349	31	22.8	Close
5	Unbalanced	Automatic	495	92	24.0	Open
6	Unbalanced	Automatic	494	145	24.0	Close
7	Unbalanced	Manual	492	92	24.1	Open
8	Unbalanced	Manual	493	140	22.8	Close

In the "manual" mode, the voltage regulator acts to maintain constant field voltage. The "automatic" mode implies both regulation of the generator terminal voltage, and shaft acceleration through modulation of the field voltage by a power system stabilizer.

INSTRUMENTATION

Figure 3-3 is a block diagram of the instrumentation for the line switching tests. Each variable was converted to a dc voltage proportional to its primary value, biased to zero at the operating point, and filtered before being recorded. The filtering for each channel was identical---a sixth order Butterworth low pass filter with the following transfer function:

$$\frac{V_{out}}{V_{in}} = \frac{1}{(1+.0155s+.0012s^2+.000000477s^3)^2}$$

The magnitude characteristic of this filter is flat to 10 Hz. The following generator variables were recorded directly on a hot pen oscillograph: shaft speed, field voltage, field current, terminal voltage, reactive power, and active power.

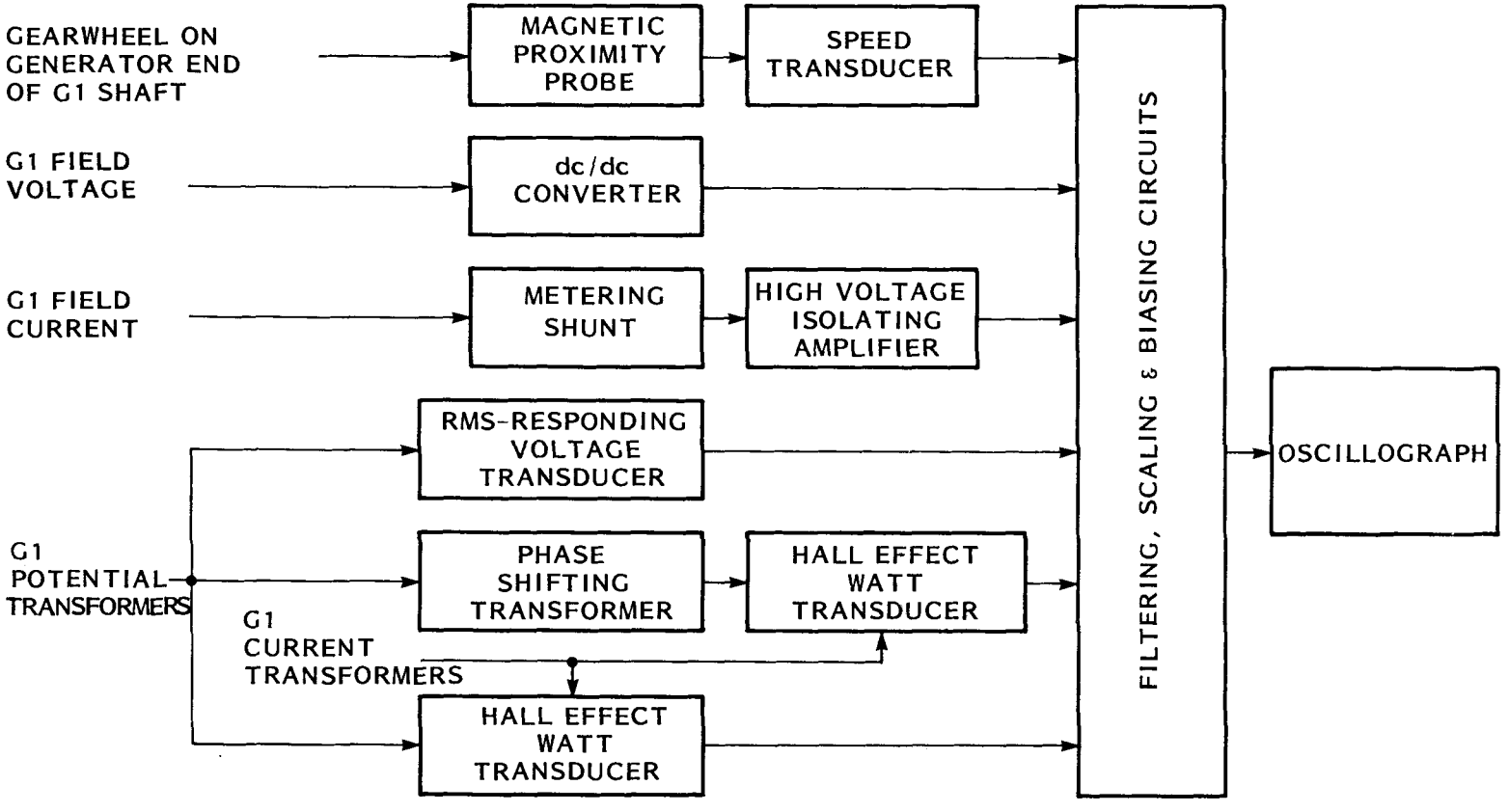

Figure 3-3. Instrumentation for Lambton Line Switching Tests.

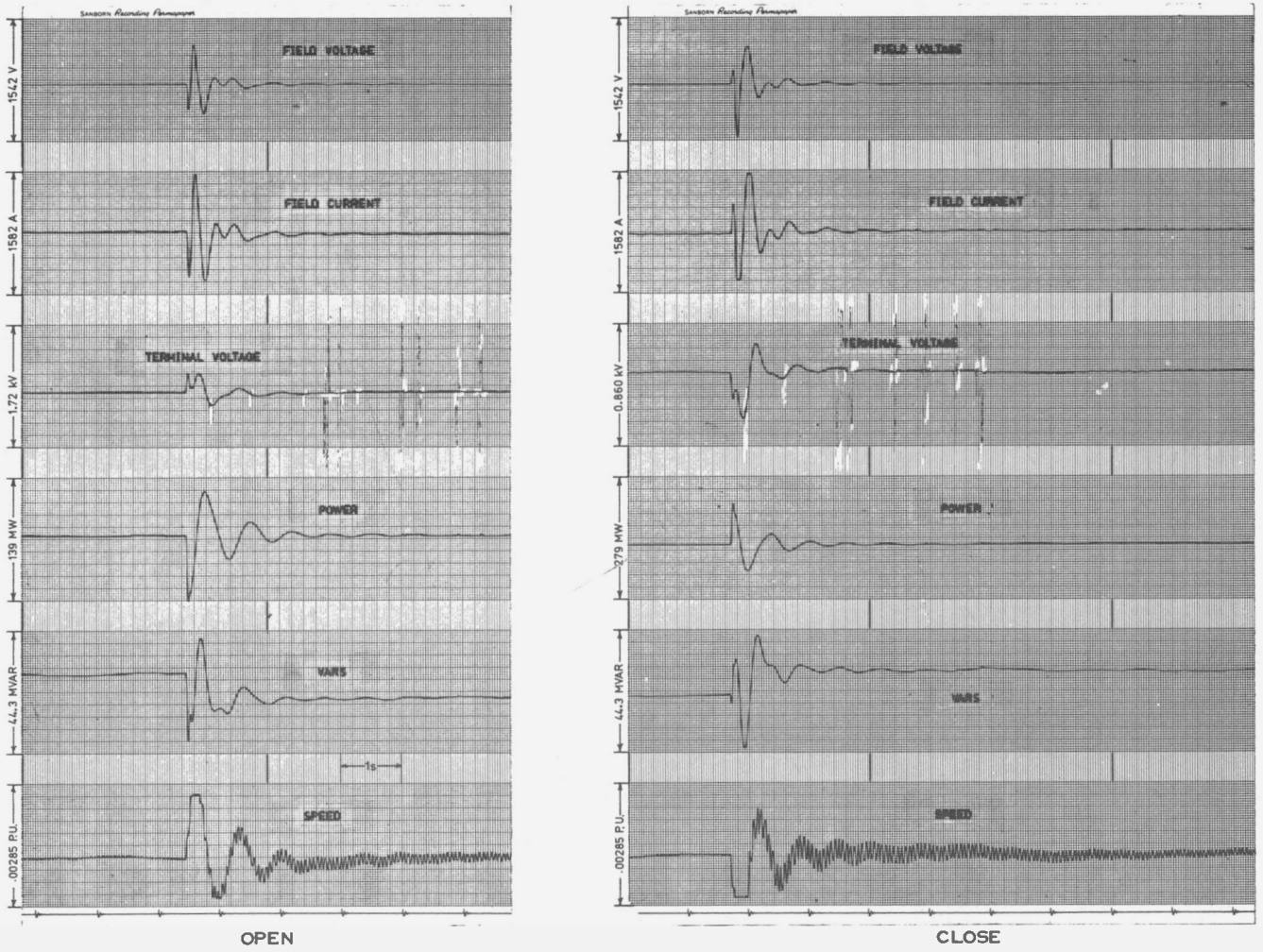

Figure 3-3. Nanticoke Line Switching Test 1, Oscillogram of Generator Variables.

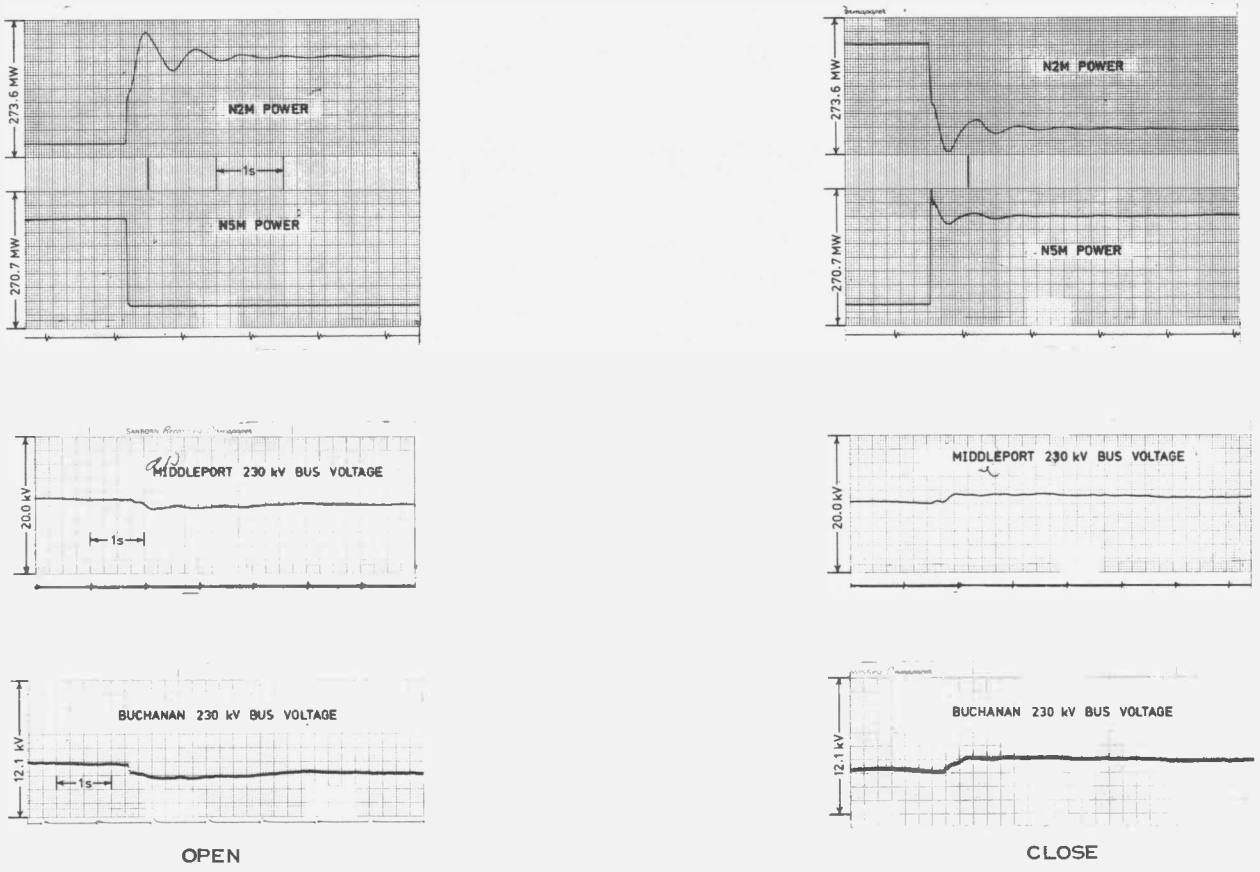

SWITCH LONG LINE (N5M)
VOLTAGE REGULATOR ON AUTO AND STABILIZER IN SERVICE

Figure 3-4. Nanticoke Line Switching Test 1, Oscillogram of External System Variables.

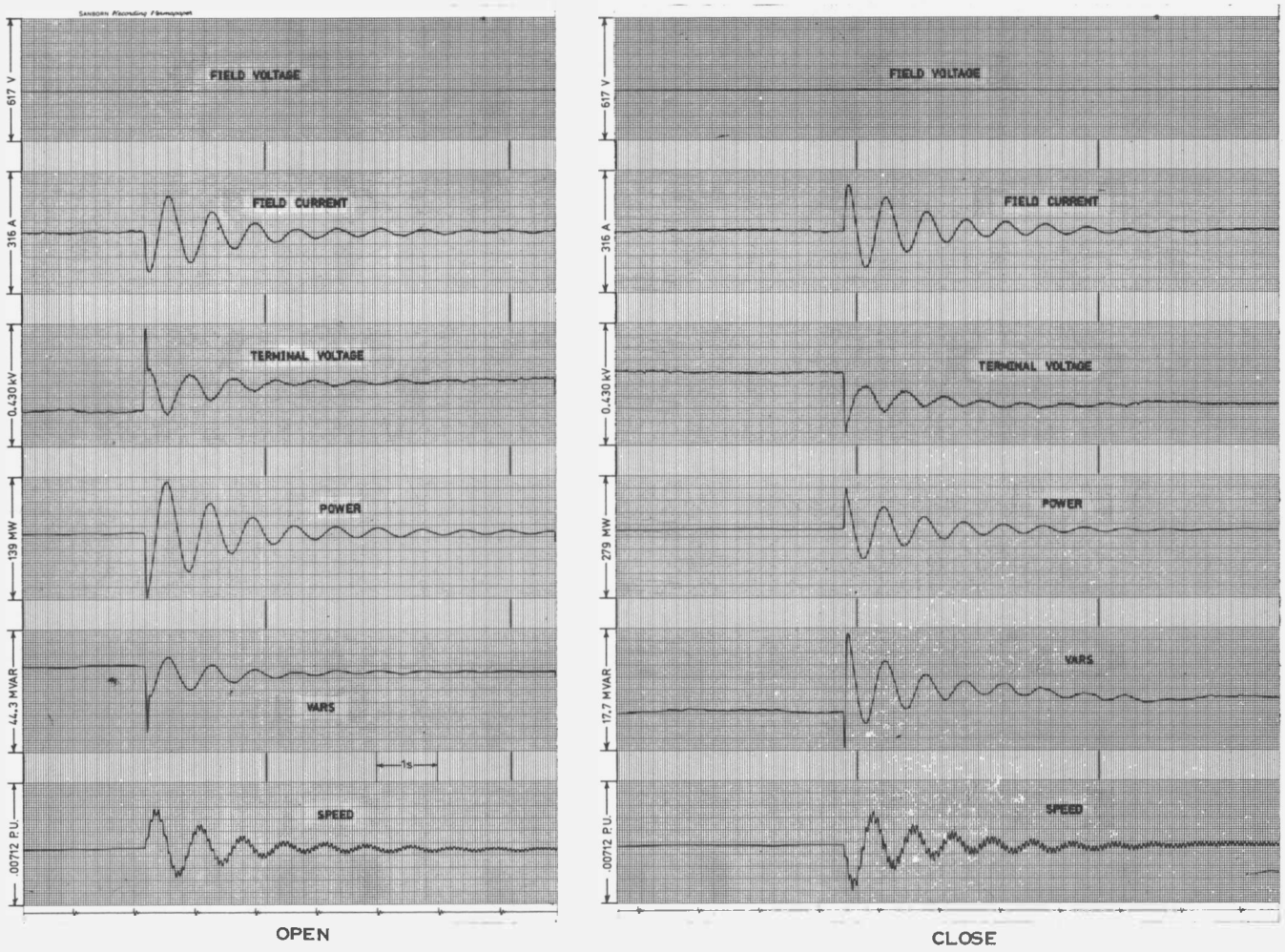

Figure 3-5. Nanticoke Line Switching Test 2, Oscillogram of Generator Variables.

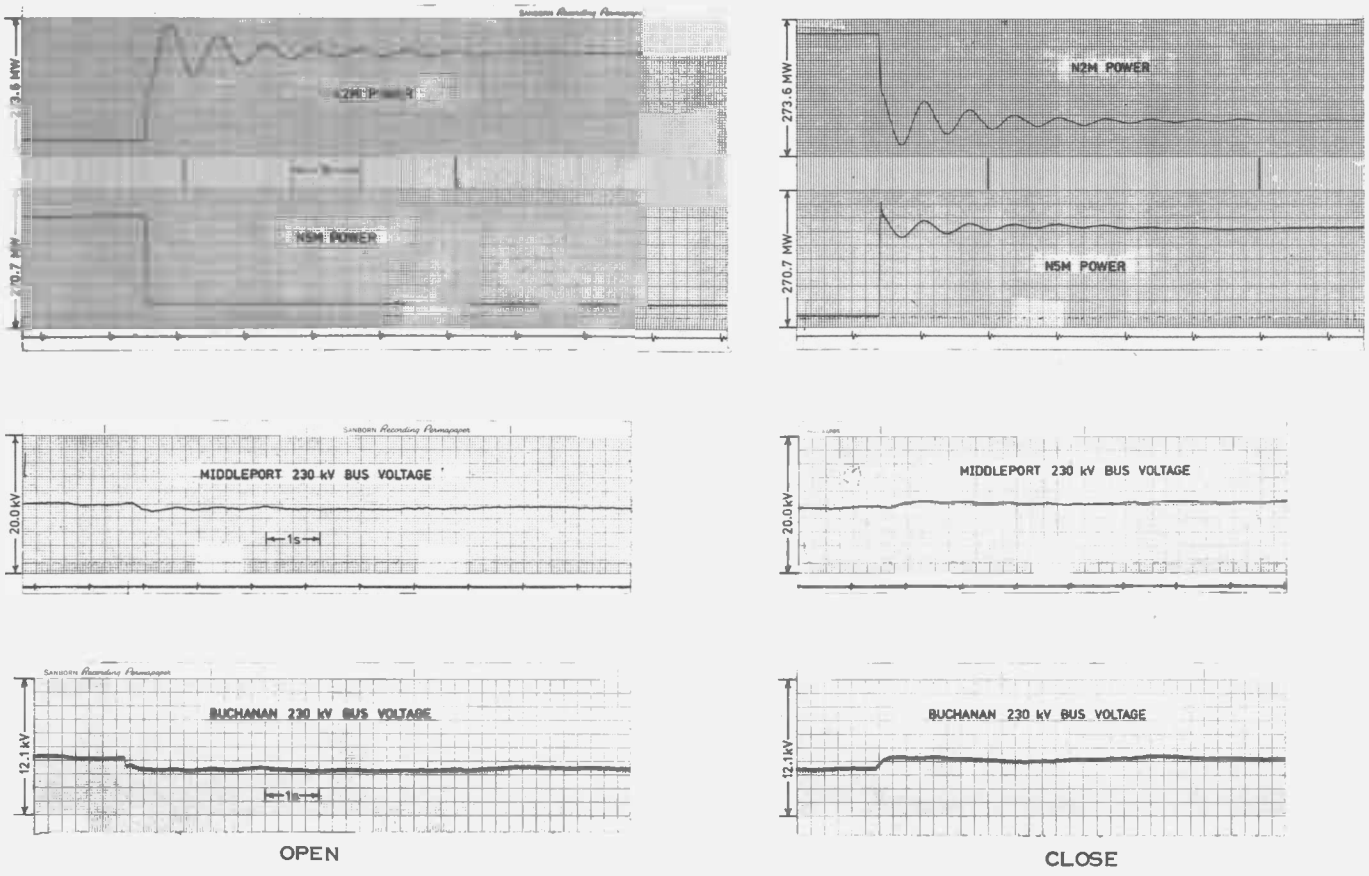

Figure 3-6. Nanticoke Line Switching Test 2, Oscillograms of External System Variables.

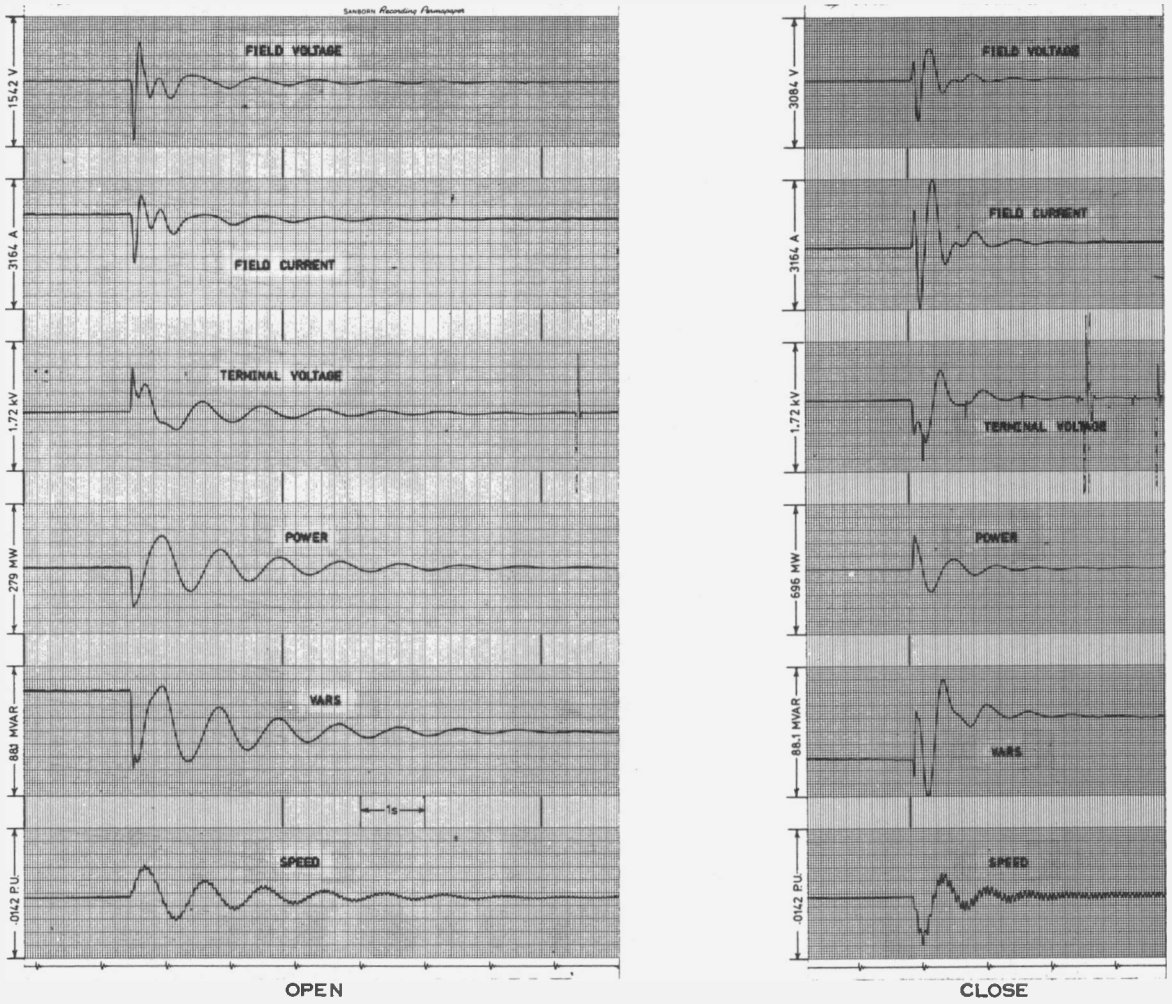

SWITCH SHORT LINE (N2M)
VOLTAGE REGULATOR ON AUTO AND STABILIZER IN SERVICE

Figure 3-7. Nanticoke Line Switching Test 3, Oscillograms of Generator Variables.

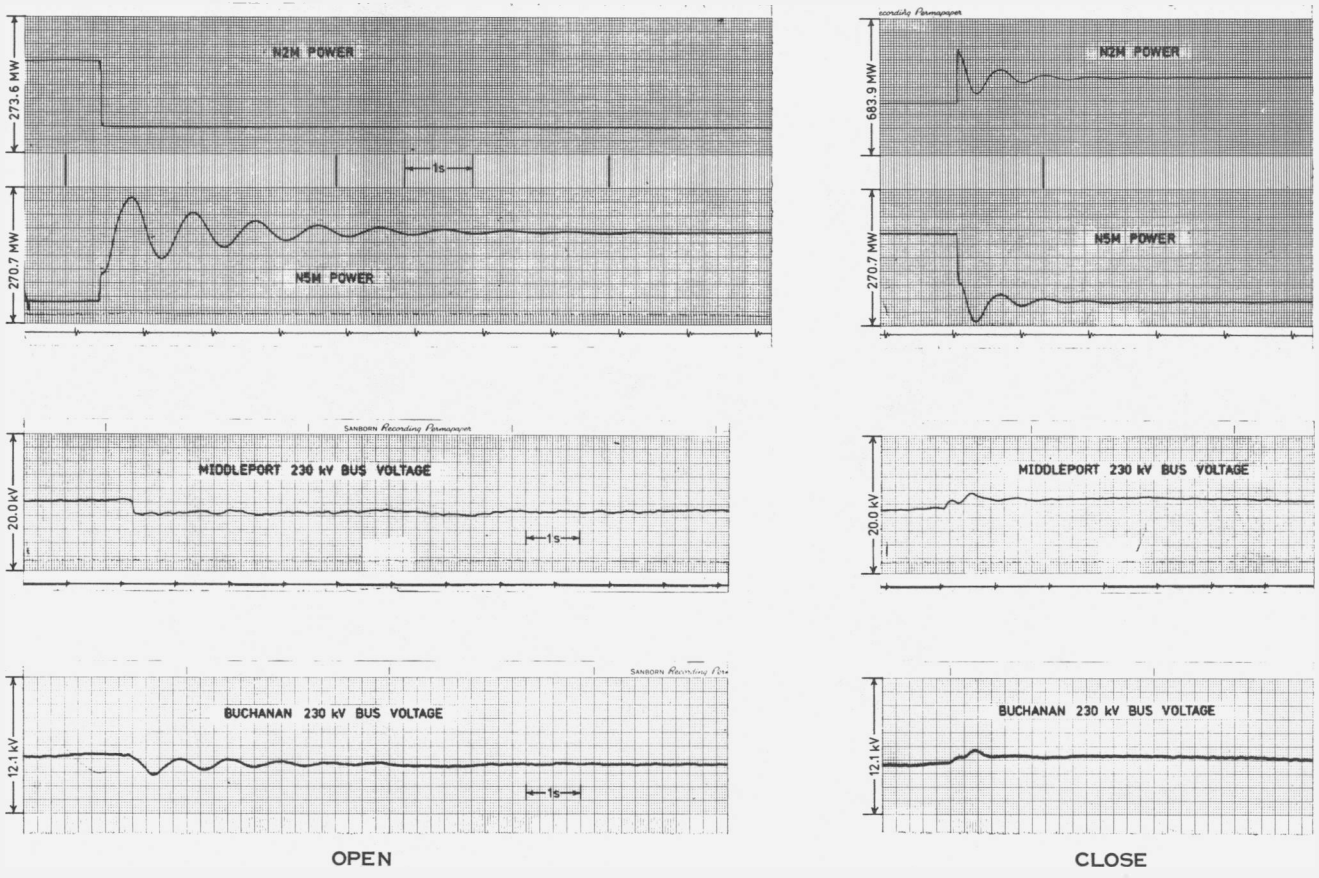

SWITCH SHORT LINE (N2M)
VOLTAGE REGULATOR ON AUTO AND STABILIZER IN SERVICE

Figure 3-8. Nanticoke Line Switching Test 3, Oscillograms of External System Variables.

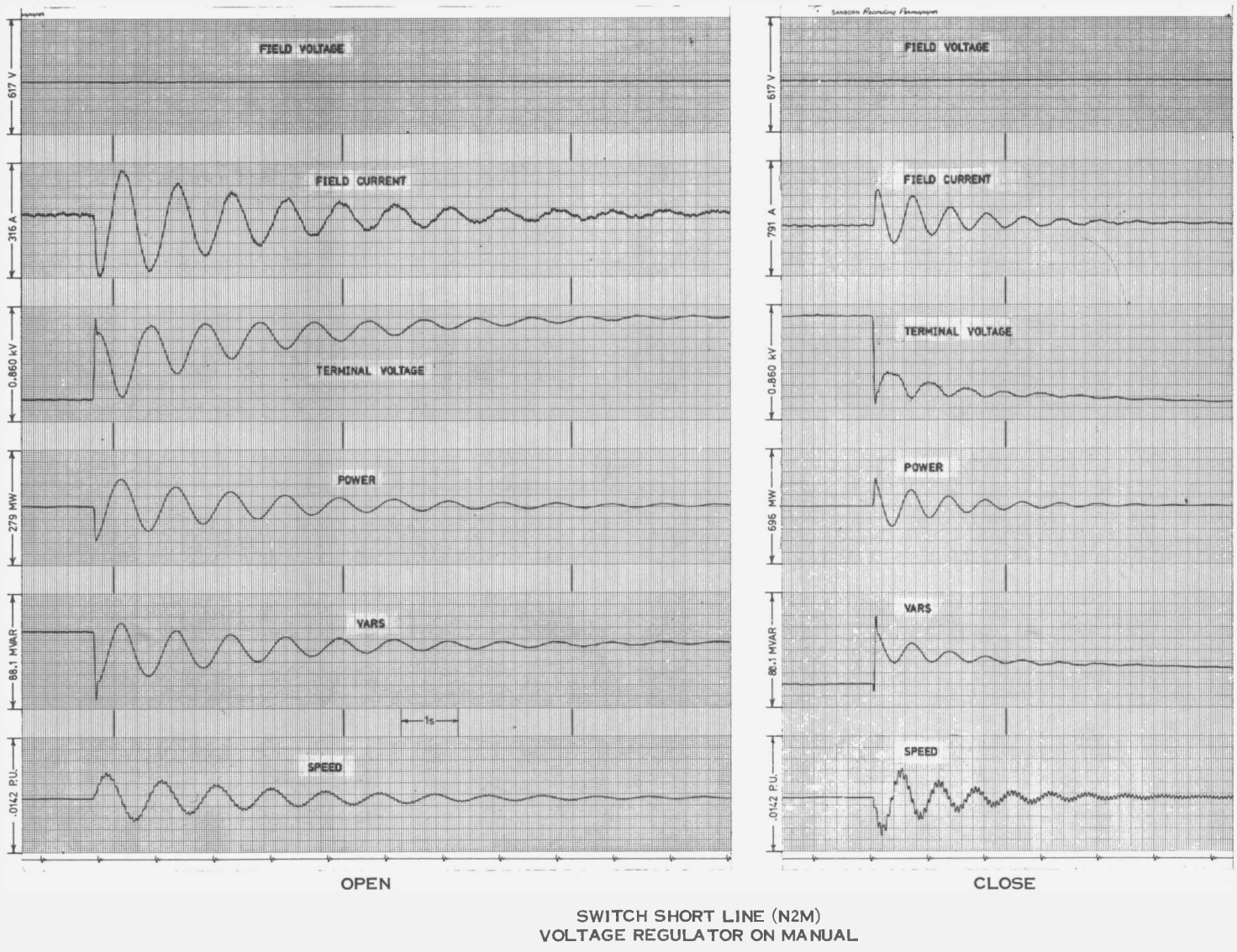

Figure 3-9. Nanticoke Line Switching Test 4, Oscillograms of Generator Variables.

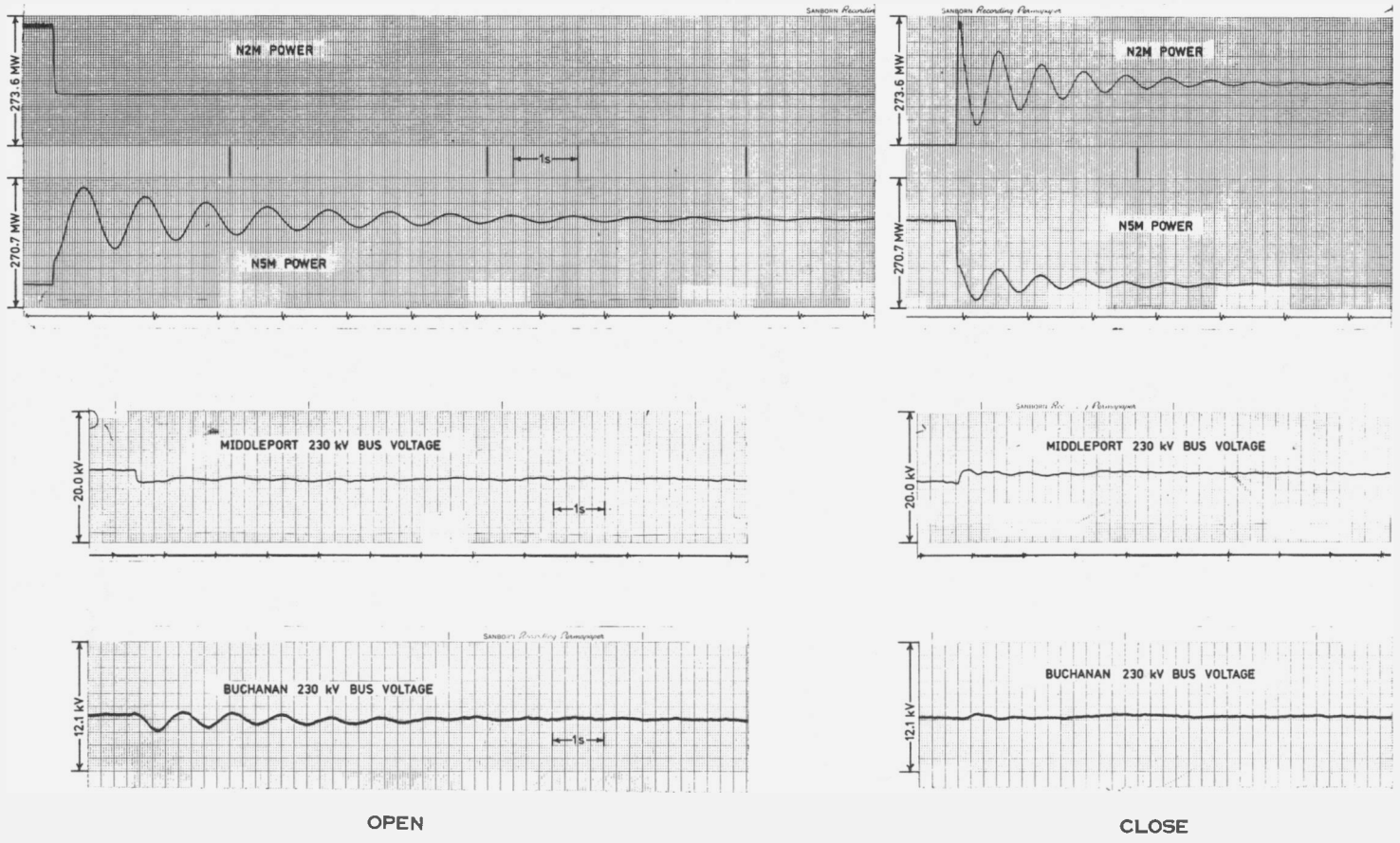

Figure 3-10. Nanticoke Line Switching Test 4, Oscillograms of External System Variables.

Section 4

ON-LINE FREQUENCY RESPONSE

TEST SET-UP

The test generator at Lambton was connected radially to the rest of the power system by two, parallel 230 kV lines, each 111 km long (Figure 4-1). Its exciter was connected to the reserve station service bus to eliminate fluctuations in its supply voltage due to swings in the terminal voltage of the test generator. The automatic voltage regulator was left in service with a reduced gain of approximately 25, but the power system stabilizer was removed to simplify the subsequent analysis.

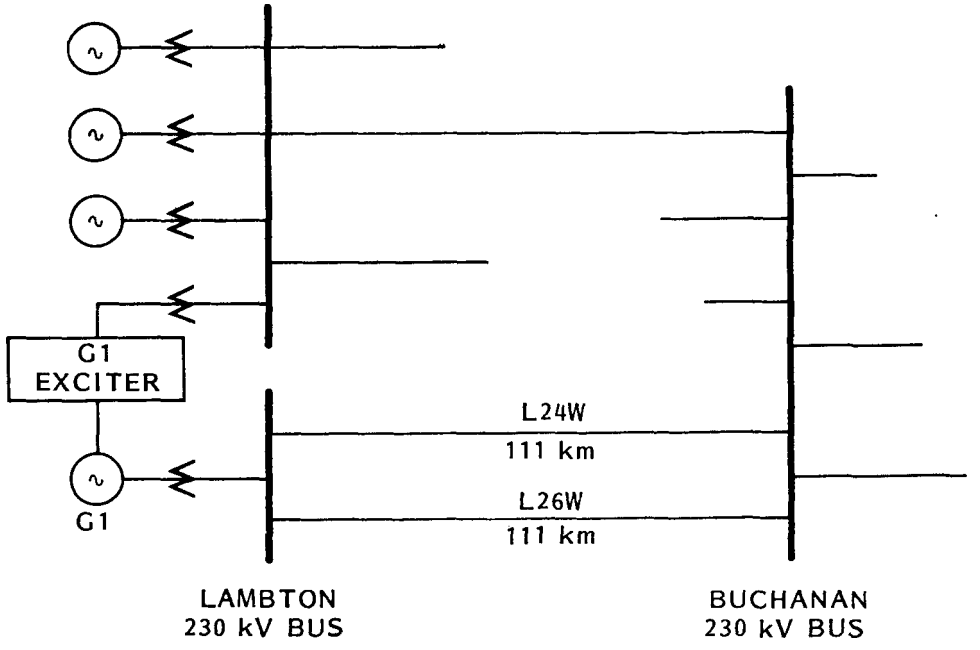

Figure 4-1. System Set-Up For Lambton On-Line Frequency Response.

With the exception of some gain changes in the signal conditioning amplifiers, the instrumentation (Figure 4-2) was identical to that used for the line switching tests described in Section 3. A frequency response analyzer was used to generate a sinusoidal test signal which was added to the voltage regulator reference to modulate the field voltage at the test frequency. It also produced a cross-correlation of each measured variable with the driving signal, from which the following transfer functions were computed:

- field voltage to field current
- field voltage to terminal voltage
- field voltage to active power
- field voltage to reactive power
- field voltage to shaft speed

Ten points were measured in each decade of frequency between 0.01 Hz and 10 Hz. The test generator was operating at 395 MW, 67 MVAR lagging, 24.2 kV during the tests. Two synchronous condensers were connected at Buchanan to maintain the 230 kV bus voltage there as constant as possible.

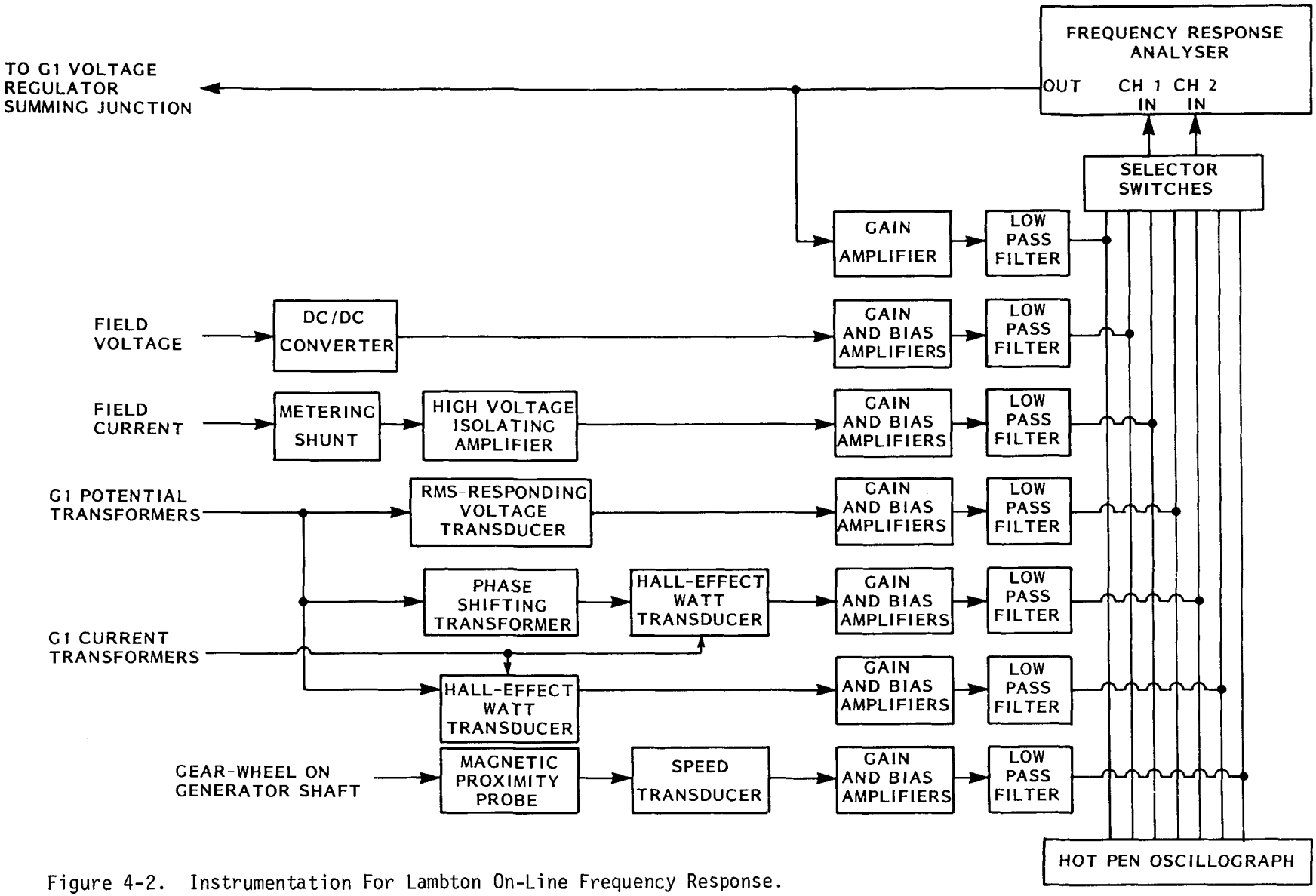

Figure 4-2. Instrumentation For Lambton On-Line Frequency Response.

RESULTS

Table 4-1 indicates the size of disturbance used at each frequency for the tests. Table 4-2 lists the magnitude and phase of each measured transfer function at each test frequency. The magnitudes of these transfer functions were normalized to the following bases:

field voltage: 114 V

field current: 1310 A

terminal voltage: 24.0 kV rms phase to phase

active power: 555.56 MVA

reactive power: 555.56 MVA

shaft speed: 120π rad/s

Figures 4-3 to 4-7 are Bode plots of the measured transfer functions. The test points in these figures are identified as follows:

- ◉ magnitude
- ⊡ phase

Table 4-1

LAMBTON ON-LINE FREQUENCY RESPONSE
PEAK DEVIATIONS OF MEASURED VARIABLES

Freq. (Hz)	Field Voltage (V)	Field Current (A)	Terminal Voltage (V rms)	Active Power (MW)	Reactive Power (MVAR)	Shaft Speed (rad/s)
0.010	5.49	65.7	349		17.4	
0.013	5.88	68.8	345		17.2	
0.016	6.16	66.4	353		17.4	
0.020	5.95	68.8	345		17.4	
0.025	6.91	68.0	349		16.6	
0.030	7.07	68.8	345		17.0	
0.040	8.41	68.8	341		17.0	
0.050	9.54	70.4	345		16.8	
0.065	11.2	72.8	337		16.2	
0.080	13.3	76.3	341		16.6	
0.10	15.0	75.4	311		15.7	0.0147
0.13	19.9	83.6	341		16.8	0.0195
0.16	22.9	86.6	322	0.255	15.7	0.0214
0.20	28.5	91.7	333	0.454	15.5	0.0303
0.25	33.9	97.1	333	0.679	15.5	0.0390
0.30	38.9	99.4	315	1.11	14.8	0.0423
0.40	54.9	124	341	2.41	16.0	0.0693
0.50	67.6	137	341	3.82	16.0	0.0824
0.65	85.0	150	345	7.45	15.1	0.122
0.80	83.1	139	287	11.4	11.2	0.148
2.0	96.5	154	114	12.9	8.90	0.0647
2.5	124	175	125	10.6	8.80	0.0423
3.0	147	194	128	9.38	8.60	0.0303
4.0	179	213	121	7.62	7.75	0.0170
5.0	196	220	109	6.27	6.83	0.0103
6.5	225	233	96	5.15	5.95	0.0050
8.0	225	220	79	4.05	4.73	0.0016
10.0	235	215	66	3.18	3.89	0.0010

Table 4-2

NORMALIZED TRANSFER FUNCTIONS FROM FIELD VOLTAGE

Freq. (Hz)	Field Current Mag (db)	Field Current Phase (deg)	Terminal Voltage Mag (db)	Terminal Voltage Phase (deg)	Active Power Mag (db)	Active Power Phase (deg)	Reactive Power Mag (db)	Reactive Power Phase (deg)	Shaft Speed Mag (db)	Shaft Speed Phase (deg)
.010	.42	-8.4	-10.40	-12.9			-3.76	-11.8		
.013	.22	-15.3	-11.10	-18.3			-4.46	-17.9		
.016	-.48	-20.2	-11.30	-26.9			-4.76	-25.1		
.020	.12	-25.9	-11.20	-33.5			-4.46	-35.8		
.025	-1.28	-29.1	-12.40	-36.5			-6.16	-35.9		
.030	-1.38	-30.3	-12.70	-39.7			-6.16	-39.8		
.040	-2.88	-34.6	-14.30	-47.4			-7.66	-48.1		
.050	-3.78	-37.9	-15.30	-53.9			-8.86	-56.2		
.065	-4.88	-39.9	-16.90	-59.0			-10.56	-58.8		
.080	-5.98	-43.2	-18.30	-64.0			-11.86	-64.4		
.100	-7.08	-43.4	-20.10	-65.7			-13.36	-67.8	-70.56	-179.8
.130	-8.68	-43.9	-21.80	-70.4			-15.26	-71.1	-70.56	-163.8
.160	-9.58	-43.1	-23.50	-72.7	-52.80	78.0	-17.06	-73.9	-70.96	-161.2
.200	-10.98	-41.2	-25.10	-75.8	-49.70	93.4	-19.06	-76.0	-69.86	-171.2
.250	-11.98	-40.0	-26.60	-78.7	-47.70	115.2	-20.56	-77.7	-69.16	-170.2
.300	-12.98	-37.6	-28.30	-78.8	-44.60	99.1	-22.16	-78.1	-69.66	-177.6
.400	-14.08	-34.4	-30.60	-80.3	-40.90	92.3	-24.46	-79.0	-68.36	-177.7
.500	-14.98	-30.3	-32.40	-81.6	-38.70	90.0	-26.26	-80.3	-68.66	-184.3
.650	-16.18	-24.6	-34.30	-83.1	-34.90	89.4	-28.76	-81.9	-67.26	-183.3
.800	-16.68	-15.4	-35.70	-83.4	-31.00	85.4	-31.16	-79.5	-65.36	-186.3
2.000	-17.08	-42.5	-45.00	-84.0	-31.20	-88.5	-34.46	-88.1	-73.86	3.3
2.500	-18.13	-37.5	-46.35	-84.9	-35.05	-93.1	-36.71	-90.6	-79.71	-.7
3.000	-18.73	-34.8	-47.65	-85.3	-37.65	-95.9	-38.41	-91.8	-84.11	-3.1
4.000	-19.63	-32.0	-49.85	-87.3	-41.15	-99.2	-41.01	-94.1	-90.81	-4.9
5.000	-20.13	-31.0	-51.55	-88.7	-43.65	-102.0	-42.91	-96.5	-96.01	-5.3
6.500	-20.83	-30.3	-53.85	-90.3	-46.55	-105.3	-45.31	-99.7	-103.51	-9.3
8.000	-21.33	-30.5	-55.55	-92.1	-48.65	-108.1	-47.31	-102.7	-113.31	-9.0
10.000	-21.93	-31.3	-57.55	-94.5	-51.15	-111.8	-49.41	-106.0	-117.41	162.1

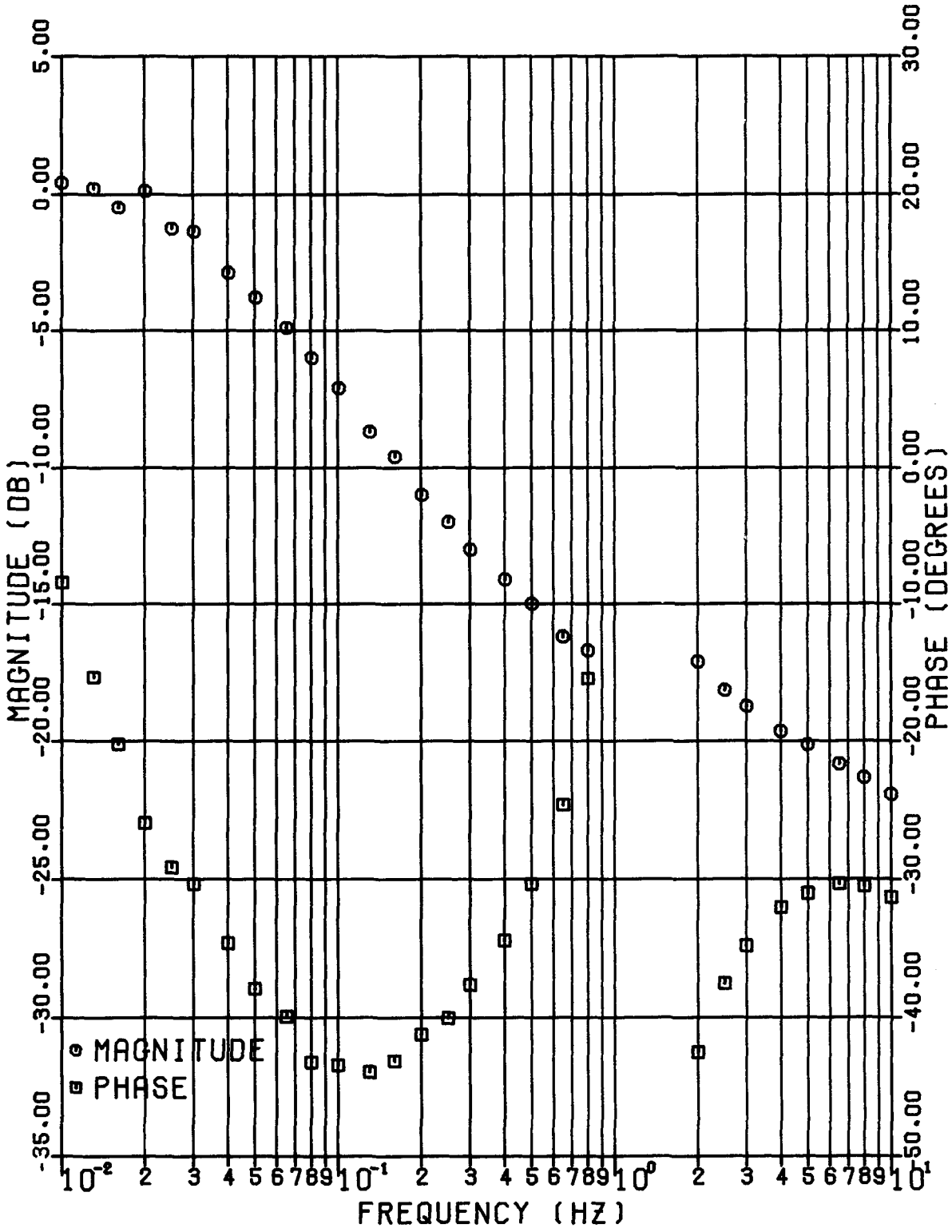

Figure 4-3. On-Line Transfer Function From Field Voltage to Field Current.

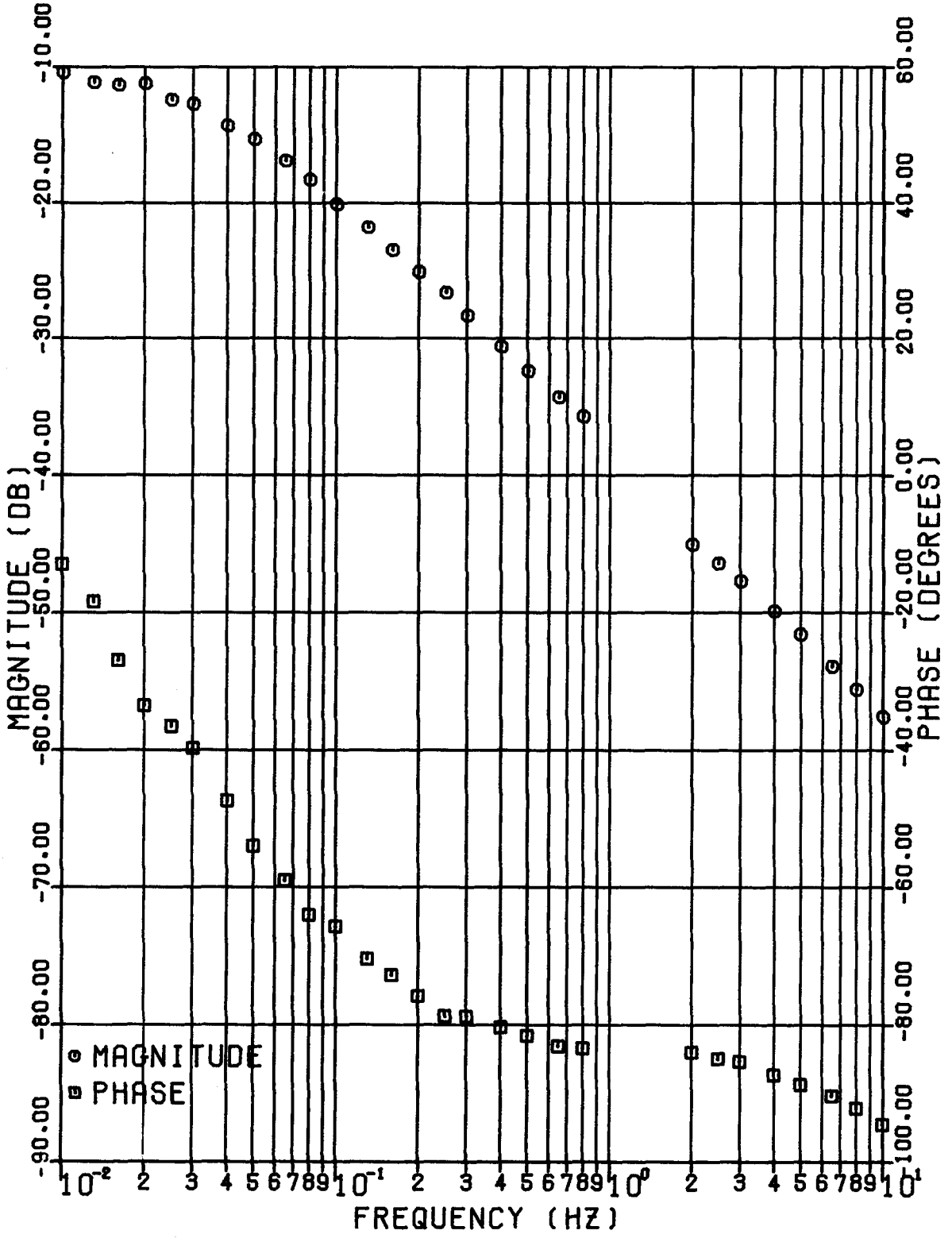

Figure 4-4. On-Line Transfer Function From Field Voltage to Terminal Voltage.

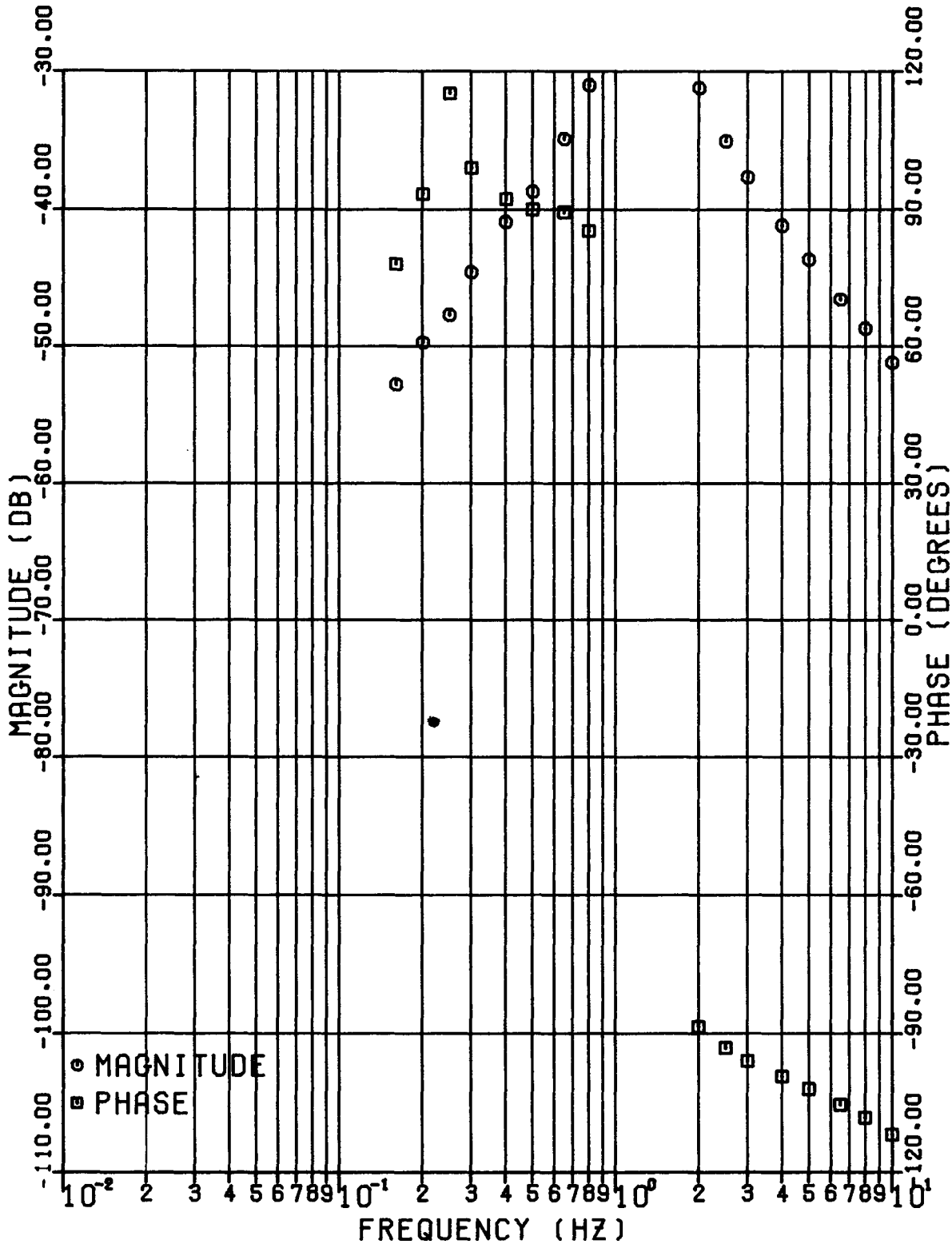

Figure 4-5. On-Line Transfer Function From Field Voltage to Active Power.

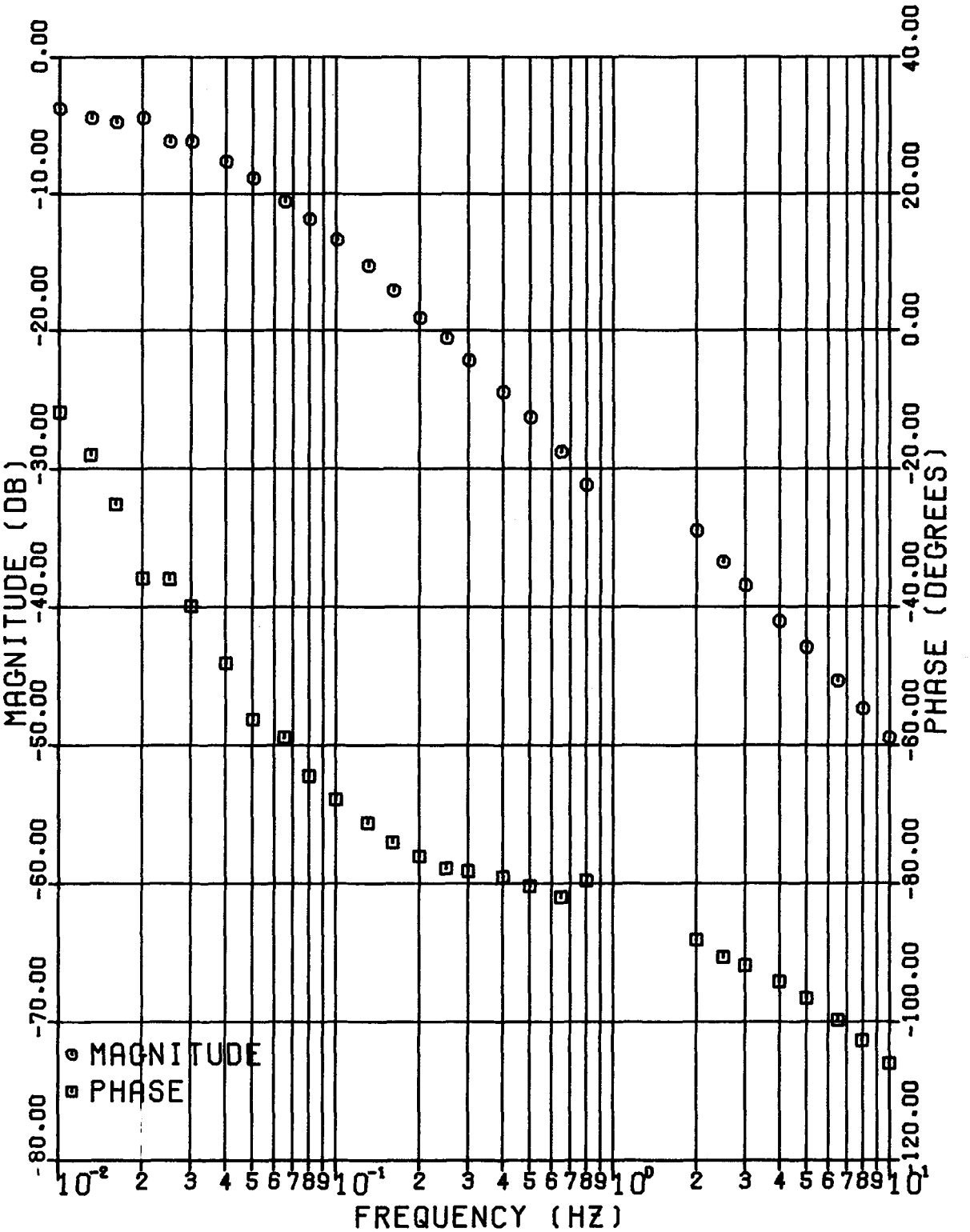

Figure 4-6. On-Line Transfer Function From Field Voltage to Reactive Power.

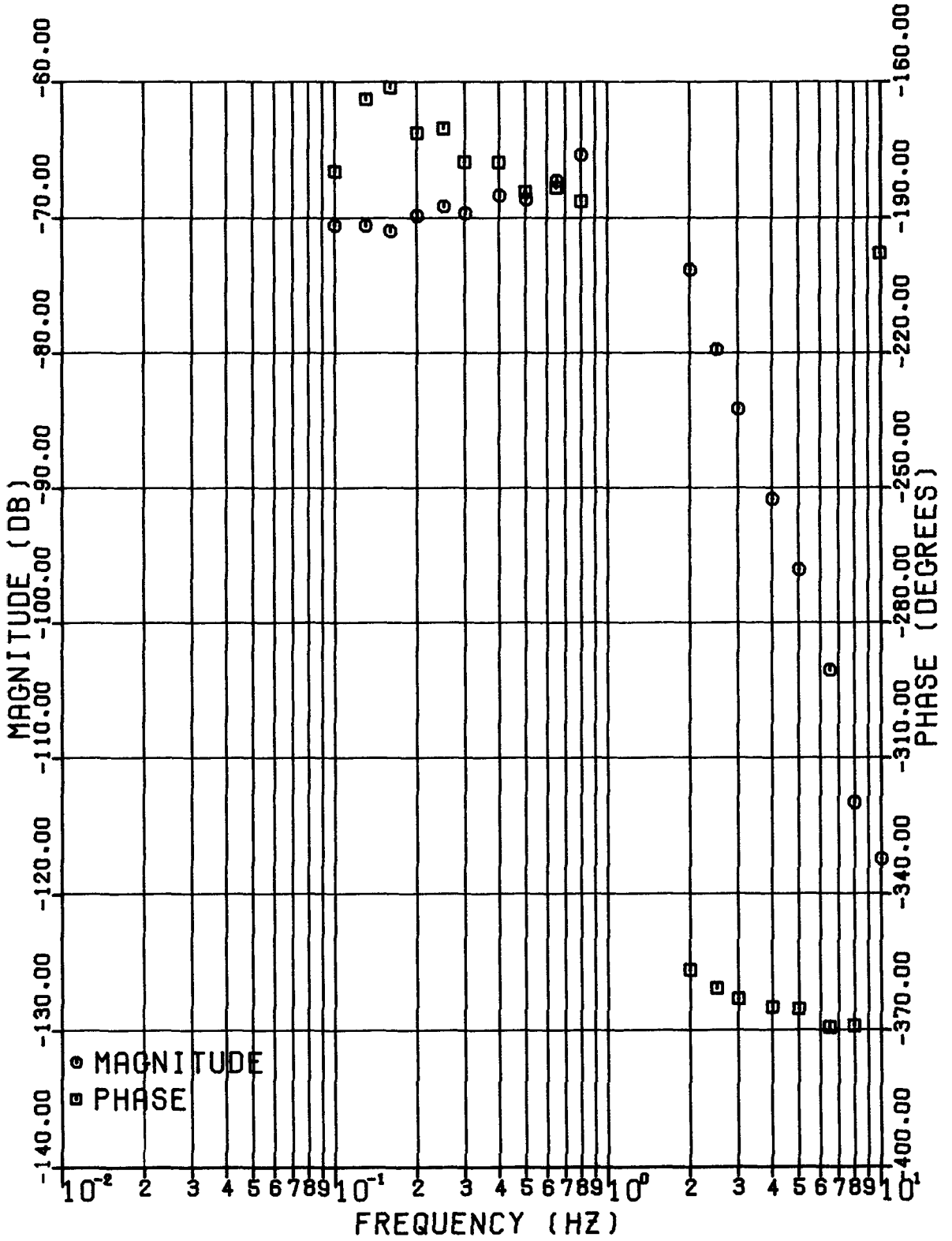

Figure 4-7. On-Line Transfer Function From Field Voltage to Shaft Speed.

Section 5

OPEN-CIRCUIT TESTS

OPEN-CIRCUIT SATURATION

The open-circuit saturation characteristic is measured on almost all synchronous generators as a part of the commissioning checks. The generator is operated at rated speed, off-line, and a measurement of terminal voltage as a function of field current is made. Typically, about ten test points are recorded.

This test was repeated at Lambton to obtain a more detailed delineation of the characteristic. Forty-nine points were measured. The objectives were to determine the slope of the air-gap line precisely and to attempt to detect any non-linearity at the low end of the curve.

A metering shunt and a dc millivoltmeter were used to measure field current, as is the standard practice. However, rather than the usual rms responding ac voltmeter, a frequency response analyzer was used to measure the generator terminal voltage.

This device has an internal oscillator which it uses as a reference. Any measurement is the result of a cross-correlation between the input variable and this internal reference, and, as such, is a measure of the fundamental component of the input variable relative to the internal oscillator frequency.

The internal oscillator of the frequency response analyzer was phase-locked to the generator terminal voltage waveform. Then, at each test point, it measured both the frequency, and the magnitude of the fundamental component of terminal voltage. This made it possible to correct each reading to 60 Hz, thus eliminating any possible errors due to rotor speed variations during the tests.

Figure 5-1 is the open-circuit saturation curve for Lambton, so obtained. The air-gap line, or linear part of the curve is well defined. From its slope, the field current required for rated terminal voltage on the air-gap line is 1310 A.

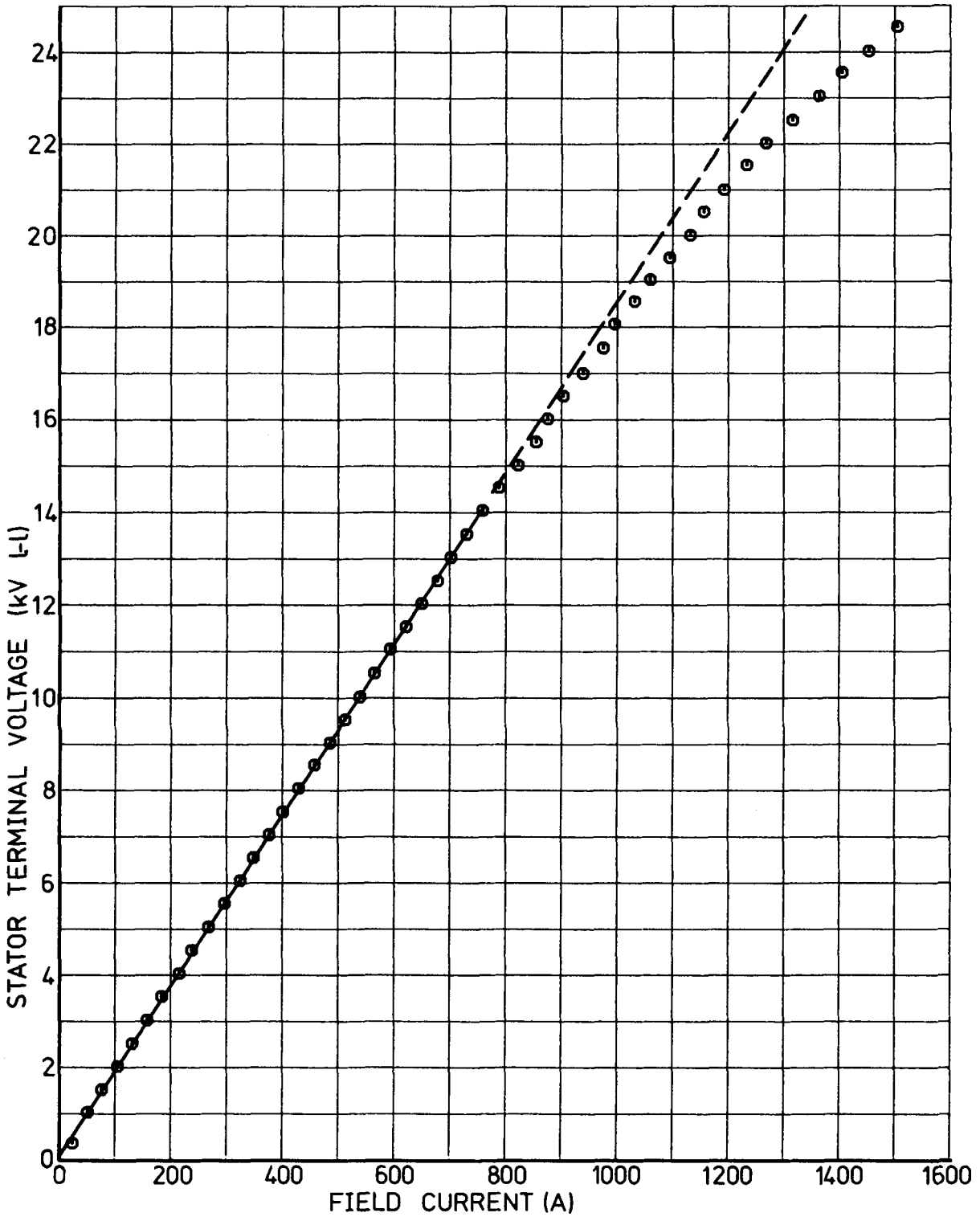

Figure 5-1. Lambton Open-Circuit Saturation Curve.

Any non-linearity at the low end of the curve was not detectable with the instrumentation used.

OPEN-CIRCUIT FREQUENCY RESPONSE

Introduction

The open-circuit frequency response of a generator is measured with the generator operating at rated speed, off line. The transfer functions between field voltage and field current, and field voltage and terminal voltage are measured by varying the field voltage a small amount in a sinusoidal fashion over a range of frequencies.

Procedure

The exciters at Lambton are a transformer-fed thyristor type. In normal operation, the exciter transformer for each unit is supplied from its own generator terminals. However, it is also possible to connect the exciter transformer to the reserve station service supply which can be fed from either the high voltage transmission system, or small combustion turbine units. To eliminate the possibility of terminal voltage excursions affecting the field voltage during the tests, the exciter on the test generator was fed from the reserve station service supply.

The generator was operated at rated speed, off line, with the automatic voltage regulator in service. The field voltage was perturbed by adding a sinusoidal test signal to the voltage regulator reference. A frequency range from .003 Hz to 10 Hz was covered. The amplitude of the test signal was adjusted to produce terminal voltage swings of approximately 1% peak to peak at each test frequency. Three runs were done at three different operating points: one at 15.0 kV, close to the linear part of the open-circuit saturation curve; one at 24.0 kV, rated terminal voltage; and one at 20.5 kV, midway between the other two points.

Instrumentation

Figure 5-2 is the instrumentation diagram for the test. A frequency response analyzer generated the sinusoidal test signal, performed a cross-correlation between the test signal and each of the measured variables, and computed the transfer functions between pairs of measured variables from the results of these cross-correlations.

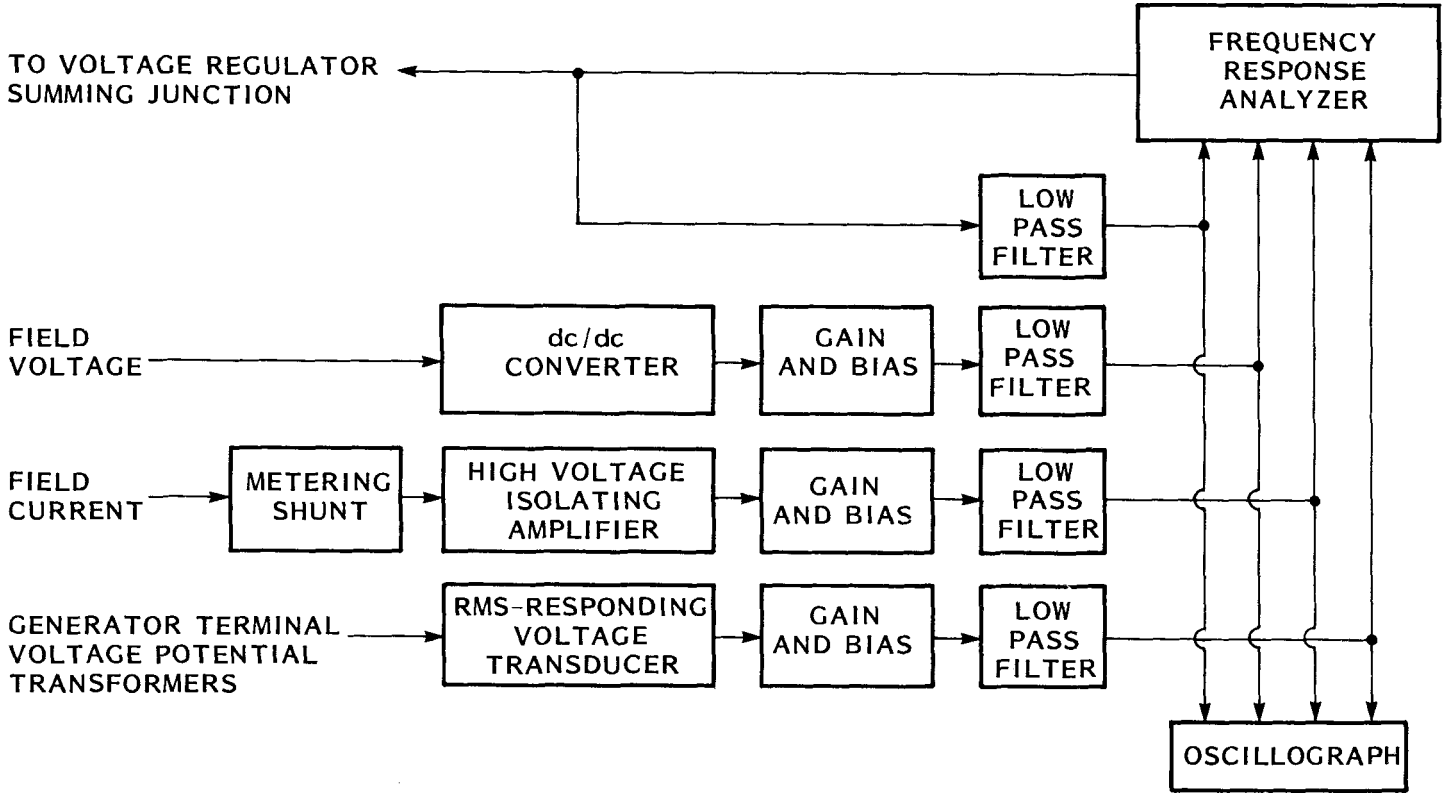

Figure 5-2. Instrumentation For Lambton Open-Circuit Frequency Response.

Field voltage was measured on the exciter output terminals with a resistive voltage divider and a dc/dc transformer type isolator. A metering shunt was installed in series with the exciter output to measure field current; a high voltage, transformer-coupled amplifier was used to provide the required isolation. Generator terminal voltage was measured with an rms responding transducer which produced a dc voltage proportional to the rms value of the terminal voltage.

The outputs from all three transducers (field voltage, field current and terminal voltage) were biased to zero at the operating point, and routed through carefully matched low-pass filters before going to the frequency response analyzer.

Results

The test data are listed in Tables 5-1 to 5-3. In each table, the first six columns after frequency are the deviations of the individual variables. The final six are the magnitude and phase of the transfer functions between: field voltage and terminal voltage, field current and terminal voltage, and field voltage and field current.

All measurements were normalized to the following bases:

field voltage, 107.4 Vdc

field current, 1310 A dc

terminal voltage, 24 kV rms phase to phase

The magnitude and phase of the three transfer functions are plotted in Figures 5-3 to 5-8. The data from all three runs is plotted on each graph to illustrate the influence of the operating point on each parameter.

Table 5-1

OPEN-CIRCUIT FREQUENCY RESPONSE AT 15.0 KV

FREQUENCY	FIELD VOLTAGE		FIELD CURRENT		TERMINAL VOLTAGE		ET/EFD		ET/IFD		IFD/EFD	
(HZ)	(DB ABOVE 1 PU)	PHASE (DEG)	(DB ABOVE 1 PU)	PHASE (DEG)	(DB ABOVE 1 PU)	PHASE (DEG)	(DB ABOVE 1 PU)	PHASE (DEG)	(DB ABOVE 1 PU)	PHASE (DEG)	(DB ABOVE 1 PU)	PHASE (DEG)
.003	-44.28	8.2	-44.28	-1.2	-45.46	-.1	-1.18	-8.3	-1.18	1.1	.00	-9.4
.005	-44.68	9.1	-44.98	2.5	-45.46	.0	-.78	-9.1	-.48	-2.5	-.30	-6.6
.007	-44.88	22.7	-44.98	-3.7	-45.46	.0	-.58	-22.7	-.48	3.7	-.10	-26.4
.010	-44.58	26.7	-44.48	9.2	-45.46	-.1	-.88	-26.8	-.98	-9.3	.10	-17.5
.013	-43.58	26.3	-44.28	5.7	-45.46	-.2	-1.88	-26.5	-1.18	-5.9	-.70	-20.6
.016	-42.58	37.0	-44.18	8.5	-45.46	-.5	-2.88	-37.5	-1.28	-9.0	-1.60	-28.5
.020	-42.08	38.8	-43.98	9.4	-45.46	-.1	-3.38	-38.9	-1.48	-9.5	-1.90	-29.4
.025	-41.78	45.9	-44.28	10.4	-45.46	-.4	-3.68	-46.3	-1.18	-10.8	-2.50	-35.5
.030	-40.48	48.7	-43.88	10.0	-45.46	-.6	-4.98	-49.3	-1.58	-10.6	-3.40	-38.7
.040	-38.68	58.4	-43.88	11.3	-45.46	-.7	-6.78	-59.1	-1.58	-12.0	-5.20	-47.1
.050	-37.38	61.9	-43.68	13.9	-45.46	-.8	-8.08	-62.7	-1.78	-14.7	-6.30	-48.0
.065	-35.58	66.1	-43.58	16.8	-45.46	-.8	-9.88	-66.9	-1.88	-17.6	-8.00	-49.3
.080	-33.88	70.2	-43.08	18.2	-45.46	-1.2	-11.58	-71.4	-2.38	-19.4	-9.20	-52.0
.100	-32.28	72.5	-42.98	21.3	-45.46	-1.7	-13.18	-74.2	-2.48	-23.0	-10.70	-51.2
.130	-30.18	75.7	-42.48	24.8	-45.46	-2.1	-15.28	-77.8	-2.98	-26.9	-12.30	-50.9
.160	-28.58	77.4	-42.18	27.3	-45.46	-2.6	-16.88	-80.0	-3.28	-29.9	-13.60	-50.1
.200	-26.68	78.5	-41.58	30.0	-45.46	-3.2	-18.78	-81.7	-3.88	-33.2	-14.90	-48.5
.250	-24.88	79.2	-40.88	33.3	-45.46	-4.2	-20.58	-83.4	-4.58	-37.5	-16.00	-45.9
.300	-23.28	79.7	-40.28	35.7	-45.46	-4.6	-22.18	-84.3	-5.18	-40.3	-17.00	-44.0
.400	-20.98	79.5	-39.18	38.1	-45.46	-6.0	-24.48	-85.5	-6.28	-44.1	-18.20	-41.4
.500	-18.88	78.7	-38.18	40.2	-45.46	-8.0	-26.58	-86.7	-7.28	-48.2	-19.30	-38.5
.650	-16.78	77.4	-37.03	40.8	-45.46	-10.4	-28.68	-87.8	-8.38	-51.2	-20.30	-36.6
.800	-14.98	75.5	-35.98	40.7	-45.46	-12.9	-30.48	-88.4	-9.48	-53.6	-21.00	-34.8
1.000	-13.18	72.9	-34.98	39.7	-45.36	-16.2	-32.18	-89.1	-10.38	-55.9	-21.80	-33.2
1.300	-11.08	68.7	-33.58	36.9	-45.36	-21.4	-34.28	-90.1	-11.78	-58.3	-22.50	-31.8
1.600	-9.38	64.2	-32.48	33.7	-45.26	-26.4	-35.88	-90.6	-12.78	-60.1	-23.10	-30.5
2.000	-7.68	58.3	-31.28	28.8	-45.16	-32.8	-37.48	-91.1	-13.88	-61.6	-23.60	-29.5
2.500	-5.88	51.0	-29.88	22.4	-45.06	-40.6	-39.18	-91.6	-15.18	-63.0	-24.00	-28.6
3.000	-4.38	43.7	-28.68	15.7	-44.86	-48.5	-40.48	-92.2	-16.18	-64.2	-24.30	-28.0
4.000	-1.88	28.6	-26.48	1.4	-44.46	-64.7	-42.58	-93.3	-17.98	-66.1	-24.60	-27.2
5.000	.22	12.0	-24.58	-14.8	-43.96	-82.3	-44.18	-94.3	-19.38	-67.5	-24.80	-26.8
6.500	2.62	-16.7	-22.18	-42.8	-43.46	-111.9	-46.08	-95.2	-21.28	-69.1	-24.80	-26.1
8.000	4.02	-49.2	-20.78	-74.9	-43.46	-145.3	-47.48	-96.1	-22.68	-70.4	-24.80	-25.7
10.000	4.52	-94.2	-20.78	-119.3	-44.66	168.9	-49.18	263.1	-23.88	288.2	-25.30	-25.1

Table 5-2

OPEN-CIRCUIT FREQUENCY RESPONSE AT 20.5 KV

FREQUENCY	FIELD VOLTAGE		FIELD CURRENT		TERMINAL VOLTAGE		ET/EFD		ET/IFD		IFD/EFD	
	(DB ABOVE		(DB ABOVE		(DB ABOVE		(DB ABOVE		(DB ABOVE		(DB ABOVE	
(HZ)	1 PU)	PHASE (DEG)	1 PU)	PHASE (DEG)	1 PU)	PHASE (DEG)	1 PU)	PHASE (DEG)	1 PU)	PHASE (DEG)	1 PU)	PHASE (DEG)
.003	-42.68	8.7	-42.48	2.9	-45.26	.5	-2.58	-8.2	-2.78	-2.4	.20	-5.8
.005	-43.28	8.4	-42.68	1.7	-45.56	-.2	-2.28	-8.6	-2.88	-1.9	.60	-6.7
.007	-42.98	10.3	-42.48	5.2	-45.46	-.2	-2.48	-10.5	-2.98	-5.4	.50	-5.1
.010	-41.28	22.4	-42.38	4.9	-45.46	-.4	-4.18	-22.8	-3.08	-5.3	-1.10	-17.5
.013	-42.18	19.5	-42.28	5.5	-45.46	-.4	-3.28	-19.9	-3.18	-5.9	-.10	-14.0
.016	-41.28	24.4	-42.48	6.0	-45.46	-.4	-4.18	-24.8	-2.98	-6.4	-1.20	-18.4
.020	-41.78	33.0	-42.48	7.2	-45.46	-.4	-3.68	-33.4	-2.98	-7.6	-.70	-25.8
.025	-40.68	39.5	-42.18	9.8	-45.46	-.5	-4.78	-40.0	-3.28	-10.3	-1.50	-29.7
.030	-39.68	43.4	-42.18	8.2	-45.46	-.7	-5.78	-44.1	-3.28	-8.9	-2.50	-35.2
.040	-37.98	51.4	-42.08	10.6	-45.46	-.8	-7.48	-52.2	-3.38	-11.4	-4.10	-40.8
.050	-36.68	55.8	-41.88	11.7	-45.46	-1.2	-8.78	-57.0	-3.58	-12.9	-5.20	-44.1
.065	-34.98	62.9	-41.78	16.1	-45.46	-1.6	-10.48	-64.5	-3.68	-17.7	-6.80	-46.8
.080	-33.58	65.5	-41.28	16.3	-45.46	-1.8	-11.88	-67.3	-4.18	-18.1	-7.70	-49.2
.100	-31.98	69.7	-40.68	17.4	-45.46	-2.2	-13.48	-71.9	-4.78	-19.6	-8.70	-52.3
.130	-29.98	73.2	-40.58	21.0	-45.46	-2.9	-15.48	-76.1	-4.88	-23.9	-10.60	-52.2
.160	-28.28	74.1	-40.18	23.3	-45.46	-3.4	-17.18	-77.5	-5.28	-26.7	-11.90	-50.8
.200	-26.58	75.2	-39.58	25.3	-45.46	-4.4	-18.88	-79.6	-5.88	-29.7	-13.00	-49.9
.250	-24.78	76.2	-39.18	28.0	-45.46	-5.3	-20.68	-81.5	-6.28	-33.3	-14.40	-48.2
.300	-23.28	76.4	-38.48	30.0	-45.56	-6.4	-22.28	-82.8	-7.08	-36.4	-15.20	-46.4
.400	-20.88	76.4	-37.58	32.6	-45.46	-8.4	-24.58	-84.8	-7.88	-41.0	-16.70	-43.8
.500	-20.38	75.1	-37.88	33.9	-46.86	-10.6	-26.48	-85.7	-8.98	-44.5	-17.50	-41.2
.650	-16.88	73.5	-35.48	34.5	-45.46	-13.4	-28.58	-86.9	-9.98	-47.9	-18.60	-39.0
.800	-15.18	71.5	-34.58	34.8	-45.46	-16.3	-30.28	-87.8	-10.88	-51.1	-19.40	-36.7
1.000	-13.28	68.7	-33.48	33.8	-45.46	-19.9	-32.18	-88.6	-11.98	-53.7	-20.20	-34.9
1.300	-11.28	64.3	-32.08	32.1	-45.46	-25.2	-34.18	-89.5	-13.38	-57.3	-20.80	-32.2
1.600	-9.58	59.9	-30.88	29.5	-45.36	-30.3	-35.78	-90.2	-14.48	-59.8	-21.30	-30.4
2.000	-7.78	54.0	-29.58	25.2	-45.36	-36.6	-37.58	-90.6	-15.78	-61.8	-21.80	-28.8
2.500	-5.98	46.4	-28.08	19.1	-45.16	-45.2	-39.18	-91.6	-17.08	-64.3	-22.10	-27.3
3.000	-4.48	38.7	-26.78	12.3	-44.96	-53.7	-40.48	-92.4	-18.18	-66.0	-22.30	-26.4
4.000	-2.08	21.8	-24.58	-3.6	-44.66	-71.7	-42.58	-93.5	-20.08	-68.1	-22.50	-25.4
5.000	-.18	3.3	-22.78	-21.7	-44.36	-91.4	-44.18	-94.7	-21.58	-69.7	-22.60	-25.0
6.500	1.92	-27.7	-20.98	-52.2	-44.36	-123.4	-46.28	-95.7	-23.38	-71.2	-22.90	-24.5
8.000	2.82	-60.3	-20.28	-84.5	-45.16	-157.0	-47.98	-96.7	-24.88	-72.5	-23.10	-24.2
10.000	3.02	-102.2	-20.78	-126.0	-46.96	-199.7	-49.98	-97.5	-26.18	-73.7	-23.80	-23.8

Table 5-3

OPEN-CIRCUIT FREQUENCY RESPONSE AT 23.7 KV

FREQUENCY	FIELD VOLTAGE		FIELD CURRENT		TERMINAL VOLTAGE		ET/EFD		ET/IFD		IFD/EFD	
(HZ)	(DB ABOVE 1 PU)	PHASE (DEG)	(DB ABOVE 1 PU)	PHASE (DEG)	(DB ABOVE 1 PU)	PHASE (DEG)	(DB ABOVE 1 PU)	PHASE (DEG)	(DB ABOVE 1 PU)	PHASE (DEG)	(DB ABOVE 1 PU)	PHASE (DEG)
.003	-38.98	2.5	-144.28	180.0	-45.56	-.5	-6.58	-3.0	98.72	-180.5	-105.30	177.5
.005	-39.38	7.0	-144.28	180.0	-45.66	-.1	-6.28	-7.1	98.62	-180.1	-104.90	173.0
.007	-39.08	5.5	-144.28	180.0	-45.66	.1	-6.58	-5.4	98.62	-179.9	-105.20	174.5
.010	-39.98	11.6	-39.68	4.6	-45.66	-.3	-5.68	-11.9	-5.98	-4.9	.30	-7.0
.013	-40.08	18.0	-40.08	5.7	-45.66	-.1	-5.58	-18.1	-5.58	-5.8	.00	-12.3
.016	-39.28	19.4	-39.68	5.8	-45.66	-.2	-6.38	-19.6	-5.98	-6.0	-.40	-13.6
.020	-38.88	29.6	-39.68	6.2	-45.56	-.8	-6.68	-30.4	-5.88	-7.0	-.80	-23.4
.025	-38.58	34.6	-39.88	8.4	-45.66	-.6	-7.08	-35.2	-5.78	-9.0	-1.30	-26.2
.030	-38.48	39.1	-39.58	7.3	-45.66	-.6	-7.18	-39.7	-6.08	-7.9	-1.10	-31.8
.040	-36.98	45.0	-39.58	11.8	-45.66	-.9	-8.68	-45.9	-6.08	-12.7	-2.60	-33.2
.050	-35.68	50.9	-39.48	12.3	-45.66	-1.1	-9.98	-52.0	-6.18	-13.4	-3.80	-38.6
.065	-34.28	56.8	-38.78	18.2	-45.66	-1.3	-11.38	-58.1	-6.88	-19.5	-4.50	-38.6
.080	-32.78	61.5	-38.88	15.9	-45.66	-1.7	-12.88	-63.2	-6.78	-17.6	-6.10	-45.6
.100	-31.28	64.8	-38.38	18.6	-45.66	-2.2	-14.38	-67.0	-7.28	-20.8	-7.10	-46.2
.130	-29.38	68.9	-37.78	22.2	-45.66	-2.8	-16.28	-71.7	-7.88	-25.0	-8.40	-46.7
.160	-27.78	71.1	-37.38	23.5	-45.66	-3.3	-17.88	-74.4	-8.28	-26.8	-9.60	-47.6
.200	-26.08	72.3	-36.88	26.3	-45.66	-4.1	-19.58	-76.4	-8.78	-30.4	-10.80	-46.0
.250	-24.28	73.6	-36.18	28.1	-45.66	-5.2	-21.38	-78.8	-9.48	-33.3	-11.90	-45.5
.300	-22.88	74.2	-35.58	29.0	-45.66	-6.4	-22.78	-80.6	-10.08	-35.4	-12.70	-45.2
.400	-20.58	74.0	-34.68	30.8	-45.66	-8.4	-25.08	-82.4	-10.98	-39.2	-14.10	-43.2
.500	-18.68	73.3	-33.88	31.9	-45.76	-10.6	-27.08	-83.9	-11.88	-42.5	-15.20	-41.4
.650	-16.58	71.4	-32.78	32.0	-45.66	-13.6	-29.08	-85.0	-12.88	-45.6	-16.20	-39.4
.800	-14.78	69.5	-31.88	31.7	-45.66	-16.7	-30.88	-86.2	-13.78	-48.4	-17.10	-37.8
1.000	-13.08	66.3	-30.88	29.9	-45.86	-22.3	-32.78	-88.6	-14.98	-52.2	-17.80	-36.4
1.300	-10.98	61.5	-29.58	26.7	-45.76	-27.1	-34.78	-88.6	-16.18	-53.8	-18.60	-34.8
1.600	-9.48	56.5	-28.48	23.1	-45.66	-32.8	-36.18	-89.3	-17.18	-55.9	-19.00	-33.4
2.000	-7.78	49.8	-27.28	17.8	-45.66	-40.5	-37.88	-90.3	-18.38	-58.3	-19.50	-32.0
2.500	-6.08	41.2	-25.98	10.5	-45.56	-50.0	-39.48	-91.2	-19.58	-60.5	-19.90	-30.7
3.000	-4.68	32.4	-24.88	2.6	-45.56	-59.7	-40.88	-92.1	-20.68	-62.3	-20.20	-29.8
4.000	-2.38	13.8	-23.03	-14.9	-45.36	-79.8	-42.98	-93.6	-22.28	-64.9	-20.70	-28.7
5.000	-.78	-6.5	-21.68	-34.3	-45.46	-101.2	-44.68	-94.7	-23.78	-66.9	-20.90	-27.8
6.500	.72	-38.3	-20.68	-65.3	-46.16	-134.3	-46.88	-96.0	-25.48	-69.0	-21.40	-27.0
8.000	1.22	-69.4	-20.58	-96.1	-47.46	-166.6	-48.68	-97.2	-26.88	-70.5	-21.80	-26.7
10.000	1.12	-108.0	-21.38	-134.1	-49.66	-206.4	-50.78	-98.4	-28.28	-72.3	-22.50	-26.1

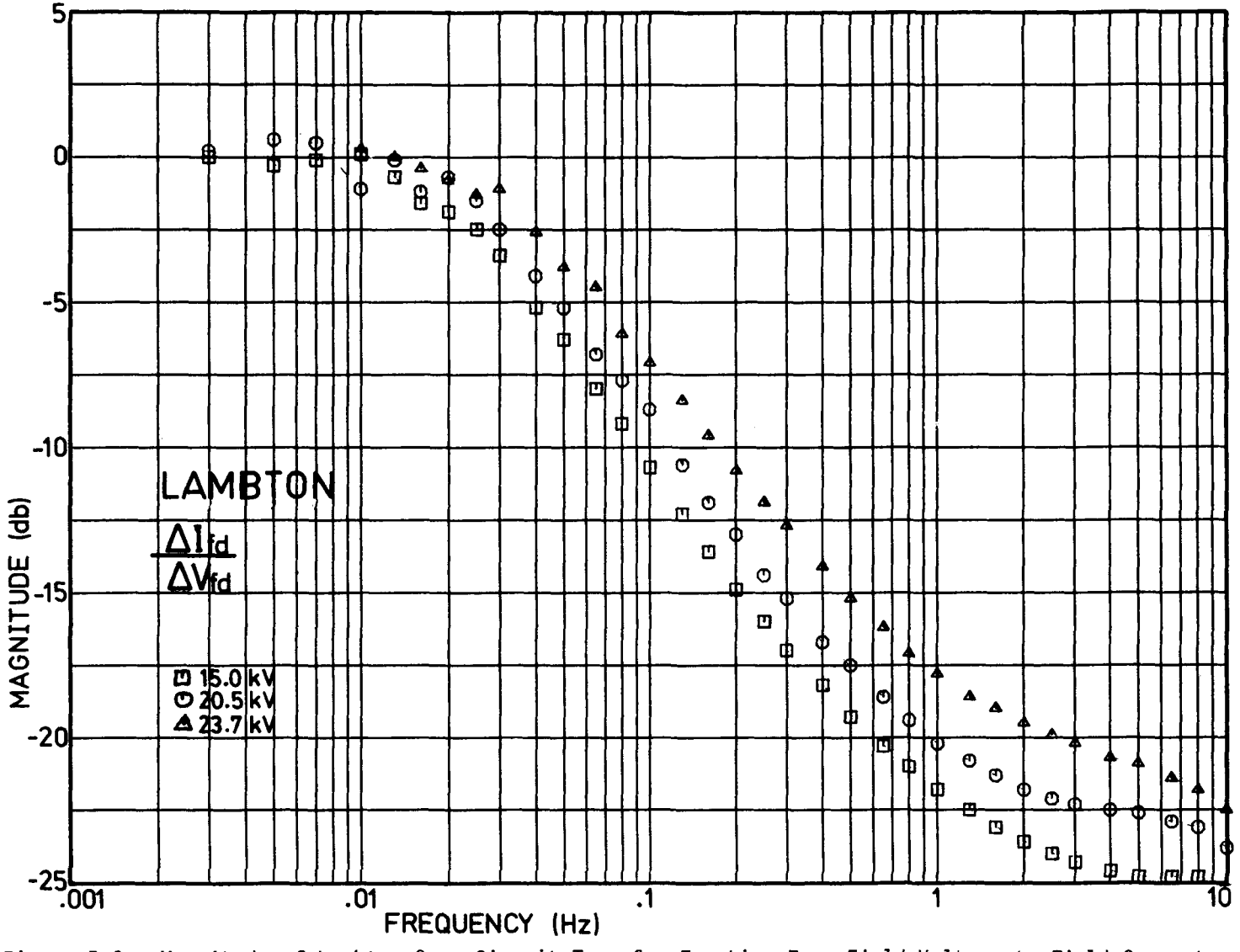

Figure 5-3. Magnitude of Lambton Open-Circuit Transfer Function From Field Voltage to Field Current.

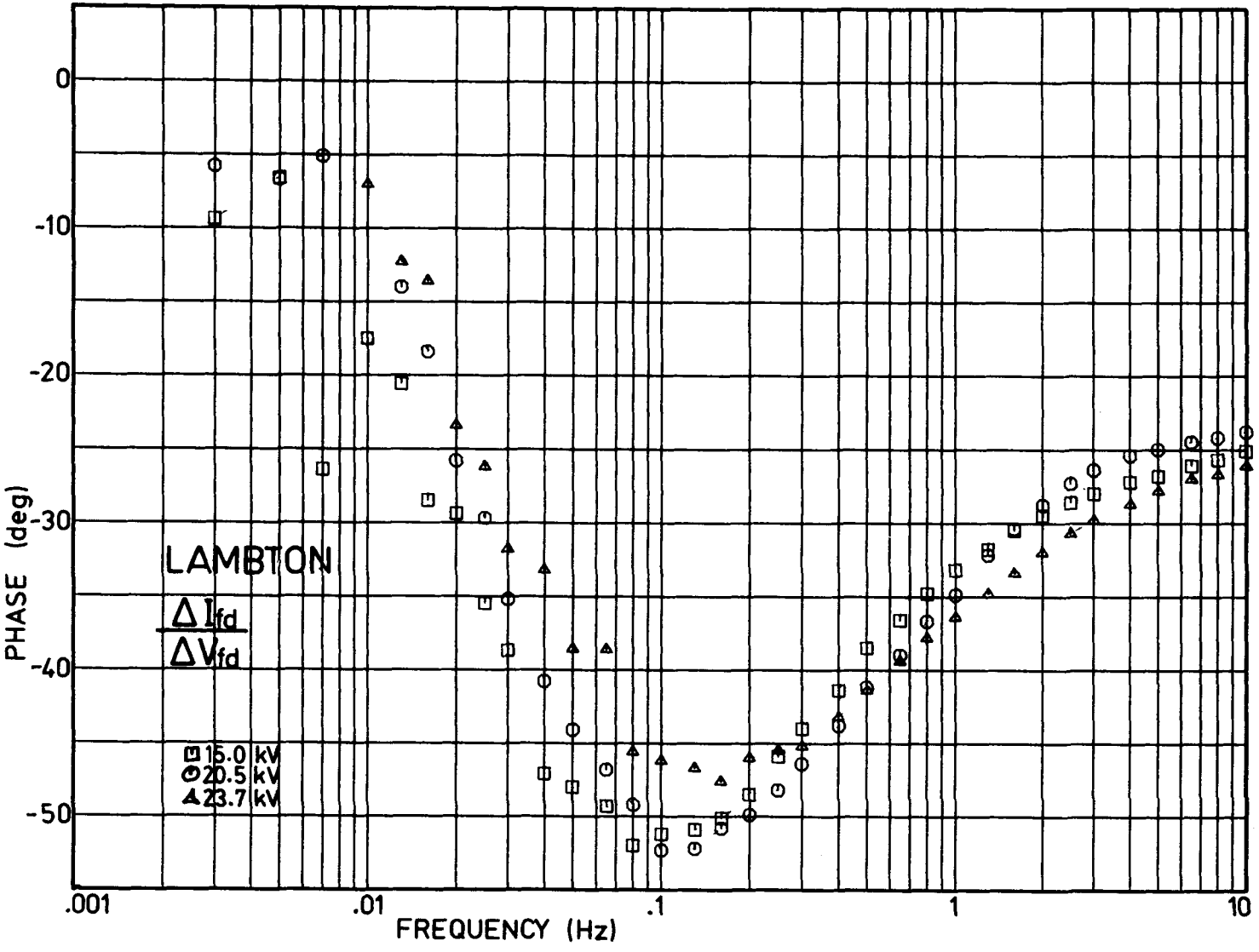

Figure 5-4. Phase of Lambton Open-Circuit Transfer Function From Field Voltage to Field Current.

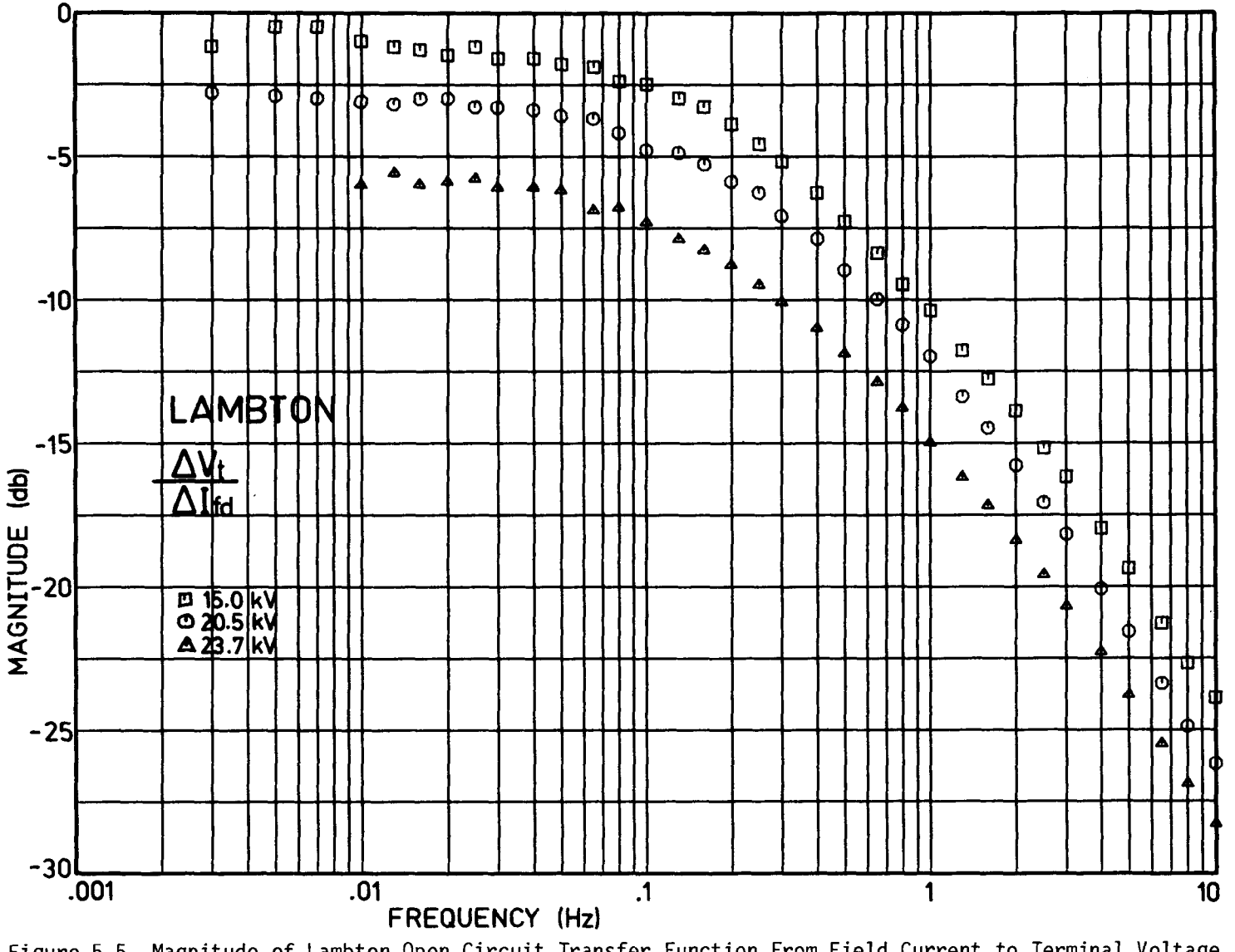

Figure 5-5. Magnitude of Lambton Open-Circuit Transfer Function From Field Current to Terminal Voltage.

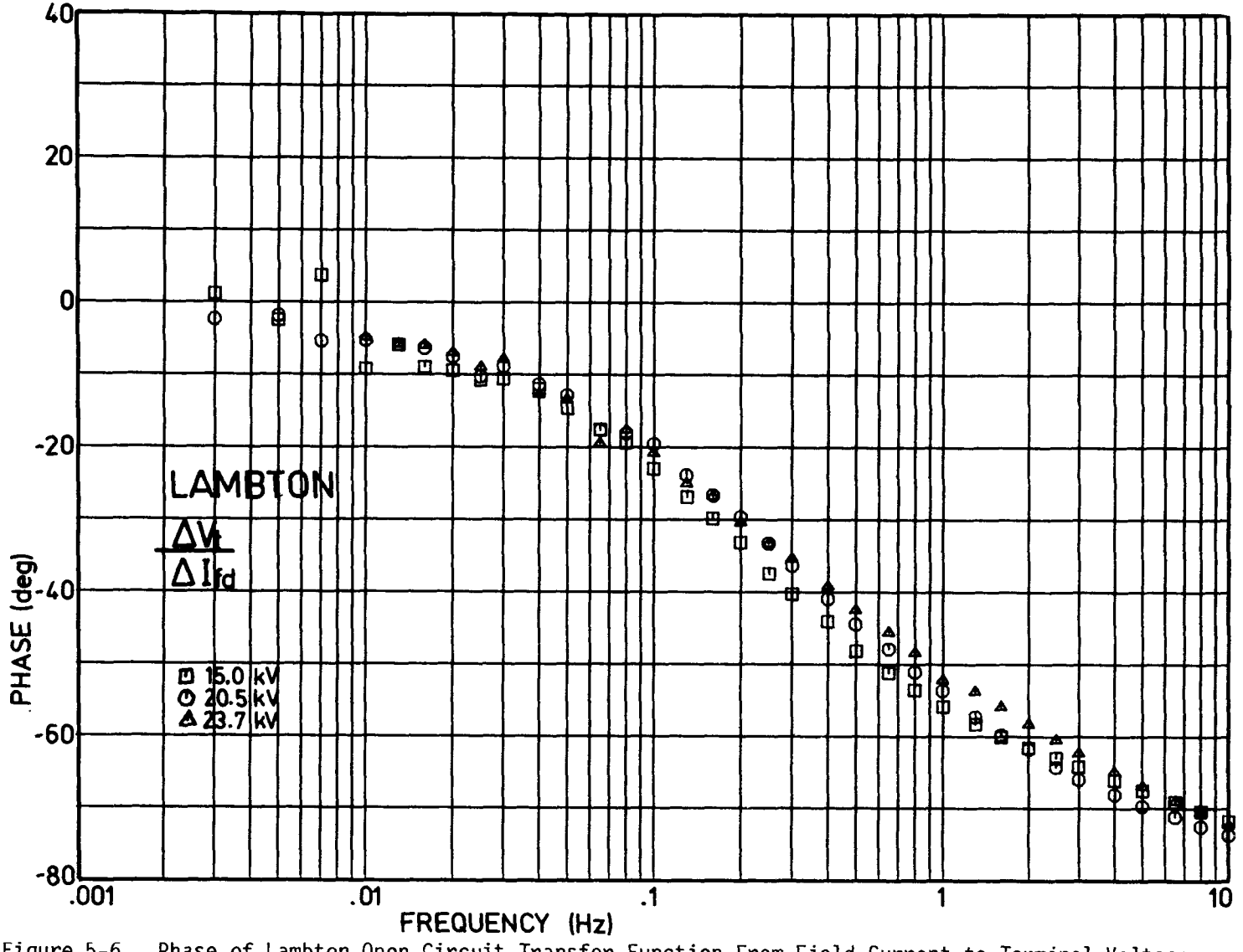

Figure 5-6. Phase of Lambton Open-Circuit Transfer Function From Field Current to Terminal Voltage.

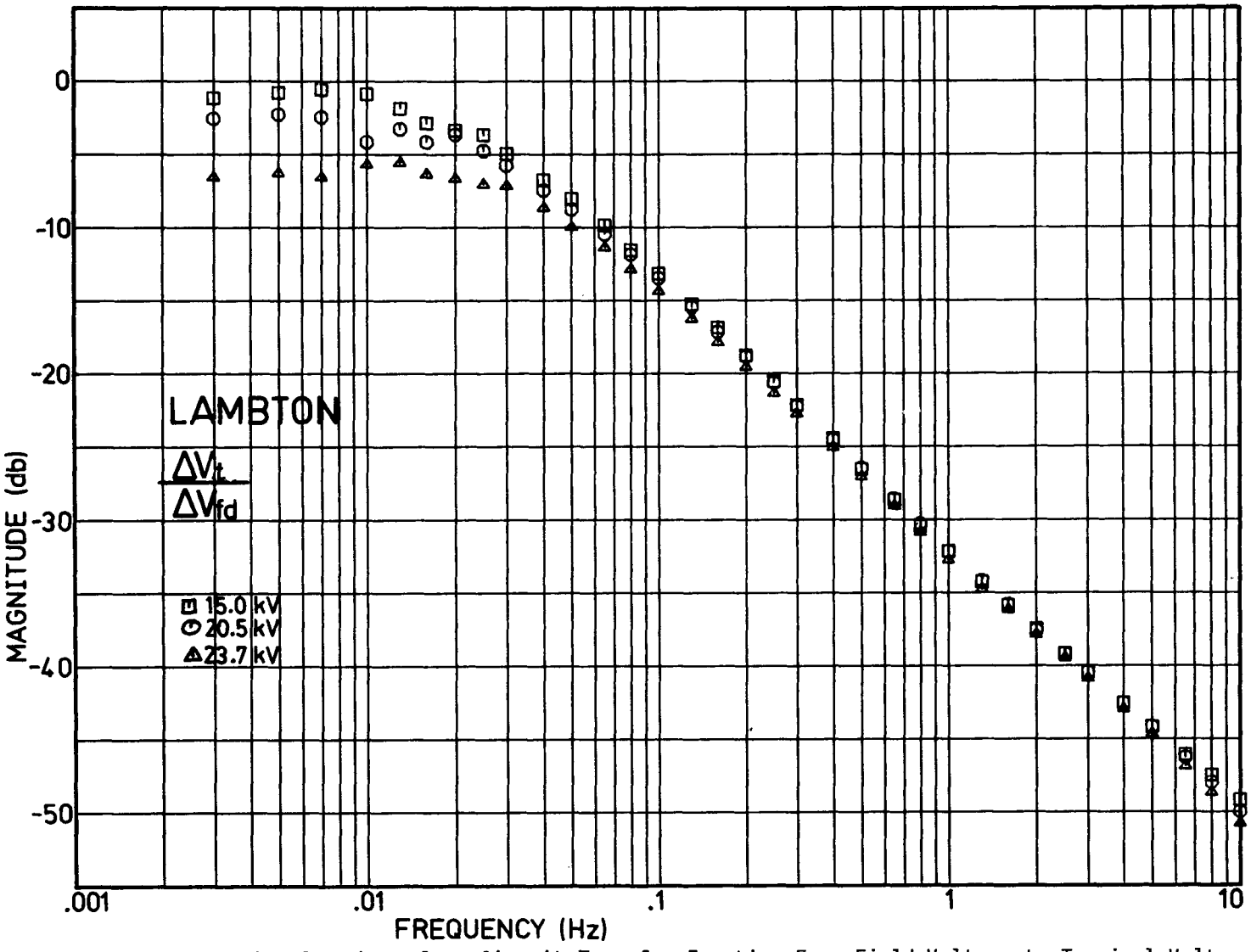

Figure 5-7. Magnitude of Lambton Open-Circuit Transfer Function From Field Voltage to Terminal Voltage.

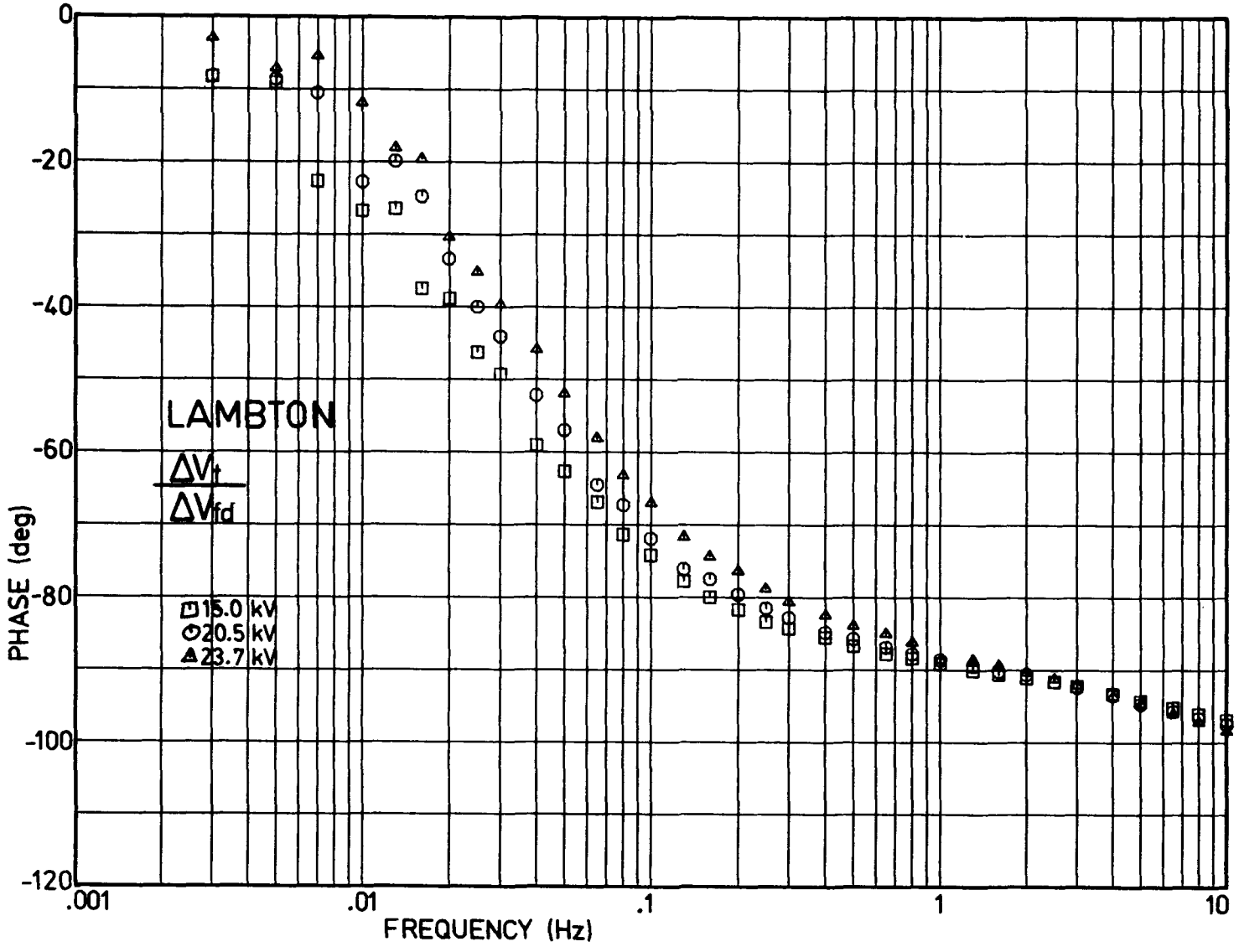

Figure 5-8. Phase of Lambton Open-Circuit Transfer Function From Field Voltage to Terminal Voltage.

LINEARITY TEST

The linearity of the open-circuit transfer function between field voltage and terminal voltage was checked. The amplitude of the field voltage swings was varied over as wide a range as possible at three selected frequencies: 0.1 Hz, 1.0 Hz, and 5.0 Hz.

The results of this test are presented in Figures 5-9 to 5-11 where the transfer functions $\Delta I_{fd}/\Delta V_{fd}$, $\Delta V_t/\Delta I_{fd}$, and $\Delta V_t/\Delta V_{fd}$, are plotted as functions of field current fluctuations. In the plots, the circles are the magnitude and the squares the phase angle of the measured transfer functions.

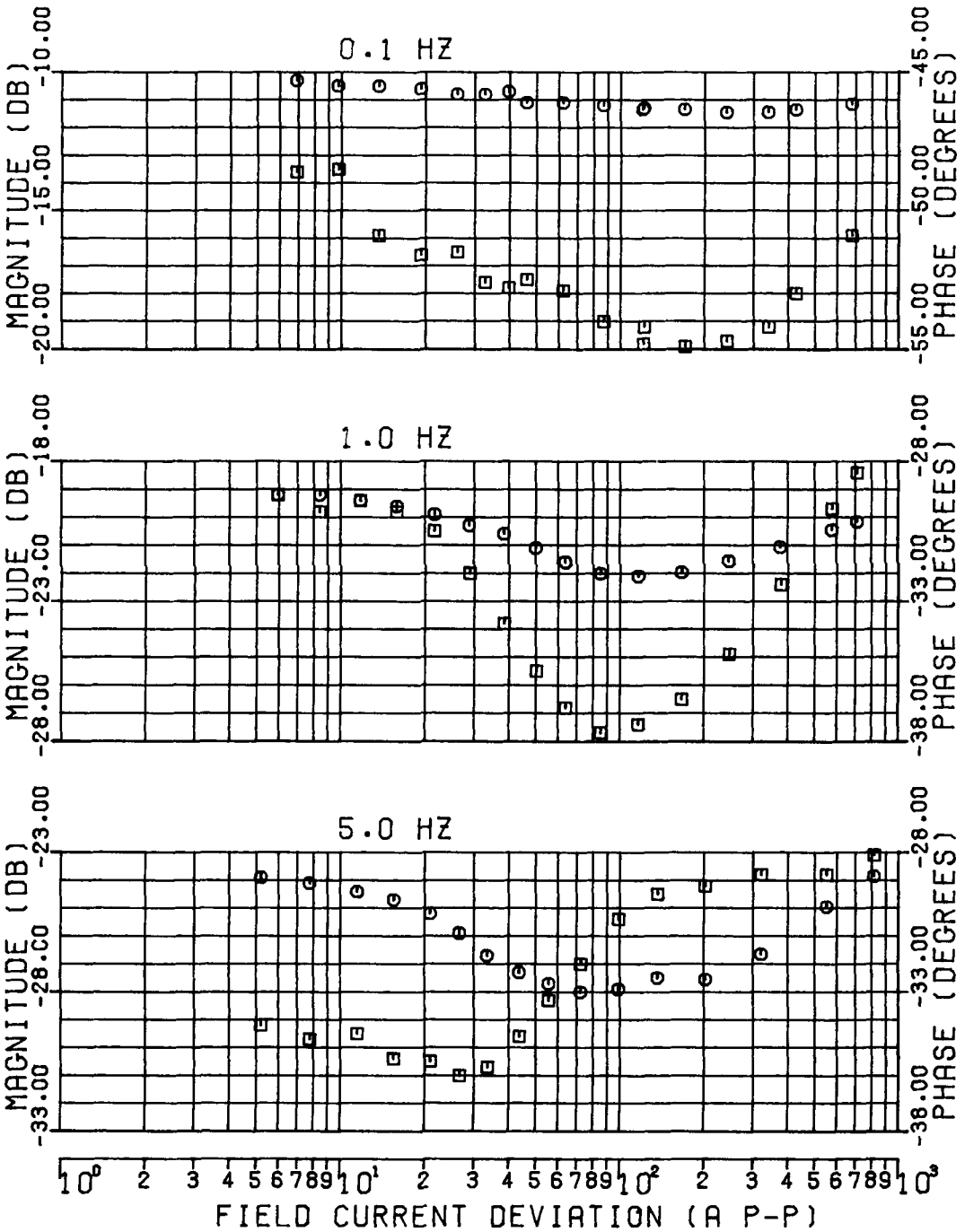

Figure 5-9. Magnitude of Lambton Open-Circuit Transfer Function From Field Voltage to Field Current as a Function of Field Current Deviation.

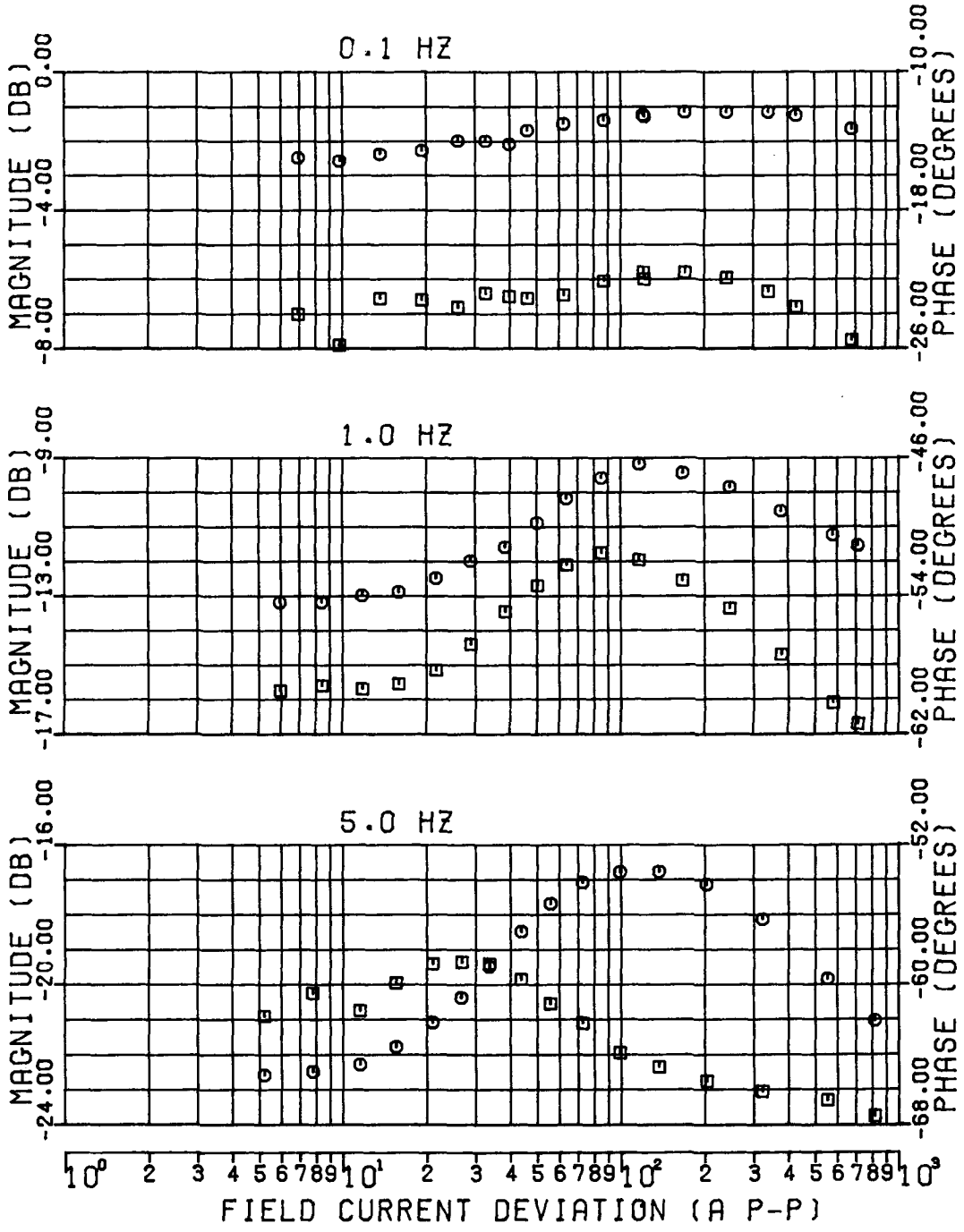

Figure 5-10. Magnitude of Lambton Open-Circuit Transfer Function From Field Current to Terminal Voltage as a Function of Field Current Deviation.

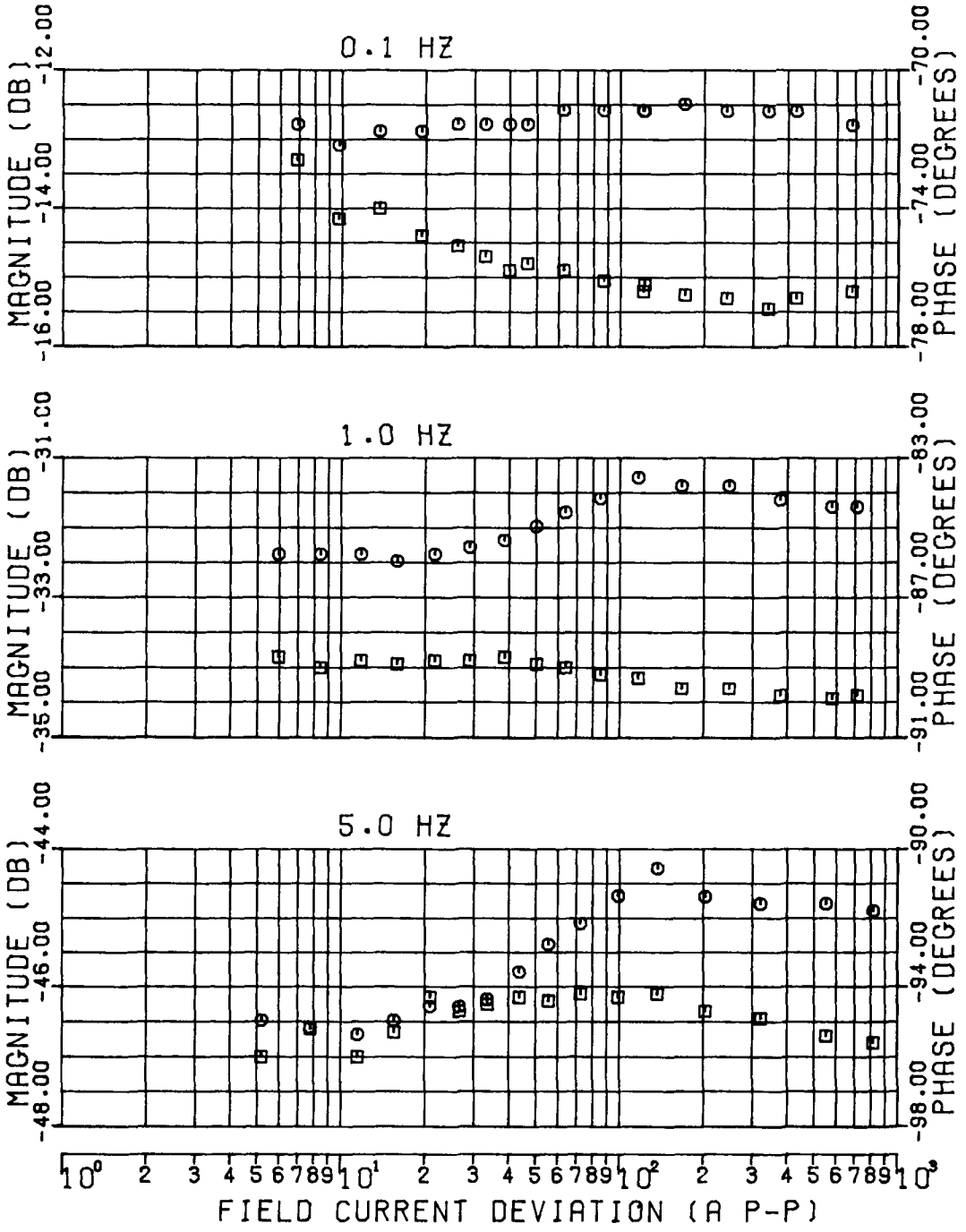

Figure 5-11. Magnitude of Lambton Open-Circuit Transfer Function From Field Voltage to Terminal Voltage as a Function of Field Current Deviation.

Section 6

STEADY STATE MEASUREMENTS

INTRODUCTION

Generator terminal quantities were measured at several steady state load points. As wide a range as possible was covered within the limits imposed by terminal voltage, core end heating and steady state stability. The purpose of the tests was to measure d- and q-axis saturation for comparison with that predicted by various saturation models.

INSTRUMENTATION

Terminal voltage, active power, reactive power, stator current, field voltage, and field current were measured with the existing transducers connected to the station computer. The generator internal angle was the only variable that required any special treatment. The output of the phase angle meter in Figure 6-1 was adjusted to zero while the generator was operating at rated speed, off line. In this condition, the terminal voltage vector is aligned with the q-axis; i.e., the internal angle is zero. With the phase shifter locked at this setting, the phase angle meter will read the internal angle when the generator is loaded.

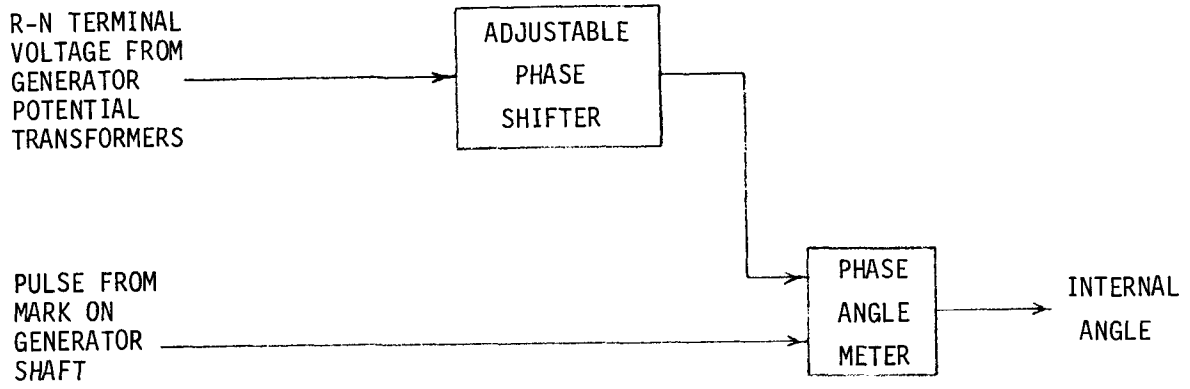

Figure 6-1. Internal Angle Measurement.

METHOD

The station computer was programmed to read the seven variables once per minute, and the generator was held at each load point for approximately five minutes. These results are listed in Table 6-1, as well as the quadrature axis synchronous reactance which was calculated from:

$$X_q = \frac{V_t^2 \sin \delta}{\sqrt{P^2 + Q^2} \cos (\delta + \phi)} \qquad (6\text{-}1)$$

where: V_t - terminal voltage

P - active power

Q - reactive power

δ - internal angle

ϕ - power factor angle

Table 6-1

LAMBTON STEADY STATE LOAD POINTS

POINT NUMBER	ACTIVE POWER (MW)	REACTIVE POWER (MVAR)	TERMINAL VOLTAGE (KV)	STATOR CURRENT (A)	FIELD CURRENT (A)	FIELD VOLTAGE (V)	INTERNAL ANGLE (DEG)	Q-AXIS REACTANCE (PU)
1	118.0	158.0	24.97	4640.	2435.	200.	11.1	1.349
2	117.5	160.3	24.99	4680.	2453.	205.	10.9	1.335
3	116.9	160.3	25.00	4680.	2448.	202.	10.8	1.333
4	116.9	171.1	25.00	4860.	2503.	207.	10.6	1.334
5	116.0	176.0	24.99	4950.	2529.	211.	10.4	1.329
6	116.1	177.6	24.99	4980.	2535.	213.	10.4	1.326
7	116.6	176.2	24.99	5000.	2539.	212.	10.4	1.320
8	116.9	178.5	25.00	5010.	2545.	212.	10.5	1.330
9	117.3	176.7	24.99	4990.	2537.	210.	10.5	1.324
10	116.6	176.2	24.99	4960.	2534.	212.	10.4	1.320
11	116.0	181.0	24.98	5100.	2578.	216.	10.3	1.316
12	115.5	194.7	24.98	5320.	2629.	218.	10.1	1.317
13	115.8	201.6	24.97	5480.	2675.	223.	9.9	1.303
14	115.8	208.0	24.97	5600.	2707.	225.	9.8	1.300
15	115.4	212.0	24.97	5700.	2735.	228.	9.6	1.282
16	115.2	215.3	24.97	5730.	2743.	230.	9.6	1.295
17	115.0	213.7	24.97	5700.	2735.	229.	9.6	1.293
18	115.3	213.9	24.95	5720.	2739.	228.	9.6	1.287
19	115.5	215.7	24.96	5760.	2749.	232.	9.7	1.297
20	115.1	215.3	24.97	5750.	2744.	228.	9.6	1.296
21	115.2	215.9	24.97	5760.	2750.	228.	9.6	1.296
22	115.2	213.7	24.97	5760.	2750.	228.	9.6	1.290
23	115.5	199.5	24.97	5440.	2664.	222.	9.9	1.302
24	115.5	201.8	24.97	5460.	2667.	222.	9.9	1.302
25	115.2	202.0	24.97	5490.	2676.	223.	9.8	1.293
26	115.4	202.8	24.97	5470.	2669.	223.	9.9	1.313
27	115.2	201.9	24.97	5480.	2671.	223.	9.2	1.178
28	115.3	204.8	24.96	5520.	2684.	226.	9.8	1.305
29	115.4	204.1	24.97	5510.	2684.	224.	9.8	1.296
30	115.4	189.6	24.99	5220.	2605.	216.	10.1	1.305
31	115.7	189.0	24.97	5220.	2606.	219.	10.1	1.310
32	115.4	186.7	24.98	5190.	2595.	218.	10.2	1.316
33	115.3	184.5	24.98	5130.	2579.	216.	10.2	1.311
34	115.6	183.7	24.99	5120.	2572.	217.	10.2	1.305
35	115.4	181.2	24.98	5070.	2565.	217.	10.2	1.307
36	115.5	181.8	24.99	5060.	2557.	212.	10.2	1.315
37	115.5	182.1	24.98	5060.	2558.	215.	10.2	1.314
38	115.4	180.5	24.98	5040.	2551.	215.	10.3	1.318
39	115.5	182.4	24.98	5080.	2562.	215	10.2	1.315
40	115.3	182.7	24.98	5080.	2569.	215.	10.2	1.319
41	115.5	183.7	24.98	5110.	2573.	215	10.2	1.312
42	115.3	184.7	24.98	5120.	2573.	214.	10.1	1.305
43	115.5	158.5	25.00	4620.	2439.	203.	10.7	1.325
44	115.3	159.2	25.01	4620.	2441.	206.	10.7	1.331
45	115.1	161.3	25.00	4670.	2452.	205.	10.6	1.321
46	115.0	160.9	25.00	4670.	2455.	207.	10.6	1.327
47	115.2	159.2	25.00	4610.	2436.	206.	10.7	1.332
48	115.1	160.5	25.01	4640.	2451.	207.	10.7	1.338
49	115.4	157.3	25.01	4600.	2436.	203.	10.7	1.324
50	114.7	157.8	25.00	4600.	2433.	205.	10.6	1.329
51	115.2	149.0	25.02	4420.	2386.	200.	10.8	1.334
52	115.1	136.5	24.88	4100.	2271.	189.	11.5	1.384
53	115.2	129.4	24.88	4100.	2268.	188.	11.5	1.360
54	115.5	129.8	24.89	4110.	2272.	189.	11.5	1.363
55	115.5	130.0	24.89	4100.	2273.	191.	11.5	1.358
56	115.7	129.9	24.88	4100.	2272.	191.	11.4	1.348
57	115.7	128.2	24.88	4090.	2268.	191.	11.5	1.354
58	115.8	127.9	24.89	4080.	2267.	189.	11.5	1.358
59	117.9	126.3	24.89	4100.	2261.	188.	11.7	1.355
60	118.2	129.3	24.89	4140.	2272.	189.	11.7	1.349
61	116.9	129.5	24.89	4110.	2272.	191.	11.6	1.358
62	116.1	127.5	24.87	4090.	2258.	189.	11.6	1.362
63	116.4	105.5	24.73	3740.	2133.	179.	12.3	1.380
64	115.7	103.6	24.73	3700.	2123.	178.	12.3	1.384
65	115.9	104.7	24.74	3720.	2131.	177.	12.3	1.381
66	116.0	105.5	24.72	3740.	2128.	178.	12.3	1.385
67	115.9	108.0	24.72	3770.	2142.	179.	12.2	1.379
68	115.5	107.6	24.72	3770.	2141.	179.	12.2	1.383
69	116.0	110.3	24.73	3810.	2158.	181.	12.2	1.380
70	116.0	108.7	24.72	3780.	2145.	179.	12.2	1.385
71	115.8	107.6	24.72	3760.	3134.	179.	12.2	1.384
72	115.7	79.9	24.53	3380.	1987.	168.	13.3	1.411
73	116.1	80.0	24.53	3390.	1978.	163.	13.3	1.411
74	116.1	79.9	24.54	3380.	1980.	166.	13.3	1.411
75	116.1	80.3	24.54	3400.	1988.	166.	13.2	1.403
76	116.0	81.1	24.54	3390.	1983.	165.	13.2	1.407
77	116.1	80.5	24.53	3410.	1989.	165.	13.2	1.403
78	116.3	56.7	24.39	3150.	1860.	155.	14.2	1.423
79	116.1	55.8	24.37	3120.	1848.	155.	14.3	1.429
80	116.1	55.5	24.37	3120.	1848.	155.	14.2	1.424

Table 6-1 (Continued)

LAMBTON STEADY STATE LOAD POINTS

POINT NUMBER	ACTIVE POWER (MW)	REACTIVE POWER (MVAR)	TERMINAL VOLTAGE (KV)	STATOR CURRENT (A)	FIELD CURRENT (A)	FIELD VOLTAGE (V)	INTERNAL ANGLE (DEG)	Q-AXIS REACTANCE (PU)
81	116.1	55.1	24.36	3120.	1841.	153.	14.3	1.434
82	116.3	52.0	24.37	3090.	1832.	152.	14.4	1.425
83	115.8	44.6	24.28	3000.	1766.	146.	14.7	1.437
84	116.2	30.0	24.20	2940.	1709.	144.	15.4	1.439
85	116.0	30.8	24.20	2940.	1713.	142.	14.7	1.373
86	116.1	32.3	24.21	2940.	1721.	144.	15.3	1.443
87	115.8	32.7	24.21	2930.	1716.	144.	15.3	1.444
88	116.0	32.8	24.21	2950.	1722.	142.	15.3	1.446
89	115.8	3.3	24.01	2870.	1566.	130.	16.9	1.474
90	116.2	0.0	23.98	2870.	1551.	129.	17.2	1.476
91	115.9	1.8	23.89	2850.	1551.	130.	17.1	1.469
92	116.0	-0.1	23.98	2870.	1545.	128.	17.2	1.478
93	116.2	-0.6	23.98	2870.	1549.	130.	17.1	1.470
94	116.3	-1.4	23.98	2870.	1544.	128.	17.3	1.476
95	116.3	-2.1	23.99	2860.	1534.	129.	17.3	1.481
96	116.0	-3.6	23.94	2870.	1508.	125.	17.4	1.482
97	116.5	-19.0	23.86	2920.	1447.	121.	18.4	1.491
98	116.4	-18.0	23.85	2930.	1452.	120.	18.4	1.489
99	116.0	-17.6	23.86	2910.	1454.	121.	18.3	1.494
100	115.9	-19.6	23.86	2920.	1443.	120.	18.5	1.499
101	116.2	-21.0	23.86	2920.	1442.	120.	18.5	1.492
102	116.0	-19.2	23.85	2910.	1452.	121.	18.3	1.486
103	116.3	-20.3	23.86	2910.	1447.	121.	18.4	1.485
104	116.2	-30.4	23.78	2990.	1381.	115.	19.2	1.495
105	116.5	-46.6	23.69	3100.	1317.	111.	20.5	1.508
106	116.9	-44.3	23.68	3110.	1327.	112.	20.3	1.502
107	115.9	-43.0	23.68	3080.	1328.	111.	20.1	1.504
108	116.1	-47.4	23.69	3110.	1311.	110.	20.4	1.507
109	116.5	-43.3	23.68	3090.	1328.	112.	20.5	1.524
110	116.1	-45.3	23.69	3090.	1319.	109.	20.3	1.508
111	116.4	-44.6	23.68	3110.	1318.	109.	20.4	1.512
112	116.6	-69.2	23.51	3380.	1206.	100.	22.5	1.523
113	116.6	-70.3	23.51	3400.	1199.	101.	22.7	1.525
114	116.4	-71.5	23.51	3410.	1194.	100.	22.7	1.522
115	116.5	-70.4	23.51	3400.	1196.	100.	22.6	1.523
116	116.4	-68.5	23.51	3380.	1204.	101.	22.5	1.526
117	116.6	-69.1	23.52	3390.	1198.	100.	22.5	1.520
118	116.3	-70.2	23.50	3390.	1204.	101.	22.6	1.523
119	116.8	-67.0	23.51	3380.	1208.	100.	22.4	1.524
120	116.7	-91.0	23.34	3730.	1101.	94.	25.0	1.538
121	116.7	-90.1	23.34	3710.	1096.	92.	24.8	1.534
122	116.5	-90.5	23.33	3710.	1100.	92.	24.9	1.535
123	116.3	-92.5	23.33	3740.	1092.	91.	25.0	1.534
124	116.3	-90.4	23.34	3710.	1100.	93.	24.8	1.535
125	116.1	-91.5	23.33	3720.	1096.	92.	24.9	1.536
126	116.3	-90.3	23.33	3710.	1101.	92.	24.9	1.538
127	116.3	-92.7	23.33	3750.	1095.	92.	25.0	1.534
128	116.3	-88.4	23.33	3680.	1106.	93.	24.7	1.537
129	116.9	-89.9	23.33	3710.	1100.	92.	24.8	1.530
130	116.7	-93.4	23.33	3780.	1083.	91.	25.1	1.535
131	116.3	-108.3	23.34	4000.	1021.	85.	26.5	1.539
132	116.6	-109.8	23.35	4020.	1023.	86.	26.6	1.534
133	116.8	-109.1	23.34	4000.	1029.	87.	26.6	1.534
134	116.9	-111.6	23.35	4050.	1018.	86.	26.8	1.535
135	116.9	-112.0	23.34	4080.	1012.	86.	26.9	1.536
136	116.9	-112.0	23.34	4050.	1017.	85.	26.8	1.532
137	116.6	-112.2	23.34	4050.	1017.	85.	26.8	1.533
138	116.6	-112.3	23.33	4060.	1016.	86.	26.9	1.535
139	116.5	-119.8	23.34	4200.	980.	83.	27.6	1.535
140	116.7	-120.7	23.34	4190.	986.	83.	27.6	1.529
141	116.6	-120.4	23.34	4200.	984.	83.	27.7	1.534
142	116.5	-120.6	23.35	4200.	981.	81.	27.7	1.535
143	116.6	-119.6	23.35	4180.	985.	83.	27.6	1.533
144	116.7	-119.6	23.34	4180.	988.	84.	27.7	1.538
145	116.9	-118.9	23.33	4200.	984.	84.	27.7	1.537
146	117.0	-117.2	23.34	4170.	990.	84.	27.5	1.536
147	116.3	-102.0	23.33	3890.	1057.	89.	25.9	1.539
148	116.6	-93.6	23.40	3740.	1097.	92.	25.0	1.535
149	116.2	-92.4	23.39	3730.	1098.	90.	24.8	1.535
150	116.6	-93.5	23.40	3750.	1095.	92.	24.9	1.534
151	131.0	-93.0	23.39	4040.	1145.	96.	27.4	1.529
152	136.2	-96.9	23.39	4180.	1146.	96.	28.5	1.519
153	137.7	-34.2	23.79	3520.	1474.	127.	22.8	1.507
154	135.3	30.2	24.31	3410.	1793.	148.	17.6	1.436
155	133.4	131.3	24.77	4540.	2336.	195.	13.4	1.376
156	132.1	171.7	24.88	5120.	2513.	205.	12.1	1.344
157	186.1	173.9	24.87	6030.	2607.	218.	16.8	1.342
158	191.5	169.4	24.88	6060.	2598.	216.	17.3	1.343
159	197.1	170.6	24.86	6160.	2610.	216.	17.8	1.344
160	204.5	169.9	24.87	6290.	2622.	217.	18.4	1.338

Table 6-1 (Continued)

LAMBTON STEADY STATE LOAD POINTS

POINT NUMBER	ACTIVE POWER (MW)	REACTIVE POWER (MVAR)	TERMINAL VOLTAGE (KV)	STATOR CURRENT (A)	FIELD CURRENT (A)	FIELD VOLTAGE (V)	INTERNAL ANGLE (DEG)	Q-AXIS REACTANCE (PU)
161	208.1	175.7	24.86	6430.	2660.	223.	18.6	1.341
162	208.8	180.1	24.86	6530.	2688.	225.	18.4	1.333
163	208.6	178.7	24.85	6510.	2682.	225.	18.4	1.333
164	210.4	178.6	24.87	6540.	2682.	223.	18.6	1.334
165	210.6	194.7	24.86	6770.	2760.	231.	18.1	1.324
166	210.0	193.0	24.86	6740.	2750.	228.	18.1	1.324
167	208.0	195.7	24.85	6750.	2763.	229.	17.8	1.321
168	207.7	196.7	24.85	6760.	2761.	231.	17.8	1.326
169	207.7	195.5	24.85	6760.	2764.	231.	17.8	1.323
170	207.8	195.1	24.85	6740.	2758.	229.	17.9	1.325
171	209.8	198.0	24.85	6830.	2781.	234.	17.9	1.323
172	210.7	197.6	24.85	6840.	2783.	233.	18.0	1.322
173	210.1	180.5	24.86	6530.	2683.	225.	18.5	1.330
174	209.3	179.4	24.85	6530.	2688.	225.	18.4	1.325
175	209.1	182.4	24.86	6550.	2696.	225.	18.3	1.329
176	209.5	182.7	24.86	6560.	2692.	226.	18.4	1.334
177	209.0	177.7	24.87	6490.	2672.	223.	18.5	1.333
178	209.7	177.1	24.86	6500.	2675.	225.	18.4	1.320
179	210.0	175.9	24.86	6480.	2664.	222.	18.6	1.333
180	209.8	174.9	24.86	6440.	2658.	221.	18.6	1.332
181	209.3	174.4	24.87	6440.	2656.	220.	18.6	1.336
182	209.6	171.5	24.87	6380.	2639.	223.	18.7	1.336
183	209.7	167.7	24.87	6340.	2624.	219.	18.9	1.339
184	209.5	168.6	24.87	6340.	2615.	217.	18.8	1.332
185	209.6	146.5	24.89	6040.	2518.	210.	19.6	1.347
186	209.4	145.2	24.88	6020.	2508.	211.	19.6	1.348
187	209.5	146.3	24.88	6030.	2511.	209.	19.6	1.347
188	209.3	145.4	24.89	6030.	2516.	210.	19.6	1.347
189	210.4	150.2	24.88	6100.	2536.	210.	19.5	1.347
190	211.1	152.4	24.88	6110.	2538.	211.	19.5	1.348
191	211.5	121.8	24.77	5790.	2387.	200.	20.8	1.362
192	211.7	130.0	24.84	5870.	2435.	203.	20.5	1.361
193	211.9	128.8	24.84	5870.	2431.	202.	20.5	1.355
194	212.7	130.9	24.84	5930.	2455.	205.	20.5	1.355
195	212.6	136.4	24.84	5960.	2467.	205.	20.3	1.359
196	214.3	134.9	24.83	5990.	2463.	207.	20.5	1.356
197	214.6	135.3	24.84	6000.	2465.	206.	20.5	1.353
198	213.0	133.5	24.83	5950.	2455.	206.	20.5	1.359
199	212.6	133.6	24.84	5940.	2453.	204.	20.4	1.357
200	212.3	108.0	24.66	5670.	2316.	195.	21.6	1.374
201	212.3	106.5	24.65	5670.	2305.	193.	21.8	1.378
202	212.8	105.4	24.65	5680.	2309.	193.	21.8	1.373
203	213.2	107.6	24.64	5700.	2312.	190.	21.8	1.376
204	213.6	106.0	24.64	5700.	2314.	193.	21.9	1.377
205	213.9	105.9	24.65	5690.	2312.	192.	21.9	1.375
206	213.7	108.2	24.65	5710.	2316.	191.	21.8	1.378
207	213.3	103.6	24.65	5650.	2297.	191.	22.0	1.379
208	213.0	82.0	24.50	5470.	2178.	183.	23.2	1.395
209	213.0	78.8	24.50	5440.	2169.	180.	23.3	1.396
210	213.3	80.2	24.50	5480.	2179.	182.	23.3	1.392
211	213.0	81.2	24.50	5460.	2178.	182.	23.2	1.395
212	212.3	80.2	24.50	5450.	2178.	182.	23.2	1.394
213	211.7	79.7	24.50	5420.	2164.	181.	23.2	1.395
214	211.3	80.7	24.50	5430.	2177.	182.	23.1	1.395
215	211.0	77.7	24.47	5390.	2140.	176.	23.3	1.399
216	211.3	56.2	24.34	5280.	2055.	172.	24.6	1.410
217	210.8	54.5	24.34	5260.	2047.	172.	24.6	1.408
218	210.4	59.1	24.33	5280.	2059.	170.	24.4	1.410
219	209.9	58.9	24.33	5280.	2067.	172.	24.3	1.405
220	210.3	61.6	24.34	5300.	2077.	172.	24.2	1.409
221	209.9	48.3	24.24	5240.	2002.	167.	25.1	1.421
222	210.4	30.9	24.12	5190.	1927.	162.	26.5	1.436
223	210.8	31.6	24.12	5200.	1928.	160.	26.4	1.430
224	211.0	31.6	24.11	5210.	1931.	159.	26.5	1.433
225	211.2	29.8	24.11	5210.	1933.	161.	26.5	1.425
226	211.1	1.4	23.87	5210.	1797.	149.	28.9	1.444
227	211.7	-2.5	23.88	5210.	1778.	147.	29.3	1.450
228	211.0	-2.7	23.88	5200.	1776.	149.	29.3	1.454
229	210.5	-4.0	23.88	5180.	1773.	148.	29.2	1.448
230	211.0	-1.3	23.87	5200.	1779.	148.	29.2	1.451
231	211.3	-0.3	23.87	5210.	1789.	149.	28.9	1.434
232	211.3	-24.4	23.72	5270.	1688.	140.	31.2	1.453
233	211.0	-24.1	23.72	5260.	1686.	139.	31.2	1.457
234	211.1	-23.4	23.72	5260.	1684.	140.	31.3	1.463
235	211.0	-22.0	23.72	5250.	1692.	140.	31.1	1.459
236	211.1	-49.0	23.55	5400.	1585.	132.	33.7	1.464
237	210.8	-47.7	23.55	5390.	1590.	132.	33.6	1.466
238	211.2	-47.8	23.56	5390.	1588.	132.	33.6	1.466
239	210.8	-48.8	23.55	5400.	1585.	132.	33.8	1.469
240	210.8	-49.0	23.55	5390.	1580.	129.	33.6	1.461

Table 6-1 (Continued)

LAMBTON STEADY STATE LOAD POINTS

POINT NUMBER	ACTIVE POWER (MW)	REACTIVE POWER (MVAR)	TERMINAL VOLTAGE (KV)	STATOR CURRENT (A)	FIELD CURRENT (A)	FIELD VOLTAGE (V)	INTERNAL ANGLE (DEG)	Q-AXIS REACTANCE (PU)
241	210.9	-48.5	23.55	5400.	1586.	130.	33.7	1.466
242	210.8	-68.1	23.42	5540.	1511.	126.	35.9	1.473
243	211.2	-64.1	23.41	5540.	1517.	125.	35.7	1.475
244	211.1	-67.8	23.42	5550.	1505.	124.	35.9	1.474
245	211.4	-69.2	23.42	5570.	1505.	124.	36.1	1.471
246	211.6	-65.7	23.42	5550.	1519.	126.	35.8	1.473
247	211.7	-63.7	23.40	5560.	1525.	125.	35.9	1.485
248	211.5	-64.8	23.40	5560.	1517.	125.	35.7	1.472
249	211.5	-63.6	23.40	5550.	1519.	125.	35.7	1.474
250	211.3	-95.9	23.19	5860.	1401.	115.	39.6	1.476
251	210.9	-94.6	23.19	5850.	1406.	117.	39.4	1.478
252	211.5	-93.5	23.19	5850.	1411.	116.	39.3	1.473
253	210.3	-93.7	23.19	5840.	1409.	117.	39.4	1.483
254	210.7	-93.1	23.19	5810.	1409.	116.	39.3	1.478
255	210.6	-92.3	23.20	5810.	1415.	119.	39.0	1.475
256	210.1	-94.4	23.18	5820.	1403.	115.	39.3	1.477
257	210.2	-94.1	23.19	5820.	1403.	118.	39.3	1.479
258	210.3	-102.3	23.19	5920.	1374.	114.	40.2	1.476
259	210.6	-109.1	23.20	5990.	1354.	111.	41.0	1.476
260	210.1	-111.5	23.18	6010.	1354.	114.	41.3	1.477
261	210.5	-110.4	23.20	6020.	1351.	111.	41.1	1.477
262	210.8	-113.4	23.19	6040.	1344.	112.	41.5	1.474
263	210.8	-113.6	23.20	6050.	1344.	110.	41.5	1.474
264	210.3	-114.2	23.19	6060.	1338.	110.	41.5	1.474
265	210.4	-111.4	23.19	6030.	1345.	110.	41.2	1.476
266	210.7	-112.9	23.19	6040.	1344.	112.	41.4	1.474
267	211.2	-112.1	23.19	6040.	1354.	111.	41.4	1.473
268	211.3	-122.4	23.17	6170.	1320.	108.	42.7	1.473
269	211.2	-131.2	23.17	6290.	1290.	106.	43.8	1.475
270	211.3	-131.5	23.18	6280.	1292.	107.	43.8	1.473
271	211.1	-134.1	23.17	6320.	1283.	105.	44.1	1.472
272	211.2	-132.7	23.17	6310.	1286.	107.	44.0	1.473
273	211.3	-132.1	23.18	6310.	1284.	105.	44.0	1.477
274	211.3	-113.7	23.16	6050.	1351.	113.	41.7	1.474
275	211.1	-104.6	23.16	5960.	1374.	114.	40.7	1.478
276	211.3	-106.3	23.16	5990.	1365.	114.	41.0	1.481
277	211.5	-31.7	23.46	5340.	1653.	136.	32.8	1.474
278	210.7	93.5	24.34	5560.	2230.	182.	22.8	1.405
279	210.3	171.9	24.86	6420.	2649.	217.	18.8	1.337
280	218.0	176.5	24.88	6610.	2688.	222.	19.3	1.336
281	224.0	175.8	24.88	6720.	2692.	223.	19.8	1.335
282	229.7	174.1	24.89	6790.	2695.	223.	20.4	1.342
283	242.1	174.9	24.88	7040.	2722.	227.	21.3	1.337
284	251.4	173.0	24.89	7200.	2738.	228.	22.0	1.334
285	250.5	174.5	24.88	7200.	2748.	227.	21.9	1.334
286	263.9	177.2	24.87	7480.	2777.	230.	22.9	1.334
287	273.2	175.7	24.87	7670.	2812.	237.	23.6	1.323
288	280.2	175.5	24.88	7790.	2819.	234.	24.1	1.324
289	282.7	173.0	24.88	7810.	2815.	234.	24.4	1.328
290	291.5	172.3	24.87	8010.	2830.	237.	25.2	1.335
291	297.8	173.9	24.87	8180.	2855.	240.	25.7	1.340
292	301.8	170.1	24.88	8150.	2839.	236.	25.8	1.311
293	301.9	212.7	24.85	8710.	3050.	254.	25.8	1.442
294	303.9	218.5	24.85	8820.	3090.	257.	24.2	1.299
295	302.7	233.5	24.84	9040.	3171.	265.	23.5	1.288
296	302.6	232.9	24.83	9010.	3158.	264.	23.6	1.293
297	303.2	235.8	24.83	9080.	3178.	267.	23.5	1.291
298	304.5	236.4	24.82	9120.	3182.	268.	23.6	1.286
299	303.8	237.7	24.84	9060.	3171.	268.	23.5	1.290
300	303.7	231.7	24.83	9030.	3157.	265.	23.7	1.292
301	303.5	234.7	24.83	9060.	3169.	266.	23.6	1.289
302	304.3	234.8	24.83	9100.	3183.	269.	23.6	1.287
303	304.7	262.1	24.98	9380.	3313.	277.	22.4	1.265
304	304.1	263.2	24.99	9440.	3338.	281.	22.3	1.263
305	304.5	260.2	24.99	9420.	3332.	282.	22.4	1.256
306	304.9	221.7	25.02	8840.	3125.	265.	23.8	1.283
307	304.6	221.9	25.02	8850.	3127.	264.	23.8	1.286
308	304.7	223.0	25.02	8850.	3126.	265.	23.7	1.285
309	304.7	221.7	25.01	8820.	3113.	261.	23.8	1.287
310	304.3	219.1	25.02	8790.	3106.	260.	23.8	1.286
311	304.9	220.7	25.01	8830.	3116.	261.	23.8	1.286
312	304.9	224.5	25.02	8850.	3127.	264.	23.7	1.288
313	305.4	222.4	25.01	8850.	3122.	263.	23.8	1.288
314	306.1	197.5	25.02	8520.	2989.	253.	24.8	1.300
315	305.6	193.7	25.02	8480.	2982.	250.	24.9	1.296
316	305.7	196.8	25.02	8540.	3005.	251.	24.7	1.295
317	305.7	197.9	25.02	8540.	3003.	254.	24.7	1.298
318	305.7	198.8	25.02	8540.	3002.	254.	24.7	1.297
319	305.9	188.1	25.03	8390.	2940.	247.	25.1	1.303
320	305.9	182.0	25.02	8360.	2932.	245.	25.3	1.297

Table 6-1 (Continued)

LAMBTON STEADY STATE LOAD POINTS

POINT NUMBER	ACTIVE POWER (MW)	REACTIVE POWER (MVAR)	TERMINAL VOLTAGE (KV)	STATOR CURRENT (A)	FIELD CURRENT (A)	FIELD VOLTAGE (V)	INTERNAL ANGLE (DEG)	Q-AXIS REACTANCE (PU)
321	305.7	173.3	25.03	8240.	2885.	241.	25.6	1.304
322	306.2	174.7	25.03	8280.	2897.	243.	25.6	1.302
323	305.7	160.3	24.96	8110.	2820.	239.	26.4	1.319
324	305.6	160.2	24.95	8140.	2817.	236.	26.4	1.316
325	307.3	162.4	24.95	8180.	2835.	239.	26.4	1.315
326	305.9	160.6	24.95	8130.	2815.	236.	26.4	1.315
327	306.0	158.8	24.96	8130.	2821.	239.	26.4	1.311
328	305.8	135.8	24.78	7940.	2692.	225.	27.9	1.339
329	307.0	134.3	24.77	7950.	2683.	225.	28.0	1.335
330	309.6	133.5	24.78	7980.	2691.	225.	28.2	1.332
331	307.6	132.3	24.78	7950.	2688.	226.	28.0	1.329
332	306.6	135.6	24.77	7950.	2691.	224.	27.9	1.336
333	307.0	131.0	24.77	7910.	2677.	223.	28.1	1.335
334	306.3	131.3	24.78	7890.	2670.	222.	28.1	1.339
335	306.1	129.5	24.78	7890.	2672.	223.	28.1	1.334
336	307.8	107.4	24.61	7800.	2569.	213.	29.7	1.350
337	306.4	109.1	24.61	7760.	2563.	214.	29.4	1.346
338	306.5	106.4	24.62	7740.	2554.	214.	29.7	1.355
339	305.6	102.5	24.63	7700.	2541.	211.	29.7	1.349
340	305.9	104.9	24.62	7740.	2558.	213.	29.6	1.349
341	306.1	103.8	24.62	7730.	2545.	212.	29.7	1.352
342	305.6	102.1	24.61	7710.	2536.	211.	29.8	1.351
343	306.2	107.9	24.63	7750.	2563.	214.	29.5	1.350
344	306.9	101.8	24.58	7710.	2520.	209.	30.0	1.356
345	306.2	81.7	24.45	7630.	2444.	203.	31.3	1.364
346	306.7	81.7	24.46	7620.	2446.	204.	31.3	1.365
347	307.3	82.6	24.46	7650.	2453.	206.	31.3	1.363
348	307.0	84.0	24.47	7650.	2462.	205.	31.2	1.365
349	306.9	69.1	24.34	7590.	2376.	198.	32.3	1.375
350	306.7	64.0	24.32	7570.	2366.	198.	32.7	1.379
351	306.7	64.9	24.32	7580.	2365.	198.	32.6	1.378
352	306.7	64.1	24.33	7570.	2374.	198.	32.7	1.379
353	305.9	65.3	24.31	7570.	2369.	198.	32.6	1.380
354	306.3	64.6	24.32	7570.	2373.	198.	32.6	1.377
355	306.0	62.5	24.32	7550.	2355.	196.	32.7	1.380
356	306.5	43.7	24.18	7530.	2282.	189.	34.3	1.388
357	306.1	43.0	24.17	7530.	2285.	190.	34.3	1.386
358	305.7	43.6	24.18	7510.	2280.	190.	34.2	1.389
359	305.4	44.3	24.18	7500.	2281.	190.	34.1	1.389
360	305.8	44.2	24.18	7510.	2281.	190.	34.3	1.393
361	306.1	43.6	24.17	7510.	2275.	190.	34.3	1.392
362	306.3	45.6	24.17	7540.	2285.	190.	34.1	1.388
363	305.6	39.9	24.18	7490.	2267.	188.	34.4	1.390
364	305.3	38.9	24.18	7480.	2259.	186.	34.4	1.388
365	305.9	23.5	24.06	7490.	2197.	183.	35.9	1.402
366	306.0	25.9	24.05	7510.	2208.	182.	35.8	1.399
367	306.3	16.2	23.99	7510.	2167.	179.	36.6	1.403
368	306.4	14.7	24.00	7510.	2162.	179.	36.7	1.402
369	305.8	13.8	24.00	7480.	2161.	180.	36.7	1.402
370	305.7	2.9	23.92	7520.	2119.	176.	37.8	1.408
371	306.4	7.5	23.92	7520.	2136.	176.	37.4	1.403
372	306.2	8.6	23.92	7530.	2137.	175.	37.4	1.410
373	307.3	-20.8	23.67	7650.	2036.	167.	40.4	1.416
374	307.0	-25.1	23.66	7630.	2008.	166.	40.7	1.415
375	306.2	-19.8	23.65	7620.	2028.	168.	40.4	1.420
376	306.5	-24.0	23.67	7630.	2018.	167.	40.6	1.416
377	306.0	-21.3	23.66	7620.	2027.	169.	40.3	1.415
378	306.8	-24.6	23.67	7630.	2022.	167.	40.6	1.414
379	306.7	-22.2	23.67	7630.	2026.	167.	40.5	1.418
380	306.2	-49.3	23.43	7770.	1933.	160.	43.6	1.426
381	305.9	-52.2	23.44	7780.	1919.	159.	43.8	1.428
382	307.0	-50.8	23.44	7780.	1931.	158.	43.7	1.424
383	306.7	-52.4	23.44	7780.	1922.	159.	43.8	1.424
384	306.2	-51.3	23.44	7760.	1927.	160.	43.7	1.425
385	306.2	-53.1	23.44	7780.	1916.	159.	43.9	1.429
386	306.2	-71.2	23.32	7910.	1852.	151.	46.0	1.430
387	306.6	-79.7	23.24	8000.	1834.	153.	47.1	1.428
388	306.4	-82.5	23.22	8010.	1820.	150.	47.5	1.431
389	306.5	-83.3	23.21	8030.	1828.	151.	47.6	1.431
390	306.7	-82.6	23.21	8030.	1832.	153.	47.4	1.427
391	306.2	-81.6	23.21	8010.	1826.	152.	47.4	1.432
392	306.2	-81.2	23.22	8000.	1827.	149.	47.4	1.434
393	306.4	-84.5	23.21	8030.	1821.	150.	47.7	1.431
394	306.5	-88.0	23.22	8050.	1810.	148.	48.1	1.432
395	306.3	-86.3	23.22	8050.	1816.	151.	47.8	1.430
396	306.4	-99.6	23.22	8140.	1776.	146.	49.3	1.431
397	307.1	-101.5	23.22	8170.	1778.	146.	49.6	1.435
398	306.4	-99.2	23.23	8140.	1779.	148.	49.3	1.434
399	306.8	-100.7	23.22	8150.	1780.	147.	49.3	1.428
400	306.3	-101.7	23.22	8150.	1776.	146.	49.4	1.427

Table 6-1 (Continued)

LAMBTON STEADY STATE LOAD POINTS

POINT NUMBER	ACTIVE POWER (MW)	REACTIVE POWER (MVAR)	TERMINAL VOLTAGE (KV)	STATOR CURRENT (A)	FIELD CURRENT (A)	FIELD VOLTAGE (V)	INTERNAL ANGLE (DEG)	Q-AXIS REACTANCE (PU)
401	306.7	-98.0	23.22	8130.	1782.	146.	49.1	1.430
402	306.4	-97.1	23.22	8110.	1788.	149.	48.9	1.426
403	306.6	-99.7	23.22	8140.	1781.	147.	49.2	1.427
404	306.1	-102.1	23.22	8140.	1774.	145.	49.4	1.426
405	306.2	-101.0	23.22	8130.	1774.	146.	49.3	1.429
406	306.4	-101.3	23.22	8140.	1776.	145.	49.4	1.430
407	306.9	-98.9	23.22	8130.	1785.	147.	49.1	1.426
408	307.0	-99.9	23.22	8140.	1787.	147.	49.2	1.425
409	307.2	-107.7	23.23	8210.	1759.	145.	50.2	1.430
410	307.6	-108.3	23.22	8240.	1759.	146.	50.3	1.428
411	307.0	-110.4	23.21	8240.	1753.	143.	50.4	1.424
412	307.8	-112.4	23.23	8270.	1755.	144.	50.6	1.425
413	307.9	-112.1	23.22	8260.	1755.	144.	50.6	1.424
414	307.5	-112.4	23.22	8260.	1753.	143.	50.5	1.421
415	308.0	-117.0	23.23	8260.	1757.	145.	50.5	1.403
416	308.1	-101.9	23.21	8200.	1782.	147.	49.6	1.426
417	308.1	-89.0	23.21	8100.	1819.	151.	48.2	1.427
418	307.4	-90.0	23.21	8090.	1814.	151.	48.3	1.429
419	306.8	-86.8	23.21	8050.	1820.	151.	47.9	1.428
420	305.8	159.6	24.78	8170.	2808.	231.	26.9	1.334
421	306.5	128.1	24.80	7860.	2662.	221.	28.2	1.338
422	306.0	124.4	24.80	7830.	2645.	218.	28.3	1.337
423	313.2	125.3	24.81	7990.	2669.	221.	28.9	1.340
424	314.1	126.0	24.81	8010.	2671.	223.	28.9	1.342
425	328.6	125.5	24.79	8340.	2711.	224.	30.0	1.334
426	333.3	125.1	24.79	8430.	2730.	229.	30.3	1.333
427	334.1	120.9	24.80	8410.	2711.	225.	30.5	1.332
428	350.0	123.5	24.79	8840.	2770.	230.	31.7	1.335
429	377.6	121.8	24.78	9420.	2851.	238.	33.6	1.327
430	391.0	126.0	24.77	9730.	2904.	244.	34.3	1.321
431	410.8	123.4	24.77	10170.	30.	248.	35.6	1.311
432	411.7	125.9	24.77	10180.	2971.	250.	35.5	1.310
433	407.4	123.9	24.77	10070.	2952.	248.	35.3	1.311
434	405.9	125.5	24.77	10030.	2957.	248.	35.1	1.310
435	407.4	126.3	24.77	10070.	2970.	250.	35.2	1.311
436	411.9	127.3	24.76	10180.	2988.	250.	35.4	1.310
437	406.0	126.7	24.77	10020.	2957.	249.	35.0	1.309
438	400.9	130.4	24.76	9960.	2954.	248.	34.6	1.313
439	402.1	131.7	24.78	9970.	2962.	248.	34.6	1.314
440	400.1	196.4	25.02	10420.	3263.	272.	30.8	1.274
44[illegible]	400.6	216.8	25.01	10640.	3357.	283.	30.1	1.273
442	398.8	234.1	25.01	10790.	3432.	291.	29.2	1.262
443	400.8	236.9	25.01	10880.	3458.	293.	29.3	1.263
444	399.7	236.8	25.00	10850.	3451.	290.	29.2	1.264
445	397.9	234.3	25.01	10770.	3434.	291.	29.2	1.264
446	397.0	231.9	25.01	10740.	3427.	292.	29.2	1.262
447	396.6	236.6	25.01	10760.	3437.	291.	29.1	1.268
448	396.9	234.4	25.01	10770.	3432.	291.	29.1	1.261
449	398.9	223.2	25.02	10650.	3379.	286.	29.7	1.269
450	398.3	222.0	25.03	10630.	3377.	286.	29.7	1.267
451	397.2	222.2	25.03	10620.	3380.	287.	29.6	1.268
452	398.3	224.2	25.02	10660.	3385.	288.	29.6	1.267
453	398.2	221.9	25.02	10650.	3384.	287.	29.7	1.266
454	397.7	225.5	25.02	10640.	3381.	285.	29.6	1.273
455	398.4	223.5	25.02	10640.	3380.	287.	29.7	1.273
456	397.7	199.0	24.88	10420.	3255.	275.	30.9	1.286
457	400.4	198.4	24.88	10500.	3262.	277.	31.1	1.282
458	400.7	197.1	24.89	10490.	3259.	274.	31.2	1.283
459	404.6	202.1	24.87	10630.	3294.	275.	31.2	1.282
460	406.9	203.0	24.87	10670.	3297.	279.	31.3	1.280
461	405.1	201.6	24.88	10620.	3288.	274.	31.2	1.277
462	403.2	174.9	24.69	10380.	3149.	268.	32.8	1.303
463	400.2	175.2	24.69	10320.	3142.	265.	32.6	1.305
464	399.3	174.3	24.69	10290.	3138.	267.	32.5	1.299
465	398.3	174.4	24.68	10300.	3140.	265.	32.6	1.308
466	400.2	176.7	24.69	10340.	3150.	264.	32.5	1.302
467	399.7	177.5	24.68	10360.	3154.	267.	32.4	1.298
468	398.5	176.8	24.70	10320.	3148.	264.	32.4	1.306
469	400.1	176.0	24.68	10370.	3151.	266.	32.6	1.304
470	407.9	176.5	24.69	10500.	3165.	264.	33.0	1.302
471	411.4	156.4	24.54	10470.	3093.	261.	34.4	1.309
472	408.1	156.1	24.57	10390.	3081.	261.	34.3	1.316
473	408.1	155.0	24.55	10390.	3078.	258.	34.4	1.316
474	409.4	156.3	24.56	10420.	3084.	260.	34.3	1.313
475	408.8	154.7	24.56	10410.	3078.	257.	34.4	1.313
476	406.5	154.1	24.56	10330.	3065.	259.	34.3	1.314
477	408.5	158.8	24.56	10420.	3095.	261.	34.1	1.310
478	404.7	132.3	24.40	10180.	2967.	252.	35.7	1.330
479	403.9	130.9	24.40	10170.	2959.	251.	35.6	1.327
480	402.6	130.0	24.41	10130.	2956.	249.	35.7	1.333

Table 6-1 (Continued)

LAMBTON STEADY STATE LOAD POINTS

POINT NUMBER	ACTIVE POWER (MW)	REACTIVE POWER (MVAR)	TERMINAL VOLTAGE (KV)	STATOR CURRENT (A)	FIELD CURRENT (A)	FIELD VOLTAGE (V)	INTERNAL ANGLE (DEG)	Q-AXIS REACTANCE (PU)
481	403.8	130.0	24.41	10140.	2951.	250.	35.7	1.330
482	402.1	130.0	24.41	10100.	2948.	247.	35.6	1.331
483	400.1	128.4	24.38	10070.	2939.	246.	35.5	1.324
484	401.2	108.4	24.25	10000.	2853.	243.	37.1	1.346
485	402.0	106.4	24.25	10000.	2845.	238.	37.3	1.345
486	402.9	104.2	24.25	10010.	2844.	241.	37.4	1.343
487	401.0	106.1	24.25	9980.	2841.	240.	37.2	1.346
488	401.2	108.2	24.25	10000.	2848.	237.	37.1	1.345
489	400.3	107.6	24.25	9960.	2845.	237.	37.1	1.345
490	400.5	104.8	24.26	9950.	2836.	237.	37.3	1.350
491	400.4	91.6	24.26	9880.	2784.	232.	38.0	1.351
492	399.8	88.2	24.26	9850.	2770.	232.	38.2	1.353
493	400.9	89.3	24.26	9890.	2782.	232.	38.1	1.348
494	400.8	88.6	24.26	9870.	2776.	235.	38.2	1.348
495	402.0	86.9	24.26	9910.	2777.	230.	38.3	1.346
496	401.3	91.7	24.24	9920.	2788.	234.	38.1	1.348
497	406.9	93.9	24.25	10060.	2816.	236.	38.3	1.346
498	407.9	92.6	24.25	10080.	2819.	237.	38.4	1.346
499	411.0	88.2	24.25	10120.	2810.	236.	38.9	1.345
500	411.1	67.3	24.26	10030.	2733.	229.	40.1	1.348
501	410.2	66.6	24.26	10000.	2724.	229.	40.1	1.349
502	408.6	63.0	24.26	9950.	2710.	226.	40.2	1.348
503	409.2	66.2	24.27	9980.	2726.	228.	40.0	1.347
504	406.0	64.5	24.26	9890.	2703.	226.	39.9	1.351
505	401.2	64.2	24.27	9780.	2695.	227.	39.6	1.352
506	400.2	59.5	24.27	9740.	2670.	224.	39.8	1.350
507	398.6	47.1	24.28	9660.	2617.	220.	40.6	1.360
508	398.0	44.4	24.28	9640.	2601.	216.	40.7	1.359
509	397.7	41.2	24.28	9620.	2592.	218.	40.8	1.358
510	397.8	41.2	24.28	9620.	2588.	215.	40.9	1.359
511	398.4	40.0	24.29	9630.	2596.	219.	41.0	1.360
512	399.0	18.5	24.13	9660.	2515.	212.	42.9	1.365
513	398.9	18.0	24.14	9660.	2517.	210.	42.9	1.367
514	400.9	17.7	24.13	9720.	2523.	210.	43.0	1.365
515	402.6	19.1	24.13	9760.	2532.	209.	43.1	1.365
516	401.9	16.9	24.14	9720.	2525.	211.	43.2	1.365
517	402.3	-2.0	24.01	9780.	2466.	204.	44.9	1.370
518	403.6	-0.1	24.01	9830.	2479.	206.	44.8	1.370
519	404.4	-0.1	24.00	9830.	2475.	207.	45.0	1.373
520	403.4	1.5	24.01	9810.	2482.	205.	44.8	1.373
521	402.6	1.7	24.00	9780.	2474.	207.	44.7	1.371
522	400.9	2.7	24.01	9760.	2469.	204.	44.6	1.375
523	399.2	0.1	24.02	9700.	2459.	204.	44.5	1.371
524	400.7	0.7	24.01	9740.	2466.	204.	44.6	1.369
525	400.2	-0.8	24.00	9740.	2460.	206.	44.8	1.375
526	399.5	-24.4	23.85	9800.	2381.	200.	46.9	1.379
527	400.0	-26.6	23.84	9830.	2388.	198.	46.9	1.366
528	401.0	-22.5	23.85	9850.	2394.	198.	46.9	1.379
529	401.3	-23.6	23.85	9860.	2390.	200.	47.0	1.381
530	402.0	-22.1	23.86	9860.	2395.	200.	46.9	1.380
531	400.7	-23.6	23.84	9850.	2389.	198.	47.0	1.379
532	400.9	-26.4	23.81	9870.	2356.	192.	47.4	1.386
533	400.2	-47.1	23.68	9950.	2315.	192.	49.4	1.386
534	400.9	-49.4	23.70	9960.	2316.	193.	49.5	1.382
535	400.7	-45.7	23.68	9950.	2324.	193.	49.2	1.383
536	401.3	-46.1	23.69	9960.	2324.	193.	49.3	1.382
537	400.1	-49.1	23.69	9940.	2314.	193.	49.5	1.385
538	400.3	-50.3	23.70	9930.	2312.	192.	49.5	1.383
539	400.7	-69.5	23.53	10100.	2258.	187.	51.9	1.391
540	400.5	-69.1	23.54	10080.	2259.	188.	51.8	1.391
541	401.3	-70.6	23.54	10110.	2263.	187.	51.9	1.388
542	399.9	-71.5	23.53	10090.	2255.	187.	51.9	1.387
543	401.7	-70.4	23.54	10130.	2265.	188.	51.9	1.387
544	406.3	-68.3	23.54	10240.	2292.	189.	52.1	1.388
545	408.0	-88.3	23.37	10470.	2231.	180.	54.5	1.390
546	409.2	-97.2	23.33	10540.	2233.	187.	55.7	1.393
547	407.8	-98.8	23.33	10490.	2221.	184.	55.5	1.387
548	403.3	-99.3	23.33	10400.	2199.	182.	55.4	1.391
549	404.3	-97.3	23.33	10420.	2213.	184.	55.3	1.390
550	404.7	-97.2	23.33	10430.	2213.	181.	55.4	1.393
551	402.8	-96.5	23.33	10370.	2205.	181.	55.2	1.394
552	401.3	-96.1	23.34	10340.	2199.	183.	55.0	1.395
553	402.0	-114.7	23.20	10530.	2163.	179.	57.4	1.396
554	401.6	-118.5	23.17	10560.	2154.	178.	57.8	1.395
555	404.8	-118.1	23.16	10650.	2172.	178.	57.9	1.390
556	403.9	-118.4	23.16	10630.	2167.	181.	57.9	1.391
557	402.7	-118.7	23.16	10600.	2156.	178.	57.8	1.390
558	401.6	-118.6	23.15	10570.	2156.	178.	57.8	1.392
559	403.1	-118.7	23.17	10590.	2162.	179.	57.8	1.389
560	404.1	-116.9	23.16	10620.	2172.	180.	57.7	1.391

Table 6-1 (Continued)

LAMBTON STEADY STATE LOAD POINTS

POINT NUMBER	ACTIVE POWER (MW)	REACTIVE POWER (MVAR)	TERMINAL VOLTAGE (KV)	STATOR CURRENT (A)	FIELD CURRENT (A)	FIELD VOLTAGE (V)	INTERNAL ANGLE (DEG)	Q-AXIS REACTANCE (PU)
561	403.8	-117.7	23.16	10610.	2169.	178.	57.8	1.391
562	402.6	-128.5	23.17	10660.	2131.	173.	58.8	1.389
563	403.6	-138.7	23.17	10760.	2123.	176.	59.8	1.387
564	404.1	-136.7	23.17	10760.	2125.	173.	59.8	1.393
565	403.0	-139.8	23.17	10760.	2119.	176.	60.0	1.391
566	401.6	-141.1	23.18	10730.	2109.	175.	60.0	1.391
567	401.2	-139.4	23.17	10720.	2115.	175.	59.8	1.390
568	402.6	-140.4	23.18	10730.	2118.	175.	59.9	1.388
569	402.3	-139.7	23.17	10750.	2118.	175.	59.9	1.390
570	402.8	-139.3	23.18	10730.	2121.	178.	59.8	1.388
571	402.0	-138.9	23.17	10720.	2114.	174.	59.9	1.391
572	403.8	-124.4	23.16	10670.	2150.	178.	58.4	1.389
573	405.5	-78.3	23.49	10260.	2311.	201.	53.0	1.387
574	406.6	28.6	24.20	9830.	2582.	213.	42.6	1.365
575	408.4	32.5	24.24	9870.	2640.	224.	42.2	1.357
576	405.6	176.5	25.05	10340.	3202.	265.	32.1	1.280
577	406.0	192.2	25.03	10470.	3256.	272.	31.4	1.278
578	402.3	191.7	25.05	10390.	3247.	269.	31.3	1.285
579	402.0	195.4	25.03	10420.	3253.	272.	31.1	1.285
580	427.3	195.5	25.03	10990.	3344.	281.	32.5	1.271
581	436.1	194.2	25.02	11140.	3357.	282.	33.1	1.274
582	435.4	193.7	25.03	11130.	3360.	283.	33.0	1.270
583	439.7	192.8	25.02	11220.	3366.	282.	33.4	1.273
584	443.1	194.4	25.01	11280.	3379.	283.	33.5	1.272
585	450.3	193.8	25.01	11430.	3398.	286.	33.9	1.269
586	451.0	193.2	25.03	11440.	3406.	289.	33.9	1.264
587	458.6	193.5	25.02	11600.	3422.	287.	34.4	1.268
588	462.8	192.4	25.02	11700.	3435.	291.	34.7	1.265
589	466.4	194.9	25.01	11810.	3462.	291.	34.8	1.267
590	473.8	193.3	25.00	11970.	3472.	294.	35.4	1.272
591	481.3	194.8	25.01	12100.	3502.	294.	35.6	1.263
592	487.8	192.7	25.01	12230.	3518.	298.	36.1	1.264
593	498.7	192.3	25.01	12470.	3552.	301.	36.6	1.261
594	506.4	192.2	25.00	12640.	3581.	301.	37.1	1.261
595	507.0	189.5	25.00	12640.	3574.	302.	37.1	1.256
596	507.5	212.4	24.98	12840.	3667.	310.	36.2	1.251
597	508.0	226.2	24.98	12990.	3743.	319.	35.6	1.244
598	508.6	241.5	24.97	13160.	3805.	320.	35.0	1.239
599	506.8	256.9	24.96	13280.	3867.	327.	34.3	1.233
600	505.6	252.7	24.96	13210.	3847.	326.	34.4	1.237
601	506.7	252.7	24.96	13220.	3853.	328.	34.4	1.231
602	505.9	252.2	24.96	13220.	3851.	326.	34.4	1.235
603	506.0	248.8	24.97	13170.	3843.	324.	34.5	1.234
604	506.2	251.7	24.97	13200.	3846.	324.	34.4	1.233
605	507.6	252.1	24.97	13200.	3854.	326.	34.5	1.239
606	506.5	251.1	24.96	13210.	3845.	327.	34.5	1.235
607	509.1	250.6	24.97	13250.	3851.	326.	34.6	1.233
608	508.4	250.2	24.97	13240.	3850.	328.	34.6	1.234
609	507.6	244.2	24.98	13150.	3815.	323.	34.8	1.238
610	508.0	244.7	24.96	13200.	3834.	325.	34.8	1.236
611	507.1	245.6	24.97	13140.	3821.	325.	34.7	1.237
612	504.9	242.1	24.97	13060.	3796.	323.	34.8	1.239
613	504.2	227.4	24.99	12890.	3726.	317.	35.4	1.248
614	505.4	227.1	24.99	12930.	3730.	316.	35.3	1.240
615	507.1	228.3	24.99	12950.	3741.	315.	35.5	1.247
616	507.4	226.4	24.98	12960.	3737.	316.	35.6	1.245
617	507.6	224.3	24.99	12950.	3735.	316.	35.7	1.247
618	508.6	225.4	24.98	13000.	3740.	318.	35.6	1.240
619	508.7	220.1	24.99	12920.	3713.	316.	35.9	1.246
620	508.6	199.0	25.00	12730.	3616.	309.	36.9	1.257
621	507.2	197.7	25.00	12710.	3610.	305.	36.7	1.249
622	507.1	198.8	25.00	12710.	3611.	304.	36.7	1.255
623	506.8	200.4	25.00	12710.	3615.	306.	36.6	1.251
624	507.7	196.5	25.00	12710.	3607.	305.	36.8	1.251
625	508.4	197.9	25.00	12720.	3612.	304.	36.9	1.255
626	508.6	196.1	25.00	12710.	3609.	304.	36.9	1.249
627	507.1	197.8	25.00	12700.	3607.	305.	36.8	1.254
628	507.7	174.2	25.00	12520.	3513.	297.	37.9	1.259
629	508.0	175.8	25.01	12540.	3516.	299.	37.8	1.258
630	508.7	179.3	25.00	12580.	3534.	298.	37.7	1.257
631	509.6	179.7	25.01	12600.	3535.	297.	37.7	1.259
632	509.4	180.9	25.01	12600.	3549.	298.	37.6	1.256
633	510.1	180.5	25.01	12630.	3547.	301.	37.6	1.255
634	511.6	181.5	25.00	12660.	3558.	300.	37.8	1.258
635	511.6	183.4	25.00	12660.	3561.	301.	37.6	1.256
636	511.3	184.6	25.00	12690.	3565.	303.	37.6	1.256
637	511.9	184.5	25.00	12710.	3571.	300.	37.5	1.251
638	511.4	185.3	25.00	12690.	3570.	300.	37.5	1.253
639	511.3	184.7	25.00	12680.	3567.	302.	37.5	1.254
640	511.6	183.7	25.01	12680.	3566.	303.	37.6	1.253

Table 6-1 (Continued)

LAMBTON STEADY STATE LOAD POINTS

POINT NUMBER	ACTIVE POWER (MW)	REACTIVE POWER (MVAR)	TERMINAL VOLTAGE (KV)	STATOR CURRENT (A)	FIELD CURRENT (A)	FIELD VOLTAGE (V)	INTERNAL ANGLE (DEG)	Q-AXIS REACTANCE (PU)
641	509.6	184.2	25.00	12640.	3559.	300.	37.5	1.254
642	509.5	183.7	25.00	12640.	3556.	301.	37.5	1.253
643	510.0	182.4	25.01	12630.	3549.	301.	37.6	1.258
644	509.1	182.4	25.00	12600.	3545.	298.	37.6	1.260
645	509.3	182.2	25.01	12640.	3553.	301.	37.5	1.255
646	508.9	183.8	25.00	12640.	3561.	301.	37.4	1.253
647	508.7	182.3	25.02	12600.	3549.	298.	37.5	1.254
648	509.9	180.3	25.01	12620.	3546.	297.	37.6	1.255
649	509.5	179.7	25.01	12600.	3540.	298.	37.6	1.255
650	508.8	181.7	25.01	12610.	3546.	302.	37.6	1.258
651	509.8	181.3	25.01	12610.	3545.	299.	37.6	1.258
652	510.3	178.4	25.00	12620.	3540.	298.	37.8	1.254
653	509.0	181.1	25.01	12590.	3535.	297.	37.6	1.255
654	508.7	178.7	25.00	12590.	3536.	297.	37.6	1.251
655	508.3	176.9	25.02	12540.	3521.	298.	37.8	1.259
656	508.4	177.8	25.00	12560.	3528.	298.	37.7	1.255
657	507.9	178.6	25.02	12550.	3531.	297.	37.6	1.258
658	507.1	177.9	25.02	12530.	3522.	298.	37.7	1.261
659	507.3	178.5	25.02	12540.	3529.	297.	37.6	1.255
660	507.9	180.5	25.01	12580.	3540.	300.	37.5	1.255
661	508.6	182.6	25.02	12590.	3543.	297.	37.5	1.255
662	508.6	179.3	25.02	12560.	3540.	297.	37.6	1.255
663	506.9	182.1	25.01	12560.	3539.	297.	37.5	1.261
664	507.8	181.3	25.00	12590.	3544.	300.	37.5	1.257
665	509.1	183.3	25.02	12610.	3557.	300.	37.5	1.255
666	509.5	184.6	25.01	12640.	3563.	300.	37.5	1.258
667	510.1	185.5	25.01	12650.	3570.	302.	37.4	1.254
668	509.1	184.5	25.01	12630.	3560.	302.	37.4	1.253
669	507.9	188.2	25.01	12630.	3570.	299.	37.2	1.257
670	508.4	192.1	25.01	12660.	3583.	304.	37.0	1.250
671	508.4	190.0	25.02	12650.	3584.	301.	37.1	1.252
672	508.1	190.1	25.02	12640.	3581.	304.	37.1	1.251
673	508.4	191.9	25.02	12680.	3596.	305.	37.0	1.250
674	509.3	191.2	25.02	12680.	3589.	301.	37.1	1.255
675	508.0	193.1	25.00	12670.	3594.	303.	37.0	1.253
676	508.6	193.9	25.02	12670.	3596.	304.	37.0	1.252
677	507.8	191.8	25.02	12650.	3587.	302.	37.0	1.254
678	507.6	191.6	25.02	12640.	3591.	304.	37.0	1.250
679	507.7	195.1	25.01	12670.	3601.	302.	36.9	1.253
680	507.7	196.6	25.01	12680.	3602.	304.	36.8	1.252
681	508.0	195.8	25.01	12690.	3607.	306.	36.9	1.252
682	508.0	196.7	25.02	12690.	3606.	304.	36.9	1.255
683	508.3	193.7	25.01	12670.	3595.	302.	37.0	1.257
684	508.6	193.1	25.02	12680.	3595.	304.	37.0	1.253
685	508.4	193.1	25.02	12680.	3597.	302.	37.0	1.253
686	507.1	193.3	25.02	12650.	3591.	304.	36.9	1.252
687	508.1	192.7	25.02	12670.	3595.	305.	37.0	1.253
688	509.3	195.7	25.02	12710.	3608.	302.	36.9	1.252
689	509.8	196.3	25.00	12740.	3610.	306.	36.9	1.250
690	510.6	195.6	25.01	12740.	3611.	306.	37.1	1.256
691	509.9	195.9	25.00	12750.	3610.	305.	36.9	1.247
692	509.5	184.7	24.89	12680.	3525.	298.	37.7	1.258
693	508.9	172.9	24.83	12620.	3502.	295.	38.3	1.263
694	507.6	173.9	24.84	12620.	3514.	296.	38.2	1.264
695	509.2	172.0	24.84	12610.	3497.	295.	38.4	1.267
696	508.7	171.3	24.85	12600.	3495.	296.	38.3	1.261
697	508.4	170.4	24.85	12580.	3490.	296.	38.4	1.267
698	508.7	171.3	24.84	12590.	3497.	294.	38.5	1.269
699	509.4	145.6	24.70	12500.	3394.	286.	40.1	1.281
700	509.3	147.3	24.70	12520.	3396.	288.	40.0	1.281
701	509.1	148.1	24.71	12510.	3397.	288.	39.9	1.281
702	508.6	144.3	24.70	12480.	3383.	286.	40.1	1.282
703	509.1	142.5	24.71	12480.	3379.	286.	40.2	1.283
704	509.7	144.4	24.69	12500.	3383.	284.	40.2	1.284
705	508.8	142.3	24.70	12470.	3373.	284.	40.2	1.280
706	508.6	119.7	24.55	12420.	3286.	278.	41.7	1.289
707	509.4	117.0	24.56	12410.	3278.	278.	41.9	1.290
708	509.5	117.7	24.56	12430.	3287.	276.	41.9	1.290
709	509.9	118.3	24.56	12430.	3283.	276.	41.9	1.290
710	509.6	118.1	24.55	12440.	3287.	277.	41.9	1.290
711	509.2	112.4	24.57	12370.	3259.	273.	42.1	1.291
712	509.5	117.2	24.55	12410.	3281.	275.	41.9	1.290
713	508.6	114.0	24.57	12360.	3262.	272.	42.0	1.292
714	508.7	114.4	24.56	12380.	3266.	277.	42.0	1.289
715	509.4	90.8	24.52	12310.	3186.	269.	43.4	1.297
716	510.8	92.0	24.51	12350.	3194.	271.	43.5	1.299
717	510.7	89.9	24.52	12330.	3186.	268.	43.6	1.298
718	509.7	89.0	24.51	12300.	3179.	266.	43.6	1.300
719	509.2	90.1	24.52	12300.	3179.	267.	43.5	1.300
720	510.7	88.8	24.52	12340.	3184.	266.	43.7	1.299

Table 6-1 (Continued)

LAMBTON STEADY STATE LOAD POINTS

POINT NUMBER	ACTIVE POWER (MW)	REACTIVE POWER (MVAR)	TERMINAL VOLTAGE (KV)	STATOR CURRENT (A)	FIELD CURRENT (A)	FIELD VOLTAGE (V)	INTERNAL ANGLE (DEG)	Q-AXIS REACTANCE (PU)
721	510.7	87.6	24.52	12330.	3183.	270.	43.7	1.296
722	509.5	87.8	24.51	12310.	3176.	266.	43.6	1.297
723	509.7	88.2	24.53	12280.	3177.	268.	43.7	1.301
724	509.4	68.7	24.40	12270.	3110.	263.	45.0	1.304
725	510.4	64.0	24.37	12300.	3095.	260.	45.5	1.311
726	509.8	65.6	24.37	12290.	3101.	262.	45.4	1.312
727	510.7	61.0	24.37	12310.	3093.	259.	45.7	1.310
728	511.0	60.6	24.36	12320.	3091.	259.	45.7	1.309
729	510.5	62.7	24.37	12310.	3093.	261.	45.6	1.312
730	510.7	60.4	24.37	12310.	3087.	259.	45.7	1.308
731	511.1	60.5	24.37	12310.	3086.	258.	45.7	1.309
732	512.4	36.9	24.31	12320.	3021.	255.	47.5	1.318
733	512.9	35.8	24.30	12350.	3019.	255.	47.6	1.316
734	512.3	36.8	24.31	12320.	3016.	252.	47.4	1.315
735	510.6	33.8	24.30	12280.	3005.	254.	47.5	1.314
736	509.7	32.7	24.30	12270.	2994.	250.	47.6	1.317
737	510.5	33.9	24.29	12290.	3004.	251.	47.5	1.314
738	510.4	16.3	24.20	12310.	2950.	250.	49.0	1.323
739	509.7	12.5	24.16	12310.	2935.	247.	49.3	1.324
740	509.5	11.4	24.15	12310.	2934.	245.	49.5	1.327
741	509.4	11.0	24.15	12300.	2932.	248.	49.5	1.326
742	509.9	11.2	24.16	12320.	2938.	248.	49.4	1.321
743	509.7	11.9	24.16	12310.	2932.	245.	49.5	1.328
744	509.7	11.7	24.13	12310.	2911.	242.	49.5	1.327
745	509.5	-16.0	23.98	12390.	2859.	241.	51.9	1.334
746	510.0	-16.2	23.99	12410.	2865.	239.	51.8	1.331
747	511.0	-14.2	23.99	12430.	2869.	242.	51.8	1.332
748	511.8	-16.8	23.98	12460.	2863.	239.	52.1	1.335
749	510.0	-16.4	23.98	12410.	2861.	241.	51.9	1.331
750	508.3	-16.6	23.98	12390.	2855.	239.	51.9	1.335
751	509.7	-15.7	23.99	12410.	2859.	239.	51.9	1.335
752	509.9	-16.2	23.98	12410.	2860.	241.	51.9	1.335
753	509.7	-36.8	23.85	12510.	2808.	237.	53.8	1.339
754	510.2	-35.7	23.85	12530.	2811.	233.	53.8	1.342
755	509.8	-37.7	23.85	12520.	2809.	234.	53.9	1.338
756	509.5	-38.5	23.85	12510.	2805.	233.	53.9	1.339
757	509.3	-36.9	23.84	12500.	2808.	236.	53.8	1.339
758	508.8	-37.4	23.85	12470.	2802.	237.	53.8	1.338
759	509.5	-35.7	23.85	12500.	2809.	236.	53.7	1.339
760	509.2	-36.0	23.85	12480.	2810.	237.	53.7	1.338
761	509.4	-36.7	23.85	12510.	2802.	235.	53.8	1.340
762	509.2	-59.8	23.68	12640.	2754.	230.	56.0	1.343
763	509.2	-59.9	23.68	12650.	2752.	229.	56.2	1.348
764	508.7	-61.3	23.67	12630.	2748.	229.	56.2	1.346
765	509.3	-60.0	23.68	12640.	2750.	229.	56.2	1.347
766	509.5	-60.5	23.66	12650.	2751.	229.	56.2	1.346
767	509.6	-60.1	23.68	12650.	2754.	230.	56.2	1.348
768	509.2	-63.5	23.67	12650.	2742.	230.	56.4	1.347
769	509.8	-64.4	23.67	12670.	2748.	229.	55.7	1.312
770	507.5	-89.0	23.51	12800.	2686.	223.	59.0	1.352
771	509.2	-88.0	23.51	12830.	2698.	226.	58.9	1.349
772	510.6	-85.6	23.51	12850.	2709.	228.	58.8	1.350
773	509.8	-86.4	23.51	12840.	2701.	227.	58.8	1.349
774	508.6	-84.9	23.51	12800.	2705.	229.	58.6	1.347
775	509.9	-82.9	23.50	12830.	2710.	225.	58.5	1.346
776	509.9	-83.2	23.51	12820.	2711.	227.	58.5	1.347
777	510.0	-83.5	23.51	12830.	2711.	227.	58.5	1.348
778	510.3	-84.2	23.52	12840.	2711.	225.	58.6	1.349
779	509.2	-108.7	23.35	13010.	2659.	221.	61.2	1.353
780	507.7	-107.3	23.35	12980.	2658.	222.	61.0	1.354
781	508.4	-109.4	23.35	13000.	2655.	221.	61.2	1.354
782	509.0	-108.0	23.34	13010.	2663.	223.	61.1	1.350
783	509.2	-108.6	23.34	13020.	2660.	220.	61.2	1.354
784	509.8	-108.3	23.35	13020.	2666.	221.	61.1	1.350
785	510.2	-124.7	23.22	13200.	2641.	219.	63.1	1.356
786	510.2	-124.7	23.17	13270.	2626.	220.	63.9	1.384
787	507.8	-132.7	23.16	13230.	2621.	219.	63.9	1.355
788	509.2	-130.9	23.16	13260.	2628.	219.	63.8	1.356
789	509.4	-130.0	23.17	13250.	2630.	218.	63.7	1.357
790	510.3	-134.9	23.17	13300.	2626.	219.	64.1	1.354
791	509.6	-132.0	23.17	13270.	2632.	218.	63.7	1.350
792	510.3	-131.3	23.16	13290.	2636.	221.	62.9	1.319
793	510.3	-112.6	23.30	13100.	2667.	223.	61.7	1.353
794	509.3	-87.0	23.51	12830.	2705.	224.	58.8	1.349
795	508.6	-95.2	23.50	12860.	2685.	225.	59.5	1.348
796	507.8	-101.7	23.51	12860.	2661.	219.	60.0	1.352
797	509.5	-139.5	23.19	13320.	2607.	219.	64.8	1.366
798	510.5	-146.0	23.17	13390.	2610.	218.	65.2	1.356
799	509.2	-146.6	23.17	13350.	2603.	219.	65.2	1.356
800	510.7	-146.4	23.16	13370.	2609.	219.	65.2	1.352

Table 6-1 (Continued)

LAMBTON STEADY STATE LOAD POINTS

POINT NUMBER	ACTIVE POWER (MW)	REACTIVE POWER (MVAR)	TERMINAL VOLTAGE (KV)	STATOR CURRENT (A)	FIELD CURRENT (A)	FIELD VOLTAGE (V)	INTERNAL ANGLE (DEG)	Q-AXIS REACTANCE (PU)
801	509.7	-147.1	23.16	13370.	2606.	218.	65.3	1.355
802	510.2	-146.8	23.16	13380.	2607.	218.	65.2	1.351
803	510.0	-147.3	23.16	13380.	2606.	219.	65.2	1.351
804	511.0	-148.0	23.16	13410.	2613.	220.	65.3	1.351
805	511.3	-148.3	23.17	13420.	2613.	217.	65.3	1.351
806	511.6	-147.0	23.16	13430.	2616.	218.	65.2	1.351
807	512.7	-147.0	23.17	13450.	2618.	219.	65.3	1.353
808	513.1	-146.2	23.16	13450.	2622.	219.	65.2	1.350
809	512.1	-144.2	23.17	13410.	2622.	220.	65.0	1.353
810	511.8	-129.9	23.16	13310.	2647.	221.	63.7	1.352
811	511.1	-44.2	23.79	12580.	2800.	231.	54.6	1.342
812	505.2	-35.3	23.86	12390.	2797.	233.	53.5	1.343
813	483.1	-40.7	23.86	11820.	2685.	225.	52.8	1.347
814	469.3	-39.6	23.87	11480.	2625.	220.	51.9	1.349
815	460.8	-40.0	23.86	11290.	2589.	217.	51.6	1.354
816	454.1	-41.3	23.88	11130.	2561.	214.	51.3	1.359
817	449.4	-39.2	23.88	11010.	2542.	210.	50.8	1.357
818	445.1	-36.7	23.90	10890.	2539.	211.	50.3	1.357
819	439.2	-37.7	23.89	10770.	2509.	210.	50.2	1.363
820	432.6	-38.1	23.91	10590.	2480.	207.	49.7	1.364
821	420.4	-38.4	23.87	10260.	2415.	200.	49.1	1.365
822	398.3	-42.3	23.89	9770.	2331.	193.	48.0	1.372
823	406.3	-42.5	23.87	10010.	2364.	196.	48.7	1.374
824	414.8	-41.3	23.88	10190.	2398.	198.	49.1	1.373
825	412.5	4.6	24.02	10020.	2552.	215.	45.0	1.366
826	408.8	174.4	25.03	10460.	3253.	268.	32.2	1.273
827	408.2	194.9	25.02	10560.	3278.	272.	31.3	1.270
828	409.3	198.0	25.02	10590.	3296.	274.	31.3	1.268
829	409.7	198.1	25.03	10610.	3307.	276.	31.3	1.268
830	410.3	209.1	25.06	10730.	3355.	280.	30.9	1.269
831	410.3	210.9	25.06	10730.	3360.	280.	30.8	1.269
832	410.6	210.5	25.06	10740.	3359.	280.	30.8	1.264
833	412.0	214.2	25.08	10800.	3381.	283.	30.8	1.269
834	414.3	214.9	25.05	10870.	3390.	285.	30.9	1.266
835	415.1	231.0	25.05	11050.	3474.	290.	30.3	1.265
836	415.2	244.1	25.04	11220.	3537.	296.	29.7	1.251
837	413.6	253.0	25.04	11350.	3600.	301.	29.1	1.237
838	416.5	258.4	25.04	11420.	3613.	301.	29.3	1.249
839	418.5	256.3	25.04	11420.	3613.	301.	29.3	1.234
840	419.4	258.3	25.03	11480.	3622.	304.	29.4	1.243
841	417.9	257.6	25.03	11440.	3612.	302.	29.4	1.248
842	419.7	255.8	25.03	11440.	3612.	302.	29.4	1.235
843	419.5	224.7	25.05	11090.	3462.	292.	30.7	1.258
844	420.4	225.4	25.06	11090.	3459.	291.	30.7	1.257
845	414.0	223.6	25.06	10940.	3430.	287.	30.5	1.267
846	413.1	223.6	25.06	10940.	3431.	286.	30.4	1.263
847	417.9	224.4	25.06	11040.	3451.	288.	30.7	1.260
848	417.3	224.2	25.05	11020.	3444.	290.	30.7	1.264
849	415.9	223.3	25.06	10990.	3443.	289.	30.6	1.263
850	414.6	220.7	25.06	10940.	3425.	286.	30.6	1.262
851	415.3	223.3	25.07	10970.	3434.	288.	30.5	1.259

Part 5

NANTICOKE TEST DATA

CONTENTS

ILLUSTRATIONS

ILLUSTRATIONS (Cont'd)

ILLUSTRATIONS (Cont'd)

TABLES

Section 1

DESCRIPTION OF GENERATOR AND STATION

THE STATION

Nanticoke Generating Station is situated on the north shore of Lake Erie approximately 50 km south of Hamilton and 90 km west of Niagara Falls.

It has an installed capacity of 4000 MW (8 identical 500 MW units). Bulk power transmission is designed to be half at 230 kV and half at 500 kV. The fuel is a mixture of U.S. and western Canadian bituminous coal which is blended on site.

THE GENERATOR

Each unit is a 2-pole, 3600 rpm machine rated at 500 MW, 0.85 power factor, and 22 kV line-to-line stator voltage. The stator winding is a direct, water-cooled type; the rotor is indirectly cooled with hydrogen.

The rotor construction is distinctly different from that of the Lambton machines. The field winding is secured by aluminum alloy slot wedges which run the full length of the rotor. The pole faces have longitudinal flexibility slots which are filled with short steel wedges. In addition to the conducting path provided by the long aluminum wedges, there is a full length copper strip (damper winding) under the wedges in every slot, including the pole faces. A tab on each end of the copper damper strips overlaps a similar one on the copper strip in each adjacent slot; these overlapping ends are clamped together by the retaining ring to form a squirrel cage underneath the slot wedges, all around the rotor.

Section 2

STATIONARY TESTS

STANDSTILL FREQUENCY RESPONSE

The following stator impedances and stator to rotor transfer functions were measured and analyzed as described in Part 1, Section 2:

$\left.\dfrac{Z_d(s)}{\dfrac{\Delta I_{fd}}{\Delta I_d}}\right\}$ On the direct axis with the field winding shorted through a metering shunt

$\left.\dfrac{Z_{do}(s)}{\dfrac{\Delta V_{fd}}{\Delta I_d}}\right\}$ On the direct axis with the field winding open

$Z_q(s)$ On the quadrature axis

An operational inductance was computed from each of the three stator impedances. The results are presented in the following tables and graphs (Tables 2-1 to 2-4 and Figures 2-1 to 2-22). With reference to the Bode plots, all magnitudes, except operational inductance, are in SI units (ohms, volts, etc) and db above 1 ohm or 1 volt, etc. The operational inductance is normalized to the generator base; so, its magnitude is in either p.u. or db above 1.0 p.u.

Magnitude and phase points are identified on the plots as follows:

- ⊙ magnitude
- ⊡ phase

TABLE 2-1

STANDSTILL FREQUENCY RESPONSE TEST DATA ON THE DIRECT AXIS WITH THE FIELD SHORTED

FREQUENCY (HZ)	D-AXIS STATOR CURRENT (A)	FIELD CURRENT (A)	DIRECT AXIS STATOR IMPEDANCE (OHM)	(DEG)	DIRECT AXIS OPERATIONAL INDUCTANCE (PU)	(DB)	(DEG)	STATOR TO FIELD TRANSFER FUNCTION (A/A)	(DB)	(DEG)
.0010	48.6	.157	.00169	.98	2.114	6.50	-1.0	.0032	-49.8	87.1
.0013	48.6	.204	.00169	1.28	2.115	6.51	-2.0	.0042	-47.5	86.2
.0016	48.6	.251	.00169	1.57	2.119	6.52	-2.6	.0052	-45.7	85.3
.0020	48.6	.312	.00169	1.95	2.107	6.47	-3.5	.0064	-43.8	83.9
.0025	48.6	.389	.00170	2.41	2.089	6.40	-4.3	.0080	-41.9	82.3
.0030	48.6	.462	.00170	2.87	2.079	6.36	-5.1	.0095	-40.4	80.9
.0040	48.6	.602	.00171	3.75	2.056	6.26	-7.7	.0124	-38.1	78.2
.0050	48.6	.750	.00172	4.58	2.036	6.17	-10.2	.0154	-36.2	75.4
.0065	48.6	.933	.00174	5.73	2.003	6.03	-13.6	.0192	-34.3	71.6
.0080	48.6	1.135	.00176	6.71	1.950	5.80	-16.0	.0234	-32.6	67.9
.0100	48.6	1.364	.00179	7.80	1.875	5.46	-19.1	.0281	-31.0	62.9
.0130	48.6	1.659	.00183	9.10	1.768	4.95	-22.9	.0342	-29.3	56.4
.0160	48.6	1.905	.00188	10.02	1.661	4.41	-26.2	.0392	-28.1	51.0
.0200	48.6	2.137	.00193	10.83	1.523	3.66	-29.7	.0440	-27.1	45.1
.0250	48.6	2.343	.00198	11.61	1.375	2.77	-32.2	.0482	-26.3	39.2
.0300	48.6	2.494	.00202	12.26	1.252	1.95	-33.6	.0513	-25.8	34.7
.0400	48.6	2.722	.00208	13.61	1.080	.67	-34.2	.0560	-25.0	28.1
.0500	48.6	2.817	.00213	14.95	.965	-.31	-33.9	.0580	-24.7	24.0
.0650	48.6	2.950	.00219	17.07	.853	-1.38	-32.2	.0607	-24.3	19.7
.0800	48.6	3.019	.00225	19.30	.784	-2.11	-30.2	.0621	-24.1	16.6
.1000	48.0	3.054	.00232	22.40	.724	-2.81	-27.2	.0636	-23.9	13.9
.1300	48.6	3.161	.00243	26.20	.661	-3.60	-24.5	.0651	-23.7	11.1
.1600	48.6	3.198	.00257	29.80	.632	-3.98	-23.0	.0658	-23.6	9.1
.2000	48.6	3.235	.00275	34.00	.602	-4.41	-21.1	.0666	-23.5	7.3
.2500	48.6	3.235	.00302	38.20	.580	-4.73	-20.1	.0666	-23.5	5.7
.3000	48.6	3.272	.00327	41.60	.560	-5.04	-19.3	.0674	-23.4	4.4
.4000	48.6	3.272	.00380	46.70	.532	-5.49	-18.4	.0674	-23.4	2.6
.5000	48.6	3.310	.00437	50.20	.515	-5.76	-18.2	.0681	-23.3	1.1
.6500	48.6	3.310	.00513	54.00	.489	-6.22	-17.7	.0681	-23.3	-.5
.8000	48.0	3.272	.00589	56.70	.470	-6.55	-17.4	.0681	-23.3	-1.7
1.0000	48.0	3.235	.00684	59.40	.449	-6.96	-16.9	.0674	-23.4	-3.2
1.3000	47.5	3.198	.00822	62.30	.426	-7.42	-16.3	.0674	-23.4	-5.1
1.6000	48.0	3.198	.00966	64.50	.413	-7.68	-15.8	.0666	-23.5	-6.6
2.0000	48.0	3.125	.01148	66.60	.398	-8.00	-15.2	.0651	-23.7	-8.5
2.5000	48.6	3.125	.01365	68.40	.383	-8.34	-14.7	.0643	-23.8	-10.5
3.0000	48.6	3.054	.01585	69.80	.373	-8.56	-14.3	.0629	-24.0	-12.3
4.0000	49.1	2.950	.02019	71.40	.359	-8.89	-13.9	.0600	-24.4	-15.2
5.0000	48.0	2.753	.02427	72.50	.347	-9.19	-13.6	.0573	-24.8	-17.4
6.5000	48.0	2.599	.03020	73.50	.334	-9.53	-13.4	.0541	-25.3	-19.8
8.0000	48.0	2.454	.03589	74.20	.323	-9.81	-13.2	.0511	-25.8	-21.4
10.0000	47.5	2.264	.04315	75.00	.312	-10.12	-12.8	.0477	-26.4	-23.0
13.0000	49.7	2.187	.05433	75.80	.303	-10.38	-12.5	.0440	-27.1	-24.4
16.0000	49.7	2.065	.06457	76.40	.293	-10.68	-12.1	.0415	-27.6	-25.1
20.0000	43.3	1.659	.07853	77.00	.285	-10.90	-11.8	.0383	-28.3	-25.6
25.0000	39.0	1.396	.09441	77.60	.274	-11.23	-11.4	.0358	-28.9	-25.9
30.0000	35.6	1.188	.11092	78.00	.269	-11.41	-11.1	.0334	-29.5	-25.7
40.0000	30.3	.922	.14290	78.80	.260	-11.70	-10.5	.0304	-30.3	-25.2
50.0000	26.4	.758	.17379	79.50	.253	-11.94	-10.0	.0287	-30.8	-24.5
65.0000	21.9	.589	.21879	80.20	.245	-12.21	-9.4	.0268	-31.4	-23.7
80.0000	18.7	.473	.26304	80.70	.240	-12.41	-8.9	.0253	-31.9	-23.2
100.0000	15.7	.380	.32362	81.20	.236	-12.55	-8.5	.0242	-32.3	-23.0
130.0000	12.6	.288	.41213	81.80	.231	-12.73	-8.0	.0228	-32.8	-23.3
160.0000	10.5	.229	.50122	82.10	.228	-12.83	-7.7	.0218	-33.2	-24.0
200.0000	8.6	.180	.60958	82.30	.222	-13.07	-7.5	.0208	-33.6	-25.4
250.0000	7.0	.136	.75863	82.40	.221	-13.10	-7.5	.0194	-34.2	-27.2
300.0000	6.0	.108	.90163	82.40	.219	-13.19	-7.5	.0181	-34.8	-29.2
400.0000	4.6	.073	1.17498	82.10	.214	-13.39	-7.8	.0160	-35.9	-32.9
500.0000	3.7	.051	1.46228	81.60	.213	-13.42	-8.3	.0139	-37.1	-36.6
650.0000	2.9	.031	1.86221	80.80	.209	-13.60	-9.1	.0108	-39.3	-43.9
800.0000	2.4	.019	2.29102	80.10	.209	-13.61	-9.9	.0078	-42.1	-55.5
1000.0000	1.9	.008	2.81857	78.50	.206	-13.74	-11.5	.0043	-47.2	-94.0

TABLE 2-2

STANDSTILL FREQUENCY RESPONSE TEST DATA ON THE DIRECT AXIS WITH THE FIELD OPEN

FREQUENCY (HZ)	D-AXIS STATOR CURRENT (A)	FIELD VOLTAGE (V)	FIELD-OPEN D-AXIS STATOR IMPEDANCE (OHM)	(DEG)	FIELD-OPEN D-AXIS OPERATIONAL INDUCTANCE (PU)	(DB)	(DEG)	STATOR TO FIELD TRANSFER IMPEDANCE (V/A)	(DB)	(DEG)
.0010	46.4		.00169	.96	2.072	6.33	-1.8			
.0013	46.4		.00169	1.25	2.065	6.30	-1.9			
.0016	46.4		.00169	1.54	2.072	6.33	-2.0			
.0020	46.4		.00169	1.93	2.077	6.35	-2.1			
.0025	46.4		.00169	2.41	2.080	6.36	-2.4			
.0030	46.4		.00169	2.90	2.088	6.39	-2.5			
.0040	46.4		.00170	3.86	2.089	6.40	-2.8			
.0050	46.4		.00170	4.77	2.069	6.32	-3.2			
.0065	46.4		.00171	6.28	2.103	6.46	-3.7			
.0080	46.4		.00172	7.00	1.916	5.65	-4.9			
.0100	46.4		.00174	9.40	2.079	6.36	-5.1			
.0130	46.4		.00177	11.87	2.056	6.26	-6.8			
.0160	46.4	.275	.00180	14.30	2.040	6.19	-7.0	.0059	-44.5	79.2
.0200	45.9	.335	.00186	17.00	2.013	6.08	-9.6	.0073	-42.7	77.4
.0250	44.8	.398	.00195	20.20	2.007	6.05	-11.8	.0089	-41.0	74.8
.0300	42.8	.447	.00202	22.50	1.926	5.69	-12.8	.0104	-39.6	72.9
.0400	49.1	.646	.00219	26.50	1.846	5.32	-15.4	.0131	-37.6	68.7
.0500	49.1	.767	.00237	29.50	1.789	5.05	-17.8	.0156	-36.1	65.5
.0650	48.6	.923	.00260	32.40	1.663	4.42	-20.0	.0190	-34.4	61.6
.0800	48.6	1.059	.00285	34.50	1.591	4.03	-22.3	.0218	-33.2	58.5
.1000	48.6	1.230	.00313	36.40	1.481	3.41	-24.0	.0253	-31.9	54.9
.1300	48.6	1.445	.00355	38.10	1.375	2.77	-26.7	.0298	-30.5	50.6
.1600	48.0	1.603	.00394	39.10	1.291	2.22	-28.8	.0334	-29.5	47.1
.2000	48.0	1.778	.00437	40.00	1.188	1.50	-30.5	.0370	-28.6	43.4
.2500	51.5	2.113	.00484	40.80	1.088	.73	-32.0	.0411	-27.7	39.7
.3000	50.3	2.213	.00525	41.40	1.005	.04	-32.9	.0440	-27.1	36.8
.4000	50.9	2.455	.00596	42.40	.883	-1.08	-34.0	.0483	-26.3	32.5
.5000	49.1	2.541	.00661	43.40	.803	-1.91	-34.4	.0517	-25.7	29.6
.6500	48.6	2.692	.00741	44.90	.710	-2.97	-34.2	.0554	-25.1	26.4
.8000	48.6	2.818	.00822	46.30	.653	-3.71	-33.9	.0580	-24.7	24.3
1.0000	48.6	2.951	.00912	48.20	.590	-4.58	-32.9	.0608	-24.3	22.3
1.3000	48.0	3.055	.01035	50.90	.526	-5.58	-31.1	.0636	-23.9	20.3
1.6000	47.5	3.126	.01162	53.20	.487	-6.25	-29.5	.0659	-23.6	19.1
2.0000	47.5	3.236	.01334	55.80	.454	-6.85	-27.8	.0682	-23.3	18.0
2.5000	48.6	3.428	.01531	58.50	.423	-7.47	-25.8	.0706	-23.0	17.8
3.0000	48.6	3.508	.01738	60.70	.404	-7.87	-24.2	.0722	-22.8	16.9
4.0000	48.0	3.589	.02138	63.90	.377	-8.47	-21.9	.0747	-22.5	16.6
5.0000	48.6	3.758	.02512	66.00	.357	-8.95	-20.4	.0774	-22.2	16.7
6.5000	48.0	3.846	.03091	68.30	.340	-9.37	-18.7	.0801	-21.9	17.2
8.0000	48.6	4.027	.03673	69.90	.330	-9.63	-17.6	.0829	-21.6	17.8
10.0000	48.0	4.169	.04365	71.40	.315	-10.04	-16.5	.0868	-21.2	18.6
13.0000	46.9	4.266	.05433	73.00	.302	-10.40	-15.3	.0909	-20.8	19.6
16.0000	46.4	4.416	.06532	74.10	.296	-10.58	-14.5	.0952	-20.4	20.4
20.0000	40.4	4.074	.07853	75.20	.285	-10.91	-13.6	.1008	-19.9	21.1
25.0000	36.8	3.936	.09551	76.10	.277	-11.14	-12.9	.1068	-19.4	21.8
30.0000	34.0	3.758	.11092	76.80	.269	-11.41	-12.3	.1106	-19.1	22.3
40.0000	28.9	3.467	.14290	77.80	.260	-11.70	-11.5	.1198	-18.4	23.1
50.0000	25.2	3.199	.17379	78.70	.253	-11.94	-10.8	.1269	-17.9	23.8
65.0000	21.2	2.884	.21879	79.50	.245	-12.21	-10.1	.1360	-17.3	24.6
80.0000	18.0	2.600	.26304	80.20	.240	-12.41	-9.4	.1441	-16.8	25.2
100.0000	15.2	2.344	.32362	80.80	.236	-12.55	-8.9	.1544	-16.2	25.5
130.0000	12.1	2.042	.41213	81.50	.231	-12.73	-8.3	.1693	-15.4	25.5
160.0000	10.1	1.841	.49548	81.70	.226	-12.93	-8.1	.1814	-14.8	25.3
200.0000	8.3	1.622	.61664	82.00	.225	-12.97	-7.8	.1944	-14.2	24.6
250.0000	6.8	1.429	.75863	82.20	.221	-13.10	-7.7	.2107	-13.5	23.6
300.0000	5.8	1.274	.90163	82.10	.219	-13.19	-7.8	.2206	-13.1	22.7
400.0000	4.4	1.047	1.17498	81.90	.214	-13.39	-8.0	.2391	-12.4	20.7
500.0000	3.6	.902	1.46228	81.60	.213	-13.42	-8.3	.2533	-11.9	19.2
650.0000	2.8	.759	1.86221	80.60	.209	-13.60	-9.3	.2714	-11.3	17.0
800.0000	2.3	.661	2.29102	79.70	.209	-13.61	-10.3	.2875	-10.8	14.9
1000.0000	1.8	.562	2.81857	78.40	.206	-13.74	-11.6	.3045	-10.3	12.4

TABLE 2-3

QUADRATURE AXIS STANDSTILL FREQUENCY RESPONSE TEST DATA

FREQUENCY (HZ)	Q-AXIS STATOR CURRENT (A)	QUADRATURE AXIS STATOR IMPEDANCE (OHM)	(DEG)	QUADRATURE AXIS OPERATIONAL INDUCTANCE (PU)	(DB)	(DEG)
.0010	44.8	.00169	.94	2.033	6.16	-2.7
.0013	44.8	.00169	1.23	2.035	6.17	-1.8
.0016	44.8	.00169	1.51	2.032	6.16	-1.2
.0020	44.8	.00169	1.89	2.032	6.16	-.7
.0025	44.8	.00169	2.35	2.027	6.14	-1.2
.0030	44.8	.00169	2.82	2.026	6.13	-1.7
.0040	44.8	.00170	3.74	2.020	6.11	-2.5
.0050	44.8	.00170	4.85	2.102	6.45	-2.9
.0065	44.8	.00171	5.87	1.966	5.87	-3.8
.0080	44.8	.00172	7.24	1.980	5.93	-4.2
.0100	44.8	.00174	9.00	1.988	5.97	-5.2
.0130	44.8	.00177	11.34	1.961	5.85	-6.9
.0160	44.8	.00180	13.49	1.926	5.70	-7.7
.0200	44.8	.00185	16.21	1.905	5.60	-9.3
.0250	44.8	.00192	19.02	1.857	5.38	-11.2
.0300	44.8	.00199	21.53	1.815	5.18	-12.4
.0400	44.8	.00214	25.68	1.747	4.84	-14.5
.0500	44.8	.00230	28.80	1.681	4.51	-16.3
.0650	44.8	.00253	32.50	1.600	4.08	-18.0
.0800	44.8	.00275	35.16	1.531	3.70	-19.5
.1000	44.3	.00302	37.70	1.440	3.17	-20.8
.1300	43.8	.00343	40.40	1.349	2.60	-22.5
.1600	43.8	.00380	42.20	1.272	2.09	-23.8
.2000	43.8	.00427	43.90	1.191	1.52	-25.1
.2500	46.9	.00479	45.50	1.108	.89	-26.0
.3000	48.0	.00525	46.80	1.039	.33	-26.5
.4000	48.0	.00617	48.60	.949	-.45	-27.3
.5000	48.0	.00692	50.10	.872	-1.19	-27.4
.6500	47.5	.00804	52.00	.799	-1.95	-27.2
.8000	47.5	.00912	53.60	.750	-2.50	-26.9
1.0000	46.9	.01035	55.20	.692	-3.20	-26.4
1.3000	46.9	.01162	57.30	.606	-4.36	-25.1
1.6000	46.4	.01396	58.90	.600	-4.43	-24.8
2.0000	45.9	.01641	60.10	.570	-4.88	-24.5
2.5000	45.9	.01906	62.30	.535	-5.44	-23.0
3.0000	46.9	.02163	63.20	.509	-5.87	-22.7
4.0000	45.9	.02692	65.00	.479	-6.40	-21.7
5.0000	47.5	.03162	66.10	.452	-6.90	-21.0
6.5000	46.9	.03891	67.40	.430	-7.34	-20.3
8.0000	46.4	.04519	68.40	.406	-7.82	-19.6
10.0000	45.9	.05309	69.20	.383	-8.34	-19.1
13.0000	43.3	.06607	70.50	.368	-8.69	-18.1
16.0000	43.3	.07853	71.30	.356	-8.98	-17.5
20.0000	43.8	.09333	72.20	.338	-9.41	-16.8
25.0000	46.4	.11221	73.00	.326	-9.74	-16.2
30.0000	43.8	.13033	73.70	.316	-10.02	-15.6
40.0000	36.8	.16597	74.80	.302	-10.41	-14.6
50.0000	28.3	.19954	75.60	.290	-10.74	-13.9
65.0000	21.7	.24833	76.50	.278	-11.11	-13.1
80.0000	18.7	.29514	77.20	.269	-11.41	-12.5
100.0000	15.7	.35895	77.80	.261	-11.65	-11.9
130.0000	12.8	.45189	78.60	.253	-11.93	-11.2
160.0000	10.8	.54958	79.10	.250	-12.03	-10.7
200.0000	8.8	.66839	79.40	.244	-12.27	-10.5
250.0000	7.3	.81289	79.60	.237	-12.50	-10.3
300.0000	6.2	.96612	79.70	.235	-12.59	-10.2
400.0000	4.8	1.25901	79.60	.229	-12.79	-10.3
500.0000	3.9	1.53119	78.70	.223	-13.02	-11.2
650.0000	3.1	1.97256	78.70	.221	-13.10	-11.3
800.0000	2.5	2.39900	77.80	.219	-13.21	-12.2
1000.0000	2.0	2.95141	76.40	.215	-13.34	-13.6

TABLE 2-4

FIELD IMPEDANCE WITH THE STATOR WINDING OPEN

FREQUENCY (HZ)	FIELD VOLTAGE (V)	FIELD CURRENT (A)	FIELD IMPEDANCE (OHM)	(DB)	(DEG)
.0010	3.72	33.48	.111	-19.10	3.6
.0013	3.80	33.48	.114	-18.90	4.7
.0016	3.72	33.48	.111	-19.10	5.7
.0020	3.72	33.48	.111	-19.10	7.2
.0025	3.72	33.10	.112	-19.00	8.8
.0032	3.76	32.72	.115	-18.80	10.8
.0040	3.80	32.35	.118	-18.60	13.1
.0050	3.89	31.98	.122	-18.30	15.9
.0063	3.98	31.61	.126	-18.00	18.9
.0079	4.22	31.61	.133	-17.50	22.2
.0100	4.42	31.25	.141	-17.00	25.5
.0130	4.68	29.50	.159	-16.00	29.0
.0160	4.90	28.50	.172	-15.30	31.7
.0200	5.19	27.53	.188	-14.50	34.4
.0250	5.50	26.29	.209	-13.60	36.8
.0300	5.75	25.11	.229	-12.80	38.6
.0400	6.10	23.17	.263	-11.60	40.3
.0500	6.38	21.87	.292	-10.70	41.7
.0650	6.68	20.18	.331	-9.60	42.4
.0800	6.92	18.61	.372	-8.60	42.2
.1000	7.16	17.37	.412	-7.70	41.5
.1300	7.33	15.66	.468	-6.60	39.8
.1600	7.50	14.79	.507	-5.90	38.0
.2000	7.67	13.64	.563	-5.00	36.2
.2500	7.76	12.73	.610	-4.30	34.6
.3000	7.85	12.02	.653	-3.70	32.9
.4000	7.94	11.22	.708	-3.00	30.3
.5000	8.04	10.59	.759	-2.40	28.9
.6500	8.04	10.11	.795	-2.00	27.6
.8000	8.13	9.66	.842	-1.50	26.8
1.0000	8.22	9.22	.892	-1.00	26.3
1.3000	8.32	8.91	.934	-.60	26.1
1.6000	8.41	8.51	.989	-.10	26.5
2.0000	8.51	8.22	1.036	.30	27.3
2.5000	8.51	7.85	1.084	.70	28.5
3.0000	8.61	7.58	1.135	1.10	29.8
4.0000	8.71	7.08	1.231	1.80	32.2
5.0000	8.81	6.60	1.334	2.50	34.4
6.5000	8.91	6.09	1.463	3.30	37.2
8.0000	9.02	5.69	1.585	4.00	39.6
10.0000	9.12	5.13	1.779	5.00	41.9
13.0000	9.23	4.52	2.042	6.20	44.3
16.0000	9.33	4.07	2.292	7.20	45.8
20.0000	9.33	3.63	2.571	8.20	47.1
25.0000	9.33	3.16	2.952	9.40	47.9
30.0000	9.33	2.85	3.275	10.30	48.4
40.0000	9.44	2.45	3.847	11.70	48.7
50.0000	9.44	2.16	4.367	12.80	48.7
65.0000	9.55	1.88	5.072	14.10	48.7
80.0000	9.55	1.70	5.625	15.00	48.8
100.0000	9.55	1.51	6.312	16.00	48.9
130.0000	9.55	1.32	7.247	17.20	49.2
160.0000	9.55	1.19	8.038	18.10	49.6
200.0000	9.55	1.06	9.019	19.10	50.2
250.0000	9.55	.93	10.237	20.20	50.9
300.0000	9.66	.85	11.354	21.10	51.5
400.0000	9.66	.72	13.340	22.50	52.5
500.0000	9.66	.64	15.141	23.60	53.6
650.0000	9.66	.55	17.585	24.90	54.8
800.0000	9.66	.49	19.731	25.90	55.8
1000.0000	9.66	.43	22.395	27.00	57.2

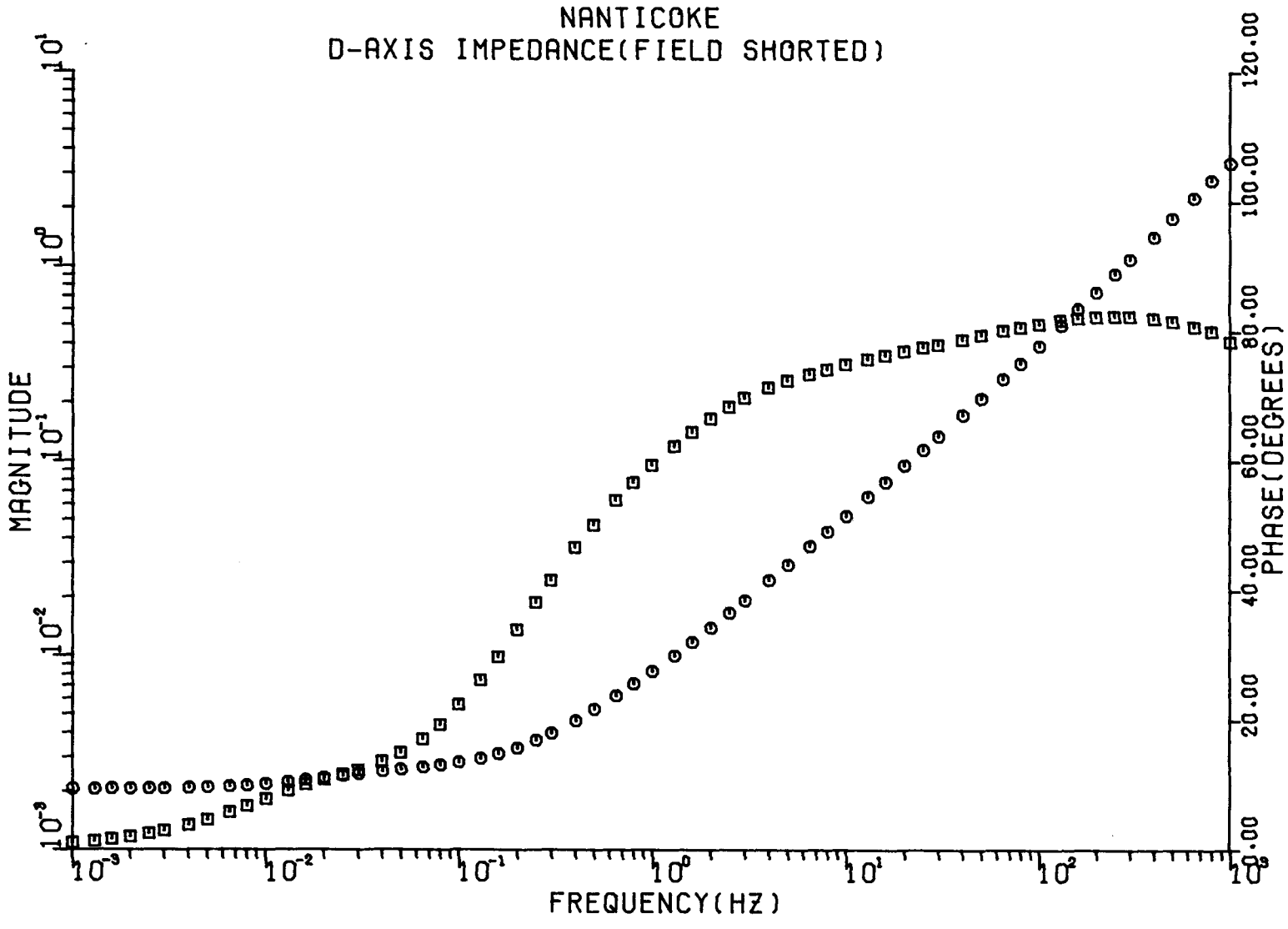

Figure 2-1. Nanticoke Direct Axis Operational Impedance, Magnitude in pu.

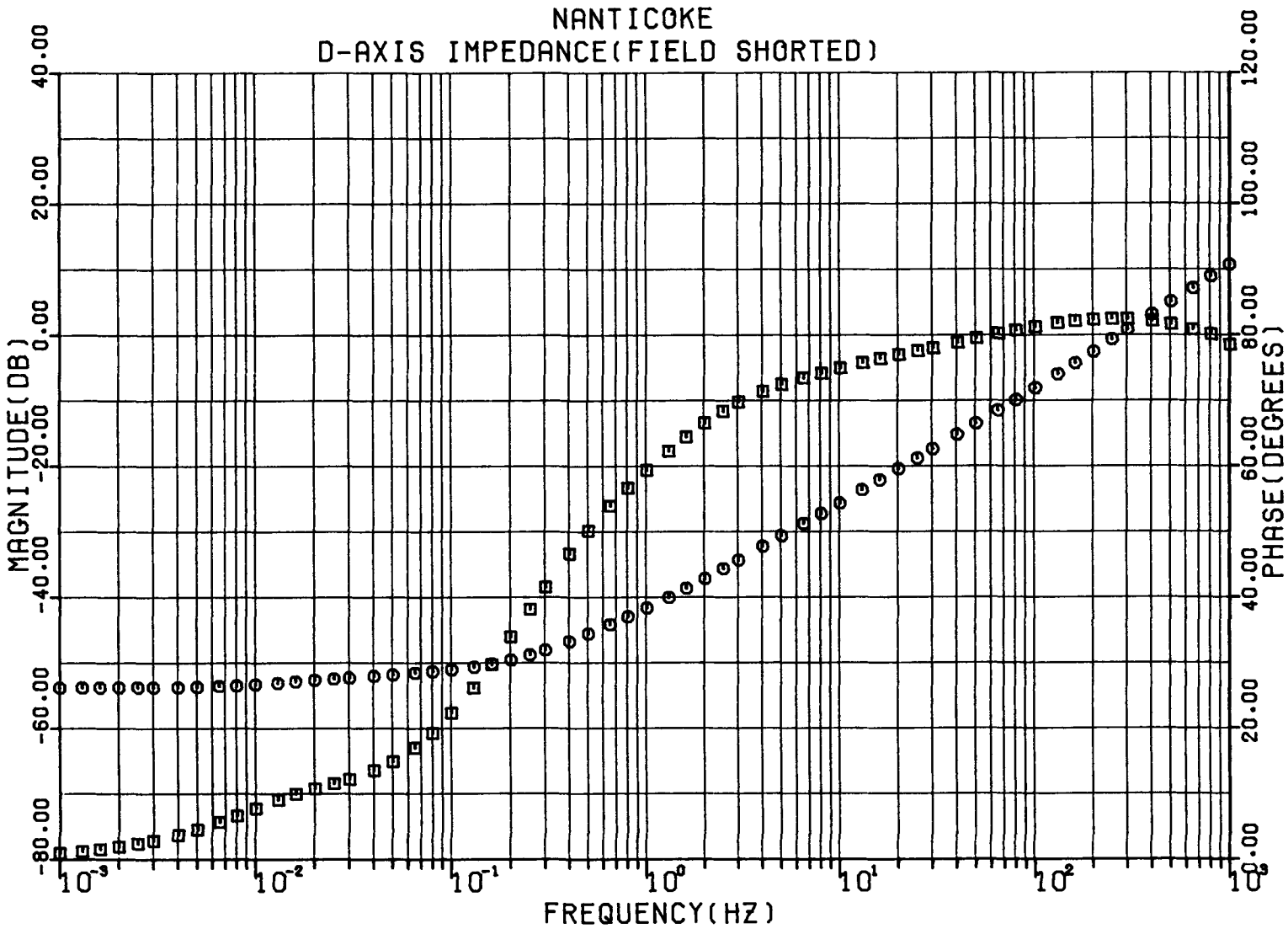

Figure 2-2. Nanticoke Direct Axis Operational Impedance, Magnitude in dB Above 1 pu.

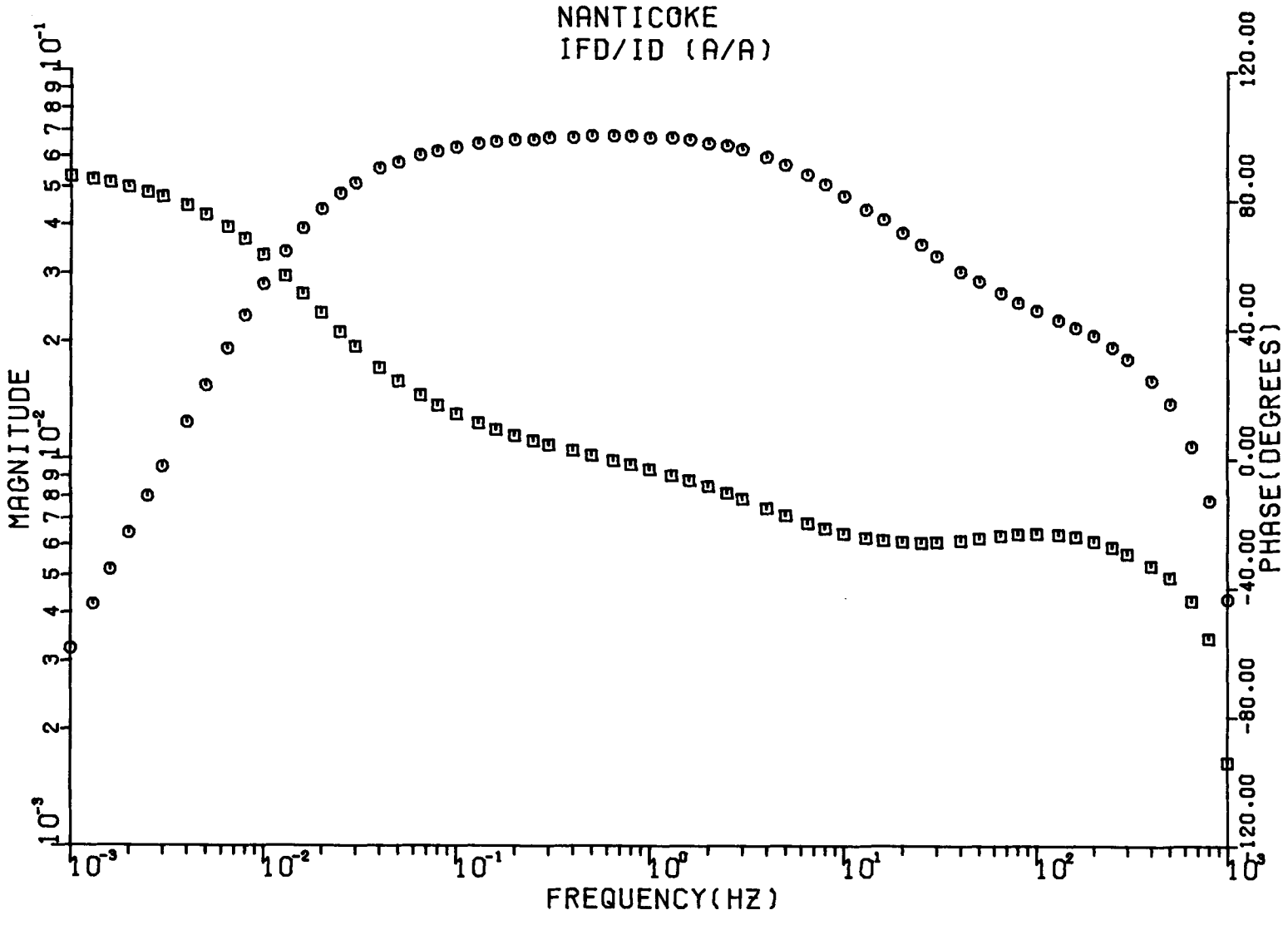

Figure 2-3. Nanticoke Stationary Stator-To-Field Transfer Function, Magnitude in A/A.

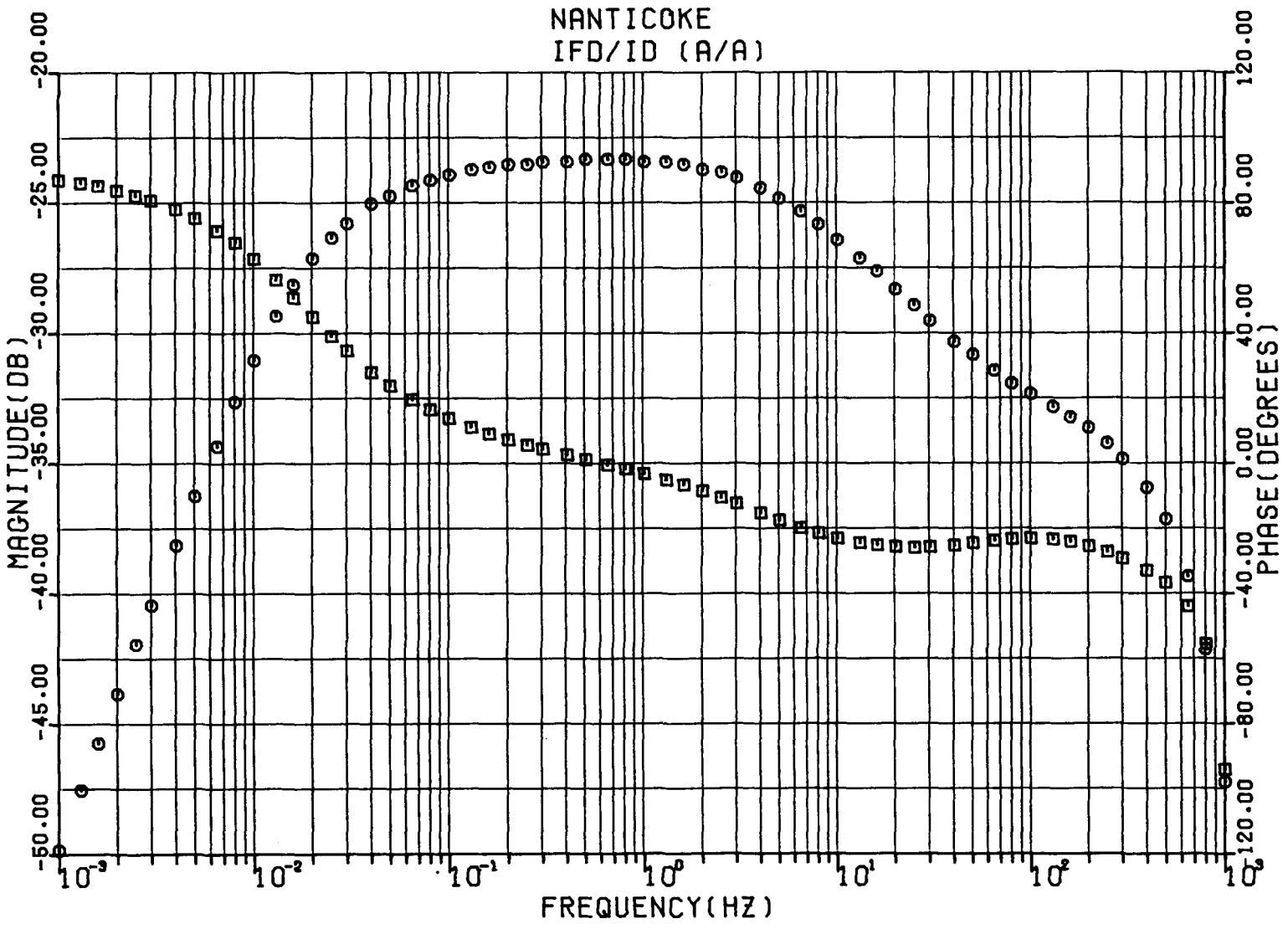

Figure 2-4. Nanticoke Stationary Stator-To-Field Transfer Function, Magnitude in dB Above 1 A/A.

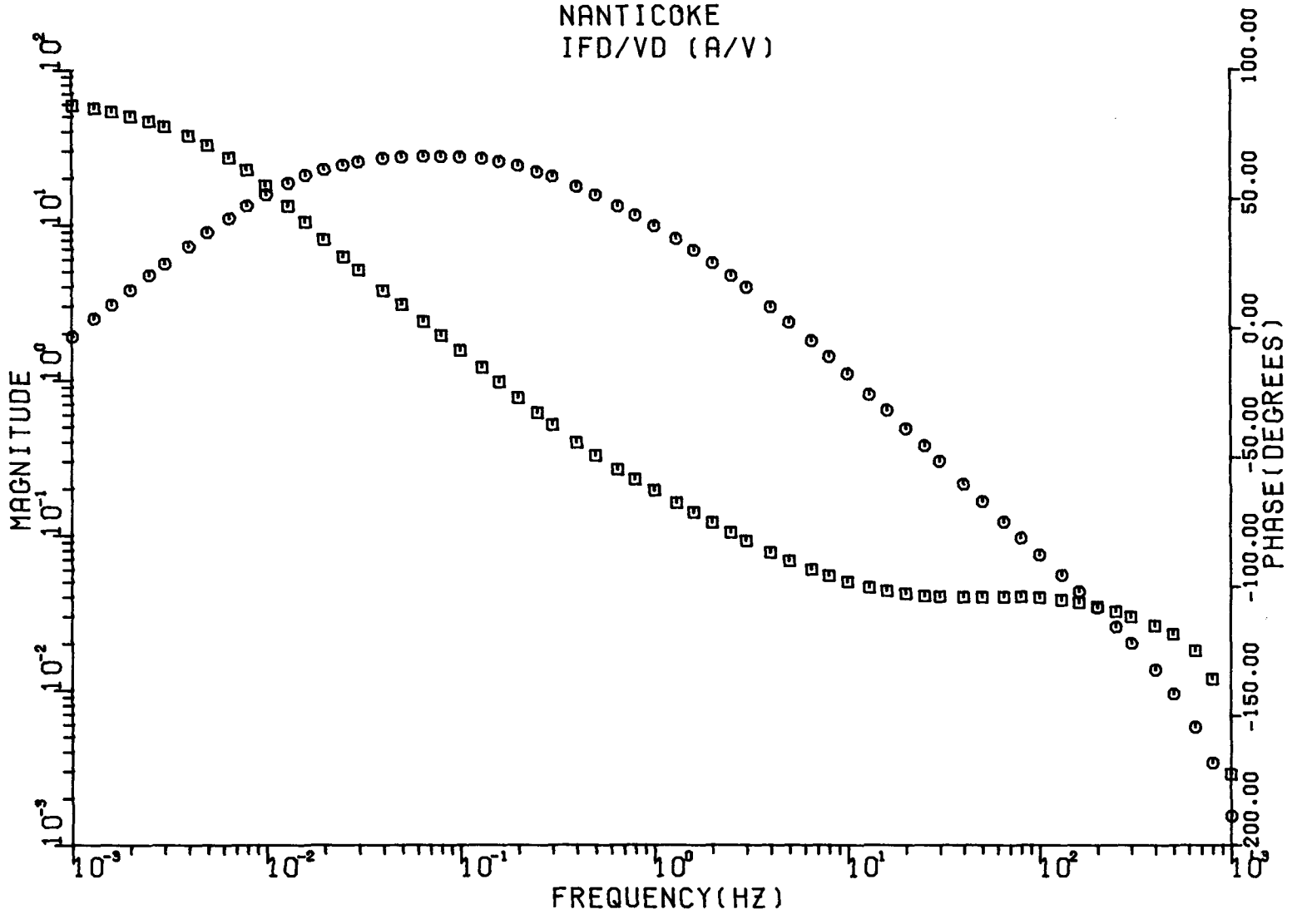

Figure 2-5. Nanticoke Stator-To-Field Transfer Admittance, Magnitude in A/V.

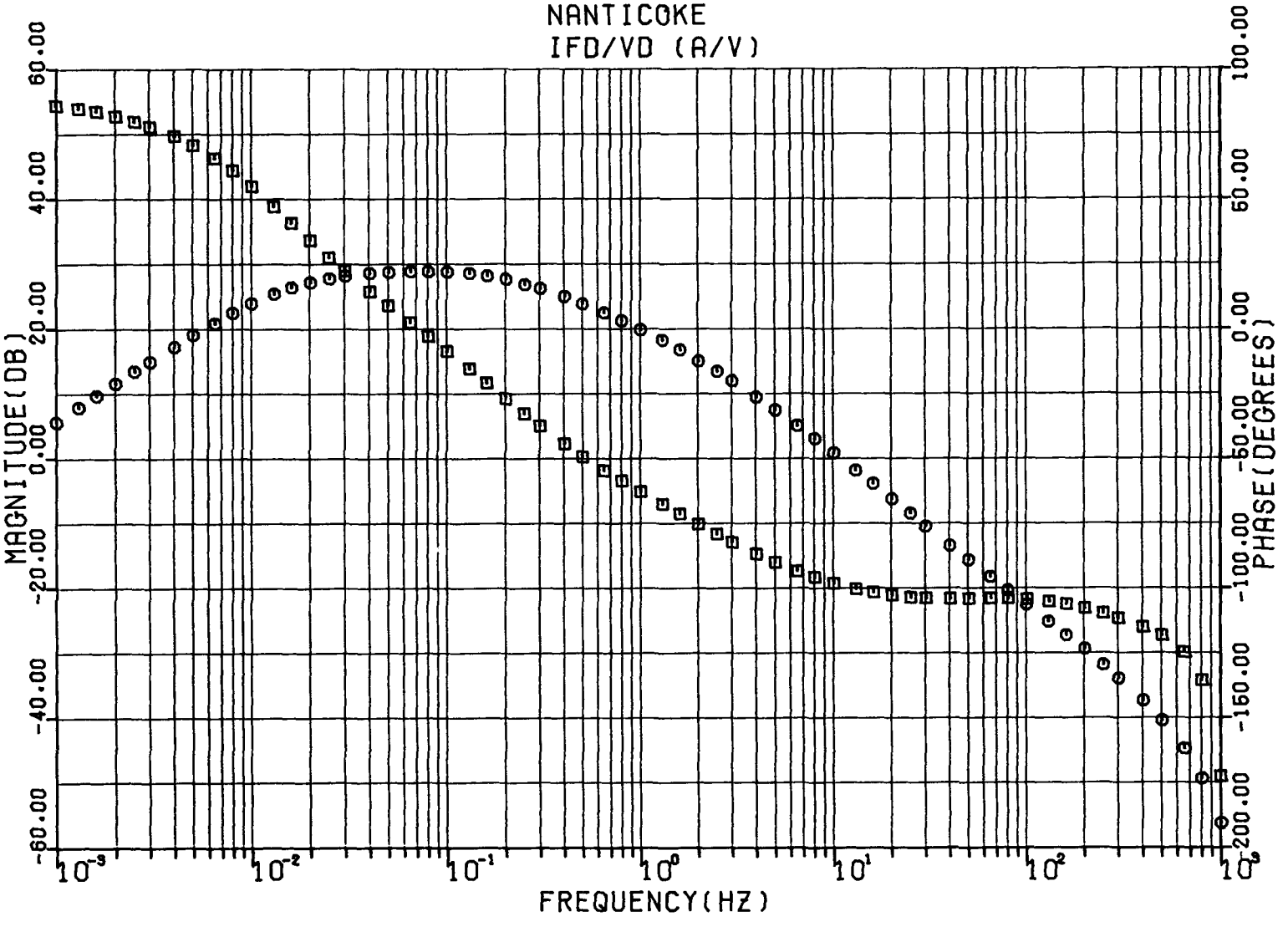

Figure 2-6. Nanticoke Stator-To-Field Transfer Admittance, Magnitude in dB Above 1 A/V.

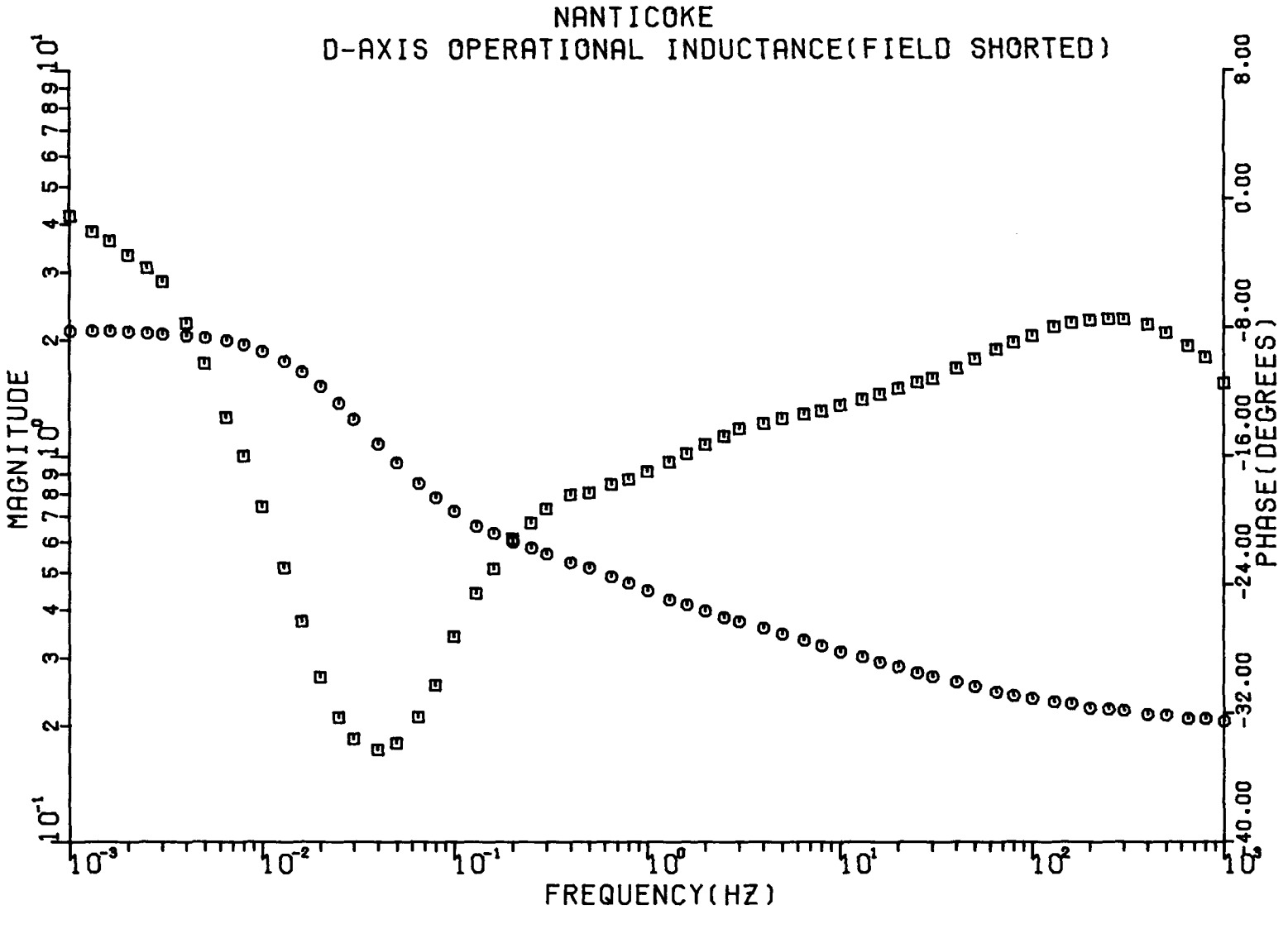

Figure 2-7. Nanticoke Direct Axis Operational Inductance, Magnitude in pu.

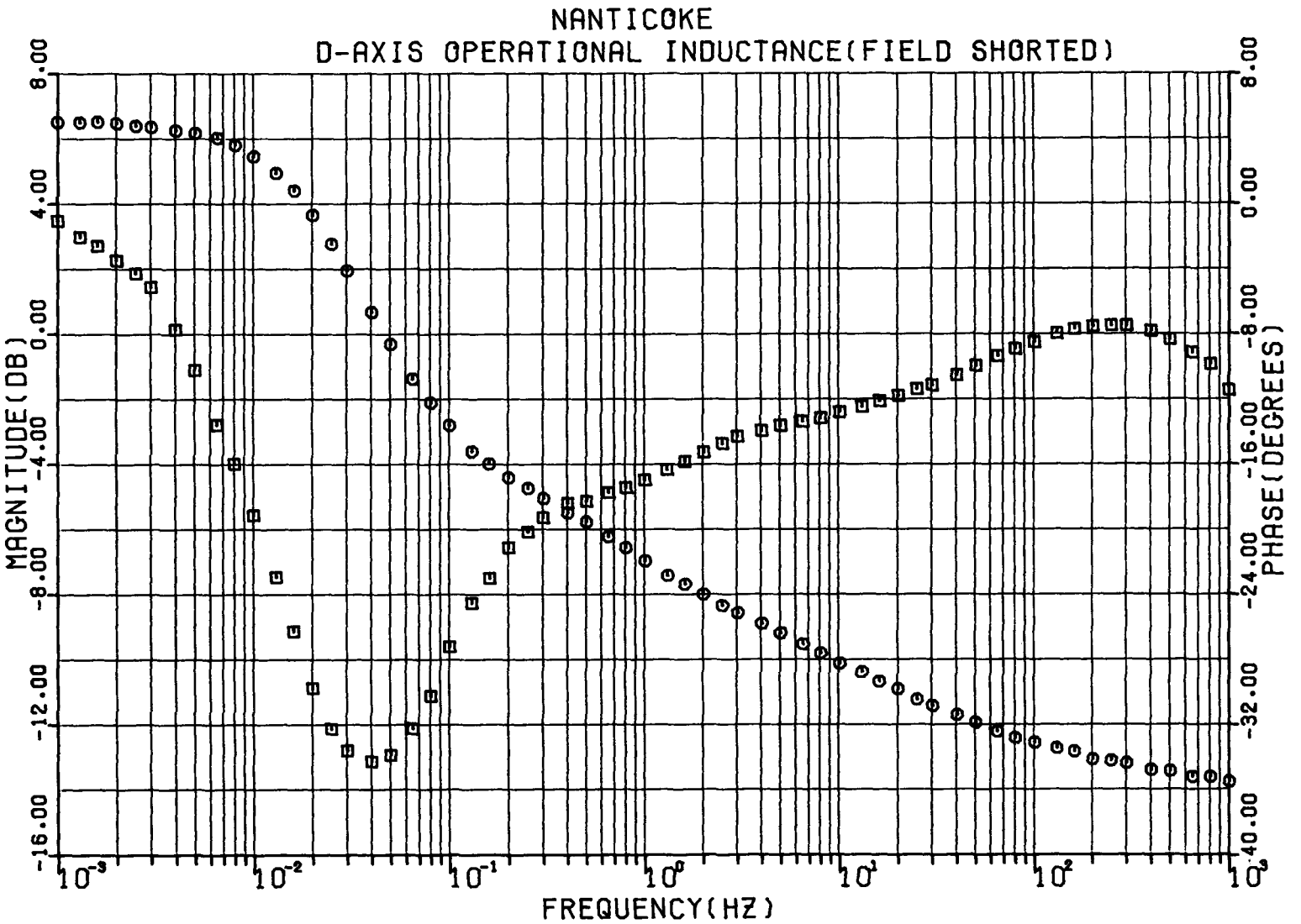

Figure 2-8. Nanticoke Direct Axis Operational Inductance, Magnitude in dB Above 1 pu.

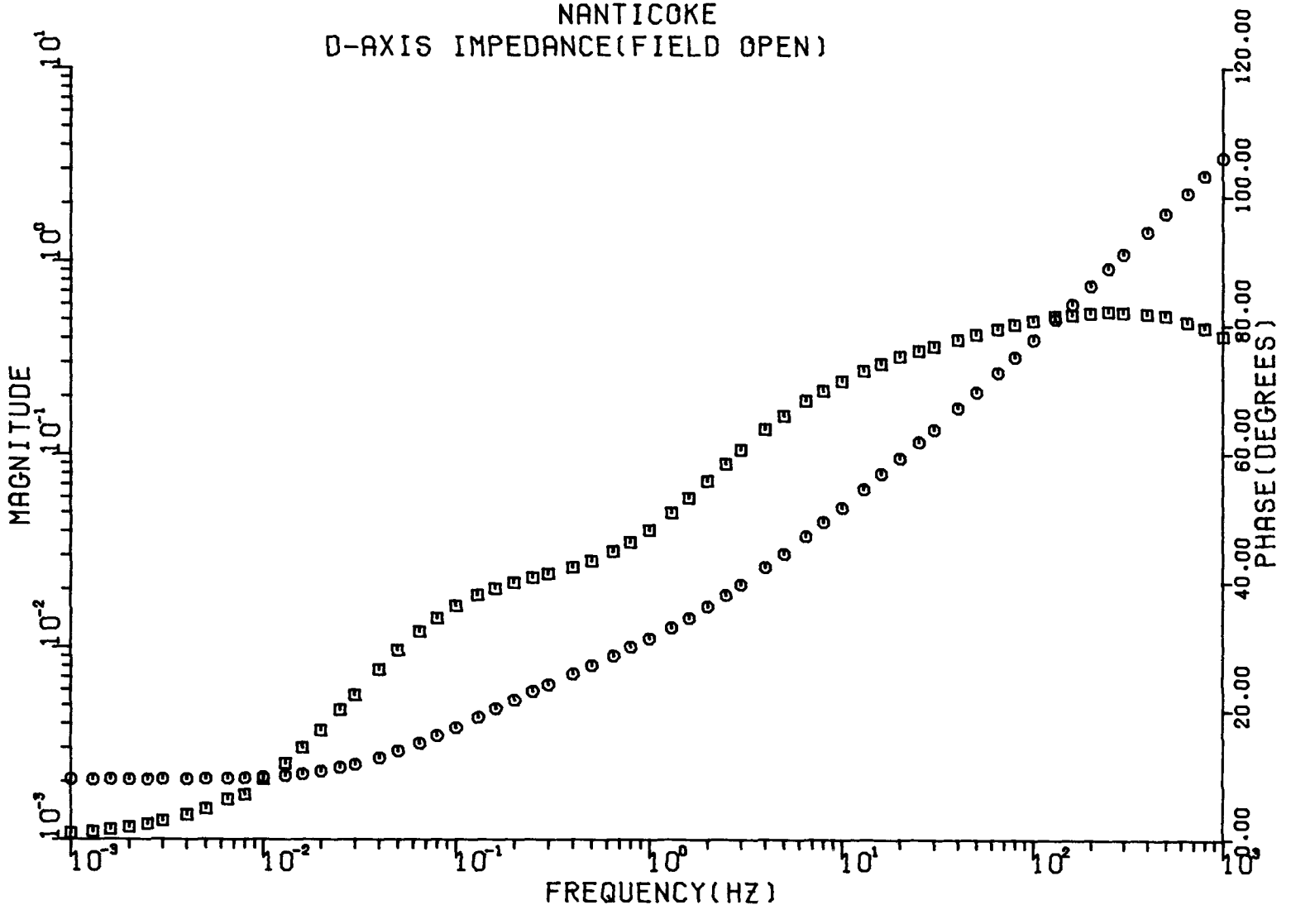

Figure 2-9. Nanticoke Open-Circuit Stator Driving Point Impedance, Magnitude in pu.

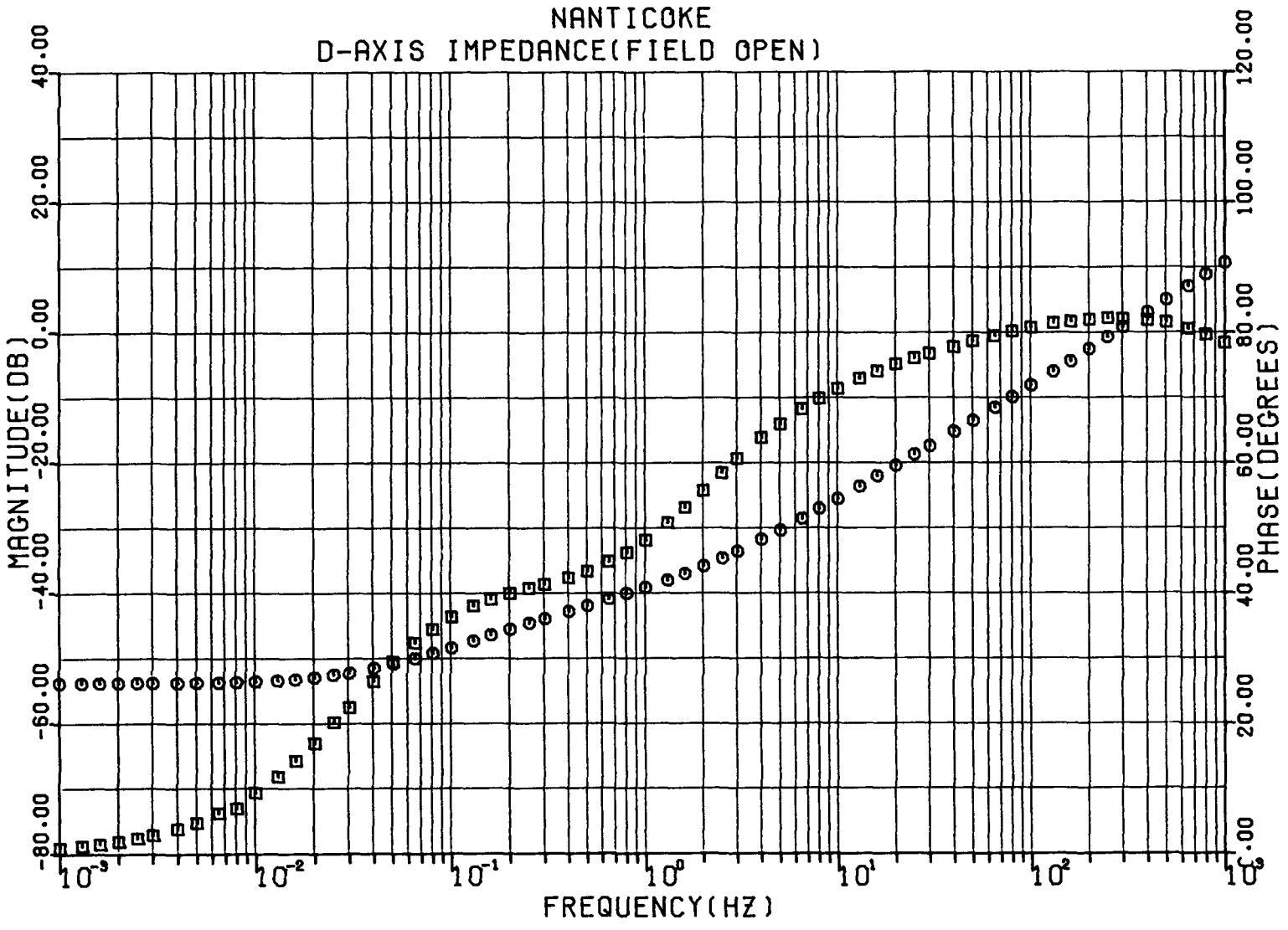

Figure 2-10. Nanticoke Open-Circuit Stator Driving Point Impedance, Magnitude in dB Above 1 pu.

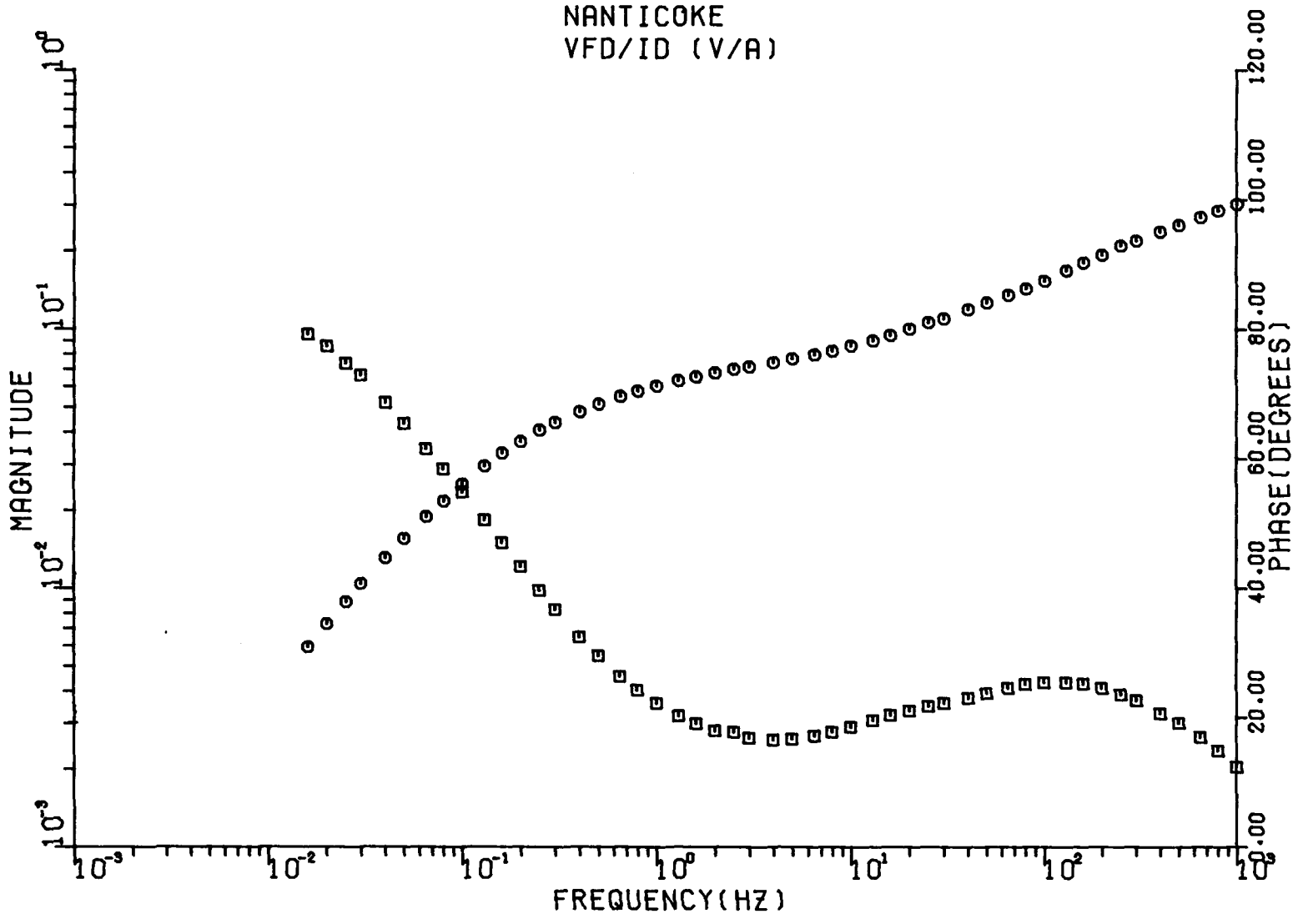

Figure 2-11. Nanticoke Stator-To-Field Transfer Impedance, Magnitude in V/A.

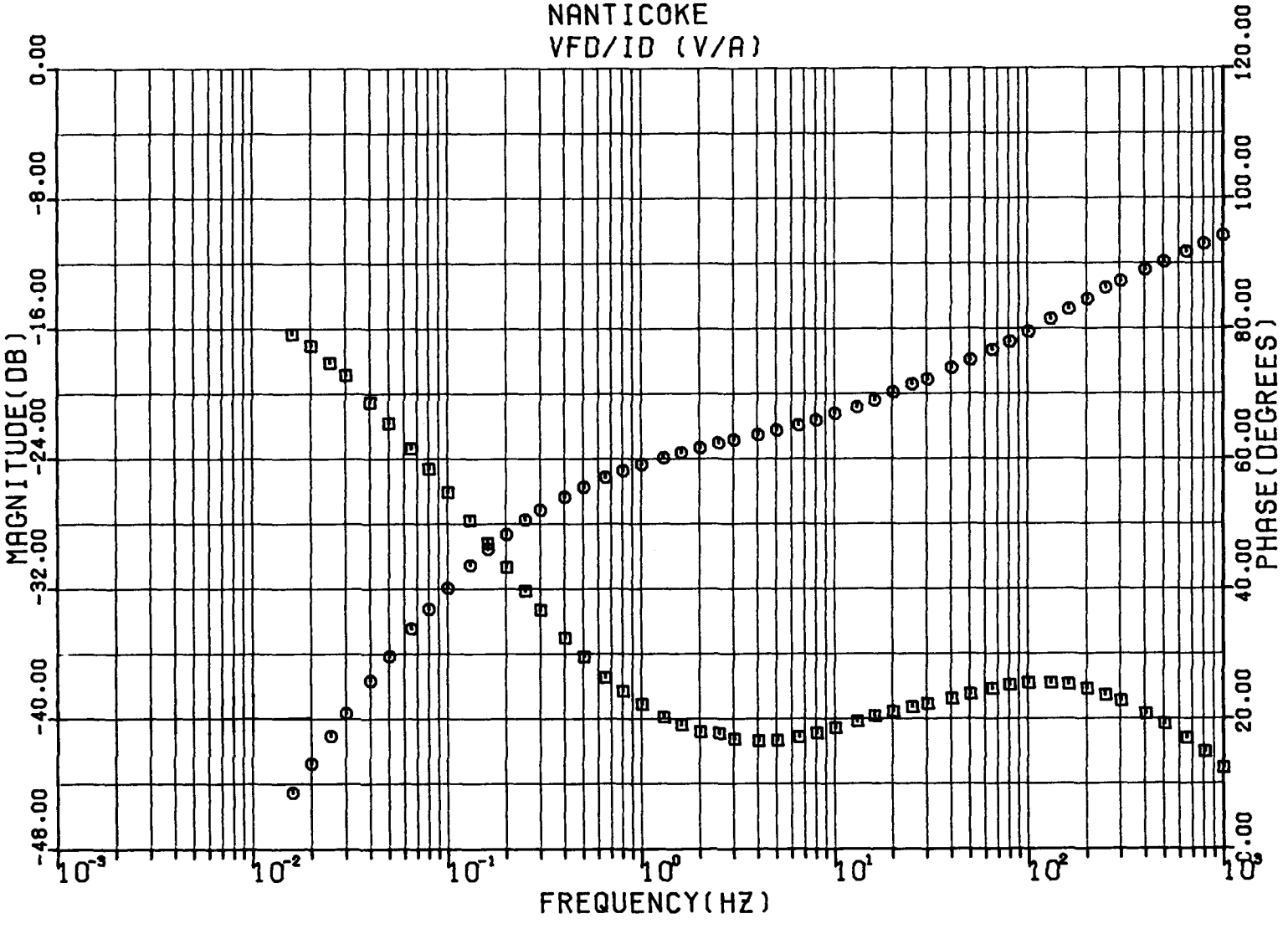

Figure 2-12. Nanticoke Stator-To-Field Transfer Impedance, Magnitude in dB Above 1 V/A.

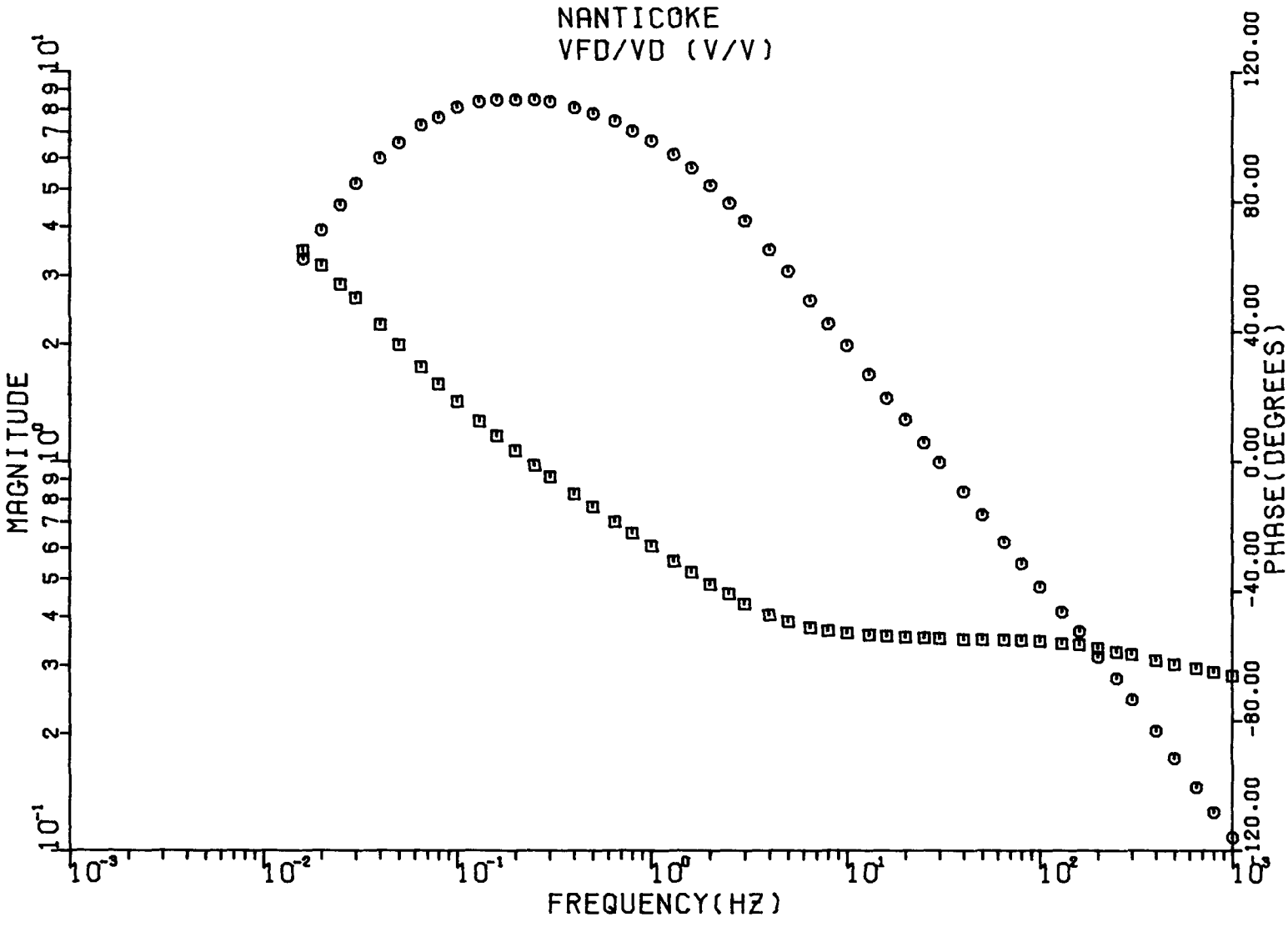

Figure 2-13. Nanticoke Open-Circuit Stator-To-Field Transfer Function, Magnitude in V/V.

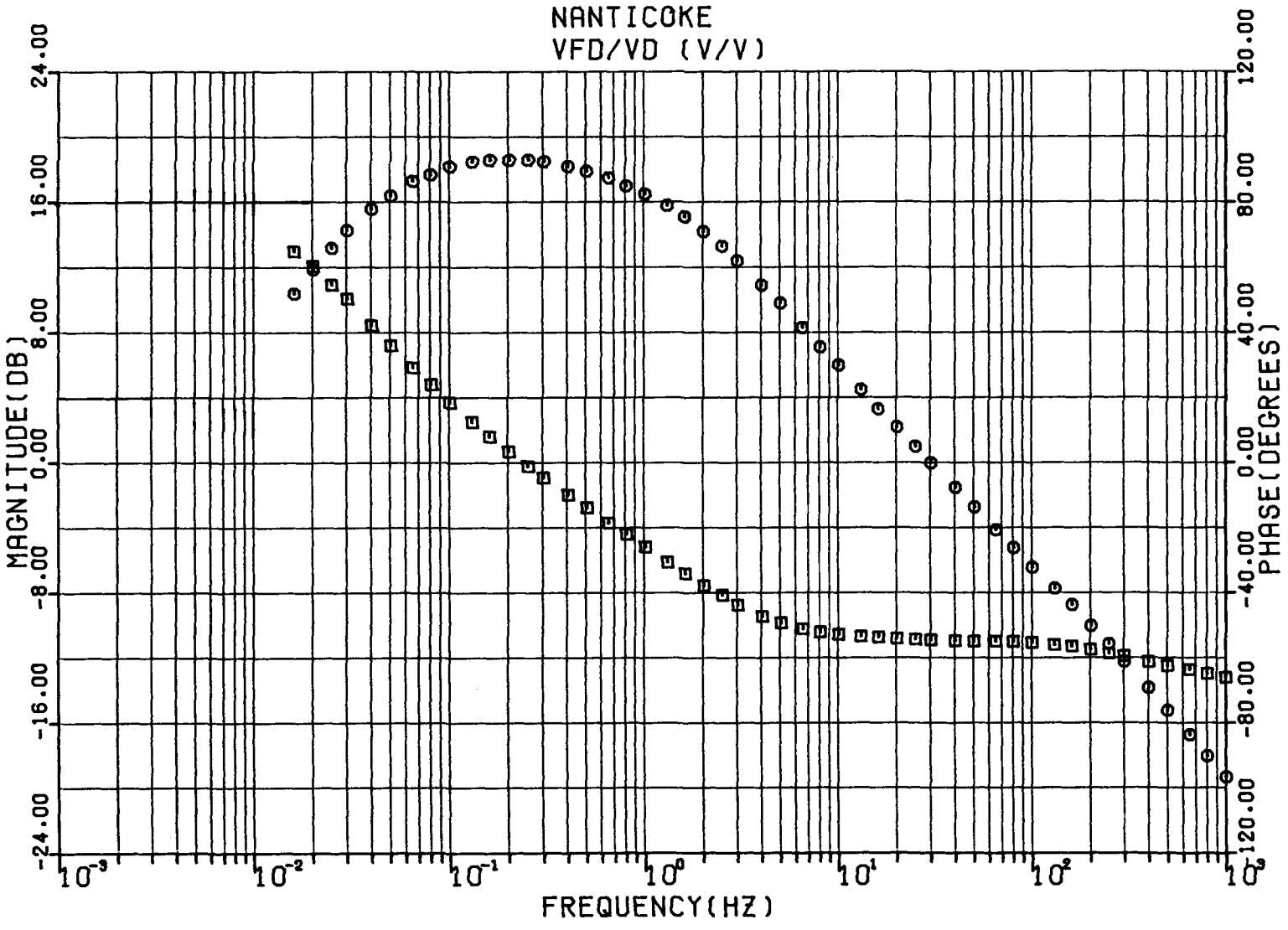

Figure 2-14. Nanticoke Open-Circuit Stator-To-Field Transfer Function, Magnitude in dB Above 1 V/V.

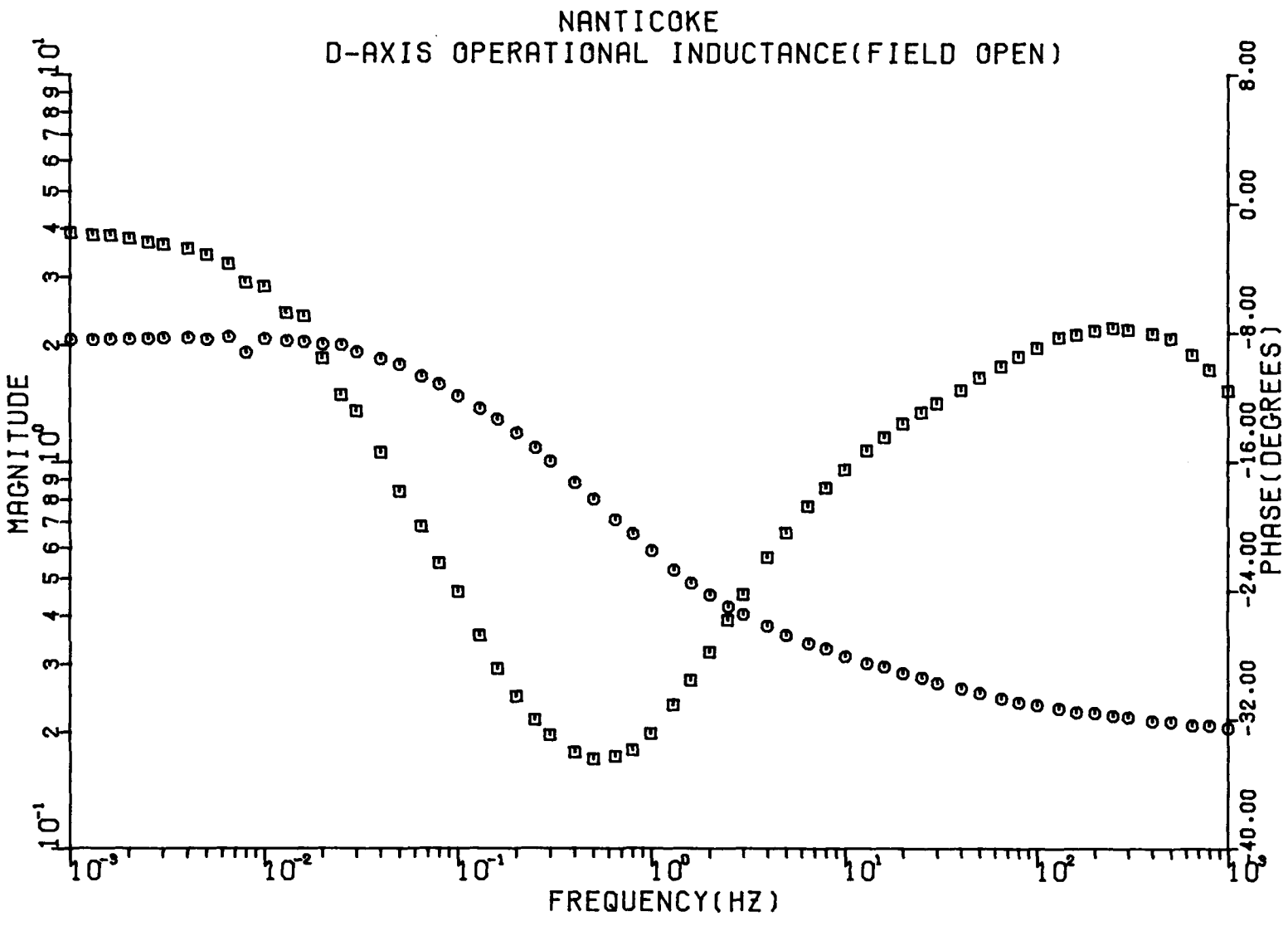

Figure 2-15. Nanticoke Open-Circuit Stator Driving Point Operational Inductance, Magnitude in pu.

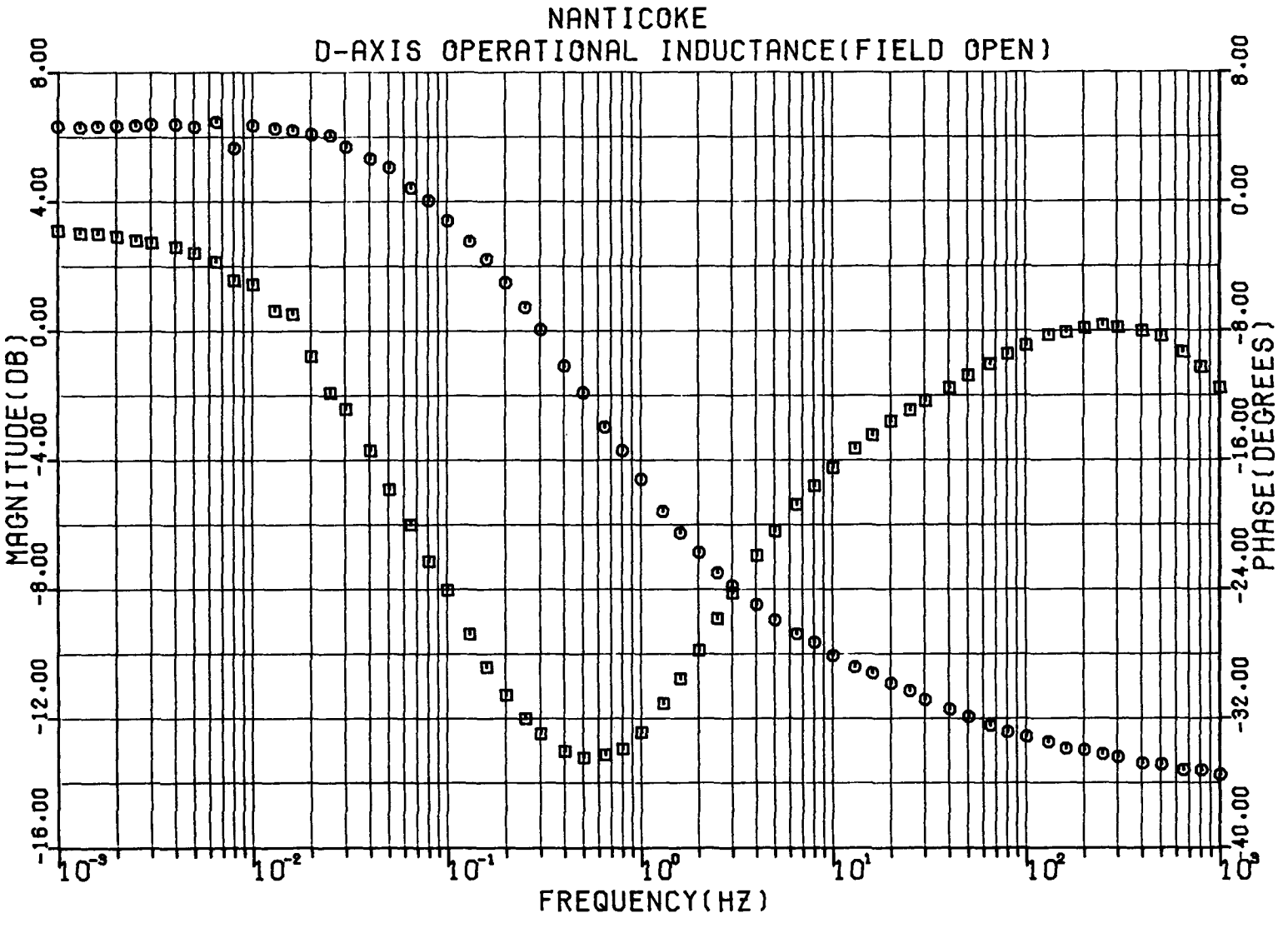

Figure 2-16. Nanticoke Open-Circuit Stator Driving Point Operational Inductance, Magnitude in dB Above 1 pu.

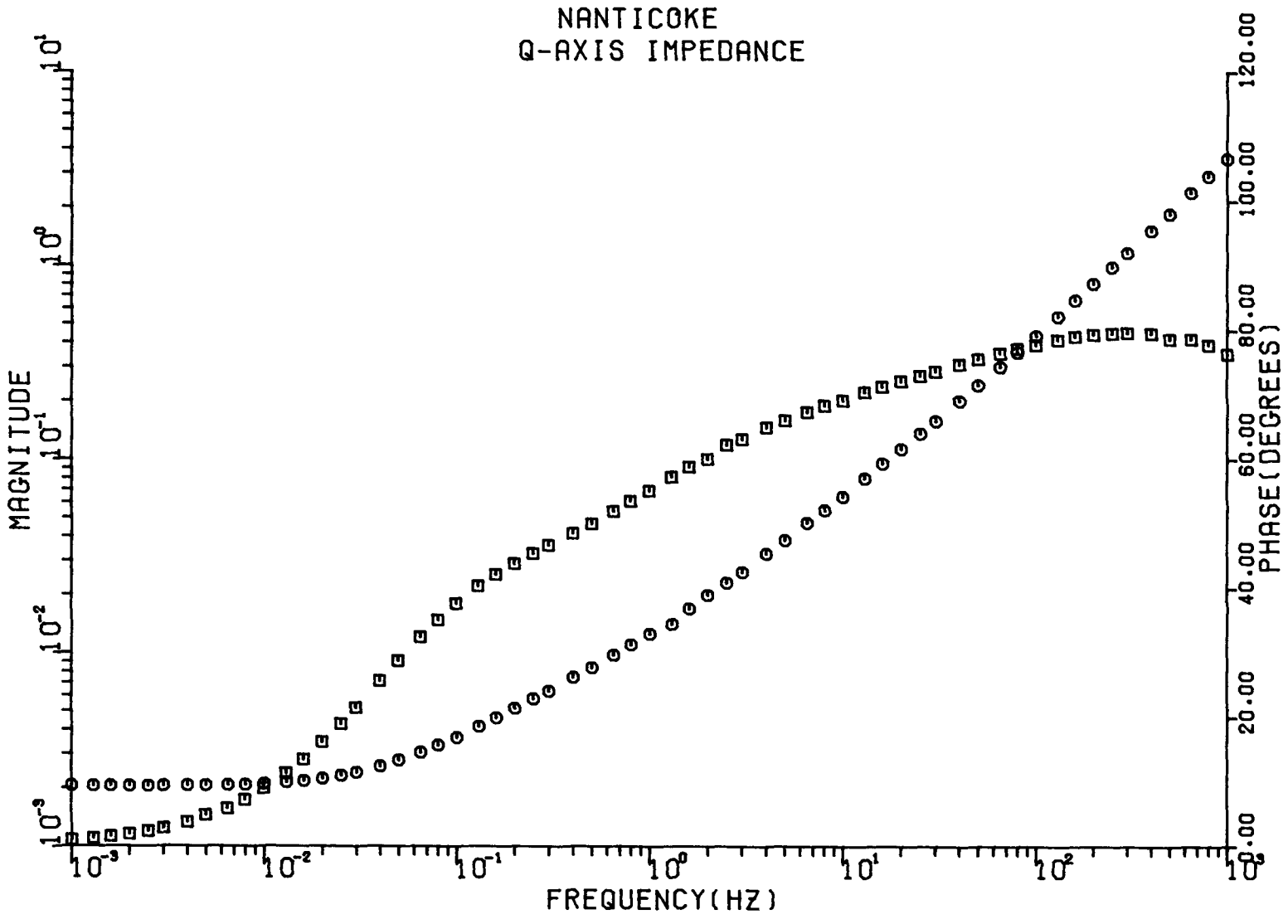

Figure 2-17. Nanticoke Quadrature Axis Operational Impedance, Magnitude in pu.

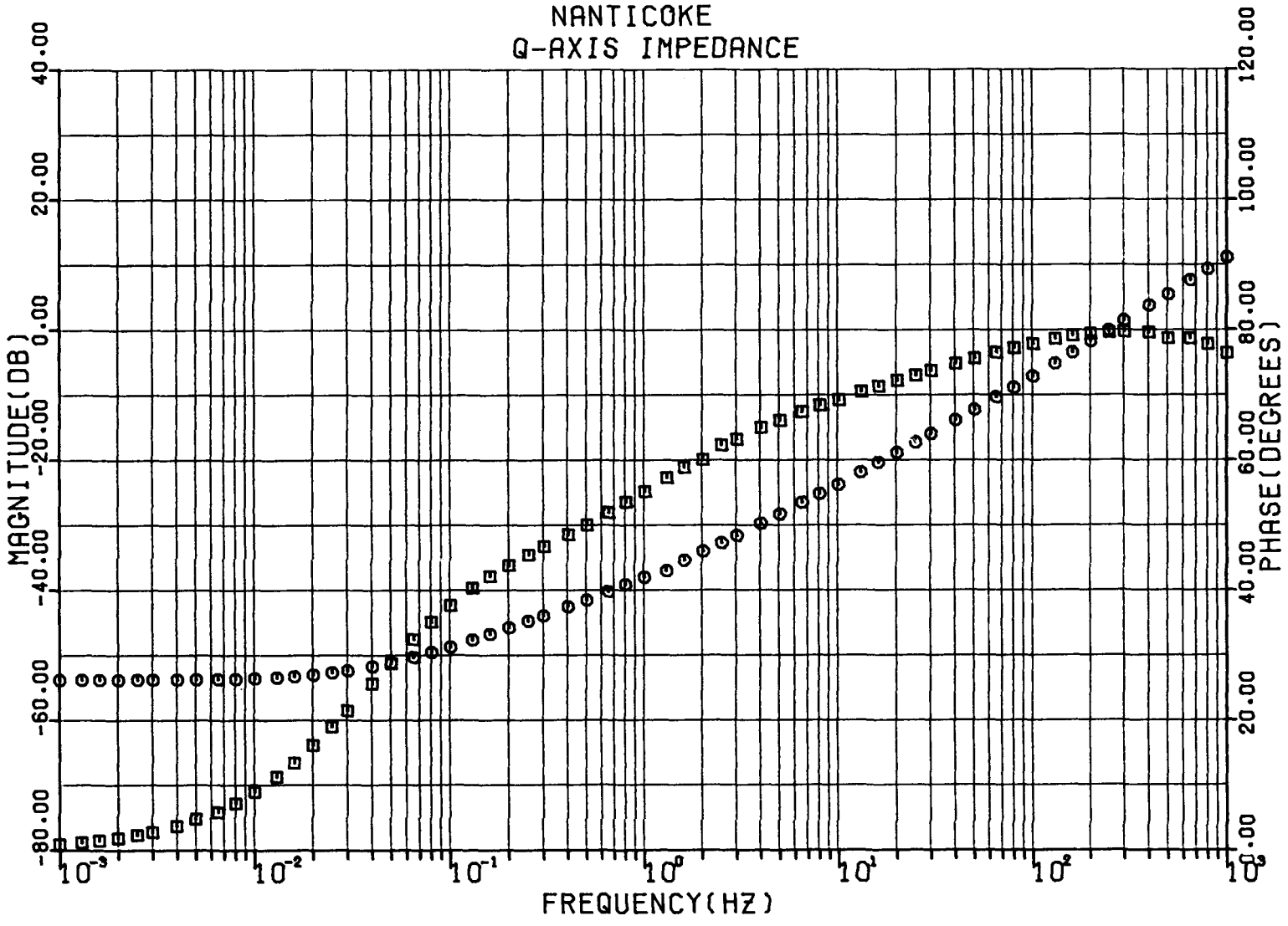

Figure 2-18. Nanticoke Quadrature Axis Operational Impedance, Magnitude in dB Above 1 pu.

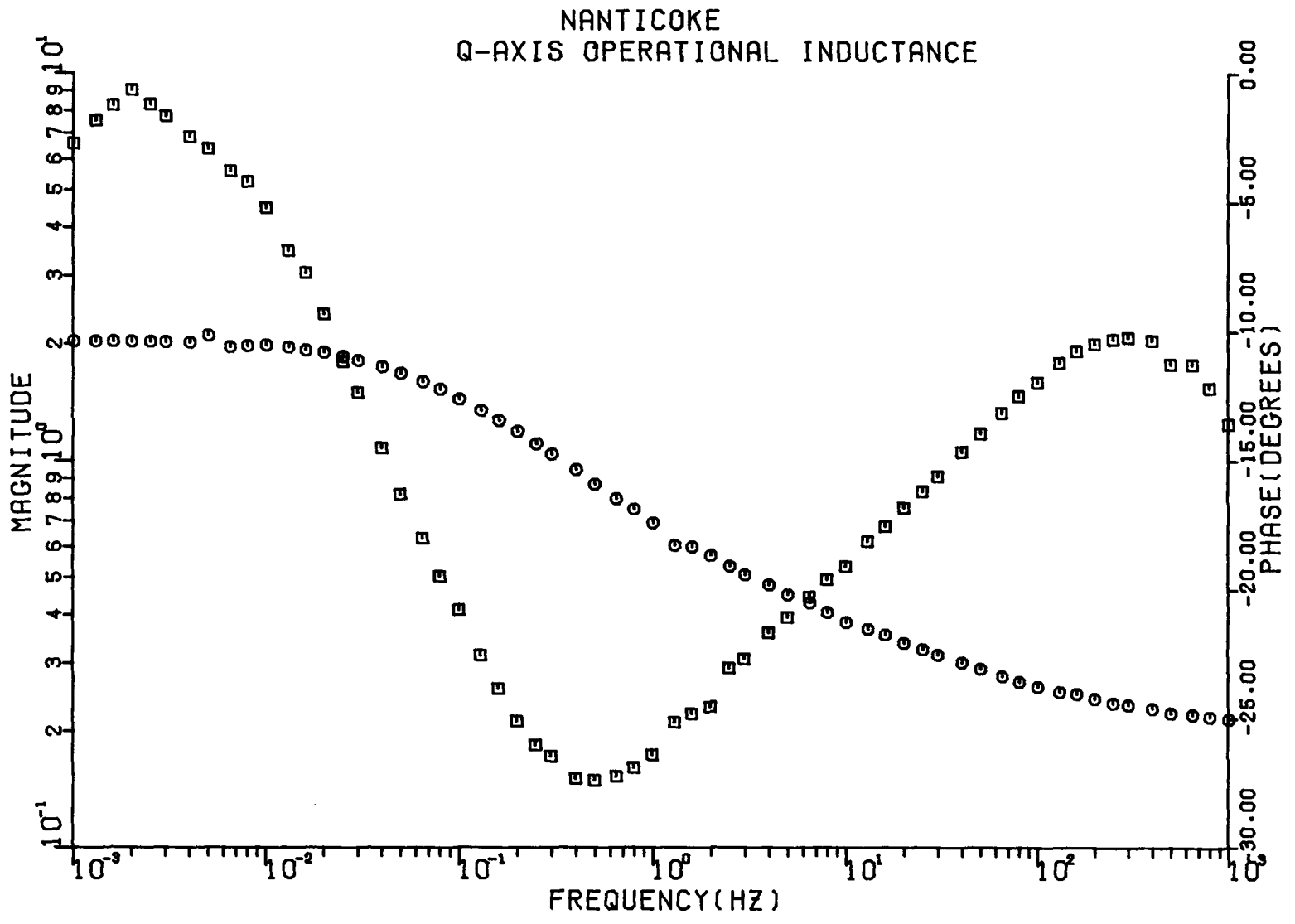

Figure 2-19. Nanticoke Quadrature Axis Operational Inductance, Magnitude in pu.

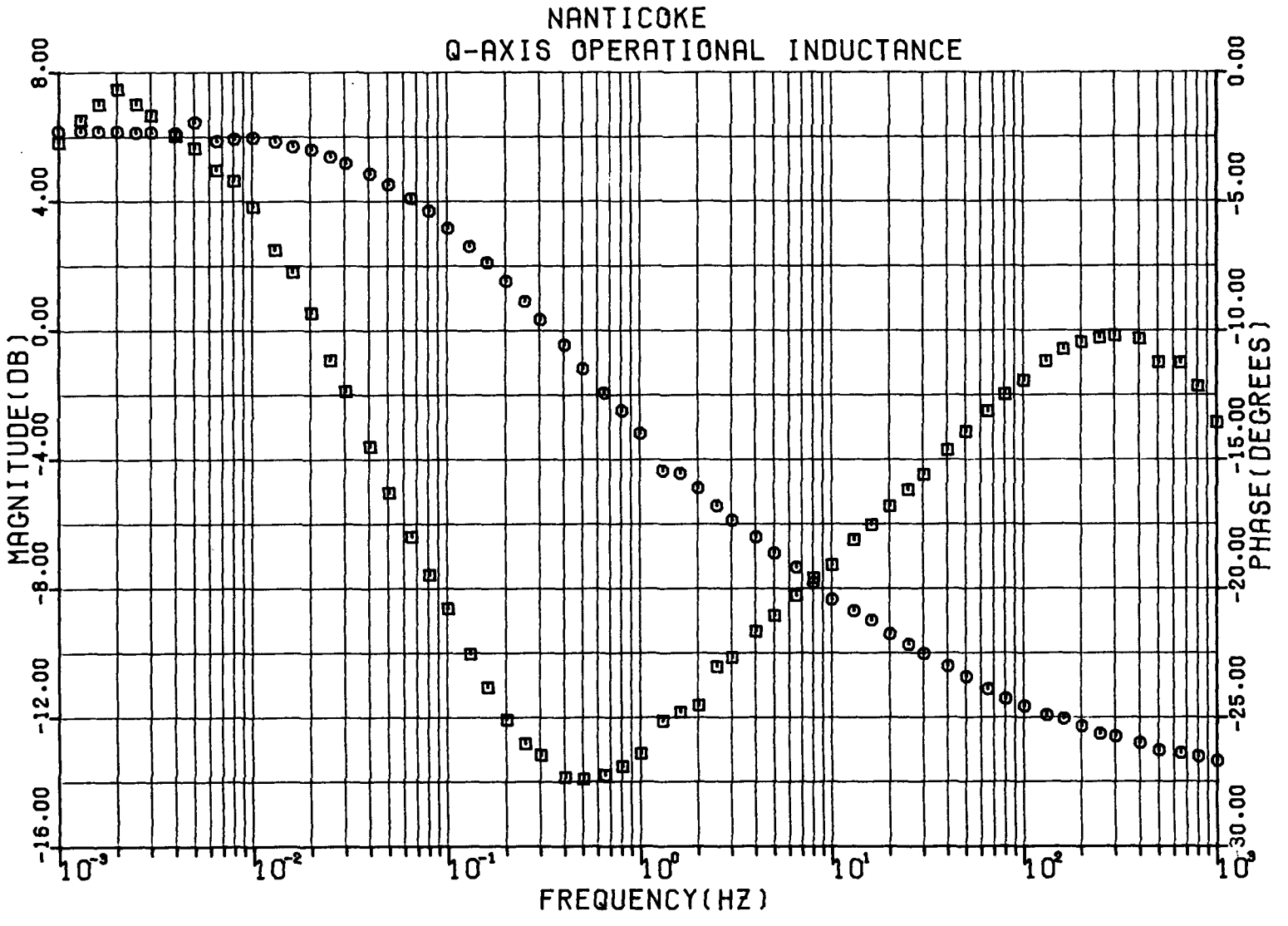

Figure 2-20. Nanticoke Quadrature Axis Operational Inductance, Magnitude in dB Above 1 pu.

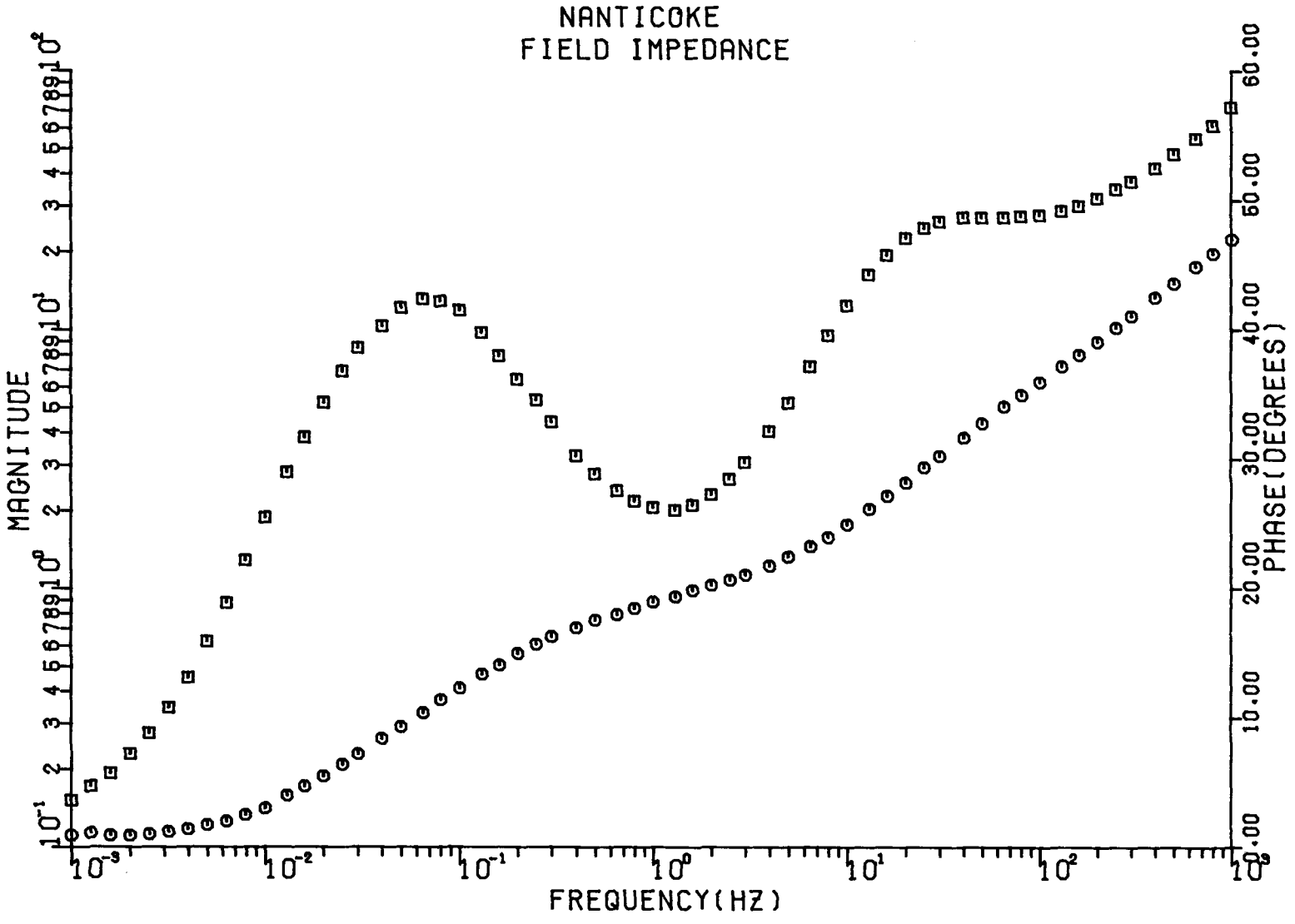

Figure 2-21. Nanticoke Open-Circuit Field Driving Point Impedance, Magnitude in Ohms.

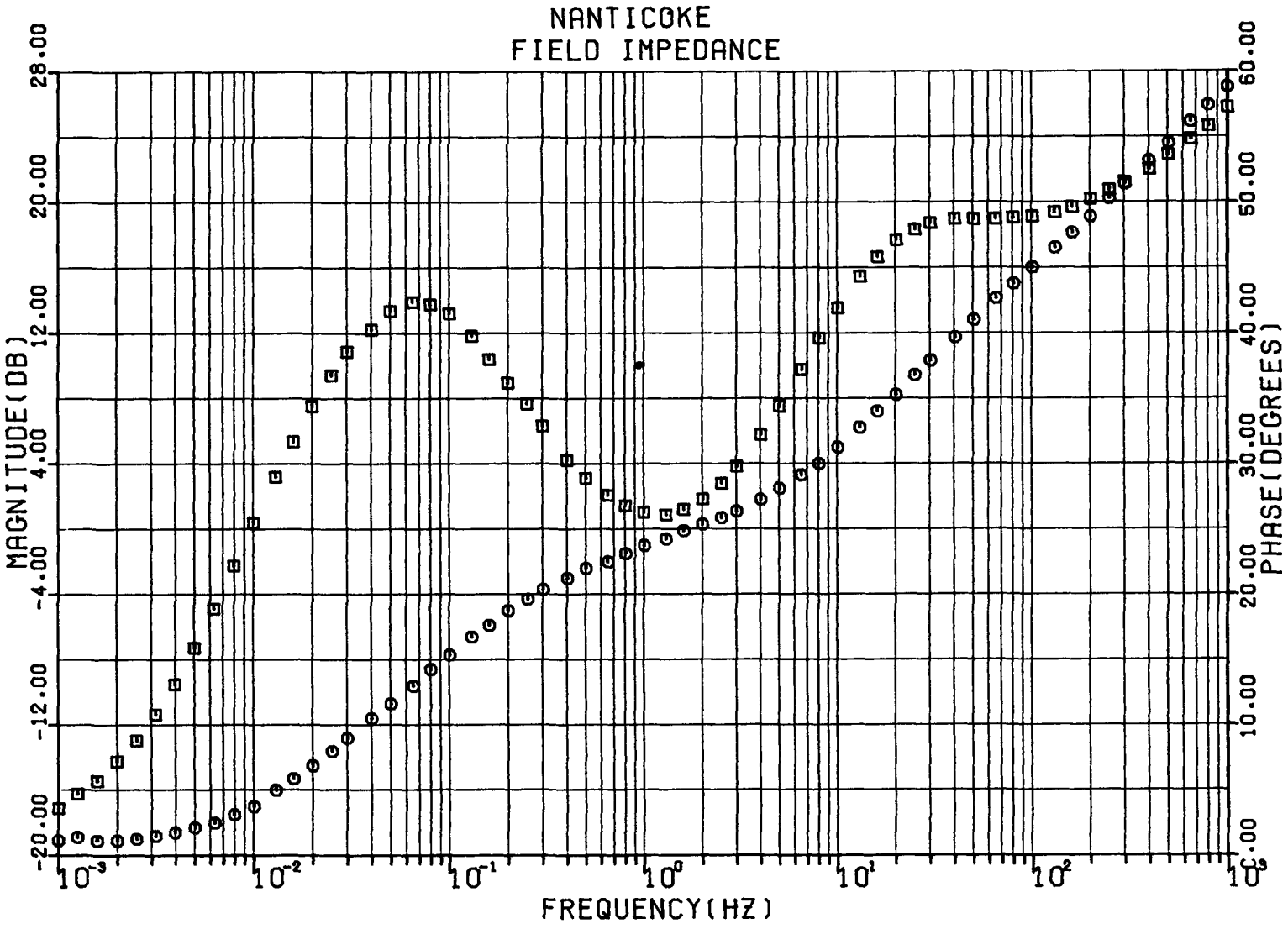

Figure 2-22. Nanticoke Open-Circuit Field Driving Point Impedance, Magnitude in dB Above 1 Ohm.

INDUCTANCE OF GENERATOR WINDINGS

Figure 2-23 is a plot of the mutual inductance between the field and one phase of the stator winding as a function of field current. The magnetic axes of the two windings were aligned during the measurements which were done by changing the level of direct current in the field and integrating the resulting induced voltage on the stator winding. The mutual inductance was then obtained from the relationship

$$L_m = \frac{\int_0^\infty e \, dt}{\Delta I_{fd}} \qquad (2\text{-}1)$$

where e is the induced voltage in the relevant stator winding. Each point in Figure 2-23 was measured from a change in field current equal to twice the corresponding value on the abscissa. In other words, a point plotted at 50 A was obtained from changes in field current between ±50 A dc.

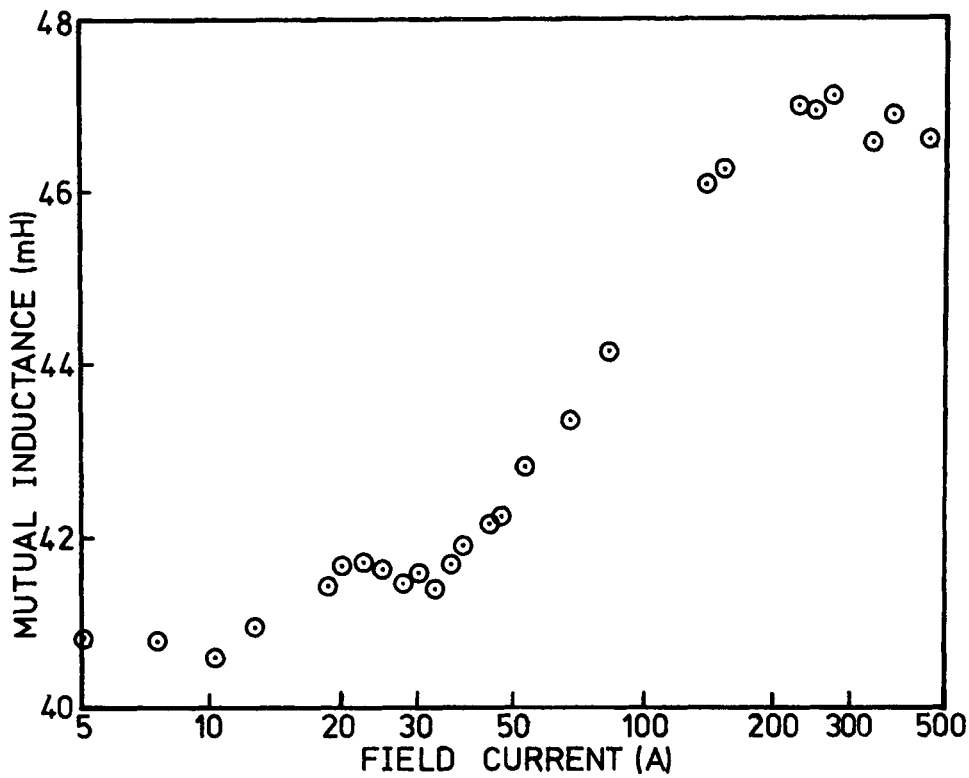

Figure 2-23. Secant Value of Mutual Inductance Between the Field and One Phase of the Stator Winding.

60 Hz FIELD IMPEDANCE

The rotor impedance, viewed from the field terminals was measured at 60 Hz over a range of currents from 0 to 34 A rms. Voltage, current and power input were recorded. From these data, the resistive and reactive components of the impedance were computed (Table 2-5 and Figures 2-24 and 2-25).

Table 2-5
NANTICOKE 60 Hz FIELD IMPEDANCE

Voltage (V)	Current (A)	Active Power (W)	Reactive Power (VAR)	R (Ω)	X (Ω)	Z (Ω)	Angle (deg)
10.53	2.28	16.48	17.46	3.17	3.36	4.62	46.6
20.00	4.24	56.16	63.54	3.12	3.53	4.72	48.5
30.90	6.42	133.09	147.1	3.23	3.57	4.81	47.9
40.30	8.36	224.8	250.9	3.22	3.59	4.82	48.1
47.90	9.86	315.2	351.7	3.24	3.62	4.86	48.1
53.20	10.80	384.8	426.6	3.30	3.66	4.93	47.9
60.00	12.12	487.2	539.8	3.32	3.68	4.95	47.9
70.10	13.96	660.0	722.5	3.39	3.91	5.02	47.5
79.80	15.64	838.8	924.1	3.43	3.78	5.10	47.7
90.20	17.44	1056.	1165.	3.47	3.83	5.17	47.8
100.0	19.08	1285.	1410.	3.53	3.87	5.24	47.6
110.0	20.40	1533.	1638.	3.68	3.94	5.39	46.9
120.1	21.90	1800.	1917.	3.75	4.00	5.48	46.8
130.0	32.40	2080.	2219.	3.80	4.05	5.56	46.8
140.0	24.90	2400.	2528.	3.87	4.08	5.62	46.4
149.9	26.05	2705.	2816.	3.99	4.15	5.75	46.1
160.0	27.30	3012.	3163.	4.04	4.24	4.86	46.4
169.9	28.80	3378.	3540.	4.07	4.27	5.90	46.3
180.0	30.15	3750.	3922.	4.13	4.32	5.97	46.2
189.5	31.15	4130.	4217.	4.26	4.35	6.08	45.6
200.0	32.50	4557.	4635.	4.31	4.39	6.15	45.4
210.0	33.85	4998.	5054.	4.36	4.41	6.20	45.3
212.0	34.10	5110.	5113.	4.39	4.40	6.22	45.0

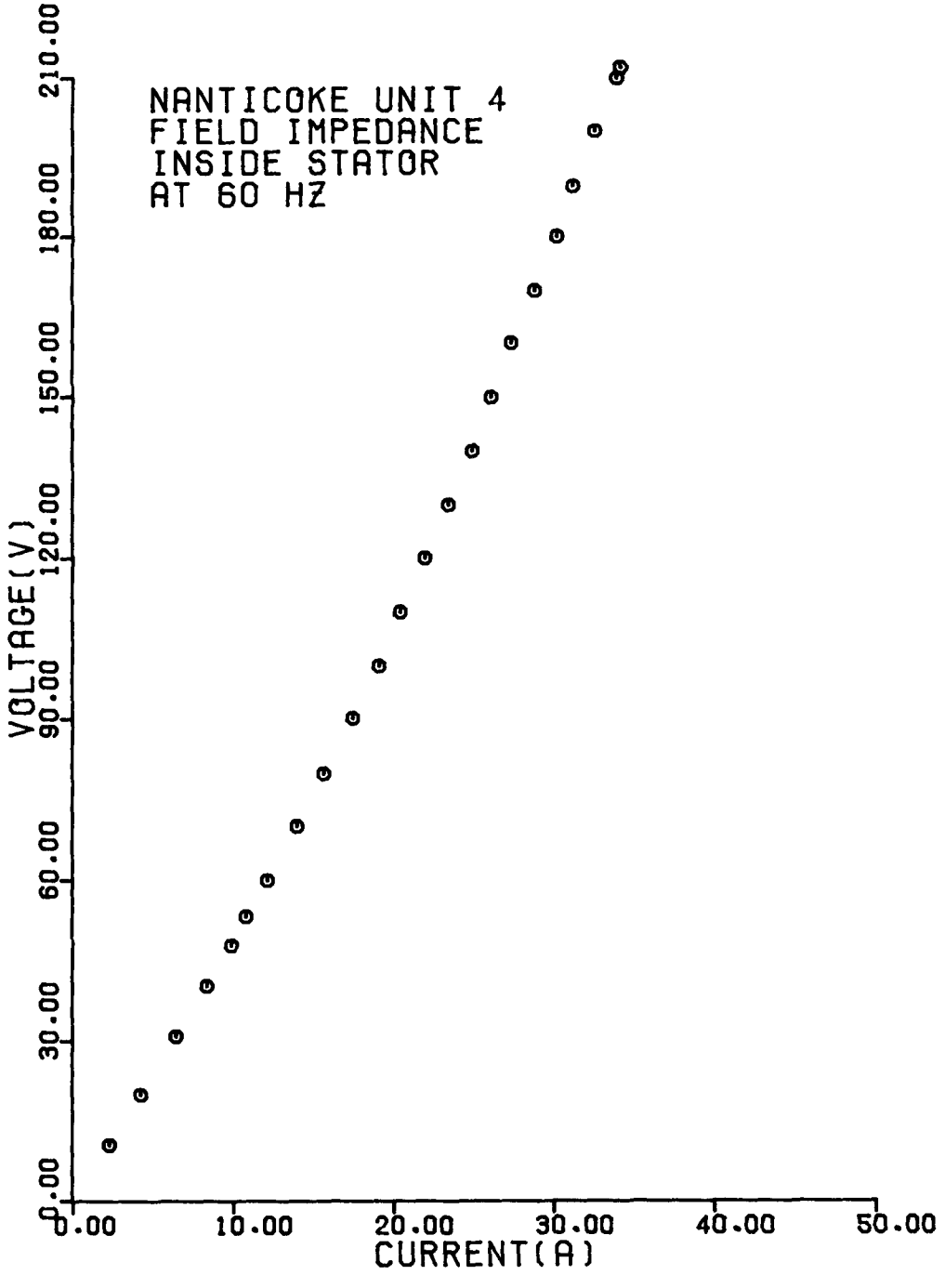

Figure 2-24. Nanticoke 60 Hz Field Impedance.

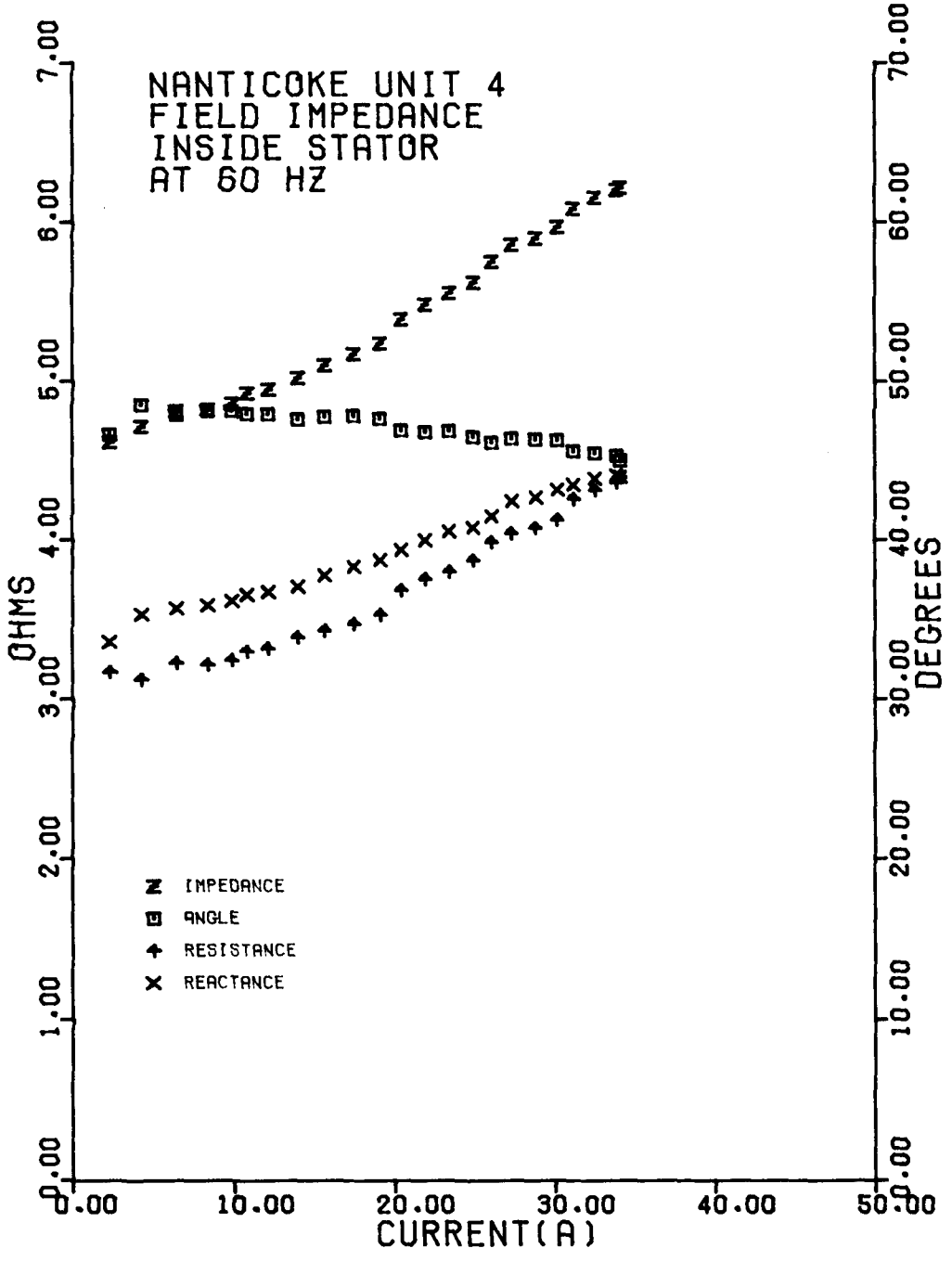

Figure 2-25. Components of Nanticoke 60 Hz Field Impedance.

Section 3

LINE SWITCHING TESTS

INTRODUCTION

A series of line switching tests was done at Nanticoke to provide a standard against which the performance of the various models of the Nanticoke generators could be judged.

SYSTEM ARRANGEMENT

The system set-up for the tests is shown in Figure 3-1. The G6 generator was connected radially to the rest of the power system by two lines. The short line, N2M, is 37 km long and runs between the 230 kV buses at Nanticoke and the Middleport transformer station. The long line formed by N5M and M32W is 133 km long and runs between the 230 kV buses at Nanticoke and the Buchanan transformer station via Middleport. The G6 exciter, a bus-fed thyristor type, was supplied from the Nanticoke 230 kV bus, as far away, electrically, as possible from the G6 terminals. The G6 load limiter was set to block any governor action during the tests.

Opening or closing either of the lines between G6 and the rest of the power system produced a sudden change in the impedance between the generator and its load. Operations involving the short line resulted in a larger disturbance to the test generator than those using the long line.

A summary of the switching operations and corresponding tests generator conditions is given in Table 3-1.

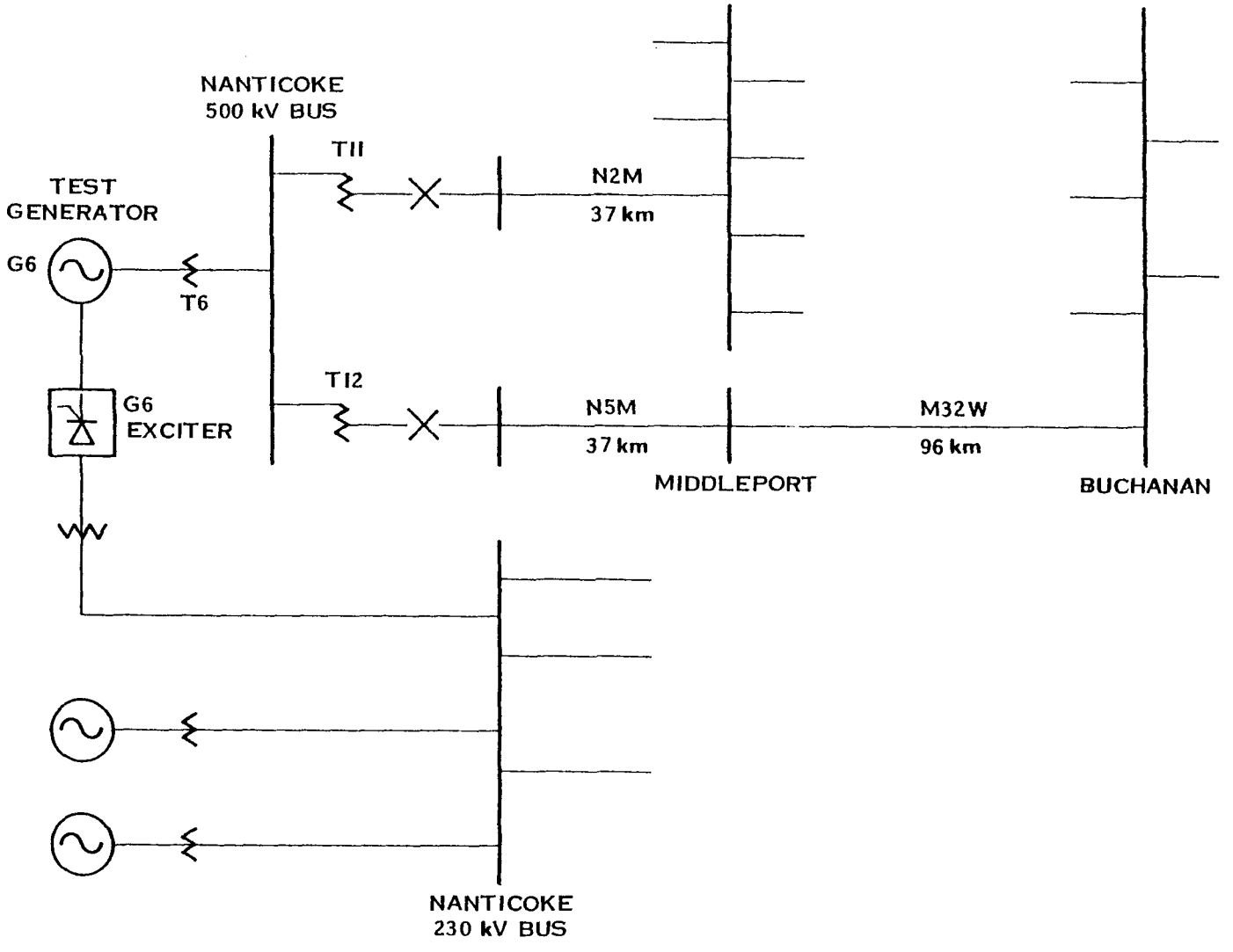

Figure 3-1. System Set-Up for Nanticoke Line Switching Tests.

Table 3-1

NANTICOKE LINE SWITCHING TESTS
SUMMARY OF OPERATIONS AND SYSTEM CONDITIONS

Test No	Time	Switching Operation	Voltage Regulator	Active Power (MW)	Reactive Power (MVAR)	Terminal Voltage (kV)	Change in External Impedance (pu on 22 kV, 588 MVA)
1-O	12:15	Open long line	Auto	299	106	22.1	0.20 to 0.48
1-C	12:18	Close long line	Auto	300	97	22.0	0.48 to 0.20
2-O	12:25	Open long line	Manual	300	108	22.0	0.20 to 0.48
2-C	12:27	Close long line	Manual	299	106	22.1	0.48 to 0.20
3-O	12:45	Open short line	Auto	301	112	22.1	0.20 to 0.87
3-C	12:55	Close short line	Auto	299	82	22.1	0.87 to 0.20
4-O	12:58	Open short line	Manual	302	112	22.1	0.20 to 0.87
4-C	13:00	Close short line	Manual	300	103	22.8	0.87 to 0.20

INSTRUMENTATION

Figure 3-2 is a block diagram of the instrumentation for the tests. Alternating current quantities were taken from existing current and potential transformers. Generator field current was measured with a shunt and a high voltage isolating amplifier. Shaft speed was measured at the outboard end of the generator shaft. Each measured variable was converted to a dc voltage proportional to its magnitude before being recorded.

RESULTS

Oscillograms of the measured transients were produced from the magnetic tape records of the tests (Figures 3-3 to 3-10).

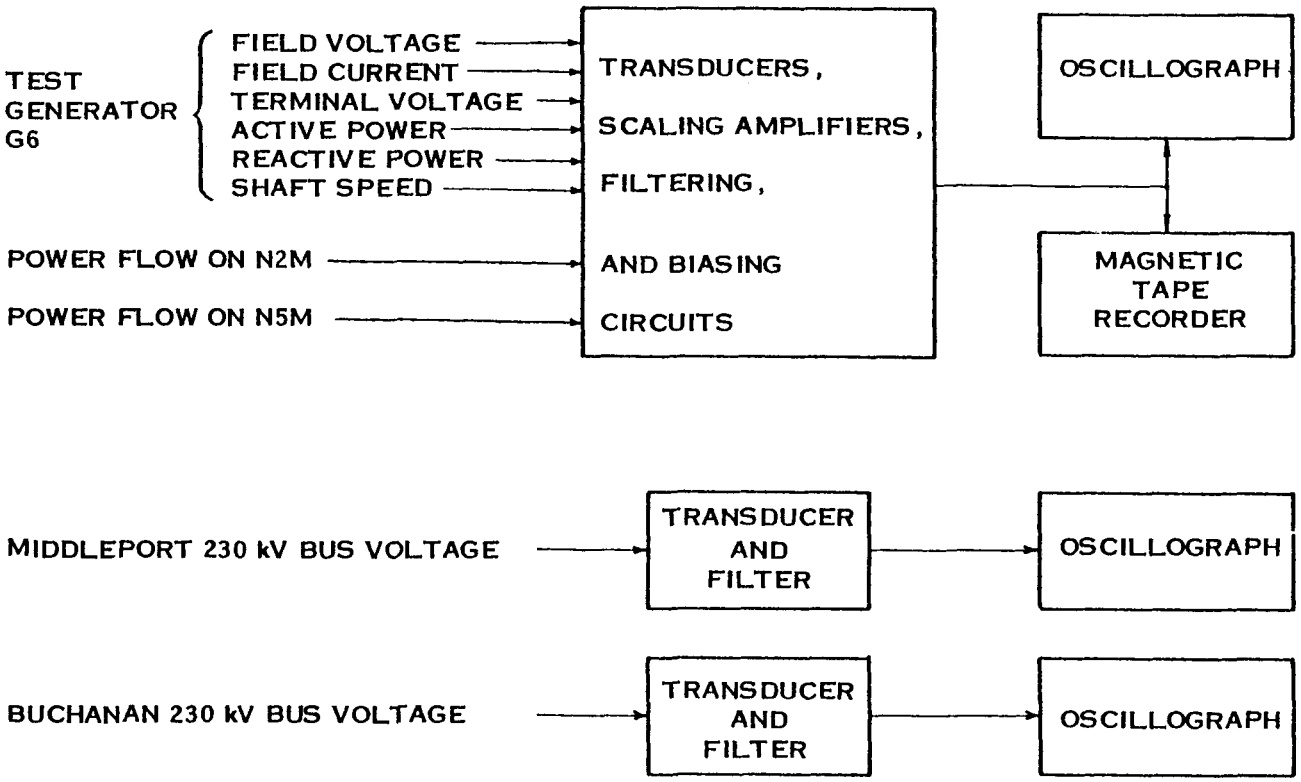

Figure 3-2. Instrumentation for Nanticoke Line Switching Tests.

Section 4

ON-LINE FREQUENCY RESPONSE

TEST ARRANGEMENT

The test generator (G6) was connected, radially, to the power system through its own 22 kV/500 kV step-up transformer, a 500 kV/230 kV autotransformer, and a single 230 kV transmission line running 45 km between Nanticoke and Middleport (Figure 4-1). The G6 exciter was supplied from the reserve station service, electrically isolated from the test generator. The load on G6 during the on-line frequency response tests was 400 MW, 120 MVAR lagging at 22.0 kV.

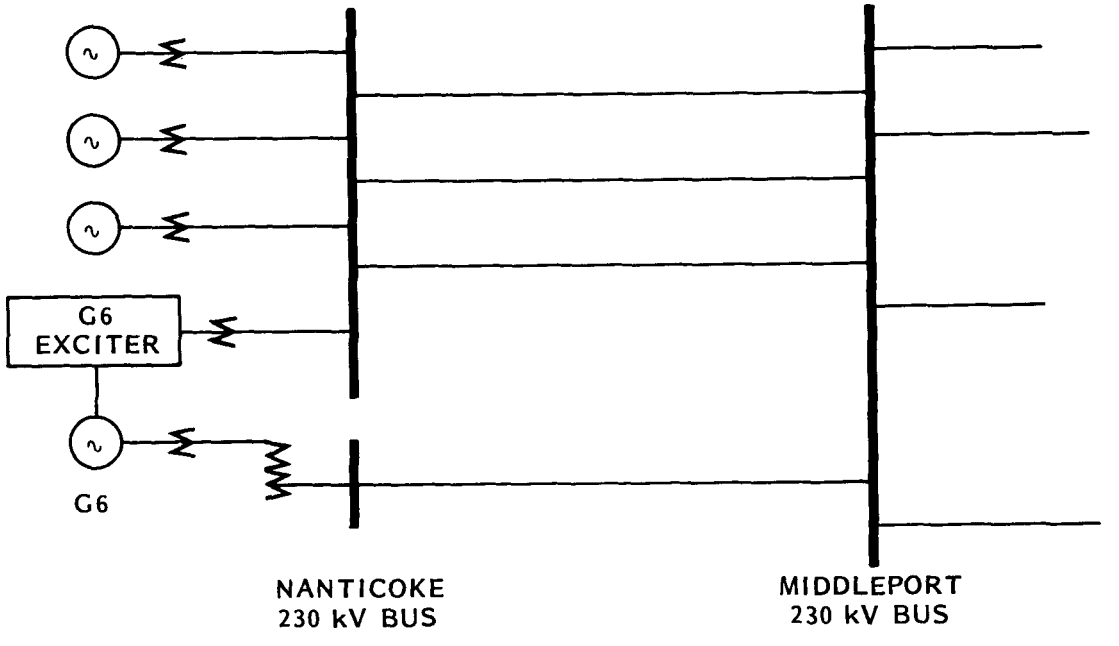

Figure 4-1. System Arrangement for Nanticoke On-Line Frequency Response.

Instrumentation for these tests was essentially the same as for the line switching tests described in Section 3, with the addition of the frequency response analyzer (Figure 4-2). A sinusoidal test signal from the frequency response analyzer was added to the voltage regulator reference to modulate the field voltage at the test frequency. The primary measuring device was the frequency response analyzer which cross-correlated each of the measured variables with the test signal to the voltage regulator. Transfer functions between field voltage and each of the other measured variables were computed from these cross-correlations. The oscillograph provided back-up records, although its principal function was that of a visual indicator to assist in controlling the test.

A frequency range from 0.01 Hz to 10 Hz was covered. The system natural frequency was between 1 Hz and 2 Hz; consequently, there is a gap in the data in this region.

RESULTS

As is evident from Table 4-1, terminal voltage swings were maintained at approximately 2% peak to peak for frequencies below 0.65 Hz. Above this, smaller deviations were tolerated in favour of maintaining linearity in the field voltage response.

The magnitude and phase of each of the measured transfer functions are listed in Table 4-2 and plotted in Figures 4-3 to 4-7.

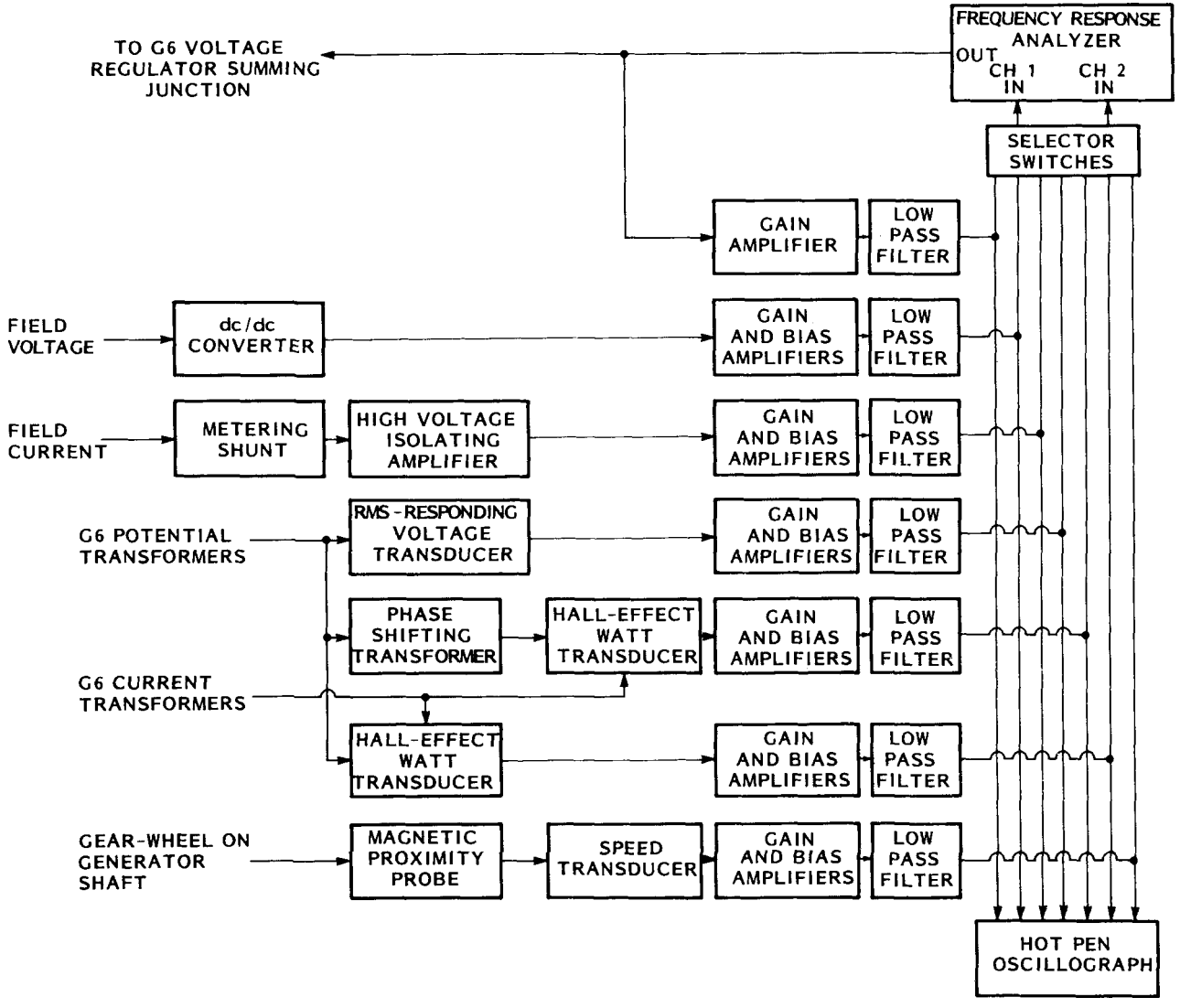

Figure 4-2. Instrumentation for On-Line Frequency Response.

Table 4-1

NANTICOKE ON-LINE FREQUENCY RESPONSE
PEAK DEVIATIONS OF MEASURED VARIABLES

Freq. (Hz)	Field Voltage (V)	Field Current (A)	Terminal Voltage (V rms)	Active Power (MW)	Reactive Power (MVAR)	Shaft Speed (rad/s)
0.010	6.62	58.5	233			
0.013	7.10	62.7	241			
0.016	6.94	61.2	241			
0.020	7.52	63.4	252		16.0	
0.025	8.15	62.0	252		15.6	
0.030	9.04	67.9	264		16.0	
0.040	10.1	65.6	246		15.1	
0.050	11.5	72.0	264		15.8	
0.058	13.7	75.4	258		16.7	
0.065	15.2	88.5	276		16.9	
0.080	18.0	92.7	283		16.9	
0.10	21.7	106	286		17.5	
0.13	24.9	109	267		16.0	
0.16	27.6	114	249		14.9	
0.20	29.6	109	225	0.342	13.1	
0.25	33.2	121	203	0.288	12.2	
0.30	31.0	108	161	0.659	9.61	
0.40	38.1	127	154	1.07	9.18	
0.50	62.5	196	212	1.95	12.1	0.0729
0.65	49.8	147	132	2.34	7.38	0.0613
0.80	47.5	137	106	3.15	5.60	0.0688
1.00	38.6	110	74.4	4.40	3.33	0.0781
1.30	16.5	50.9	26.4	4.40	1.33	0.0553
2.00	40.0	92.7	22.2	3.84	2.39	0.0322
2.50	55.9	119	26.4	3.05	2.39	0.0198
3.00	92.7	185	35.6	3.38	3.08	0.0181
4.00	179	318	48.6	4.02	3.92	0.0151
5.00	156	252	30.0	2.26	2.44	0.0048
6.50	150	217	19.8	1.39	1.58	0.0025
8.00	128	167	11.5	0.839	0.929	0.0010
10.0	99.3	115	6.2	0.375	0.487	0.0003

Table 4-2

NORMALIZED TRANSFER FUNCTIONS FROM FIELD VOLTAGE

Freq. (Hz)	Field Current Mag (db)	Field Current Phase (Deg)	Terminal Voltage Mag (db)	Terminal Voltage Phase (deg)	Active Power Mag (db)	Active Power Phase (deg)	Reactive Power Mag (db)	Reactive Power Phase (deg)	Shaft Speed Mag (db)	Shaft Speed Phase (deg)
.010	1.28	-6.9	-13.94	-14.1						
.013	1.28	-12.3	-14.24	-22.0						
.016	1.28	-10.4	-14.04	-25.9						
.020	.88	-16.1	-14.34	-28.5			-6.85	-29.7		
.025	-.02	-19.5	-15.04	-36.8			-7.75	-35.2		
.030	-.12	-23.4	-15.54	-40.2			-8.45	-40.5		
.040	-1.42	-25.7	-17.14	-50.0			-9.95	-49.8		
.050	-1.72	-27.2	-17.64	-54.9			-10.65	-54.9		
.058	-2.82	-29.2	-19.34	-60.1			-11.65	-62.9		
.065	-2.32	-24.7	-19.64	-59.0			-12.45	-57.8		
.080	-3.42	-27.0	-20.94	-63.1			-13.95	-63.5		
.100	-3.82	-27.1	-22.44	-65.1			-15.25	-65.3		
.130	-4.82	-24.8	-24.24	-70.0			-17.25	-70.9		
.160	-5.32	-25.2	-25.74	-72.5			-18.75	-73.8		
.200	-6.32	-22.6	-27.24	-76.0	-52.13	89.2	-20.45	-75.1		
.250	-6.42	-21.6	-29.14	-77.2	-54.63	126.9	-22.05	-78.3		
.300	-6.82	-20.1	-30.54	-78.9	-46.83	99.2	-23.55	-80.0		
.400	-7.22	-21.0	-32.74	-84.7	-44.43	97.4	-25.75	-84.2		
.500	-7.72	-19.9	-34.24	-87.6	-43.53	88.3	-27.65	-87.0	-68.19	-191.1
.650	-8.24	-19.7	-36.36	-91.7	-39.95	81.0	-29.97	-88.8	-67.71	-193.5
.800	-8.44	-19.3	-37.86	-95.1	-36.95	74.2	-31.97	-92.2	-66.31	162.9
1.000	-8.54	-18.1	-39.16	-100.1	-32.25	66.5	-34.67	-95.0	-63.41	153.8
1.300	-7.84	-20.0	-40.76	-132.5	-24.85	20.0	-35.27	-73.7	-59.01	98.9
2.000	-10.34	-32.3	-49.96	-107.6	-33.75	-109.1	-37.87	-112.2	-71.41	-26.6
2.500	-11.04	-32.2	-51.36	-114.6	-38.65	-117.9	-40.77	-118.7	-78.51	-32.3
3.000	-11.64	-33.4	-53.16	-119.1	-42.15	-123.5	-42.97	-123.5	-83.71	-40.5
4.000	-12.64	-35.4	-56.16	-126.4	-46.35	-131.6	-46.57	-131.6	-91.01	-54.3
5.000	-13.44	-37.0	-59.16	-131.3	-50.15	-141.5	-49.47	-138.2	-99.71	-56.2
6.500	-14.44	-38.5	-62.46	-137.8	-54.05	-147.2	-52.97	-145.8	-105.11	-43.1
8.000	-15.34	-39.3	-65.76	-141.8	-57.05	-153.2	-56.17	-149.6	-111.51	-28.6
10.000	-16.34	-39.4	-68.96	-144.6	-61.85	-157.2	-59.57	-156.5	-120.21	55.7

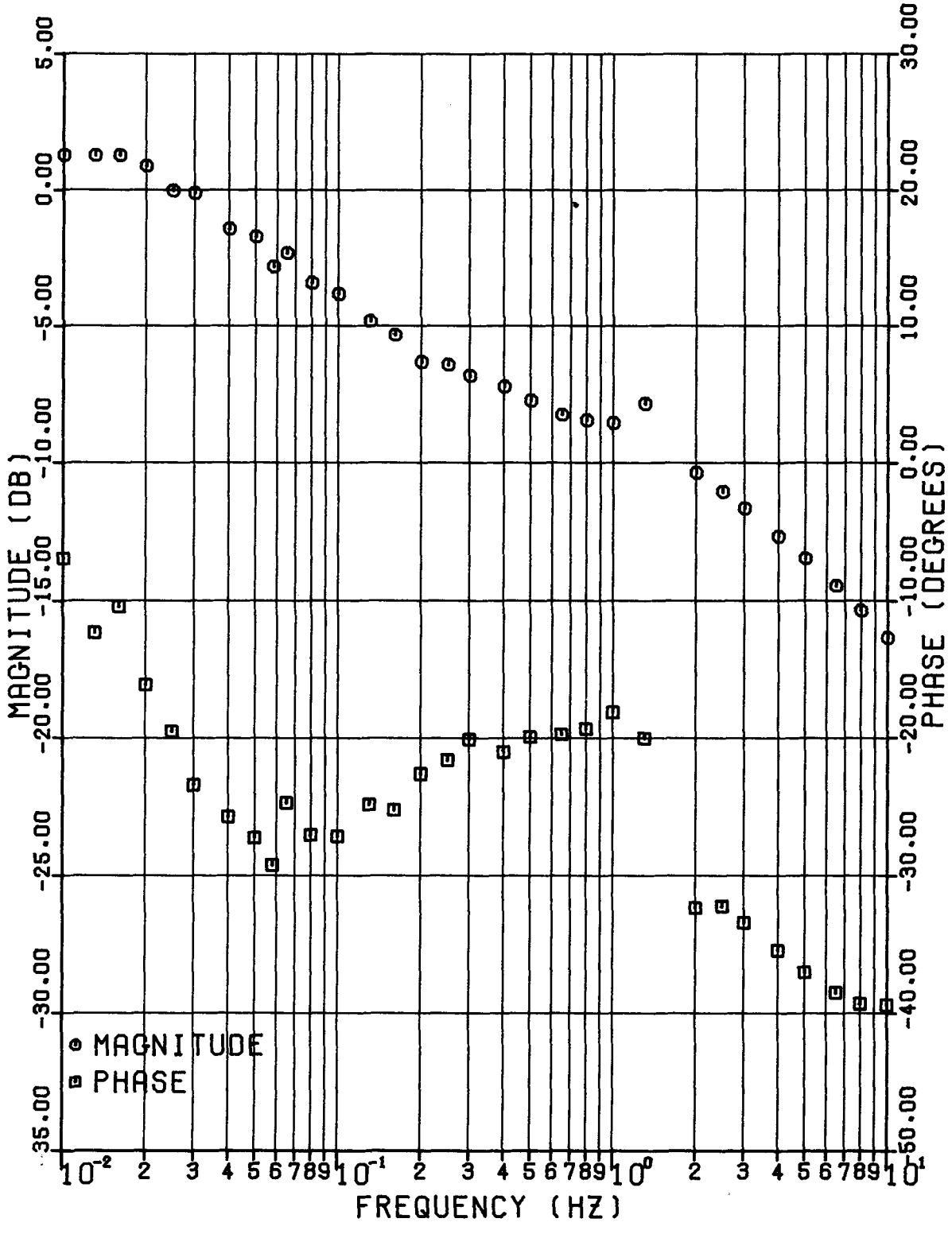

Figure 4-3. Nanticoke On-Line Transfer Function From Field Voltage to Field Current.

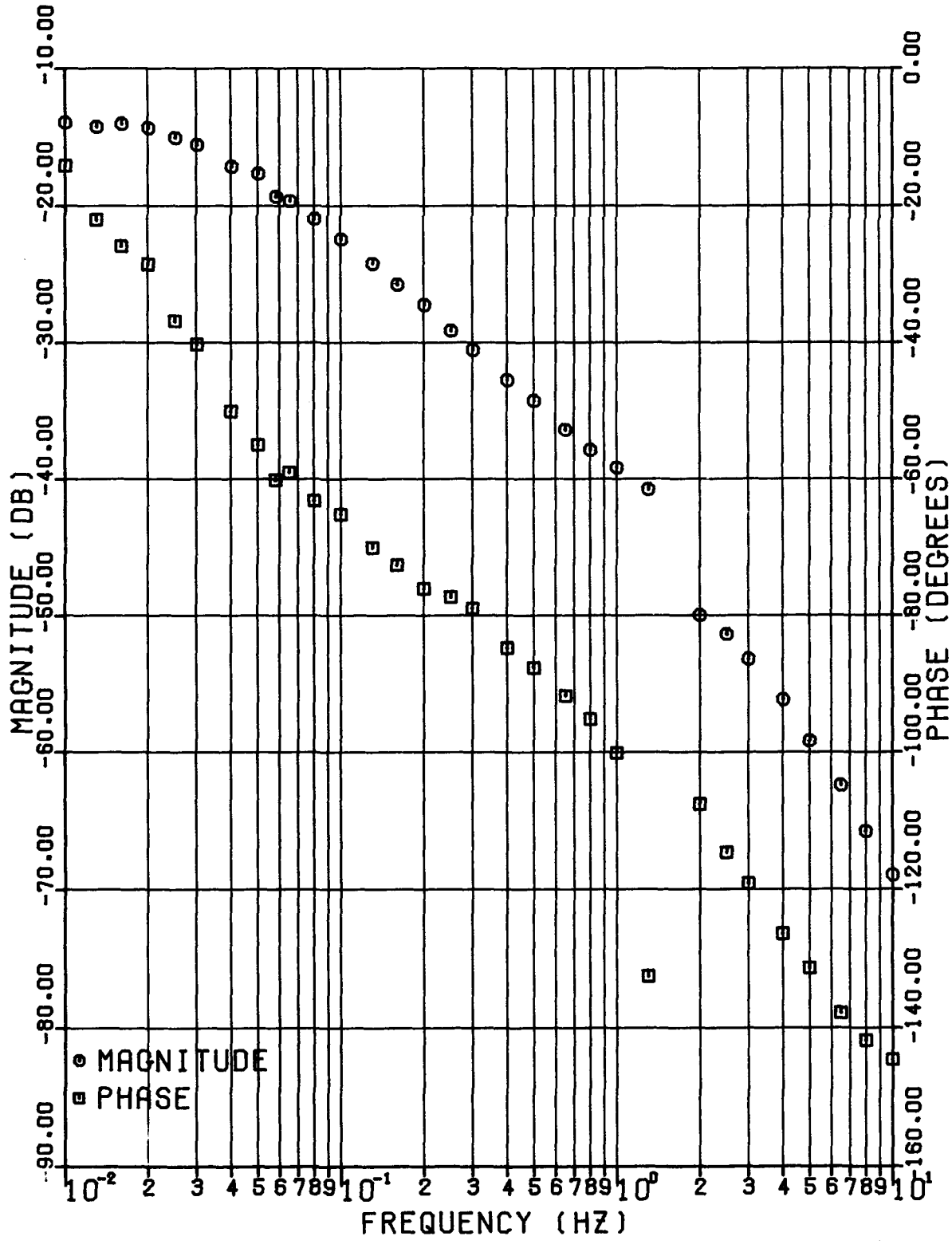

Figure 4-4. Nanticoke On-Line Transfer Function From Field Voltage to Terminal Voltage.

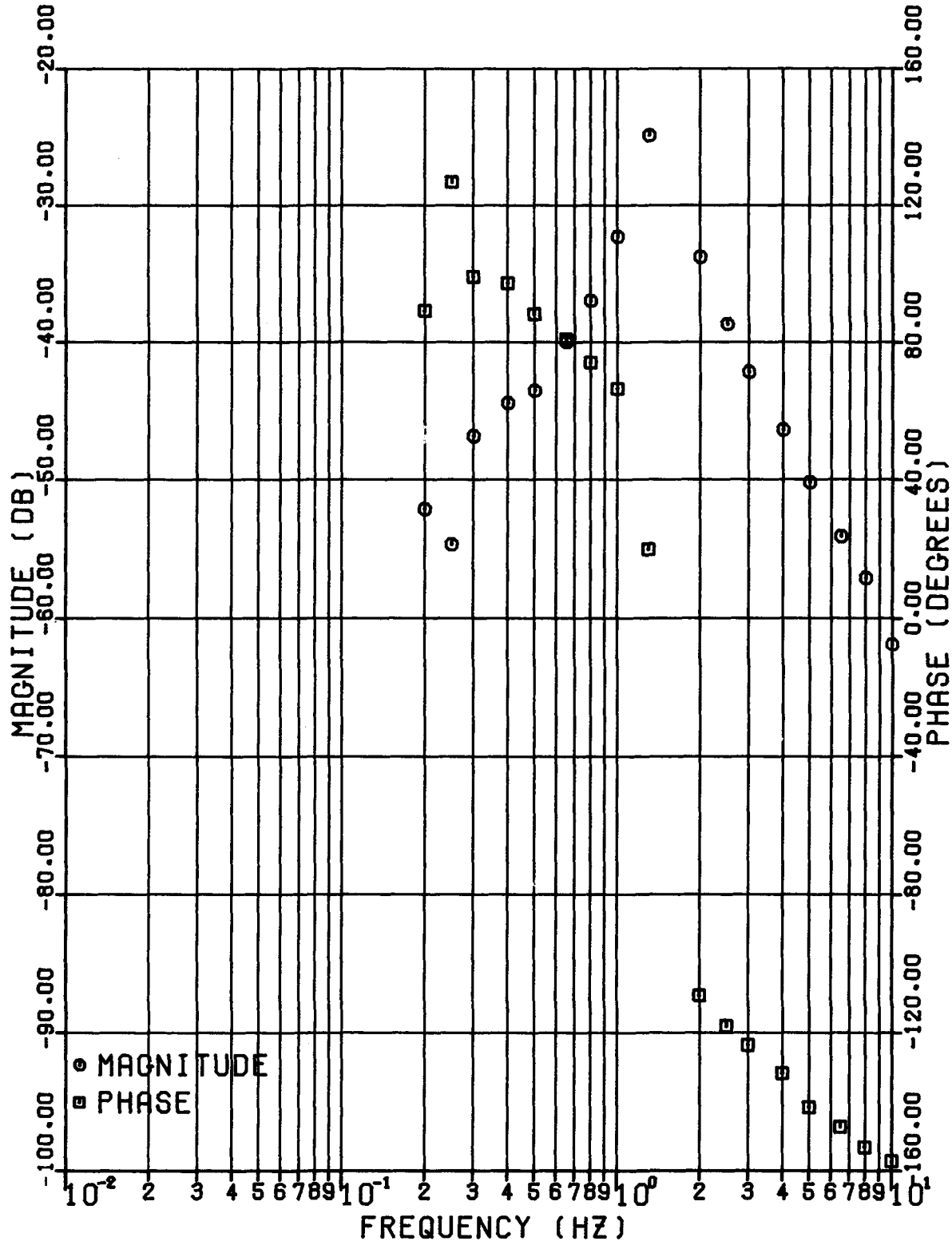

Figure 4-5. Nanticoke On-Line Transfer Function From Field Voltage to Active Power.

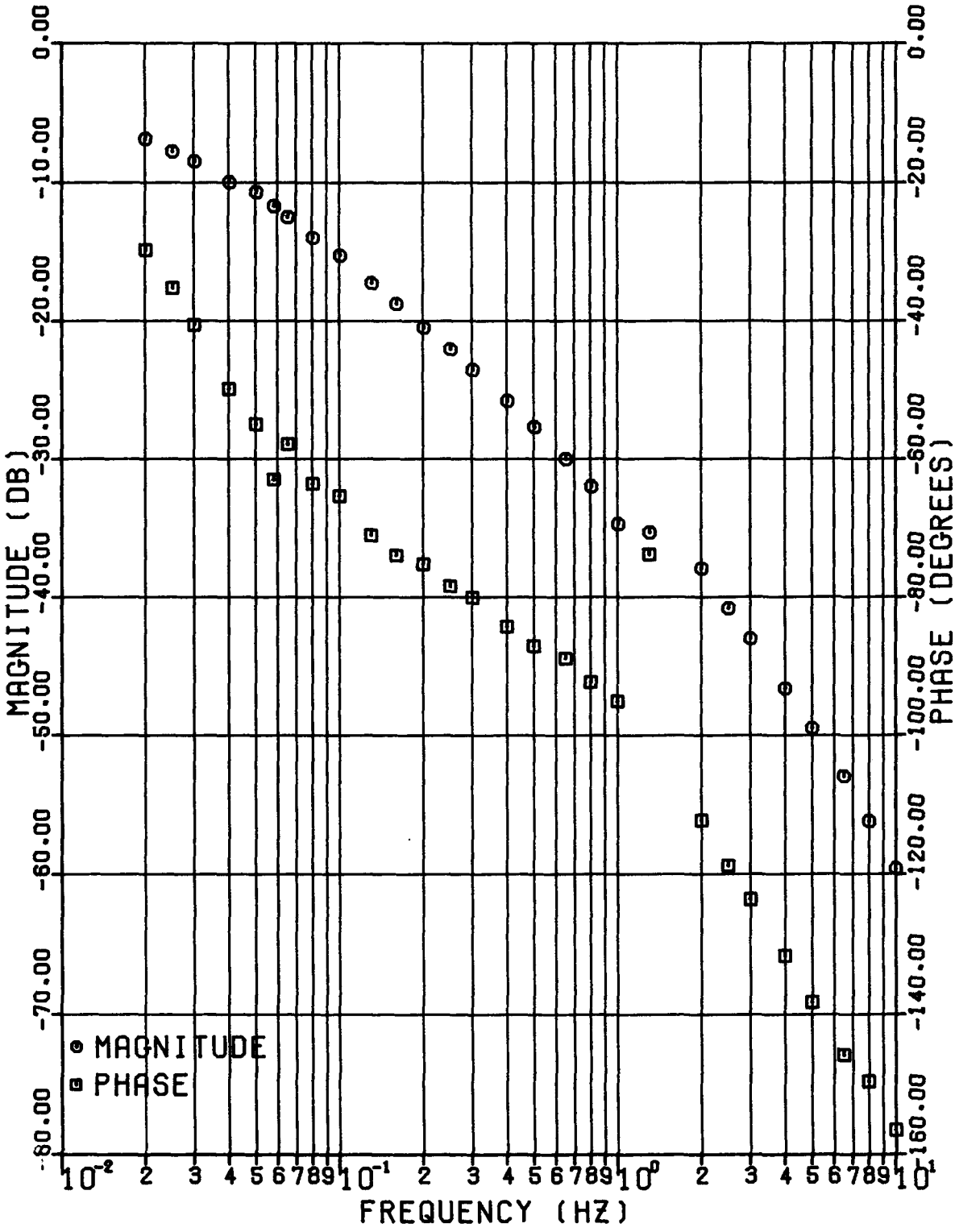

Figure 4-6. Nanticoke On-Line Transfer Function From Field Voltage to Reactive Power.

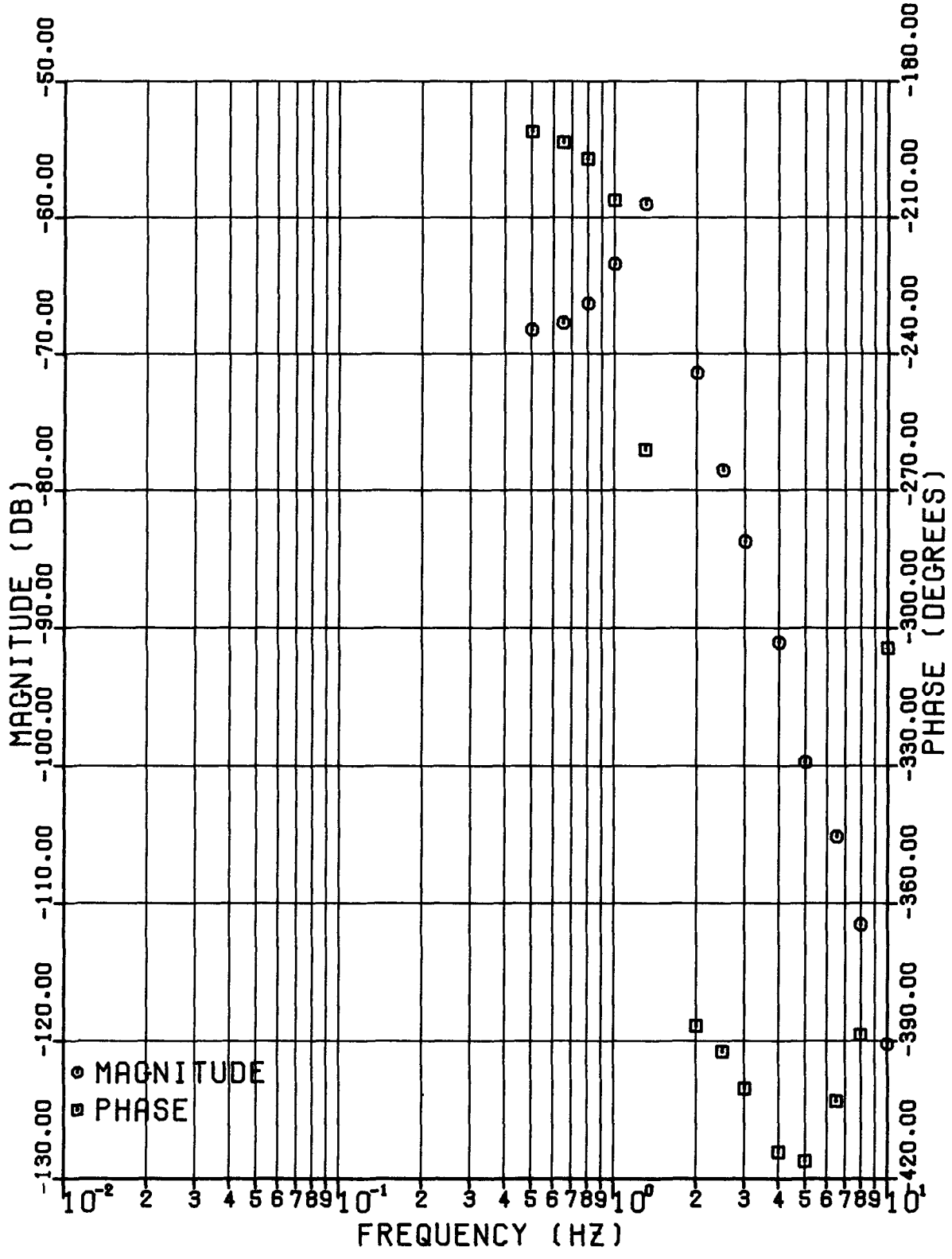

Figure 4-7. Nanticoke On-Line Transfer Function From Field Voltage to Shaft Speed.

Section 5

OPEN-CIRCUIT TESTS

OPEN-CIRCUIT SATURATION

The conventional open-circuit saturation characteristic was measured with the generator operating at rated speed, off line. Particular attention was paid to the linear part of the curve to ensure an accurate determination of the air-gap line.

Generator field current was obtained directly from a shunt and a dc millivoltmeter. The stator terminal voltage was measured with a Solartron 1172 frequency response analyzer. The internal oscillator of the frequency response analyzer was synchronized to the generator's terminal voltage waveform, thus enabling the instrument to measure both the frequency and the magnitude of the fundamental component of this voltage.

Since the magnitude of the terminal voltage is a function of both field current and rotor speed, all readings were corrected to 60 Hz. Figure 5-1 is the open-circuit saturation curve for Nanticoke obtained by this method. The slope of the linear part of the curve (air-gap line) fixes the field current required for 1.0 p.u. terminal voltage on the air-gap line at 980 A.

OPEN-CIRCUIT FREQUENCY RESPONSE

Test Procedure

The transfer functions between field voltage and field current, and field voltage and terminal voltage were measured with the generator operating at rated speed, off line. A frequency range of 0.003 Hz to 10 Hz was covered. The machine was perturbed by adding a sinusoidal voltage, at the test frequency, to the voltage regulator reference. Terminal voltage excursions were held as close to 1% peak to peak as possible. However, above 3 Hz, it was not possible to do this within the exciter's maximum voltage capability. Between 3 and 10 Hz, the test signal magnitude was adjusted to produce the maximum field voltage excursions possible without hitting the exciter ceiling.

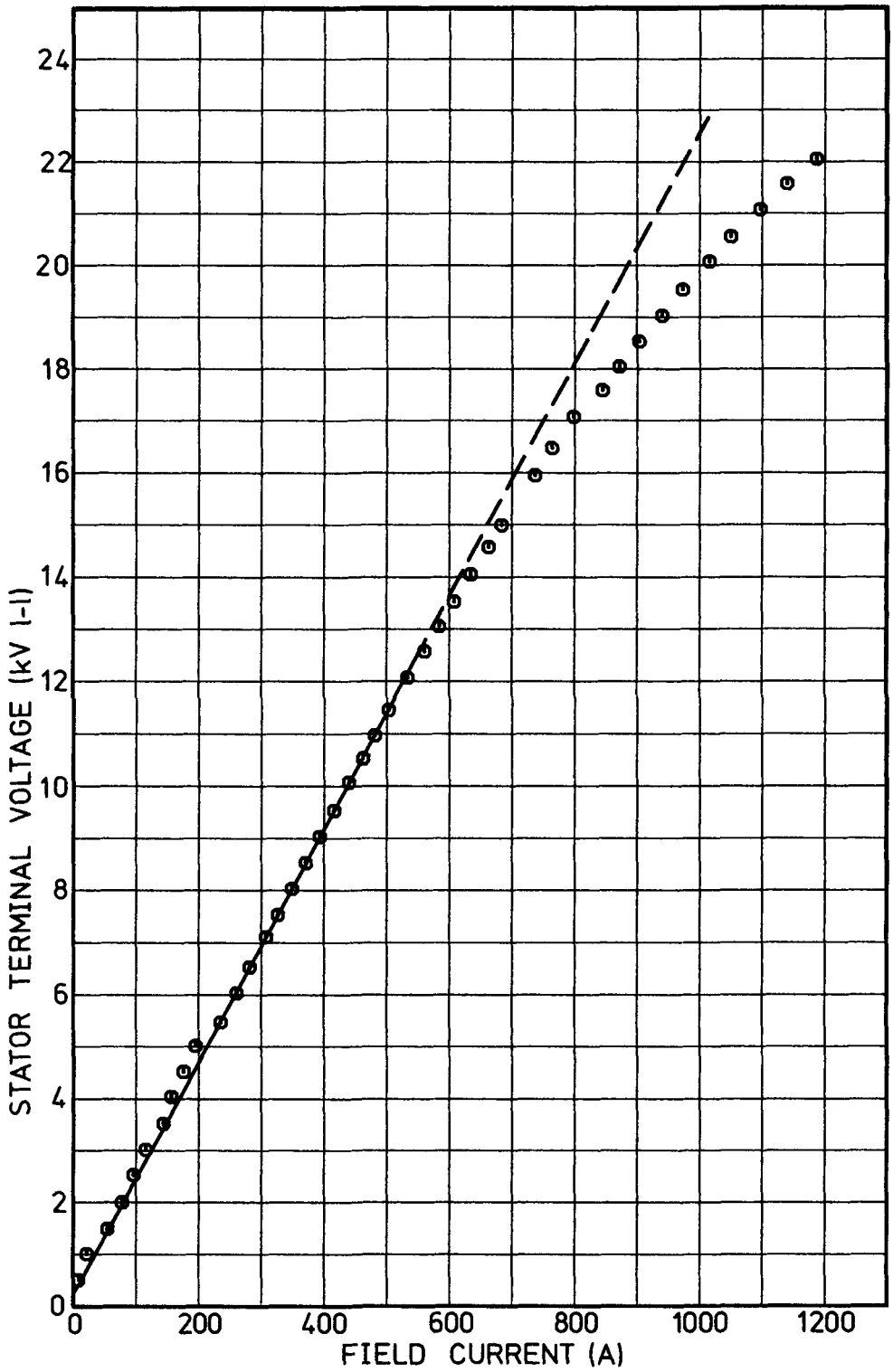

Figure 5-1. Nanticoke Open-Circuit Saturation Curve.

For all tests, the exciter, which is a transformer-fed thyristor type, was supplied from the reserve station service bus rather than by its normal connection to the generator terminals. This scheme eliminated any fluctuation in the exciter supply voltage due to terminal voltage swings. The automatic voltage regulator was in service at all times.

Three runs were done, one at 22.0 kV (rated voltage), one at 10.0 kV (on the linear part of the open-circuit saturation curve), and one at 18.0 kV, between the other two operating points.

Instrumentation

The block diagram in Figure 5-2 shows the instruments and transducers used for the open-circuit frequency response test. A frequency response analyzer generated the test signal and computed the magnitude and phase of the two transfer functions $\frac{\Delta I_{fd}}{\Delta V_{fd}}$ and $\frac{\Delta V_t}{\Delta V_{fd}}$ by cross-correlating the measured variables with the test signal.

Results

Figures 5-3 to 5-8 and Tables 5-1 to 5-3 are the Bode plots of the measured transfer functions and tabulations of the test data. All data has been normalized to the following bases:

field voltage: 108.6 V dc

field current: 980 A

terminal voltage: 22.0 kV rms phase to phase

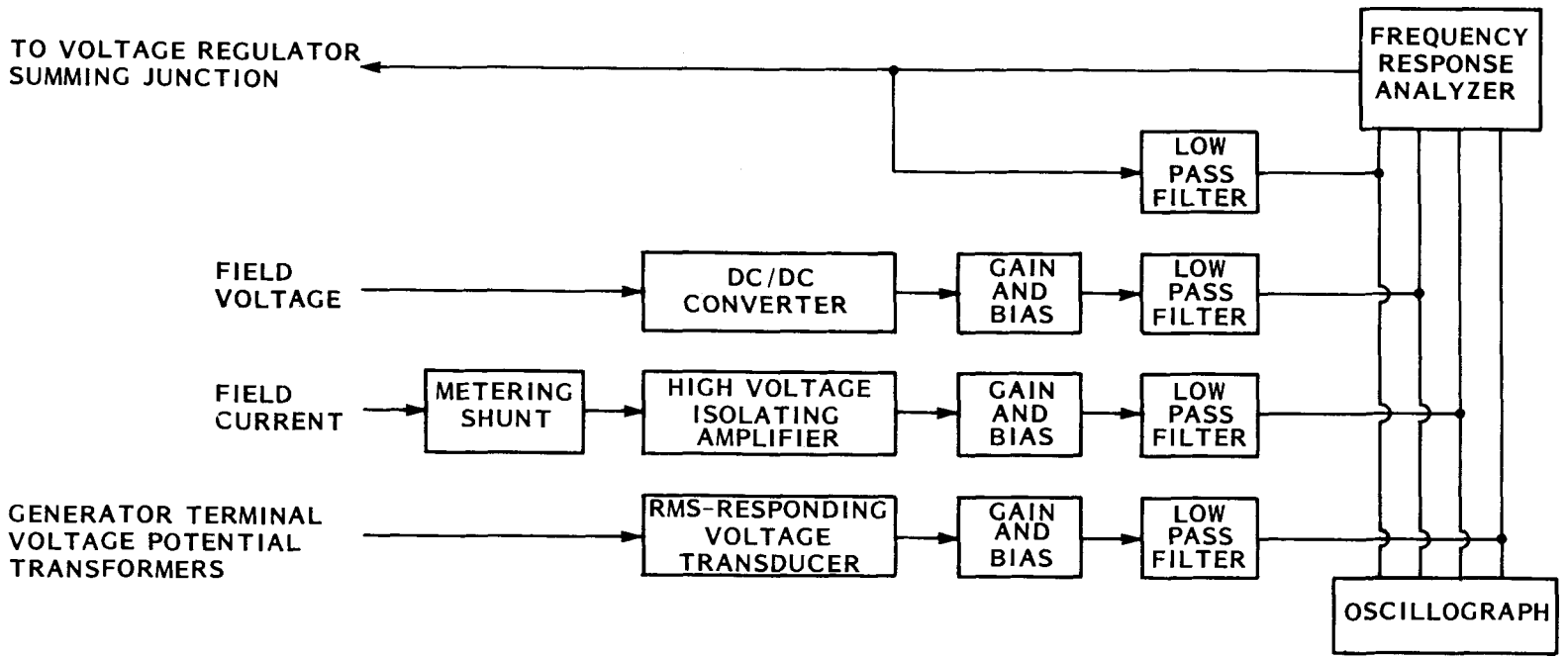

Figure 5-2. Instrumentation for Nanticoke Open-Circuit Frequency Response Test.

Table 5-1

OPEN-CIRCUIT FREQUENCY RESPONSE AT 10.0 KV

FREQUENCY	FIELD VOLTAGE		FIELD CURRENT		TERMINAL VOLTAGE		ET/EFD		ET/IFD		IFD/EFD	
(HZ)	(DB ABOVE 1 PU)	PHASE (DEG)	(DB ABOVE 1 PU)	PHASE (DEG)	(DB ABOVE 1 PU)	PHASE (DEG)	(DB ABOVE 1 PU)	PHASE (DEG)	(DB ABOVE 1 PU)	PHASE (DEG)	(DB ABOVE 1 PU)	PHASE (DEG)
.003	-46.60	9.3	-127.53	360.0	-47.81	-.3	-1.21	-9.6	79.72	-360.3	-80.93	350.7
.005	-46.60	17.9	-45.63	20.0	-47.91	-.3	-1.31	-18.2	-2.28	-20.3	.97	2.1
.008	-45.90	23.0	-44.23	3.1	-48.11	-.1	-2.21	-23.1	-3.88	-3.2	1.67	-19.9
.010	-45.50	30.2	-44.53	13.0	-48.11	-.2	-2.61	-30.4	-3.58	-13.2	.97	-17.2
.013	-44.70	36.2	-42.53	24.5	-48.01	.3	-3.31	-35.9	-5.48	-24.2	2.17	-11.7
.016	-44.00	42.5	-44.33	35.1	-48.01	.0	-4.01	-42.5	-3.68	-35.1	-.33	-7.4
.020	-43.10	49.1	-46.83	21.6	-48.11	-.4	-5.01	-49.5	-1.28	-22.0	-3.73	-27.5
.025	-41.90	54.9	-44.33	23.7	-48.91	-.5	-7.01	-55.4	-4.53	-24.2	-2.43	-31.2
.030	-40.70	57.6	-44.83	31.0	-48.11	-.5	-7.41	-58.1	-3.28	-31.5	-4.13	-26.6
.040	-38.80	64.4	-43.63	36.5	-48.01	-.9	-9.21	-65.3	-4.38	-37.4	-4.83	-27.9
.050	-37.20	68.8	-42.33	37.6	-48.01	-1.0	-10.81	-69.8	-5.68	-38.6	-5.13	-31.2
.065	-35.30	73.0	-41.53	46.3	-48.11	-1.0	-12.81	-74.0	-6.58	-47.3	-6.23	-26.7
.080	-33.70	75.5	-40.93	48.9	-48.11	-1.3	-14.41	-76.8	-7.18	-50.2	-7.23	-26.6
.100	-31.90	77.7	-39.43	54.6	-48.01	-1.8	-16.11	-79.5	-8.58	-56.4	-7.53	-23.1
.130	-29.80	80.8	-38.03	56.0	-48.01	-2.3	-18.21	-83.1	-9.98	-58.3	-8.23	-24.8
.160	-28.10	82.0	-36.83	60.0	-48.01	-2.8	-19.91	-84.8	-11.18	-62.8	-8.73	-22.0
.200	-26.20	84.3	-35.33	64.0	-48.01	-3.6	-21.81	-87.9	-12.68	-67.6	-9.13	-20.3
.250	-24.40	86.0	-34.13	66.3	-48.11	-4.2	-23.71	-90.2	-13.98	-70.5	-9.73	-19.7
.300	-22.70	86.9	-32.73	67.8	-48.01	-5.0	-25.31	-91.9	-15.28	-72.8	-10.03	-19.1
.400	-20.30	89.1	-30.53	68.8	-47.91	-7.2	-27.61	-96.3	-17.38	-76.0	-10.23	-20.3
.500	-18.10	91.1	-28.73	70.0	-47.81	-8.7	-29.71	-99.8	-19.08	-78.7	-10.63	-21.1
.650	-15.60	92.5	-26.73	69.8	-47.71	-11.1	-32.11	-103.6	-20.98	-80.9	-11.13	-22.7
.800	-13.40	93.2	-25.03	70.0	-47.71	-13.8	-34.31	-107.0	-22.68	-83.8	-11.63	-23.2
1.000	-11.20	93.8	-23.23	67.9	-47.61	-17.5	-36.41	-111.3	-24.38	-85.4	-12.03	-25.9
1.000	-11.80	93.8	-23.72	68.2	-48.21	-17.6	-36.41	-111.4	-24.49	-85.8	-11.92	-25.6
1.300	-8.60	93.5	-21.22	63.9	-47.81	-24.6	-39.21	-118.1	-26.59	-88.5	-12.62	-29.6
1.600	-6.30	91.8	-19.72	59.3	-47.71	-30.0	-41.41	-121.8	-27.99	-89.3	-13.42	-32.5
2.000	-5.00	87.2	-19.22	51.5	-49.01	-39.9	-44.01	-127.1	-29.79	-91.4	-14.22	-35.7
2.500	-.70	77.0	-16.02	38.0	-47.61	-55.7	-46.91	-132.7	-31.59	-93.7	-15.32	-39.0
3.000	1.80	56.7	-14.42	14.8	-47.51	-80.0	-49.31	-136.7	-33.09	-94.8	-16.22	-41.9
4.000	5.70	-19.0	-12.12	-63.9	-47.71	-164.0	-53.41	-145.0	-35.59	-100.1	-17.82	-44.9
5.000	8.40	-56.6	-10.62	-103.7	-48.31	-206.9	-56.71	-150.3	-37.69	-103.2	-19.02	-47.1
6.500	11.70	-76.8	-8.62	-125.6	-48.81	-233.4	-60.51	-156.6	-40.19	-107.8	-20.32	-48.8
8.000	11.50	-102.1	-10.02	-152.2	-52.11	-263.6	-63.61	-161.5	-42.09	-111.4	-21.52	-50.1
10.000	12.30	-129.1	-10.42	-179.8	-54.81	-295.9	-67.11	-166.8	-44.39	-116.1	-22.72	-50.7

Table 5-2

OPEN-CIRCUIT FREQUENCY RESPONSE AT 18.0 KV

FREQUENCY	FIELD VOLTAGE		FIELD CURRENT		TERMINAL VOLTAGE		ET/EFD		ET/IFD		IFD/EFD	
(HZ)	(DB ABOVE 1 PU)	PHASE (DEG)	(DB ABOVE 1 PU)	PHASE (DEG)	(DB ABOVE 1 PU)	PHASE (DEG)	(DB ABOVE 1 PU)	PHASE (DEG)	(DB ABOVE 1 PU)	PHASE (DEG)	(DB ABOVE 1 PU)	PHASE (DEG)
.004	-41.30	5.3	-40.03	7.9	-44.21	-.1	-2.91	-5.4	-4.18	-8.0	1.27	2.6
.007	-40.70	14.5	-40.73	2.9	-44.21	.5	-3.51	-14.0	-3.48	-2.4	-.03	-11.6
.008	-40.60	17.3	-40.83	10.8	-44.31	-.1	-3.71	-17.4	-3.48	-10.9	-.23	-6.5
.010	-39.70	22.8	-40.23	9.6	-44.31	.0	-4.61	-22.8	-4.08	-9.6	-.53	-13.2
.013	-39.20	30.9	-39.93	8.7	-44.21	-.1	-5.01	-31.0	-4.28	-8.8	-.73	-22.2
.016	-38.80	36.2	-39.83	16.0	-44.31	-.3	-5.51	-36.5	-4.48	-16.3	-1.03	-20.2
.020	-38.10	40.8	-39.03	18.7	-44.31	-.2	-6.21	-41.0	-5.28	-18.9	-.93	-22.1
.025	-37.10	47.8	-39.03	20.7	-44.31	-.6	-7.21	-48.4	-5.28	-21.3	-1.93	-27.1
.030	-35.90	52.2	-38.73	29.5	-44.21	-.6	-8.31	-52.8	-5.48	-30.1	-2.83	-22.7
.040	-34.50	59.3	-38.13	32.4	-44.31	-.4	-9.81	-59.7	-6.18	-32.8	-3.63	-26.9
.050	-32.80	63.2	-37.53	31.6	-44.31	-.5	-11.51	-63.7	-6.78	-32.1	-4.73	-31.6
.065	-31.00	68.7	-37.13	39.0	-44.31	-.9	-13.31	-69.6	-7.18	-39.9	-6.13	-29.7
.080	-29.40	72.8	-35.93	42.2	-44.21	-1.4	-14.81	-74.2	-8.28	-43.6	-6.53	-30.6
.100	-27.80	74.4	-35.13	48.9	-44.21	-1.9	-16.41	-76.3	-9.08	-50.8	-7.33	-25.5
.130	-25.70	77.7	-33.33	49.9	-44.31	-2.2	-18.61	-79.9	-10.98	-52.1	-7.63	-27.8
.160	-24.10	80.5	-32.33	54.8	-44.21	-3.0	-20.11	-83.5	-11.88	-57.8	-8.23	-25.7
.200	-22.10	82.4	-30.73	60.3	-44.31	-3.4	-22.21	-85.8	-13.58	-63.7	-8.63	-22.1
.250	-20.30	84.1	-29.73	63.1	-44.21	-4.0	-23.91	-88.1	-14.48	-67.1	-9.43	-21.0
.300	-18.70	85.1	-28.43	64.6	-44.21	-5.4	-25.51	-90.5	-15.78	-70.0	-9.73	-20.5
.400	-16.30	86.8	-26.33	66.6	-44.11	-7.0	-27.81	-93.8	-17.78	-73.6	-10.03	-20.2
.500	-14.20	88.2	-24.63	67.6	-44.11	-8.5	-29.91	-96.7	-19.48	-76.1	-10.43	-20.6
.650	-11.80	89.5	-22.53	68.1	-44.01	-11.1	-32.21	-100.6	-21.48	-79.2	-10.73	-21.4
.800	-9.70	90.0	-20.83	67.4	-43.91	-14.2	-34.21	-104.2	-23.08	-81.6	-11.13	-22.6
1.000	-7.40	90.6	-18.93	66.0	-43.71	-17.8	-36.31	-108.4	-24.78	-83.8	-11.53	-24.6
1.000	-7.40	90.5	-19.03	65.9	-43.71	-17.7	-36.31	-108.2	-24.68	-83.6	-11.63	-24.6
1.000	-11.40	90.5	-22.73	66.0	-47.71	-17.8	-36.31	-108.3	-24.98	-83.8	-11.33	-24.5
1.300	-8.30	90.2	-20.33	62.8	-47.71	-21.3	-39.41	-111.5	-27.38	-84.1	-12.03	-27.4
1.600	-5.60	88.7	-18.13	58.9	-46.71	-29.9	-41.11	-118.6	-28.58	-88.8	-12.53	-29.8
2.000	-2.10	84.8	-15.43	52.0	-45.81	-39.2	-43.71	-124.0	-30.38	-91.2	-13.33	-32.8
2.500	2.30	75.7	-12.03	39.8	-44.21	-54.0	-46.51	-129.7	-32.18	-93.8	-14.33	-35.9
3.000	6.00	58.0	-9.13	19.9	-42.81	-76.8	-48.81	-134.8	-33.68	-96.7	-15.13	-38.1
4.000	10.10	-13.2	-6.43	-54.3	-42.81	-155.8	-52.91	-142.6	-36.38	-101.5	-16.53	-41.1
5.000	12.60	-55.2	-4.83	-97.7	-43.41	-203.5	-56.01	-148.3	-38.58	-105.8	-17.43	-42.5
6.500	14.80	-81.8	-3.93	-125.4	-45.11	-236.5	-59.91	-154.7	-41.18	-111.1	-18.73	-43.6
8.000	16.00	-101.2	-3.83	-145.2	-47.01	-260.6	-63.01	-159.4	-43.18	-115.4	-19.83	-44.0
10.000	15.90	-128.6	-5.13	-173.2	-50.51	-292.8	-66.41	-164.2	-45.38	-119.6	-21.03	-44.6

Table 5-3

OPEN-CIRCUIT FREQUENCY RESPONSE AT 22.0 KV

FREQUENCY	FIELD VOLTAGE		FIELD CURRENT		TERMINAL VOLTAGE		ET/EFD		ET/IFD		IFD/EFD	
(HZ)	(DB ABOVE 1 PU)	PHASE (DEG)	(DB ABOVE 1 PU)	PHASE (DEG)	(DB ABOVE 1 PU)	PHASE (DEG)	(DB ABOVE 1 PU)	PHASE (DEG)	(DB ABOVE 1 PU)	PHASE (DEG)	(DB ABOVE 1 PU)	PHASE (DEG)
.007	-35.10	11.8	-34.02	3.8	-42.51	-.1	-7.41	-11.9	-8.49	-3.9	1.08	-8.0
.010	-35.00	18.4	-34.72	8.4	-42.61	.2	-7.61	-18.2	-7.89	-8.2	.28	-10.0
.013	-34.70	22.7	-35.12	10.2	-42.61	-.2	-7.91	-22.9	-7.49	-10.4	-.42	-12.5
.016	-34.30	26.3	-34.32	7.8	-42.61	-.4	-8.31	-26.7	-8.29	-8.2	-.02	-18.5
.020	-33.90	31.8	-35.22	14.0	-42.61	-.3	-8.71	-32.1	-7.39	-14.3	-1.32	-17.8
.025	-33.10	37.6	-34.82	16.0	-42.61	-.4	-9.51	-38.0	-7.79	-16.4	-1.72	-21.6
.030	-32.60	42.4	-34.42	15.1	-42.61	-.6	-10.01	-43.0	-8.19	-15.7	-1.82	-27.3
.040	-31.20	50.5	-33.82	23.2	-42.61	-.7	-11.41	-51.2	-8.79	-23.9	-2.62	-27.3
.050	-29.80	55.8	-33.82	25.7	-42.61	-1.0	-12.81	-56.8	-8.79	-26.7	-4.02	-30.1
.065	-28.20	61.8	-32.72	30.6	-42.61	-1.0	-14.41	-62.8	-9.89	-31.6	-4.52	-31.2
.080	-26.80	66.1	-32.12	36.1	-42.61	-1.4	-15.81	-67.5	-10.49	-37.5	-5.32	-30.0
.100	-25.10	69.4	-31.12	41.5	-42.61	-1.8	-17.51	-71.2	-11.49	-43.3	-6.02	-27.9
.130	-23.10	73.6	-29.82	46.2	-42.61	-2.4	-19.51	-76.0	-12.79	-48.6	-6.72	-27.4
.160	-21.50	76.4	-28.92	51.4	-42.51	-3.7	-21.01	-80.1	-13.59	-55.1	-7.42	-25.0
.200	-19.80	78.5	-27.72	52.2	-42.61	-3.7	-22.81	-82.2	-14.89	-55.9	-7.92	-26.3
.250	-17.90	80.5	-26.32	57.0	-42.61	-4.5	-24.71	-85.0	-16.29	-61.5	-8.42	-23.5
.300	-16.40	82.0	-25.12	58.7	-42.51	-5.6	-26.11	-87.6	-17.39	-64.3	-8.72	-23.3
.400	-13.90	83.8	-23.22	61.1	-42.61	-6.6	-28.71	-90.4	-19.39	-67.7	-9.32	-22.7
.400	-15.00	84.0	-24.22	61.9	-43.61	-7.1	-28.61	-91.1	-19.39	-69.0	-9.22	-22.1
.500	-13.00	85.6	-22.62	62.8	-43.41	-9.2	-30.41	-94.8	-20.79	-72.0	-9.62	-22.8
.500	-13.10	85.7	-22.62	63.2	-43.51	-9.1	-30.41	-94.8	-20.89	-72.3	-9.52	-22.5
.650	-10.60	87.0	-20.72	63.7	-43.41	-11.9	-32.81	-98.9	-22.69	-75.6	-10.12	-23.3
.650	-10.50	86.9	-20.62	63.4	-43.71	-11.3	-33.21	-98.2	-23.09	-74.7	-10.12	-23.5
.800	-8.50	87.5	-19.12	63.4	-43.31	-14.3	-34.81	-101.8	-24.19	-77.7	-10.62	-24.1
1.000	-6.30	87.4	-17.32	62.1	-43.21	-18.6	-36.91	-106.0	-25.89	-80.7	-11.02	-25.3
1.000	-6.30	87.5	-17.32	61.8	-43.21	-18.1	-36.91	-105.6	-25.89	-79.9	-11.02	-25.7
1.300	-3.30	87.4	-14.92	59.1	-42.71	-24.5	-39.41	-111.9	-27.79	-83.6	-11.62	-28.3
1.600	-.60	85.4	-12.72	54.6	-42.11	-30.9	-41.51	-116.3	-29.39	-85.5	-12.12	-30.8
2.000	2.80	81.2	-10.02	47.6	-41.21	-40.7	-44.01	-121.9	-31.19	-88.3	-12.82	-33.6
2.500	3.60	71.4	-10.02	34.9	-43.11	-56.1	-46.71	-127.5	-33.09	-91.0	-13.62	-36.5
3.000	.50	54.6	-13.72	15.8	-48.41	-77.5	-48.91	-132.1	-34.69	-93.3	-14.22	-38.8
4.000	1.90	-6.7	-13.62	-48.9	-50.91	-146.0	-52.81	-139.3	-37.29	-97.1	-15.52	-42.2
5.000	3.00	-50.9	-13.72	-95.3	-52.91	-195.6	-55.91	-144.7	-39.19	-100.3	-16.72	-44.4
6.500	4.20	-81.3	-13.72	-127.4	-55.51	-232.1	-59.71	-150.8	-41.79	-104.7	-17.92	-46.1
8.000	5.30	-102.7	-13.62	-149.8	-57.51	-257.9	-62.81	-155.2	-43.89	-108.1	-18.92	-47.1
10.000	6.30	-129.4	-13.72	-177.3	-60.11	-289.7	-66.41	-160.3	-46.39	-112.4	-20.02	-47.9

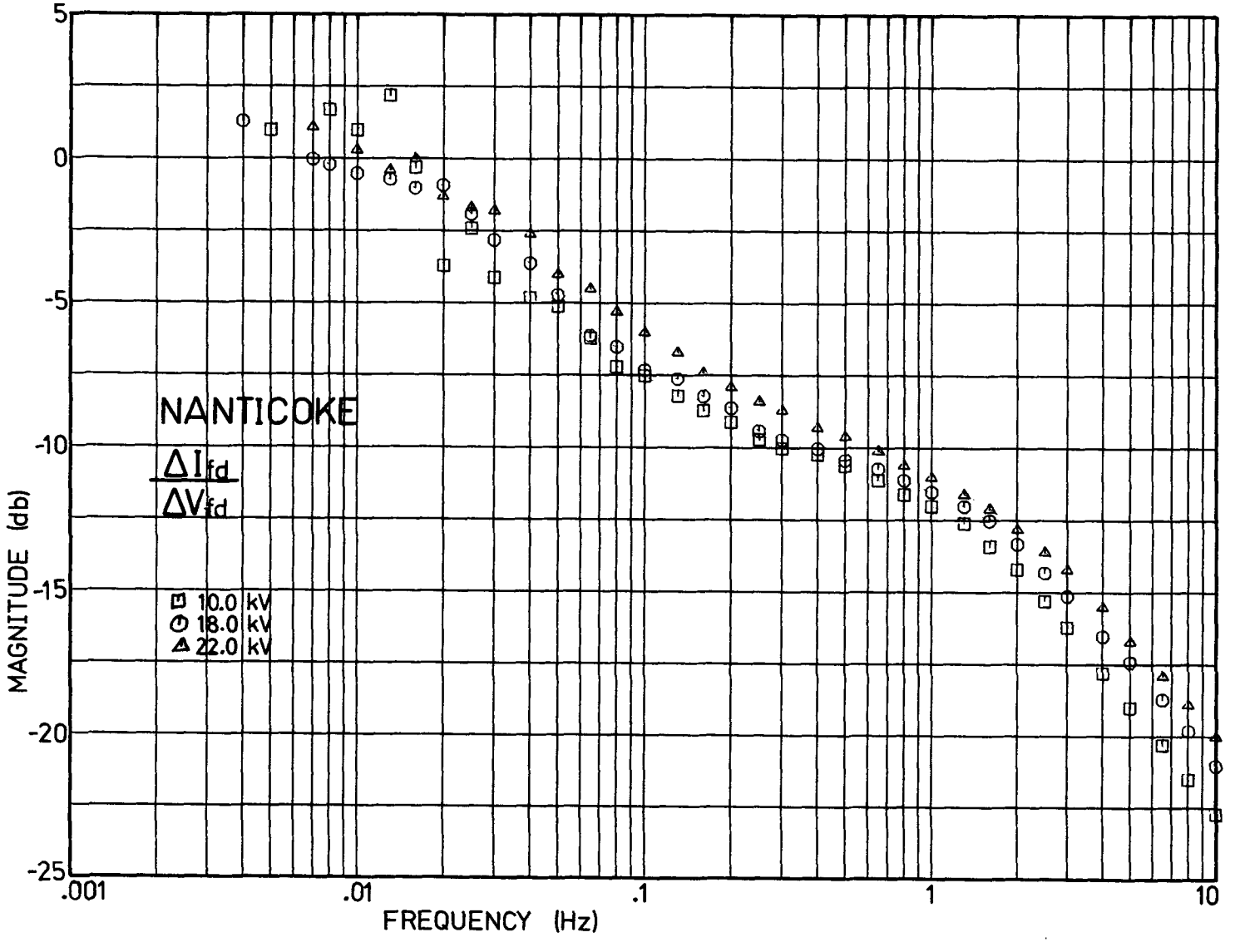

Figure 5-3. Magnitude of Nanticoke Open-Circuit Transfer Function From Field Voltage to Field Current.

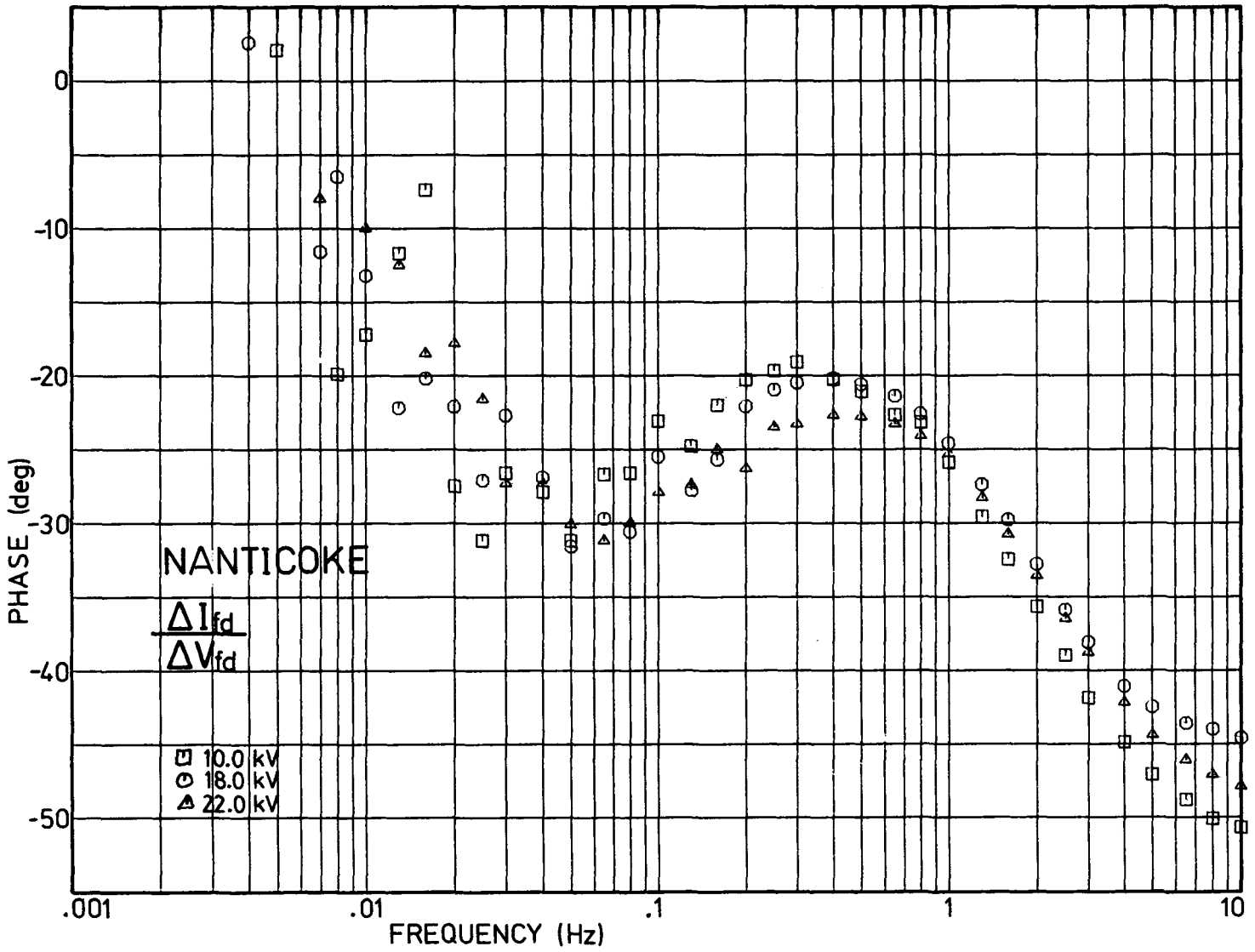

Figure 5-4. Phase of Nanticoke Open-Circuit Transfer Function From Field Voltage To Field Current.

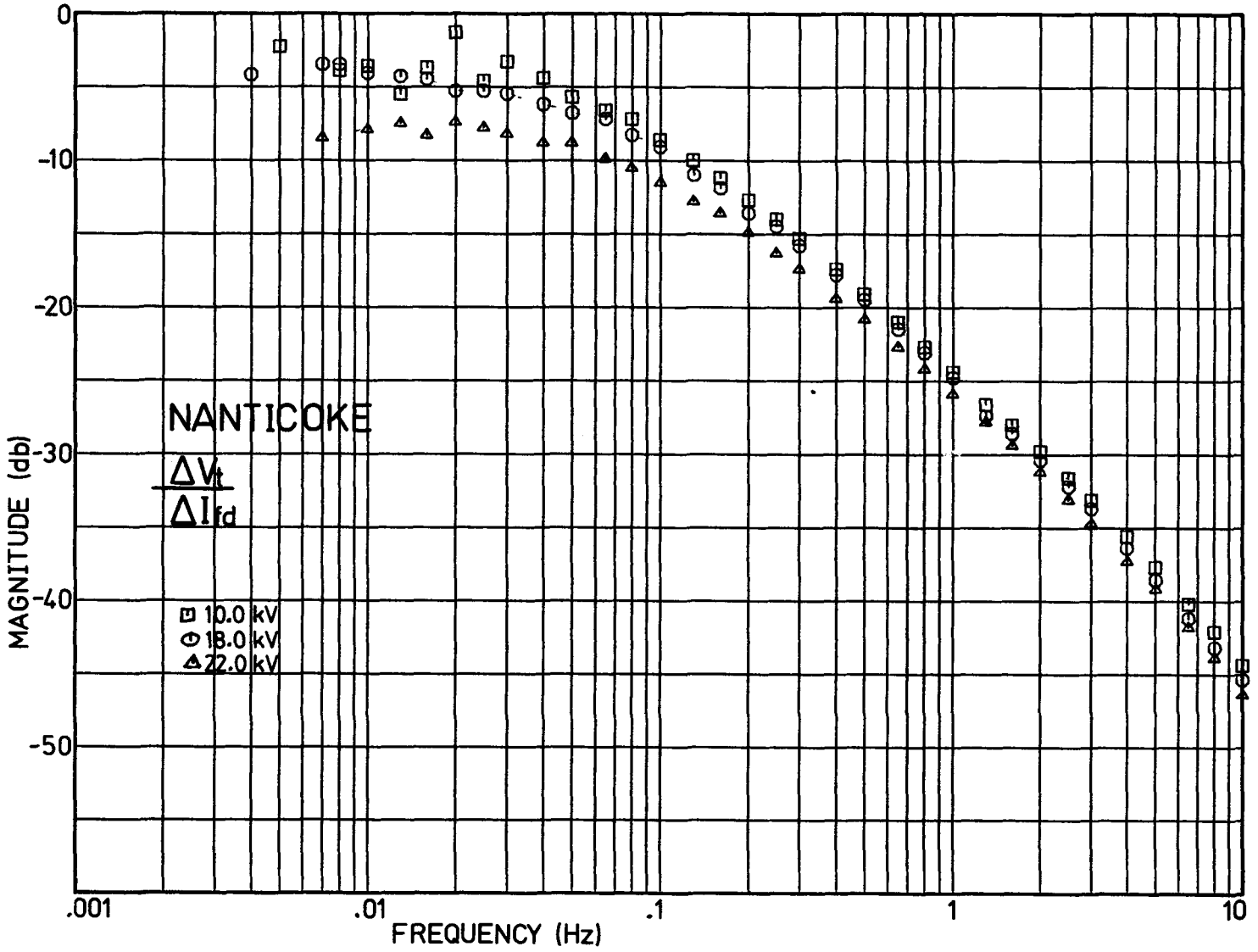

Figure 5-5. Magnitude of Nanticoke Open-Circuit Transfer Function From Field Current To Terminal Voltage.

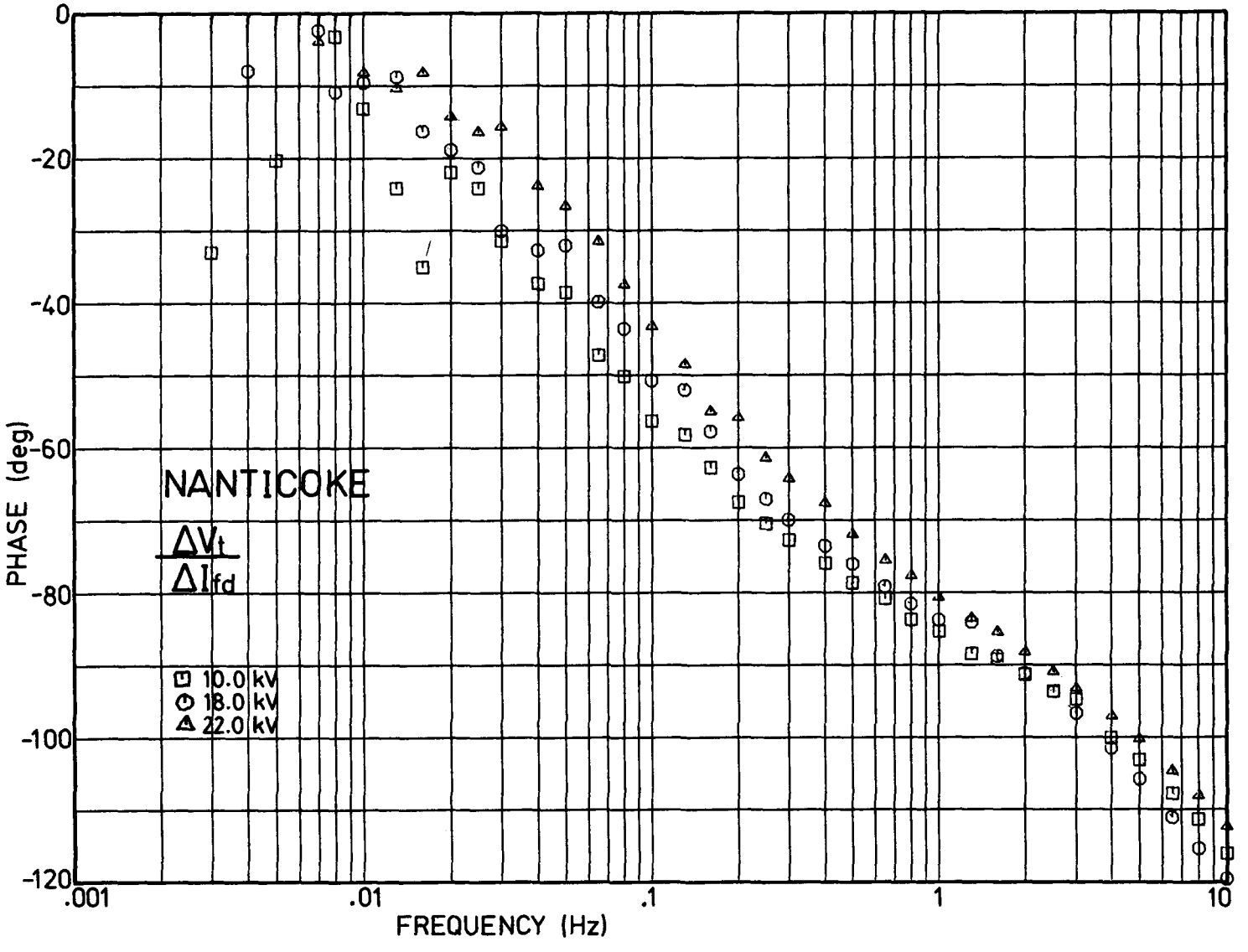

Figure 5-6. Phase of Nanticoke Open-Circuit Transfer Function From Field Current to Terminal Voltage.

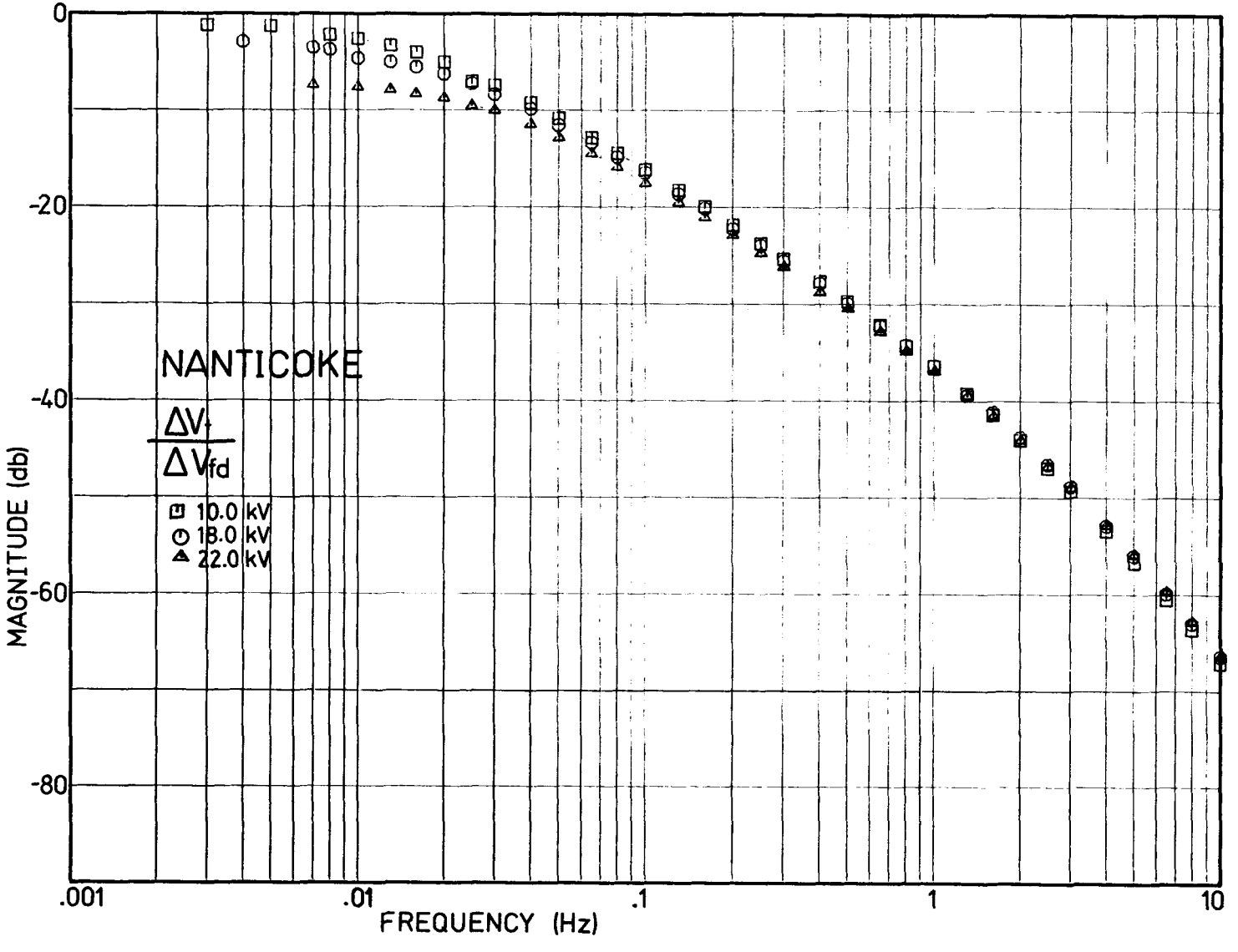

Figure 5-7. Magnitude of Nanticoke Open-Circuit Transfer Function From Field Voltage to Terminal Voltage.

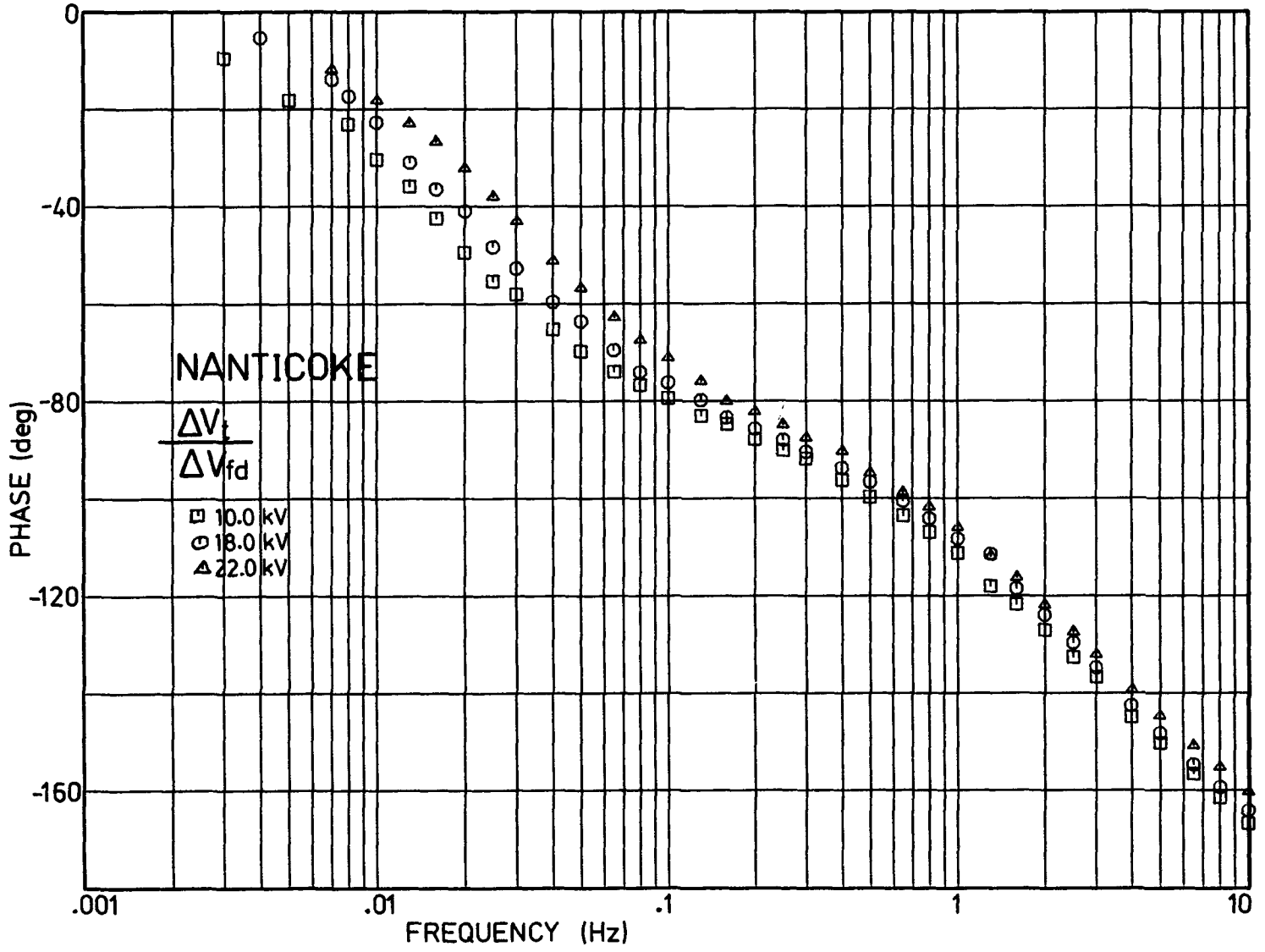

Figure 5-8. Phase of Nanticoke Open-Circuit Transfer Function From Field Voltage to Terminal Voltage.

LINEARITY TEST

The generator was operated at rated speed, off line at a nominal terminal voltage of 10 kV which is in the unsaturated region on the open-circuit saturation curve. At three selected frequencies, 0.2 Hz, 1.0 Hz and 5.0 Hz, the field voltage was varied, sinusoidally, over as wide an amplitude range as practical. The open-circuit transfer functions among field voltage, field current, and terminal voltage were measured at each of the three frequencies as functions of the field current modulation (Figures 5-9 to 5-11).

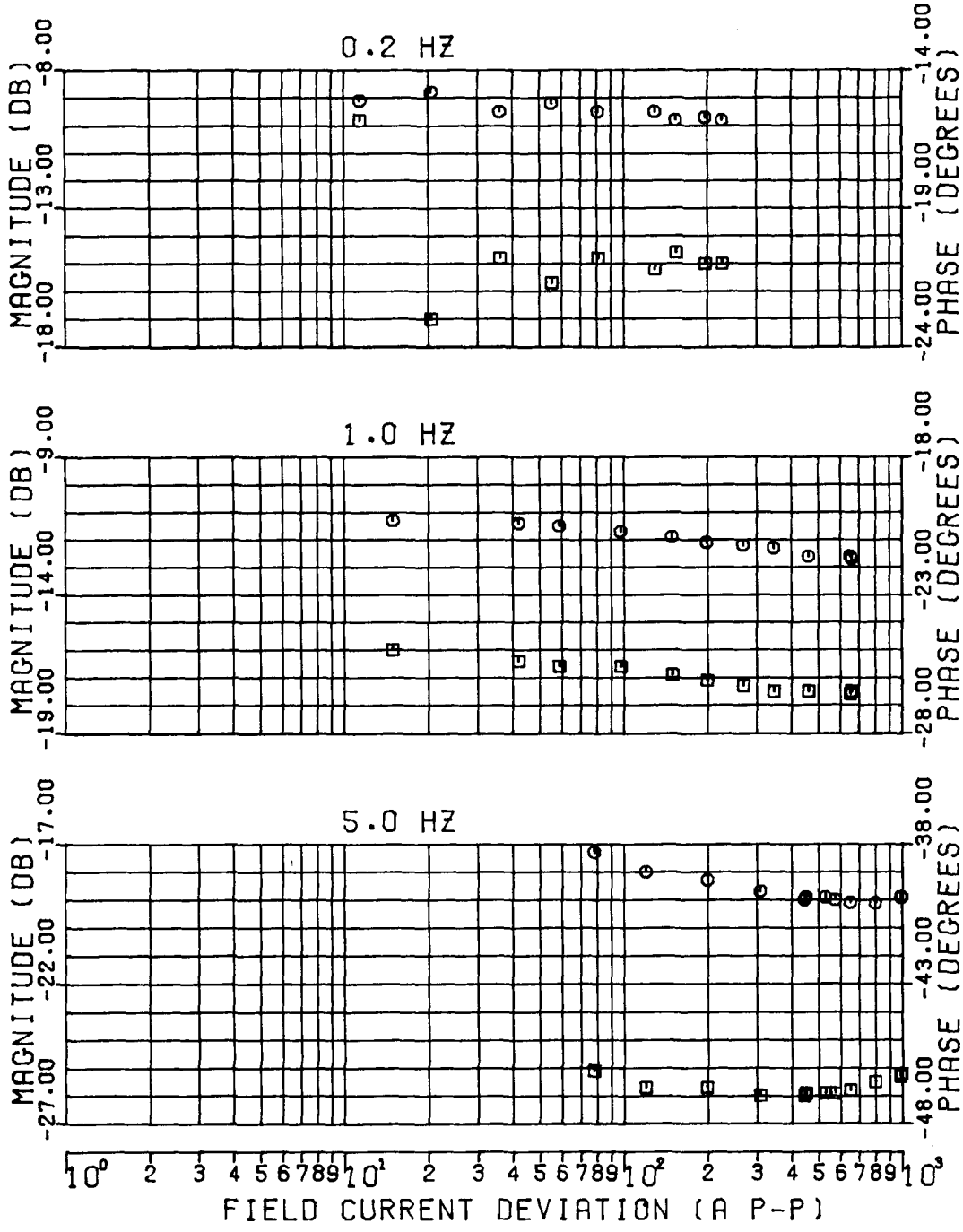

Figure 5-9. Nanticoke Open Circuit Transfer Function From Field Voltage to Field Current as a Function of Field Current Deviation.

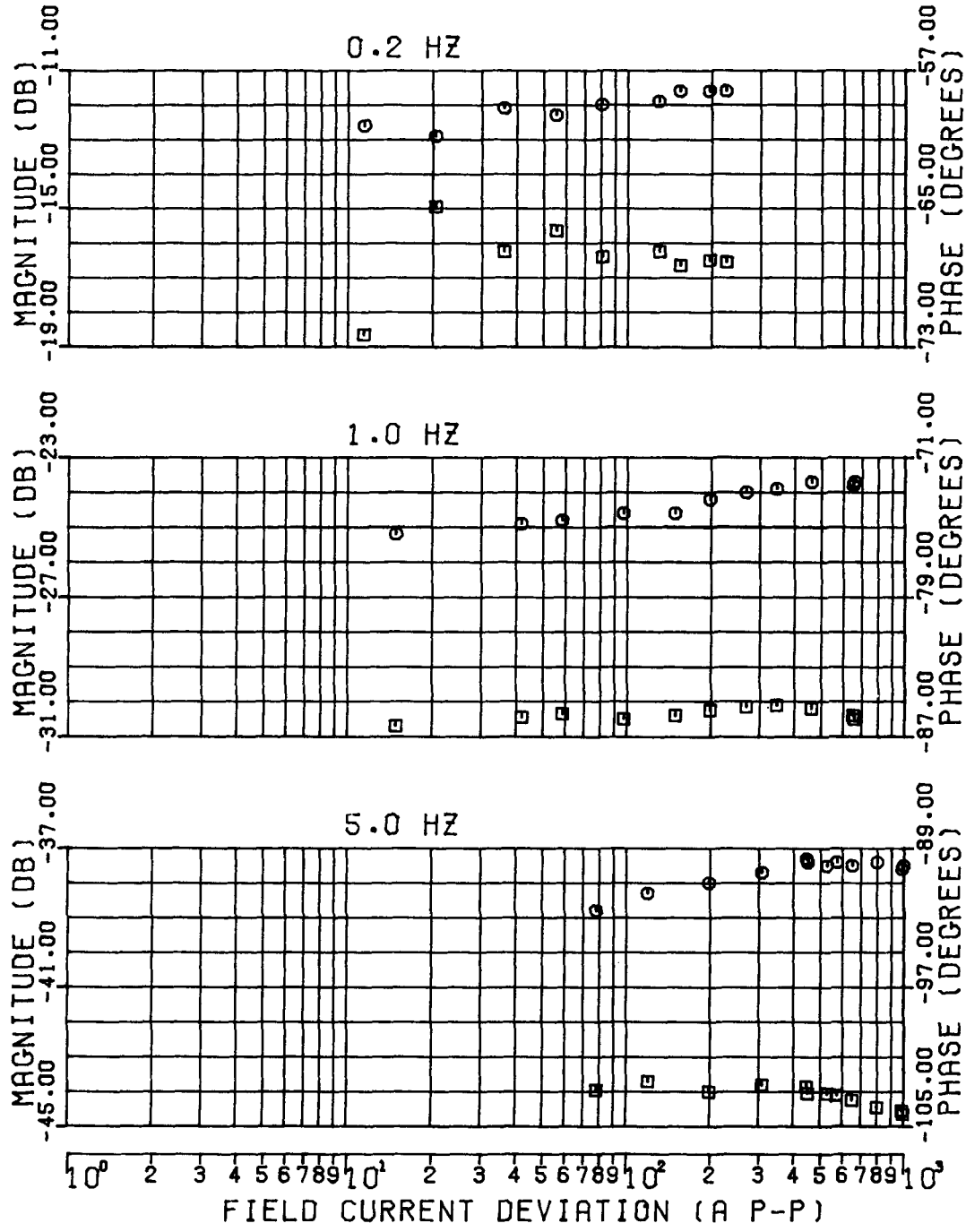

Figure 5-10. Nanticoke Open-Circuit Transfer Function from Field Current to Terminal Voltage as a Function of Field Current Deviation.

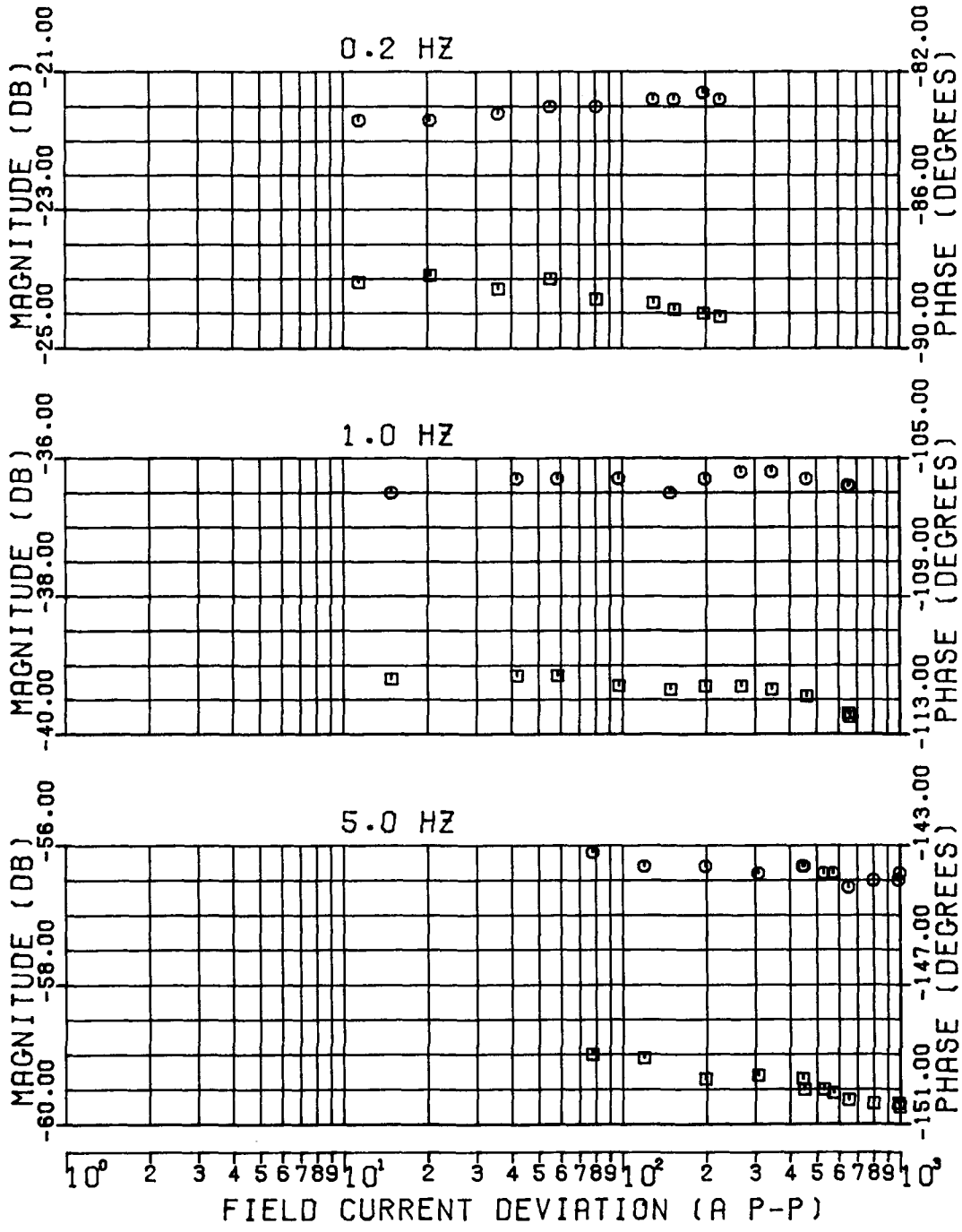

Figure 5-11. Nanticoke Open-Circuit Transfer Function from Field Voltage to Terminal Voltage as a Function of Field Current Deviation.

Section 6

STEADY STATE MEASUREMENTS

Steady state load point measurements similar to those described for Lambton were done at Nanticoke in 1975, prior to the start of this contract. Operating restrictions on the station at that time limited the permissible range of loads somewhat. In particular, no leading power factor tests were possible. However, useful data was still obtained for the normal operating range of the unit (Table 6-1).

TABLE 6-1

NANTICOKE STEADY STATE LOAD POINTS

Active Power (MW)	Reactive Power (MVAR)	Terminal Voltage (kV)	Stator Current (kA)	Field Current (A)	Internal Angle (deg)	Q-Axis Synchronous Reactance (pu)
100	39	21.25	2.83	1365	16.0	1.77
200	95	21.63	5.77	1813	24.6	1.66
200	80	21.52	5.62	1739	25.6	1.67
200	60	21.36	5.47	1643	27.3	1.69
200	40	21.23	5.36	1558	28.9	1.70
201	31	21.14	5.37	1520	29.8	1.69
300	99	21.58	8.23	2059	33.7	1.61
299	85	21.45	8.17	2003	34.7	1.61
298	70	21.38	8.07	1943	36.0	1.63
299	63	21.30	8.08	1918	36.7	1.63
300	42	21.17	8.02	1835	38.8	1.65
298	30	21.10	7.95	1791	39.8	1.66
299	17	21.00	7.99	1750	41.4	1.66
300	7	20.90	8.06	1721	42.8	1.67
403	140	21.77	11.10	2504	38.0	1.53
396	129	21.67	10.90	2444	38.6	1.55
401	107	21.57	10.89	2377	40.5	1.56
400	102	21.53	10.86	2358	40.8	1.56
402	85	21.40	10.85	2304	42.5	1.58
504	159	21.79	13.77	2858	42.5	1.47
499	145	21.68	13.61	1800	43.3	1.48
499	133	21.59	13.58	2753	44.3	1.49
500	122	21.47	13.59	2732	45.3	1.50
500	112	21.42	13.57	2699	46.1	1.51